

Topics in Current Chemistry Collections

Rocco Mazzeo *Editor*

Analytical Chemistry for Cultural Heritage

 Springer

Topics in Current Chemistry Collections

Journal Editors

Massimo Olivucci, Siena, Italy and Bowling Green, USA

Wai-Yeung Wong, Hong Kong

Series Editors

Hagan Bayley, Oxford, UK

Kendall N. Houk, Los Angeles, USA

Greg Hughes, Codexis Inc, USA

Christopher A. Hunter, Cambridge, UK

Kazuaki Ishihara, Nagoya, Japan

Michael J. Krische, Austin, Texas

Jean-Marie Lehn, Strasbourg, France

Rafael Luque, Córdoba, Spain

Jay S. Siegel, Tianjin, China

Joachim Thiem, Hamburg, Germany

Margherita Venturi, Bologna, Italy

Chi-Huey Wong, Taipei, Taiwan

Henry N.C. Wong, Hong Kong

Vivian Wing-Wah Yam, Hong Kong

Chunhua Yan, Beijing, China

Shu-Li You, Shanghai, China

Aims and Scope

The series Topics in Current Chemistry Collections presents critical reviews from the journal Topics in Current Chemistry organized in topical volumes. The scope of coverage is all areas of chemical science including the interfaces with related disciplines such as biology, medicine and materials science.

The goal of each thematic volume is to give the non-specialist reader, whether in academia or industry, a comprehensive insight into an area where new research is emerging which is of interest to a larger scientific audience.

Each review within the volume critically surveys one aspect of that topic and places it within the context of the volume as a whole. The most significant developments of the last 5 to 10 years are presented using selected examples to illustrate the principles discussed. The coverage is not intended to be an exhaustive summary of the field or include large quantities of data, but should rather be conceptual, concentrating on the methodological thinking that will allow the non-specialist reader to understand the information presented.

Contributions also offer an outlook on potential future developments in the field.

More information about this series at <http://www.springer.com/series/14181>

Rocco Mazzeo

Editor

Analytical Chemistry for Cultural Heritage

With contributions from

Matthias Alfeld • Willemien Anaf • Ludovic Bellot-Gurlet
Uwe Bergmann • Sylvain Bernard • Loïc Bertrand • Irene Bonacini
Ilaria Bonaduce • Bruno Brunetti • David Caramelli • Laura Cartechini
Francesca Casadio • Céline Daher • Ilaria Degano • Brenda Doherty
Aurélien Gourrier • Massimo Guardigli • Koen Janssens
Martina Lari • Stijn Legrand • Federica Marone • Rocco Mazzeo
Costanza Miliani • Mara Mirasoli • Francesca Modugno • Letizia Monico
Jacopo La Nasa • Wout De Nolf • Gert Nuyts • Melissa Palmieri
Maria Perla Colombini • Lucia Pitzurra • Silvia Prati • Ina Reiche
Erika Ribechini • Aldo Roda • Aldo Romani • Francesca Rosi
Philippe Sciau • Giorgia Sciutto • Antonio Sgamellotti • Mathieu Thoury
Manuela Vagnini • Stefania Vai • Geert Van der Snickt
Mark Van Strydonck • Frederik Vanmeert • Jo Verbeeck
Marc Vermeulen • Karolien De Wael • Martina Zangheri



Springer

Editor
Rocco Mazzeo
Department of Chemistry
University of Bologna
Bologna, Italy

Originally published in *Top Curr Chem (Z)*, Volume 374 (2016),
© Springer International Publishing Switzerland 2016

ISSN 2367-4067 ISSN 2367-4075 (electronic)
Topics in Current Chemistry Collections
ISBN 978-3-319-52802-1 ISBN 978-3-319-52804-5 (eBook)
DOI 10.1007/978-3-319-52804-5

Library of Congress Control Number: 2016963803

© Springer International Publishing AG 2017

This work is subject to copyright. All rights are reserved by the Publisher, whether the whole or part of the material is concerned, specifically the rights of translation, reprinting, reuse of illustrations, recitation, broadcasting, reproduction on microfilms or in any other physical way, and transmission or information storage and retrieval, electronic adaptation, computer software, or by similar or dissimilar methodology now known or hereafter developed.

The use of general descriptive names, registered names, trademarks, service marks, etc. in this publication does not imply, even in the absence of a specific statement, that such names are exempt from the relevant protective laws and regulations and therefore free for general use.

The publisher, the authors and the editors are safe to assume that the advice and information in this book are believed to be true and accurate at the date of publication. Neither the publisher nor the authors or the editors give a warranty, express or implied, with respect to the material contained herein or for any errors or omissions that may have been made. The publisher remains neutral with regard to jurisdictional claims in published maps and institutional affiliations.

Printed on acid-free paper

This Springer imprint is published by Springer Nature
The registered company is Springer International Publishing AG
The registered company address is: Gewerbestrasse 11, 6330 Cham, Switzerland

Contents

Editorial	vii
Rocco Mazzeo	
Emerging Approaches in Synchrotron Studies of Materials from Cultural and Natural History Collections	1
Loïc Bertrand, Sylvain Bernard, Federica Marone, Mathieu Thoury, Ina Reiche, Aurélien Gourrier, Philippe Sciau, Uwe Bergmann	
Non-invasive Investigations of Paintings by Portable Instrumentation: The MOLAB Experience	41
B. Brunetti, C. Miliani, F. Rosi, B. Doherty, L. Monico, A. Romani, A. Sgamellotti	
Non-Invasive and Non-Destructive Examination of Artistic Pigments, Paints, and Paintings by Means of X-Ray Methods	77
Koen Janssens, Geert Van der Snickt, Frederik Vanmeert, Stijn Legrand, Gert Nuyts, Matthias Alfeld, Letizia Monico, Willemien Anaf, Wout De Nolf, Marc Vermeulen, Jo Verbeeck, Karolien De Wael	
New Frontiers in Application of FTIR Microscopy for Characterization of Cultural Heritage Materials	129
S. Prati, G. Sciutto, I. Bonacini, R. Mazzeo	
Raman Spectroscopy of cultural heritage Materials: Overview of Applications and New Frontiers in Instrumentation, Sampling Modalities, and Data Processing	161
Francesca Casadio, Céline Daher, Ludovic Bellot-Gurlet	
Immunochemical Micro Imaging Analyses for the Detection of Proteins in Artworks.	213
Giorgia Sciutto, Martina Zangheri, Silvia Prati, Massimo Guardigli, Mara Mirasoli, Rocco Mazzeo, Aldo Roda	
Immunochemical Methods Applied to Art-Historical Materials: Identification and Localization of Proteins by ELISA and IFM.	241
Laura Cartechini, Melissa Palmieri, Manuela Vagnini, Lucia Pitzurra	

Trends in High Performance Liquid Chromatography for Cultural Heritage	263
Ilaria Degano, Jacopo La Nasa	
Analytical Approaches Based on Gas Chromatography Mass Spectrometry (GC/MS) to Study Organic Materials in Artworks and Archaeological Objects	291
Ilaria Bonaduce, Erika Ribechini, Francesca Modugno, Maria Perla Colombini	
DNA Sequencing in Cultural Heritage	329
Stefania Vai, Martina Lari, David Caramelli	
Radiocarbon Dating	347
Mark Van Strydonck	

Editorial

Rocco Mazzeo¹

© Springer International Publishing Switzerland 2016

The conservation–restoration of cultural heritage is undoubtedly a field of interdisciplinary collaboration among professionals with different educational backgrounds and professional experience. To this purpose, a mutual understanding among conservator–restorers, archaeologists, art historians, architects, conservation scientists—and chemists in particular—is needed for a proper safeguarding of cultural properties. Indeed, recent decades have seen the involvement of an increasing number of chemists because of the importance of diagnostic studies and research into conservation materials and treatments. I am pretty much convinced that the vast array of works of art representing the highest forms of human production provides important occasion for knowledge advancement, promoting close interactions among disciplines seemingly far removed from each other, such as chemistry and art history or archaeology.

Cultural heritage, one of the higher expressions of human activities, makes use of a variety of materials that have yet to be identified, and this is why every single work of art systematically involves issues that typically belong to chemistry. This happens from the very moment of the creation of a work of art, and continues towards the period in which chemistry determines the rate of transformation, ageing, degradation and sometimes the complete disappearance of the artefact. It was therefore predictable that chemistry and the other scientific disciplines would be asked to be involved in the safeguarding of cultural heritage.

To this end, chemists apply examination of works of art using both advanced analytical methods and conservation science, which is concerned with the

This article is part of the Topical Collection “Analytical Chemistry for Cultural Heritage”.

✉ Rocco Mazzeo
rocco.mazzeo@unibo.it

¹ Department of Chemistry “Giacomo Ciamician”, Microchemistry and Microscopy Art Diagnostic Laboratory, University of Bologna, Via Selmi 2, 40126 Bologna, Italy

physical/material aspects of works of art, their deterioration and conservation. Scientific examination and conservation science both rely on measurements central to analytical chemistry for cultural heritage, that branch of chemistry concerned with determining the qualitative and quantitative identity of heritage materials.

Today, analytical chemistry plays a key role in the characterization of the nature of heritage materials, the study of ancient production techniques, the understanding of causes and mechanisms of degradation, and the development and performance evaluation of restoration materials and methods. It also supports archaeological and historical interpretations through archaeometric studies aimed at characterizing ancient materials, the way in which they were produced, and their provenance, authenticity and dating.

Unfortunately, the systematic involvement of science in general, and chemistry and analytical chemistry in particular, dates back only four decades. In fact, even though the first contributions of science to the study of works of art occurred at the beginning of the last century, it was a cautious entry, independent of the efforts and capacities of the first pioneers, who were few in number and with very limited resources available. However, starting in the 1950s, the application of science, and particularly chemistry, to conservation became increasingly systematic, although poorly coordinated if compared with the extent and complexity of the problems raised by the conservation of cultural heritage.

Nowadays, analytical chemistry as applied to cultural heritage is a recognized discipline that covers many advanced and complex aspects of chemical research, as highlighted by the publication of peer-reviewed journal special issues such as those on characterization of paintings [1], analytical chemistry in cultural heritage [2], advanced techniques in art conservation [3] and a recently published critical review on analytical chemistry in the field of cultural heritage [4].

While offering as broad a view as possible, a panorama of the most advanced analytical methodologies and procedures applied to the characterization, origin and mechanisms of heritage materials decay, this collection of *Topics in Current Chemistry* cannot be comprehensive, but I'm convinced it demonstrates their key role in conservation research.

An innovative contribution to this topical collection deals with synchrotron-based techniques. In fact, although photon-based speciation has been applicable mainly to inorganic materials, novel developments based on scanning transmission X-ray microscopy (STXM) and deep UV photoluminescence bring new opportunities to study speciation in organic and hybrid materials at a sub-micrometre spatial resolution.

Moreover, in the context of the characterization of pigments subject to natural degradation, synchrotron facilities are able to elucidate the chemical transformation that has taken place. In particular, the combination of micro X-ray fluorescence (μ -XRF) with related methods such as micro X-ray absorption spectroscopy (μ -XAS), micro X-ray diffraction (μ -XRD), Fourier transform infrared microscopy (μ -FTIR) and/or Raman microscopy have proven themselves quite suitable for such studies. Since microscopic investigation of a relatively limited number of minute paint samples may not yield information representative of the entire work of art, new methods for macroscopic imaging, such as those based on X-ray fluorescence

scanning and full-field hyperspectral imaging, have been developed and are presented and discussed.

The challenge of analysing works of art in situ by means of portable non-invasive analytical techniques including XRF, mid- and near-FTIR, UV–Vis and Raman spectroscopy, as well as XRD, are discussed in detail, along with their impact on our understanding of painting materials and execution techniques. Readers will find successful applications for both point analyses and hyperspectral imaging approaches. More challenging applications, such as the identification of organic pigments, where the synergistic use of FTIR, UV–Vis and Raman spectroscopy can lead to satisfactory results, are also presented and discussed.

Notwithstanding the utility of non-invasive analytical techniques and their use in situ, they cannot provide a detailed stratigraphic characterization of the materials constituting works of art. This is particularly true when organic-based components must be identified and spatially located. In this regard, the most recent decades have seen the development and use of advanced micro-invasive analytical techniques. It is worth mentioning the progress achieved by high-performance liquid chromatography (HPLC) in the detection of dyestuffs, enzyme-linked immunosorbent assay (ELISA), immunofluorescence microscopy (IFM) and immunochemical imaging techniques for protein-based materials, and gas chromatography mass spectrometry (GC/MS) in the detection of organic materials in ancient as well as modern and contemporary works of art. In fact, all these analytical techniques have been substantially improved in terms of both new sample preparation procedures, which allow a greater number of heritage materials to be examined, and interpretation of results, thanks to the great support provided by chemometric multivariate analyses.

The field of Raman and FTIR spectroscopy in art and archaeology has experienced massive, vital growth since its first application to heritage materials. Despite the many reviews available in the literature, this is the first time that extensive coverage has been devoted to advanced spectral processing and the contributions of chemometrics to the furtherance of spectroscopic studies of works of art. Raman spectroscopy is also increasingly being used to uncover structure–property relationships of artistic and archaeological materials at the microscale and to reconstruct ancient technologies. Surface-enhanced Raman spectroscopy (SERS) is now an established tool in the analytical chemist’s toolkit, while new developments in spatially offset Raman spectroscopy (SORS) and widefield imaging are expected. At the same time, a new and very promising field is the development of enhanced FTIR methods for detecting trace components in micro extracts, allowing the detection of extractable organic compounds from about 0.1 mg of sample such as natural and synthetic dyes.

Despite initial scepticism, radiocarbon dating has gained considerable importance over the last decades. In fact, art objects made of textile, ivory, stucco, paper or parchment and polychrome statues can now be dated. To this end, the introduction of accelerator mass spectrometry (AMS), which enables the amount of sample to be confined in 1 mg of carbon and reduces counting time to 50 min, has proven to be revolutionary, particularly when applied to the dating of precious art objects.

Another important research issue, which is well presented in this topical collection, concerns DNA sequencing as applied to anthropology, archaeozoology, molecular evolution and population genetics. A dramatic improvement in DNA methodologies has occurred in recent years, yielding to a revolution that has allowed the recovery of even complete genomes from highly degraded samples, with the possibility of going back in time 400,000 to 700,000 years. The application to individual identification of famous personalities such as King Richard III confers to paleogenetics an important role in cultural heritage studies.

It can certainly be said that analytical chemistry has had and will continue to have an impact on all aspects of cultural heritage knowledge, from historical studies, material degradation and characterization, to conservation and fruition.



References

1. Mazzeo R, Roda A (2008) *Anal Bioanal Chem* 392(1–2):27–28
2. Mazzeo R, Roda A, Prati S (2011) *Anal Bioanal Chem* 399:2885–2887
3. Brunetti BG, Sgamellotti A (2010) *Acc Chem Res* 43(6):693–694
4. Madariaga JM (2015) *Anal Methods* 7:4848–4876

Emerging Approaches in Synchrotron Studies of Materials from Cultural and Natural History Collections

Loïc Bertrand^{1,2} · Sylvain Bernard³ · Federica Marone⁴ ·
Mathieu Thoury^{1,2} · Ina Reiche^{5,6} · Aurélien Gourrier^{7,8,9} ·
Philippe Sciau¹⁰ · Uwe Bergmann¹¹

Received: 17 September 2015 / Accepted: 24 November 2015 / Published online: 4 January 2016
© Springer International Publishing Switzerland 2015

Abstract Synchrotrons have provided significant methods and instruments to study ancient materials from cultural and natural heritages. New ways to visualise (surfacic or volumic) morphologies are developed on the basis of elemental, density and refraction contrasts. They now apply to a wide range of materials, from historic artefacts to paleontological specimens. The tunability of synchrotron beams owing to the high flux and high spectral resolution of photon sources is at the origin of the main chemical speciation capabilities of synchrotron-based techniques. Although, until recently, photon-based speciation was mainly applicable to inorganic materials, novel developments based, for instance, on STXM and deep UV photoluminescence bring new opportunities to study

✉ Loïc Bertrand
loic.bertrand@synchrotron-soleil.fr

- ¹ IPANEMA, CNRS, Ministère de la Culture et de la Communication, Université Paris-Saclay, 91192 Gif-sur-Yvette, France
- ² Synchrotron SOLEIL, BP 48 Saint-Aubin, 91192 Gif-sur-Yvette, France
- ³ IMPMC, CNRS UMR 7590, Sorbonne Universités, MNHN, UPMC, IRD UMR 206, 61 rue Buffon, 75005 Paris, France
- ⁴ Swiss Light Source, Paul Scherrer Institut, 5232 Villigen, Switzerland
- ⁵ Rathgen-Forschungslabor, Staatliche Museen zu Berlin-Stiftung Preußischer Kulturbesitz, Schloßstraße 1a, 14059 Berlin, Germany
- ⁶ Sorbonne Universités, UPMC University Paris 06, CNRS, UMR 8220, Laboratoire d'archéologie moléculaire et structurale (LAMS), 4 place Jussieu, 75005 Paris, France
- ⁷ Université Grenoble Alpes, LIPHY, 38000 Grenoble, France
- ⁸ CNRS, LIPHY, 6 rue Jules Horowitz, 38043 Grenoble, France
- ⁹ European Synchrotron Radiation Facility, 38043 Grenoble Cedex, France
- ¹⁰ CEMES, CNRS UPR 8011, Université de Toulouse, 29 rue J. Marvig, 31055 Toulouse, France
- ¹¹ Stanford PULSE Institute, SLAC National Accelerator Laboratory, Menlo Park, CA 94025, USA

speciation in organic and hybrid materials, such as soaps and organometallics, at a sub-micrometric spatial resolution over large fields of view. Structural methods are also continuously improved and increasingly applied to hierarchically structured materials for which organisation results either from biological or manufacturing processes. High-definition (spectral) imaging appears as the main driving force of the current trend for new synchrotron techniques for research on cultural and natural heritage materials.

Keywords Synchrotron · Palaeontology · Cultural heritage · Archaeometry · Imaging

Abbreviations

CT	Computed tomography
DUV	Deep ultraviolet
EELS	Electron energy loss spectroscopy
EPMA	Electron probe micro-analysis
FF	Full field
FIB	Focused ion beam
FOV	Field of view
FTIR	Fourier-transform Infrared spectroscopy
Ga	Gigaannum
Ma	Megaannum
Myr	Million year
NEXAFS	Near edge X-ray absorption fine structure (=XANES)
PIXE	Proton induced X-ray emission
PL	Photoluminescence
Pps	Projected pixel (voxel) size on the sample plane
qsSAXSI	Quantitative scanning SAXS imaging
ROI	Region of interest
SAXS	Small-angle X-ray scattering
SC	Semi-conductor
SEM	Scanning electron microscopy
SR	Synchrotron radiation
STXM	Scanning transmission X-ray microscopy
TEM	Transmission electron microscopy
Vis	Visible
XANES	X-ray absorption near edge structure
XAS	X-ray absorption spectroscopy
XRD	X-ray diffraction
XRF	X-ray fluorescence

1 Introduction: New Methodologies to Study Ancient Materials

The three main drivers of the complexity of ancient materials are their complex chemical composition, their multiscale heterogeneity, and the contrast in relative abundance in their individual components [20]. During characterisation, such

complexity is addressed by *dynamics* in its general meaning—either spatial, spectral, or intensity-wise, in order to identify, characterise and discriminate traces over large scales [29]. The main specificities of the synchrotron radiation source—polychromaticity, high flux, low divergence, small source size, stability, “calculability” of the source, and polarisation—are well adapted to addressing these challenges [20]. Investigations using synchrotron methods are generally coupled to a range of laboratory approaches.

In the past decade, several articles reviewed the potential of synchrotron radiation (SR) techniques for heritage studies. Cotte et al. discussed the benefits of synchrotron-based FTIR and X-ray absorption spectroscopy for a better identification, discrimination and mapping of paint materials (pigments, binders, alteration products) across historical cross sections collected from easel and mural paintings, and archaeological artefacts [57, 58]. In recent reviews, Bertrand et al. discussed recent application of synchrotron techniques to cultural heritage and archaeology. The main fields of application of synchrotron techniques in the field were shown to concern the study of alteration and corrosion processes, identification of raw materials and technologies used to produce archaeological artefacts and art objects, and, to a lesser extent, investigation of current or novel stabilisation, conservation and restoration practices [27]. The trends were discussed on a methodological and instrumentation perspective, particularly focusing on the use of microfocused hard X-ray spectroscopy (absorption, fluorescence, diffraction), full-field X-ray tomography and infrared spectroscopy [20].

Several specific reviews were also produced for categories of ancient materials. One of the earliest and most developed groups of materials studied using synchrotron techniques is paint materials (artists’ pigments, binders and extenders, alteration compounds such as metal soaps and oxidation products of pigments); these materials are studied to describe mechanisms of physicochemical alteration, acquire information on technical art history, or obtain knowledge on artists’ and workshop practices [56, 103].

The use of synchrotron techniques to study ancient metallurgical samples was reviewed by Young et al. [186], while Manso et al. discussed application to paper-based materials [122]. The study of fossil specimens from natural history collections is a flourishing application of synchrotron-based imaging, owing in particular to the application and adaptation of high-resolution micro-tomographic techniques to paleontological and paleoanthropological specimens [8, 71, 156, 173–175]. In addition, a range of new raster-scanning techniques is gradually being adapted to the study of fossil specimens [89].

In the present article, we discuss recent applications based on the subjective selection of recent research works that show promise for further extension in the field of ancient materials sciences. We have deliberately chosen not to attempt to exhaustively cover all significant ongoing developments. Rather, the present contribution aims at providing a concise view of areas that could be further developed and adapted to a wider range of topics concerning ancient materials, as well as neighbouring fields of research such as environmental sciences.

The main trend observed is the generalisation of *high-definition imaging* as the core approach to tackle the heterogeneity of heritage materials across several orders

of magnitude in length scale. Among other promising developments, we discuss developments towards a finer discrimination and high-resolution mapping of heterogenous hybrid (organic–inorganic) compounds across ancient cross-sections, and the acquisition and processing of accurate structure- and texture-related information on ancient mineral materials with a strong hierarchical architecture.

2 Morphologies through Density and Chemical Contrasts

The development of high-definition imaging, particularly in the X-ray range, has been extremely significant for the heritage field in the past 5–10 years. This resulted from new setups, data collection and data analysis strategies reaching a mature stage within laboratory environments and at large-scale facilities; in particular, synchrotrons. We discuss here complementary approaches that apply to the imaging of both bulk artefacts (generally centimeter to decimeter-sized, low spatial resolution) and samples (down to submillimetric size, high to very high resolution). For such approaches, two main data collection strategies predominate: full-field imaging and raster-scanning. We have selected representative examples of both 3D microtomography and fast XRF scanning. Detailed images are used to correlate (spatially-resolved) local contrasts with the morphology of the sample, which can be further associated with information from other characterisation techniques. They also allow to search and analyse details within large areas (volumes) of samples, and to discover unexpected characteristics of the studied materials on-the-go.

2.1 Visualising 3D Internal Morphologies through Tomographic Microscopy

Two-dimensional X-ray microscopy has existed for many years and is still an important tool for the non-destructive investigation of a large variety of samples, including precious or rare objects [33]. The gained information is, however, cumulative and the absolute position of the interaction along the beam path cannot be uniquely determined. Access to the third dimension is achieved by the acquisition of a number of object views taken at different angles, which are subsequently combined using analytic [106] or iterative tomographic reconstruction algorithms. Insight into volumetric information has opened up numerous new possibilities for addressing old and new scientific questions, with a tremendous increase in the number of studies in the field making use of this technique.

In their interaction with matter, X-rays, as a consequence of the photoelectric effect, are attenuated according to the Beer-Lambert law:

$$I(Z, E) = I_0(E) \exp\left(-\int \mu(Z, E) dz\right) \quad (1)$$

where $I(Z, E)$ and $I_0(E)$ are the beam intensities after and before the specimen under investigation, respectively, E is the beam energy and Z the atomic number [7]. The main material property determining the absorption characteristics of a specimen is its linear attenuation coefficient μ related to the imaginary part β of the refraction

index $n(Z, E) = 1 + \beta(Z, E)i - \delta(Z, E)$ by $\mu = 4\pi\beta/\lambda$, where λ is the radiation wavelength [7].

Absorption contrast tomographic microscopy, as a consequence of the strong dependency of μ on $Z(\propto Z^4)$, is particularly suited to investigate samples composed of materials with contrasting densities and Z numbers larger than 10 [e.g. alkaline earth metals (Mg and Ca), transition metals (Fe, Co...), metalloids (Si) and halogens (Br, Cl, I...)]. Highest contrast is obtained by ad-hoc energy selection of the X-ray beam ensuring optimal penetration depth into the studied material ($\mu \propto E^{-3}$).

In paleontology, tomographic microscopy has revolutionized the study of fossils, giving access to 3D morphological, and to some extent, chemical information with unprecedented spatial resolution, in a non-destructive manner [59]. Insights into fossil anatomy, development and preservation can be obtained in a high throughput way, and reconstruction of extinct organisms, fossilized flowers, seeds and fruits from incomplete remains is strongly facilitated. Computer-assisted treatment of 3D digital data sets is also very useful to virtually extract delicate fossils embedded in rocks or matrices that are difficult to dissolve or remove without damaging the object of interest [50]. In addition to the wealth of morphological and chemical information, 3D digital reconstructions also permit functional analysis studies and testing of longstanding debates. With digital 3D reconstructions of the mandible of two of the earliest mammaliaformes and applying classical mechanics and finite element modelling, it was, for instance, possible to test hypotheses regarding the functional and dietary specialisation of these primitive mammalians. The results suggest that early lineage splitting and ecomorphological adaptation of skull and jaw occurs from the early stages of mammalian evolution [84]. 3D digital data sets, with the possibility to virtually remove layers or in-fill negative spaces, are also extremely valuable to investigate the possible taphonomic processes leading at times to very cryptic fossilized specimens. *Virtual taphonomy* is an attractive tool, easing their identification [165]. For instance, in early fruits from the sedge family, only the hard endocarp is usually preserved, while the same part in modern specimens is typically buried below a succession of soft layers lost during the fossilisation process. With virtual taphonomy, these various layers can be digitally peeled off, revealing the previously hidden, and therefore difficult to guess surface morphology of the endocarp. Access to this information makes classification of fossil specimens easier and more reliable.

The great potential of X-ray tomographic microscopy for the study of manuscripts has been demonstrated in several works, where scrolls have been virtually *unrolled* and subsequently deciphered (e.g. [119, 126]). In fact, many ancient documents have experienced heavy degradation hindering any manipulation, unwrapping or page flipping. The digitization in these works has been feasible, thanks to the particular chemistry of the used ink (“iron gall” ink), with a formulation containing a sufficient amount of iron to produce considerable contrast to distinguish the ink from its support. The same approach is also being used in the framework of the “Venice Time Machine” program (<http://dhvenice.eu>). The aim is to digitize all books and manuscripts of the “Archivio di Stato” in Venice, in a fast and safe way. The chemistry of the used inks for administrative documents is,

however, mostly poorly known. Although also mostly based on the “iron gall” formulation, the chemical composition, and in particular, the iron content of these black inks, varies a lot between documents spanning several centuries, and even within the same manuscript. In most cases, the iron content is sufficient for character detection, and proof-of-principle studies demonstrated page-by-page deciphering of a small book [2, 3] (Fig. 1). Analogously, images and sound could be recovered from degraded acetate films, impossible to unreel because of the film sticking to itself as a consequence of the breakdown of acetate to acetic acid. Since silver is responsible for the images in black and white movies, the contrast against the acetate support provided by X-rays should be sufficiently high to extract the pictures. In a proof-of-concept study, Davis & Mills demonstrated the feasibility with an X-ray tube, by recovering a few seconds of the opening of the British Gaumont News, sound included [62].

Synchrotron-based absorption contrast tomographic microscopy is constantly finding new applications. For instance, Bertini et al. investigated Iron Age Scottish glass beads, unraveling their internal morphology (e.g. 3D shape, size, number and distribution of gas bubbles and crystals, the filling of bubbles, characterization and spatial distribution of different materials within the beads) in a non-destructive manner, leading to conclusions on manufacturing techniques and location, as well as pyro-technological development of ancient communities [19].

When X-ray absorption is low or a specimen consists of materials with similar densities and/or Z numbers, different X-ray-matter interaction mechanisms can be exploited to enhance the contrast in the object under study. X-rays are in fact not only attenuated by matter, but also refracted at material interfaces, albeit by only a tiny angle. This angle is related to the real part δ of the index of refraction n , according to $\alpha = \int \frac{\partial \delta(x,y)}{\partial x} dz$ and is proportional to the gradient of the phase $\phi(x,y)$ of the refracted beam [32], e.g. $\alpha = \frac{\lambda}{2\pi} \frac{\partial \phi(x,y)}{\partial x}$. The refraction angle can be accurately determined using different phase contrast techniques, belonging mostly to three main categories: free-space propagation [45, 167], interferometry [31, 131, 182] and analyzer systems [43, 63]. All methods have advantages and disadvantages, for instance in terms of sensitivity, spatial resolution and practicality.

In the case of ancient papyrus scrolls carbonized during the Vesuvian eruption in 79 AD, black carbon-based ink is difficult to distinguish from the carbonized substrate using purely absorption contrast, due to the similar densities of the materials [128]. Instead, free space propagation phase contrast helps in this task. In fact, if the X-rays impinging on the sample are (partially) coherent, the refracted beam interferes with the direct beam downstream from the specimen. A characteristic interference pattern, typically known as Fresnel fringes, can be observed at the object interfaces, facilitating the discrimination of object domains with similar densities. Because the boundary visibility in particular is intensified in this way, this method is commonly called edge enhancement. Despite its simplicity, it is routinely used for the study of delicate charcoaled and lignified fossils, such as spores, flowers and seeds (e.g. [79]), and for virtual dissection of fossil wood permineralized with pyrite to facilitate the characterization at the submicrometer level [172]. In particular, this approach has proved invaluable to map fine

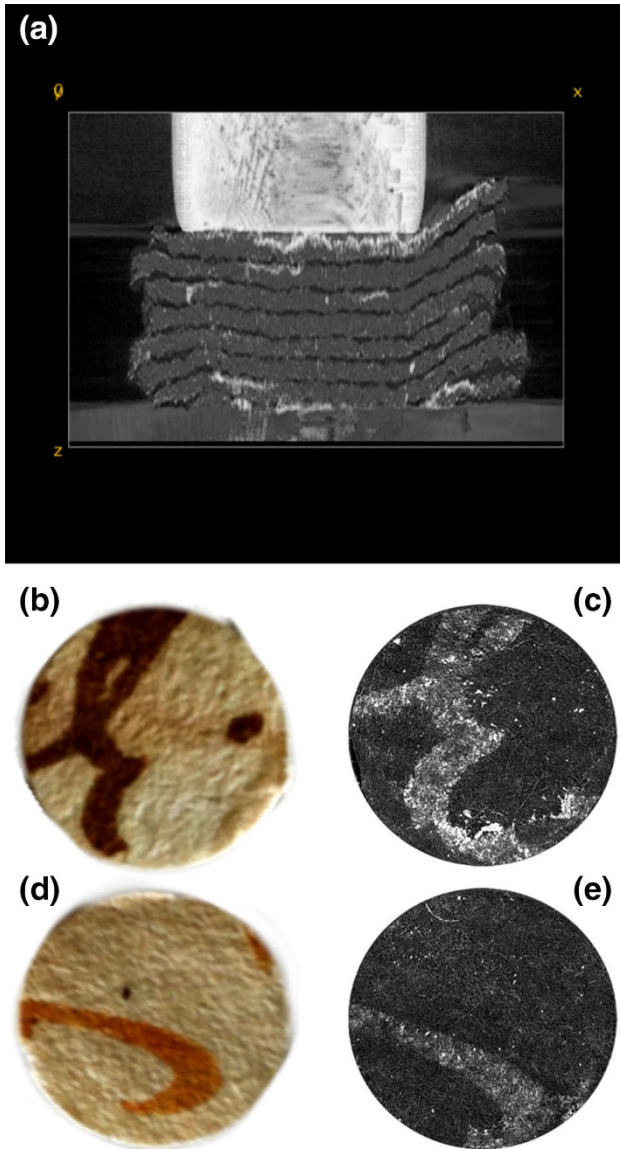


Fig. 1 X-ray tomographic microscopy of a 1679 Italian document. Several specimen fragments (0.8 cm diameter) have been stacked to simulate a small volume. **a** Vertical cut through the 3D reconstructed data set; the bright area at the *top* represents a small magnet used to keep the fragments in place. **b, d** Photographs of two different characters written with iron gall (**b**) and Hg-containing (**d**) ink. **c, e** The same two characters read from the digital volume by virtual slicing the tomographic data set. Data collected at the TOMCAT beamline [170] at the SLS-PSI; Energy: 15 keV, voxel size: 6.5 μm . *Source:* Reproduced with permission from [2]

laminations in enamel and dentine. This is important for studying fossilized hominid and primate teeth (e.g. [166]) providing insight into the evolution of human growth and development.

Fresnel fringes do not only highlight interfaces, but can also contribute to boost area contrast, and therefore enormously facilitate segmentation using straightforward global thresholding methods as opposed to more complex phase retrieval procedures. Several phase retrieval algorithms exist, based on different approximations [36, 46, 88, 114]. The single distance phase retrieval approach after Paganin et al. [136], thanks to its practicality and robustness, is one of the most used algorithms for the investigation of natural history (e.g. [80, 132]) and cultural heritage artefacts, although it lacks quantitiveness and the high frequencies in the tomographic reconstructions are partially damped. To overcome these drawbacks, more accurate algorithms exist [46]. Yet they generally require the acquisition of tomographic data sets at multiple distances and rather complex post-processing workflows [155]. In selected applications, holotomography gave superior results. With this technique, it was, for instance, possible to reveal the skull and brain in 300 Ma old fish, despite the small density difference between the pristine rock matrix and the regions preserving small amounts of soft tissue [141].

Currently, progress in the X-ray imaging field is made towards improved spatial and temporal resolution. With a projection microscope, it has in fact been possible to go beyond the typical spatial resolution in the sub-micrometer range of state-of-the-art hard X-ray microtomography end-stations based on a parallel beam geometry. Moreau et al. revealed non-destructively, with the required spatial resolution in the order of hundred nanometers, features (e.g. organization, size and shape) of in-situ pollen grains in 100 Ma old flowers, critical for plant classification [132]. Comparable resolution and truly quantitative electron density distributions can be achieved using ptychography: at each angular position, the sample is scanned across a coherent, often highly structured, X-ray beam while diffraction patterns are collected. By exploiting the redundancy provided by the overlapping adjacent probe spots and iterative phase retrieval algorithms [147], the effects of the sample can be successfully separated from those of the structured illumination. Visualization with this emerging technique of cellular and sub-cellular features in apatite preserved tubular fossils, enabled the reassessment of the phylogenetic affinity of these extant organisms [60].

Increased temporal resolution, compared to the typical few minutes required at most microtomography endstations for a tomographic scan, could be valuable for the investigation of dynamic processes involving natural history or historical objects. At third generation synchrotron sources, the high brilliant beams coupled to CMOS detectors permit the acquisition of all projections necessary for a tomographic reconstruction in less than a second [130], enabling the investigation of the evolution of the 3D microstructure through time. Although time-resolved experiments remain rare in the cultural heritage field, this technique could bring valuable information for the understanding of degradation processes observed, for instance, on paintings (through exposure to light, heat sources and humidity in a uncontrolled manner), in particular if such phenomena could be simulated and

accelerated for research purposes. For instance, Ferreira et al. documented with synchrotron-based tomographic microscopy the destructive effect of calcium soap migration in paintings and suggested a formation mechanism [73]. Time-resolved tomographic investigations could be very useful for testing these ideas and improving our understanding of the dynamics of formation and migration of these aggregates, especially if ad hoc materials can be prepared and artificially subjected to different environmental conditions. The same is true for conservation techniques of historical objects, where the effects of physical and chemical treatments, in particular at the micrometer level, are still poorly understood.

2.2 Imaging Flat Artefact and Samples through Fast XRF Raster-Scanning

Highly resolved spatial information about the chemical composition of cultural and natural artefacts can be valuable in many different aspects. In paintings and manuscripts, it can reveal the elemental composition of colours and inks. This can help in uncovering obscured drawings or writings, or reveal information about the origin, authenticity, degradation and age of the artefact. In natural history artefacts, such as fossilized animals or plants, it can reveal biomarkers of the original life form, including soft tissue not seen in the visible image of the fossil. This can lead to a better understanding of the colouration, anatomy, diet or even health of the original animal, as well as fossilization, chemical pathways and replacements.

X-ray fluorescence (XRF) detection is one of the most sensitive non-destructive techniques for analysis and quantification of the chemical elements in a sample, specifically those at low concentrations. Here, a beam of X-rays of sufficiently high energy (short wavelength) impinges on the sample and knocks out an inner-shell electron from the elements of interest (Fig. 2, top left). The hole created in the inner shell is filled by a second electron from an outer shell, which, as a result, can emit a secondary X-ray photon, the so called XRF (Fig. 2, middle left). The energy of the XRF signal corresponds to the difference of the binding energies of the two electrons involved. As each chemical element has electrons in shells with binding energies that are unique, it also has a unique spectrum of XRF lines at characteristic energies. Whether a fluorescence line lends itself to an XRF analysis is defined by three criteria: (1) the incident X-ray intensity and the XRF signal must be sufficiently strong to be detectable, (2) the incident and XRF photon energy has to be high enough to penetrate and exit the matrix of the sample, and (3) the energy of the XRF line must be discernable from that of other chemical elements in the sample. In practice, for most elements up to the third row transition metals, the $K\alpha$ lines (resulting from an electron in the L shell filling a hole in the K shell) are best suited for XRF imaging, since they have the strongest signal and highest X-ray energy and hence penetration (Fig. 2, center). For heavier elements, such as lead for example, L lines fall into the practical energy range. XRF analyses often focus on trace metals, as they are chemically important and have distinct XRF lines with enough penetration power. Of the lighter elements, especially potassium, sulfur, chlorine and calcium play an important role if the matrix of the artefact allows for enough XRF signal penetration and extraction.

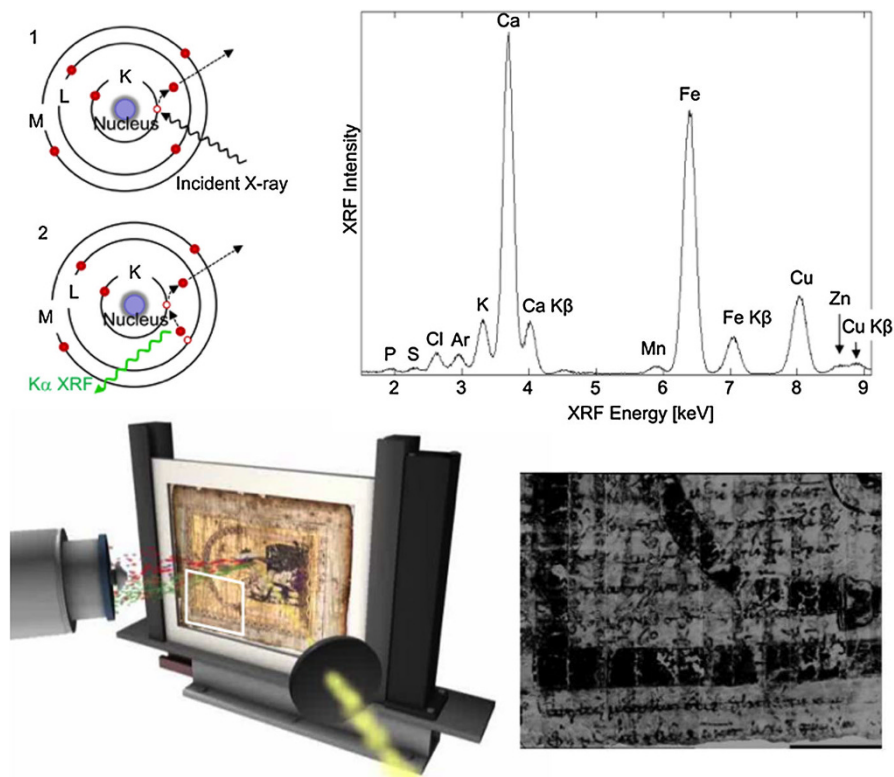


Fig. 2 Concept of XRF imaging. *Top left* In the XRF process, an inner shell electron is knocked out by the incident beam (1), and the XRF photon is emitted after the hole is filled from an out electron (2). *Top right* The XRF spectrum taken from the Archimedes Palimpsest [11]. *All lines* are $K\alpha$ unless labeled otherwise. *Bottom left* Concept of the rapid scan XRF imaging setup. The incident X-ray beam is collimated to the desired sized and the sample is mounted on a scanning stage. The detector is typically mounted at a 90° angle to the incident X-ray beam and the XRF signal for each pixel is recorded on-the-fly as the sample is raster scanned continuously in the horizontal while stepping up vertically at the end of each line. *Bottom right* Iron XRF map of the area indicated by the white box revealing the Archimedes writings

The real power of XRF comes to fruition when combining its tremendous elemental sensitivity with high spatial resolution to create a two dimensional chemical map of an artefact (Fig. 2, right). This has driven the development of continuous rapid-scan XRF imaging setups making use of the small, intense, and collimated X-ray beams produced at modern synchrotron facilities. Here, artefacts of various sizes can be scanned in a matter of a few hours to produce multi megapixel high-resolution 2D chemical maps. Motivated by the challenge of imaging the hidden writings in the Archimedes Palimpsest, the first setup at SSRL used 10 ms readout times and a smaller scanning stage limited to the size of a single folio. The system was then further optimized in readout speed, and the addition of larger scanning stages was later used to image the Thermopolis Archaeopteryx, one of the best-preserved specimens of this icon fossil. Currently, an imaging setup with a

readout speed of up to 2 ms per pixel and scanning speeds of up to 50 mm/s is operational and available for users beamline 6-2 at SSRL. At this setup a $30 \times 30 \text{ cm}^2$ object imaged at $100 \text{ }\mu\text{m}$ beam diameter spatial resolution can be scanned in about 5 h, resulting in a 9-megapixel, high-resolution digital chemical map of up to 15 different elements. Details about the instrumentation are discussed in references [10–14, 139, 154, 185]. Smaller objects can also be imaged at about $1 \text{ }\mu\text{m}$ resolution with a slower system at various stations worldwide. There are plans underway at SSRL to build a new setup that covers a range of beam sizes ($1\text{--}100 \text{ }\mu\text{m}$) as well as scanning speeds. Here, the whole artefact can first be imaged at lower resolution, and once some areas of interest are identified, they can be studied at higher resolution without the need to move to a different instrument (Sam Webb, *private communication*). Furthermore, slower acquisition might be used when the aim is collecting low-intensity signals from trace elements such as some transition metals, heavy metals or rare earths. In such case, full XRF spectra need to be collected and processed to extract meaningful signal intensity and map elemental concentration across entire fossil morphologies [90, 92].

Such XRF imaging can be further coupled to scans in the excitation energy to collect speciation-based information, such as to study the chemical environment of target elements. Gueriau et al. used this approach to the so-called *cerium anomaly*, where direct X-ray absorption-based speciation of cerium and respective concentration in rare earth elements (from XRF) provide palaeo-environmental information regarding the burial milieu and processes [91]. A similar approach was used by Cook et al. to determine and validate the speciation of strontium within whole archaeological fish otoliths [51, 52].

Alternately, XRF imaging instruments with resolutions ranging to well below the micrometer range are used for very small samples, and very large XRF scanning systems have been developed for the chemical mapping of paintings using both synchrotron and commercial X-ray sources [4, 5, 68, 104]. The commercial instruments [4] are based on X-ray tubes and do not have the speed, sensitivity, and spatial resolution of the synchrotron-based systems, but they have the advantage that the artefacts do not have to be moved from the museum and that they can be used for long periods of time. In addition to advances in scanning hardware and readout electronics, new, faster and more efficient XRF detectors are being developed [152, 153]. All these developments will help to further broaden the use of XRF imaging methods as a very powerful tool for cultural and natural heritage studies.

3 Heterogeneity in Organic Materials

Synchrotron techniques were reported thus far to be mostly suited to the advanced study of ancient inorganic materials. From early on, however, synchrotron experiments were used to trace elemental analysis in organic materials, or to probe the short- and long-range order of ancient fibrillar organic molecules, such as hair and wool keratins [22]. Methodological developments in the X-ray range, particularly at low energy ($<1 \text{ keV}$) where the 1s electron binding energies of

carbon, oxygen and nitrogen are attained, in the UV/visible and in the infrared bring new capabilities regarding speciation-based identification, discrimination and mapping of organics or hybrid (organic–inorganic) compounds in ancient materials. We will discuss below two techniques, deep UV photoluminescence and scanning transmission X-ray microscopy, where very high spatial resolution can be attained, and that are currently undergoing significant development. Both approaches are also applicable to a large class of inorganic compounds, such as transition metals and semiconductors, respectively, but application to the recognition of spectroscopic signatures of organic or hybrid-type compounds is particularly underlined here.

3.1 Multiscalar Imaging of Heritage Materials Using UV Photoluminescence

Spontaneous emission or *luminescence* is the process by which an electron from an atom, molecule, or crystal in an excited state undergoes a transition to a lower energy state, e.g. the ground state, with emission of a photon. The process involves transition from a non- or anti-bonding to a bonding or lone-pair orbital in a molecule, or from the conduction to the valence band in crystals. At thermal equilibrium, the rate of absorption is equal to that of spontaneous plus stimulated emissions. This allows defining the relationship between Einstein's coefficients B_{12} , A_{21} , and B_{21} , respectively. In the UV/Vis domain, the nature of the emission phenomenon is principally spontaneous, whereas this is no longer true at lower frequencies.

Solid-state photoluminescence originates from excited states of electronic energy levels, and thus provides a variety of information on the physicochemistry of the material studied. For semiconducting materials, direct information on the band gap energy and on the amount and nature of impurities, or other type of crystal defects, is accessible. Photoluminescence can also provide direct signature of organic groups, such as amino acids tryptophan (2-amino-3-(1H-indol-3-yl) propanoic acid, Trp) and tyrosine (2-amino-3-(4-hydroxyphenyl) propanoic acid, Tyr). The spectroscopic response of these two well-known π -conjugated luminophores can also be used as an indirect probe of their chemical environment.

The luminescence phenomenon can be described by means of its spectral and temporal components. Emission and excitation spectra inform on the distribution of probability of the transition between the excited and ground states, and the luminescence quantum yield reflects the fraction of photons emitted by a material relative to that absorbed. In turn, the radiative lifetime is the time window during which the emission of photons can be observed. Both the spectral and temporal components of the luminescence signal can therefore be exploited to separate, identify, and characterise species within complex mixtures.

Photoluminescence has been exploited in the field of Cultural Heritage, archaeology and paleontology since the first quarter of the 20th century as a practical means to increase contrast between materials at the surface of artworks or paleontological specimens. Repaints and restorations can result in significantly distinct luminescence response captured by photography [149]. Similar approaches were used to enhance contrast and visualize morphological patterns in fossils [110]. Over the last 10 years, development of new imaging setups has allowed for the

gathering of spatial distribution and spectral information on materials' emission properties over artworks, using multispectral or lifetime approaches [40, 134, 179].

Based on these approaches, a new synchrotron-based method has been developed to study the photoluminescence of semiconductor artists' pigments at the microscale using excitation wavelengths ranging from the deep ultraviolet (DUV) up to the visible range (Vis). The aim was to access the heterogeneity of their emission properties as a signature of manufacturing processes. This development was inspired by pioneer work making use of a confocal raster-scanning setup coupled to a UV synchrotron beam to study the microscale distribution of the steroid coumestrol in single Leydig cells [82].

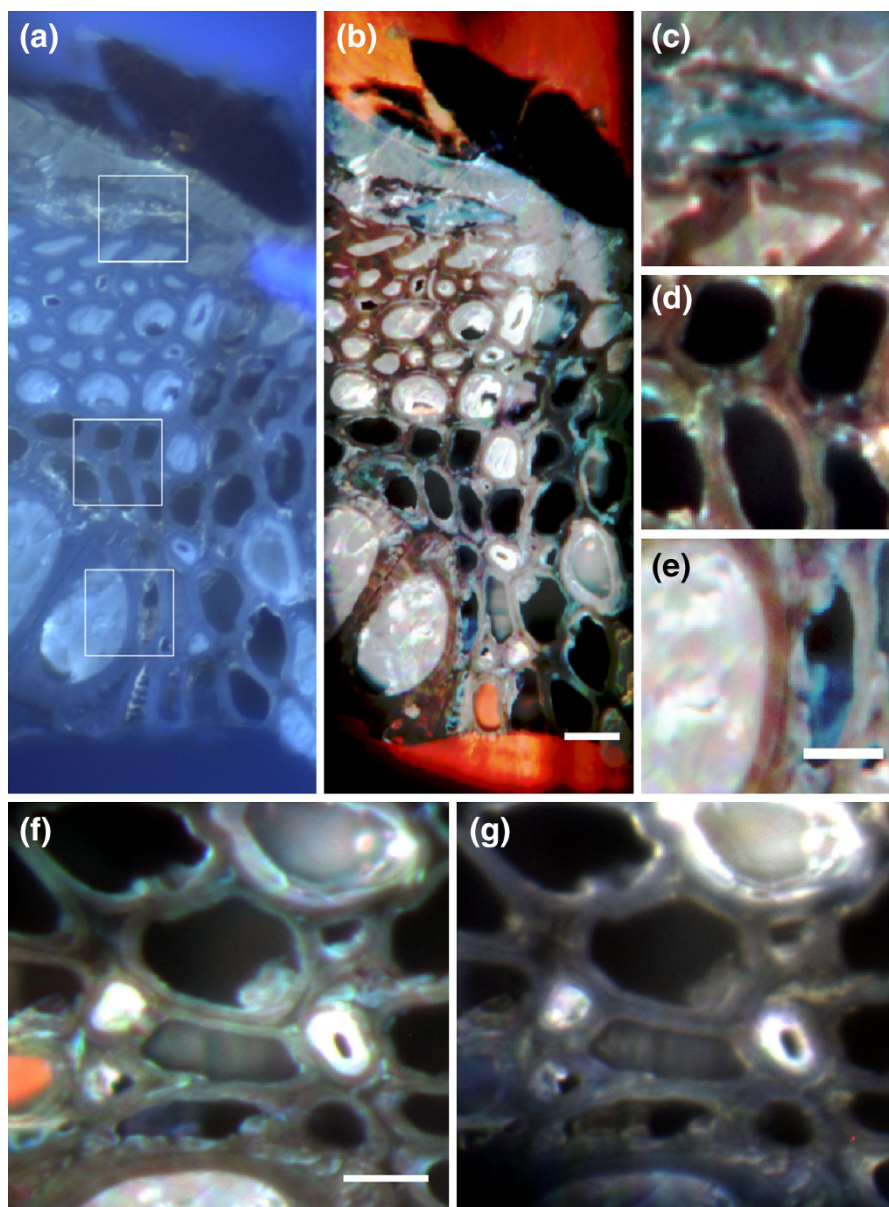
A dedicated branch has been developed at the DISCO beamline of the SOLEIL synchrotron to perform imaging at high spatial resolution and exploit the tunability of the synchrotron source. The full-field imaging setup developed at the DISCO beamline was built around an Axio Observer Z1 inverted microscope (Carl Zeiss MicroImaging, Jena, Germany). The exhaustive description of this home-made setup is available in the literature [28].

Optimisation of the excitation range in the DUV offers new capabilities to analyze historical samples, as shown below on one of the earliest surviving Italian lutes, made by Laux Maler before 1552 in Bologna (Musée de la musique, Paris; inv. num. E.2005.3.1; Fig. 3) [70].

Synchrotron DUV PL does not require specific sample preparation and can be performed at ambient atmosphere. The only constraint is the depth of field of high-numerical aperture objectives, which is below one micrometer in the DUV range. The surface quality and the planarity of the sample surface should be well controlled to ensure an accurate focus of the images collected. In the example shown here, the sample was embedded in methacrylate-based Technovit 2000LC resin (Heraeus Kulzer), and its surface was prepared using an ultra-microtome so that a satisfactory optical contact could be obtained between the sample and the quartz slide.

The full-field approach using (multiband) detection in multiple spectral bands is well-adapted to the collection of low quantum yield PL signals. Hyperspectral detection is much less compatible with detecting weak emission with high signal-to-noise ratio (SNR) images. Multiband detection also allows optimising the integration time for images collected in distinct spectral bands. This is a crucial asset, since the quantum yield may vary strongly from one material to another, in the 10^{-1} – 10^{-6} range. In addition, visualising PL in distinct bands offers new possibilities to exalt contrasts between materials. For example, strata of the coating film in the Laux Maler appear homogeneous using the conventional UV epiluminescence microscope. However, compositional contrasts between strata are strongly enhanced using multiband detection in SR DUV PL (Fig. 3a). The contrast of luminescence between the secondary walls and the middle lamella (Fig. 3e–g) also greatly improves the description of the microstructure of the wood cell walls.

The tunability of wavelength (i.e. energy) available with the synchrotron source between 200 and 600 nm is a powerful parameter to enhance contrast between PL properties of distinct materials. Figure 3g, h illustrates the impact of the excitation



wavelength; PL under excitation at 275 nm clearly allows an optimized localisation of the organic embedding medium that has penetrated within the sample.

DUV excitation allows accessing the intrinsic PL properties of specific organic compounds without requiring any labelling or marking to enhance the signal. Within wood, luminescence from the secondary walls shows a quite broad emission band peaking around 340–400 nm when excited in the 240–320 nm range (Fig. 3d). This signature is consistent with the presence of lignin.

Fig. 3 Comparison between standard epiluminescence and synchrotron full-field multiband imaging on a cross section sample of the Laux Maler surface coating, one of the earliest surviving Italian lutes. **a** Visible epiluminescence light microscopy collected with 365-nm mercury excitation. **b** Spatially-registered false-colour RGB image constructed from synchrotron full-field multiband imaging under 275 nm excitation with colour designation: *blue* 500, 20 nm FWHM, *green* 465, 30 nm FWHM, *red* 380, 15 nm FWHM. Image intensity levels in each channel were adjusted using equalisation stretch. 40 μm . **c–e** Detailed areas, corresponding to those indicated by *white rectangles* in **a**. *Scale bar* 20 μm . Image intensity levels in each channel were adjusted using a Gaussian stretch. **f** Detailed areas using similar excitation and emission parameter as in **b–e** using a 2–98 % stretch. **g** Detailed area similar to **f** under 340 nm excitation and colour designation *blue* 425, 30 nm FWHM, *green* 465, 30 nm FWHM, *red* 480, 17 nm FWHM. *Scale bar* 40 μm

Finally, one of the main assets of the technique is the capability to image large areas of hundreds of sq. micrometers at a high spatial resolution. In the configuration used in the current set up on the DISCO beamline, the minimum pps is 153 nm with a 100 \times objective, NA = 1.25. In such configuration, the Rayleigh criterion leads to a resolution of 244 nm at a wavelength of 500 nm, which is almost ideally imaged with that pps. The ratio between the spatial resolution attainable and the size of the area probed is in the range of 10^3 – 10^4 . This high spatial dynamics allows a clear comparison of the luminescence of distinct wood cells (Fig. 3b).

DUV photoluminescence micro-imaging offers promising capabilities for the analysis of a broader range of materials, such as proteinaceous materials or semiconducting artists' pigments. PL provides a distinct source of contrast than that attainable under IR or X-ray excitation to characterise ancient materials at the submicroscale [179].

DUV micro-imaging allows probing intrinsic photoluminescence contrasts of organic materials at submicroscale over wide areas. Attaining such spatial dynamics is a crucial improvement for the study of heterogeneous systems. Imaging the spatial distribution of minute compounds in their environment within micro-samples can be the clue to better understand the physicochemical processes induced during alteration processes, or to identify original materials used during the creation process of artists or craftsmen. The use of low flux ($\sim 10^{12}$ ph/s) minimizes flux-dependant (rather than dose-dependant) radiation-induced side effects. It can also be considered as an efficient probe to monitor radiation damages that occur during ion, electron, and X-ray microanalyses [24, 83, 179].

The main limitation of the technique is either due to the very low quantum yields of PL of certain materials, or to the broadness of emission bands that prevent them from being used as reliable signatures to identify specific compounds. Further developments of the approach will soon allow collecting hyperspectral PL cubes collected with a small wavelength step. This will permit new speciation capabilities in full-field mode.

3.2 Identifying Organic Signatures through Scanning Transmission X-ray Microscopy

Paleontological specimens are remnants of once living organisms, and as such, may preserve ancient biogenic organic molecules. The study of these organics may provide crucial insights regarding the chemical evolution of life at the molecular

level over geological times (e.g. [18, 35, 89]). Similarly, cultural heritage samples are mixtures of various materials and organics such as substrates, binding media and pigments. In addition to better constraining the fabrication of these artefacts, the study of these organics may allow deepening our knowledge about customs of ancient civilizations [20, 29]. Yet, the heterogeneity, complexity, diversity and scarcity of organics within paleontological and ancient cultural heritage materials make it difficult to characterize their molecular structure [25, 28, 89].

Synchrotron-based scanning transmission X-ray microscopy (STXM) offers spatially resolved information on the molecular structure of organics at the submicrometric scale. STXM experiments at the carbon absorption edge allows both microscopic observations, i.e. in situ mapping organic (biogeo)chemical heterogeneities at a 15-nm spatial resolution, and spectroscopic measurements, i.e. recording carbon X-ray absorption near edge structure (C-XANES or C-NEXAFS) spectra at the same spatial scale. STXM experiments thus consist in collecting hyperspectral maps from which C-XANES data can be extracted [53]. Absorption peaks of C-XANES spectra provide information on the molecular structure of the investigated organics as they correspond to transitions from inner shell 1s electrons to both unoccupied antibonding π^* and low-lying σ^* orbitals and thus are sensitive indicators of the local chemical bonding environment surrounding the measured carbon atoms [74, 102, 133, 168].

STXM is highly complementary to infrared spectroscopy and UV/Vis absorption/luminescence techniques and offers several advantages [58, 81]. STXM experiments do not require organics to be extracted from the sample inorganic matrix. Plus, STXM-based C-XANES spectroscopy allows the direct detection of functional groups rather than chemical bonds, thus facilitating the identification of organics [133, 168]. Due to the directness of the signal, C-XANES data collected on different organic-rich specimens can be easily compared [53]. Even though infrared spectroscopy is well known for the richness of chemical information it can provide, its diffraction-limited spatial resolution is restricted to a few micrometers, conferring a clear advantage to STXM-based C-XANES spectroscopy for the study of organic-rich samples exhibiting submicrometric biogeochemical heterogeneities [58, 97]. As absorption of ultraviolet and visible light by organics is restricted to certain functional groups (chromophores) and as UV/Vis spectra result from the superposition of electronic, rotational and vibrational transitions, the use of STXM-based XANES spectroscopy allows a more direct identification of organics within paleontological and cultural heritage specimens [20, 138]. While TEM-based electron energy loss spectroscopy (EELS) may be used to obtain chemical information almost comparable to C-XANES data with even a better spatial resolution, this technique suffers (in addition to inevitable radiation damages) from a spectral resolution that remains too low to distinguish among various C bonding environments separated by only a few tenths of an eV [34, 98].

Similarly to all electric-dipole transition spectroscopies, C-XANES spectroscopy adheres to Beer's law. Variations in peak intensities directly result from variations in concentration of the functional groups absorbing at these specific energies. The intensity of a given peak is related to the concentration of the functional group through the specific oscillator strength of the corresponding electronic transition

[74, 102]. Yet, as oscillator strengths are not precisely known, the absolute concentrations of functional groups cannot be estimated quantitatively. Nevertheless, assuming that the oscillator strength of a given functional group is essentially the same in different organic compounds, relative concentrations can be discussed qualitatively by normalizing C-XANES spectra to the total carbon amount (corresponding to the absorption over the 320–350 eV range).

Despite these unique capabilities, rare are the studies having explored the advantages of STXM for the characterization of organics within cultural heritage specimens. Animated by other motivations, Hernandez-Cruz et al. have investigated the local orientation of silk fibers of a *Bombyx mori* cocoon using STXM-based C-XANES spectroscopy [94]. Their results have demonstrated that, in addition to provide information of the molecular structure of organics, STXM allows quantitatively mapping the orientation of fibers within a representative protein sample. This methodology has then been successfully applied by Rousseau et al. to investigate the dragline silk microstructure produced by *Nephila clavipes* orb-weaving spiders, which has allowed them to better constrain the structure-property relationships of silk samples [151]. More recently, Willneff et al. have used XANES spectroscopy to investigate the impact of cleaning process (soiling removal) on paint film surfaces through a variety of wet treatments using aqueous or hydrocarbon solvent systems [184]. Similarly, Rouchon et al. [150] have used STXM to document, at the submicrometric scale, the penetration of iron gall ink within cellulosic paper fibers similar to those of ancient manuscripts as well as the subsequent degradation of the cellulosic compounds of these paper fibers. Although these studies have been performed on analogues rather than on cultural heritage specimens, they illustrate the capabilities of STXM and C-XANES spectroscopy for the study of organics within such artefacts.

Of note, the main difficulty associated with the study of organics from cultural heritage specimens is that they may have suffered a diversity of decay chemical reactions. As organics within these samples may exhibit diverse degrees of ageing, their recognition and discrimination may be challenging. This is even worse for paleontological specimens: biogenic organic molecules may indeed experience multiple stages of degradation induced by a combination of biological, chemical, and physical factors during geological time scales [18, 89]. The general paleobiological perception has long been that burial-induced biomolecule degradation processes are detrimental to the chemical preservation of biogenic organics in rocks. Yet, using STXM-based C-XANES spectroscopy, Bernard et al. have reported the persistence of partially degraded sporopollenin compounds within ~ 230 -Ma fern spores having experienced more or less intense metamorphism during burial down to depths of about 40 km [16, 17]. More recently, the use of STXM at the carbon and nitrogen absorption edges has allowed Cody et al. [47] to evidence the (partial) preservation of chitin-protein complexes within ~ 310 and ~ 420 -Ma arthropod cuticles. Following a similar approach, Ehrlich et al. [72] have demonstrated the preservation of chitin within ~ 500 -Ma Burgess Shale sponges despite burial at depths of ~ 10 km.

The recognition of bacterial signals within sub-modern samples using STXM is quite straightforward as illustrated on Fig. 4 [9, 117, 127, 146]. Yet, in rocks, the

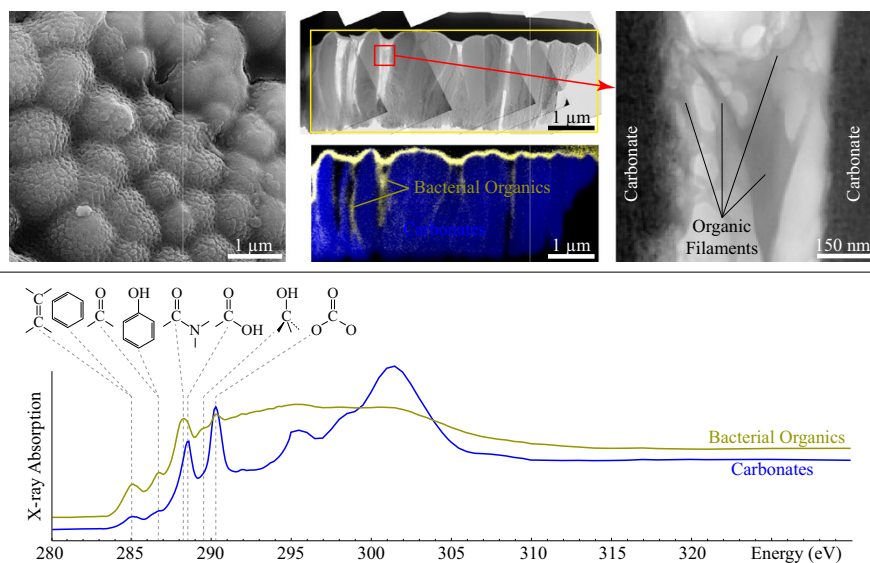


Fig. 4 STXM characterization of epibiotic calcifying bacterial colonies observed on the cuticle of a specimen of *Farfantepenaeus brevivirostris* (Kingsley, 1878, MNHN.IU.Na8524) from La Paz Bay, Mexico. *Top left* SEM image of the calcifying bacterial colony. *Top center* TEM image and STXM compositional map of the ultrathin FIB foil extracted from the calcifying bacterial colony showing the spatial distribution of carbonates (blue) and bacterial organics (yellow). *Top right* TEM image of a detail of the ultrathin FIB foil. Organic filaments appear in dark. *Bottom* C-XANES spectra of organics and carbonates composing the ultrathin FIB foil. Peaks at 285.1, 286.7, 288.2, 288.6, 289.5 and 290.3 eV are attributed to electronic transitions of carbon involved in aromatic or olefinic, phenolic, amidyl, carboxylic, hydroxylated and carbonate groups, respectively

recognition of such signals may become difficult. Via STXM experiments, Cosmidis et al. have managed to evidence the preservation of biogenic organic signatures within fossilized biominerals of bacterial origin in ~ 25 and ~ 60 -Ma phosphorites [54, 55]. De Gregorio et al. [64] have reported STXM-based C-XANES data collected on organic microstructures from the 3.5-Ga Apex cherts, but the significant degradation experienced by these organics during fossilization and burial makes it challenging to unambiguously assess their biogenicity. Better understanding the impact of fossilization and burial-induced degradation processes on organic signatures has thus recently emerged as a major scientific challenge. Using STXM to characterize the organic residues of laboratory experiments, Li et al. [118] and Picard et al. [137] have documented the nature and the extent of the transformations that may experience microorganisms during burial, thus providing new milestones towards a better mechanistic understanding of biogenic molecule degradation processes.

STXM has not yet had its golden age, as illustrated by a number of recent methodological advances, including notably protocols to precisely estimate N/C and O/C atomic ratios of organics at the submicrometric scale through the collection of C-, N- and O-XANES data [6, 47]. In addition, it has recently become possible to image frozen hydrated specimens at temperatures as low as 100 K using cryo-STXM

[123, 135, 181], as well as to perform 3D STXM experiments by combining STXM with angle-scan tomography [135, 181]. STXM thus holds great promise to contribute to the current challenges of reconstructing the original molecular structure of organics preserved within paleontological and cultural heritage materials.

4 Hierarchical Architecture of Materials

The heterogeneity of ancient materials is often multi-scalar, as specific physico-chemical laws govern the formation and stability of their structure at successive discrete length scales. Such hierarchical architecture often has a significant impact on materials properties (resistance to stress, optical response), and chemical reactivity during short- and long-term alteration. The architecture of such materials can be *directly* documented by microscopy techniques (such as electron and optical microscopy), and *indirectly* probed through structural methods, such as X-ray (and neutron) diffraction and small-angle scattering. We selected here two examples with distinct origins of the multiscale organisation. In archaeological bones and ivory, ordering results from tight biological control during biomineralisation. In ancient ceramics, controlled manufacturing process can lead to a thoroughly structured material, in which distinct structural levels bring complementary clues to understand the *chaîne opératoire* (manufacturing sequence) employed by past craftsmen.

4.1 Quantitative SAXS Raster-Scanning of Archaeological Samples

Scattering of radiation arises from discontinuities in the exposed media at the level of the radiation wavelength [142]. This can be used as a source of contrast, as for dark field imaging methods. Furthermore, a rigorous analysis of the spatial (and temporal) distribution of scattered radiation may provide very accurate structural information [169]. Because of the strong degree of structural hierarchy and heterogeneity of biological materials [78, 112], one major complication associated with their analysis is the requirement to combine nanoscale sensitivity with microscopic to macroscopic field of view. This point is not trivial when considering archaeological objects, as, except for permafrost conditions, they are degraded over time due to complex biophysicochemical alteration processes. Those processes are multi-factorial, non-linear in time and produce additional inhomogeneities in the materials (see e.g. [15, 49, 93, 143, 144]). Thus, the necessity to analyse the nanoscale properties with biologically, chemically and physically relevant statistics becomes quite stringent when dealing with, for example, archaeological bone and ivory.

In the case of X-ray scattering at small angles (SAXS), electron density fluctuations can be probed at the nanometer scale. This is ideal to study bone-like materials that consist of collagen fibrils of ~ 100 nm in diameter, mechanically reinforced by $\sim 5 \times 50 \times 100$ nm³ nanocrystals of carbonated hydroxyapatite mineral [61, 113, 140, 190]. As a consequence, the SAXS signal observed for bone, antler, dentin or ivory is dominated by the contrast between the mineral

nanocrystals and the surrounding collagen. The nanocrystal envelope (shape, size and 3D organization of the nanocrystals) can then be derived from 2D SAXS patterns [39, 75–77, 99, 189]. This intense signal is overlaid on a weaker one arising from density fluctuations within the microfibril organization, such that, if the mineral density is sufficiently low, this signal also becomes visible in the scattering patterns.

With SAXS, the average structural information is obtained while the details of the distribution of nanocrystals properties within the probed volume are not. This is a strong limitation for bone studies, since the microfibrils organization may differ significantly depending on the histological position, micro-architecture, and macroscopic anatomical characteristics.

In order to overcome this limitation, spatially-resolved measurements can be conducted. While such measurements would take 20–60 min and allow resolving micro-architectural details using laboratory microbeams (photon flux: $\sim 10^{4-6}$ ph s⁻¹, beam diameter: 50–300 μm), acquisition only takes a few (milli)seconds using synchrotron radiation (photon flux: $\sim 10^{9-12}$ ph s⁻¹), for bone or dentin sections of ~ 50 – 100 μm thick. An additional advantage of the high brilliance of SR sources is that adequate X-ray optics can be used to considerably reduce the beam size down to as low as 50 nm for scattering experiments, despite the loss of photons resulting from the focusing process [145, 158]. Thus, fast scanning SAXS allows mapping large sample regions with high accuracy. One obvious problem, common to other scanning imaging methods, is the handling, storage and analysis of the large amount of data generated during the experiments (currently 10^{4-6} 2D frames). This entails the need for automatic data analysis schemes that, ultimately, result in a more classical imaging approach, i.e. with little or no a priori user input for the reduction of the 2D scattering signal to a scalar metric representing a nanoscale structural parameter in quantitative scanning SAXS imaging (qsSAXSI) [87, 180].

The nano- to macroscale structural features of bones, coupled to their chemical and isotopic composition, provide essential biogenic signatures characteristic of the living and environmental conditions that the individuals experienced during their lifetimes. Hence, the archaeological records based on these materials constitute important archives of our past that can be exploited to better understand skills, cognitive capabilities and life styles in ancient societies (see e.g. [30, 37, 38, 187, 188]).

The potential benefit of qsSAXSI for such purposes can be illustrated by a recent experiment performed on artificially heated bone at temperatures below 300 °C, which covers a wide range of actions linked to specific socio-cultural behaviors such as cooking or tool manufacturing. In the archaeological record, many traces of heating can be found on bone or dentin artefacts, as evidenced by colour changes and increased mechanical fragility [42, 163, 164, 171]. However, the heating process can also be accidental [109] and other diagenetic phenomena may lead to similar changes [41, 108]. Therefore, reliable markers of heat-induced structural modifications are required. To decouple the heating effects from other diagenetic processes, a common strategy is to study the heat induced changes in a controlled

environment on modern samples. Many such studies have been conducted in a large temperature range, typically $\sim 50\text{--}1000^\circ\text{C}$ (e.g.[95, 96, 148]). However, at the macroscopic level, the most drastic changes were reported below 300°C [107] in the form of an important weight loss ($>30\%$) and shrinkage, as well as an increased fragility of the bone samples. Unfortunately, the colour changes are very weak in this range, which makes it challenging to distinguish heated from non-heated artefacts. Nevertheless structural modifications are expected to occur in this range.

Recently, Chadefaux and Reiche established a link between the macroscopic and microscopic changes with a growth and disorganization of the mineral nanocrystals in bovine bone. However, due to the limited field of view of TEM measurements, it is not clear whether the data are representative of modifications that may have occurred at different histological locations [41].

To clarify this matter, qsSAXSI measurements were performed at the cSAXS beamline of the Swiss Light Source on transverse sections of bovine bone of $200\ \mu\text{m}$ in thickness over the full cortical shell $\sim 11.5\ \text{mm} \times 1.5\ \text{mm}^2$. The scans were performed in steps of $50 \times 20\ \mu\text{m}^2(\text{H} \times \text{V})$ with a beam size of $\sim 25 \times 6\ \mu\text{m}^2(\text{H} \times \text{V})$, which is below the characteristic length scale of the histological features ($\sim 100\ \mu\text{m}$). In this experiment, the use of a fast, highly sensitive detector (Pilatus 2M) allowed recording 172,500 frames in $\sim 2.4\ \text{h}$ (50 ms/frame with a beam flux of $\sim 5 \times 10^{10}\ \text{ph s}^{-1}$ at $\lambda = 0.667\ \text{\AA}$) for each sample. Figure 5b shows the qsSAXSI images of the average nanocrystal thickness (T) for sample sections heated at 100, 150, 170, 190, 210, 250 $^\circ\text{C}$ during 1 h. T is a standard parameter in the SAXS analysis of bone [77]. While the dimensions of nanocrystals have been found to vary substantially in the literature, there is a global consensus on the fact that they are essentially platelet-shaped with a highly reproducible thickness of 2–6 nm, depending on animal species. This is therefore one of the most stable metrics to characterize the evolution of mineral nanocrystal size in healthy and pathological conditions [86]. A significant rise in average particle thickness upon heating can be observed in Fig. 5b by the increase in image brightness [85]. This trend can be further quantified by calculating the histograms of the gray levels of the image, i.e. of the distribution of T -values across the image (Fig. 5c). In fact, an exponential increase is found in Fig. 5d even at temperatures below 300°C . The width of the histograms T_{FWHM} also increases significantly, meaning that there is a higher range of nanocrystal sizes throughout the sample. The changes in both parameters imply that the particle growth process upon heating is heterogeneous throughout the tissue. Such criteria can, therefore, be used to identify heated bone remains from archaeological contexts and seem to be good markers for the determination of the heat temperature. Very valuable information can be obtained using synchrotron qsSAXSI with higher spatial resolution (i.e. beam size $<10\ \mu\text{m}$) since the images of T can be related to the histological features observed using other modalities, e.g. light microscopy.

This analytical scheme can also be used to study diagenetic alterations at sub-micrometer level. This is particularly useful to assess whether or not the macroscopic preservation state reflects the level of conservation at smaller hierarchical scales down to the molecular level. This question was at the focus of

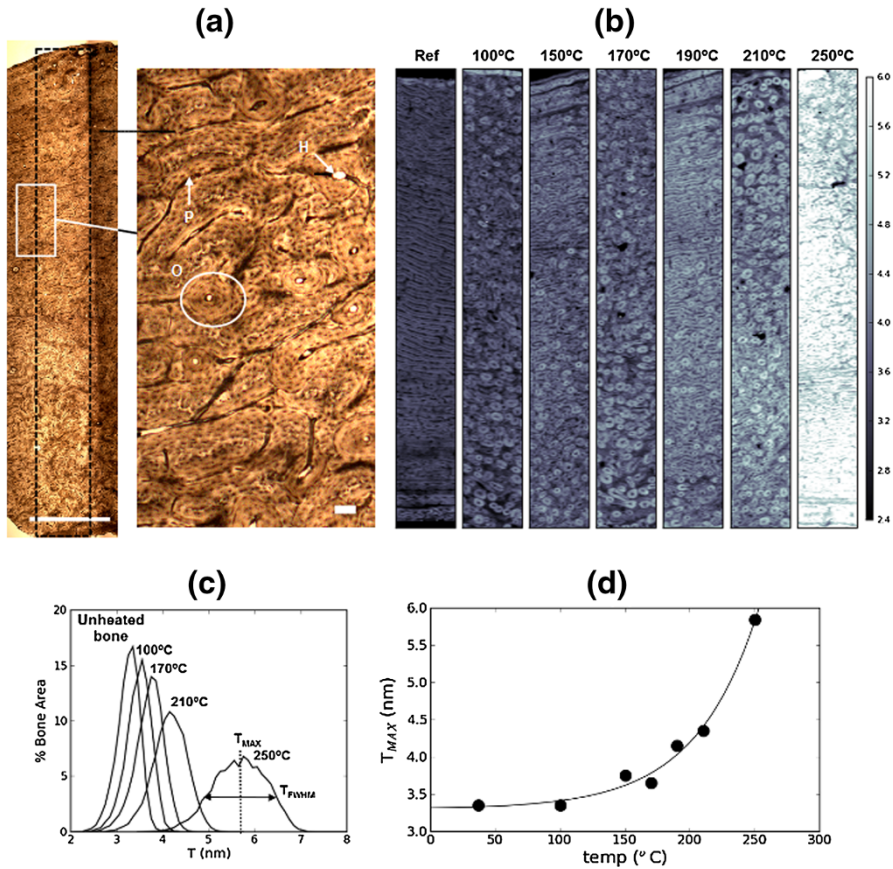


Fig. 5 **a** Optical micrograph of a transverse section of bovine bone used as control (Ref) for this study and magnified image of a sub region of the sample showing the typical features of interest: an osteon (O) and a fibrolamellar bone packet (P). The *scale bars* are, respectively, 1 mm and 50 μm ; **b** qsSAXSI images of the T -parameter for samples heated at increasing temperatures towards the *right*. The images are all displayed with the same colour scale range for T (nm) in order to highlight the increase in brightness and, thus, in T values; **c** the histograms of the images shown in **b** are displayed as a function of temperature; **d** the value of the maximum of the histograms, T_{MAX} , is plotted as a function of temperature, revealing a strong increase in mineral nanocrystal thickness

a recent study of the ivory structure of elephant tusks found in a shipwreck at the site “Les Poulins”, North Brittany, France [1]. Quantitative scanning SAXS imaging measurement were performed at the MySpot beamline of the BESSY II synchrotron radiation facility (HZB, Helmholtz-Zentrum Berlin für Materialien und Energie, Berlin, Germany). This study first showed that the thickness of the mineral nanocrystals is increased in the archaeological samples compared to the modern ones. Secondly, local fluctuations in the thickness were observed between the innermost part of the tusk (pulp) to the outermost region (the cement). While those changes could have been evidenced by TEM, it is important to note that the analysis was performed over the full transverse radius of $\sim 2\text{--}8$ cm, which is clearly beyond the reach of TEM related methods. Finally, the qsSAXSI analysis also revealed that

the degree of alignment of the nanocrystals and, hence, of the collagen microfibrils was well conserved, albeit with minor local fluctuations.

Although only qsSAXSI applications to the study of bone and ivory are discussed in the present contribution, the method could be used to study a much broader class of materials. The only requirement is that the object must consist of heterogeneities at the nanoscale. The main advantage is the extent of the regions of analysis, which is orders of magnitude higher than other nanoprobe methods. Typical applications include nanocomposite materials such as biominerals, including seashells and corals. This is also the case for a number of purely organic biological materials (e.g. wood, hair). Finally, materials containing nano-sized inclusions (ceramics, metals) are also very good candidates. Overall, the potential of qsSAXSI is huge, and it can be foreseen that the increased number of beamlines allowing scanning-SAXS with micro- and nanobeams will provide new opportunities for cultural heritage studies.

4.2 Combining Poly- and Monochromatic μ -XRD to Study Operating Sequences

X-ray diffraction is one of the most efficient techniques to study the crystallographic composition and the structure of materials. Early on, it was used to determine the mineralogical composition of archaeological and historical artefacts [105, 183]. With the development of synchrotron facilities, X-ray diffraction techniques have significantly evolved (focused beam, time resolved and in-situ measurements, *etc.*), and the cultural heritage community has greatly benefitted from these improvements [157]. For instance, the ability to work with a small quantity of material while keeping a very good angular resolution was a key element in the quantitative study of Egyptian cosmetics by powder XRD [69]. Recently, this technique has contributed to probing the rare ϵ - Fe_2O_3 phase in ancient Jian ceramics [66].

High brightness and high spectral flux of the X-ray sources, associated with the ability to focus it in order to get very small beams with sufficient X-ray intensity to detect a diffraction in an acceptable amount of time (< a few min), opened the new field of crystallographic mapping [100]. Today, new generation synchrotron facilities can provide micrometer or submicrometer beam sizes in a routine manner permitting the record of high spatial resolution maps. X-ray diffraction is much more sensitive to crystal orientation than spectrometry techniques. In fact, diffraction conditions are very restrictive and only specific orientations with regard to the incident beam can give reliable diffraction patterns. With a monochromatic beam, diffraction patterns can be obtained by rotating the crystal (single crystal diffraction technique) or by placing a large (ideally infinite) number of randomly oriented crystals in the beam in order to have enough crystallites in diffraction condition (X-ray powder diffraction technique). The first technique is not suitable for scanning polycrystalline materials while the second requires the crystallite size to be much smaller than the X-ray beam size. For example, with a micrometer-size beam (e.g. $1\ \mu\text{m} \times 1\ \mu\text{m}$), only nanocrystals (< $100\ \mu\text{m}$) can fulfil the powder diffraction conditions. In many cases, archaeological or historical artefacts are constituted of heterogeneous materials in which several crystalline phases coexist in a wide grain size distribution. Because of the restriction mentioned above, only the nanometric

phases can be mapped at high resolution (1 μm step size or less) using a monochromatic beam.

An attractive solution to study polycrystalline compounds with a spatial resolution inferior to the grain size is to use a polychromatic beam. Indeed, the diffraction condition is also wavelength dependent. This is the Laue diffraction technique, which can be used to analyse a stationary single crystal in any orientation. The main principles of this old technique are well described in most of crystallographic books. Laue diffraction takes full advantage of the wide energy bandpass X-ray spectra delivered at a synchrotron light source and can easily be combined with microbeams. This technique is a very efficient method to probe crystals of variable size inside a heterogeneous matrix [101, 176].

Over the last 10 years, Laue micro-diffraction has been successfully applied to map grain orientation and crystal strains in various polycrystallized and composite materials [111, 178]. However only a limited number of studies have concerned cultural heritage materials up to now. For instance, the distribution of micrometric-sized quartz crystals in the coating layer of terra sigillata potteries was determined using Laue microdiffraction [159]. Liu et al. reported the presence of $\text{BaCuSi}_2\text{O}_6$ crystals (Chinese Purple) in the paintings decorating Terra Cotta Warriors from the Qin dynasty, where Laue micro-diffraction was used to investigate the orientation and the distribution of the grains in the pigment [120]. Similar methodology has also been applied to the study of colour pigments from an ancient Egyptian coffin (747–600 BC), where the potential of Laue micro-diffraction for mineralogical phase identification was addressed [121].

In the crystallographic study of archaeological materials constituted of several amorphous and crystallized phases with diverse grain sizes, Laue diffraction has also its limitations. Indeed, this technique is not suitable for analysing small crystals with respect to a micrometer beam size (e.g. crystal size smaller than 500 nm with a 1×1 sq. micrometer beam), which are inversely properly analysed using X-ray powder diffraction. The hybrid approach developed at some synchrotron facilities where both monochromatic powder microdiffraction and Laue microdiffraction methods can be combined on the same experimental set-up gives a powerful tool for extracting structural information over the full spatial range [177]. Quite recently, this approach was used to investigate at the micrometer scale the structure of different types of ancient materials [67]. To do so, mappings of the interesting regions were performed on beamline 12.3.2 at the ALS (USA), one of the few beamlines over the world offering the possibility to switch between monochromatic and polychromatic modes quickly and without changing the position of the focal point on the sample.

The red coatings (slips) of Roman potteries (Terra sigillata and pre-sigillata) result from the transformation during firing of an iron oxide-rich material obtained after decantation of clay materials [161]. A fragment of a sigillata with a high-quality gloss coating is shown on Fig. 6a. The morphology difference between the body and the coating is shown on the corresponding optical image of the cross-section (Fig. 6). The complementarities between powder and Laue diffraction techniques are illustrated through the four following image patterns (Fig. 6c, d). Well-defined powder diffraction rings are recorded in monochromatic mode from

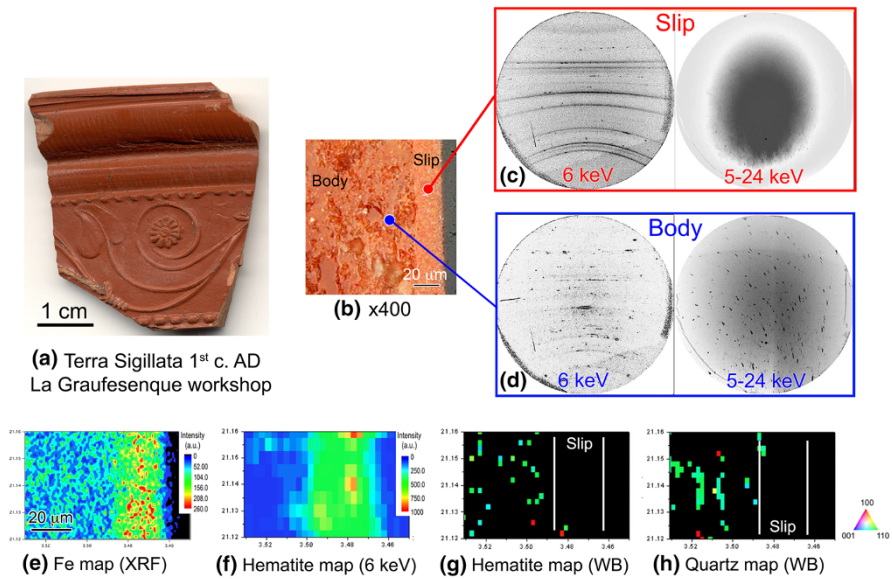


Fig. 6 Example of complementary use of poly- and monochromatic X-ray micro-diffraction concerning a Terra sigillata sherd performed on beamline 12.3.2 at ALS (USA) and presented in Dejoie et al. [67]. Details are given in the text

the slip of sigillata ceramics, while no diffraction signal is recorded in Laue mode (Fig. 6). This confirms that the coating is mainly composed of nanocrystalline phases (corundum and hematite) dispersed in a glassy matrix [162]. On the other hand, the information obtained in monochromatic mode with a microbeam from the body of the ceramic is quite complex (Fig. 6d). Highly spotty diffraction rings are observed, indicating the presence of larger crystals ($>1\mu\text{m}$), together with nanocrystalline phases. In this case, a Laue pattern may provide better quantitative crystallographic information.

The distribution of iron obtained by X-ray fluorescence is shown in Fig. 6e. The distribution of hematite obtained from both powder diffraction ($E = 6\text{ keV}$) and Laue diffraction (white beam, 5–24 keV) is presented on Fig. 6f, g, respectively. These maps reveal that hematite $\alpha - \text{Fe}_2\text{O}_3$ under a nanocrystalline form is mainly located in the slip where the iron content is higher. The repartition of hematite at the micrometric scale is quite homogeneous in the slip, which contains only very few micrometric crystals. Both the homogeneous spatial repartition and the small size dispersion of hematite crystal in the slip are conferring their characteristic deep-red colour to Terra sigillata wares. Contrary to the hematite phase formed during the firing process, quartz (Fig. 6h) is already present in the raw clay materials and then poorly affected by the heating and cooling stages. Consequently, it can be used as a key element for obtaining information about the clay preparation process; in particular, the settling and decantation steps. The quantity of large quartz crystals ($1-10\mu\text{m}$) was found to be much higher in pre-sigillata than in sigillata, in accordance with a change in the clay preparation process to produce high quality sigillata.

Another example is the thermal treatment of flints carried out by the Chassey culture that settled in Vaucluse region (France) during the fourth millennium BC [116]. These flints are essentially constituted of a matrix of nanometric quartz in which a few larger detritic quartz are included. By separating the diffracted signals coming from the nano- and the micrometer-scale, the monochromatic/Laue hybrid approach allowed for the first time evidencing of both a relaxation of the residual strain in large crystals during the thermal treatment and a domain size increase for the nanocrystalline part.

Combining Laue and monochromatic microdiffraction on a same instrument allows for probing the existence, or absence, of micrometric and/or nanometric phases, and interpreting the associated crystallographic structures in the sample probed volume. However, although the 2D description of the structure at the micrometer scale of the material is established, the depth information is still missing. This could be achieved by implementing 3D methods developed on non-rotating samples [115]. In the different examples presented, the investigations were performed at a micrometer scale, but with the development of nano-beams, one can soon expect to be able to carry out such studies with a higher spatial resolution. With sub-micrometric beams probing a few tens of nanometers, Laue diffraction will be the technique of choice to study crystal by crystal most of crystalline phases of the material, while powder X-ray diffraction will focus on the few additional nanocrystallized phases (crystal size ≤ 10 nm). A more quantitative analysis of the structure, from both monochromatic and Laue data [65], could also provide additional details on these heterogeneous and complex materials.

Coupling of structural methods with FF-XANES (full-field X-ray absorption near edge structure) spectroscopy where full-field images are collected while varying the incident energy of the beam across a characteristic absorption edge is promising. The later technique was recently successfully used to investigate iron oxide repartitions in Greek and Roman ceramics. It showed that the differences among iron oxide repartitions (slip surface, slip core, interface slip/body and body) could be related to the firing processes [44, 124, 125, 160]. Both the large analyzed area (1 mm²) and the submicrometer resolution of the technique are well adapted to the investigation of particles on representative areas, at a spatial resolution allowing the study of the repartition and association and of transition metals.

5 Conclusion

All the above examples took benefit from high-definition 2D or 3D images. Such images result from collection of data over large fields of view (typically tens of millimeters to tens of centimeters) sampled at a high spatial resolution (of typically hundreds of nanometers to hundreds of micrometers). Unprecedented high-resolution chemical and speciation-oriented description of samples and artefacts surfaces and volumes over large fields of views now enables studying inclusions, cracks, abnormalities and defects that often play the lead role in material behaviour and bring essential clues towards the recognition of manufacturing processes; in a

Table 1 Typical experimental parameters available at the end stations used to produce the works described in the present article

Experiment	Energy range (keV)	Lateral dimension (μm)	pps (μm^2)	Nature of information collected
Tomographic microscopy	8–250	Few hundreds of μm to few tens of cm	$(0.05\text{--}50)^2$	Internal morphology; porosity
Fast XRF raster-scanning	2.4–23	1×1 up to $500 \times 600 \text{ mm}^2$	$(1\text{--}100)^2$	Elementary composition
UV/visible photoluminescence	200–800 nm 1.5–6.2 eV	Few centimeters	$(0.15)^2$	Molecular and ionic signatures; SC signature and defects
Scanning transmission X-ray microscopy	0.2–2	Hundreds	$(0.015)^2$	Chemical speciation
Quantitative SAXS raster-scanning	7–25	$(0.1\text{--}50)^2$	$(20\text{--}9500)^2$	Size, shape and relative organization of nanoscale heterogeneities
Poly- and monochromatic $\mu\text{-XRD}$	5–24	80×40	Laue: 2×2 (1 s/point) mono.: 3×5 (90 s/point)	Structural and textural properties

Lateral dimension typical diameter of FOV or of the raster-scanned area, *pps* typical projected pixel (voxel) size, *mono.* monochromatic, *SC* semi-conductor

word, allowing ‘looking for traces’. It also provides context to such information and answers the need, well-identified in ancient materials, to search for “needles in haystacks” [153]. Imaging can also contribute to establishing the statistical relevance and validation on the collected or even averaged data (e.g. [51] in stratified archaeological biominerals). In physics terms, it provides the ability to describe a material over successive length scales, and correlate the information from different length scales to obtain information on processes (manufacturing, alteration, *etc.*), a capability that can be designated as *spatial dynamics* [20, 29].

The tunability of the synchrotron source is also essential in many ongoing developments. It can either be exploited *statically*, by optimisation of the excitation energy (3D tomography, structural methods, XRF), or *dynamically*, by scanning (or performing Fourier-transform with respect to a reference beam) over a significant spectral range in *excitation* spectroscopies (DUV photoluminescence, X-ray absorption spectroscopy, *etc.*). As discussed earlier, the latter spectroscopies are extremely sensitive to changes in chemical properties and environment of selected atoms or moieties. Coupling of high-definition imaging with excitation spectroscopies provides a range of new *spectral imaging* approaches where the distribution of a specific signature can be mapped across a sample or artefact morphology (Table 1).

This requires fast full-field imaging of large images or fast scans in position (x , y , z), with parallel scans in incident (emission) energy. The question of the

ultimate spot size attained may be less of a question as imagers with projected pixel sizes as small as a few micrometers to tens of nanometers are now starting to become operational, if not routine, in many energy ranges. However, compromises have to be made between the desired step and beam sizes (or pixel size), lateral dimensions of images, number of energy positions to collect and process data in reasonable time, while minimising the risk of radiation-induced changes.

The question of radiation damage may well become the main dimensioning parameter for a number of reasons. (1) In order to attain a certain number of counts with a certain noise, the incoming *number of photons* will have to be identical, albeit over a smaller area. The flux density is certainly not the only parameter governing radiation-induced side effects, but one of the central ones, and an increase in flux density can lead to dramatic changes in the chemistry or magnitude of effects; for instance, when charges or heat build up locally instead of being dissipated by the material. (2) As the question of imaging large areas of samples or objects becomes a major component in many investigations, significant areas of samples or artefacts may be put at risk. Irradiating centimetric areas may induce significant change in the colour perception of an irradiated artefact that would not be perceived after microscale analysis, or may considerably modify the chemistry of samples, comparably to effects induced under scanning electron microscopy. (3) An interconnecting method along carefully crafted analytical protocols is often needed, and irradiation can induce unexpected changes downstream, such as observed in Fig. 7. (4) Vastly increased flux densities can be attained at modern installations using undulator- or wiggler-based instruments. For these reasons, most of the experiments performed on heritage materials may end up being limited primarily by the risk of local alteration of samples, hence requiring more research efforts to be undertaken in the field [28, 129].

Another significant ubiquitous constraint is sample preparation, which has also become a major transverse interest for the field. For high-definition imaging, specific efforts are needed to overcome limitations to make samples suited both to high-resolution and large-area imaging. The conjunction of both goals is not straightforward, and may require, for instance, attaining low roughness across very wide sample surfaces. In many cases, sample contamination should be as limited as possible during preparation. Popular ways are the use of unsupported sections, avoiding embedding media, or using low chemical impact intermediate layers to isolate samples from mounting resins. Coupling distinct analytical approaches puts additional constraints to sample preparation. When working on a single cross-section, this raises the need of ensuring compatibility between the distinct, and sometimes quite adverse, requirements originating from each technique. Areas where previous irradiation was performed need either to be identifiable, or to be recorded accurately at the sample (artefact) level. The long-term recording of this information when samples are not sacrificed is a very significant issue with no current solution when involving microscale characterisation. Working on successive cross-sections prepared a similar way (e.g. successive sections prepared through ultramicrotomy) raises the need of ensuring comparability between analysed areas from successive sections. When the thickness of the sections exceeds the size of

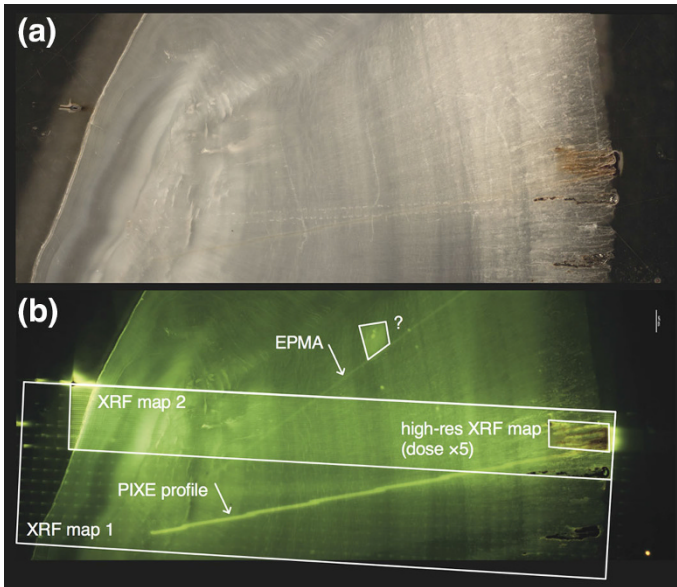


Fig. 7 Radiation-induced side effects from various techniques used to study archaeological fish otoliths. Ancient otoliths are used as palaeo-environmental proxies of water salinity and temperature [52]. They are primarily made of aragonite CaCO_3 . Light microscopy images under visible (a) and UV (b) illumination. Note the emissions resulting from irradiation for the various techniques used: electron probe micro-analysis and particle-induced X-ray emission profiles, low-energy high-flux synchrotron XRF maps. High intensity spots on the border of the XRF maps denote locations where longer point acquisitions were performed, mostly before launching collection of maps. The *question mark* indicates an area where a previous analysis was performed but was not reported, although it is likely to impact further investigation. Images courtesy P. Cook (IPANEMA)

characteristic details studied through microscale imaging, this approach becomes even less reliable.

Processing large multi-dimensional data sets is a challenge. For instance, collecting photoluminescence maps at several excitation and emission wavelengths, e.g. data in Echard et al. ,is four-dimensional and can generate many additional maps when decomposing these data on the basis of specific spectroscopic signatures [70]. This raises logistical issues, and also new practical and theoretical problems of exploration, processing and representation. This is of course not only a constraint, as developments will offer ample opportunities to take the most benefit of the collected hypervolumes, while current approaches favor the parallel and independent processing of connected data (e.g. see discussion in [26, 48] where approaches are developed to cluster spectral data through hierarchical procedures, and to perform unsupervised classification through conditional density estimation and penalized likelihood model selection to regularise spectral images).

This has led to a number of significant research programs, such as European (COST G8, CHARISMA, IPERION CH) and national initiatives. The sixth edition of the *Synchrotron and neutrons in art and archaeology* (SR2A) conference, established since 2005, and dedicated sessions in conferences such as Technart,

showed a significant increase in number of attendees, and demonstrated a broader extension of the user community towards more ambitious projects gathering transdisciplinary expertise [21].

To conclude, very significant improvements have occurred, thanks to the development of synchrotron-based imaging approaches to study artefacts and samples from cultural and natural collections and sites. These developments now expand over the whole spectral range accessible at synchrotron facilities, from the far infrared to hard X-rays. They also bring new capabilities over almost all elemental, chemical, structural and morphological approaches at unprecedented resolution over very large fields of view. New practical and theoretical developments are therefore needed to obtain the best benefit of these new capabilities, which will surely be the focus of this interdisciplinary work in the coming years.

Acknowledgments The IPANEMA platform is jointly developed by CNRS, the French Ministry of Culture and Communication and MNHN, and benefits from a CPER grant (MENESR, Région Ile-de-France) [23]. IPANEMA and Synchrotron SOLEIL are supported by the Research Infrastructures activity IPERION CH of the Horizon2020 Programme of the EU (Grant Agreement No. 654028). Support from the ERC project PaleoNanoLife (P.I.: F. Robert), the PATRIMA LabEx and within the agreement between the MNHN and IPANEMA is acknowledged. LB and UB acknowledge support from the France–Stanford Center for Interdisciplinary Studies Program. Portions of this research were carried out at the Stanford Synchrotron Radiation Lightsource (SSRL), a user facility of the U.S. Department of Energy (DOE), Office of Basic Energy Sciences. The work performed on the 12.3.2 beamline was supported by the Director, Office of Science, Office of Basic Energy Sciences of the US Department of Energy, who operates ALS under contract No. DE-AC02-05CH11231.

References

1. Albéric M, Gourrier A, Müller K, Zizak I, Wagermaier W, Fratzl P, Reiche I (2014) Early diagenesis of elephant tusk in marine environment. *Palaeogeogr Palaeoclimatol Palaeoecol* 416:120–132
2. Albertin F, Astolfo A, Stampanoni M, Peccenini E, Hwu Y, Kaplan F, Margaritondo G (2015) Ancient administrative handwritten documents: X-ray analysis and imaging. *J Synchrotron Radiat* 22(2):446–451. doi:10.1107/S1600577515000314
3. Albertin F, Astolfo A, Stampanoni M, Peccenini E, Hwu Y, Kaplan F, Margaritondo G (2015) X-ray spectrometry and imaging for ancient administrative handwritten documents. *X-ray Spectrom* 44(3):93–98
4. Alfeld M, Pedroso JV, van Eikema Hommes M, Van der Snickt G, Tauber G, Blaas J, Haschke M, Erler K, Dik J, Janssens K (2013) A mobile instrument for in situ scanning macro-XRF investigation of historical paintings. *J Anal At Spectrom* 28(5):760–767
5. Alfeld M, Siddons DP, Janssens K, Dik J, Woll AR, Kirkham R, van de Wetering E (2013) Visualizing the 17th century underpainting in Portrait of an old man by Rembrandt van Rijn using synchrotron-based scanning macro-XRF. *Appl Phys A* 111(1):157–164. doi:10.1007/s00339-012-7490-5
6. Alleon J, Bernard S, Remusat L, Robert F (2015) Estimation of nitrogen-to-carbon ratios of organics and carbon materials at the submicrometer scale. *Carbon* 84:290–298
7. Als-Nielsen J, McMorrow D (2011) Elements of modern X-ray physics, 2nd edn. Wiley, New York
8. Barbi M, Tokaryk T, Tolhurst T (2014) Synchrotron radiation as a tool in paleontology. *Phys Can* 70(1):8–12
9. Benzerara K, Menguy N, López-García P, Yoon TH, Kazmierczak J, Tyliczszak T, Guyot F, Brown GE (2006) Nanoscale detection of organic signatures in carbonate microbialites. *Proc Nat Acad Sci* 103(25):9440–9445
10. Bergmann U (2007) Archimedes brought to light. *Phys World* 20:39–42. doi:10.1038/435257a

11. Bergmann U (2011) Imaging with X-ray fluorescence. In: Netz R, Noel W, Wilson N, Tchernetska N (eds) *The archimedes palimpsest*, vol 1, chap. 6. Cambridge University Press, Cambridge
12. Bergmann U, Knox KT (2009) Pseudo-color enhanced X-ray fluorescence imaging of the archimedes palimpsest. In: *IS&T/SPIE electronic imaging*. International Society for Optics and Photonics, pp 724702–724702
13. Bergmann U, Manning PL, Wogelius RA (2012) Chemical mapping of paleontological and archaeological artifacts with synchrotron X-rays. *Ann Rev Anal Chem* 5(1):361–389. doi:10.1146/annurev-anchem-062011-143019
14. Bergmann U, Morton RW, Manning PL, Sellers WI, Farrar S, Huntley KG, Wogelius RA, Larson P (2010) Archaeopteryx feathers and bone chemistry fully revealed via synchrotron imaging. *Proc Natl Acad Sci USA* 107(20):9060–9065. doi:10.1073/pnas.1001569107
15. Berna F, Matthews A, Weiner S (2004) Solubilities of bone mineral from archaeological sites: the recrystallization window. *J Archaeol Sci* 31(7):867–882
16. Bernard S, Benzerara K, Beyssac O, Brown GE Jr, Stamm LG, Durringer P (2009) Ultrastructural and chemical study of modern and fossil sporoderms by scanning transmission X-ray microscopy (STXM). *Rev Palaeobot Palynol* 156(1–2):248–261. doi:10.1016/j.revpalbo.2008.09.002
17. Bernard S, Benzerara K, Beyssac O, Menguy N, Guyot F, Brown GE Jr, Goffe B (2007) Exceptional preservation of fossil plant spores in high-pressure metamorphic rocks. *Earth Planet Sci Lett* 262(1–2):257–272. doi:10.1016/j.epsl.2007.07.041
18. Bernard S, Papineau D (2014) Graphitic carbons and biosignatures. *Elements* 10:435–440
19. Bertini M, Mokso R, Krupp EM (2014) Unwinding the spiral: discovering the manufacturing method of iron age scottish glass beads. *J Archaeol Sci* 43:256–266
20. Bertrand L, Cotte M, Stambanoni M, Thoury M, Marone F, Schöder S (2012) Development and trends in synchrotron studies of ancient and historical materials. *Phys Rep* 519(2):51–96. doi:10.1016/j.physrep.2012.03.003
21. Bertrand L, Dillmann P, Reiche I (2015) Synchrotron radiation and neutrons in art and archaeology 2014 (editorial). *J Anal At Spectrom* 30:540–541. doi:10.1039/C5JA90006A
22. Bertrand L, Doucet J, Dumas P, Simionovici A, Tsoucaris G, Walter P (2003) Microbeam synchrotron imaging of hairs from Ancient Egyptian mummies. *J Synchrotron Rad* 10(5):387–392. doi:10.1107/S0909049503015334
23. Bertrand L, Languille MA, Cohen SX, Robinet L, Gervais C, Leroy S, Bernard D, Le Penne C, Josse W, Doucet J, Schöder S (2011) European research platform IPANEMA at the SOLEIL synchrotron for ancient and historical materials. *J Synchrotron Rad* 18(5):765–772. doi:10.1107/S090904951102334X
24. Bertrand L, Réfrégiers M, Berrie B, Echard JP, Thoury M (2013) A multiscale photoluminescence approach to discriminate among semiconducting historical zinc white pigments. *Analyst* 138(16):4463–4469. doi:10.1039/C3AN36874B
25. Bertrand L, Réguer S, Doucet J (2007) Le synchrotron, un outil polyvalent pour l'étude chimique des matériaux du patrimoine (Synchrotron: a versatile tool for the chemical study of heritage materials). *Act Chim* 312–313:105–111
26. Bertrand L, Robinet L, Cohen SX, Sandt C, Le Hô AS, Soulier B, Lattuati-Derieux A, Echard JP (2011) Identification of the finishing technique of an early eighteenth century musical instrument using FTIR spectromicroscopy. *Anal Bioanal Chem* 399(9):3025–3032. doi:10.1007/s00216-010-4288-1
27. Bertrand L, Robinet L, Thoury M, Janssens K, Cohen SX, Schöder S (2012) Cultural heritage and archaeology materials studied by synchrotron spectroscopy and imaging. *Appl Phys A* 106(2):377–396. doi:10.1007/s00339-011-6686-4
28. Bertrand L, Schöder S, Anglos D, Breese MBH, Janssens K, Moïni M, Simon A (2015) Mitigation strategies for radiation damage in the analysis of ancient materials. *Trends Anal Chem* 66:128–145. doi:10.1016/j.trac.2014.10.005
29. Bertrand L, Thoury M, Anheim E (2013) Ancient materials specificities for their synchrotron examination and insights into their epistemological implications. *J Cult Heritage* 14(4):277–289. doi:10.1016/j.culher.2012.09.003
30. Bocherens H, Polet C, Toussaint M (2007) Palaeodiet of Mesolithic and Neolithic populations of Meuse Basin (Belgium): evidence from stable isotopes. *J Archaeol Sci* 34(1):10–27
31. Bonse U, Hart M (1965) An x-ray interferometer with long separated interfering beam paths. *Appl Phys Lett* 7(4):99–100. doi:10.1063/1.1754330

32. Born M, Wolf E (1999) Principles of optics: electromagnetic theory of propagation, interference and diffraction of light. Cambridge University Press, Cambridge
33. Branco W (1906) Die Anwendung der Röntgenstrahlen in der Paläontologie. der Königl. Akad. der Wiss, Verlag
34. Braun A, Huggins FE, Shah N, Chen Y, Wirick S, Mun SB, Jacobsen C, Huffman GP (2005) Advantages of soft X-ray absorption over TEM-EELS for solid carbon studies—a comparative study on diesel soot with EELS and NEXAFS. *Carbon* 43:117–124
35. Briggs DE, Summons RE (2014) Ancient biomolecules: their origins, fossilization, and role in revealing the history of life. *BioEssays* 36(5):482–490
36. Bronnikov AV (2002) Theory of quantitative phase-contrast computed tomography. *J Opt Soc Am A* 19(3):472–480
37. Buckley M, Kansa SW, Howard S, Campbell S, Thomas-Oates J, Collins M (2010) Distinguishing between archaeological sheep and goat bones using a single collagen peptide. *J Archaeol Sci* 37(1):13–20
38. Buckley M, Walker A, Ho SYW, Yang Y, Smith C, Ashton P, Oates JT, Cappellini E, Koon H, Penkman K, Elsworth B, Ashford D, Solazzo C, Andrews P, Strahler J, Shapiro B, Ostrom P, Gandhi H, Miller W, Rancey B, Zylber MI, Gilbert MTP, Prigodich RV, Ryan M, Rijdsdijk KF, Janoo A, Collins MJ (2008) Comment on “protein sequences from mastodon and tyrannosaurus rex revealed by mass spectrometry”. *Science* 319(5859):33. doi:10.1126/science.1147046. <http://www.sciencemag.org/content/319/5859/33.3.abstract>
39. Burger C, Zhou H, Wang H, Sics I, Hsiao BS, Chu B, Graham L, Glimcher MJ (2008) Lateral packing of mineral crystals in bone collagen fibrils. *Biophys J* 95(4):1985–1992
40. Casini A, Lotti F, Picollo M, Stefani L, Aldrovandi A (2003) Fourier transform interferometric imaging spectrometry: a new tool for the study of reflectance and fluorescence of polychrome surfaces. *Conservation science 2002: papers from the conference held in Edinburgh, Scotland 22–24 May 2002*. Archetype Publications, Edinburgh, Scotland, pp 249–253
41. Chadeaux C., Reiche I. (2009) Archaeological bone from macro-to nanoscale: heat-induced modifications at low temperatures. *J Nano Res* 8:157–172. *Trans Tech Publ*
42. Chadeaux C, Vignaud C, Chalmin É, Robles-Camacho J, Arroyo-Cabrales J, Johnson E, Reiche I (2009) Color origin and heat evidence of paleontological bones: case study of blue and gray bones from San Josecito Cave. *Mexico Am Miner* 94(1):27–33. doi:10.2138/am.2009.2860
43. Chapman D, Thomlinson W, Johnston RE, Washburn D, Pisano E, Gmur N, Zhong Z, Menk R, Arfelli F, Sayers D (1997) Diffraction enhanced x-ray imaging. *Phys Med Biol* 42(11): 2015–2025. <http://stacks.iop.org/0031-9155/42/2015>
44. Cianchetta I, Trentelman K, Maish J, Saunders D, Foran B, Walton M, Sciau P, Wang T, Pouyet E, Cotte M, Meirer F, Liu Y, Pianetta P, Mehta A (2015) Evidence for an unorthodox firing sequence employed by the Berlin Painter: deciphering ancient ceramic firing conditions through high-resolution material characterization and replication. *J Anal At Spectrom* 30(3):666–676. doi:10.1039/C4JA00376D
45. Cloetens P, Barrett R, Baruchel J, Guigay JP, Schlenker M (1996) Phase objects in synchrotron radiation hard X-ray imaging. *J Phys D Appl Phys* 29(1):133–146
46. Cloetens P, Ludwig W, Baruchel J, van Dyck D, van Landuyt J, Guigay JP, Schlenker M (1999) Holotomography: quantitative phase tomography with micrometer resolution using hard synchrotron radiation X-rays. *Appl Phys Lett* 75(19):2912–2914. doi:10.1063/1.125225
47. Cody GD, Gupta NS, Briggs DEG, Kilcoyne ALD, Summons RE, Kenig F, Plotnick RE, Scott AC (2011) Molecular signature of chitin-protein complex in Paleozoic arthropods. *Geology* 39(3):255–258. doi:10.1130/G31648.1
48. Cohen SX, Pennec EL (2014) Unsupervised segmentation of spectral images with a spatialized gaussian mixture model and model selection. *Oil Gas Sci Technol* 69(2):245–260
49. Collins M, Nielsen-Marsh C, Hiller J, Smith C, Roberts J, Prigodich R, Wess T, Csapo J, Millard A, Turner-Walker G (2002) The survival of organic matter in bone: a review. *Archaeometry* 44(3):383–394
50. Collinson ME, Smith SY, Manchester SR, Wilde V, Howard LE, Robson BE, Ford DS, Marone F, Fife JL, Starnpanoni M (2012) The value of x-ray approaches in the study of the messel fruit and seed flora. *Palaeobiodiversity Palaeoenvironments* 92(4):403–416
51. Cook PK, Dufour É, Languille MA, Mocuta C, Réguer S, Bertrand L (2015) Strontium speciation in archaeological otoliths. *J Anal At Spectrom*. doi:10.1039/C5JA00426H

52. Cook PK, Languille MA, Dufour É, Mocuta C, Tombret O, Fortuna F, Bertrand L (2015) Biogenic and diagenetic indicators in archaeological and modern otoliths: potential and limits of high-definition synchrotron micro-XRF elemental mapping. *Chem Geol* 414:1–15. doi:10.1016/j.chemgeo.2015.08.017
53. Cosmidis J, Benzerara K (2014) Soft X-ray scanning transmission spectromicroscopy. In: DiMasi E, Gower LB (eds) *Biom mineralization Sourcebook: characterization of biominerals and biomimetic materials*, chap. 8. CRC Press, Boca Raton, Florida, USA, pp 115–134
54. Cosmidis J, Benzerara K, Gheerbrant E, Esteve I, Bouya B, Amaghaz M (2013) Nanometer-scale characterization of exceptionally preserved bacterial fossils in Paleocene phosphorites from Ouled Abdoun (Morocco). *Geobiology* 11(2):139–153. doi:10.1111/gbi.12022
55. Cosmidis J, Benzerara K, Menguy N, Arning E (2013) Microscopy evidence of bacterial microfossils in phosphorite crusts of the Peruvian shelf: Implications for phosphogenesis mechanisms. *Chem Geol* 359:10–22
56. Cotte M, Checroun É, Mazel V, Solé VA, Richardin P, Taniguchi Y, Walter P, Susini J (2009) Combination of FTIR and X-rays synchrotron-based micro-imaging techniques for the study of ancient paintings. A practical point of view. *e-Preserv. Science* 6:1–9
57. Cotte M, Dumas P, Taniguchi Y, Checroun É, Walter P, Susini J (2009) Recent applications and current trends in Cultural Heritage Science using synchrotron-based Fourier transform infrared micro-spectroscopy. *C R Phys* 10(7):590–600. doi:10.1016/j.cry.2009.03.016
58. Cotte M, Susini J, Dik J, Janssens K (2010) Synchrotron-based X-ray absorption spectroscopy for art conservation: looking back and looking forward. *Acc Chem Res* 43(6):705–714. doi:10.1021/ar900199m
59. Cunningham JA, Rahman IA, Lautenschlager S, Rayfield EJ, Donoghue PC (2014) A virtual world of paleontology. *Trends Ecol Evol* 29(6):347–357
60. Cunningham JA, Vargas K, Pengju L, Belivanova V, Marone F, Martínez-Pérez C, Guizar-Sicairos M, Holler M, Bengtson S, Donoghue PC (2015) Critical appraisal of tubular putative eumetazoans from the Ediacaran Weng'an Doushantuo biota. *Proc R Soc B* 282(1812):20151169
61. Currey JD (2002) *Bones: structure and mechanics*. Princeton University Press, Princeton
62. Davis GR, Mills D (2014) Brute force absorption contrast microtomography. In: Stock SR (ed) *Developments in X-ray tomography IX*, SPIE optical engineering and applications, p 92120L. International Society for Optics and Photonics
63. Davis T, Gao D, Gureyev T, Stevenson A, Wilkins S (1995) Phase-contrast imaging of weakly absorbing materials using hard X-rays. *Nature* 373(6515):595–598
64. De Gregorio BT, Sharp TG, Flynn GJ, Wirick S, Hervig RL (2009) Biogenic origin for earth's oldest putative microfossils. *Geology* 37(7):631–634
65. Dejoie C, McCusker LB, Baerlocher C, Kunz M, Tamura N (2013) Can Laue microdiffraction be used to solve and refine complex inorganic structures? *J Appl Crystallogr* 46(6):1805–1816
66. Dejoie C, Sciau P, Li W, Noé L, Mehta A, Chen K, Luo H, Kunz M, Tamura N, Liu Z (2014) Learning from the past: rare ε -Fe₂O₃ in the ancient black-glazed Jian (Tenmoku) wares. *Sci Rep* 4(4941). doi:10.1038/srep04941
67. Dejoie C, Tamura N, Kunz M, Goudeau P, Sciau P (2015) Complementary use of monochromatic and white-beam X-ray micro-diffraction for the investigation of ancient materials. *J Appl Cryst* 48. doi:10.1107/S1600576715014983
68. Dik J, Janssens K, van der Snickt G, van der Loeff L, Rickers K, Cotte M (2008) Visualization of a lost painting by Vincent van Gogh using synchrotron radiation based X-ray fluorescence elemental mapping. *Anal Chem* 80:6436–6442. doi:10.1021/ac800965g
69. Dooryhée É, Martinetto P, Walter P, Anne M (2004) Synchrotron X-ray analyses in art and archaeology. *Rad Phys Chem* 71(3–4):863–868. doi:10.1016/j.radphyschem.2004.04.129
70. Echard JP, Thoury M, Berrie BH, Séverin-Fabiani T, Vichi A, Didier M, Réfrégiers M, Bertrand L (2015) Synchrotron DUV luminescence micro-imaging to identify and map historical organic coatings on wood. *Analyst* 140(15):5344–5353. doi:10.1039/C5AN00483G
71. Edwards N, Wogelius RA, Bergmann U, Larson P, Sellers W, Manning P (2013) Mapping prehistoric ghosts in the synchrotron. *Appl Phys A* 111(1):147–155
72. Ehrlich H, Rigby JK, Botting J, Tsurkan M, Werner C, Schwille P, Petrášek Z, Pisera A, Simon P, Sivkov V et al (2013) Discovery of 505-million-year old chitin in the basal demosponge *Vauxia gracilenta*. *Sci Rep* 3:3497

73. Ferreira ESB., Boon JJ, Stampanoni M, Marone F (2011) Study of the mechanism of formation of calcium soaps in an early 20th-century easel painting with correlative 2D and 3D microscopy. In: Proceedings of 16th ICOM-CC triennial conference, Lisbon, Portugal, September 19–23, 2011
74. Francis J, Hitchcock A (1992) Inner-shell spectroscopy of p-benzoquinone, hydroquinone, and phenol: distinguishing quinoid and benzenoid structures. *J Phys Chem* 96(16):6598–6610
75. Fratzl P, Fratzl-Zelman N, Klaushofer K, Vogl G, Koller K (1991) Nucleation and growth of mineral crystals in bone studied by small-angle X-ray scattering. *Calcif Tissue Int* 48(6):407–413
76. Fratzl P, Gupta HS, Paris O, Valenta A, Roschger P, Klaushofer K (2005) Diffracting “stacks of cards”—some thoughts about small-angle scattering from bone. In: Scattering methods and the properties of polymer materials. Springer, New York, pp 33–39
77. Fratzl P, Schreiber S, Klaushofer K (1996) Bone mineralization as studied by small-angle X-ray scattering. *Connect Tissue Res* 34(4):247–254
78. Fratzl P, Weinkamer R (2007) Nature’s hierarchical materials. *Prog Mat Sci* 52(8):1263–1334. doi:10.1016/j.pmatsci.2007.06.001
79. Friis EM, Marone F, Pedersen KR, Crane PR, Stampanoni M (2014) Three-dimensional visualization of fossil flowers, fruits, seeds, and other plant remains using synchrotron radiation x-ray tomographic microscopy (srxtm): new insights into cretaceous plant diversity. *J Paleontol* 88(4):684–701
80. Friis EM, Pedersen KR, Marone F (2014) *Arcellites punctatus* sp. nov.: a new megaspore from the early cretaceous of portugal studied using high resolution synchrotron radiation X-ray tomographic microscopy (SRXTM). *Grana* 53(2):91–102
81. Garino C, Borfecchia E, Gobetto R, van Bokhoven JA, Lamberti C (2014) Determination of the electronic and structural configuration of coordination compounds by synchrotron-radiation techniques. *Coord Chem Rev* 277:130–186
82. Gerritsen HC, van der Oord CJR, Levine YK, Munro HI, Jones GR, Shaw DA, Rommerts FF (1994) Fluorescence imaging and time-resolved spectroscopy of steroid using confocal synchrotron radiation microscopy. In: Lakowicz JR (ed) Time-resolved laser spectroscopy in biochemistry IV, vol 2137. Los Angeles, CA
83. Gervais C, Thoury M, Reguer S, Mass J (2015) Radiation damages during synchrotron X-ray microanalyses of prussian blue and zinc white historic paintings: detection, mitigation and integration. *Appl Phys A* 121(3):949–955
84. Gill PG, Purnell MA, Crumpton N, Brown KR, Gostling NJ, Stampanoni M, Rayfield EJ (2014) Dietary specializations and diversity in feeding ecology of the earliest stem mammals. *Nature* 512(7514):303–305
85. Gourrier A, Bunk O, Müller K, Reiche I (2011) Artificially heated bone at low temperatures: a quantitative scanning-small-angle X-ray scattering imaging study of the mineral particle size. *ArcheoSciences Revue d’archéométrie* 35:191–199
86. Gourrier A, Li C, Siegel S, Paris O, Roschger P, Klaushofer K, Fratzl P (2010) Scanning small-angle X-ray scattering analysis of the size and organization of the mineral nanoparticles in fluorotic bone using a stack of cards model. *J Appl Crystallogr* 43(6):1385–1392
87. Gourrier A, Wagermaier W, Burghammer M, Lammie D, Gupta HS, Fratzl P, Riekel C, Wess TJ, Paris O (2007) Scanning X-ray imaging with small-angle scattering contrast. *J Appl Cryst* 40:S78–S82
88. Groso A, Abela R, Stampanoni M (2006) Implementation of a fast method for high resolution phase contrast tomography. *Opt Exp* 14(18):8103–8110
89. Gueriau P, Bernard S, Bertrand L (2016) Synchrotron advanced imaging of paleontological specimens. *Elements* 12(1) (in press)
90. Gueriau P, Bertrand L (2015) Deciphering exceptional preservation of fossils through trace elemental imaging. *Microsc Today* 23(3):2–6. doi:10.1017/S1551929515000024
91. Gueriau P, Mocuta C, Bertrand L (2015) Cerium anomaly at microscale in fossils. *Anal Chem* 87(17):8827–8836. doi:10.1021/acs.analchem.5b01820
92. Gueriau P, Mocuta C, Dutheil DB, Cohen SX, Thiaudière D, The OT1 consortium, Charbonnier S, Clément G, Bertrand L (2014) Trace elemental imaging of rare earth elements discriminates tissues at microscale in flat fossils. *Plos One* 9(1):e86946
93. Hedges RE (2002) Bone diagenesis: an overview of processes. *Archaeometry* 44(3):319–328
94. Hernández Cruz D, Rousseau ME, West MM, Pézolet M, Hitchcock AP (2006) Quantitative mapping of the orientation of fibroin β -sheets in *B. mori* cocoon fibers by scanning transmission X-ray microscopy. *Biomacromolecules* 7(3):836–843

95. Hiller JC, Thompson TJU, Evison MP, Chamberlain AT, Wess TJ (2003) Bone mineral change during experimental heating: an X-ray scattering investigation. *Biomaterials* 24(28):5091–5097. doi:10.1016/S0142-9612(03)00427-7
96. Hiller JC, Wess TJ (2006) The use of small-angle X-ray scattering to study archaeological and experimentally altered bone. *J Archaeol Sci* 33(4):560–572. doi:10.1016/j.jas.2005.09.012
97. Hitchcock A, Morin C, Heng Y, Cornelius R, Brash J (2002) Towards practical soft X-ray spectromicroscopy of biomaterials. *J Biomater Sci Polym Ed* 13(8):919–937
98. Hitchcock AP, Dynes JJ, Johansson G, Wang J, Botton G (2008) Comparison of NEXAFS microscopy and TEM-EELS for studies of soft matter. *Micron* 39:311–319
99. Holmes JM, Beebe RA, Posner AS, Harper RA (1970) Surface areas of synthetic calcium phosphates and bone mineral. *Exp Biol Med* 133(4):1250–1253
100. Ice GE, Budai JD, Pang JW (2011) The race to X-ray microbeam and nanobeam science. *Science* 334(6060):1234–1239
101. Ice GE, Pang JW (2009) Tutorial on X-ray microLaue diffraction. *Mat Charact* 60(11):1191–1201
102. Ishii I, Hitchcock A (1988) The oscillator strengths for C1s and O1s excitation of some saturated and unsaturated organic alcohols, acids and esters. *J Elect Spectrosc Relat Phenom* 46(1):55–84
103. Janssens K, Alfeld M, Van der Snickt G, De Nolf W, Vanmeert F, Radepon M, Monico L, Dik J, Cotte M, Falkenberg G, Miliani C, Brunetti BG (2013) The use of synchrotron radiation for the characterization of artists' pigments and paintings. *Ann Rev Anal Chem* 6(1):399–425. doi:10.1146/annurev-anchem-062012-092702
104. Janssens K, Dik J, Cotte M, Susini J (2010) Photon-based techniques for nondestructive subsurface analysis of painted cultural heritage artifacts. *Acc Chem Res* 43(6):814–825. doi:10.1021/ar900248e
105. Jarcho S (1964) Lead in the bones of prehistoric lead-glaze potters. *Am Antiq* 30(1):94–96
106. Kak A, Slaney M (2001) Principles of computerized tomographic imaging. Society of Industrial and Applied Mathematics, Philadelphia, USA
107. Kalsbeek N, Richter J (2006) Preservation of burned bones: an investigation of the effects of temperature and pH on hardness. *Stud Conserv* 51(2):123–138
108. Koon H, Nicholson R, Collins M (2003) A practical approach to the identification of low temperature heated bone using tem. *J Archaeol Sci* 30(11):1393–1399
109. Koon H, O'Connor T, Collins M (2010) Sorting the butchered from the boiled. *J Archaeol Sci* 37(1):62–69
110. Krueger KK (1974) The use of ultraviolet light in the study of fossil shells. *Curator Mus J* 17(1):36–49
111. Kunz M, Chen K, Tamura N, Wenk HR (2009) Evidence for residual elastic strain in deformed natural quartz. *Am Mineral* 94(7):1059–1062
112. Lakes R (1993) Materials with structural hierarchy. *Nature* 361(6412):511–515
113. Landis WJ, Glimcher MJ (1978) Electron diffraction and electron probe microanalysis of the mineral phase of bone tissue prepared by anhydrous techniques. *J Ultrastruct Res* 63(2):188–223
114. Langer M, Cloetens P, Pacureanu A, Peyrin F (2012) X-ray in-line phase tomography of multi-material objects. *Optics Lett* 37(11):2151–2153
115. Larson B, Yang W, Ice G, Budai J, Tischler J (2002) Three-dimensional X-ray structural microscopy with submicrometre resolution. *Nature* 415(6874):887–890
116. Léa V (2005) Raw, pre-heated or ready to use: discovering specialist supply systems for flint industries in mid-Neolithic (Chassey culture) communities in southern France. *Antiquity* 79(303):51–65
117. Li J, Benzerara K, Bernard S, Beyssac O (2013) The link between biomineralization and fossilization of bacteria: insights from field and experimental studies. *Chem Geol* 359:49–69
118. Li J, Bernard S, Benzerara K, Beyssac O, Allard T, Cosmidis J, Moussou J (2014) Impact of biomineralization on the preservation of microorganisms during fossilization: An experimental perspective. *Earth Planet Sci Lett* 400:113–122
119. Lin Y, Seales WB (2005) Opaque document imaging: building images of inaccessible texts. In: Tenth IEEE international conference on computer vision, 2005. ICCV 2005, vol 1, pp 662–669. IEEE
120. Liu Z, Mehta A, Tamura N, Pickard D, Rong B, Zhou T, Pianetta P (2007) Influence of Taoism on the invention of the purple pigment used on the Qin terracotta warriors. *J Archaeol Sci* 34:1878–1883. doi:10.1016/j.jas.2007.01.005

121. Lynch PA, Tamura N, Lau D, Madsen I, Liang D, Strohschnieder M, Stevenson AW (2007) Application of white-beam X-ray microdiffraction for the study of mineralogical phase identification in ancient egyptian pigments. *J Appl Cryst* 40:1089–1096. doi:10.1107/S0021889807041003
122. Manso M, Carvalho M (2009) Application of spectroscopic techniques for the study of paper documents: a survey. *Spectrochim Acta B* 64(6):482–490. doi:10.1016/j.sab.2009.01.009 10th Rio Symposium on Atomic Spectrometry
123. Maser J, Osanna A, Wang Y, Jacobsen C, Kirz J, Spector S, Winn B, Tennant D (2000) Soft X-ray microscopy with a cryo scanning transmission x-ray microscope: I. Instrumentation, imaging and spectroscopy. *J Microsc* 197(1):68–79
124. Meirer F, Cabana J, Liu Y, Mehta A, Andrews JC, Pianetta P (2011) Three-dimensional imaging of chemical phase transformations at the nanoscale with full-field transmission x-ray microscopy. *Synchrotron Radiat* 18(5):773–781
125. Meirer F, Liu Y, Pouyet E, Fayard B, Cotte M, Sanchez C, Andrews JC, Mehta A, Sciau P (2013) Full-field XANES analysis of Roman ceramics to estimate firing conditions—a novel probe to study hierarchical heterogeneous materials. *J Anal At Spectrom* 28:1870–1883
126. Mills D, Samko O, Rosin P, Thomas K, Wess T, Davis GR (2012) Apocalypto: revealing the unreadable. In: Stock SR (ed) *Developments in X-ray tomography VIII, SPIE Optical Engineering and Applications*, vol 8506. International Society for Optics and Photonics, San Diego, California, USA, p 85060A
127. Miot J, Li J, Benzerara K, Sougrati MT, Ona-Nguema G, Bernard S, Jumas JC, Guyot F (2014) Formation of single domain magnetite by green rust oxidation promoted by microbial anaerobic nitrate-dependent iron oxidation. *Geochim Cosmochim Acta* 139:327–343
128. Mocella V, Brun E, Ferrero C, Delattre D (2015) Revealing letters in rolled Herculaneum papyri by X-ray phase-contrast imaging. *Nat Comm* 6:5895
129. Moini M, Rollman C, Fleskes R (2014) Molecular level effects of natural aging, as well as chemical and radiation exposures on museums' proteinaceous specimens. In: *Proceedings of American Society for mass spectrometry meeting 2013*
130. Mokso R, Marone F, Haberthür D, Schittny J, Mikuljan G, Isenegger A, Stampanoni M (2011) Following dynamic processes by X-ray tomographic microscopy with sub-second temporal resolution. In: *The 10th international conference on X-ray microscopy*, vol 1365. AIP Publishing, New York, pp 38–41
131. Momose A (1995) Demonstration of phase-contrast X-ray computed tomography using an X-ray interferometer. *Nucl Instrum Methods Phys Res Sect A* 352(3):622–628
132. Moreau JD, Cloetens P, Gomez B, Daviero-Gomez V, Néraudeau D, Lafford TA, Tafforeau P (2014) Multiscale 3D virtual dissections of 100-million-year-old flowers using X-ray synchrotron micro- and nanotomography. *Microsc Microanal* 20(1):305–312. doi:10.1017/S1431927613014025
133. Myneni SC (2002) Soft X-ray spectroscopy and spectromicroscopy studies of organic molecules in the environment. *Rev Mineral Geochem* 49(1):485–579
134. Nevin A, Osticioli I, Anglos D, Burnstock A, Cather S, Castellucci E (2007) Raman spectra of proteinaceous materials used in paintings: a multivariate analytical approach for classification and identification. *Anal Chem* 79(16):6143–6151. doi:10.1021/ac070373j
135. Obst M, Schmid G (2014) 3D chemical mapping: application of scanning transmission (soft) X-ray microscopy (STXM) in combination with angle-scan tomography in bio-, geo-, and environmental sciences. *Methods Mol Biol* 1117:757–781
136. Paganin D, Mayo S, Gureyev T, Miller P, Wilkins S (2002) Simultaneous phase and amplitude extraction from a single defocused image of a homogeneous object. *J Microsci Oxford* 206(1):33–40
137. Picard A, Kappler A, Schmid G, Quaroni L, Obst M (2015) Experimental diagenesis of organo-mineral structures formed by microaerophilic Fe(II)-oxidizing bacteria. *Nat Commun* 6:6277
138. Pons MN, Le Bonté S, Potier O (2004) Spectral analysis and fingerprinting for biomedica characterisation. *J Biotechnol* 113(1):211–230
139. Popescu BFG, George MJ, Bergmann U, Garachtchenko AV, Kelly ME, McCrea RP, Lüning K, Devon RM, George GN, Hanson AD et al (2009) Mapping metals in Parkinson's and normal brain using rapid-scanning X-ray fluorescence. *Phys Med Biol* 54(3):651
140. Posner AS (1969) Crystal chemistry of bone mineral. *Physiol Rev* 49(4):760–92
141. Pradel A, Langer M, Maisey JG, Geffard-Kuriyama D, Cloetens P, Janvier P, Tafforeau P (2009) Skull and brain of a 300-million-year-old chimaeroid fish revealed by synchrotron holotomography. *Proc Natl Acad Sci USA* 106(13):5224–5228. doi:10.1073/pnas.0807047106

142. Pusey PN (2002) Introduction to scattering experiments. Scattering methods applied to soft condensed matter, Neutrons, X-rays and light, pp 3–21
143. Reiche I, Favre-Quattropiani L, Vignaud C, Bocherens H, Charlet L, Menu M (2003) A multi-analytical study of bone diagenesis: the Neolithic site of Bercy (Paris, France). *Meas Sci Technol* 14(9):1608
144. Reiche I, Lebon M, Chadefaux C, Müller K, Le Hô AS, Gensch M, Schade U (2010) Microscale imaging of the preservation state of 5,000-year-old archaeological bones by synchrotron infrared microspectroscopy. *Anal Bioanal Chem* 397(6):2491–2499. doi:10.1007/s00216-010-3795-4
145. Riekel C, Burghammer M, Müller M (2000) Microbeam small-angle scattering experiments and their combination with microdiffraction. *J Appl Cryst* 33(3):421–423. doi:10.1107/S0021889899014375
146. Robin N, Bernard S, Miot J, Blanc-Valleron MM, Charbonnier S, Petit G (2015) Calcification and diagenesis of bacterial colonies. *Minerals* 5(3):488–506
147. Rodenburg JM, Hurst AC, Cullis AG (2007) Transmission microscopy without lenses for objects of unlimited size. *Ultramicroscopy* 107(2–3):227–31. doi:10.1016/j.ultramic.2006.07.007
148. Rogers K, Daniels P (2002) An X-ray diffraction study of the effects of heat treatment on bone mineral microstructure. *Biomaterials* 23(12):2577–2585
149. Rorimer JJ (1931) Ultra-violet rays and their use in the examination of works of art. Metropolitan Museum of Art, New-York, USA
150. Rouchon V, Bernard S (2015) Mapping iron gall ink penetration within paper fibres using scanning transmission X-ray microscopy. *J Anal At Spectrom* 30(3):635–641. doi:10.1039/C4JA00358F
151. Rousseau ME, Hernández Cruz D, West MM, Hitchcock AP, Pézolet M (2007) Nephila clavipes spider dragline silk microstructure studied by scanning transmission X-ray microscopy. *J Am Chem Soc* 129(13):3897–3905
152. Ryan C, Kirkham R, Hough R, Moorhead G, Siddons D, de Jonge M, Paterson D, Geronimo GD, Howard D, Cleverley J (2010) Elemental X-ray imaging using the Maia detector array: the benefits and challenges of large solid-angle. *Nucl Instrum Meth A* 619(1–3):37–43. doi:10.1016/j.nima.2009.11.035
153. Ryan C, Siddons D, Kirkham R, Li Z, de Jonge M, Paterson D, Kuczewski A, Howard D, Dunn P, Falkenberg G et al (2014) Maia X-ray fluorescence imaging: capturing detail in complex natural samples. In: 499 (ed) *J Phys Conf Ser* 1:012002. IOP Publishing
154. Sadeghi B, Bergmann U (2010) The codex of a companion of the prophet and the qurān of the prophet. *Arabica* 57:343–436
155. Sanchez S, Ahlberg PE, Trinajstić KM, Mirone A, Tafforeau P (2012) Three-dimensional synchrotron virtual paleohistology: a new insight into the world of fossil bone microstructures. *Microsc Microanal* 18(05):1095–1105
156. Scherf H (2013) Computed tomography in paleoanthropology—an overview. *Archaeol Anthropol Sci* 5(3):205–214. doi:10.1007/s12520-013-0128-5
157. Schreiner M, Frühmann B, Jembrih-Simbürger D, Linke R (2004) X-rays in art and archaeology: an overview. *Powder Diff* 19(1):3–11. doi:10.1154/1.1649963
158. Schroer CG, Kurapova O, Patommel J, Boye P, Feldkamp J, Lengeler B, Burghammer M, Riekel C, Vincze L, van der Hart A et al (2005) Hard x-ray nanoprobe based on refractive X-ray lenses. *Appl Phys Lett* 87(12):124,103
159. Sciau P, Goudeau P, Tamura N, Dooryhée É (2006) Micro scanning X-ray diffraction study of Gallo-Roman Terra Sigillata ceramics. *Appl Phys A* 83(2):219–224. doi:10.1007/s00339-006-3512-5
160. Sciau P, Leon Y, Goudeau P, Fakra SC, Webb S, Mehta A (2011) Reverse engineering the ancient ceramic technology based on X-ray fluorescence spectromicroscopy. *J Anal At. Spectrom* 26(5):969–976
161. Sciau P, Relaix S, Mirguet C, Goudeau P, Bell AMT, Jones RL, Pantos E (2008) Synchrotron X-ray diffraction study of phase transformations in illitic clays to extract information on sigillata manufacturing processes. *Appl Phys A* 90(1):61–66. doi:10.1007/s00339-007-4249-5
162. Sciau P, Relaix S, Roucau C, Kihn Y, Chabanne D (2006) Microstructural and microchemical characterization of Roman period Terra sigillate slips from archaeological sites in Southern France. *J Am Ceram Soc* 89(3):1053–1058. doi:10.1111/j.1551-2916.2005.00827.x
163. Shahack-Gross R, Bar-Yosef O, Weiner S (1997) Black-coloured bones in hayonim cave, israel: differentiating between burning and oxide staining. *J Archaeol Sci* 24(5):439–446

164. Shipman P, Foster G, Schoeninger M (1984) Burnt bones and teeth: an experimental study of color, morphology, crystal structure and shrinkage. *J Archaeol Sci* 11(4):307–325
165. Smith SY, Collinson ME, Rudall PJ, Simpson DA, Marone F, Stampanoni M (2009) Virtual taphonomy using synchrotron tomographic microscopy reveals cryptic features and internal structure of modern and fossil plants. *Proc Natl Acad Sci USA* 106(29):12013–12018
166. Smith TM, Tafforeau P, Le Cabec A, Bonnin A, Houssaye A, Pouech J, Moggi-Cecchi J, Manthi F, Ward C, Makaremi M et al (2015) Dental ontogeny in pliocene and early pleistocene hominins. *PLoS One* 10:e0118,118
167. Snigirev A, Snigireva I, Kohn V, Kuznetsov S, Schelokov I (1995) On the possibilities of X-ray phase contrast microimaging by coherent high-energy synchrotron radiation. *Rev Sci Instrum* 66(12):5486–5492
168. Solomon D, Lehmann J, Kinyangi J, Liang B, Heymann K, Dathe L, Hanley K, Wirick S, Jacobsen C (2009) Carbon (1s) NEXAFS spectroscopy of biogeochemically relevant reference. *Soil Sci Soc Am J* 73(6):1817–1830
169. Spalla O (2002) General theorems in small-angle scattering. Neutrons, X-rays and light: scattering methods applied to soft condensed matter. Lindner and Zemb, North-Holland, Elsevier edition
170. Stampanoni M, Groso A, Isenegger A, Mikuljan G, Chen Q, Bertrand A, Henein S, Betemps R, Frommherz U, Böhler P, Meister D, Lange M, Abela R (2006) Trends in synchrotron-based tomographic imaging: the SLS experience. In: Bonse U (ed) *Developments in X-ray tomography V*, Proceedings of SPIE, vol 6318, p 63180M. SPIE. doi:10.1117/12.679497
171. Stiner MC, Kuhn SL, Weiner S, Bar-Yosef O (1995) Differential burning, recrystallization, and fragmentation of archaeological bone. *J Archaeol Sci* 22(2):223–237
172. Strullu-Derrien C, Kenrick P, Tafforeau P, Cochard H, Bonnemain JL, Le Hérissé A, Lardeux H, Badel E (2014) The earliest wood and its hydraulic properties documented in c. 407-million-year-old fossils using synchrotron microtomography. *Bot J Linn Soc* 175(3):423–437
173. Sutton MD (2008) Tomographic techniques for the study of exceptionally preserved fossils. *Proc Roy Soc B* 275(1643):1587–1593
174. Tafforeau P, Boistel R, Boller E, Bravin A, Brunet M, Chaimanee Y, Cloetens P, Feist M, Hozowska J, Jaeger JJ, Kay RF, Lazzari V, Marivaux L, Nel A, Nemoz C, Thibault X, Vignaud P, Zabler S (2006) Applications of X-ray synchrotron microtomography for non-destructive 3D studies of paleontological specimens. *Appl Phys A* 83(2):195–202. doi:10.1007/s00339-006-3507-2
175. Tafforeau P, Smith TM (2008) Nondestructive imaging of hominoid dental microstructure using phase contrast X-ray synchrotron microtomography. *J Human Evol* 54(2):272–278. doi:10.1016/j.jhevol.2007.09.018
176. Tamura N, Celestre R, MacDowell A, Padmore H, Spolenak R, Valek B, Chang NM, Manceau A, Patel J (2002) Submicron X-ray diffraction and its applications to problems in materials and environmental science. *Rev Sci Instrum* 73(3):1369–1372
177. Tamura N, Kunz M, Chen K, Celestre R, MacDowell A, Warwick T (2009) A superbend X-ray microdiffraction beamline at the advanced light source. *Mater Sci Eng A* 524(1):28–32
178. Tamura N, MacDowell AA, Spolenak R, Valek BC, Bravman JC, Brown WL, Celestre RS, Padmore HA, Batterman BW, Patel JR (2003) Scanning X-ray microdiffraction with submicrometer white beam for strain/stress and orientation mapping in thin films. *J Synchrotron Rad* 10(2):137–143. doi:10.1107/S0909049502021362
179. Thoury M, Echard JP, Réfrégiers M, Berrie B, Nevin A, Jamme F, Bertrand L (2011) Synchrotron UV-visible multispectral luminescence micro-imaging of historical samples. *Anal Chem* 83(5):1737–1745. doi:10.1021/ac102986h
180. Wagermaier W, Gourrier A, Aichmayer B (2013) Understanding hierarchy and functions of bone using scanning X-ray scattering methods. In: *Materials design inspired by nature: function through inner architecture*, pp 46–73. RSC
181. Wang Y, Jacobsen C, Maser J, Osanna A (2000) Soft X-ray microscopy with a cryo scanning transmission X-ray microscope: II. Tomography. *J Microsc* 197(1):80–93. doi:10.1046/j.1365-2818.2000.00629.x
182. Weitkamp T, Diaz A, David C, Pfeiffer F, Stampanoni M, Cloetens P, Ziegler E (2005) X-ray phase imaging with a grating interferometer. *Opt Exp* 13(16):6296–6304
183. Weymouth JW (1973) X-ray diffraction analysis of prehistoric pottery. *Am Antiq* 38(3):339–344
184. Willneff E, Ormsby B, Stevens J, Jaye C, Fischer D, Schroeder S (2014) Conservation of artists' acrylic emulsion paints: XPS, NEXAFS and ATR-FTIR studies of wet cleaning methods. *Surf Interface Anal* 46(10–11):776–780

185. Wogelius RA, Manning PL, Barden HE, Edwards NP, Webb SM, Sellers WI, Taylor KG, Larson PL, Dodson P, You H, Da-qing L, Bergmann U (2011) Trace metals as biomarkers for eumelanin pigment in the fossil record. *Science* 333(6049):1622–1626. doi:10.1126/science.1205748. <http://www.sciencemag.org/content/333/6049/1622.abstract>
186. Young ML (2012) Archaeometallurgy using synchrotron radiation: a review. *Rep Prog Phys* 75(3):036,504. doi:10.1088/0034-4885/75/3/036504
187. Zazzo A, Balasse M, Patterson WP (2006) The reconstruction of mammal individual history: refining high-resolution isotope record in bovine tooth dentine. *J Archaeol Sci* 33(8):1177–1187
188. Zazzo A, Lebon M, Quiles A, Reiche I, Vigne JD (2015) Direct dating and physico-chemical analyses cast doubts on the coexistence of humans and dwarf hippos in cyprus. *PLoS One* 10(8):e0134,429
189. Zhou H, Burger C, Sics I, Hsiao BS, Chu B, Graham L, Glimcher MJ (2007) Small-angle X-ray study of the three-dimensional collagen/mineral superstructure in intramuscular fish bone. *Applied crystallography*
190. Ziv V, Weiner S (1994) Bone crystal sizes: a comparison of transmission electron microscopic and X-ray diffraction line width broadening techniques. *Connect Tissue Res* 30(3):165–175

Non-invasive Investigations of Paintings by Portable Instrumentation: The MOLAB Experience

B. Brunetti^{1,2} · C. Miliani^{1,2} · F. Rosi² ·
B. Doherty² · L. Monico² · A. Romani^{1,2} ·
A. Sgamellotti^{1,2}

Received: 18 October 2015 / Accepted: 17 December 2015 / Published online: 3 February 2016
© Springer International Publishing Switzerland 2016

Abstract The in situ non invasive methods have experienced a significant development in the last decade because they meet specific needs of analytical chemistry in the field of cultural heritage where artworks are rarely moved from their locations, sampling is rarely permitted, and analytes are a wide range of inorganic, organic and organometallic substances in complex and precious matrices. MOLAB, a unique collection of integrated mobile instruments, has greatly contributed to demonstrate that it is now possible to obtain satisfactory results in the study of a variety of heritage objects without sampling or moving them to a laboratory. The current chapter describes an account of these results with particular attention to ancient, modern, and contemporary paintings. Several non-invasive methods by portable equipment, including XRF, mid- and near-FTIR, UV–Vis and Raman spectroscopy, as well as XRD, are discussed in detail along with their impact on our understanding of painting materials and execution techniques. Examples of successful applications are given, both for point analyses and hyperspectral imaging approaches. Lines for future perspectives are finally drawn.

Keywords X-ray fluorescence · Raman spectroscopy · FTIR · UV–Vis spectroscopy · Pigment · Binding media

✉ B. Brunetti
bruno@dyn.unipg.it

¹ Centro di Eccellenza SMAArt (Scientific Methodologies Applied to Archaeology and Art), Università degli Studi di Perugia, Via Elce di Sotto 8, 06123 Perugia, Italy

² Istituto CNR di Scienze e Tecnologie Molecolari (CNR-ISTM), Via Elce di Sotto 8, 06123 Perugia, Italy

1 Introduction

In recent decades there has been a growing interest in the applications of analytical chemistry for the study of heritage materials. Through scientific examinations, satisfactory answers have been given to numerous problems of a multidisciplinary nature, such as the clarification of historical art and archaeological questions (i.e. execution techniques, attribution, dating, provenance), the assessment of the state of conservation of artefacts, the establishment of the best conditions to avoid or slow down alterations, as well as the monitoring of the behaviour of artwork materials during and after restoration [1, 2].

These studies were carried out in the past mostly by micro-destructive methods using minimal samples, taken from marginal areas of the artwork during restoration, in order to mitigate the visual impact of the operation. In other cases, the first relevant non-invasive analytical approaches were experimented by moving artifacts, such as manuscripts or small paintings, into a scientific laboratory, and exploiting bench-top instrumentation (e.g. micro-Raman spectrometers) [3, 4] or accelerators and large scale facility methods [5–8].

However, a large portion of historical patrimony consists in immovable objects that cannot be moved from their usual location (e.g. monuments, sculptures, buildings) and, even in the case of movable patrimony (including precious paintings, ceramics, gems, manuscripts, etc.), curators normally avoid moving artworks to a laboratory due to the risk to their integrity and high insurance costs. For such reasons, many efforts over the years have been oriented towards the design and set up of innovative mobile instruments with sensitivity and specificity comparable to their bench-top counterparts, achieving the best compromise between efficiency and portability in order to apply a method based on bringing the laboratory to the object and not vice versa.

Such an in situ, non-invasive approach, being able to get valuable information without altering or moving the object, registered an immediate success, leading to a rapid diffusion of the use of portable instrumentation that produced in recent years: (a) a significant change in diagnostic practices, (b) a net increase of scientific inputs in heritage studies and (c) a positive modification in the relationships between curators, conservators, and scientists, thus permitting a common language to be established and partnership strengthened.

After the first national Italian applications and the pioneering and successful MOLAB (mobile laboratory) experience of the European projects Eu-ARTECH (2004–2009) [9] and CHARISMA (2009–2014) [10], where a set of integrated portable instrumentations were offered to European users for in situ measurements, more and more mobile tools and facilities flourished in different countries that now permit users, through the national and European IPERION CH programmes [11], to exploit integrated portable instruments able to non-invasively obtain satisfying results in the study of a variety of heritage objects and relative inorganic and organic materials.

In this chapter, following a short general introduction on the limitations and advantages intrinsic to the use of compact portable instrumentation for analytical

applications, selected experimental results are presented, mostly obtained in recent works by MOLAB [12]. The aim is to show actual performances of the non-invasive approach in the study of atomic and molecular composition of artwork materials, with particular focus on pigments, colorants and binding media in ancient and modern paintings.

More recently, following the success of point analyses, innovative chemical imaging techniques at the macro scale have been also experimentally applied for in situ examination of paintings. Indications are given on perspectives for future developments along this direction.

2 Portable Spectroscopic Instrumentation: Benefits and Drawbacks

Passing from bench-top instrumentation to the compact and manageable equipment for in situ measurements some limitations may be incurred in term of performance, due to the miniaturization of optical and electronic components and constraints in the setup geometry. Nevertheless, the performance of portable spectroscopic instruments has greatly improved in the past decade, narrowing the gap between portable and bench-top instruments.

Relevant issues can arise regarding spectral interpretation due to the optical and matrix effects that are present each time a signal is recorded in backscattering, emission, or reflection mode from materials having a complex, heterogeneous, and often multi-layered character, as occurs in polychromies.

However, the use of a variety of equipment, a non-invasive approach, and the accurate preliminary work carried out in the laboratory prior to the in situ campaign can overcome these limitations. In fact, observations coming from a manifold of analytical techniques, each overcoming intrinsic limitations of the others, can provide extensive and complementary information. In addition, since non-invasive measurements do not require any contact with the examined object, they can be carried out all over the painted surface on a virtually infinite number of points, obtaining numerous integrative and representative data. Finally, the preparatory work carried out in the laboratory on mock-up samples allows a better understanding of the spectra to be achieved, and interpretation models to be built which include matrix effects. In conclusion, when all this information is jointly analyzed, a more thorough understanding of the paint chemical composition can be achieved than in the case of laboratory analyses on few samples, often consisting of specimens sampled from the borders of lacunae or close to the frame.

In this section, the analytical technique most frequently applied for non-invasive in situ investigations are introduced and, for each, advantages and limitations are presented. The techniques are: X-ray fluorescence (XRF), mid- and near Fourier transform infrared (FTIR) analysis in reflection mode, Raman spectroscopy (with and without a microscope), ultraviolet–visible–near infrared (UV–Vis–NIR) absorption and fluorescence spectroscopies, and X-ray diffraction (XRD).

2.1 X-ray Fluorescence

X-ray fluorescence (XRF) spectrometry allows for a rapid determination of the elemental composition of a material. The technique is particularly efficient for the study of high- Z elements in low Z -matrixes. As a mobile tool, it has been extensively used for analysis in art and archaeology since the early 1970s and, therefore, represents the first technique to be historically exploited for intensive in situ non-invasive investigations [13–15].

Today, it is a primary tool universally exploited as a first approach to any study carried out in situ. Throughout the years, it has provided answers to a huge number of questions regarding manufactures in art, revealing specific aspects of the working practice of ancient masters [16–18].

A main limitation of XRF for in situ analyses is that only qualitative results are generally obtained, because matrix effects related to diffusion, re-absorption, and Auger ionization do not allow for reliable quantifications. This is particularly true in the case of complex layered structures, as occurs in paintings. Only in few favourable cases, has the modelling of the X-ray's absorption through different layers allowed for determining composition and thickness of paint layers on the basis of $K\alpha/K\beta$ or $L\alpha/L\beta$ intensity ratios. This method was successfully applied in situ to estimate the thickness of layers in a painting by Marco d'Oggiono, a pupil of Leonardo da Vinci, and on the *Mona Lisa* in the Louvre Museum, to determine how Leonardo achieved a barely perceptible gradation of facial tones from light to dark (the Leonardo *sfumato*) [19–21].

2.2 Reflection Infrared Spectroscopy

Reflection FTIR spectroscopy, from the near-IR (NIR) range up to 400 cm^{-1} , is the most informative and reliable molecular technique among the MOLAB array of methods [22–32].

In the medium infrared range (mid-FTIR, $4000\text{--}400\text{ cm}^{-1}$), the matrix effect appears with large spectral distortions, both in band shape and position, that can affect the interpretation of reflection spectra [33, 34]. Reflection mid-FTIR spectroscopy from a complex and optically thick surface (as that of a painting) generally includes the collection of both diffuse (from the volume) and specular (from the surface) reflection with a variable and unpredictable ratio that basically depends on the roughness of the examined surface as well as on the optical properties of the investigated materials. In particular, the specular reflection is governed by Fresnel's law and, accordingly, is a function of both the absorption index (k) and refractive index (n) [35]. As a consequence, reflection spectra of organic compounds typically show derivative profiles (resembling the refractive index dependence on wavenumber), while reflection spectra of many inorganic compounds (sulfates, carbonates, phosphates, silicates, etc.) are often distorted by the inversion of those fundamental bands that show $k \gg n$ [28].

On the other hand, the diffuse reflection is governed by Kubelka–Munk's law and depends on the absorption index and scattering coefficient (s). In diffuse reflection,

the spectral distortions are smaller and concern mainly the relative intensity of bands. Typically, weak absorption bands increase in their relative intensity with respect to stronger absorption bands especially when laying at high wavenumbers. Consequently, overtones and combination bands, usually neglected in transmission mode can be profitably exploited in reflection mode with substantial advantage, especially when the fundamental bands of the fingerprint regions are obscured by overlap with other signals [27, 28]. Moreover, diffuse reflection can also determine the enhancement of absorption bands related to minor components, allowing (in favourable cases) for a fine discrimination between pigments made of similar main chemical structure, as, for example, natural and synthetic ultramarine blue [36] or lamp and bone black [23].

In the NIR region (near-FTIR, 7000–4000 cm^{-1}), reflection spectra are dominated by diffuse (volume) reflection because the absorption indices of materials are generally rather low. As a drawback, near-FTIR spectra generally show poor specific profiles generated by an overlap of overtone and combination modes. Nevertheless, this spectral range proved to be useful for a non-invasive, initial classification of binding media and other natural polymers [37, 38].

Another important advantage is related to the higher penetration depth of near-FTIR with respect to mid-FTIR that makes it sensitive and exploitable to also characterize the binding media in the presence of a (preferably thin) layer of varnish, whose signal would prevail in the mid-infrared range.

A wide database of reflection spectra recorded on model paints composed of a variety of pigments and binders (different materials and different surface roughness) allowed distinctive information to be registered and classified, suitable for a correct interpretation of the mid- and near-FTIR spectral features during diagnostic campaigns [22–34].

Great advantage of portable FTIR instrumentation (mid and near) lies in the good performances of the available mobile instruments, that are comparable to those of standard bench-top equipment.

2.3 UV–Vis–NIR Absorption and Emission

UV–Vis–NIR reflection spectroscopy (typically in the range 190–1700 nm) in configuration with optical fibres (known as FORS—fiber optic reflectance spectroscopy) is a well-established technique for the characterization of pigments and colorants in works of art. It has the advantage of being easy to apply and it requires short acquisition times (few seconds). In addition, there is a wide commercial availability of truly portable and relatively inexpensive instrumentation.

Despite the advantages, some shortcomings prevent the reliable use of FORS as a self-consistent analytical tool. In particular, reflectance spectra in the UV–Vis–NIR range features broad bands related to electronic transitions (besides a few vibrational bands in the NIR) and, therefore, they have an intrinsically lower fingerprinting ability when compared with spectra obtained with other molecular spectroscopic techniques, such as FTIR or Raman spectroscopy. However, although in some cases it cannot allow unambiguous identification, its straightforward

applicability makes it an ideal spectroscopic method in a multi-technique analytical approach.

Early publications on the topic (without optical fibres) date back to the 1930s [39]. Since then, it has been widely used alone (typically applied with extension to the NIR range up to 2500 nm) or in combination with other techniques for the study of paintings [40–42] and illuminations in manuscripts [43–45].

More recently, UV–Vis–NIR fluorescence spectroscopy has been exploited as an additional non-invasive tool to investigate coloured materials in paintings, manuscripts and other polychromies [46]. Its use is particularly advisable when organic dyes and/or pigments are present with rather good emission quantum yield. As for absorption electronic bands, the corresponding emissions are usually quite broad (i.e. several tens of nanometers full width at half-maximum, [FWHM]). This often causes overlapping among emissions from distinct fluorophores and makes it difficult to distinguish among them, thus reducing the specificity of spectrally based discrimination. In addition, the spectral properties of a fluorophore can vary depending on its microenvironment (e.g. binding media, mixture with other pigments) with further complications. Nevertheless, on the basis of in-depth studies in the laboratory (in solution, solid state and, finally, on paint models) it has been demonstrated that its fluorescence properties may be used to identify anthraquinone dyes (differentiating between those of animal or vegetal origin) [47], oxazines [48], indigoids [49], flavonoids and carotenoid dyes [50]. In addition, a few inorganic pigments (e.g. zinc white [51], Cd-based pigments [52, 53], and Egyptian blue [54]) show rather specific emission bands (the latter two in the NIR range) which can be exploited for their non-invasive identification.

Here, the limitations produced by matrix effects are related to self-absorption, that is, absorption by the fluorophore itself of the emitted light, thus erasing a variable portion of the emission spectrum on the short wavelength side. The problem of the correction for self-absorption of fluorescence spectra collected on pictorial works has been addressed, and a method for the treatment of the fluorescence signals has been first developed for luminophore dispersed in an opaque layer [55] and then extended for luminophore in a translucent layer on a coloured background (i.e. glazing technique) [56].

With the aim of increasing the specificity of emission UV–Vis–NIR spectroscopy toward the molecular recognition of dyes and organic pigments, the exploitation of fluorescence kinetic parameters has been recently proposed. In fact, kinetic analysis of emission decay curves can be used to distinguish among different compounds that have similar fluorescence spectra and may aid in the identification of the molecular species by comparison with known standards [57, 58].

Notably, a prototype system for integrated measurements of UV–Vis–NIR reflection spectroscopy (investigating the absorption properties), steady-state fluorescence, and luminescence lifetimes is currently applied in MOLAB interventions to record on the same spot, *in situ*, the full photo-physical behaviour of dyes and pigments on painted surfaces [59].

2.4 Raman Spectroscopy

Drawbacks and successes of portable Raman spectrometers for in situ non-invasive applications have been widely discussed in a recent review paper with a rich, extended bibliography [60]. Much more than for bench-top applications, molecular fluorescence represents the main inconvenience for non-invasive Raman spectroscopy, especially when analysing paint layers rich of (oxidised) organic components. In the case of a micro-spectrometry setup, no portable confocal microscopes are available and this implies the occurrence of matrix effects producing a high fluorescence background that obscures the weak Raman features. This limitation is obviously also present in the case of direct use of optical fibres (i.e. measurements without a microscope).

Other inconveniences arise from the compactness of portable systems, implying a reduced optical path and, therefore, a lower spectral range and resolution than in bench-top instruments. Furthermore, shields or correction systems for the daylight are not always available and, in case of use of scaffoldings, vibrations of the support of the spectrometer can seriously impede the recording of spectra. A final relevant drawback is that extreme attention must be paid in regulating the laser power, since the surface of the artefacts may be thermally and/or photochemically altered. This is obviously valid both for portable and bench-top instrumentation; however, it is evident that measurements carried out directly on the surface of a precious artwork (i.e. a painting masterpiece) require much more caution than laboratory investigation on samples. This calls for careful preliminary studies prior to the in situ campaign to search for the best compromise between safety of operation and intensity of scattering signals [61].

In general, Raman spectroscopy has proved to be a very successful technique for in situ studies of illuminations in manuscripts (low fluorescence, due to the generally high pigment/binder ratio), glasses, enamels, metals, but less for panel and canvas paintings. In case of mural paintings, the diffuse presence of organic protectives and/or consolidants, applied in restoration, as well as problems related to vibrations and defocusing, still usually limits in situ Raman spectroscopy applications.

As for bench-top instruments, to overcome fluorescence, a great advantage is offered by the use of high-wavelength lasers, which are able to reduce or eliminate electronic excitation, as, for example, those at 785 nm (diode laser) or those more recently introduced in a portable dispersive setup emitting at 1064 nm (Nd:YAG laser). However, due to the ν^4 dependence of Raman intensity, the sensitivity of spectra acquired using a near-infrared excitation is generally very low.

2.5 X-ray Diffraction

XRD is the most reliable method for the identification of minerals or synthetic crystalline materials. In principle, it represents the fundamental technique to complement chemical analyses by XRF and vibrational spectroscopy (FTIR and Raman). However, applications of portable XRD systems for in situ non-invasive measurements are scarce, mostly due to the severe geometrical restrictions of the in situ experimental setups that introduce numerous drawbacks. The characteristics

of existing XRD systems for heritage applications have been recently reviewed and the performances of each system compared [62]. These instruments are, apart from two single cases, based on angular dispersion XRD (AD-XRD) and consist of conventional goniometer-type diffractometers in which data are obtained by scanning the detector and/or the X-ray source [62–64], or systems that make use of two-dimensional (2D) detectors, such as charge-coupled devices (CCDs) [65, 66] or imaging plates, [67–69] that allow for the recording of diffraction data without mechanical movements.

The positioning of the instrument with respect to the surface to be analyzed is a critical parameter. For example, referring to the two latter systems, the source (a selectable X-ray tube) illuminates a small spot on the sample surface at 10° incidence and the 2D detector is set at the nearest distance from the spot. Thus, steric hindrances inevitably introduce limits in the 2θ angular range of the detected signals, which are 10° – 60° and 20° – 55° for the two systems, respectively, with 0.25° – 0.3° angular resolution [41]. A higher 2θ scan range (24° – 134°) with 2θ resolution of 0.12° is available in another system that uses a goniometer. However, the beam size that defines the spatial resolution is higher [62]. In all cases, due to the low intensities of the diffracted beams, in situ XRD analyses require acquisition times that are much longer than for the other non-invasive techniques, amounting to 30 min or even much more, sometimes hours, to achieve one single acceptable spectrum. A final drawback of non-invasive XRD is that shifts of the diffraction 2θ angles can be recorded, mainly due to the different depth of the crystals of the minerals to be detected (e.g. the crystals of the pigments). This is a disadvantage that, in principle, could be turned into an advantage when information on the depth of the pigment layers is required [70].

The advantage of XRD is that the technique is well established, diffraction phenomena are theoretically well understood (data can be theoretically simulated from crystal structure data), and a complete reference database is available as a powder diffraction file (PDF) supplied by the International Centre for Diffraction Data (ICDD). All these features make XRD a profitable technique to complement the data acquired in situ by FTIR and Raman spectroscopy, provided that a long-term analytical campaign is planned (several days), due to the requested long accumulation time for each point of measurement.

A drastic reduction of the data acquisition time (one or two orders of magnitude) is, in principle, possible when energy dispersive XRD (ED-XRD) is used, based on polychromatic excitation (using the *brehmstrahlung* X-rays that are filtered off in conventional X-ray tubes) and X-ray energy dispersive detection (i.e. using the same detector for XRF measurements). This approach represents a possible alternative to AD-XRD for in situ heritage applications [70–73]. However, in this approach, some complications arise: first, the quantities that regulate the scattered intensity depends on the energy; second, the spectral resolution depends not only on the angular divergence of the X-ray beam, but also on the energy resolution of the detector; third and most important, XRD and XRF peaks are recorded together in the same spectrum, sometimes overlapping, an inconvenience that can be avoided by changing the detection angle, reintroducing in some way the necessity of a mechanical angular movement. For these reasons, instruments able to carry out both

angular and energy dispersive XRD have been assembled with the purpose of taking advantages of both ED-XRD (shorter time and higher energy penetration) and AD-XRD (higher d resolution).

The first in situ application of a double ED and AD-XRD system was carried out in Japan to investigate a bronze mirror from the Eastern Han Dynasty (25–220 AD) and the painted statue of “Tamonten holding a stupa” from the Heian Period (794–1192 AD) [71]. Two new prototypes have been very recently set up and successfully tested at ICP-Elettra, showing promising results [73].

3 In Situ Experimental Results

MOLAB has been operative in Italy and Europe for around 15 years (started in 2001, with a national project dedicated to the monitoring of the state of conservation of the David of Michelangelo [74]) and, during these years, great experience has been accumulated with a total number of more than two hundred studies on different types of heritage artworks, including paintings, bronze and stone sculptures, manuscripts, and ceramics [12].

On the basis of this experience, selected examples of results are presented in this section on the identification of pigments, dyes, and binders in paintings. It will be also shown how an important, key passage for the success of the MOLAB measurements is represented by the preliminary work developed in the laboratory prior to the in situ campaign.

Using a protocol that starts with XRF measurements, followed in the order by (a) near- and mid-FTIR, (b) UV–Vis absorption and emission, (c) Raman spectroscopy, and (d) XRD, it can be assessed that the general characterization of the execution technique of a painter [identification of pigments and family of binder(s)] can be achieved today through direct measurements on the work of art, without any sampling. The necessity of a few micro-samples is restricted to the solution of specific problems, as the characterization of the paint stratigraphy or the determination of the detailed nature of binder(s) and colorants [22–25].

Successful applications of in situ non-invasive approaches for the study of painting techniques have been carried out on masterpieces of different periods and schools, as Renaissance paintings by Raphael [16], Perugino [17], Leonardo, on impressionist and post-impressionist paintings by Cézanne [25], Renoir [23] and Van Gogh [3, 75, 76], and on contemporary paintings by Picasso [77], Burri [78] Mondrian [79], De Stael, and many others.

3.1 Non-invasive Characterization of Pigments

3.1.1 Identification of Ancient Masters' Palette

Among these studies, an exemplary characterization of ground and pigments has been carried out at the Royal Museum of Fine Arts of Antwerp on the triptych *Christ among Singing and Music Playing Angels* by the Flemish painter Memling [80]. The painting, dated ca. 1487–'90, is composed of three panels (ca.



Fig. 1 The mobile laboratory, MOLAB, during the campaign at the Royal Fine Art Museum of Antwerp for the study of the triptych *Christ among Singing and Music Playing Angels* (ca. 1487–'90), by H. Memling. The analytical work is proceeding simultaneously applying different techniques. The instruments rotate in front of each panel in order to investigate the selected areas with all the available equipment

2 m × 1.5 m, each) which depict Christ in the clouds, surrounded by 16 angels, singing and playing different musical instruments. The study has been carried out through a long-term analytical campaign, in occasion of the restoration of the painting, when the varnish was removed. In Fig. 1, the MOLAB laboratory setup at the Royal Museum of Fine Arts is shown.

Together with XRF, reflection mid- and near-FTIR, absorption and emission (steady-state and time-resolved) UV–Vis spectroscopies, and XRD were exploited. Non-invasive Raman spectroscopy was not used in this case, because scattering was fully covered by a large fluorescence background induced by the binding medium.

Preliminary to the study of pigments, the presence of a small lacuna (ca. 0.2 cm²) in the paint, that left the underlying ground uncovered (Fig. 2), permitted the materials in the ground layer(s) to be first investigated by mid-FTIR and XRD, without interferences from the paint. The presence of both gypsum (CaSO₄·2H₂O) and chalk (CaCO₃) in the ground layers was clearly revealed by mid-FTIR through the combination and overtone bands at 2200 [27] and 2500 cm⁻¹, [25, 81] respectively. XRD spectra, collected in these areas, confirmed the presence of both compounds, as shown in Fig. 2.

The discovery of gypsum was rather unexpected. According to this finding, Memling here combined the practice of the Western and Northern European artists to use chalk for the ground, with the habits of the Mediterranean School, known to employ gypsum for the same purpose [82]. Although it remains not fully established if the two compounds were mixed or separated in two layers, the occurrence of gypsum as a preparation layer was confirmed by FTIR measurements which clearly indicated the presence of calcium sulfate not only from areas with emerging ground (lacunae), but also from several undamaged areas, through the paint (see, for

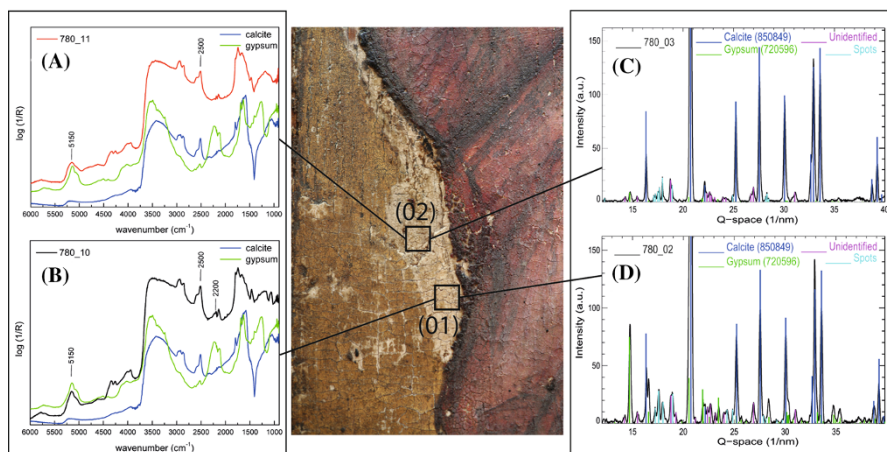


Fig. 2 Identification of calcium carbonate and gypsum by both mid-FTIR (a, b) and XRD (c, d) from two areas (01 and 02) of a lacuna in the paint in Fig. 1 (modified from Ref. [80])

example, the spectra reported in Fig. 3: a broad signal at 5150 cm^{-1} , ascribable to OH combination band of hydrated calcium sulphate [27]).

The figures represented in the three panels of the painting were characterised by a wide variety of colours and shades that were achieved by the painter combining different pigments. The variegate chromatic effects were created through specific mixtures or overlayers, especially on the wings and robes of the playing and singing angels.

Essential for the unambiguous molecular identification of pigments and mixtures in these complex areas was the complementary information originated from mobile FTIR, XRD, and UV–Vis absorption and emission spectroscopy. It was found that in the wings and robes of the angels, shades from light blue to deep purple were achieved by combining azurite, $2\text{CuCO}_3\cdot\text{Cu}(\text{OH})_2$ (identified by FTIR and XRD) with a variety of other pigments, such as bone black (identified by FTIR), lead white (revealed by FTIR and XRD), lead–tin yellow type I (revealed by XRD) and/or an organic red lake, most probably madder lake (identified by UV–Vis absorption and emission spectral profiles).

These pigments, together with natural ultramarine (present only in precious details), cinnabar and/or red ochre (in the incarnates), yellow, and brown ochre composed the full palette of the painter.

In more detail, azurite was characterized by reflection mid-FTIR via the combination bands of both the copper carbonate (structured signal at 2500 cm^{-1}) and copper hydroxide moiety (doublet at 4244 and 4373 cm^{-1}) [28] (see Fig. 3); lead white was mainly identified by the $\nu_1 + \nu_3$ combination band of cerussite (PbCO_3) and hydrocerussite [$2\text{PbCO}_3\cdot\text{Pb}(\text{OH})_2$] at 2410 and 2428 cm^{-1} , respectively; while carbon black of animal origin was identified through a small sharp signal at 2010 cm^{-1} [28].

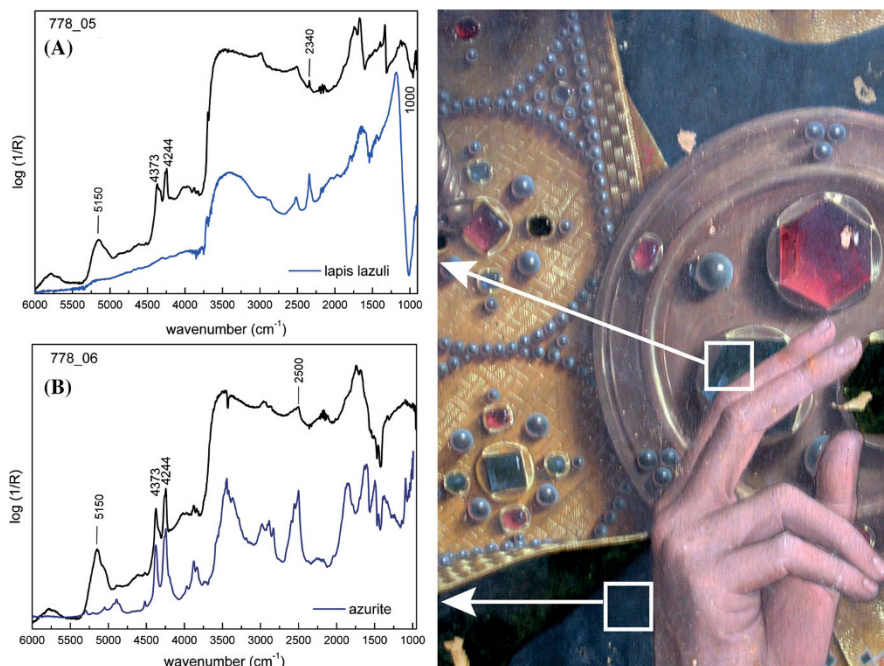


Fig. 3 Mid-FTIR reflection spectra recorded on two areas of the garment of Christ (see Fig. 1). Spectrum A (black line) illustrates the presence of both azurite and natural lapis lazuli in the highlights of the blue gems, while only azurite was found to characterise the blue colour of the garment (spectrum B, black line). Blue lines reference spectra of lapis lazuli and azurite (modified from Ref. [80])

XRD ascertained and confirmed the presence of the mineral azurite in the wings and robes of most of the angels and the presence of both hydrocerussite and cerussite in lead white. In dark blue areas of the robes, where mid-FTIR spectra showed the presence of carbon black, XRD established the presence of graphite, intermixed with the blue paint to produce a darker shade.

The combined use of XRF and XRD also indicated that the feathers in the rainbow-coloured wings of some angels were obtained by combining azurite with lead–tin yellow. The latter pigment, not visible by reflection FTIR spectroscopy, was also found in lighter yellow areas, on the mantle of one of the angels, where a combination of Pb and Sn was revealed by XRF, and XRD ascertained the presence of a crystalline phase of lead–tin oxide, in particular, lead–tin yellow type 1.

Examinations of deep purple areas suggested that this colour was obtained by combining azurite with a red organic pigment (layered and/or intermixed). Reflection UV–Vis emission and absorption spectroscopy succeeded in specifying the vegetal origin of an anthraquinone dyestuff, representative of madder lake. This lake was identified by the structured shape of the absorption band, with typical features at 510 and 540 nm, as well as the maximum of the emission band at 600 nm (Fig. 4) [47, 59]. The identification was also confirmed by the time decay

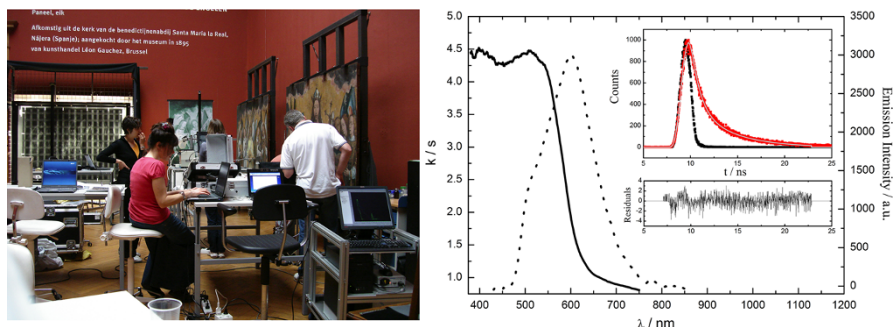


Fig. 4 *Left* preparation of the measurement with the portable system for absorption/fluorescence measurements. *Right* absorption (full line) and fluorescence emission spectra (dotted line) recorded in a deep purple area. In the inset, fluorescence decay time (red dots), excitation source (black dots), fitting curve (thin grey line), and distribution of residuals (bottom). Excitation wavelength: $\lambda = 455$ nm. Emission max. $\lambda = 620$ nm (rearrangement from Ref. [80])

values that were of ca. 1 and 4 ns (1, 2 and 4.3 ns of standard madder lake in oil [57]).

Colours tending to orange, such as the feathers in the wing of one angel, were obtained by a combination of vermilion with lead–tin yellow, as demonstrated by XRD and XRF.

Light blue paint was obtained by combining azurite with variable ratios of lead white. However, mid-FTIR spectra collected on the highlights of the blue gems decorating the cloak of Christ, revealed together with azurite, a broader absorption band inverted by a *reststrahlen* effect, in the range $900\text{--}1100\text{ cm}^{-1}$, corresponding to the Si–O antisymmetric stretching vibration, and a sharp stretching band at 2340 cm^{-1} assigned to the CO_2 stretching mode (Fig. 3). The distinctive incidence of silicates, together with the presence of CO_2 , is an evident marker of the presence of natural lapis lazuli. The entrapment of CO_2 in the β -cage of the sodalite framework of lazurite is related to the geological genesis of the mineral [36]. The presence of lazurite over-imposed to azurite was fully confirmed by the XRD spectra, recorded in the same area (data not shown).

A summary of the obtained results is reported in Table 1, with an indication of the analytical techniques relevant for the identification. In the table, the results obtained by MOLAB in the study of another triptych by H. Memling, *The Last Judgement* of the National Museum of Gdansk [83] are also reported. The comparison highlights a substantial analogy of the materials used by Memling in the two artworks.

In conclusion, it has been shown that the integration of elemental, vibrational, electronic, and XRD analytical techniques now permits a general description of the materials used by the artist to be obtained in situ without any sampling, with a satisfying identification of the inorganic pigments used, accompanied by good indications of the presence of organic pigments and colorants.

Table 1 Hans Memling's use of pigments and ground from the MOLAB non-invasive studies of *Christ among Singing and Music Playing Angels* in the Royal Fine Art Museum of Antwerp and *The Last Judgement* triptych in the National Museum of Gdansk (Adapted from Ref. [83])

Area of interest	<i>Christ among Singing and Music Playing Angels</i> (Antwerp) [80]	<i>The Last Judgement</i> triptych (Gdansk) [83]	Analytical techniques ¹
Ground	Calcium carbonate and gypsum	Calcium carbonate	XRF, mid- and near-FTIR, XRD
Blue	Lapis lazuli (only gems of the Christ mantle)	Lapis lazuli (precious details)	Mid-FTIR, XRD
	Azurite (with black carbon in darker areas)	Azurite	XRF, mid-FTIR, XRD
	Smalt	–	XRF, near-FTIR
Green	Cu-based pigments	Cu-based pigments	XRF
	Azurite and lead–tin yellow	–	XRF, mid-FTIR, XRD
Yellow	Lead–tin yellow (I)	Lead–tin yellow (I)	XRF, XRD
	Yellow ochre	Yellow ochre	XRF, XRD, mid-FTIR
Red/orange	Cinnabar	Cinnabar	XRF, UV–Vis absorption
Purple	Madder lake	Madder lake	UV–Vis fluorescence emission (steady state and time resolved)
Brown	Ochre	Ochre	XRF, XRD
White	Lead white (hydrocerussite and cerussite)	Lead white (hydrocerussite and cerussite)	Mid-FTIR, XRD
Black	Bone black	–	Mid-FTIR
Incarnates	Ochre and/or cinnabar with lead white	Ochre and/or cinnabar with lead white	XRF, UV–Vis absorption, mid-FTIR, XRD
Gilding	Pure gold by mixtion or by bole, goethite and quartz	Pure gold by mixtion	XRF, XRD
Binder ²	Lipidic (weak signal of proteins only in some areas with thin paint)	Lipidic (weak signal of proteins in some areas)	Mid-FTIR

¹ Portable XRD results refer only to the Antwerp painting

² See Sect. 3.2 for details on binding media identification

3.1.2 Non-invasive Discrimination of Pigments Showing Varieties in Composition and Structures

The non-invasive in situ approach has been recently demonstrated to be suitable for the diagnostic identification of pigments that show varieties of compositions and structures. This is the case, for example, of the so-called lead antimonates, which are known to be characterized by a pyrochlore structure, $\text{Pb}_2\text{Sb}_2\text{O}_7$ (Naples yellow), where the replacement of Sb by various elements gives rise to formulation varieties $\text{Pb}_2\text{Sb}_{2-x}\text{Y}_x\text{O}_{7-x/2}$ ($\text{Y} = \text{Sn}, \text{Zn}, \text{Fe}, \text{Pb}$) that correspond to different yellow hues [84–86]. This is also the case of the cadmium sulfide pigments, which share a common structure based on CdS, but partial substitutions of Cd or S with elements

as Zn, Hg, and Se lead to a variety of tonalities from yellow to orange and red [52, 53].

The discrimination among formulations and structures of these series of pigments, within the same family, is not straightforward, because their spectroscopic properties usually show strong similarities. In addition, XRD could not always be applied because synthetic historical pigments have often been prepared by imperfectly controlled reactions, producing not only crystalline but also highly disordered phases. In this case, the exploitation of vibrational spectroscopy can be particularly helpful, confirming FTIR and Raman spectroscopy in particular, as specifically suitable techniques for non-invasive in situ discrimination of the possible varieties.

The Raman spectrum of pure Naples yellow ($\text{Pb}_2\text{Sb}_2\text{O}_7$) displays a typical feature, that consists of strong band at about 510 cm^{-1} related to the symmetric stretching of the SbO_6 octahedra [85]. The same Raman scattering mode, in a modified pyrochlore showing orange color, appears split in two bands, one again at 510 cm^{-1} (but much less intense) and another around 450 cm^{-1} , with further modifications occurring in the low wavenumber region. On the basis of a structural study on standards of lead antimonate yellows, these spectral features have been demonstrated to be distinctive of a doped pyrochlore with Sb partially substituted by Zn or Sn [86, 87].

Yellow CdS is a semiconductor with a direct band gap of 2.41 eV (512 nm at room temperature) [88] whose color can be tuned from yellow to light-yellow hues by partially substituting cadmium with zinc in the crystal lattice, thus forming solid solutions of cadmium zinc sulfide ($\text{Cd}_{1-x}\text{Zn}_x\text{S}$) [89]. Alternatively, co-precipitation with variable amounts of selenium leads to the formation of cadmium sulfo-selenide solid solutions ($\text{CdS}_{1-x}\text{Se}_x$) characterized by tonalities ranging from orange to red [89]. The resonance-enhanced longitudinal optical Raman modes have been shown to be linearly dependent on the Se and Zn molar fraction of the ternary solid solutions. These linear relationships are exploitable for the in situ identification of the composition of ternary pigments by resonance Raman spectroscopy.

In addition to these cases, the study of lead chromates and lead chromate–sulfate co-precipitates has attracted specific interest, since their possible identification via vibrational spectroscopy (i.e. IR and Raman) and XRD. These substances compose the series of pigments known as chrome yellows that were often used by painters of the late nineteenth century, as the impressionists and post-impressionists. They show tonalities that range from yellow-orange to pale-yellow according to their chemical composition (PbCrO_4 ; $\text{PbCr}_{1-x}\text{S}_x\text{O}_4$, with $0 < x < 0.8$) [90, 91]. Another form of lead chromate-based pigment is the co-precipitate with lead oxide and is commonly known as chrome orange [$(1 - x)\text{PbCrO}_4 \cdot x\text{PbO}$] due to its deep orange shade.

From the crystallographic point of view, PbCrO_4 and chrome orange show monoclinic structures, while that of PbSO_4 is orthorhombic. It follows that a structural change in $\text{PbCr}_{1-x}\text{S}_x\text{O}_4$ co-precipitates is observed with increasing sulfur content: when x exceeds 0.4–0.5, a modification from a monoclinic to an orthorhombic structure takes place [95, 96].

Van Gogh himself, in the letters to his brother Theo and to his friend Emile Bernard (letters n. 593, 595, 684, 687, 710, 863), mentions the use of three varieties of lead chromate-based pigments, namely chrome yellow types I, II, and III, probably corresponding to pale-yellow (S-rich $\text{PbCr}_{1-x}\text{S}_x\text{O}_4$), yellow-orange (PbCrO_4) and orange $[(1-x)\text{PbCrO}_4 \cdot x\text{PbO}]$ hues [92–94].

It has been demonstrated that the darkening observed for chrome yellows, caused by the photo-reduction of original chromates to Cr(III) compounds, is favoured when the pigment is present in the orthorhombic S-rich form $\text{PbCr}_{1-x}\text{S}_x\text{O}_4$ ($x > 0.4$) [75, 95–98]. Thus, the possibility to distinguish among different forms of lead chromate-based pigments and to map their location all over the surface of a painting is relevant for the assessment of the areas subject to a major risk of degradation.

In $\text{PbCr}_{1-x}\text{S}_x\text{O}_4$ solid solutions, the chromate to sulfate substitution leads to a volume decrease of the monoclinic unit cell at a low sulfate concentration and to a change of the crystalline structure from monoclinic to orthorhombic with increasing sulfur content. These modifications strongly affect the fundamental vibrational bands of these materials (with changes of shape and wavenumber position of these signals), making Raman and infrared spectroscopies suitable techniques for their direct discrimination, even when using a non-invasive in situ approach.

As is visible in Fig. 5, in the Raman spectra collected by a portable instrument with a 785 nm laser excitation on a series of paint models, the chromate bending multiplet [ν_2/ν_4 ($\text{Cr}_2\text{O}_4^{2-}$)] appears to be strongly affected by the sulfate substitution, showing a clear shift of band positions and a modification of band shapes related to the change of the crystalline structure. Additionally, the symmetric stretching band of both sulfate [$\nu_1(\text{SO}_4^{2-})$] and chromate [$\nu_1(\text{CrO}_4^{2-})$] moieties shifts slightly toward higher energy, as a function of the sulfate amount. Another relevant effect of the chromate to sulfate substitution is the decrease of the Raman scattering cross-section.

Based on the knowledge developed by the study of the laboratory model paints, non-invasive Raman spectroscopy has been successfully applied in situ to study a series of paintings by Van Gogh conserved at the Van Gogh Museum in Amsterdam, namely *Sunflowers gone to seed*, *Bank of the Seine*, and *Portrait of Gauguin* (Fig. 5). In *Sunflowers gone to seed*, the spectrum acquired from a yellow-orange area shows the presence of monoclinic PbCrO_4 . The spectrum from a greenish yellow area of *Bank of the Seine* shows again the spectral features of the monoclinic PbCrO_4 , with the additional presence of a signal at 1050 cm^{-1} indicating a mixture with lead white. Finally, in a light yellow area of *Portrait of Gauguin*, the chrome yellow pigment is identified as the unstable S-rich $\text{PbCr}_{1-x}\text{S}_x\text{O}_4$ ($x \sim 0.5$). The presence of the sulfate component is well-evidenced by the $\nu_1(\text{SO}_4^{2-})$ band at 976 cm^{-1} and changes of shape and positions of $\nu_1(\text{CrO}_4^{2-})$ and ν_2/ν_4 ($\text{Cr}_2\text{O}_4^{2-}$) modes.

The presence of lead chromates and unstable lead chromate–sulfate co-precipitates has been recently found by non-invasive in situ measurements also on the Van Gogh's famous *Sunflowers* painting, in the Van Gogh Museum of Amsterdam [76].

These results unequivocally demonstrated that Van Gogh employed different types of lead chromate–sulfate solid solutions, either in undiluted form or in

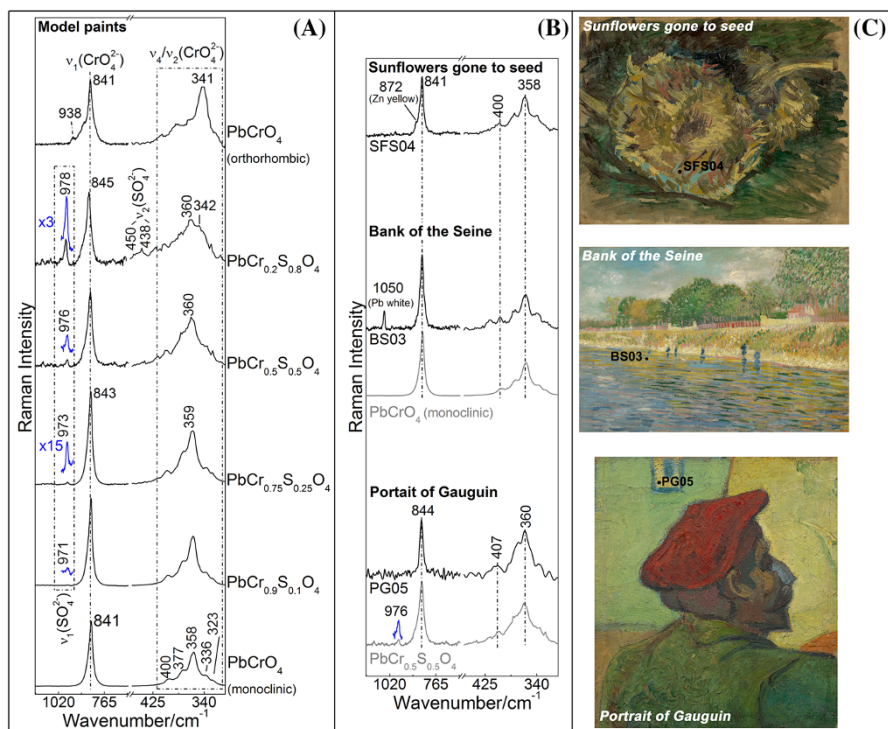


Fig. 5 Raman spectra collected using the MOLAB portable device (excitation line $\lambda = 785.0$ nm) from: **a** oil paint model samples made up of different chrome yellow pigments with different compositions and structures and **b** from yellow areas of the paintings *Sunflowers gone to seed*, *Bank of the Seine* and *Portrait of Gauguin* by Vincent van Gogh (all at the Van Gogh Museum in Amsterdam). **c** Photo of the paintings (from top to bottom) with indication of the corresponding in situ Raman spectroscopy measurement points (rearrangement from Ref. [61])

mixtures with other pigments (such as lead white, as shown above, red lead and vermilion). He also used other chromate-based compounds such as chrome orange $[(1-x)\text{PbCrO}_4 \cdot x\text{PbO}]$ and zinc yellow $(\text{K}_2\text{O} \cdot 4\text{ZnCrO}_4 \cdot 3\text{H}_2\text{O})$. All such information are essential to curators to implement adequate measures of preventive conservation [99].

3.1.3 Identification of Synthetic Organic Pigments

The synthetic manufacture of organic dyes was greatly developed following the discovery of Perkin's mauve in 1856, distinguishing routes to produce brightly colored lake pigments which were widespread from the late nineteenth century. These lakes were later supplemented by the introduction of the first water-insoluble organic pigments, namely the β -naphthol pigments, and then many others [100]. It is due to their wide use in contemporary paintings that the identification of synthetic dyes attracted considerable interest in recent years, leading to a source of literature exploiting the use of various chromatographic and spectro analytical techniques,

namely high-performance liquid chromatography (HPLC), infrared and Raman spectroscopy techniques [79, 101–104].

Mobile Raman spectroscopy can give a decisive contribution to the identification of synthetic organic pigments when used in integrated applications with other mobile techniques as XRF and FTIR. For example, identification of red azo β -naphthols occurred in an extensive campaign by MOLAB on paintings by Alberto Burri dating from 1948 to 1975, belonging to the Collezione Albizzini (Città di Castello, Italy). Within the campaign, the use of synthetic red organic pigments by Burri was identified in two paintings, *Rosso* (1950) and *Rosso Gobbo* (1954), exploiting data from in situ XRF, FTIR and Raman spectroscopy (using a portable micro-setup equipped with a 532 nm laser excitation).

In the painting *Rosso* (1950), the generic presence of a red organic pigment was revealed by UV–Vis fluorescence, which showed a maximum emission around 630 nm. Being, however, insufficient to identify the nature of the pigment, the study was deepened by exploiting a combination of non-invasive XRF and mid-FTIR techniques. By XRF examination, these areas showed a weak but clear amount of chlorine, whose presence was strictly related to the observed red regions (Fig. 6a, gray line). The same areas, examined by mid-FTIR in reflection mode, revealed specific distorted bands, consisting of derivative-like bands that corresponded to those observed on both reflection and transmission spectra on the standard of pigment red 4 (PR4; Fig. 6b).

This pigment is one of the four commercially available red azo β -naphthols, PR1, PR3, PR4, and PR6, which are characterized by a common structure where the azo function ($-N=N-$) is bound to a naphthol group and to a 2,4-substituted aromatic ring which features different substitutions for each pigment [100]. In particular, only PR4 (chlorinated para red) and PR6 (parachlor red) show chlorine as an aromatic ring substituent, although in different positions. This finding allowed the presence of PR1 and PR3 to be excluded in the examined painting, circumscribing the possibilities to PR4 or PR6. In spite of the fact that the FTIR spectrum recorded on *Rosso* showed features very similar to those of the PR4 standard and in agreement with literature data [103], the lack of a reference infrared spectrum of the positional isomer PR6 did not allow a discrimination of the two pigments with absolute certainty.

In another painting of Burri, *Rosso Gobbo* (1954), mid-FTIR spectroscopy suggested the possible presence of the same red organic pigment. However, more diverse than in the previous case, no secure PR4 distinctive features appeared in FTIR (see Fig. 6b, black line) nor in XRF spectra, where a peak at 2.65 keV corresponding to the chlorine $K\alpha$ emission (Fig. 6a, inset) was too weak to be assigned to chlorine with certainty. While XRF and FTIR did not permit an unambiguous identification, here, micro-Raman spectroscopy measurements on the same areas of the painting (Fig. 6c, black line) showed scattering features very similar to those of the two red azo β -naphthols PR4 and PR3 (Fig. 6c, gray and light gray lines). Further comparison of the recorded spectra with the standards indicated that the observed strong signal at about 1580 cm^{-1} is present in PR4 and absent in PR3. Furthermore, following Raman spectroscopy literature data [103, 104] it has been possible to distinguish between the red azo β -naphthol pigments PR4 and PR3

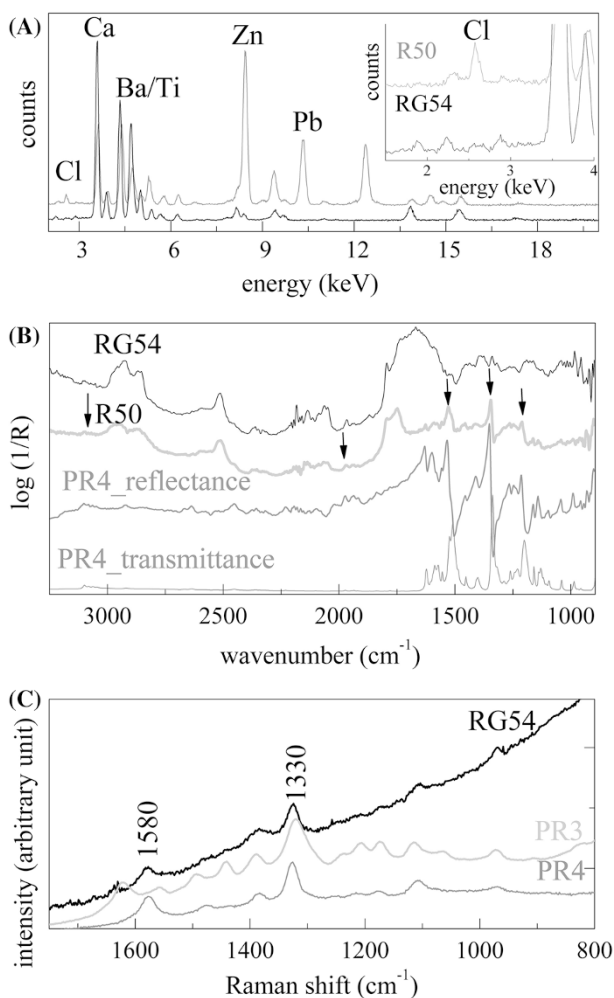


Fig. 6 XRF spectra recorded on red areas of the paintings *Rosso* (R50 gray line) and *Rosso Gobbo* (RG54 black line) by A. Burri; *inset* enlarged view of the energy range 1.5–4 keV; **b** reflection mid-FTIR spectra collected on the red areas of the paintings *Rosso* (R50 gray line) and *Rosso Gobbo* (RG54 black line) compared with the reflection and transmission mid-FTIR spectra of PR4 standard; **c** micro-Raman spectrum collected on a red area of the painting *Rosso Gobbo* (RG54 black line) compared with the spectra of PR3 (light gray line) and PR4 (gray line) standards (from Ref. [78])

based upon the relative intensities of the intense bands at about 1330 and 1200 cm^{-1} . These findings lead to the exclusion of *toluidine red* (PR3) and also *para red extra light* (PR1), which are characterized by different ring substitutes and different Raman spectroscopy scatterings, confirming the use by Burri of the *chlorinated para red* (PR4) or the positional isomer *parachlor red* (PR6).

It should be mentioned that the identification of highly fluorescent natural and synthetic organic dye components, often encountered in ancient, modern, and contemporary paintings respectively, provide a challenging analytical task for

conventional Raman spectroscopy in a non-invasive set-up as well as bench-top applications. For this reason, in recent years, the potential of surface-enhanced Raman spectroscopy (SERS) methodologies for the ultrasensitive detection of organic dyes, colorants and pigments used by artists has been widely exploited and appreciated. The introduction of this analytical tool in the field of heritage research has significantly improved the chances of successfully identifying dyes on minute samples. Furthermore, research efforts have been undertaken towards the development of an analytical methodology to apply SERS directly to the painting surface. Minimally invasive SERS substrates have been proposed based on silver-doped methylcellulose removable gels specifically devised for use when investigating organic dyes and pigments in paint layers, providing an enhancement of Raman spectroscopy signals of about 10^3 – 10^4 [102, 105, 106].

3.2 Non-invasive Identification of Binding Media and Other Polymers

Chromatographic techniques (such as gas chromatography mass spectrometry [GC–MS], pyrolysis gas chromatography mass spectrometry [Py–GC/MS], and HPLC) have been proven to be the most suitable and consolidated analytical methods for the full chemical characterization of natural and synthetic polymers (binders) in paint micro-samples. Often these analyses are profitably preceded by FTIR measurements on the same micro-samples, as a rapid method for a preliminary characterization of the polymers, with possible indications on the presence of pigments and fillers. In fact, binding media, basically proteins, glycosides, and lipids, in ancient art and a wide range of synthetic polymers in contemporary art show fairly distinctive vibrational features in the infrared range [107–110].

Non-invasive reflection FTIR spectroscopy has, therefore, significant diagnostic potentialities and, even in the presence of distortion effects due to the mixing of specular and diffuse reflection or overlaps by pigment absorption bands, it has been demonstrated to be a suitable technique for in situ discrimination of different families of binders, such as lipids, proteins, and alkyd, vinyl, or acrylic resins, without any sampling [12, 111].

3.2.1 Preliminary Laboratory Tests

To facilitate diagnostics, detailed studies have been carried out on the most relevant features of near and mid-FTIR reflection spectra of binders in ancient and modern art [22, 24, 37, 111, 112]. The investigation was performed recording reflection spectra on paint reconstructions made of organic media (acrylic emulsion, polyvinyl acetate resin, alkyd resin, drying oil, and proteinaceous tempera) mixed with several pigments. This was done to better interpret any possible overlap of relevant vibrational absorption bands of pigments and binders in the region of interest of the spectra.

Spectral features relevant for diagnostics have been observed in three different regions of the infrared spectrum.

First, the so-called fingerprint region (between 2000 and 400 cm^{-1}) mainly containing the fundamental modes of binders, as the carbonyl stretching mode (1740–1730 cm^{-1}), the amide I, II and III bands (1680–1200 cm^{-1}), the CH bending modes (1380–1480 cm^{-1}), the symmetric stretching C–O–C mode (1300–1200 cm^{-1}), and the C–O and C–C stretching modes and C=C deformations (1200–700 cm^{-1}).

Second, the range between 3500 and 2800 cm^{-1} that includes the CH and NH stretching modes of the organic binders. In particular, this range can be relevant for the detection of proteinaceous media thanks to the amide A (at ca. 3300 cm^{-1}) and amide B (at ca. 3070 cm^{-1}) bands [113] which, although not always visible, are quite characteristic of polypeptide structures.

Third, the portion of the spectrum between 6000 and 3900 cm^{-1} corresponding to the near infrared, mainly including combination and overtone bands of organic compounds (CH, C=O, NH, C–O functional groups).

It has been noted that in the fingerprint region, vinyl and acrylic spectra show derivative-shaped profiles, while proteins and oils, and to a lesser extent alkyds, feature more broad bands (still distorted with respect to the transmission mode spectra). Thus, it can be inferred that for vinyl and acrylic films, the surface reflection is dominant while for the others there is a substantial contribution of volume reflection, the difference being most probably related to the different absorption coefficient of the polymers influencing the degree of light penetration. Diversely, the other two regions at higher wavenumbers are characterized by a prevalence of diffuse reflection. Generally, the presence of a pigment has the effect of increasing the contribution from volume reflection with a moderate broadening of the derivative shape that is stronger for the bands positioned at higher wavenumbers. Due to the possible coexistence of specular reflection and diffuse reflection, it is not advisable to transform the reflectance spectra via the Kramers–Kronig algorithm.

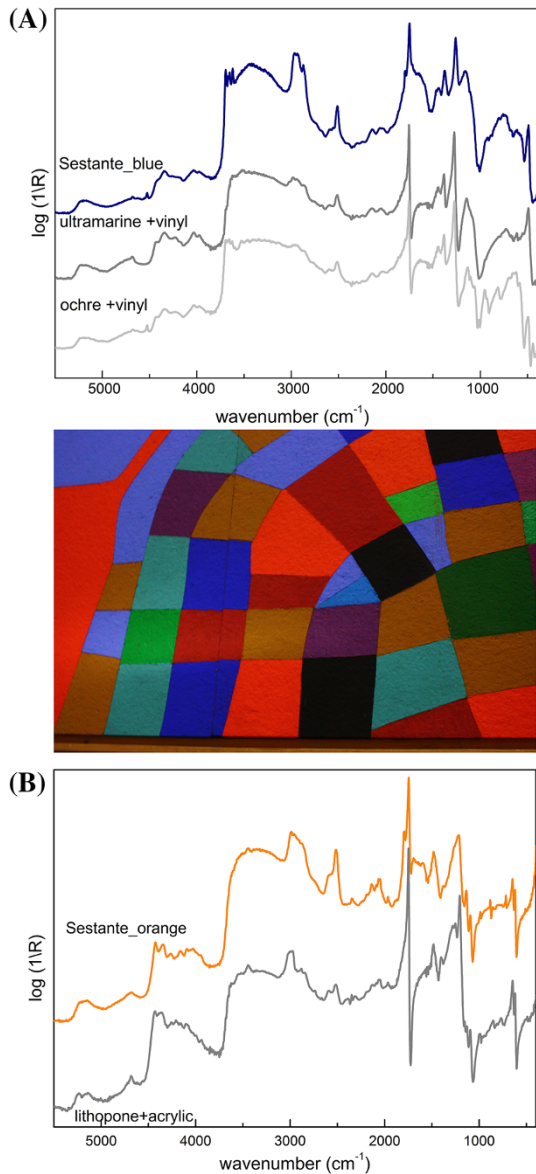
When all these features are taken into account, in spite of the spectral distortions arising from the sum of the specular and diffuse reflection related to the pigment-binder mixture and the overlaps with pigment bands, it is possible to individuate diagnostic bands for each polymeric compound that can be exploited for its non-invasive identification directly on ancient and modern paintings.

3.2.2 Examples of In Situ Studies

An initial example of the MOLAB analytical campaign is Memling's triptych, as presented in Fig. 1. In this case, the near-FTIR investigations registered C–H combination bands at 4260 cm^{-1} ($\nu_s\text{CH} + \delta\text{CH}$) and 4340 cm^{-1} ($\nu_a\text{CH} + \delta\text{CH}$), attributable to lipids [37], on all of the points measured on the three panels. The presence of lipids pointed towards the use of a drying oil and/or egg yolk as a binding medium. Weak protein signals (4595 cm^{-1} , first overtone νCO amide I + amide II; 4880 cm^{-1} , $(\nu + \delta)\text{NH}$) [37] were exclusively registered in some small, damaged paint areas, where the inner ground layer emerged, probably bound by glue [80].

A further example is within the study of the painting *Sestante 10* by Alberto Burri, a modern painting which is part of a series created by the artist in 1982, characterized by geometrical figures of different colour, shape, and surface roughness (Fig. 7). Here, the use of different binders in different figures was found. As shown in Fig. 7a, the spectrum recorded from a blue area showed features clearly attributable to a vinyl binder, with the contribution of both diffuse and

Fig. 7 Detail of the painting *Sestante 10* by A. Burri. **a** reflection FTIR spectrum recorded in the indicated *blue area*. **b** reflection FTIR spectrum recorded on the indicated *red area* (see text)



specular reflected light, leading to a mixed derivative/positive shape. In addition, the comparison with reference models of ultramarine blue and ochre in a vinyl medium, together with other standard reference spectra for fillers (see Fig. 7a), allowed the presence of compounds, such as gypsum, calcium carbonate and kaolin to be detected. Diversely, the spectrum of Fig. 7b, recorded in a red area, perfectly fitted the reference spectrum from a standard of acrylic binder and lithopone, also reported in the figure. The similarity of the spectral profiles included the presence of the carbonyl band at about 1740 cm^{-1} , the weaker CH bending at about 1460 cm^{-1} and the acrylic marker band $\nu(\text{CC})$ with inflection point around 1175 cm^{-1} .

The exploitation of a large database of reference spectra for the interpretation of the relevant infrared reflection features recorded on paintings of several contemporary artists led very recently to the in situ characterisation of binding media in masterpieces by Hartung, Capogrossi, Turcato, Afro and other twentieth-century Italian artists [111].

4 New Perspectives: In Situ Chemical Imaging

The recent development of advanced methods for element-selective or species-selective imaging of painted surfaces has opened new perspectives for the non-invasive in situ study of paintings. In fact, through these methods, the distribution of elements or molecular moieties all over the entire painting can be drawn, giving relevant information on composition and distribution of materials at the surface and sub-surface of the paint. The information obtained profitably integrates the data by point analyses, significantly improving the understanding of the artist's creative process (in some cases, including the identification of underpaintings).

Imaging methods for the study of elemental and molecular distributions on the microscale are currently available in scanning electron microscopes or IR and Raman micro-spectrometers or at specific micro-analysis synchrotron beam lines. The extension of these imaging techniques to the macroscopic scale (large surface of several square centimetres) for in situ non-invasive studies is not straightforward and different approaches have been put recently into practice, each one with appropriate advantages and limitations. Some of these methods are full-field imaging methods, employing cameras or image plates sensitive to the range of the electromagnetic spectrum of interest, while others are based on a scanning-mode approach, using well-collimated beams over the painting.

4.1 X-ray Fluorescence Imaging

A scanner for macroscopic X-ray fluorescence imaging has been recently implemented by Alfeld et al. [114] at Antwerp University to determine the distribution of pigments on paintings over large areas. Although scanning conditions can be varied, the scanner consists of an XZ motor stage in a typical setup, covering a surface of $60 \times 25\text{ cm}^2$, on which a 10-W Rh anode transmission tube is mounted, together with a set of energy dispersive XRF detectors. In the scanning process, a typical 0.8-mm lead pinhole collimator is employed as a beam-defining optic,

yielding a beam size of ca. 1.2 mm at the surface of the paint. The scanning is carried out with a variable step size of 0.5–1 mm, with a variable dwell time.

Another macro-XRF scanner has become commercially available in recent years from Bruker Nano GmbH (Berlin, Germany) under the name M6-Jetstream. This system consists of an X-ray tube mounted with a silicon-drift-detector on an XZ motor stage. Through scanning, the distribution image of the main elements that compose the surface and sub-surface paint layers in an area of $80 \times 60 \text{ cm}^2$ is obtained. The primary beam size can be varied between $50 \mu\text{m}$ and 1 mm, although high-resolution scans are only possible in areas of limited size [115].

Alfeld et al. [115] have employed the Antwerp prototype and tested the Bruker M6-Jetstream to carry out measurements on artworks of several painters. In particular, with the Antwerp macro-XRF scanner, several paintings by van Gogh, Goya, Memling, Rembrandt, amongst others [116, 117], have been investigated.

Due to the penetrative character of X-rays, the results obtained have been profitably exploited, not simply to draw the distribution of elements (and related pigments) over the surface, but also to reveal distinct features of underpaintings. In fact, when pigments used in underpaintings have a fairly different atomic composition with respect to those at the surface, the plot of the distribution of specific elements leads to underpaint images that emerge with a better clarity than achievable by traditional radiographies or IR reflectographies. In studies of works by Van Gogh [118], Goya [119] and Rembrandt [120, 121], paintings that were erroneously believed to be lost were found below the visible surface.

4.2 Hyperspectral infrared imaging

Delaney et al. have recently described the use of high-sensitivity, portable hyperspectral cameras suitable for the examination of paintings, drawings, and manuscripts' illuminations. These cameras can operate in various wavelength ranges, in the visible and near-IR (up to 2500 nm), and are characterized by high spectral (2.4–4 nm) and spatial resolutions (0.2–0.1 mm/pixel) [122–126].

These visible and near-infrared imaging spectroscopy systems have been exploited to identify and display the distribution of various pigments, utilizing electronic transitions, vibrational combination/overtone modes, and near-infrared luminescence. By this method, through in situ measurements, the pigments used by Picasso in the *Harlequin Musician* (1924), [122] part of the collection of the National Gallery of Art, Washington D.C., were identified and mapped. The results took significant advantage by the extension of imaging reflection spectroscopy up to 2500 nm and by the inclusion of luminescence imaging spectroscopy data. In addition, the combination with site-specific in situ analysis, such as XRF, strongly supported the achievement of a robust pigment identification and their mapping.

Very recently, the coupling of macro-XRF scanning and hyperspectral NIR imaging have been also attempted, showing the high potentiality of integrating the two imaging approaches to identify and map artist materials in an early Italian Renaissance panel painting [127].

In addition to the study of pigments, hyperspectral imaging in the near IR range has been also experimented to test the performance of the method for the study of

binders. The possible identification of these organic materials and their distribution throughout the painted surface has been demonstrated, exploiting the combinations and higher harmonics of the fundamental bands typical of the fingerprint mid-IR region which fall within the near-IR range. These chemical signatures include bands associated with CH, OH, NH and carbonyl groups. The method has been shown to be suitable for the mapping of egg yolk as binder in an early fifteenth-century illuminated manuscript attributed to Lorenzo Monaco [124] and the selective use of animal glue and egg yolk in a Cosme' Tura painting, dated 1475 (Fig. 8) [125, 127].

A recent work opened promising perspectives also towards the exploitation of hyperspectral imaging in the mid-IR range. A novel hyperspectral imager (model HI90, Bruker Optics, Portland, OR, USA), originally developed for the remote identification and localization of pollutants in the atmosphere, [128] was adapted for hyperspectral imaging of paintings, and used for identification and mapping of binding media on the painting *Sestante 10* (1982) by Alberto Burri already mentioned in Sect. 3.2 (see Fig. 7) [129]. The system, based on a focal plane array mercury–cadmium–telluride (MCT) detector with 256×256 pixels, operates in the range $900\text{--}1300\text{ cm}^{-1}$, permitting the recording of mid-IR spectra to be carried out at each pixel, with 4-cm^{-1} resolution. The system couples the focal plane array

Fig. 8 Visible image and chemical map for Gabriel panel of Cosme' Tura's *The Annunciation with Saint Francis and Saint Louis of Toulouse* (Samuel H. Kress Collection, 1952.2.6, National Gallery of Art, Washington D.C.). *Left* Colour image. *Right* False-colour image showing the locations of binding media. Egg yolk binder (*red*) maps mainly to Gabriel's red robe. Glue binder (*blue*) maps to areas of the face and feet. Azurite in a glue binder (*green*) and malachite in an egg yolk binder (*yellow*) map to the sky and *dark green* tunic and wings, respectively. Reproduced from [125] with permission from The Royal Society of Chemistry



detector with an interferometer and, exploiting the multiplex advantage, allows for recording a complete hyperspectral data cube in one single measurement of a few tens of seconds.

With a setup based on 128×128 pixels, three areas (ca. $9 \times 9 \text{ cm}^2$) of the large painting ($250 \times 360 \text{ cm}^2$) were analyzed on site at the Ex-Seccatoi del Tabacco (Citta' di Castello, Italy), where the painting is in permanent exhibition, through measurements that required 80 s per each cube.

Within the same areas explored by the HI90, point-analysis measurements have been also carried out with a portable FTIR spectrometer (Alpha-R, Bruker Optics, Portland, OR, USA) with the aim to validate the assignment made on the basis of the spectral data recorded at each pixel. These measurements revealed the excellent quality of the spectra collected by the hyperspectral imaging system, since the HI90 brightness temperature profiles recorded at each pixel were comparable to the corresponding Alpha-R reflection spectra (Fig. 9a, b).

The selective use by Burri of different binders to paint different areas of the *Sestante 10* cellotex panel was clearly put in evidence. In Fig. 9a, the visible image of a $9 \times 9 \text{ cm}^2$ detail of *Sestante 10* is shown. The brightness temperature (BT) difference image, reported in Fig. 9b, shows the distribution of an acrylic binder in the red–orange sector, while the BT difference image shown in Fig. 9c, indicates the use of a vinyl binder common to the red, ochre, blue, cyan, and purple coloured areas.

Exploring the potentiality of spectroscopically imaging the mid-IR range, Legrand et al. [130] tested advantages and limitations of a prototype macroscopic mid-FTIR scanner. The scanning system consisted of a Bruker Alpha FTIR

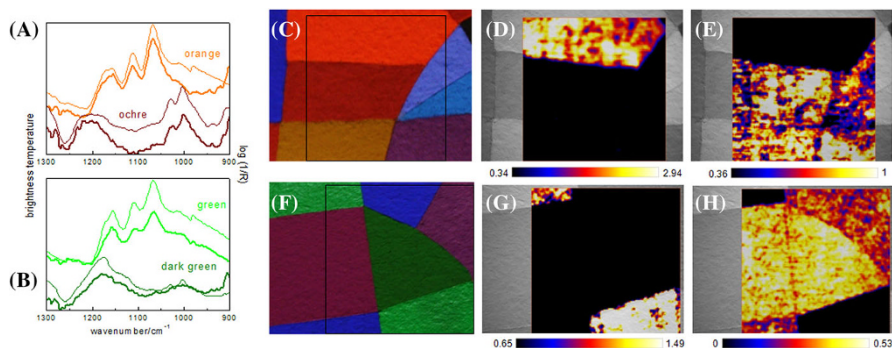


Fig. 9 a, b Comparison of the spectral profiles recorded with the HI90 (*thick lines*) and the ALPHA-R spectrometer (*thin lines*) for the *orange*, *ochre*, *green* and *dark green* sectors of the painting *Sestante 10* by A. Burri (the *rectangles* highlight the spectral range considered for the chemical mapping). c, f Images of two details of the painting. The *black rectangle* highlights the areas investigated with the HI90 system (ca. $9 \times 9 \text{ cm}^2$). d, g False-colour representations of the difference in the mean brightness temperature between 1154 and 1167 cm^{-1} and the mean brightness temperature between 1197 and 1209 cm^{-1} representing the acrylic medium distribution. e, h False-colour representation of the difference in the mean brightness temperature (measured in Kelvin) between 1250 and 1255 cm^{-1} and the mean brightness temperature between 1220 and 1230 cm^{-1} , representing the vinyl binder distribution (rearrangement from [129])

spectrometer that was moved all along the XZ plane in front of the painting, while FTIR spectra were recorded in reflection mode. Since this device scans the object point-by-point, the recording of full spectra over an extended mid-IR-range (7500–400 cm^{-1}) at each position is possible, identifying the compounds present and visualizing their distribution based on their fingerprint features. In one of the performance tests of the system, spectra were recorded on a detail ($8 \times 8 \text{ cm}^2$) of an unvarnished folk-art panel painting of Antillean origin (probably twentieth century). The obtained mid-FTIR chemical distributions were compared and integrated with the elemental distributions recorded from macroscopic XRF imaging measurements on the same area, finding good correlations. The crossing of the data by the two approaches allowed a wide and satisfying visualization of pigment distributions in red, orange, yellow, green, and blue areas [130].

A comparison between the performances of the two full-field and macro-scanning approaches in mid-FTIR reveal complementary limits and potentials.

A substantial advantage of the macro-FTIR scanning configuration is that full spectra are recorded at each position all over the surface of the painting in the whole range from 7500 to 400 cm^{-1} , obtaining a large quantity of exploitable data. However, a major important limitation of the prototype macro-FTIR scanner is the time required to record a hyperspectral dataset that can amount to numerous days for large surfaces. Nevertheless, many possibilities are available to improve this aspect, including the use of a more powerful source of mid-IR radiation and of larger beam focusing and/or collection optics for the reflected radiation. A great advantage of the full-field configuration of the Bruker HI90 is the fact that the time necessary to record all the spectra in the examined $9 \times 9 \text{ cm}^2$ areas (16,384 spectra) amounts only to 80 s. A major limitation of the HI90 instrument is in the short wavenumber range that can be explored in the present configuration. This limit is expected to be overcome in the future with extension to larger wavenumber ranges.

An additional significant limitation of mid-IR imaging, in both full-field and macro-scanning approaches, lays in the fact that it can be significantly applied only to unvarnished paintings or to paintings where the varnish has been removed. Fortunately, for many paintings under restoration, the varnish is at least partially removed in the preliminary phases of the intervention.

All the innovative data acquired in the most recent years on macroscopic chemical imaging by XRF and near- and mid-IR spectroscopy open new significant perspectives for the in situ non-invasive study of paintings. In particular, in situ macro-XRF imaging is expected to become a widely diffused technique in the near future, due to both the availability of commercial instrumentation and the straightforward and reliable interpretation of elemental spectra. On the other side, both near and mid-IR imaging represent powerful techniques that can deliver complementary information on the distribution of inorganic and organic materials which cannot be detected or identified in a unique manner by means of XRF elemental data. In particular, they can give information on natural and synthetic binders otherwise impossible to be non-invasively mapped.

Further related research is currently in development for the setup of new methods for the in situ identification and mapping of chemical components on large areas of paintings. Of great interest are those regarding macro-XRD imaging, where

laboratory experiments based on application of synchrotron radiation sources lead to encouraging successful results [131, 132]. Using synchrotron light, high-energy (80–120 keV) XRD imaging has been recently experimented for the non-invasive measurement (in transmission mode) of crystalline phase distributions in paintings. Potentials and limitations of the experimented technique have been demonstrated using an authentic sixteenth-century painting as well as model paintings [132]. Very recently, promising preliminary experimentations have been carried out for the transfer of the technique from the synchrotron to a compact prototypical system suitable for in situ applications [117].

5 Conclusions

The results on the most recent in situ application of non-invasive methodologies outlined in this paper clearly show how the integration of data from different analytical techniques can successfully overcome the intrinsic limitation of each single spectroscopic method when applied on heterogeneous samples. At the same time, an accurate and systematic preliminary work on test samples allows for overcoming complications imposed by specific optical and matrix effects, making a satisfactory interpretation of reflection spectra possible.

The presented *modus operandi*, optimized after years of technological advances and experience, is based on exploring the atomic and the molecular levels, probing either electronic or vibrational properties (inducing absorption, emission and/or scattering phenomena), and employing techniques that are sensitive to highly or poorly ordered systems. The method allows today's researchers to successfully identify pigments in paintings with adequate certainty and completeness, fully avoiding sampling. In addition, through the exploitation of reflection near- and mid-FTIR spectroscopy, the family of natural binders widely used in ancient art (lipidic, proteic, glucosidic) can be disclosed, as well as of synthetic resins, as vinyl, acrylic, and alkyd, largely employed in contemporary art. Recently, thanks to accurate and detailed preliminary laboratory tests on a wide set of pigment specimens it has also become possible in some cases to distinguish composition and structures among a variety of inorganic pigments belonging to an extended series of compounds sharing the same chemical class, such as the series of chromate–sulfate coprecipitates, cadmium sulfides and lead antimonates. In this case, appropriate information is obtained by Raman spectroscopy through measurements that do not require long accumulation times nor specific arrangements, apart from control of the power of the radiation used. The unique advantage of Raman spectroscopy is the possibility to identify partial or totally amorphous phases frequently encountered in cases of pigments synthesized in ancient times.

More challenging is the identification of organic pigments. In this case, however, the synergic use of techniques such as FTIR, UV–Vis and Raman spectroscopy can lead to satisfactory results. In particular, while UV–Vis absorption and fluorescence can indicate a colorant's family, Raman spectroscopy can directly lead, in case of good scattering cross sections, to its unambiguous molecular identification. Interesting perspectives are opened by the rapid affirmation of SERS techniques,

although this approach for non-invasive in situ applications still remains at the experimental level.

Significant advances in the non-invasive in situ study of painting materials is represented by the chemical imaging techniques. A prototype macro-XRF scanner has been set up and exploited to identify and map the distribution of elements (and related pigments) over the surface of numerous paintings, as well as to reveal distinct features of underpaintings, with a clearness obtained better than that obtained by other traditional imaging techniques. By this method, paintings originally believed to be lost were brought to new light.

The most significant perspectives of further advancements rely on the infrared hyperspectral imaging. In the near-IR, the most recent hardware and software achievements allowed successful results to be obtained. A few cases of integrating macro-XRF and hyperspectral near-IR imaging have been also successfully experimented.

However, much work remains to be done for the development of methods in the mid-IR where the systems experimented to date have shown interesting solutions, but with problems still existing for data acquisition times, for the systems based on surface scanning, for extension of the explorable wavelength range, and for the full-field systems. In both cases, good perspectives for improvement are open, which rely on the use of a more powerful source of mid-IR radiation and better focusing and collection optics for the reflected radiation in case of the scanning method and on the introduction of new detectors for the full-field approach.

Acknowledgments The MOLAB activities described in this work were possible thanks to the support of the European Commission, through the Research Infrastructure projects Eu-ARTECH (FP6-RH3-CT-2004-506171) and CHARISMA (FP7-GA n. 228330) and of the Laboratorio di Diagnostica di Spoleto. The authors are grateful to several researchers that contributed to MOLAB activities: C. Anselmi, D. Buti, L. Cartechini, A. Chieli, A. Daveri, F. Gabrieli, C. Grazia, P. Moretti, F. Presciutti, M. Vagnini. Kind permission from J. Wiley and Sons to reproduce Fig. 5 (from Ref. [61]) and rearrange Fig. 9 (from Ref. [129]) is acknowledged. Figures 2, 3 and 4 are reproduced from Ref. [80] and Fig. 8 from Ref. [125] with permission of the Royal Society of Chemistry.

References

1. Brunetti BG, Clark AJ, Sgamellotti A (eds) (2010) Advanced techniques in art conservation. *Acc Chem Res* 43(6):693-4
2. Sgamellotti A, Brunetti BG, Miliani C (eds) (2014) Science and art. The painted surface. The Royal Society of Chemistry, Cambridge
3. Clark RJH (1995) Raman microscopy: application to the identification of pigments on medieval manuscripts. *Chem Soc Rev* 24:187-196
4. Burgio L, Ciomartan DA, Clark RJH (1997) Pigment identification on medieval manuscripts, paintings and other artefacts by Raman microscopy: applications to the study of three German manuscripts. *J Mol Struct* 405:1-11
5. MacArthur JD, Del Carmine P, Lucarelli F, Mandò PA (1990) Identification of pigments in some colours on miniatures from the medieval age and early Renaissance. *Nucl Instr Meth B* 45:315-321
6. Wagner W, Neelmeijer C (1995) External proton beam analysis of layered objects. *Fresenius J Anal Chem* 353:297-302
7. Brissaud I, Guilló A, Lagarde G, Midya P, Calligaro T, Salomon J (1999) Determination of the sequence and thicknesses of multilayers in an easel painting. *Nucl Instr Meth B* 155:447-452

8. Janssens K, Vittiglio G, Deraedt I, Aerts A, Vekemans B et al (2000) Use of microscopic XRF for non-destructive analysis in art and archaeometry. *X-Ray Spectrom* 29:73–91
9. Eu-ARTECH, Access, research and technology for the conservation of the European Cultural Heritage, 6th FP RII3-CT-2004-506171 (2004–2009). www.euartech.org
10. CHARISMA, Cultural heritage advanced research infrastructures: synergy for a multidisciplinary approach to conservation, 7th FP GA n. 228330 (2009–2014). www.charismaproject.eu
11. IPERION CH, Integrated platform for the European Research Infrastructure on Cultural Heritage, H2020 RIA n. 654028 (2014–2015). www.iperionch.eu
12. Miliani C, Rosi F, Brunetti BG, Sgamellotti A (2010) In situ non-invasive study of artworks: The MOLAB multi-technique approach. *Acc Chem Res* 43:728–738
13. Cesareo R, Frazzoli FV, Mancini C, Sciuti S, Marabelli M, Mora P, Rotondi P, Urbani G (1972) Non-destructive analysis of chemical elements in paintings and enamels. *Archaeometry* 14:65–78
14. Hall ET, Schweizer F, Toller PA (1973) X-ray fluorescence analysis of museum objects: a new instrument. *Archaeometry* 15:53–78
15. Moiola P, Seccaroni C (2000) Analysis of art objects using a portable X-ray fluorescence spectrometer. *X-Ray Spectrom* 29:48–52
16. Brunetti BG, Seccaroni C, Sgamellotti A (eds) (2004) *The painting technique of Pietro Vannucci, called il Perugino*. Nardini, Firenze
17. Roy A, Spring M (eds) (2007) *Raphael's painting technique: working practice before Rome*. Nardini, Firenze
18. Menu M, Ravaud E (eds) (2009) *Andrea Mantegna painting technique*. Special issue of *Techne*. C2RMF, Paris
19. de Viguerie L, Solé VA, Walter Ph (2009) Multilayers quantitative X-ray fluorescence analysis applied to easel paintings. *Anal Bioanal Chem* 395:2015–2020
20. Bonizzoni L, Galli A, Poldi G, Milazzo M (2007) In situ non-invasive EDXRF analysis to reconstruct stratigraphy and thickness of Renaissance pictorial multilayers. *X-Ray Spectrom* 36:55–61
21. del Viguerie L, Walter Ph, Laval E, Mottin B, Solé VA (2010) Revealing the sfumato technique of Leonardo da Vinci by X-Ray fluorescence spectroscopy. *Angew Chem Int Ed* 49:6125–6128
22. Miliani C, Rosi F, Borgia I, Benedetti P, Brunetti BG, Sgamellotti A (2007) Fiber-optic Fourier Transform mid-infrared reflectance spectroscopy: A suitable technique for in situ studies of mural paintings. *Appl Spectrosc* 61:293–299
23. Miliani C, Rosi F, Burnstock A, Brunetti BG, Sgamellotti A (2007) Non-invasive in situ investigations versus micro-sampling: a comparative study on a Renoir's painting. *Appl Phys A* 89:849–856
24. Rosi F, Daveri A, Miliani C, Verri G, Benedetti P, Piqué F, Brunetti BG, Sgamellotti A (2009) Non-invasive identification of organic materials in wall paintings by fiber optic reflectance infrared spectroscopy: a statistical multivariate approach. *Anal Bioanal Chem* 395:2097–2106
25. Rosi F, Burnstock A, Van den Berg KJ, Miliani C, Brunetti BG, Sgamellotti A (2009) A non-invasive XRF study supported by multivariate statistical analysis and reflectance FTIR to assess the composition of modern painting materials. *Spectrochim. Acta A* 71:1655–1662
26. Kahrim K, Daveri A, Rocchi P, de Cesare G, Cartechini L, Miliani C, Brunetti BG, Sgamellotti A (2009) The application of in situ mid-FTIR fibre-optic reflectance spectroscopy and GC–MS analysis to monitor and evaluate painting cleaning. *Spectrochim Acta A* 74:1182–1188
27. Rosi F, Daveri A, Doherty B, Nazzareni S, Brunetti BG, Sgamellotti A, Miliani C (2010) On the use of overtone and combination bands for the analysis of the $\text{CaSO}_4\text{-H}_2\text{O}$ system by mid-infrared reflection spectroscopy. *Appl Spectrosc* 64:956–963
28. Miliani C, Rosi F, Daveri A, Brunetti BG (2012) Reflection infrared spectroscopy for the non-invasive in situ study of artists' pigments. *Appl Phys A* 106:295–307
29. Buti D, Rosi F, Brunetti BG, Miliani C (2013) In-situ identification of copper-based green pigments. *Anal Bioanal Chem* 405:2699–2711
30. Doherty B, Daveri A, Clementi C, Romani A, Bioletti S, Brunetti BG, Sgamellotti A, Miliani C (2013) The Book of Kells: A non-invasive MOLAB investigation by complementary spectroscopic techniques. *Spectrochim Acta A* 115:330–336
31. Daveri A, Doherty B, Moretti P, Grazia C, Romani A, Fiorin E, Brunetti BG, Vagnini M (2015) An uncovered XIII century icon: Particular use of organic pigments and gilding techniques highlighted by analytical methods. *Spectrochim Acta A* 135:398–404

32. Buti D, Domenici D, Miliani C, García Sáiz C, Gómez Espinoza T, Jiménez Villalba F, Verde Casanova A, Sabiá de la Mata A, Romani A, Presciutti F, Doherty B, Brunetti BG, Sgamellotti A (2014) Non-invasive investigation of a pre-Hispanic Maya screenfold book: The Madrid Codex. *J Archaeol Sci* 42:166–178
33. Fabbri M, Picollo M, Porcinai S, Bacci M (2001) Mid-infrared fiber-optics reflectance spectroscopy: A non-invasive technique for remote analysis of painted layers. Part I: Technical setup. *Appl Spectrosc* 55:420–427
34. Fabbri M, Picollo M, Porcinai S, Bacci M (2001) Mid-infrared fiber-optics reflectance spectroscopy: A non-invasive technique for remote analysis of painted layers. Part II: Statistical analysis of spectra. *Appl Spectrosc* 55:428–433
35. Griffiths P, De Haseth JA (2007) *Fourier transform infrared spectrometry*, 2nd edn. Wiley, New York
36. Miliani C, Daveri A, Brunetti BG, Sgamellotti A (2008) CO₂ entrapment in natural ultramarine blue. *Chem Phys Lett* 446:148–151
37. Vagnini M, Miliani C, Cartechini L, Rocchi P, Brunetti BG, Sgamellotti A (2009) FT-NIR spectroscopy for non-invasive identification of natural polymers and resins in easel paintings. *Anal Bioanal Chem* 395:2107–2118
38. Jurado Lopez A, Luque De Castro MD (2004) Use of near-infrared spectroscopy in a study of binding media in paintings. *Anal Bioanal Chem* 380:706–771
39. Wendlandt WW, Hecht HG (1966) *Reflectance spectroscopy*. Interscience Publishers, New York
40. Bacci M, Baldini F, Carlá R, Linari R, Picollo M, Radicati B (1993) Colour analysis of the Brancacci Chapel frescoes. *Appl Spectrosc* 47:399–402
41. Bacci M, Casini A, Cucci C, Picollo M, Radicati B, Vervat M (2003) Non-invasive spectroscopic measurements on the “Il ritratto della figliastra” by Giovanni Fattori: identification of pigments and colorimetric analysis. *J Cult Herit* 4:329–336
42. Bacci M, Picollo M, Trumpy G, Tsukada M, Kunzelman D (2007) Non-invasive identification of white pigments on 20th-century oil paintings by using fiber optic reflectance spectroscopy. *J Am Inst Conserv* 46:27–37
43. Bruni S, Caglio S, Guglielmi V, Poldi G (2008) The joined use of non-invasive spectroscopic analyses – FTIR, Raman, visible reflectance spectrometry and EDXRF – to study drawings and illuminated manuscripts. *Appl Phys A* 92:103–108
44. Ricciardi P, Delaney J, Facini M, Glinsman L (2013) Use of imaging spectroscopy and in situ analytical methods for the characterization of the materials and techniques of 15th century illuminated manuscripts. *J Am Inst Conserv* 52:13–29
45. Aceto M, Agostino A, Fenoglio G, Idone A, Gulmini M, Picollo M, Ricciardi P, Delaney JK (2014) Characterisation of colourants on illuminated manuscripts by portable fibre optic UV–visible-NIR reflectance spectrophotometry. *Anal Methods* 6:1488–1500
46. Romani A, Clementi C, Miliani C, Favaro G (2010) Fluorescence Spectroscopy: A Powerful Technique for the Noninvasive Characterization of Artwork. *Acc Chem Res* 43:837–846
47. Clementi C, Doherty B, Gentili P, Miliani C, Romani A, Brunetti BG, Sgamellotti A (2008) Vibrational and electronic properties of painting lakes. *Appl Phys A* 92:25–33
48. Clementi C, Miliani C, Romani A, Favaro G (2006) In situ fluorimetry: A powerful noninvasive diagnostic technique for natural dyes used in artefacts Part I. Spectral characterization of orcein in solution, on silk and wool laboratory-standards and a fragment of Renaissance tapestry. *Spectrochim Acta, Part A* 64:906–912
49. Miliani C, Romani A, Favaro G (1998) Spectrophotometric and fluorimetric study of some anthraquinoid and indigoid colorants used in artistic paintings. *Spectrochim Acta, Part A* 54:581–588
50. Buti D (2009) Ph.D. Thesis, University of Firenze
51. Clementi C, Rosi F, Romani A, Vivani R, Brunetti BG, Miliani C (2012) Photoluminescence properties of zinc oxide in paints: A study of the effect of self-absorption and passivation. *Appl Spectrosc* 66:1233–1241
52. Rosi F, Grazia C, Gabrieli F, Romani A, Paolantoni M, Vivani R, Brunetti BG, Colombari Ph, Miliani C (2016) UV–Vis-NIR and micro Raman spectroscopies for the non destructive identification of Cd_{1-x}Zn_xS solid solutions in cadmium yellow pigments. *Microchem J* 124:856–867
53. Grazia C, Rosi F, Gabrieli F, Romani A, Paolantoni M, Vivani R, Brunetti BG, Colombari Ph, Miliani C (2016) A multitechnique approach for investigating the composition of ternary CdS_{1-x}Se_x solid solutions employed as artists’ pigments. *Microchem J* 125:279–289


54. Accorsi G, Verri G, Bolognesi M, Armaroli N, Clementi C, Miliani C, Romani A (2009) The exceptional near-infrared luminescence properties of cuprorivaite (Egyptian blue). *Chem Commun* 3392–3394
55. Clementi C, Miliani C, Verri G, Sotiropoulou S, Romani A, Brunetti BG, Sgamellotti A (2009) Application of the Kubelka-Munk correction for self-absorption of fluorescence emission in carmine lake paint layers. *Appl Spectrosc* 63:1323–1330
56. Simonot L, Thoury M, Delaney JK (2011) Extension of the Kubelka-Munk theory for fluorescent turbid media to a non-opaque layer on a background. *J Opt Soc Am* 28:1349–1357
57. Romani A, Clementi C, Miliani C, Brunetti BG, Sgamellotti A, Favaro G (2008) Portable equipment for luminescence lifetime measurements on surfaces. *Appl Spectrosc* 62:1395–1399
58. Nevin A, Cesaratto A, Bellei S, D'Andrea C, Toniolo L, Valentini G, Comelli D (2014) Time-Resolved Photoluminescence Spectroscopy and Imaging: New Approaches to the Analysis of Cultural Heritage and Its Degradation. *Sensors* 14:6338–6355 **and references therein**
59. Romani A, Grazia C, Anselmi C, Miliani C, Brunetti BG (2011) New portable instrument for combined reflectance, time-resolved and steady-state luminescence measurements on works of art. In: Pezzati L, Salimbeni R (eds) *SPIE Proceedings* Vol. 8084: O3A: Optics for Arts, Architecture, and Archaeology III. doi:10.1117/12.889529
60. Colomban Ph (2012) The on-site/remote Raman analysis with mobile instruments: a review of drawbacks and success in cultural heritage studies and other associated fields. *J Raman Spectrosc* 43:1529–1535
61. Monico L, Janssens K, Hendriks E, Brunetti BG, Miliani C (2014) Raman study of different crystalline forms of PbCrO_4 and $\text{PbCr}_{1-x}\text{S}_x\text{O}_4$ solid solutions for the non-invasive identification of chrome yellows in paintings: a focus on works by Vincent van Gogh. *J Raman Spectrosc* 45:1034–1045
62. Nakai I, Abe Y (2012) Portable X-ray powder diffractometer for the analysis of art and archaeological materials. *Appl Phys A* 106:279–293
63. Gatto Rotondo G, Romano FP, Pappalardo G, Pappalardo L, Rizzo F (2010) Nondestructive characterization of fifty various species of pigments of archaeological and artistic interest by using the portable X-ray diffraction system of the LANDIS laboratory of Catania (Italy). *Microchem J* 96:252–258
64. Romano FP, Pappalardo L, Masini N, Pappalardo G, Rizzo F (2011) The compositional and mineralogical analysis of fired pigments in Nasca pottery from Cahuachi (Peru') by the combined use of the portable PIXE-alpha and portable XRD techniques. *Microchem J* 99:449–453
65. Chiari G (2008) Saving art in situ. *Nature* 453:159
66. Sarrazin P, Chiari G, Gailhanou M (2008) A portable non-invasive XRF/XRD instrument for the study of art objects. *Adv X-Ray Anal* 52:175–186
67. Gianoncelli A, Castaing J, Ortega L, Dooryhée E, Salomon J, Walter Ph, Hodeau JL, Bordet P (2008) *X-Ray Spectrom* 37:418–423
68. Duran A, Perez-Rodríguez JL, Espejo T, Franquelo ML, Castaing J, Walter Ph (2009) *Anal Bioanal Chem* 395:1997–2004
69. Pages-Camagna S, Laval E, Vigears D, Duran A (2010) Non-destructive and in situ analysis of Egyptian wall paintings by X-ray diffraction and X-ray fluorescence portable systems. *Appl Phys A* 100:671–675
70. Chiari G (2010) Analyzing stratigraphy with a dual XRD/XRF instrument. Denver X-ray conference abstracts. http://www.dxcicdd.com/10/DXC_list_abstract.asp
71. Uda M, Ishizaki A, Satoh R, Okada K, Nakajima Y, Yamashita D, Ohashi K, Sakuraba Y, Shimono A, Kojima D (2005) Portable X-ray diffractometer equipped with XRF for archaeometry. *Nucl Instr Meth B* 239:77–84
72. Mendoza Cuevas A, Perez Gravie H (2011) Portable energy dispersive X-ray fluorescence and X-ray diffraction and radiography system for archaeometry. *Nucl Instrum Methods A* 633:72–78
73. Mendoza Cuevas A, Bernardini F, Gianoncelli A, Tuniz C (2015) Energy dispersive X-ray diffraction and fluorescence portable system for cultural heritage applications. *X-Ray Spectrom* 44:105–115
74. Bracci S, Falletti F, Matteini M, Scopigno R (eds) (2004) *Exploring David. Diagnostic tests and state of conservation*. Giunti, Firenze
75. Monico L, Janssens K, Miliani C, Brunetti BG, Vagnini M et al (2013) Degradation process of lead chromate in paintings by Vincent van Gogh studied by means of spectromicroscopic methods. 3.

- Synthesis, characterization, and detection of different crystal forms of the chrome yellow pigment. *Anal Chem* 85:851–859
76. Monico L, Janssens K, Hendricks E, Vanmeert F, Van der Schnickt G, Cotte M, Falkenberg G, Brunetti BG, Miliani C (2015) Evidence for degradation of the chrome yellows in Van Gogh Sunflowers: a study by non-invasive methods and synchrotron radiation-based X-ray techniques. *Angew Chem Int Ed* 54:13923–13927
 77. Casadio F, Miliani C, Rosi F, Romani A, Anselmi C, Brunetti BG, Sgamellotti A, Andral JL, Gautier G (2013) Scientific investigations on an important corpus of Picasso paintings in Antibes: New insights into technique, conditions and chronological sequence. *J Am Inst Conserv* 52:184–204
 78. Rosi F, Miliani C, Clementi C, Kahrim K, Presciutti F, Vagnini M, Manuali V, Daveri A, Cartechini L, Brunetti BG, Sgamellotti A (2010) An integrated spectroscopic approach for the non-invasive study of modern art materials and techniques. *Appl Phys A* 100:613–624
 79. Van Bommel MR, Janssen H, Spronk R (eds) (2012) *Inside out Victory Boogie Woogie. A material history of Mondrian's masterpiece.* Amsterdam University Press, Amsterdam
 80. Van der Snickt G, Miliani C, Janssens K, Brunetti BG, Romani A, Rosi F, Walter Ph, Castaing J, De Nolf W, Klaassen L, Labarque I, Wittermann R (2011) Material analyses of “Christ with singing and music-making angels”, a late 15th C panel painting attributed to Hans Memling and assistants: Part I. non-invasive in situ investigations. *J Anal At Spectrom* 26:2216–2229
 81. Ricci C, Miliani C, Brunetti BG, Sgamellotti A (2006) Non-invasive identification of surface materials on marble artifacts with fiber optic mid-FTIR reflectance spectroscopy. *Talanta* 61:1221–1226
 82. Gettens RJ, Mrose ME (1954) Calcium Sulphate Minerals in the Grounds of Italian Paintings. *Stud Conserv* 1:174–189
 83. Szmelter I, Cartechini L, Romani A, Pezzati L (2014) Multi-criterial studies of the masterpiece The Last Judgement, attributed to H. Memling, at the National Museum of Gdansk. In: Sgamellotti A, Brunetti BG, Miliani C (eds) *Science and art. The painted surface.* The Royal Society of Chemistry, Cambridge
 84. Hradil D, Grygar T, Hradilova J, Bezdicka P, Grunwaldova V, Fogas I, Miliani C (2007) Micro-analytical identification of Pb-Sb-Sn yellow pigment in historical European paintings and its differentiation from lead tin and Naples yellows. *J Cult Herit* 8:377–383
 85. Rosi F, Manuali V, Miliani C, Brunetti BG, Sgamellotti A, Grygar T, Hradil D (2009) Raman scattering features of lead pyroantimonate compounds. Part I: XRD and Raman characterization of Pb₂Sb₂O₇ doped with tin and zinc. *J Raman Spectrosc* 40:107–111
 86. Rosi F, Manuali V, Grygar T, Bezdicka P, Brunetti BG, Sgamellotti A, Burgio L, Seccaroni C, Miliani C (2011) Raman scattering features of lead pyroantimonate compounds: implication for the non-invasive identification of yellow pigments on ancient ceramics. Part II. In situ characterisation of Renaissance plates by portable micro-Raman and XRF studies. *J Raman Spectrosc* 42:407–414
 87. Cartechini L, Rosi F, Miliani C, D'Acapito F, Brunetti BG, Sgamellotti A (2011) Modified Naples yellow in Renaissance majolica: study of Pb–Sb–Zn and Pb–Sb–Fe ternary pyroantimonates by X-ray absorption spectroscopy. *J Anal At Spectrom* 26:2500–2507
 88. Fiedler I, Bayard MA (1986) Cadmium yellow orange and red. In: Feller RL (ed) *Artist's Pigments, a handbook of their history and characteristics, vol 1.* Cambridge University Press, Cambridge, pp 65–108
 89. Huckle WG, Swigert GF, Wiberley SE (1966) Cadmium Pigments. Structure and Composition. *Ind Eng Chem Prod Res Dev* 5:362–366
 90. Kirby J, Stonor K, Roy A, Burnstock A, Grout R, White R (2003) *Seurat's Painting Practice: Theory, Development and Technology.* Natl Gallery Tech Bull 24:4–37
 91. Van der Snickt G, Janssens K, Schalm O, Aibéo C, Klouft H, Alfeld M (2010) James Ensor's pigment use: artistic and material evolution studied by means of portable X-ray fluorescence spectrometry. *X-Ray Spectrom* 39:103–111
 92. Hendriks E (2006) In: Hendriks E, Van Tilborgh L (eds) *New Views on Van Gogh's development in Antwerp and Paris: an integrated art historical and technical study of his paintings in the Van Gogh Museum.* University of Amsterdam, Amsterdam, pp 149–150
 93. Kühn H, Curran M (1986) Chrome yellow and other chromate pigments. In: Feller RL (ed) *Artists' pigments: a handbook of their history and characteristics, vol 1.* Cambridge University Press, Cambridge, pp 187–200
 94. Eastaugh N, Walsh V, Chaplin T, Siddall R (2004) *The pigment compendium (CD-ROM).* Elsevier, Amsterdam

95. Monico L, Van der Snickt G, Janssens K, De Nolf W, Miliani C, Verbeeck J, Tian H, Tan H, Dik J, Radepont M, Cotte M (2011) Degradation process of lead chromate in paintings by Vincent van Gogh studied by means of synchrotron X-ray spectromicroscopy and related methods. 1. Artificially aged model samples. *Anal Chem* 83:1214–1223 **and references therein**
96. Monico L, Van der Snickt G, Janssens K, De Nolf W, Miliani C, Dik J, Radepont M, Hendriks E, Geldof M, Cotte M (2011) Degradation process of lead chromate in paintings by Vincent van Gogh studied by means of synchrotron X-ray spectromicroscopy and related methods. 2. Original paint layer samples. *Anal Chem* 83:1224–1231 **and references therein**
97. Monico L, Janssens K, Miliani C, Van der Snickt G, Brunetti BG, Cestelli Guidi M, Radepont M, Cotte M (2013) Degradation Process of Lead Chromate in Paintings by Vincent van Gogh Studied by Means of Spectromicroscopic Methods. 4. Artificial aging of model samples of co-precipitates of lead chromate and lead sulfate. *Anal Chem* 85:860–867
98. Monico L, Janssens K, Vanmeert F, Cotte M, Brunetti BG, Van der Snickt G, Leeuwestein M, Salvant Plisson J, Menu M, Miliani C (2014) Degradation process of lead chromate in paintings by Vincent van Gogh studied by means of spectromicroscopic methods. Part 5. Effects of non-original surface coatings into the nature and distribution of chromium and sulfur species in chrome yellow paints. *Anal Chem* 86:10804–10811
99. Monico L, Janssens K, Cotte M, Romani A, Sorace L, Grazia C, Brunetti BG, Miliani C (2015) Synchrotron-based X-ray spectromicroscopy and electron paramagnetic resonance spectroscopy to investigate the redox properties of lead chromate pigments under the effect of the visible light. *J Anal At Spectrosc* 30:2024
100. Herbst W, Hunger K (2004) Industrial organic pigments production, properties, applications. Wiley, New York
101. Van Bommel MR, Vanden Berghe I, Wallert AM, Boitelle R, Wouters J (2007) High-performance liquid chromatography and non-destructive three-dimensional fluorescence analysis of early synthetic dyes. *J Chromatogr A* 1120:260–272
102. Doherty B, Vagnini M, Dufourmantelle K, Sgamellotti A, Brunetti BG, Miliani C (2014) A vibrational spectroscopic and principal component analysis of triarylmethane dyes by comparative laboratory and portable instrumentation. *Spectrochim Acta A* 12:292–305
103. Sherrer NC, Stephan Z, Francoise D, Annette F, Renate K (2009) Synthetic organic pigments of the 20th and 21st century relevant to artist's paints: Raman spectra reference collection. *Spectrochim Acta A* 73:505–524
104. Vandenebe P, Moens L, Edwards HGM, Dams R (2000) Raman spectroscopic database of azo pigments and application to modern art studies. *J Raman Spectrosc* 31:509–517
105. Doherty B, Brunetti BG, Sgamellotti A, Miliani C (2011) A detachable SERS active cellulose film: a minimally invasive approach to the study of painting lakes. *J Raman Spectrosc* 42:1932–1938
106. Doherty B, Presciutti F, Sgamellotti A, Brunetti BG, Miliani C (2014) Monitoring of optimized SERS active gel substrates for painting and paper substrates by unilateral NMR profilometry. *J Raman Spectrosc* 45:1153–1159
107. Learner TJ (2004) Analysis of modern paints. Research in conservation. Getty Conservation Institute, Los Angeles
108. Cappitelli F, Learner T, Chiantore O (2002) An initial assessment of thermally assisted hydrolysis and methylation—gas chromatography/mass spectrometry for the identification of oils from dried paint films. *J Anal Appl Pyrolysis* 63:339–348
109. Silva MF, Doménech-Carbó MT, Fuster-Lopéz L, Martín-Rey S, Mecklenburg MF (2009) Determination of the plasticizer content in poly(vinyl acetate) paint medium by pyrolysis–silylation–gas chromatography–mass spectrometry. *J Anal Appl Pyrolysis* 85:487–491
110. Peris-Vicente J, Baumer U, Stege H, Lutzenberger K, Gimeno Adelantado JV (2009) Characterization of commercial synthetic resins by Pyrolysis-Gas Chromatography/Mass Spectrometry: Application to modern art and conservation. *Anal Chem* 81:3180–3187
111. Rosi F, Daveri A, Moretti P, Brunetti BG, Miliani C (2016) Interpretation of mid and near-infrared reflection properties of synthetic polymer paints for the non-invasive assessment of binding media in twentieth-century pictorial artworks. *Microchem J* 124:898–908
112. Ploeger R, Chiantore O, Scalapone D, Poli T (2011) Mid-infrared fiber-optic reflection spectroscopy analysis of artists' alkyd paints on different supports. *Appl Spectrosc A* 65:429–435
113. Barth A, Zscherp C (2002) What vibrations tell us about proteins. *Q Rev Biophys* 35:369–430

114. Alfeld M, Janssens K, Dik J, de Nolf W, van der Snickt G (2011) Optimization of mobile scanning macro-XRF systems for the in situ investigation of historical paintings. *J Anal At Spectrom* 26:899–909
115. Alfeld M, Pedroso JV, Hommes MV, van der Snickt G, Tauber G, Blaas J, Haschke M, Erler K, Dik J, Janssens K (2013) A mobile instrument for in situ scanning macro-XRF investigation of historical paintings. *J Anal At Spectrom* 28:760–776
116. Janssens K, Dik J, Cotte M, Susini J (2010) Photon-Based Techniques for Nondestructive Sub-surface Analysis of Painted Cultural Heritage Artifacts. *Acc Chem Res* 43:814–825
117. Legrand S, Vanmeert F, Van der Snickt G, Alfeld M, De Nolf W, Dik J, Janssens K (2014) Examination of historical paintings by state-of-the-art hyperspectral imaging methods: from scanning infra-red spectroscopy to computed X-ray laminography. *Herit Sci* 2:13 **and references therein**
118. Alfeld M, van der Snickt G, Vanmeert F, Janssens K, Dik J, Appel K, van der Loeff L, Chavannes M, Meedendorp T, Hendriks E (2013) Scanning XRF investigation of a Flower Still Life and its underlying composition from the collection of the Kroller-Muller Museum. *Appl Phys A* 111:165–175
119. Bull D, Krekeler A, Alfeld M, Dik J, Janssens K (2011) An intrusive portrait by Goya. *Burlingt Mag* 153:668–673
120. Alfeld M, De Nolf W, Cagno S, Appel K, Siddons DP, Kuczewski A, Janssens K, Dik J, Trentelman K, Walton M, Sartorius A (2013) Revealing hidden paint layers in oil paintings by means of scanning macro-XRF: a mock-up study based on Rembrandt's "An old man in military costume". *J Anal At Spectrom* 28:40–43
121. Trentelman K, Janssens K, van der Snickt G, Szafran Y, Woollett AT, Dik J (2015) Rembrandt's "An old man in military costume" the underlying image re-examined. *Appl Phys A*. doi:10.1007/s00339-015-9426-3
122. Delaney JK, Zeibel JG, Thoury M, Littleton R, Palmer M, Morales KM, de la Rie ER, Hoenigswald A (2010) Visible and Infrared imaging spectroscopy of Picasso's Harlequin musician: mapping and identification of artist materials in situ. *Appl Spectrosc* 64:584–594
123. Thoury M, Delaney JK, de la Rie ER, Palmer M, Morales K, Krueger J (2011) Near-infrared luminescence of cadmium pigments: in situ identification and mapping in paintings. *Appl Spectrosc* 65:939–951
124. Ricciardi P, Delaney JK, Facini M, Zeibel JG, Picollo M, Lomax S, Loew M (2012) Near infrared reflectance imaging spectroscopy to map paint binders in situ on illuminated manuscripts. *Angew Chem Int Ed* 51:5607–5610
125. Dooley KA, Lomax S, Zeibel JG, Miliani C, Ricciardi P, Hoenigswald A, Loew M, Delaney JK (2013) Mapping of egg yolk and animal skin glue paint binders in Early Renaissance paintings using near infrared reflectance imaging spectroscopy. *Analyst* 138:4838–4848
126. Muir K, Langley A, Bezur A, Casadio F, Delaney JK, Gautier G (2012) Scientifically investigating Picasso's suspected use of Ripolin house paints in still life, 1922, and the red armchair, 1931. *J Am Inst Conserv* 52:156–172
127. Dooley KA, Conover DM, Deming Glinesman L, Delaney JK (2014) Complementary Standoff Chemical Imaging to Map and Identify Artist Materials in an Early Italian Renaissance Panel Painting. *Angew Chem Int Ed* 53:13775–13779
128. Sabbah S, Harig R, Rusch P, Eichmann J, Keens A, Gerhard J (2012) Remote sensing of gases by hyperspectral imaging: system performance and measurements. *Opt Eng* 51:111717
129. Rosi F, Miliani C, Braun R, Harig R, Sali D, Brunetti BG, Sgamellotti A (2013) Noninvasive analysis of paintings by mid-infrared hyperspectral imaging. *Angew Chem Int Ed* 52:5258–5261
130. Legrand S, Alfeld M, Vanmeert F, De Nolf W, Janssens K (2014) Macroscopic reflection Fourier Transformed Mid-Infrared (MA-rFTIR) scanning, a new technique for in situ imaging of painted cultural artefacts. *Analyst* 139:2489–2498
131. Doryhee F, Anne M, Bardies I, Hodeau JL, Martinetto P, Rondot S, Salomon J, Waughan GBM, Walter Ph (2005) Non-destructive synchrotron X-ray diffraction mapping of a Roman painting. *Appl Phys A* 81:663–667
132. De Nolf W, Dik J, Van der Snickt G, Wallert A, Janssens K (2011) High energy X-ray powder diffraction for the imaging of (hidden) paintings. *J Anal At Spectrom* 26:910–916

Non-Invasive and Non-Destructive Examination of Artistic Pigments, Paints, and Paintings by Means of X-Ray Methods

Koen Janssens¹  · Geert Van der Snickt^{1,2} ·
Frederik Vanmeert¹ · Stijn Legrand¹ ·
Gert Nuyts¹ · Matthias Alfeld^{1,3} · Letizia Monaco^{1,4} ·
Willemien Anaf^{1,5,7} · Wout De Nolf^{1,6} ·
Marc Vermeulen^{1,7} · Jo Verbeeck⁸ · Karolien De Wael¹

Received: 15 May 2016 / Accepted: 21 October 2016 / Published online: 21 November 2016
© Springer International Publishing Switzerland 2016

Abstract Recent studies are concisely reviewed, in which X-ray beams of (sub)micrometre to millimetre dimensions have been used for non-destructive analysis and characterization of pigments, minute paint samples, and/or entire paintings from the seventeenth to the early twentieth century painters. The overview presented encompasses the use of laboratory and synchrotron radiation-based instrumentation and deals with the use of several variants of X-ray fluorescence (XRF) as a method of elemental analysis and imaging, as well as with the combined use of X-ray diffraction (XRD) and X-ray absorption spectroscopy (XAS). Microscopic XRF is a variant of the method that is well suited to visualize the elemental distribution of key elements, mostly metals, present in paint multi-layers, on the length scale from 1 to 100 μm inside micro-samples taken from paintings. In the context of the characterization of artists' pigments subjected to natural degradation, the use of methods limited to elemental analysis or imaging usually is not sufficient to elucidate the chemical

This article is part of the Topical Collection “Analytical Chemistry for Cultural Heritage”.

✉ Koen Janssens
koen.janssens@uantwerpen.be

- ¹ AXES Research Group, Department of Chemistry, University of Antwerp, Antwerp, Belgium
- ² Conservation/Restauration Department, University of Antwerp, Antwerp, Belgium
- ³ Laboratoire d'Archéologie Moléculaire et Structurale, Pierre and Marie Curie, Paris, France
- ⁴ Department of Chemistry, Biology and Biotechnologies, Centro SMAART and CNR-ISTM, University of Perugia, Perugia, Italy
- ⁵ Royal Museum of Fine Arts, Brussels, Brussels, Belgium
- ⁶ Experimental Division, European Synchrotron Radiation Facility, Grenoble, France
- ⁷ Royal Institute for Cultural Heritage, Brussels, Belgium
- ⁸ EMAT Research Group, Department of Physics, University of Antwerp, Antwerp, Belgium

transformations that have taken place. However, at synchrotron facilities, combinations of μ -XRF with related methods such as μ -XAS and μ -XRD have proven themselves to be very suitable for such studies. Their use is often combined with microscopic Fourier transform infra-red spectroscopy and/or Raman microscopy since these methods deliver complementary information of high molecular specificity at more or less the same length scale as the X-ray microprobe techniques. Since microscopic investigation of a relatively limited number of minute paint samples, taken from a given work of art, may not yield representative information about the entire artefact, several methods for macroscopic, non-invasive imaging have recently been developed. Those based on XRF scanning and full-field hyperspectral imaging appear very promising; some recent published results are discussed.

Keywords X-ray fluorescence · X-ray diffraction · X-ray absorption · Synchrotron radiation · Paintings · Pigments

1 Introduction

Starting from pre-historic times, human artists have always felt the urge to depict their surrounding world on various substrates by using colored materials of different types. Historical paintings, such as, for example, prehistoric cave paintings, are often called “windows on the past” and have allowed later generations to imagine how former human societies looked and/or functioned. Historical paintings, therefore, are an enormously valuable part of the cultural legacy we have inherited from past generations.

There is a general belief that paintings are complex, but essentially static assemblages of widely different (in)organic materials. However, at, or just below, the seemingly placid surface of these works of art, chemical reactions are taking place that slowly alter the chemical make-up of the paint layers. While some of these reactions are the result of intimate contact between the different materials, most are driven forward by external physicochemical factors. A prime stimulus for reduction–oxidation (redox) reactions is light absorption by colored substances (molecules) in the ultraviolet (UV) and visible (VIS) range. Such reactions can lead to spontaneous in situ formation of secondary chemicals that will often differ in their macroscopic properties (such as color, volume, porosity) from the original materials. Both the organic components of paint (protein-, saccharide- or lipid/oil-based binding media, organic dyes, etc.) and/or the inorganic components (mostly pigments based on metal ions) may be affected. Another important factor in paint degradation is the often cyclic variation in relative humidity, which causes condensation and re-evaporation of minute moisture droplets within the microporous, age-cracked paint layers. The latter can act as miniature galvanic cells in which redox reactions can occur at the interface between pigment grains, binding medium, and water. In addition, phenomena such as crystallization of salts, the leaching of metal cations from pigment grains, and in situ formation of metal soaps can gradually undermine the mechanical integrity of paint materials [1]. Cycles of condensation/evaporation may also transport secondary alteration compounds

towards the surface, leading to the formation of weathering crusts. These crusts can be partly crystalline; almost all have a color and texture that is quite different from the original material.

When considering the inorganic materials employed as pigments by artists from the fifteenth to the eighteenth century, a relatively limited evolution can be observed over time. This is because the chemistry of pigment synthesis was fairly limited in this period, with the majority of inorganic materials used as pigments still being naturally occurring minerals. Only in cases of a few exceptions, such as lead white and smalt, the chemical technology was sufficiently advanced that specific colored inorganic materials of high quality and chemical stability could be synthesized in controlled circumstances.

Since the trade in artists' pigments was well spread, it was possible for artists to purchase different varieties of the same pigment, often of significantly different quality and price; in the case of mineral species, these quality differences are related to different geographical origins and/or the grain selection/purification method to convert mineral finds into finely ground pigment powder.

Among the pigments employed by fifteenth to seventeenth century fine art painters in the Low Countries, such as Jan Van Eyck (1390–1441), Hans Memling (1430?–1494), Quinten Matsys (1466–1530), Pieter Brueghel the Elder (1525?–1569), Pieter Paul Rubens (1577–1640), Anthony Van Dyck (1599–1641), Rembrandt van Rijn (1606–1669), Jan Davidz. de Heem (1606–1684), and Johannes Vermeer (1632–1675), a few fall in a special category. For these, in many historical paintings, a significant level of chemical alteration of either the pigment grains themselves or of the paint they are part of is observed. It concerns, for example, the pigment smalt (a blue, cobalt-doped type of potassium-rich glass), vermilion red (mercury sulphide, HgS , also known as cinnabar in its mineral form, a pigment used since antiquity), orpiment and realgar (both arsenic sulphides, respectively As_2S_3 and As_4S_4), and lead white (usually a mixture of cerussite, PbCO_3 , and hydrocerussite, $2\text{PbCO}_3 \cdot \text{Pb}(\text{OH})_2$). Smalt is a very frequently employed blue pigment that turns greyish/pink upon alteration. Since smalt is often used as part of large surfaces (for example, in a blue sky, in blue clothing of saintly figures, in the darker backgrounds of indoor scenes) its discoloration can have a profound influence of the general outlook and color balance of the painting. This is, for example, the case in a number of paintings by Jan Matsys (1509–1573) and Rembrandt van Rijn. A less strong, but notable change in color can take place with vermilion red, where the originally bright red surface may darken; in addition, the blackened parts of the paint often become covered with white precipitates. In a number of works by the baroque-era painters P.P. Rubens and Pieter Brueghel the Younger (1564–1636), such discolorations have been observed. The yellow/orange pigments composed of arsenic sulphides such as realgar and orpiment have a reputation of being fugitive, i.e., one assumes them to be converted by the action of light and humidity to gaseous/volatile As-containing compounds, supposedly causing the yellow-orange tinting power of these paints to slowly disappear. The seventeenth century painter J. Davidz. de Heem frequently employs the bright orange orpiment as part of his intricate flower pieces while in the Rembrandt

paintings *The Nightwatch* and *The Jewish Bride*, realgar is for example employed for painting yellow/golden highlights of the fabrics.

Near the end of the nineteenth century, a number of scientific and technical innovations such as the industrial synthesis of new pigments (with bright, more saturated hues) and the introduction of the paint tube (allowing easy distribution and use of industrially produced artistic paints) set the stage for a significant artistic revolution. Indeed, several masters of modern art, such as Joseph M.W. Turner (1775–1851), John Constable (1776–1837), Camille Pissarro (1830–1903), Paul Cézanne (1839–1906), Vincent van Gogh (1853–1890), George Seurat (1859–1891), and James Ensor (1860–1949) avidly made use of the new possibilities the recently available pigments and paints offered for expressing themselves.

Among the many colors employed by Vincent Van Gogh, the use of yellow pigments becomes very important after 1885. While in his early period (1883–1885/6), he employed mainly Naples yellow (lead antimonate) or light hued earth pigments, in the second half of his career (when he worked in Paris, Arles, and St. Remy, 1885–1890), he frequently employs both chrome yellow and cadmium yellow [2]. As becomes clear from his correspondence [3], chrome yellows are among Van Gogh's favored pigments, featuring in some of his most important paintings from the French period (1886–1890), such as, for example, the *Sunflowers* series of paintings. Already during his lifetime, Vincent van Gogh was aware of the lack of stability of chrome yellow (see letter nr. 595 from 1898 [3]). In this respect, cadmium yellow had a better reputation; however, recent investigations have revealed that also this pigment may change its hue under the influence of time and environmental agents. Its degradation behavior has been/is being studied in works of art by Vincent Van Gogh, Henri Matisse (1869–1954), and Edvard Munch (1863–1944). The final pigment to be discussed here is minium or red lead (Pb_3O_4); Van Gogh and his contemporaries sometimes employed this orange-red pigment. This substance, frequently used outside artists' workshops to protect metals from corrosion, tends to become either white or black, as a function of its chemical environment.

In order to assess better the current and future state of a painted work of art, it is highly relevant to have a good understanding of the alteration processes that gradually affect the materials it consists of. Many of these alteration phenomena only become visible after an extended period of time and are caused by slow acting (physico-)chemical transformations in multi-component and multi-phase chemical systems that only gradually move towards equilibrium. Redox processes have been identified as being responsible for alteration of a number of inorganic pigments. A lot of these reactions involved include a photo-activation step and, therefore, require (sufficiently energetic) light falling on the painting (surface). The secondary compounds formed in this manner generally are present as micrometer-thin layers, at or just below the paint surface. Advanced analytical methods that allow to distinguish between subtly different compounds or valence states of the same transition metal in these micrometer-thin and superficial alteration layers and that at the same time are able to provide information on the distribution of such secondary compounds, are therefore mandatory tools for art-conservation research [4].

Traditionally, to study the chemical make-up of painted artworks in detail, (minute) paint samples are collected. These tiny samples can be taken using five

standard “microdestructive” techniques: scalpels or lancets (e.g. [5]); gentle cotton bud (Q-tip) abrasion (e.g. [6]); microdrilling (involving a 100–200 μm diameter bore) (e.g. [7]); or laser ablation, the ablated materials being collected on microscope slides (e.g. [8]). These techniques remove only minute amounts of material and any damage is effectively invisible to the naked eye; they, therefore, do not disturb the esthetic experience of the artwork. Moreover, microdestructive sampling is mostly limited to areas where paint losses have already occurred. The extracted material often comprises the entire stack of micrometre-thick paint layers at a given position. To examine the minute samples, one or more non-destructive microanalytical methods may be employed before undertaking additional analytical investigations that involve the chemical digestion of the sampled material, or any other wet-chemical operation. Prior to microanalysis, multilayered paint samples are typically embedded in resin, cross-sectioned and then polished. Alternatively, the different materials/layers in a paint sample may be carefully separated from each other under the microscope for separate analysis.

The range of analytical techniques available to painting researchers is now fairly extensive and the methods can be used to characterize a painting’s materials in detail. They include the following: optical microscopy (OM), scanning electron microscopy coupled with energy dispersive X-ray spectrometry (SEM-EDX) [9], micro-Fourier transform infrared spectroscopy (μ -FTIR) ([10]), micro-Raman spectroscopy (μ -RS) [11, 12], high-pressure liquid chromatography (HPLC), gas chromatography coupled with mass spectrometry (GCMS), and pyrolysis GCMS (Py-GCMS) [5, 13–15]. To complement these analytical methods there are chemical imaging techniques such as synchrotron radiation (SR)-based micro-X-ray fluorescence (μ -XRF) [16], micro-X-ray absorption near-edge spectroscopy (μ -XANES) spectroscopy ([17]), micro-X-ray powder diffraction (μ -XRPD) [18], and synchrotron radiation micro-Fourier transform infrared spectroscopy (SR- μ -FTIR). SR-based photoluminescence is a relative new addition to this series [19]. Often, combinations of these methods are required to fully understand the paints’ chemistry [20, 21]. This was also the case for a number of the investigations described below.

Micrometers below a painting’s surface, a wealth of information may be present about the creative process followed by the artist while making the work of art. The manner in which a painted work of art was created, its conservation, and exhibition history may leave material traces behind, for example, in the layer-by-layer build-up of the artwork. However, this stratigraphic information, comprising structural and compositional aspects, is usually not easy to obtain in a non-invasive manner. Next to the visible surface layers, subsurface layers may include underdrawings, underpaintings, and adjustments made in the course of painting. Together, all these layers determine the current appearance of the work of art. In a growing number of cases conservators have discovered abandoned compositions underneath paintings, illustrating the artist’s practice of reusing a canvas or panel. Imaging methods that can “read” this hidden information without any damage to the artwork are, therefore, valuable tools for art-historical research [22]. The standard methods for studying the inner structure of painted works of art are X-ray radiography (XRR) and infrared reflectography (IRR), both penetrative illumination techniques that are optionally complemented with the

microscopic analysis of cross-sectioned paint samples. Since these methods all have their limitations, recently, a number of fundamentally new approaches based on X-rays for imaging the buildup of hidden paint layers systems (and for analyzing small samples thereof) have been put into practice. Two major motivations can be discerned for the development of such analytical methods: (a) the desire to know more about the creative process and/or the artist's way of working that have led to a given artefact and (b) the need to assess and predict the current and future condition of a work of art. Motivation (a) is essentially of art-historical nature and seeks to reconstruct (better) the *past/history* of an artwork while motivation (b) is more strongly linked to preventive conservation and to conservation technology and, therefore, mostly concerned with *the future* of the artwork [17]. It should be duly noted, however, that for conservation, also an understanding of the history of a work of art and the artist's intent is fundamental, since it provides the basis for assessing the current condition of the artwork and for deciding which might be the most appropriate interventions [23].

A comprehensive understanding of the paints used in a work of art, therefore, requires information from across the painting's surface, as well as on their ordering as a function of depth [23]. To complement the detailed information that can be gathered from a limited number of (possibly non-representative) paint cross sections, mobile versions of different non-invasive spectroscopic methods can be used to investigate a (much) larger number of locations on a work of art. By means of portable XRF (PXRF), element signatures can be swiftly recorded from all differently colored areas of a painting, allowing indirect inferences to be made on which pigments were used throughout. Similarly, portable RS and FTIR equipment can be used in a complementary manner to record molecular spectroscopic data and to assess the presence of any organic constituents (e.g. [24]). More recently, several X-ray and visible/near infrared (VIS/NIR) based non-invasive imaging methods have been developed and successfully employed to document the composition of *complete* paintings [25–27]. They can be considered the state-of-the-art equivalents of the two imaging methods that have been routinely employed in subsurface investigation of paintings for several decades: infrared reflectography (IRR) and X-ray radiography (XRR). Some of these exploit a scanning mode of operation (see Fig. 1) and include the techniques of macroscopic X-ray fluorescence (MA-XRF) [26], macroscopic X-ray diffraction (MA-XRD) [28], macroscopic Fourier transform infrared scanning in reflection mode (MA-rFTIR) [29], and VIS/NIR imaging [30]. Camera-based analytical approaches include hyperspectral imaging in the visible range (350–700 nm), the near-infrared range (NIR; 0.7–1.7 μm), and the short-wave infrared range (SWIR; 1.7–2.5 μm) [27].

In what follows, after outlining a number of X-ray based methods of analysis suitable for studying pigment degradation phenomena, we describe a number of recent studies aimed at unraveling the degradation pathways these pigments are subjected to. Here, the ability to determine the speciation of the inorganic metallic compounds on the (sub)microscopic scale is often highly valuable, as this speciation state often alters during degradation processes. We also briefly describe recently developed methods of chemical imaging by means of which the distribution of pigments in paintings can be visualized. It is often interesting to combine both methods for local (speciation) analysis and large scale chemical imaging in a study of a particular work of art.

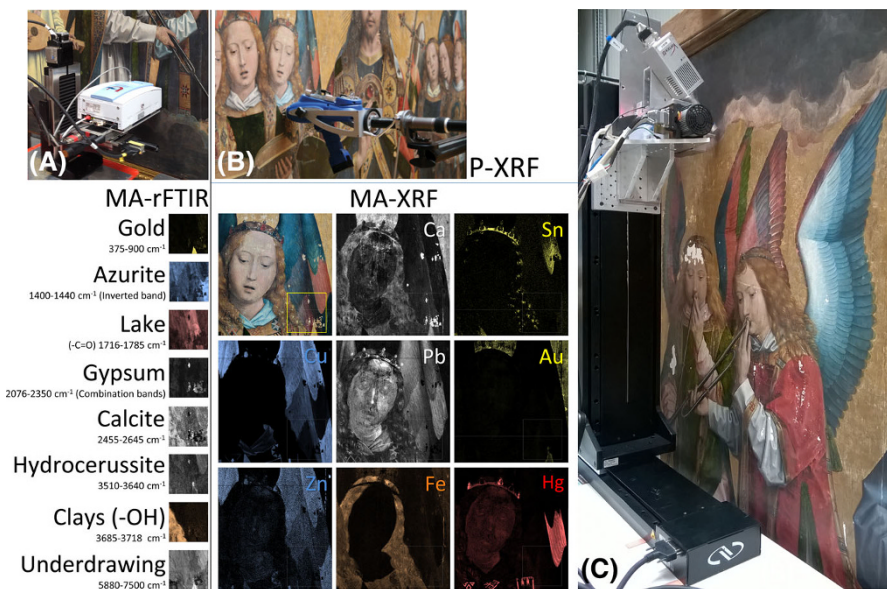


Fig. 1 *Christ with singing and music-making Angels*, Hans Memling (1430–1495, Royal Museum of Fine Arts, Antwerp, Belgium, panels 779, 778, and 780; oil on panel). **a** MA-rFTIR scanner in front of panel 779; **b** PXRF-analysis of the chest-area of Angel #8, panel 778. **c** MA-XRF scanner, scanning part of panel 780, and resulting elemental maps. The FTIR maps shown in **a** correspond to the white rectangle in the MA-XRF maps shown in **c**. Adapted from [21]

2 X-ray Based Methods of Analysis

X-ray fluorescence analysis (XRF) is a well-established method of (semi-)quantitative elemental analysis that is based on the ionization of the atoms of the material being irradiated by an energetic beam of primary X-rays. XRF on heritage and archaeological samples is mainly used in reflection geometry to probe the stratigraphy of polished cross-sections of micro-samples or the exposed surfaces of objects. The energy of the fluorescent photons is the difference in energy between the vacancy that is the result of the ionization process and the electronic state of the electron filling the vacancy [16, 31]. In this manner, the characteristic radiation emitted by the ionized atoms contains information on the nature and the abundance of the elemental constituents present. The technique is particularly efficient for studying high atomic number (high-Z) elements in low-Z matrices. Analysis of the XRF spectra involves identification of the elements present from the fluorescence lines observed and estimation of their net intensity; the latter are in principle proportional to the abundance of the corresponding chemical elements. (Semi-)quantitative analysis usually involves more complex calculations as initial absorption of the X-ray beam and absorption of the fluorescent photons in the material has to be modeled by taking the (expected) matrix composition into account in an iterative fashion [32–34]. Since XRF meets a number of the requirements of the “ideal method” for non-destructive analysis of cultural heritage materials [35], analysis of objects of artistic and/or archaeological value with

conventional XRF is fairly common. It is in fact one of the most often applied methods for obtaining qualitative and semi-quantitative information on such objects. Several textbooks cover the fundamental and methodological aspects of the method and its many variants [36].

The variants of XRF that are most relevant for the analysis of painted works of art or of micro-samples taken from such artifacts are (1) PXRF, (2) the X-ray microprobe (XMP), involving the combined use of μ -XRF/ μ -X-ray absorption spectroscopy (μ -XAS) and/or of μ -XRF/ μ -XRD, usually based on synchrotron radiation, and (3) MA-XRF imaging.

Portable XRF (PXRF): prior to analyzing painted works of art with more sophisticated methods, as a means of first exploration or screening of the artifacts, the use PXRF, sometimes also called handheld XRF (HXRF or HHXRF) is usually very relevant [37]. Various compact, battery operated devices of this kind are now commercially available [38–43] next to a number of self-built systems [44–47]. One of these is shown in Fig. 1b. Since the interaction of individual photons of a specific energy with single atoms of given atomic number can be very well described, in principle, any form of X-ray fluorescence and, therefore, also PXRF, has the potential of being used for (semi-)quantitative analysis. Several calibration schemes and variants thereof have been developed since the 1970s [48]. Over the past decade, PXRF instruments have allowed non-invasive analyses to be conducted in museums around the world, on virtually any size artifact, producing data for up to several hundred samples per day. However, questions have been raised about the sensitivity, precision, and accuracy of these devices, and the limitations and advantages stemming from performing surface analysis on (often) heterogeneous objects made in obsidian, ceramics, metals, bone, and painted materials have been discussed [49]. In the next paragraph, a number of recently published studies in which PXRF was part of the set of analytical methods employed is outlined. Considering that in PXRF-based studies, the interpretation of the spectral data obtained from complex, multilayered (paint) systems can be problematic, usually the advantages of PXRF have been exploited in combination with other, more surface-specific and/or molecule-specific methods of analysis, in particular vibrational spectroscopies such as Raman and FTIR (micro)spectroscopy.

PXRF has been used extensively both for documentation, as well as for authentication purposes [50] of works of art of different historical periods. The painting materials used in prehistoric rock art have been characterized by PXRF, usually in combination with more specific methods (of molecular spectroscopy) [51–53]. To characterize the materials and stratigraphies of an Egyptian coffin in the Museo Civico Archeologico of Bologna (Italy), restored several times in the past, a two-step approach involving both non-invasive and micro-invasive analysis techniques was used [54]. The in situ, portable spectroscopies employed included XRF, fibre optics reflectance spectroscopy (FORS), and FTIR. This multi-technique approach allowed to reveal many differences in the composition of the (calcite, CaCO_3) ground layer and to identify the pigments in the original [cinnabar, orpiment, red clay, Egyptian blue ($\text{CaCuSi}_4\text{O}_{10}$), and copper-based greens] and restored zones [lead white, Naples yellow ($\text{Pb}(\text{SbO}_3)_2/\text{Pb}_3(\text{SbO}_4)_2$), cerulean blue ($\text{CoO}\cdot n\text{SnO}_2$), azurite ($2\text{CuCO}_3\cdot\text{Cu}(\text{OH})_2$)] of the coffin. In order to resolve

remaining doubts about the presence of specific pigments in superimposed layers, a few micro-fragments of paint were removed and analyzed using benchtop methods. PXRF was combined with portable RS, Diffuse reflectance infra-red Fourier transform spectroscopy (DRIFTS) and other methods for studying two wall paintings in the Naples Archaeological Museum. The artefacts were extracted ca. 150 years ago from Marcus Lucretius' house in Pompeii, showing the result of the interaction of H₂S gas (expelled during the eruption of Vesuvius) on the painting materials [55]. The efflorescence on the walls of the house and the extracted wall paintings were also studied [56]. The painted surface of plasters withdrawn from different areas of the Villa dei Quintili (Rome, Italy) were examined in a similar manner [57]. A combined XRF/XRD portable instrument was used to study the pigment palette in the paints of the vaults of the Courtyard of Lions in the Alhambra Palace (Granada, Spain), identifying (among others) cinnabar and hematite (Fe₂O₃) in the red hues, in combination with hydrocerussite in the flesh tones while lazurite ((Na,Ca)₈[(S,Cl,SO₄,OH)₂(Al₆Si₆O₂₄)]), azurite, and malachite (CuCO₃·Cu(OH)₂) were encountered in, respectively, the blue and green areas [58]. Nubian wall paintings (from churches in southern Egypt and northern Sudan) from the seventh to fourteenth century were analyzed with a combination of PXRF and LA-ICP-MS, allowing the identification of the raw materials employed [59]. On a thirteenth century icon covered by a nineteenth century painting, an extensive campaign of non-invasive analytical investigations was carried out using PXRF, FORS, UV–VIS absorption and emission, allowing the documentation of the gilding techniques employed and formulation new hypotheses regarding thirteenth century painting techniques and materials [60]. To document the use of powdered bismuth (Bi) in Late Gothic paintings and polychromic sculptures, PXRF was used together with SEM-EDX and optical microscopy [61]. A combination of portable FTIR, Raman, and XRF was used to identify the rare minerals crocoite (PbCrO₄) and mimetite (Pb₅(AsO₄)₃Cl) in medieval Bohemian murals [62], probably as a result of the degradation of the pigments orpiment (As₂S₃) and minium (Pb₃O₄). The same methods were also employed to determine the nature of the painting materials present in Memling's polyptych *Angels Singing and Playing Music* [63] (see Fig. 1), allowing the assessment of the manner in which this painter employed a limited set of pigments and dyes to accomplish a great variety of color and optics effects. With the aim of establishing it better into its historical context, a portable XRF–XRD system was employed to analyze a fifteenth century illuminated parchment from the Archive of the Royal Chancellery in Granada [64]. This revealed the presence of gold and silver, lead tin oxide yellow (Pb(Sn,Si)O₃/Pb₂SnO₄), azurite, vermilion, minium, and malachite. Also, the materials employed by Pieter Brueghel the Elder in the painting *Mad Meg* were studied by means of PXRF and other methods [65], identifying the use of copper resinate green, smalt blue, vermilion red, and lead white; these findings confirm the hypotheses about “an economic way of painting” by Brueghel. The gold dust, gold leaf, and the materials used for the gilding of two miniature portraits on copper support from the Evora Museum collection (Portugal) were examined and analyzed by stereomicroscopy, Raman, and FTIR microspectroscopies, SEM-EDX, PXRF, and liquid chromatography coupled to diode array and mass spectrometric detection [66]. The pigments and binding media

employed in Sorolla's gouache sketches for the Library of the Hispanic Society of America, New York City, NY, USA have been studied by means of a combination of PXRF, SEM-EDX, and FTIR analysis, showing that a rich palette of pigments was used to manufacture these nineteenth century artists' materials [67]. With the aim of documenting the evolution in the pigment use of the late nineteenth century/early twentieth century. Belgian painter James Ensor, and to correlate this technical evolution with stylistic developments, a systematic survey was conducted mainly based on PXRF [68]. A series of non-invasive analyses employing PXRF, portable RS, and FTIR were combined with benchtop micro-Raman and SEM-EDX investigations to study the complicated mixtures encountered in paintings by E. Munch and F. Kupka, highlighting the need to employ combinations of methods in order to arrive at unambiguous pigment identifications [69]. Other works of modern painters were examined to verify their authenticity [70] or document their pigment usage [71–75].

Microscopic XRF (μ -XRF) is a branch of XRF that has been developed since 1990 [76], mainly thanks to the use and increasing availability of (a) synchrotron radiation (SR) and (b) various devices for efficient focusing of X-rays [16, 77]. It can obtain information on the local elemental composition of inhomogeneous samples. At synchrotron facilities, a variety of micro- or nanofocus optics, based on refraction [78, 79], diffraction [80, 81], or total reflection [82, 83] of X-rays, is currently in use to create small beams with energies in the 1–100 keV range and with diameters of typically 0.1–1 μ m. In laboratory μ -XRF instruments, mostly polycapillary lenses are employed for focusing [84–86], providing focused X-ray beams that usually are 10–30 μ m in diameter [87]. Among the commercial apparatus currently available, there are some specifically developed for the local investigation of works of art [88]. By incorporation of additional degrees of freedom of the measuring head, the analysis of Antique manuscripts [89, 90] and bronzes [91, 92], Medieval paintings [93], Chinese porcelain [94], and Baroque-era drawings [95] has become possible.

A specific sub-type of micro-XRF investigations are those employing a confocal excitation-detection geometry [96]. In this case, the recorded XRF signals stem from a well-defined cube-like "sampling" volume that is situated at the intersection of the X-ray optical devices positioned between X-ray source and sample (defining the primary beam) and between sample and X-ray detector (defining the direction from which XRF signals can enter the detector) [97]. Often, polycapillary optics are employed for the latter purpose [98, 99]. By moving the sample through this sampling volume, local information on the elemental composition of the material being investigated can be obtained. Sequential series of confocal XRF measurements along lines and planes allows to visualize the distribution of chemical elements of interest in one or two dimensions, creating, for example, virtual depth profiles, and two- or three-dimensional distributions inside the materials of interest [23, 100, 101]. After its original introduction at synchrotron radiation facilities [97, 101–105], the feasibility of performing confocal XRF measurements using tube sources was demonstrated by several groups around the world [106–110], along with appropriate deconvolution, quantification, and simulation models [111–118]. Several papers have been recently been published where confocal XRF

measurements are exploited for sub-surface examination of painted works of art [119–124], next to pottery [125], coins [86], stained glass [126, 127], painted metal sheet [128], and natural rock samples [129].

About 10–15 years ago, the main advantages of SR-based μ -XRF for the study of archaeological and artistic materials (such as glass, inks, enamel, metals) were considered to be its quantitative and non-destructive character combined with the possibility to perform trace analysis at the 1–10 ppm-level for transition element metals [130]. At that time, the combined use of μ -XRF with μ -XAS and μ -XRD was described as an interesting development [131]. Currently, this multi-modal approach has become standard practice at SR facilities, where the role of μ -XRF is still central, but often no longer of major importance. X-ray microprobes (XMPs), i.e., synchrotron beam lines that allow the combined use of these methods are nowadays present at all SR facilities. Recent review papers [21, 132–134] indicate that they are well-established, non-destructive analytical tools that are successfully employed in a large variety of application fields such as materials science/quality control, environmental science, geology, and life sciences, as well as in cultural heritage investigations. **Figures 2** and **3** show spectral data and chemical maps derived from degraded paint micro samples. For the investigation of (altered) paint layer samples, also SR-based μ -FTIR is being increasingly used as a complementary method; in addition to the identification of organic components (binders, varnishes) it provides specific

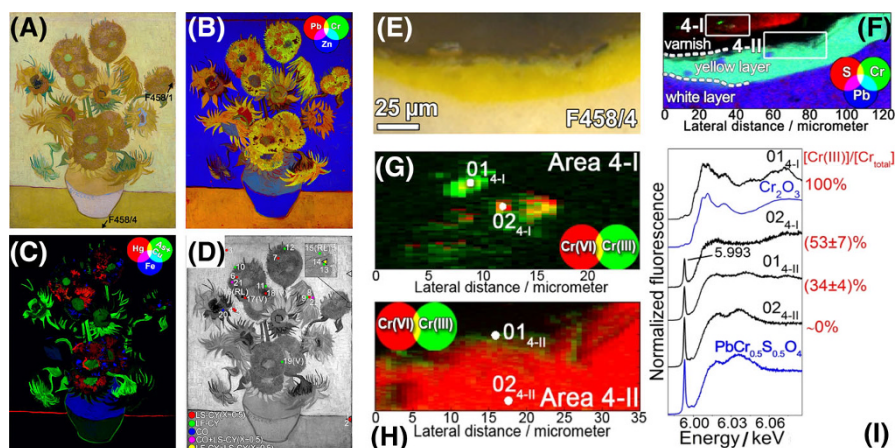


Fig. 2 **a** Photograph of *Sunflowers* by Van Gogh (Aries, 1889; Van Gogh Museum, Amsterdam, the Netherlands); sampling spots are also shown. RGB composite MA-XRF maps of **b** Pb/Cr/Zn and **c** Hg/As + Cu/Fe. **d** Raman and IR distribution of different CY types (LS-CY: light-sensitive chrome yellow ($\text{PbCr}_{1-x}\text{S}_x\text{O}_4$, with $x > 0.4$); LF-CY: light-fast chrome yellow (monoclinic PbCrO_4); CO: chrome orange ($[(1-x)\text{PbCrO}_4 \cdot x\text{PbO}]$). *Triangles* show the location of FTIR analyses; “V” and “RL” indicate spots containing also vermilion and red lead. The *white circle* denotes the location where only red lead was identified. **e** Photomicrograph detail of sample F458/4 where SR μ -XRF/ μ -XANES analysis of **f–i** were performed. RGB SR μ -XRF images of **f** S/Cr/Pb [map size: $124 \times 51.2 \mu\text{m}^2$; pixel size ($h \times v$): $1 \times 0.25 \mu\text{m}^2$; energy: 6.090 keV]. **g, h** RG Cr(VI)/Cr(III) chemical state maps [pixel size ($h \times v$): $0.7 \times 0.2 \mu\text{m}^2$] and **i** XANES spectra collected from areas indicated in **g, b**. Maps of (**g, h**) were acquired in the regions shown in **f**. Adapted from [156]

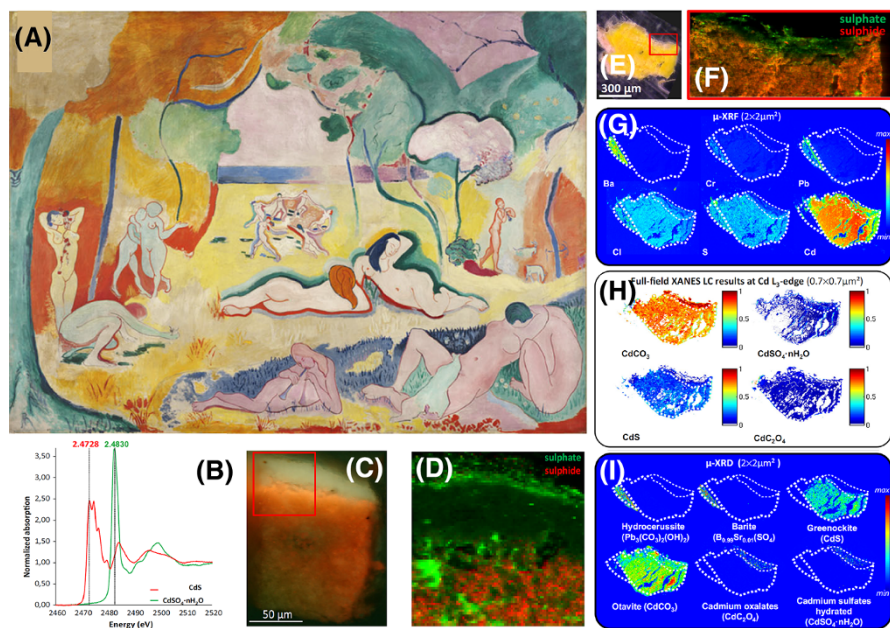


Fig. 3 **a** *Le bonheur de vivre* (aka *The Joy of Life*, 1905–1906, oil on canvas, 176.5 × 240.7 cm, The Barnes Foundation, BF719) by Henri Matisse; **b** S-K_α edge XANES of cadmium yellow (CdS, in red) and its transparent/colourless oxidation product (CdSO₄·nH₂O, in green); **c**, **e** Optical photographs of paint cross sections taken from **a**; **d**, **f** Compound sulphide (red)/sulphate (green) map of the areas indicated by the red rectangle in **c** and **e** (step size: 1 × 1.2 μm²); **g**–**i** XRF, full-field XANES and XRD maps of the sample shown in **e**. Adapted from [222]

information on the presence of counter ions such as carbonates, sulfates, and oxalates where μ-XRF and μ-XAS mostly yield data on the metal ions themselves.

SR-based XMPs have proven their value over more conventional combinations of microanalytical methods, especially for the characterization of degradation products that are formed in thin layers (smaller than 10 μm in thickness) at the surface of weathered archaeological and/or artistic materials and artifacts. Since individual paint layers in paint stratigraphies may be only a few micrometres in thickness, the lateral resolution offered by laboratory μ-XRF is not always sufficient to extract all relevant information; thus, the collection of elemental maps from paint cross sections using SEM-EDX at a typical lateral resolution of 1 μm is still preferred. Occasionally, μ-XRF has been used for this purpose, and then mostly in combination with other laboratory-based methods that provide complementary information [135, 136]. Since the use of (focussed beams of) synchrotron radiation exposes the materials under investigation to elevated doses of radiation, not all materials can be examined without beam damage [137]; phenomena such as gradual loss of crystallinity, beam-induced oxidation or reduction have been observed in several cases [138–140].

X-ray absorption spectroscopy (XAS) is based on the absorption of X-rays by materials in the vicinity of the absorption edge of one of its constituting elements. The technique provides chemical speciation, i.e. information on the coordination

sphere of the selected absorbing element (the central atom). The tunability of the synchrotron emission with typical bandwidths $\Delta E/E$ smaller than 10^{-3} – 10^{-4} , i.e. in the (fractional) eV range for hard X-rays, permits the fine scanning of individual element absorption edges. Synchrotron beam line setups are usually optimized to continuously scan the primary beam energy E with a fixed exit of the beam over the desired energy range (a few tens of electron volts for XANES or a few hundred eV for extended X-ray absorption fine structure (EXAFS) spectroscopy). Due to the high absorbance of many materials encountered at energies below 20 keV most X-ray absorption experiments for cultural heritage and archaeology are performed using XANES in fluorescence detection mode by collecting the X-ray signal typically over some tens of eVs. The XANES fingerprint that is obtained is compared to that of known reference compounds and in many situations the unknown fingerprint spectra can be described by a linear combination of the spectra of the references (see for example Fig. 2i or 3b). By recording μ -XRF maps at a limited number of energies along the XANES spectrum and appropriate transformation of the resulting intensity distributions, it is possible to obtain species-specific maps (see for example Fig. 3b). Several reviews on the use of XANES for cultural heritage investigations are available [17, 20].

X-ray diffraction (XRD): the main use of XRD for the study of paintings and pigments stems from the fact that identification and quantification of crystalline phases in complex mixtures is possible. Via appropriate optics, an X-ray micro-beam of medium to low divergence (typically <3 mrad) is generated that allows a paint sample or an entire artifact either in transmission or in reflection geometry to be irradiated (see Fig. 4). Such beams may be generated at synchrotron facilities using various optics, but also by using laboratory X-ray sources and, e.g., double focusing mirrors. The powder diffraction rings are usually recorded with a two-dimensional detector and then azimuthally integrated (Fig. 4e, f), yielding a radial profile (scattering intensity vs. scattering angle 2θ or momentum transfer Q). Each phase inside the sample gives rise to a series of diffraction rings that appear as sharp peaks in the radial profile. This “fingerprint” can be compared with databases and used to identify the phases present. A possible overlap between the diffraction peaks makes this process more difficult. In a number of cases, also Rietveld analysis [141] is performed in order to extract quantitative information.

Macroscopic X-ray fluorescence (MA-XRF) imaging is a large scale variant of μ -XRF that has come in use since 2008 when it transpired that hidden/overpainted layers in paintings can be revisualized in this manner; significantly more (pictorial and chemical) information can be obtained than by means of X-ray radiography [142]. It involves the relatively fast scanning of a work of art relative to an X-ray source and XRF-detector assembly. Either the latter assembly is moved in front of the stationary artwork (mobile MA-XRF scanners) or vice versa. With typical dwell times of 50–200 ms per point, a (very) large number of XRF spectra (of the order of one to several million spectra/artwork) are recorded, yielding (after appropriate spectrum evaluation [143]) large-scale elemental maps (see Figs. 1c, 2b, c, 7c, d, 8, 9d, 10b). While its development started at a synchrotron facility [144], at which also the first studies were realized [142, 145–148], relatively soon mobile MA-XRF instruments were developed that allowed performing scanning experiments in the

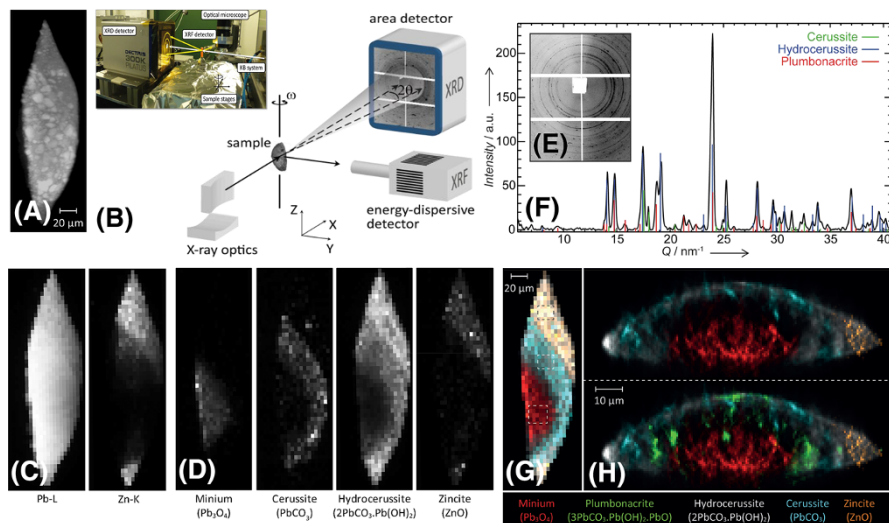


Fig. 4 **a** XRR image (obtained via X-ray absorption tomography) of a minium pustule removed from the surface of “Wheat stacks under a cloudy sky”, V. van Gogh (Kröller-Müller Museum, Otterlo, the Netherlands). **b** Schematic and photograph of scanning XRF/XRD setup employed at Beamline P06 of PETRA-III. **c** XRF and **d** XRD 2D distribution images of the severed pustule (map size: $80 \times 55 \mu\text{m}^2$). **e** 2D X-ray diffractogram of a plumbonacrite-rich location and **f** corresponding Q-space spectrum showing the peaks of various lead carbonates. **g** Color reconstructions of the projected and **h** the internal crystalline distribution of the paint sample. Pixel size: $45 \mu\text{m}^2$ (in **c**, **d**, and **g**); $11 \mu\text{m}^2$ (in **h**). Adapted from [163]

museum or picture gallery where the works of art are normally on display or are conserved [26, 149, 150]. With these MA-XRF scanners, it was possible to examine a great variety of artworks by well-known artists such as Rubens [22], Rembrandt [151–153], Vermeer [154], Goya [155], Van Gogh [145, 156], Magritte [157], Mondriaan [158] and Pollock [159], and to discover new information on their artistic history and on their current state of conservation. Several X-ray instrumentation manufacturers and research institutions have recently described MA-XRF scanners of their own making [27, 160].

3 Multimodal X-ray-Based Identification and Degradation Studies of Artists’ Pigments

3.1 Pigments As Semi-Conductor Materials

Most of the artists’ pigments of which the spontaneous degradation behavior are described below are semiconductors. These are materials in which, upon absorption of photons, electrons can be promoted from the valence to the conduction band, leaving behind positive holes (see Fig. 5a). As illustrated in Fig. 5b, near the surface of the material, band bending can take place, which may lead to either electrons or positive holes being “injected” in the adjacent materials. The (in)stability of these

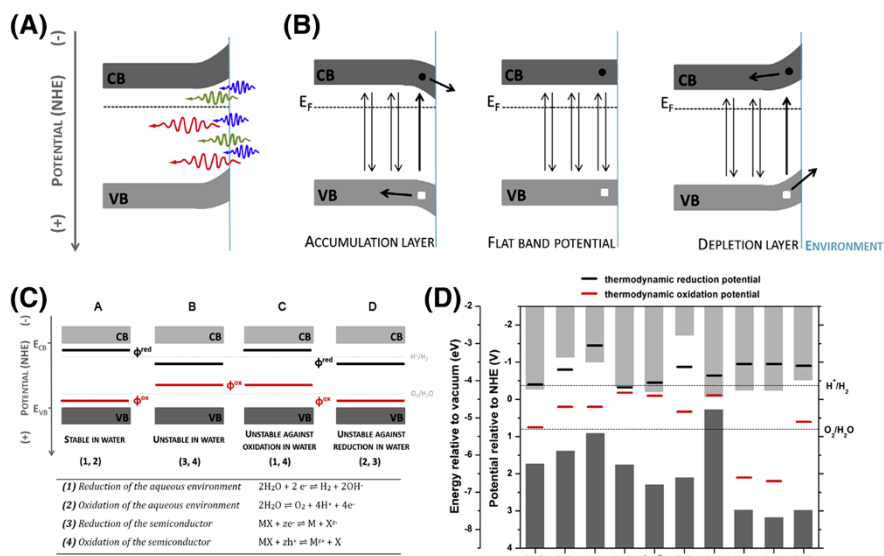


Fig. 5 **a** Indication of the penetration depth of blue (≈ 450 nm), green (≈ 510 nm), and red (≈ 650 nm) light. **b** Band bending for n -type semiconductors under illumination: accumulation layer (negative surface charge), flat band potential and depletion layer (positive surface charge, most common for n -type semiconductors). Arrows indicate either recombination of generated electron-hole pairs, or charge separation in the presence of an electric field induced by band bending. **c** Schematic overview on the stability of semiconductors in water. Oxidation and reduction potentials of a semiconductor relative to the oxidation and reduction potential of H_2O . **d** Oxidation and reduction potentials relative to the NHE and vacuum level for relevant semiconductor pigments or pigment degradation products in aqueous solution at pH 7 (pH 8.5 for ZnO), plotted versus the valence (dark grey columns) and conduction (light grey columns) band edge positions at pH 7. Adapted from [161]

pigments and the nature of the corresponding chemical transformations may be better understood/predicted by considering the positions of the valence band maximum (VBM) and conduction band minimum (CBM) in relation to their thermodynamic oxidation and reduction potential (ϕ_{ox} and ϕ_{red}) and that of water (see Fig. 5c) [161, 162]. In this manner, the positions of ϕ_{ox} and ϕ_{red} can be used for a fast screening of the stability of semiconductor pigments towards photo-induced corrosion in an aqueous/humid environment. This theoretical approach corresponds well with experimental data on pigment permanence and degradation phenomena found in the literature. By experimentally recording the photo-induced reduction or oxidation current emitted by the irradiated pigment/paint in an electrochemical setup that mimics the real environment of the degrading paint, the influence of potentially harmful environmental parameters (e.g., the wavelength and intensity of the exciting light, the type of solvent, its pH, the concentration of metal-binding ligands such as Cl^- and HCO_3^-) can be rapidly determined. It provides an experimental way of assessing whether or not a semi-conductor pigment is prone to photo-induced oxidation or reduction, with the advantage that it is much faster than more traditional approaches based on artificial ageing of paint model samples. Accelerated weathering experiments on such materials usually are time-consuming, limiting the number of environmental factors of which the influence can

systematically be examined. Moreover, during the long time period of artificial aging, the possibility exists that several chemical transformation processes (e.g. an initial photo-induced redox reaction followed by the precipitation of the released metal ions with suitable anions) may be taking place so that only their compound effect can be observed [163]. As concrete examples, the degradation behavior of the pigments cadmium yellow (CdS) and vermilion (α -HgS) were discussed in greater detail [162, 164, 165].

3.2 Pigment Degradation Studies Related to Fifteenth–Seventeenth Century Works of Art

Vermilion red (α -HgS) is a very frequently used semi-conductor pigment from the neolithic period onwards. It has been mined prehistorically and historically in China, Japan, Europe, and the Americas to extract metallic mercury (Hg^0) for use in metallurgy, as a medicine or preservative, and as a red pigment for (body) painting and in ceramics [166]. It is a pigment that features a complex multistep degradation pathway. Chlorine and sulfur K-edge μ -XANES investigation were combined with μ -XRD to determine the alteration mechanism that causes red pigment to acquire a grayish-black aspect (see Fig. 6) [167]. Paint fragments from Rubens paintings and from wall paintings in the Monastery of Pedralbes in Spain have also been examined [168–170]. Whereas elemental analyses of the degradation products revealed, along with mercury and sulfur, the presence of chlorine, XRD identified (in addition to α -HgS) calomel (Hg_2Cl_2) and the mercury-, sulfur-, and chlorine-containing minerals corderoite (α - $\text{Hg}_3\text{S}_2\text{Cl}_2$) and kenhsuite (γ - $\text{Hg}_3\text{S}_2\text{Cl}_2$). These observations are consistent with S- and Cl-edge XANES data. The resulting maps reveal a clear stratification between the primary mercury compounds (α -HgS) and the secondary species that arose from the interaction with environmental chlorine, leading the authors to hypothesize that α -HgS first takes up Cl, thereby converting into one or more $\text{Hg}_3\text{S}_2\text{Cl}_2$ phases. These light-sensitive compounds, following the loss of sulfur atoms, can be transformed into Hg_2Cl_2 , whereas sulfide ions oxidize into sulfate ions. The final step may involve the UV-induced disproportionation of Hg_2Cl_2 to HgCl_2 and may cause metallic mercury to turn white calomel into a grayish-black substance. No evidence for this transformation could be found with X-ray methods, although some relevant data were recorded via secondary ion mass spectrometry [171]. To study in greater detail the principle environmental factors (light, presence of halides) influencing the instability of red mercury sulfide and to better understand the chemical equilibria governing the formation and evolution of the different degradation compounds, a thermodynamic study of the Hg–S–Cl–H₂O system was made in combination with theoretical considerations and experimental ageing experiments [172]. The latter were performed in O₂-rich and O₂-poor circumstances (see Fig. 6d, e). From these it could be concluded that Hg(0), α - $\text{Hg}_3\text{S}_2\text{Cl}_2$, and Hg_2Cl_2 can be formed from the reaction of α -HgS with ClO(g). Artificial aging experiments were carried out on model samples following the conditions assessed in the first part, in order to reproduce natural ageing observed on red mercury sulfide. Similarly to degradation compounds detected on original works of art, mercury chlorine compounds such as calomel and corderoite were identified on the surface of

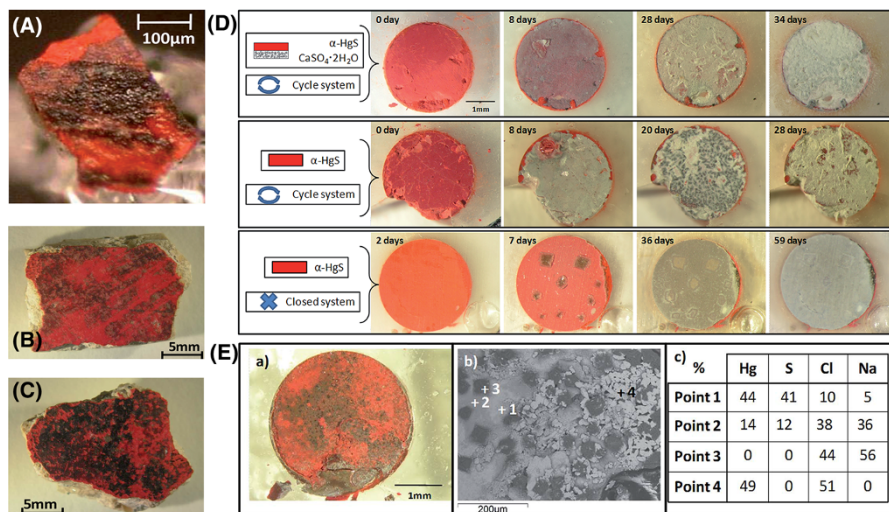
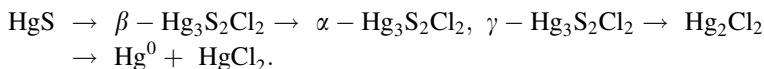


Fig. 6 Photographs of paint micro-fragments taken from: **a** *The Adoration of the Magi*, a painting by P. P. Rubens, Royal Museum of Fine Arts, Antwerp, Belgium; **b, c** a Roman fresco from *Villa delle Torre*, near Pompeii, Italy. **d** Pellets aged with NaOCl solution and light at different times of ageing: (*top panel*) two-layered vermilion/gypsum pellet, aged in a cyclic system; single-layered vermilion pellet, aged in (*middle panel*) cyclic and (*bottom panel*) closed system; **e** Visible and local backscattered electron (BSE) image of two-layered vermilion/NaCl pellet, aged with NaOCl in a closed system; the table shows quantitative SEM analyses results performed on the four points shown in the BSE image (in atomic percentage; Hg, S, Cl, and Na concentrations were normalized to a total of 100%; C, O, and Al data not shown here). Adapted from [170]

α -HgS model samples when exposed to light and a sodium hypochlorite solution. Together with these compounds, sulfates were detected as well, and more particularly gypsum ($\text{CaSO}_4 \cdot 2\text{H}_2\text{O}$) when Ca was originally present in the model sample. These experiments also showed that light is a necessary factor to obtain degradation. From the relevant Pourbaix diagrams, it follows that both calomel and corderoite can be formed at basic pH, which is consistent with their formation in the presence of NaOCl solution (pH 12) during artificial ageing experiments. These compounds appear to be formed simultaneously, but the visual aspect of the samples changed during the course of the ageing experiments, showing different steps and colors. In order to remain stable, corderoite needs chlorine to be always available as a reagent. In the case of aging in O_2 -rich circumstances, corderoite after some time disappeared and was converted into calomel. It, therefore, appears that corderoite is an intermediate product in the reaction of the formation of calomel from α -HgS. Mapping of cross-sections obtained from the artificially aged samples revealed a multi-layered structure similar to the ones observed on altered works of art, with mercury chloride compounds on top of red mercury sulfide layers and sulfates at the surface of the samples. Compounds containing both S and Cl are found in intermediate layers. Concerning the visual aspect of the degradation of red mercury sulfide, the different compounds detected on the pellets and on historical paintings (calomel, corderoite, kenhshuite, gypsum) explain the observed white/purple colors, but not the black one. The attribution of the black colour to meta-cinnabar (β -HgS)

turned out to be unfounded. Theoretical spectroscopic results have indicated that none of the minerals identified as degradation compounds on mercury sulfide samples is intrinsically gray or black [165]. The presence of elemental mercury was proposed as a by-product of the photo-induced mechanism that causes the darkening of the paintings. In some conditions, the formation of Hg^0 from HgS is indeed thermodynamically favorable. By means of electrochemical methods [164, 173], the formation of metallic mercury from HgS by the joint action of light and chloride ions could be experimentally demonstrated. All the above consideration could be brought together in the following sequence of chemical transformations:



By means of a combination of laboratory-based experiments and thermodynamic modeling, the mechanism(s) and kinetics of cinnabar alteration in fresco applications was further clarified, specifically the role of light, humidity, and chlorine ions. Additionally, possible pathways and preventive and remedial conservation treatments during or immediately following excavation were explored to inhibit or retard darkening of cinnabar pigmented fresco surfaces [174].

Arsenic sulfide pigments (As_xS_y) are yellow (orpiment, As_2S_3) to orange-red (realgar, As_4S_4) p-type semi-conductors that have been used as wall painting pigments since antiquity, especially in Asia or Egypt [175, 176] and in illuminated manuscripts [177–179]. They have been used less extensively in Europe where less toxic or easier-to-use alternatives, such as lead–tin yellow, lead chromate, or cadmium yellow, were available and preferred. Nonetheless, both orpiment and realgar are frequently found in easel paintings, especially during the Venetian renaissance era and in still life or portrait details [180]. It is not also uncommon to find them in sculptures or decorative art objects [181]. Their sensitivity to light and resulting photo-oxidation in works of art is well described and often identified [182–184]: realgar ($\alpha\text{-As}_4\text{S}_4$, monoclinic, red) first becomes para-realgar ($\beta\text{-As}_4\text{S}_4$, monoclinic, yellow) which then turns into arsenolite (As_2O_3 , white) while orpiment (As_2S_3 , yellow-gold) directly turns into arsenolite [176, 180, 182, 185, 186]. In oil paintings, the chemical degradation of emerald green ($\text{Cu}(\text{C}_2\text{H}_3\text{O}_2)_2 \cdot 3\text{Cu}(\text{AsO}_2)_2$) and of arsenic sulfide pigment have arsenic trioxide (As_2O_3) as a common degradation end product. In such paintings where this degradation takes place, arsenic is no longer confined to the pigment particles, but is detected via elemental X-ray analysis throughout the whole paint system, e.g., at layer interfaces, in varnishes, around iron- and aluminium-containing particles, and in the wood structure of a panel painting. The migrated arsenic is thought to be transported within the paint system as arsenic trioxide in aqueous form (H_3AsO_3) by the same mechanism as its transport in groundwater in the environment. In environmental studies, the oxidation of $\text{As}(+\text{III})$ to $\text{As}(+\text{V})$ is well documented; dispersed arsenic in paintings released from degraded pigments can, therefore, be a marker for water-linked transport processes [180]. In a cross section from *A Stone Cartouche with a Garland of Flowers* (1655) by the Flemish seventeenth century painter Daniel Seghers (1590–1661), a combination of FTIR and Raman microscopy and XANES

investigations was employed to identify and image the two oxidation states of the arsenic sulfide pigment and its secondary compounds—arsenite [As(+III), undegraded] and arsenate [As(+V), degraded]. This painting presented unquestionable signs of alteration as the yellow roses, originally painted using a mixture of arsenic sulfide and ochre, became transparent over time. The As-K edge μ -XANES spectra and maps collected from the cross section left no doubt that As(+V) compounds are effectively present while some of the corresponding Raman data are consistent with this [187]. Some indications are already available that the mineral schultenite (PbHAsO_4) can be formed in situ; a positive identification of this degradation compound by means of XRD could be realized in several seventeenth century paintings by J. De Heem (unpublished data).

Smalt was commonly used as a pigment by artists between the sixteenth and eighteenth centuries. It is a powdered blue potash glass colored by cobalt ions that easily degrades in oil paint, causing sometimes dramatic chromatic changes in the appearance of oil paintings. In many cases, reflection light microscopy demonstrated the presence of partially discolored smalt particles with a remaining blue core [188] (for an example, see Fig. 9b, c). The composition of smalt can vary considerably depending on the manufacturing process and the elements that are present in the raw materials in addition to the essential glass components silica, potassium oxide, and cobalt. It is known from historical documentary sources that smalt was available to artists in various grades with different color intensities, but it can be difficult to distinguish between pigment that is degraded and that which has always been rather grey in hue. Quantitative analysis of smalt pigment by SEM-EDX has proved to be a useful method of distinguishing between deteriorated and well preserved pigment based on the potassium content [189]. A typical pattern was encountered in a sample from Paolo Fiammingo's *The Sons of Boreas Pursuing the Harpies* (National Gallery London, NG 5467) [190]. In the upper layer of the cross section, where the smalt is mixed with lead white, it is well preserved and contains around 13–14 w% K_2O . The smalt in the lower layer, which was mixed with only a little lead white, is degraded: the paint appears yellowish; the pigment has lost its color almost entirely and contains only 1–2% K_2O . In order to investigate the changes in the structure and environment around the cobalt ion on deterioration and to further the understanding of the basis of the loss of color, particles of well-preserved and altered smalt in micro-samples from paintings in the National Gallery, London, and the Louvre Museum, Paris, were analyzed using XAS at the Co K-edge [191]. XANES and EXAFS measurements showed that in intense blue particles, the cobalt is predominantly present as Co(+II) in tetrahedral coordination, whereas in colorless, altered smalt the coordination number of Co(+II) in the glass structure is increased, and there is a shift from tetrahedral toward octahedral coordination. The extent of this shift correlates clearly with the alkali content, indicating that it is caused by leaching of potassium cations, which act as charge compensators and stabilize the tetrahedral coordination of the cobalt ions that is responsible for the blue color. The same samples were analyzed complementarily by using vibrational techniques such as μ -RS and SR-FTIR microscopy [192]. Comparison of the resulting spectra with those from modern smalt, together with spectral decomposition and correlation with quantitative SEM-EDX analysis, shed

new light on the role of the various cations in the silicate structure. Important modifications in the structure of the pigment on alteration were revealed, in particular the leaching of alkali ions and the formation of silanol groups, which subsequently condense to create new bridging Si–O–Si bonds and molecular water in the glass. The degradation mechanism and progressive deterioration of smalt were reproduced while also a theoretical explanation for the connection between the discoloration process and structural atomic changes around the Co atom was provided [193].

From antiquity, the pigment ultramarine was prepared by grinding the semi-precious stone lapis lazuli (containing the mineral lazurite) into powder. It was one of the most expensive artists' pigments throughout history. Lapis lazuli is composed of various minerals, among which aluminosilicates of the sodalite group. The most notable is the mineral lazurite $(\text{Na,Ca})_8(\text{Al}_6\text{Si}_6\text{O}_{24})(\text{SO}_4,\text{S},\text{Cl})_2$ in which the cations and anions are trapped within the aluminosilicate framework. The pigment obtains its color from the fact that S_2^- and S_3^- anions are present inside the sodalite β -cages. Evidence of entrapment of carbon dioxide in the natural pigment from Afghanistan was found by Miliiani et al. [194], indicated by the IR absorption band at 2340 cm^{-1} and a low frequency satellite corresponding to the $^{13}\text{CO}_2$ isotopologue. The thermal behavior of natural ultramarine was studied by FTIR, UV–vis spectroscopy, and XRD, from 300 to 1120 K. Measurements showed that CO_2 and the encapsulated S_3^- chromophore behave in the same way during the heating experiment, starting to be released only at about 670 K when the apertures of the sodalite β -cages became larger as an effect of temperature. The absorption at 2340 cm^{-1} can be used as a reliable discriminant between Afghan (the most probable source prior to the nineteenth century for Western artworks) and artificial ultramarine, a fact of great interest when dealing with the authentication of artworks. Recently, the possibility was investigated to distinguish lapis lazuli of different geographic provenance based on their S–K edge XANES spectrum [195]. All examined lapis lazuli samples feature a S-XANES profile consistent with S_3^- being the dominant species (which considered to be the main responsible for the blue colour); however, also indications for the presence of species such as S_4^{2-} , S_4^- , and S_8 are apparent, depending on the origin of the material. However, the heterogeneity of the natural rocks hampers the straightforward association of one specific S K-edge XANES spectrum to a region of provenance. The blue pigments used on altarpieces in the fifteenth century in Catalonia and Crown of Aragon are principally composed of the mineral azurite. To a lesser extent, lapis lazuli was used and occasionally in the background areas and for outlining the principal figures; indigo (of vegetal origin) was used for the chromatic preparation layer. Data from several altarpieces belonging to well-known artists of that time were analyzed by SR-XRD, benchtop FTIR and SR-FTIR microscopy, RS, and SEM-EDX. XRD and SR-FTIR proved to be especially useful. The application of several layers with decreasing particle size, starting with azurite and finishing with lapis lazuli relates these artworks van Eyck's "Adoration of the Mystic Lamb" [196]. Synthetic ultramarine shares many properties with its natural form. Both natural and synthetic ultramarine have long been considered to be highly stable to light and compatible with other pigments. With both pigment forms, in some circumstances, a grey-black

to greyish/yellow discoloration of ultramarine-containing paint may be observed. In historical paintings, this phenomenon is known as “ultramarine disease” and is generally attributed to a break-up of the binding medium. In a recent study on color changes resulting from the interaction of various inorganic pigments with acrylic binding media under UV irradiation, ultramarine blue was found to have a very significant influence on alkyd resin paint, including a loss of blue color [197]. The opening of the sodalite cages of ultramarine [198] can cause its chromophoric S-anions to be released, leading to a loss of color of the pigment itself. Recently, Al-K edge XANES was employed to investigate the white discoloration of synthetic ultramarine in twentieth century paintings [199]. In degraded areas (induced by exposure during 1 min to 3 M HCl), the Al K-edge XANES featured an additional peak, corresponding to octahedral, six coordinated aluminium; in undegraded ultramarine, only the signature from AlO_4 units, part of intact β -cages, are observed. From this difference, it may be possible to conclude that the degradation of ultramarine may involve the removal of Al from the aluminosilicate network.

3.3 Alteration of Late Nineteenth/Early Twentieth Century Artists' Pigments

Below, we describe a number of recent case studies where a combination of X-ray and vibrational spectromicroscopic methods, sometimes together with more conventional laboratory-based analysis techniques, was used to shed light onto the degradation mechanism of pigments employed by artists such as James Ensor, Henri Matisse, Vincent van Gogh, and contemporary artists. The degradation behavior of various yellow pigments such as chrome yellow (PbCrO_4 or $\text{PbCr}_{1-x}\text{S}_x\text{O}_4$ with $x \leq 0.8$), zinc yellow ($\text{K}_2\text{O} \cdot 4\text{ZnCrO}_4 \cdot 3\text{H}_2\text{O}$), cadmium yellow ($\text{CdS}/\text{Cd}_{1-x}\text{Zn}_x\text{S}$), and Naples yellow [$\text{Pb}(\text{SbO}_3)_2 \cdot \text{Pb}_3(\text{Sb}_3\text{O}_4)_2$] were investigated by means of μ -XAS and/or related methods, in addition, the degradation of minium (aka red lead, Pb_3O_4) and Prussian blue [$\text{MFe}^{\text{III}}[\text{Fe}^{\text{II}}(\text{CN})_6] \cdot x\text{H}_2\text{O}$, with $\text{M}=\text{K}^+$, NH_4^+ , or Na^+].

To elucidate the reasons for the darkening of the originally bright chrome yellow (CY) paint in works by Van Gogh (see Fig. 2), a combination of μ -XRF, S, and Cr K-edge μ -XANES together with scanning transmission electron microscopy coupled to energy electron loss spectroscopy (STEM-EELS) was employed [156, 200–207]. This alteration proved to be caused by the surface reduction of Cr(+VI) to Cr(+III), but was very hard to document in a convincing manner using a combination of electron microscopy, Raman, and FTIR spectromicroscopies only. In samples taken from various paintings and in artificially aged CY paint of that period, Cr(+III) species were found, usually at the boundary between the paint and varnish layers and in sulfur-rich areas (see Fig. 2h). μ -XANES profiling and mapping (Fig. 2e–g) allowed the determination of the superficial brown coating that is 2–3 μm in thickness and contains non-crystalline Cr(III) compounds such as $\text{Cr}_2\text{O}_3 \cdot 2\text{H}_2\text{O}$, $\text{Cr}_2(\text{SO}_4)_3 \cdot \text{H}_2\text{O}$, and/or $(\text{CH}_3\text{CO}_2)_7\text{Cr}_3(\text{OH})_2$ [200]. The high sensitivity towards darkening of this material could be traced back to the presence of monoclinic and/or orthorhombic $\text{PbCr}_{1-x}\text{S}_x\text{O}_4$ ($0 \leq x \leq 0.8$) co-precipitate phases that are less stable than monoclinic (S-free) PbCrO_4 [203–209]. A change from the

monoclinic to the orthorhombic structure is observed in $\text{PbCr}_{1-x}\text{S}_x\text{O}_4$ when x exceeds 0.4 [202, 208].

To gain a deeper understanding of the behavior of the different types of chrome yellows, a series of oil paint models was prepared and characterized using a variety of methods before and after photochemical aging. The materials were obtained by employing commercial and in-house synthesized powders of PbCrO_4 and $\text{PbCr}_{1-x}\text{S}_x\text{O}_4$ co-precipitates with different x values [202, 203]. Also, samples of 100-year-old commercial paint were subjected to aging and the resulting differences investigated at the micro- and nanoscale [200, 207]. In parallel, a large series of around 20 original chrome yellow paint samples, taken from paintings by Vincent van Gogh and some of his contemporaries were characterized [202]. By combining the results obtained from paint models and original paint samples, a number of conclusions could be reached:

- (a) Among the aged model oil paints, only those composed of a sulfate-rich orthorhombic $\text{PbCr}_{1-x}\text{S}_x\text{O}_4$ co-precipitate showed a significant darkening after photochemical aging. Cr K-edge μ -XANES investigations the formation of up to about 60% of Cr(+III) species in the outer layer of the most altered sample [203]. On the contrary, negligible alteration effects were observed when sulfate species (such as PbSO_4 and BaSO_4) were absent from the crystalline structure or were merely mechanically mixed with the original chrome yellow pigment. Only when the sulfate ions are inside the lead chromate crystal structure itself, the darkening phenomenon was apparent. This finding is attributed to a difference in solubility of the chromate compounds that becomes higher when their crystalline structure changes from monoclinic to orthorhombic [203]. By means of XRD, RS, and FTIR, it is possible to make clear the distinction between the different above-mentioned forms of chrome yellows [202, 208].
- (b) an evaluation of the influence of the wavelength (range) of UV–visible light on the photochemical reduction of the lead chromate-based pigments was also performed. Light-sensitive sulfur-rich/orthorhombic $\text{PbCr}_{1-x}\text{S}_x\text{O}_4$ ($x \sim 0.75$) co-precipitate was exposed to ranges of UV ($240 \leq \lambda \leq 400$ nm), UVA-VIS ($\lambda \geq 300$ nm), blue ($335 \leq \lambda \leq 525$ nm), and red ($\lambda \geq 570$ nm) light [203]. These experiments demonstrated that it is possible to slow down the darkening of this material by minimizing its exposure to wavelengths shorter than about 525 nm.
- (c) The above-mentioned forms of chrome yellow (both stable and less stable) were identified on about 20 embedded paint micro-samples originating from paintings by Van Gogh and some of his contemporaries. It was also possible to demonstrate that the identification of these different forms of chrome yellow is possible by carrying out non-invasive in situ analyses, i.e., by employing portable Raman and FTIR instrumentation. For example, in Van Gogh's paintings *Portrait of Gauguin* (Van Gogh Museum, Amsterdam, the Netherlands) and *Falling Leaves* (Les Alysamps, Kröller-Müller Museum, Otterlo, The Netherlands) the presence of the more light-sensitive $\text{PbCr}_{1-x}\text{S}_x\text{O}_4$ type of chrome yellow could be identified [202, 208].

By means of EELS, nanoscale maps of Cr(+VI), Cr(+III), and S(+VI)-containing species before and after light exposure of a historical light-sensitive chrome yellow paint were obtained [207]. This allowed a relatively simple degradation model to be proposed. Considering that this paint originally consists of nanograins of PbCrO_4 , $\text{PbCr}_{1-x}\text{S}_x\text{O}_4$, and PbSO_4 fixed in a porous network of cross-linked oil-based binder in which micro droplets of aqueous solution can be present, this model assumes that the degradation starts via an initial dissolution of CrO_4^{2-} ions into the aqueous phase. In their turn, these ions can react with the organic binder (oil) at those locations where the binder network and the water phase are in contact, thus oxidizing the binder material; this results in a reduction of the chromate ions to Cr(+III) compounds. The redox reaction is followed by precipitation of Cr_2O_3 as nanometer-thin outer layers on the surface of all particles that are present. Because of the leaching of chromate ions from the particles, several core-shell structures can be formed in situ on/in the particles.

An integrated approach based on a combination of diffuse reflectance UV-VIS, SR μ -XRF/ μ -XANES, and electron paramagnetic resonance (EPR) spectroscopies was used to study the photo-redox process in chrome yellows under the influence of monochromatic light of different wavelengths and several white light sources [205]. EPR spectroscopy was used as a complementary tool to SR-based X-ray methods due to its sensitivity for revealing species containing one or more unpaired electrons and for distinguishing different coordination geometries of paramagnetic centers, such as Cr(+V)-species. Semi-quantitative indications about the darkening of the paint surface were obtained by UV-VIS spectroscopy. The Cr speciation data highlighted that the reduction process was favored not only by (blue) wavelengths in the 400–460 nm range (i.e., where the pigment shows its maximum absorption), but also by (green) light in the 490–530 nm range. The first evidence of the presence of Cr(+V)-intermediates in the $\text{Cr}(+\text{VI}) \rightarrow \text{Cr}(+\text{III})$ reduction reaction was also gathered; this allowed the risks of inducing photo-degradation of the 490–530 nm wavelength range to be explained.

In order to distinguish between the transformations induced by specific relative humidity (RH)/temperature conditions (i.e., >50% RH and a fixed temperature of 40 °C) and exposure to light, monoclinic PbCrO_4 , and orthorhombic $\text{PbCr}_{0.2}\text{S}_{0.8}\text{O}_4$ were subjected to separate or combined thermal and photo-chemical ageing protocols [206]. Diffuse reflectance UV-VIS and FTIR spectroscopies were used to obtain information associated with chromatic changes and the formation of organo-metal degradation products at the paint surface in combination with the above-mentioned Cr-speciation techniques. Under the thermal aging conditions employed, Pb(+II)-carboxylates and reduced Cr-compounds (in abundance of up to about 35% at the surface) were identified in the lead chromate-based paints. The tendency of chromates to become reduced increased with increasing moisture levels and was favored for the orthorhombic $\text{PbCr}_{0.2}\text{S}_{0.8}\text{O}_4$ compound. In the case of thermally aged paint models, a higher relative abundance of Cr(+V)-species were observed than in the case of the equivalent photo-degraded material where mainly Cr(+III) species were encountered. In paint models first subjected to a thermal treatment and then exposed to light, compounds ascribable to the oxidation of the organic binder

were detected for all chrome yellow types investigated; however, the initial thermal treatment increased the tendency toward photo-reduction of the $\text{PbCr}_{0.2}\text{S}_{0.8}\text{O}_4$ pigment only. For this light-sensitive compound, the variation in thickness of the photo-altered layer (containing ca 70% of reduced forms of Cr) as a function of moisture levels could be attributed to a surface passivation phenomenon taking place prior to photochemical aging.

Three micro-samples from two varnished paintings by Van Gogh and a waxed low relief by Gauguin (all originally uncoated) were examined with the aim of better understanding whether or not the application of the top coating influenced the morphological and/or physicochemical properties of the chrome yellow paint underneath [204, 209]. In all samples studied, regardless of the nature of the coatings (resins or wax), μ -XRF and Cr-K edge μ -XANES measurements showed that Cr(+III) alteration products were present in the form of grains inside the coating (generally enriched in S-species); the Cr(+III) compounds were also homogeneously spread at the paint surface. Inside the coating and within the grains, the alteration compounds were present in abundance up to 70 and 100%, respectively, and were identified as Cr(+III)-sulfates and -oxides. The distribution of Cr(+III) species may be explained by mechanical friction caused by brush-application of the coating that picked up and redistributed superficially formed grains of secondary Cr-compounds, likely already present in the reduced state as result of the photodegradation process. On the basis of the study of varnished chrome yellow paint models, no evidence could be found of an actively Cr-reducing role of the varnish or of superficial S-species.

Firm evidence for the chemical alteration of chrome yellow pigments in Van Gogh's *Sunflowers* (Van Gogh Museum, Amsterdam; see Fig. 2) was recently presented [156]. Noninvasive in situ vibrational spectroscopic analysis at several spots on the painting was combined with SR-based μ -XRD, μ -Raman, and μ -FTIR investigations of two paint micro samples to reveal the presence of lightfast PbCrO_4 and light-sensitive $\text{PbCr}_{1-x}\text{S}_x\text{O}_4$ (with x approximately equal to 0.5). Cr(+III)-compounds, products of this degradation process, were found at the interface between the paint and the varnish (see Fig. 2h). Selected locations of the painting with the highest risk of color modification by chemical deterioration of chrome yellow were identified; see also Sect. 4 below.

The production records for lead chromate pigments present in the nineteenth century archive database of Windsor & NewtonTM (W&N) for the manufacture of their artists' materials, were recently systematically studied [210]. W&N produced essentially three pigment types: (a) lemon/pale chrome yellow, based on solid solutions of lead chromate and lead sulphate [$\text{Pb}(\text{Cr},\text{S})\text{O}_4$], (b) middle or pure monoclinic lead chromate (PbCrO_4), and (c) deep lead chromate that contains the latter admixed with basic lead chromate (Pb_2CrO_5), accounting for 53, 22, and 21% of the production, respectively. Production recipes for primrose yellow (4%) resulted in mixed crystals with a high percentage of lead sulphate. Each pigment type is characterized by only one or two main synthetic pathways; process variations reveal a systematic and thorough search for a high-quality durable product. A comparison of the chemical composition of pigment reconstructions with early W&N oil paint tubes showed that their records entitled "pale" and "lemon"

correlated with the pigment tubes labelled chrome yellow while the records “middle” and “deep” corresponded with the tubes labeled “chrome deep”.

Some of the properties of the chrome yellow varieties containing variable amounts of S have been examined by employing density functional theory (DFT) calculations in order to better understand their photo-degradation behavior [211]. The results show that the mixed $\text{PbCr}_{1-x}\text{S}_x\text{O}_4$ and the native PbCrO_4 share a similar electronic structure, although an energy up-shift of the conduction band is computed by both increasing the amount of sulfate and passing from the monoclinic to the orthorhombic phase. The calculations suggest that, when the degradation would be considered to be purely an electron-exchange phenomenon, the Cr(+VI) photo-reduction would more difficult for compounds with high sulfur concentration and an orthorhombic phase. In reality, however, the opposite is true. Thus, it is likely that the degradation is more strongly influenced by other factors, such as a different solubility and/or (nano-)morphology of the $\text{PbCr}_{1-x}\text{S}_x\text{O}_4$ materials. Another theoretical study attempts to answer the question whether or not the degradation of $\text{PbCr}_{1-x}\text{S}_x\text{O}_4$ is purely a surface phenomenon; also, the question whether the bulk properties of the sulfur-rich pigment material trigger the process is still open [212]. First-principles calculations were employed to investigate the role of sulfur in defining bulk properties such as structure, stability, and optical properties of the materials. The calculations support the hypothesis that an initial local segregation of lead sulfate could take place. This material would then absorb UV light, thus providing the necessary energy for subsequent reduction of chromate ions into the greenish chromic oxide. To date, no experimental evidence to support this was found.

The darkening of zinc yellow ($\text{K}_2\text{O}\cdot 4\text{ZnCrO}_4\cdot 3\text{H}_2\text{O}$), as observed in *A Sunday at La Grande Jatte* (G. Seurat, 1884, Art Institute of Chicago, Chicago, IL, USA) was studied by a combination of EELS and Cr-K edge XANES on artificially aged model paint samples and on original micro paint samples [213, 214]. To observe changes, more corrosive circumstances that needed for chrome yellows were needed, involving a combination of SO_2 gas, 50/90% humidity and light. Next to Cr(+III) species also dichromate ions [containing Cr(+VI)] were found as degradation products.

Cadmium yellow ($\text{CdS}/\text{Cd}_{1-x}\text{Zn}_x\text{S}$) is another class of yellow pigments frequently employed in the early twentieth century by painters such as Henri Matisse, James Ensor, Edvard Munch, and Vincent van Gogh. Cd-based pigments share a common hexagonal wurtzite structure in which cadmium and sulfur can be partially substituted to generate ternary phases with a wide range of colors from pale yellow to deep red. Among them, in $\text{CdS}_{1-x}\text{Se}_x$ solid solutions, the substitution of sulfur by selenium decreases the valence-to conduction energy gap, hereby modifying the color toward orange and red tonalities. UV–VIS–NIR and Raman micro-spectroscopies have been used for investigating the composition of ternary $\text{Cd}_{1-x}\text{Zn}_x\text{S}$ and $\text{CdS}_{1-x}\text{Se}_x$ solid solutions employed as artists' pigments [215, 216]. The goal was the determination of the solid solution stoichiometry of a series of Cd-containing paints, by exploiting the linear dependence of some absorption, emission, and scattering properties with the pigment composition. The high sensitivity of Raman spectroscopy to local compositional and structural heterogeneity permitted to

formulate a hypothesis about the possible presence of quaternary solid solutions based on the substitution of cadmium by zinc ($\text{CdS}_{1-x}\text{Zn}_x\text{S}_{1-y}\text{Se}_y$) in commercial pigments and by barium ($\text{CdS}_{1-x}\text{Ba}_x\text{S}_{1-y}\text{Se}_y$) in historical paints. By employing a combination of S K-edge μ -XANES and μ -XRD, it was established that the oxidation of the pigment cadmium yellow (α -CdS) to cadmium sulphate ($\text{CdSO}_4 \cdot \text{H}_2\text{O}$) (white/transparent) was the chemical transformation responsible for the loss of the bright yellow color in a painting by J. Ensor [217]. In a follow-up paper [218], the same authors discovered that another chemical pathway has given rise to the formation of an orange-grey superficial crust in a painting by Van Gogh called *Flowers in a Blue Vase* (1887, KMM), containing the grey/white mineral anglesite (PbSO_4) and cadmium oxalate. The chemical and physical alterations of cadmium yellow (CdS) paints in *Henri Matisse's Le bonheur de vivre* (aka *The Joy of Life*, 1905–1906, The Barnes Foundation, Philadelphia, PA, USA), shown in Fig. 3a, have been recognized since 2006, when a survey by portable X-ray fluorescence identified this pigment in all altered regions of the monumental painting. This alteration is visible as fading, discoloration, chalking, flaking, and spalling of several regions of light to medium yellow paint. Similar secondary Cd-compounds (see Fig. 3h), such as CdCO_3 , $\text{CdSO}_4 \cdot n\text{H}_2\text{O}$ (Fig. 3c–f), and CdC_2O_4 (Cd-oxalate) as found in the Ensor and Van Gogh paintings have been identified [219–221]. By using a combination of μ -XRF (Fig. 2g), 2D full-field XANES imaging (Fig. 2h), μ -XRPD (Fig. 3i), and FTIR imaging of the altered paint layers, the question was addressed what the roles of cadmium carbonates and cadmium sulfates are found in the altered paint layers [222]. These compounds have often been assumed to be photo-oxidation products, but could also be residual starting reagents from an indirect wet process synthesis of CdS. In thin sections of altered cadmium yellow paints from *Le bonheur de vivre* the distribution of various cadmium compounds confirms that cadmium carbonates and sulphates are photo-degradation products. On the other hand, in *Flower Piece* (1906, H. Matisse, The Barnes Foundation), the cadmium carbonates appear to be remnants of the CdS manufacturing process, where CdCO_3 is the starting reagent. By employing TOF–SIMS species-specific mapping of degraded paint samples, three categories of inorganic and organic components could also be co-localized throughout *i*: (1) species relating to the preparation and photo-induced oxidation of CdS yellow pigments, (2) varying amounts of long-chain fatty acids present in both the paint and primary ground layer, and (3) specific amino acid fragments, possibly relating to the painting's complex restoration history [223].

As of the 1840s, cadmium zinc sulfides were extensively employed by nineteenth and twentieth century artists. The direct band gap of CdS is 2.42 eV, but can be modulated by the progressive substitution of Cd with Zn, resulting in pale yellow cadmium zinc sulfide pigments. Rosi et al. developed an analytical methodology for the non-destructive identification of different forms of yellow $\text{Cd}_{1-x}\text{Zn}_x\text{S}$ solid solutions based on electronic and vibrational spectroscopies such as XRF, μ -RS, reflection mode UV–VIS–NIR, VIS–NIR emission spectroscopy, and XRD. Six commercial CdS-based pigments and four historical pigments from the early twentieth century were examined. The reflection behavior in the VIS range and the emission profiles in the VIS and NIR ranges reflected the pigment composition

while μ -RS allows to monitor the short range disorder in the CdS lattice caused by Zn substitution. Information on the stoichiometry of the solid solutions and on their local structure could be obtained via XRD and by employing different Raman on/off resonance excitation conditions [215].

Minium or red lead (Pb_3O_4) is another frequently employed pigment by Van Gogh and contemporary artists. This orange–red pigment has been used since Antiquity. It contains both Pb^{2+} and Pb^{4+} -ions and has sometimes been observed to lose its red color. These transformations are either described as darkening of the pigment caused by the formation of either plattnerite (β - PbO_2) or galena (PbS) or as whitening by which red lead is converted into anglesite (PbSO_4) or (hydro)cerussite ($2\text{PbCO}_3 \cdot \text{Pb}(\text{OH})_2$; PbCO_3). By examining a degraded paint sample from Van Gogh's *Wheat Stacks under a Cloudy Sky* (1889, KMM) by means of conventional 2D and tomographic XRPD, it was possible to elucidate the degradation mechanism of minium and identify a missing link compound [163]. The degradation process was understood to be induced by absorption of 550 nm (or shorter) wavelengths, promoting electrons from the valence to the conduction band of minium. These electrons may reduce $\text{Pb}(+\text{IV})$ to $\text{Pb}(+\text{II})$. The in situ formed Pb^{2+} (perhaps in the form of PbO) then captures CO_2 (either atmospheric or the result of oxidation of the paint binding medium) to form various lead carbonates. Next to the frequently encountered cerussite and hydrocerussite, a very rare lead mineral, plumbonacrite ($3\text{PbCO}_3 \cdot \text{Pb}(\text{OH})_2 \cdot \text{PbO}$), was revealed to be present. The location of this compound was revealed via XRPD-tomography (Fig. 4b) of a hemispherical paint protrusion, at the centre of which a partially degraded grain of minium was present (see Fig. 4g, h). Evidence for the presence of a series of consecutive equilibria, gradually transforming plumbonacrite into cerussite via hydrocerussite was found. In a follow-up paper, the influence of several parameters on the tendency towards degradation of minium such as (a) a surplus of PbO inside the red lead material itself, (b) the pH, and (c) the concentration of available HCO_3^- or CO_3^{2-} -ions was investigated [224]. For demonstrating the photoactivity of the pigment, an electrochemical setup with a minium-modified graphite electrode (C | Pb_3O_4) was used. It could be confirmed that minium behaves as a *p*-type semiconductor, photoactive during illumination, and inactive in the dark. Raman measurements confirm the formation of degradation products. The photo-activity of the semiconductor pigment is partly defined by the presence of PbO impurities; these introduce new states in the original band gap. It was experimentally evidenced that the presence of PbO particles in minium leads to an upward shift of the valence band, reducing the band gap. Thus, upon photoexcitation, the electron/hole separation is more easily initialized. The $\text{PbO}/\text{Pb}_3\text{O}_4$ composite electrodes demonstrate a higher reductive photocurrent compared to the photocurrent registered at pure PbO or Pb_3O_4 -modified electrodes. In the presence of bicarbonate ions, a significantly higher photoreduction current is recorded because the PbO that is formed in situ reacts further to become hydrocerussite. It could be shown that the presence of bicarbonates in the environment stimulates the photodecomposition process of minium and plays an important role in the degradation process.

The fading of modern pigments based on Prussian blue blues [$\text{MFe}^{\text{III}}[\text{Fe}^{\text{II}}(\text{-CN})_6] \cdot x\text{H}_2\text{O}$, with $\text{M}=\text{K}^+$, NH_4^+ or Na^+], another class of pigments frequently

employed by Van Gogh [2] and other artists [69, 225], in the presence of various white pigments has also been investigated [138, 226–230]. Painted samples were studied by UV–VIS, Fe K-edge X-ray absorption, ^{57}Fe transmission Mössbauer spectroscopy, and attenuated total reflectance (ATR) infrared spectroscopy. XAS revealed an effective decrease in the iron coordination number in the aged samples, which, combined with Mössbauer data, suggest a reduction of the surface iron ions in the Prussian blue upon exposure to light.

4 State-of-the-Art X-ray-Based Chemical Imaging of Painted Works of Art

4.1 Macroscopic X-ray Fluorescence Imaging (MA-XRF)

In a number of recent papers, the results obtained via MA-XRF were compared to those obtained by other methods providing elemental distribution information on the square meter scale. Next to XRR, also neutron activation autoradiography (NAAR) provides information of this kind [231]. Given the differences between XRR, MA-XRF, and NAAR in the fundamental physical phenomena exploited, a theoretical comparison of their capabilities is not straightforward and critical comparisons of their use on the same painting were not available until recently. While NAAR images tend to be more difficult to interpret because they usually contain contributions from more than one element/pigment, MA-XRF maps provide more direct and intuitive information on the distribution of pigments. The different mechanism by which the images are created also affects the sharpness of the resulting image. In NAAR, for example both the copper and mercury radionuclides produce high-energy radiation. In the case the photographic film not in direct contact with the paint, the path the electrons must bridge between paint and film can cause blurring of the NAAR images. By contrast, MA-XRF images that are obtained by scanning can be much sharper in such cases. However, the absorption of characteristic XRF radiation emitted by elements in underlying paint layers by overlying strata may significantly influence the maps.

During the investigation of Rembrandt's painting *Susanna and the Elders* (Gemäldegalerie, Berlin, Germany), XRR, NAAR, and MA-XRF data were juxtaposed [232]. In the XRR images, which are dominated by the Pb distribution, many *pentimenti* (i.e., intentional changes to the composition, made by the original artist) are visible, but given the complex genesis of the painting, their identification in the radiograph was not straightforward. The painting features a considerable number of overpainted features and a wide range of pigments with different elemental tracers, including earth pigments (Mn/Fe), azurite (Cu), lead white (Pb), vermilion (Hg), and smalt (Co, As) are present. MA-XRF suffers from few spectral overlaps and the scanning of the painting was performed in a few tens of hours and in situ, i.e. in the museum itself. NAAR required the stay of the painting at a nuclear research facility for several weeks while inter-element interferences are more difficult to resolve. Moreover, only a limited number of elements contribute to the acquired autoradiographs, most notably Mn, Cu, As, Co, Hg, and P while highly

relevant elements such as (K), Ca, Fe, and Pb do not show up in the NAAR images. However, NAAR provides a higher lateral resolution and is less hindered by absorption in covering layers, which makes it the only method capable of visualizing P in lower paint layers. Comparison of the MA-XRF Pb and Hg distribution of *Susanna and the Elders* suggest, for example, that the first Elder's hand was repositioned several times.

Another painting by Rembrandt that was studied by both MA-XRF and NAAR is *An Old Man in Military Costume* (1630–31) in the J. Paul Getty Museum (Los Angeles, CA, USA) [151]. The objective of the study was to virtually reconstruct the hidden portrait below the one that is now visible. The challenge of reconstructing the overpainted figure in *An Old Man in Military Costume* was significantly advanced by the judicious combined use of imaging methods. XRR provided information on part of the face and the area of the eyes since it largely reflects the distribution of lead white. NAAR provided a strong image of the face and cloak of the underlying figure, along with an indication of the chemical composition. The single-element distribution maps produced by MA-XRF provided additional details into the shape of the underlying image and the composition of the pigments used. The underlying figure's face proved to be richer in mercury than the face of the figure on the surface. Likewise, the cloak of the underlying figure was found to be richer in copper than the surface figure although the nature of the copper-containing pigment could not be determined from these data. The use of iron earth pigments, specifically, Si-rich umbers, came forth from complementary information provided by the NAAR and MA-XRF maps; more specifically, the MA-XRF Fe distribution revealed the shape of the first portrait's gorget or collar. These data were used to create a false color digital reconstruction, yielding the most detailed representation of the underlying painting to date. This new reconstruction, and associated information on the pigments employed in both the upper and lower images serves to invigorate the art-historical discussion on the exact nature of the concealed figure and its significance in Rembrandt's oeuvre.

NAAR and XRF imaging were also used in the investigation of *The Reading Hermit* (1630), allegedly painted by Rembrandt [233].

Gradually, the elemental mapping capabilities of MA-XRF are being employed for the investigation of works of art other than oil paintings. Its applicability for investigating stained-glass windows inside a conservation studio was assessed by analyzing a well-studied late-medieval panel from the City Museum of Bruges (Belgium), showing Saint George and Saint Michael (see Fig. 7) [234]. Although accurate quantification of components is not feasible with this analytical imaging technique, plotting the detected intensities of K versus Ca in a scatter plot allowed distinguishing glass fragments of different compositional types within the same panel (Fig. 7c1–c4). In particular, clusters in the Ca/K correlation plot revealed the presence of two subtypes of potash glass and three subtypes of high lime-low alkali (HLLA) glass. MA-XRF results proved to be consistent with previous semi-quantitative SEM-EDX analyses on two glass micro-samples and theories on glass production in the Low Countries formulated in literature. A bi-plot of the intensities of the more energetic Rb-K versus Sr-K emission lines yielded a similar glass type differentiation and presented a suitable alternative in case the Ca/K signal ratio is

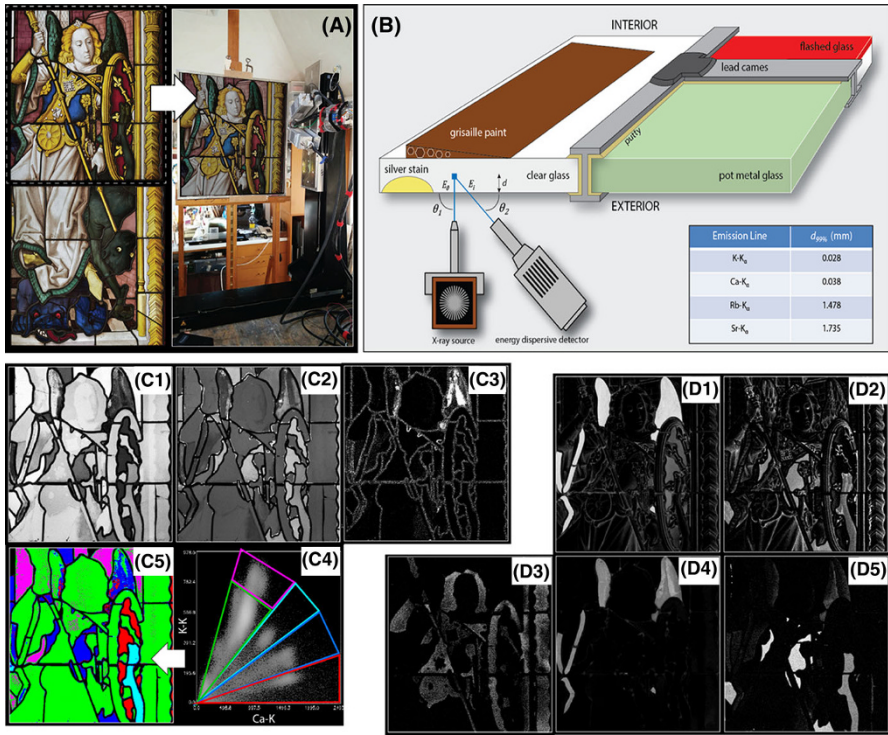


Fig. 7 Stained glass window from the collection of the City Museum of Bruges showing Saint Michael, dated ca. 1490, in front of the MA-XRF scanner; **b** schematic of build-up of a stained glass window and measurement geometry on interior side. The table lists sampling depths for different XRF energies; Elemental maps collected from the interior side: **c1** K, **c2** Ca, and **c3** S; **c4** Ca vs K-K α intensity scatter diagram with pixels clusters indicated; **c5** Locations of color-coded pixel clusters. Elemental maps collected from the interior side: **d1** Cu and **d2** Co; from the exterior side: **d3** Ag, **d4** Cu, and **d5** Co. Adapted from [234]

affected by superimposed weathering crusts. The MA-XRF maps permitted the identification of the chromophores responsible for the green, blue and red glass colors. In addition, by contrasting MA-XRF Maps from the interior with exterior side of the window, it was possible to discriminate between glass panes made in colored pot metal glass (i.e., glass that is colored throughout the pane) and those made in multi-layered flashed glass (i.e., colorless glass covered with one or more thin, intensely colored glass coatings). The benefit of obtaining compositional information from the entire surface, as opposed to point analysis, was illustrated by the discovery of what appears to be a green cobalt glass feature (see Fig. 7d) that was previously missed on this well-studied stained-glass window, both by connoisseurs and spectroscopic sample analysis. Generally, the major benefit is the ability to acquire compositional data from the entire surface in a non-invasive way. In addition, the ensuing chemical data can be presented in a visual way, hence making their interpretation easier for non-XRF specialists. However, in contrast with conventional SEM-EDX and μ -XRF point analyses on samples, MA-XRF experiments do not provide accurate quantitative composition information on the

different glass components. Although essentially qualitative in nature, the resulting insights are particularly useful for conservators who are typically interested in an efficient discrimination of the historical phases in one specific window rather than in the exact chemical composition of the different glass types present. The mobile aspect of the instrument allows performing the experiments directly inside a conservation studio and the ensuing elemental distribution maps can also serve as functional working drawings during the actual treatment. However, the lack of absolute concentration data of the various glass constituents does prevent inter-comparison of MA-XRF data obtained from different stained-glass windows. In this framework, combining the MA-XRF maps with SEM-EDX analyses on a limited number of samples is expected to be particularly relevant. Moreover, by creating MA-XRF maps, sampling locations for SEM-EDX investigations can be selected in a highly substantiated way. Thus, the number of micro-samples required for obtaining a comprehensive compositional overview of the glass types present in a glass window can be minimized and the resulting sample data can be extrapolated to the rest of the glass surface in a more confident manner.

The benefits and limitations of employing MA-XRF for the study of manuscript illuminations were recently discussed [235]. As a representative example of this type of objects, a fifteenth century Italian manuscript fragment from the collection of the Fitzwilliam Museum in Cambridge (UK) was investigated. MA-XRF scanning of this fragment was undertaken to gain insight into the materials and techniques of Renaissance illuminators and to help answer specific questions regarding its authorship and place of execution, currently considered to be either Bologna or Rome. The non-invasive analysis permitted to reconstruct the palette employed by the anonymous illuminator and highlighted the likely use of two unusual pigments: an arsenic sulphide glass and a manganese (hydr)oxide. Identification of the latter would have been difficult without an elemental Mn map, which showed no overlap with the Fe distribution, excluding the presence of umber pigments, widely used and, therefore, less distinctive of a specific artist or school. The use of manganese oxides as black pigments as hitherto been identified almost exclusively in easel paintings by a number of sixteenth century artists working in northern and central Italy, such as Perugino, with whom the unknown artist of the manuscript fragment shows stylistic affinities. Although MA-XRF could not provide a definite answer to the question of geographic origin, this kind of analysis did offer strong support to securely place the fragment within a specific artistic milieu. In order to realize a more precise and more reliable pigment identification on these type of artefacts, MA-XRF scanning is best combined with a series of RS or XRD point measurements.

MA-XRF was used together with optical coherence tomography (OCT) for the inspection of a late sixteenth century illuminated parchment manuscript (a gradual), originating from the Convent of the Benedictine Sisters in Lviv (Ukraine) (Fig. 8) [236]. It was employed both for mapping the elemental distribution over large parts of the folios (which included illuminated initials; see Fig. 8a–d), for quantitative analysis of the composition of the smalt pigment, and for documenting changes in the composition of the iron gall ink on different pages. OCT, by providing cross-sectional images of painted details, helped to interpret the XRF results. Of the two

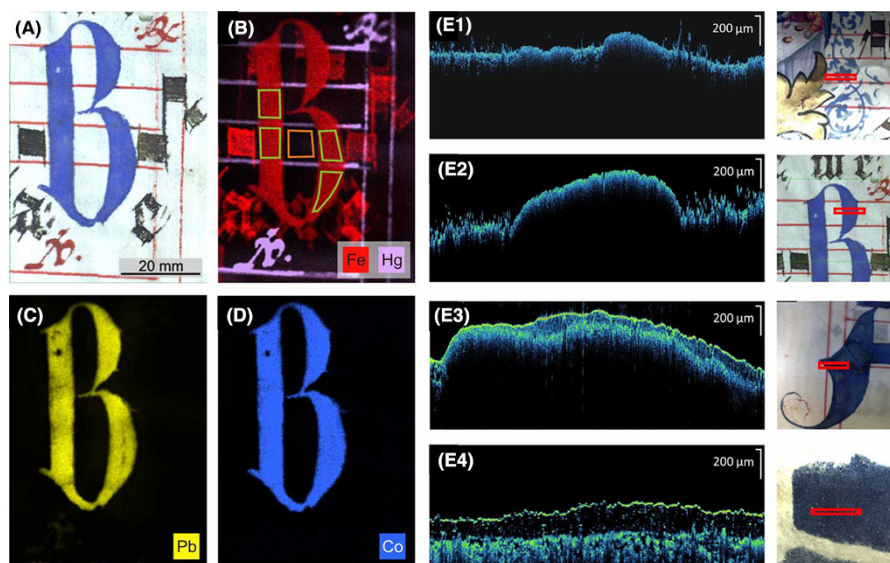


Fig. 8 **a** Optical photograph and elemental maps of **b** Fe, Hg, **c** Pb, and **d** Co a capital “B” from a sixteenth century gradual, originating from a Benedictine Convent (Lviv, Ukraine) **e** OCT profiles of several details of blue-lettering (*red rectangles*). Adapted from [236]

non-invasive techniques, MA-XRF appeared to be the more useful. As opposed to the local approach employed with PXRF, the ability of MA-XRF to scan large areas allows for a more general characterization of the object, not restricted to small regions of examination or to the collection of samples from them. OCT also yields images of relatively large structures; Fig. 8e shows virtual OCT cross sections of different locations on the manuscript. However, OCT suffers, due to the high scattering properties of historic parchment, from the drawback that the information retrieved is relatively limited.

To illustrate the interplay between spectroscopic methods for non-invasive imaging, for point measurements and for microscopic pigment identification/imaging, their combined use for a full characterization of the fifteenth century work of art, *Christ with Singing and Music-Making Angels*, by Hans Memling was described [21]. This involved the recording of MA-XRF and MA-rFTIR maps (see Fig. 1), providing information on Memling’s painting and colour rendering technique. For example, vermilion red was used in the cloak embroidery and in the bright red parts of the wings of some of the angels, while at a lower concentration level, it was also present in the flesh tones of the faces. In the more purplish tones, madder lake was the major colorant, sometimes mixed with azurite. The latter pigment was also employed in all blueish areas. For the hair of the angels, clay-containing earth pigments (Fe, e.g. from goethite) were employed, with lead tin yellow for the highlights. The worn gilded background features high Au and reflected infrared signals but also Ca and Fe signals, both of which originate from an underlying adhesive bole layer. In Fig. 1c, a composite of the relevant MA-XRF

elemental maps is shown. In the examined areas, almost no indications of *pentimenti* were encountered.

4.2 Studies Combining Large-Scale Chemical Imaging and Microscopic Paint Sample Analysis

Next to the use of MA-XRF and related methods for subsurface visualization of overpainted representations, this chemical form of imaging of paintings is also increasing being used as part of pigment degradation studies. Below a number of investigations are described where macroscopic chemical imaging is combined with microscopic analyses of minute paint samples.

4.2.1 Identification and Localization of Different Smalt Types in “Saul and David”, Rembrandt

The painting *Saul and David* shown in Fig. 9, is thought to date from c. 1652 and previously was attributed to Rembrandt van Rijn and/or his studio. It is a complex work of art, recently subjected to an intensive conservation treatment and associated investigation [153]. It was anticipated that its analysis would shed light on authenticity questions and Rembrandt’s role in the creation of the painting. The painting was thought to have been started in a colorful style characterized by great detailing and smooth handling of the paint. In contrast, the adjustments made to the painting during the second stage are painted very loosely; some scholars are in doubt whether this second stage was executed by Rembrandt—some of his assistants may have completed the work. It would seem that the painter was experimenting with the use of smalt in this second phase, since it was found over much of the painting, not only in the blue areas of the turban, which belong to the first phase. The extensive use of smalt, especially in mixtures with bone black, lakes, and earth pigments is considered typical of Rembrandt’s late painting technique. Its pigment combination was not only useful to create coloristic effects, but also for its drying properties and to give bulk and texture to the paint. As part of the investigation into the authenticity of the curtain area, a number of paint micro-samples were examined with light microscopy (LM) and SEM-EDX. Given that the earth, smalt, and lake pigments used in the painting could not be imaged with traditional imaging techniques, the entire painting was also examined with state-of-the-art non-invasive imaging techniques. Special attention was devoted to the presence of cobalt-containing materials, specifically the blue pigment smalt, considered characteristic for the Rembrandt’s late artistic production [152]. The painting and a selected number of MA-XRF distribution maps, recorded prior to removal of overpaint and darkened varnish layers, are shown in Fig. 9a, d, respectively. From the Fe and Co distribution maps, it is immediately clear that the upper right canvas piece (part γ) painted in a monochrome dark tone does not show the same origin as the canvas sections of *Saul and David* (parts α and β , respectively). Both Co and Fe appear to be present throughout the γ area at high abundance; the joins between the various sub-parts, as well as the entire γ -section were uniformly covered with an Fe- and Co-containing paint in order to dissimulate

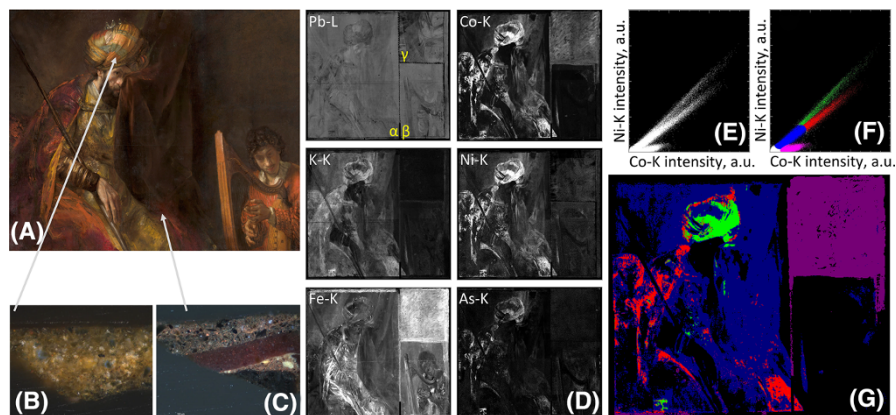


Fig. 9 *Saul and David* by Rembrandt, (c. 1652, 126 × 158 cm, Royal Museum Mauritshuis, Den Haag, the Netherlands, inv. no. MH621, oil on canvas); **b, c** Optical micrographs of two paint cross sections (locations indicated); **d** MA-XRF maps (1656 × 1311 pixels) of various elements present in the painting; **e** Ni-K vs. Co-K XRF intensity scatter plot; **f** as E, color codes: *green*: “high Ni”, *red*: “medium Ni”, *magenta*: “low Co/Ni”, *blue*: “rest”; **g** location map of color-coded pixels. Adapted from [152]

the differences with sections α and β . The Co map of the α -section demonstrates that smalt was extensively used in the areas of the turban, the curtain, Saul’s garments and his chair. K is associated with smalt, but also with red lake (likely from alum or KOH added during its production). The Fe-distribution in the α -section is quite different from the other elements since it is dominated by the earth pigment-containing areas, where the Fe concentration is much higher than in smalt (where it is of the order of a few wt%). The Co map has a patchy appearance at the left and bottom of the picture, areas corresponding to Saul’s cloak, which initially appears to have extended over the chair. The lighter (higher intensity) areas in the Co map correspond to the thicker/more intact smalt-rich paint. Paint cross-sections (Fig. 9c) from the dark patchy areas in the scans of Saul’s show the presence of an incomplete smalt-rich top paint layer applied on top of red lake glazes. The partial removal of the smalt paint from Saul’s garment and chair is most likely due to a misinterpretation during a past restoration, where a restorer tried to recover the bright red color of Saul’s cloak, obscured by a discolored and darkened smalt layer. In the Ni:Co correlation plot (Fig. 9e, f), the existence of smalt characterized by various distinct Ni:Co ratios is clearly visible. Next to the “medium Ni” group of pixels (labeled red in Fig. 9f), a smaller group of pixels (labelled green) is present characterized by a Ni:Co ratio that is ca. 25% higher than in the “medium Ni” group. This “high Ni” group of pixels is situated in Saul’s turban and some small parts of his clothing. The “medium Ni” group of smalt pixels corresponds to patchy areas of paint of uneven thickness that are present in Saul’s garment in sections α and β . The pixels belonging to the curtain area in the background between the figures of Saul and David, generally showing both a low Co and Ni intensity, were labelled blue. In magenta, a fourth group of pixels, characterized by a very low Ni to Co XRF intensity ratio is also visible in Fig. 9g, corresponding to the paint used to cover the canvas insert γ [153]. Microscopic examination of paint samples from this

section showed that Co is not present in the form of smalt pigment particles but in a more finely divided state, dispersed through the layer. The Co material was likely added to the nineteenth century overpaint as drying agent. In sections α and β however, the Co and Ni are definitely present inside coarsely ground smalt particles. The difference between the “medium Ni” and “high Ni” areas could also be found back in the quantitative SEM-EDX data of paint samples from both areas (shown in Fig. 9b, c). From analysis of a series individual smalt particles it was possible to infer that (a) the leaching process significantly decreases the K_2O content of the glass, typically from a level of 10–16 to 2–5 wt% while it does not seem to have a large effect on the observed NiO:CoO concentration ratio; (b) the two average NiO:CoO ratios obtained in both areas of the painting are significantly different at the 99% confidence level: the “turban area” particles on average show a mean NiO:CoO concentration ratio of 0.35 ± 0.06 (1 s) that is significantly higher than the average ratio of the particles in the “garment area” where it is 0.28 ± 0.07 . This observation is consistent with the MA-XRF scatter plots of Fig. 9e–g, were in the turban area, a Ni:Co intensity ratio that is ca. 25% higher than that in the garment area is observed. In this manner the combination of quantitative SEM-EDX analysis and MA-XRF scanning revealed that three types of Co-containing materials are present in the Saul and David painting.

4.2.2 Evidence for Pigment Degradation in “Sunflowers” by V. Van Gogh

The *Sunflowers* painting shown in Fig. 2 was painted by Vincent Van Gogh in Arles in 1888–89 as part of a series of seven, all depicting a bouquet of sunflowers in an earthenware pot. The extent to which spontaneously occurring color changes have influenced today’s outlook of the paintings has been questioned, while previous studies showed that CYs ($PbCr_{1-x}S_xO_4$ with variable sulfate content x) are prone to darkening due to (photo-)reduction. The formation of reduced Cr is more favored for sulfate-rich, lemon-yellow, orthorhombic $PbCr_{1-x}S_xO_4$ varieties of the pigment (with $x > 0.4$) than for the orange-yellow, monoclinic $PbCrO_4$ that is the most lightfast of these materials [200, 202, 203, 205, 206]. A combination of non-invasive methods such as MA-XRF, FTIR, and RS were performed in situ on the version of *Sunflowers* owned by the Van Gogh Museum (Fig. 2a). Microscopic investigation of minute paint samples was undertaken (1) to assess the extent to which the painting contains lightfast $PbCrO_4$ (henceforth denoted as LF-CY) and light sensitive S-rich $PbCr_{1-x}S_xO_4$ ($x > 0.4$) (LS-CY), and (2) to determine whether or not these pigments have been subject to a reduction process [156]. The MA-XRF maps of the painting (Fig. 2b, c) show that Pb and Cr are the main elemental constituents of the sunflower petals, the orange corollas and the table area. In the pale yellow background, Zn is the predominant element (Fig. 2b), suggesting the presence of zinc white (ZnO), while Pb and Cr are present in a significantly lesser quantities. In some of the ochre and orange tones of the sunflower petals, besides Pb and Cr, Hg, and/or Cu and As were also found (Fig. 2c), due to the presence of vermilion (HgS) and/or emerald green [$3Cu(AsO_2)_2 \cdot Cu(CH_3COO)_2$]. In areas of the sunflower petals and the upper region of the vase with no or very little Pb and Cr, Fe is the main constituent element instead, indicating the use of a yellow ochre (Fe-

hydroxide based pigment). All the above-mentioned pigments are frequently encountered in works by Van Gogh. In the green(ish) areas, besides Cu and As, Pb and Cr are sometimes found together too, suggesting the use of mixtures or overlapping brush strokes of emerald green and CYs. The Pb- L_{α} :Cr- K_{α} XRF intensity ratio changes throughout the painting (Fig. 2b), suggesting a distribution of different CY types. However, the presence of other Pb- and/or Cr-based pigments, also frequently used by Van Gogh, such as red lead (Pb_3O_4), lead white [$PbCO_3$, $Pb_3(CO_3)_2(OH)_2$], or viridian green ($Cr_2O_3 \cdot 2H_2O$), and variations of the paint thickness (giving rise to self-absorption of variable magnitude), could also cause a change in the Pb- L_{α} :Cr- K_{α} intensity ratio. No meaningful S-distribution maps could be recorded, mainly due to the spectral overlap between the S-K and Pb-M XRF signals and the limited MA-XRF sensitivity for these signals. More reliable insights into the distribution of the different types of CY were obtained by performing vibrational spectroscopic and structural analyses at a select number of points on the surface of the *Sunflowers* painting (see Fig. 2d for a summary of the results). In the light yellow table area, non-invasive Raman and reflection mid-FTIR analyses revealed the presence of LS-CY ($x \approx 0.5$). This finding was confirmed by SR-based μ -XRD and vibrational spectroscopic analysis of a sample from the region (F458/4). In the Zn-rich pale yellow background, Raman spectroscopy (Fig. 2d) again demonstrated the presence of LS-CY ($x \approx 0.5$). For the sunflower petals, various CYs appear to have been used. While in the light yellow areas, a type of LS-CY very similar to that detected in the table and background was identified by Raman spectroscopy, on the other hand, in the ochre-yellow petals, the presence of LF-CY (i.e., monoclinic $PbCrO_4$) was observed. Occasionally, this is mixed with LS-CY or red lead. Chrome orange and vermilion red are sometimes also present in the darker/orange petals. SR-based μ -XRD and μ -Raman mapping experiments of regions of interest of one of the studied paint samples (F458/1) confirmed the non-invasive analyses: LF-CY is the chief constituent of the orange-yellow shades, while LS-CY ($x \approx 0.5$) is the main phase in the lighter yellow hues. Clear indications for the gradual conversion of Cr(+VI) to Cr(+III) were found. Next to Cr(+III)-rich particles, Cr(+III)-species are present as a 2–3 μ m thick layer right at the varnish/paint interface. Here, the relative abundance of Cr(+III) is around 35%, decreasing to 0% when going deeper inside the yellow paint. This pattern is very similar to that previously observed in photochemically aged LS-CY ($x > 0.4$) paint models [200, 203, 205, 206]. In summary, the non-invasive identification and macro-scale level distribution of the light-sensitive chrome yellow in the *Sunflowers* painting in combination with analysis of paint micro samples has permitted to identify selected locations with the highest probability/risk of color change due to Cr(+VI) reduction and to provide the first evidence on the conservation state of chrome yellow in selected regions of the painting.

4.2.3 Combining MA-XRF and VNIR Hyperspectral Imaging for the Study of *Le Portrait, R. Magritte*

Diffuse reflectance imaging spectroscopy can be used to separate and identify many artist pigments by virtue of their unique electronic transitions and vibrational

features in the visible to reflective near infrared (400–2500 nm) [27, 157, 237–240]. When combined with MA-XRF scanning results, a more complete identification and mapping of artists' materials is possible [27].

“Le portrait” (*The Portrait*, 1935, The Museum of Modern Art (MoMA), New York City, NY, USA), shown in Fig. 10, is a painting by Belgian surrealist artist René Magritte (1898–1967). It is a classic example of Magritte’s imagery, characterized by the realistic representation of ordinary objects made surreal by context or their relationship to each other. In the corresponding XRR image, an underlying composition is visible, showing the head and torso of a female nude. A similarity between the figure in the XRR image and the upper left quarter of a painting by Magritte entitled “La pose enchantée” (*The Enchanted Pose*), presumed lost, can be recognized. Preliminary in situ analyses by means of PXRF suggested the presence of a chromium based pigment in the sky and of an iron oxide based pigment in the darker areas of the female face. To gain a more thorough and overall depiction of the hidden layer, MA-XRF was used to identify and map the distribution of key chemical elements representative of pigments commonly found in artists’ paintings, thus revealing information on the color palette employed by Magritte while painting “La pose enchantée”. Secondly, visible and near infrared (VNIR) hyperspectral imaging was performed to complement the information obtained by XRR and MA-XRF, both with respect to the hidden figure and to Magritte’s palette in both pictorial layers [157].

The results of these investigations are summarized in Fig. 10. The Pb distribution map (Fig. 10b) bears a significant and expected resemblance to the X-radiography, but is no longer encumbered by the stretcher and hardware and thus easier to interpret. The brushstrokes around the bottle confirm that the bottle was painted right on the top of original painting and that the background around it was painted afterwards. The female

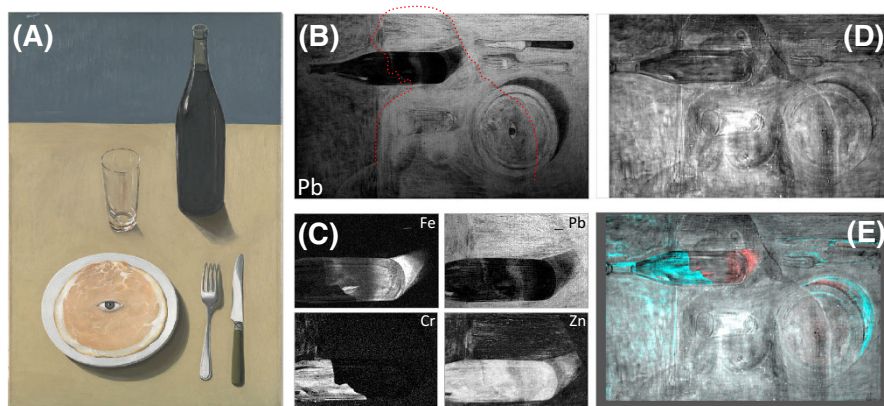


Fig. 10 **a** “Le portrait”, René Magritte (*The Portrait*, 1935; oil on canvas, 73.3×50.2 cm²; Metropolitan Museum of Modern Art—(c) C. Herscovici/Artists Rights Society (ARS), New York, USA); **b** rotated MA-XRF Pb-L map; **c** different detailed MA-XRF of the facial area with adjusted contrast; **d** first transmission mode NIR eigenimage of 1000–1500 nm spectral region (after histogram equalization); **e** composite image obtained by overlaying the image of **d** with Cr (light blue), Fe + Hg (red) MA-XRF maps. Adapted from [157]

figure is visible in the Pb map, showing that this element is more abundant in the highlights of her face and body. The Zn distribution map, looking like the negative of the Pb map, suggests the presence of this element in the ground layer. The dark color used in the bottle appears to stem mainly from carbon black, as Ca and P appear co-localized; Magritte used this pigment also in other paintings. Next to K and Fe, also Cd is detected in the black. It is not unusual for Magritte to modify the tonality of his blacks by mixing with other colors, such as cadmium yellow, in his palette. The same elements are also present in the dark green used to paint the shadow of the plate, the haft of the knife and the top of the bottle. The relative proportions vary slightly as does the green tonality. No other element related to the inorganic green pigment could be identified, suggesting the green was produced by mixing bone black with cadmium yellow, painted over the blue sky of the hidden painting. In subsequent measurements diffuse reflectance spectroscopy (DRS) supports the use of a cadmium yellow in the dark glass of the bottle, its shadow and in the knife handle given the observation of a sharp transition edge at 470 nm, consistent with the presence of CdS [241]. The Cr XRF signals, recorded in the shadow of the plate and knife and in the top half part of the bottle, only, suggest that Magritte did not use a chromium oxide green pigment as part of the top-level blue nor in the dark paint of the bottle and shadows. Rather, this element is present in the sky of the underlying painting, its X-ray fluorescence likely to be totally blocked by the lead white in the top ochre paint while the top blue paint and especially the black and dark green paint are (partially) transparent for Cr XRF radiation. No metallic elements (such as Co, Cu, Fe) were detected that could relate to the blue color on the top half of the painting using the MA-XRF scanning. This rules out many blue pigments such as cobalt, Prussian or cerulean blue; however, ultramarine blue ($\text{Na}_{8-10}\text{Al}_6\text{Si}_6\text{O}_{24}\text{S}_{2-4}$) cannot be ruled out (Na, Al, Si, and S, characteristic elements of ultramarine, are all difficult or impossible to detect in typical MA-XRF experimental conditions). PXRF measurements using a He flush revealed weak peaks for Al and Si, supportive of the assignment of ultramarine. DRS measurements of the blue background revealed a broad absorption centered at 597 nm and a peak reflectance at 483 nm, also consistent with the presence of ultramarine blue. The green shifted reflectance maximum may in part be due to a contribution of the chrome oxide below. The red color of the slice of ham and of the eyelid were rendered with vermilion red; this pigment was also used in the underlying composition, in highlights over the nose and lips of the nude (Fig. 10c, e). The MA-XRF Fe and Pb maps as well as the diffuse reflectance measurements show that the rest of the figure was painted with an iron oxide based red pigment and lead white for the highlights. NIR hyperspectral imaging of the painting (400–2450 nm wavelength range) in transmission mode was found to give more information about the pictorial features of the prior painted composition than imaging in reflectance mode. Principle component analysis (PCA) analysis, followed by histogram equalization was used to maximize the clarity of the features from the earlier painting [242, 243]. The appearance of the nude woman corresponds well to the photograph of the prior painting. In the spectral region from 1450 to 1680 nm, Minimum Noise Fraction PCA (MNF-PCA) yields a first eigenimage (Fig. 10d) that shows more of the sketches of the pictorial elements. Figure 10e clearly illustrates the complementary nature of MA-XRF and VNIR imaging. While in the darker areas, the XRF signals from the lower

figure can more easily reach the XRF detector that is positioned in a reflection geometry, the opposite is true for the NIR signals that were recorded in transmission. The lighter, more lead white-rich paint is more transparent for the NIR photons while the dark, boneblack-rich areas efficiently absorb the NIR radiation. In this particular case, both imaging methods together are capable of revealing all details of the face, showing the characteristic enlarged lips, nose, ears and eyes that are expected. In a similar study on a Degas portrait, it was possible by employing XRF data alone, to faithfully reconstruct the original colours of the overpainted face [244].

5 Conclusions

In this review, an overview was presented of recent developments regarding the characterization of pigmented materials used by painters from the seventeenth to early twentieth century based on various forms of X-ray-based spectroscopic and imaging analysis. XRF covers a wide range of instrumentation that can be profitably employed for this type of investigations, ranging from fairly compact and cost-effective portable devices to sophisticated synchrotron beam lines where elemental imaging with submicroscopic lateral resolution is possible. Microscopic XRF is well suited to visualize the elemental distribution of key elements, mostly metals, present in paint multilayers on the length scale from 1 to 100 μm inside paint micro-samples taken from paintings. In the context of the characterization of the pigments that suffer from spontaneous degradation, the use of methods limited to elemental analysis or imaging usually is not sufficient to elucidate the chemical transformations that have taken place. However, at synchrotron facilities, combinations of $\mu\text{-XRF}$ with related methods such as $\mu\text{-XAS}$ and $\mu\text{-XRD}$ have proven themselves to be very suitable for such studies. Their use is often associated with $\mu\text{-FTIR}$ and $\mu\text{-RS}$ spectroscopy since these methods deliver complementary information on the molecular nature of the materials present, at more or less the same length scale as the X-ray microprobe techniques. The combined use of these methods has allowed elucidating the degradation pathways of some of the pigments frequently employed by fifteenth to twentieth century painters such as P.P. Rubens, Rembrandt van Rijn, V. van Gogh, J. Ensor, and H. Matisse. Some of these studies are now started to be combined with mapping of the distribution of pigments on the square metre scale.

References

1. Cotte M, Checroun E, De Nolf W, Taniguchi Y, De Viguier L, Burghammer M, Walter P, Rivard C, Salomé M, Janssens K, Susini J (2016) Lead soaps in paintings: friends or foes? *Stud Conserv*. doi:10.1080/00393630.2016.1232529
2. Hendriks E (2011) Van Gogh's working practice: a technical study. In: Van Tilborgh L, Hendriks E (eds) *Vincent Van Gogh Paintings 2: Antwerp & Paris, 1885–1888*. Lund Humphries Publishers Ltd., London, pp 90–143
3. Jansen L, Luijten H, Bakker N (2009) *Vincent van Gogh—The Letters*. <http://www.vangoghletters.org>. Thames & Hudson Ltd., London

4. Janssens K, Alfeld M, Van der Snickt G, De Nolf W, Vanmeert F, Radepont M, Monico L, Dik J, Cotte M, Falkenberg G, Miliani C, Brunetti BG (2013) The use of synchrotron radiation for the characterization of artists' pigments and paintings. *Ann Rev Anal Chem* 6(6):399–425
5. Colombini MP, Modugno F (2004) Characterisation of proteinaceous binders in artistic paintings by chromatographic techniques. *J Sep Sci* 27:147–160
6. Vandenebeele P, Wehling B, Moens L, Dekeyzer B, Cardon B, von Bohlen A, Klockenkamper R (1999) Pigment investigation of a late-medieval manuscript with total reflection X-ray fluorescence and micro-Raman spectroscopy. *Analyst* 124:169–172
7. Wess TJ, Drakopoulos M, Snigirev A, Wouters J, Paris O, Fratzl P, Collins M, Hiller J, Nielsen K (2001) The use of small-angle X-ray diffraction studies for the analysis of structural features in archaeological samples. *Archaeometry* 43:117–129
8. Cesaratto A, D'Andrea C, Nevin A, Valentini G, Tassone F, Alberti R, Frizzi T, Comelli D (2014) Analysis of cadmium-based pigments with time-resolved photoluminescence. *Anal Methods* 6:130–138
9. Antunes V, Jose Oliveira M, Vargas H, Serrao V, Candeias A, Carvalho ML, Coroado J, Mirao J, Dias L, Longelin S, Seruya AI (2014) Characterization of glue sizing under calcium carbonate ground layers in Flemish and Luso-Flemish painting—analysis by SEM-EDS, mu-XRD and mu-Raman spectroscopy. *Anal Methods* 6:710–717
10. Lluveras A, Boulerand S, Roque J, Cotte M, Giraldez P, Vendrell-Saz M (2008) Weathering of gilding decorations investigated by SR: development and distribution of calcium oxalates in the case of Sant Benet de Bages (Barcelona, Spain). *Appl Phys Mater Sci Process* 90:23–33
11. Bell IM, Clark RJH, Gibbs PJ (1997) Raman spectroscopic library of natural and synthetic pigments (pre-similar to 1850 AD). *Spectrochim Acta Part A Mol Biomol Spectrosc* 53:2159–2179
12. Van Der Snickt G, De Nolf W, Vekemans B, Janssens K (2008) mu-XRF/mu-RS vs. SR mu-XRD for pigment identification in illuminated manuscripts. *Appl Phys A Mater Sci Process* 92:59–68
13. Andreotti A, Bonaduce I, Colombini MP, Gautier G, Modugno F, Ribechini E (2006) Combined GC/MS analytical procedure for the characterization of glycerolipid, waxy, resinous, and proteinaceous materials in a unique paint microsample. *Anal Chem* 78:4490–4500
14. Colombini MP, Andreotti A, Bonaduce I, Modugno F, Ribechini E (2010) Analytical strategies for characterizing organic paint media using gas chromatography/mass spectrometry. *Acc Chem Res* 43:715–727
15. Degano I, Ribechini E, Modugno F, Colombini MP (2009) Analytical methods for the characterization of organic dyes in artworks and in historical textiles. *Appl Spectrosc Rev* 44:363–410
16. Janssens K, Adams F, Rindby A (2000) Microscopic X-ray fluorescence analysis. Wiley, Chichester
17. Cotte M, Susini J, Dik J, Janssens K (2010) Synchrotron-based X-ray absorption spectroscopy for art conservation: looking back and looking forward. *Acc Chem Res* 43:705–714
18. De Nolf W, Janssens K (2010) Micro X-ray diffraction and fluorescence tomography for the study of multilayered automotive paints. *Surf Interface Anal* 42:411–418
19. Thoury M, Echard JP, Refregiers M, Berrie B, Nevin A, Jamme F, Bertrand L (2011) Synchrotron UV-visible multispectral luminescence microimaging of historical samples. *Anal Chem* 83:1737–1745
20. Bertrand L, Robinet L, Thoury M, Janssens K, Cohen SX, Schoder S (2012) Cultural heritage and archaeology materials studied by synchrotron spectroscopy and imaging. *Appl Phys A Mater Sci Process* 106:377–396
21. Janssens K, Legrand S, Van der Snickt G, Vanmeert F (2016) Virtual archaeology of altered paintings: multiscale chemical imaging tools. *Elements* 12:39–44
22. Janssens K, Dik J, Cotte M, Susini J (2010) Photon-based techniques for nondestructive subsurface analysis of painted cultural heritage artifacts. *Acc Chem Res* 43:814–825
23. Alfeld M, Broekaert JAC (2013) Mobile depth profiling and sub-surface imaging techniques for historical paintings—a review. *Spectrochim Acta Part B* 88:211–230
24. Miliani C, Rosi F, Brunetti BG, Sgamellotti A (2010) In situ noninvasive study of artworks: the MOLAB multitechnique approach. *Acc Chem Res* 43:728–738
25. Daffara C, Parisotto S, Mariotti PI (2015) Mid-infrared thermal imaging for an effective mapping of surface materials and sub-surface detachments in mural paintings: integration of thermography and thermal quasi-reflectography. In: Pezzati L, Targowski P (eds) *Optics for arts, architecture, and archaeology V*

26. Alfeld M, Janssens K, Dik J, de Nolf W, van der Snickt G (2011) Optimization of mobile scanning macro-XRF systems for the in situ investigation of historical paintings. *J Anal At Spectrom* 26:899–909
27. Dooley KA, Conover DM, Glinsman LD, Delaney JK (2014) Complementary standoff chemical imaging to map and identify artist materials in an early italian renaissance panel painting. *Angew Chem Int Edit* 53:13775–13779
28. De Nolf W, Dik J, Van der Snickt G, Wallert A, Janssens K (2011) High energy X-ray powder diffraction for the imaging of (hidden) paintings. *J Anal At Spectrom* 26:910–916
29. Legrand S, Alfeld M, Vanmeert F, De Nolf W, Janssens K (2014) Macroscopic Fourier transform infrared scanning in reflection mode (MA-rFTIR), a new tool for chemical imaging of cultural heritage artefacts in the mid-infrared range. *Analyst* 139:2489–2498
30. Daffara C, Pampaloni E, Pezzati L, Barucci M, Fontana R (2010) Scanning multispectral IR reflectography SMIRR: an advanced tool for art diagnostics. *Acc Chem Res* 43:847–856
31. Beckhoff B, Kanngiesser B, Langhoff N, Rainer W, Helmut W (2006) *Handbook of practical X-ray fluorescence analysis*. Springer, Berlin
32. Vincze L, Somogyi A, Osan J, Vekemans B, Torok S, Janssens K, Adams F (2002) Quantitative trace element analysis of individual fly ash particles by means of X-ray microfluorescence. *Anal Chem* 74:1128–1135
33. Vincze L, Janssens K, Adams F, Jones KW (1995) A general monte carlo simulation of energy-dispersive X-ray fluorescence spectrometers.3. Polarized polychromatic radiation, homogeneous samples. *Spectrochim Acta Part B At Spectrosc* 50:1481–1500
34. Vincze L, Janssens K, Vekemans B, Adams F (1999) Monte Carlo simulation of X-ray fluorescence spectra: part 4. Photon scattering at high X-ray energies. *Spectrochim Acta Part B At Spectrosc* 54:1711–1722
35. Lahanier C, Amsel G, Heitz C, Menu M, Andersen HH (1986) Proceedings of the international workshop on ion-beam analysis in the arts and archaeology—Pont-A-Mousson, Abbaye Des Pre-montres, France, February 18–20, 1985—Editorial. *Nucl Instrum Methods Phys Res Sect B Beam Interact Mater At* 14: R7–R8
36. Van Grieken R, Markowicz A (2002) *Handbook of X-ray spectrometry*. Marcel Dekker, New York
37. Van der Linden V, Meesdom E, Devos A, Van Dooren R, Nieuwdorp H, Janssen E, Balace S, Vekemans B, Vincze L, Janssens K (2011) PXRF, mu-XRF, Vacuum mu-XRF, and EPMA Analysis of Email Champeve Objects Present in Belgian Museums. *Microsc Microanal* 17:674–685
38. Carvalho ML, Karydas A, Piorek S (2010) Special issue: the use and application of handheld and portable XRF spectrometers. *X-Ray Spectrom* 39:77
39. Potts PJ, Ramsey MH, Carlisle J (2002) Portable X-ray fluorescence in the characterisation of arsenic contamination associated with industrial buildings at a heritage arsenic works site near Redruth, Cornwall, UK. *J Environ Monit* 4:1017–1024
40. Jones MC, Williams-Thorpe O, Potts PJ, Webb PC (2005) Using field-portable XRF to assess geochemical variations within and between dolerite outcrops of Preseli, south Wales. *Geostand Geoanal Res* 29:251–269
41. Piorek S (1997) Field-portable X-ray fluorescence spectrometry: past, present, and future. *Field Anal Chem Technol* 1:317–329
42. Piorek S (2004) Ieee, Portable X-ray fluorescence analyzer for the first level screening of materials for prohibited substances, 2005 International Conference on Asian Green Electronics: Design for Manufacturability and Reliability, Proceedings, pp 7–13
43. Piorek S, Puusaari E, Piorek E, McCann B (1999) Identification and quantitative analysis of alloys using x-ray fluorescence analyzer with a silicon “p-i-n” diode detector. In: Fernandez JE, Tartari A (eds) EDXRS-98: Proceedings of the European Conference on Energy Dispersive X-Ray Spectrometry 1998. Editrice Compositori, Bologna, p 280
44. Pages-Camagna S, Laval E, Vigears D, Duran A (2010) Non-destructive and in situ analysis of Egyptian wall paintings by X-ray diffraction and X-ray fluorescence portable systems. *Appl Phys A Mater Sci Process* 100:671–681
45. Eveno M, Moignard B, Castaing J (2011) Portable apparatus for in situ X-ray diffraction and fluorescence analyses of artworks. *Microsc Microanal* 17:667–673
46. Kriznar A, Munoz V, de la Paz F, Respaldiza MA, Vega M (2011) Portable XRF study of pigments applied in Juan Hispalense’s 15th century panel painting. *X-Ray Spectrom* 40:96–100
47. Migliori A, Bonanni P, Carraresi L, Grassi N, Mando PA (2011) A novel portable XRF spectrometer with range of detection extended to low-Z elements. *X-Ray Spectrom* 40:107–112

48. Kenna TC, Nitsche FO, Herron MM, Mailloux BJ, Peteet D, Sritrairat S, Sands E, Baumgarten J (2011) Evaluation and calibration of a Field Portable X-Ray Fluorescence spectrometer for quantitative analysis of siliciclastic soils and sediments. *J Anal At Spectrom* 26:395–405
49. Tykot RH (2016) Using nondestructive portable X-ray fluorescence spectrometers on stone, ceramics, metals, and other materials in museums: advantages and limitations. *Appl Spectrosc* 70:42–56
50. Galli A, Bonizzoni L (2014) True versus forged in the cultural heritage materials: the role of PXRF analysis. *X-Ray Spectrom* 43:22–28
51. Beck L, Rousseliere H, Castaing J, Duran A, Lebon M, Moignard B, Plassard F (2014) First use of portable system coupling X-ray diffraction and X-ray fluorescence for in situ analysis of prehistoric rock art. *Talanta* 129:459–464
52. Pitarch A, Ruiz JF, de Vallejuelo SFO, Hernanz A, Maguregui M, Madariaga JM (2014) In situ characterization by Raman and X-ray fluorescence spectroscopy of post-Paleolithic blackish pictographs exposed to the open air in Los Chaparros shelter (Albalate del Arzobispo, Teruel, Spain). *Anal Methods* 6:6641–6650
53. Dayer L, d'Errico F, Garcia-Moreno R (2014) Searching for consistencies in Chatelperronian pigment use. *J Archaeol Sci* 44:180–193
54. Bracci S, Caruso O, Galeotti M, Iannaccone R, Magrini D, Picchi D, Pinna D, Porcinai S (2015) Multidisciplinary approach for the study of an Egyptian coffin (late 22nd/early 25th dynasty): combining imaging and spectroscopic techniques. *Spectrochim Acta Part A Mol Biomol Spectrosc* 145:511–522
55. Madariaga JM, Maguregui M, Castro K, Knuutinen U, Martinez-Arkarazo I (2016) Portable Raman, DRIFTS, and XRF analysis to diagnose the conservation state of two wall painting panels from pompeii deposited in the Naples National Archaeological Museum (Italy). *Appl Spectrosc* 70:137–146
56. Madariaga JM (2015) Analytical chemistry in the field of cultural heritage. *Anal Methods* 7:4848–4876
57. Crupi V, Galli G, La Russa MF, Longo F, Maisano G, Majolino D, Malagodi M, Pezzino A, Ricca M, Rossi B, Ruffolo SA, Venuti V (2015) Multi-technique investigation of Roman decorated plasters from Villa dei Quintili (Rome, Italy). *Appl Surf Sci* 349:924–930
58. Gomez-Moron MA, Ortiz P, Martin-Ramirez JM, Ortiz R, Castaing J (2016) A new insight into the vaults of the kings in the Alhambra (Granada, Spain) by combination of portable XRD and XRF. *Microchem J* 125:260–265
59. Syta O, Rozum K, Choinka M, Zielinska D, Zukowska GZ, Kijowska A, Wagner B (2014) Analytical procedure for characterization of medieval wall-paintings by X-ray fluorescence spectrometry, laser ablation inductively coupled plasma mass spectrometry and Raman spectroscopy. *Spectrochim Acta Part B At Spectrosc* 101:140–148
60. Daveri A, Doherty B, Moretti P, Grazia C, Romani A, Fiorin E, Brunetti BG, Vagnini M (2015) An uncovered XIII century icon: particular use of organic pigments and gilding techniques highlighted by analytical methods. *Spectrochim Acta Part A Mol Biomol Spectrosc* 135:398–404
61. Cečhak T, Trojek T, Sefcu R, Chlumska S, Trestikova A, Kotrly M, Turkova I (2015) The use of powdered bismuth in Late Gothic painting and sculpture polychromy. *J Cult Herit* 16:747–752
62. Hradil D, Hradilova J, Bezdicka P, Svarcova S, Cermakova Z, Kosarova V, Nemeč I (2014) Crocoite PbCrO_4 and mimetite $\text{Pb}_5(\text{AsO}_4)_3\text{Cl}$: rare minerals in highly degraded mediaeval murals in Northern Bohemia. *J Raman Spectrosc* 45:848–858
63. Van der Snickt G, Miliani C, Janssens K, Brunetti BG, Romani A, Rosi F, Walter P, Castaing J, De Nolf W, Klaassen L, Labarque I, Wittermann R (2011) Material analyses of 'Christ with singing and music-making Angels', a late 15th-C panel painting attributed to Hans Memling and assistants: part I. non-invasive in situ investigations. *J Anal At Spectrom* 26:2216–2229
64. Duran A, Lopez-Montes A, Castaing J, Espejo T (2014) Analysis of a royal 15th century illuminated parchment using a portable XRF-XRD system and micro-invasive techniques. *J Archaeol Sci* 45:52–58
65. Van de Voorde L, Van Pevenage J, De Langhe K, De Wolf R, Vekemans B, Vincze L, Vandenberghe P, Martens MPJ (2014) Non-destructive in situ study of "Mad Meg" by Pieter Bruegel the Elder using mobile X-ray fluorescence, X-ray diffraction and Raman spectrometers. *Spectrochim Acta Part B At Spectrosc* 97:1–6

66. Veiga A, Teixeira DM, Candeias AJ, Mirao J, Manhita A, Miguel C, Rodrigues P, Teixeira JG (2015) Micro-analytical study of two seventeenth century gilded miniature portraits on copper. *Microchem J* 123:51–61
67. Roldan C, Juanes D, Ferrazza L, Carballo J (2016) Characterization of Sorolla's gouache pigments by means of spectroscopic techniques. *Radiat Phys Chem* 119:253–263
68. Van der Snickt G, Janssens K, Schalm O, Aibeo C, Kloust H, Alfeld M (2010) James Ensor's pigment use: artistic and material evolution studied by means of portable X-ray fluorescence spectrometry. *X-Ray Spectrom* 39:103–111
69. Kosarova V, Hradil D, Hradilova J, Cermakova Z, Nemeč I, Schreiner M (2016) The efficiency of micro-Raman spectroscopy in the analysis of complicated mixtures in modern paints: munch's and Kupka's paintings under study. *Spectrochim Acta Part A Mol Biomol Spectrosc* 156:36–46
70. Kajiya EAM, Campos P, Rizzutto MA, Appoloni CR, Lopes F (2014) Evaluation of the veracity of one work by the artist Di Cavalcanti through non-destructive techniques: XRF, imaging and brush stroke analysis. *Radiat Phys Chem* 95:373–377
71. Cardeira AM, Longelin S, Costa S, Candeias A, Carvalho ML, Manso M (2014) Multi-analytical characterisation of D'Apres Cormon by Jose Veloso Salgado. *Nucl Instrum Methods Phys Res Sect B Beam Interact Mater At* 331:271–274
72. Izzo FC, Capogrosso V, Gironde M, Alberti R, Mazzei C, Nodari L, Gambirasi A, Zendri E, Nevin A (2015) Multi-analytical non-invasive study of modern yellow paints from postwar Italian paintings from the International Gallery of Modern Art Ca Pesaro, Venice. *X-Ray Spectrom* 44:296–304
73. Trojek T, Trojkova D (2015) Several approaches to the investigation of paintings with the use of portable X-ray fluorescence analysis. *Radiat Phys Chem* 116:321–325
74. Cardeira AM, Longelin S, Costa S, Candeias A, Carvalho ML, Manso M (2016) Analytical characterization of academic nude paintings by Jose Veloso Salgado. *Spectrochim Acta Part A Mol Biomol Spectrosc* 153:379–385
75. Epley BA, Rogge CE (2015) Prior states: evolution of composition and color in two Barnett Newman paintings. *Appl Phys A Mater Sci Process* 121:987–998
76. Janssens K, Vekemans B, Vincze L, Adams F, Rindby A (1996) A micro-XRF spectrometer based on a rotating anode generator and capillary optics. *Spectrochim Acta Part B At Spectrosc* 51:1661–1678
77. Vincze L, Janssens K, Adams F, Rindby A, Engstrom P (1998) Interpretation of capillary generated spatial and angular distributions of x rays: theoretical modeling and experimental verification using the European Synchrotron Radiation Facility Optical beam line. *Rev Sci Instrum* 69:3494–3503
78. Schroer CG, Boye P, Feldkamp JM, Patommel J, Samberg D, Schropp A, Schwab A, Stephan S, Falkenberg G, Wellenreuther G, Reimers N (2010) Hard X-ray nanoprobe at beamline P06 at PETRA III. *Nucl Instrum Methods Phys Res Sect A Accel Spectrom Detect Assoc Equip* 616:93–97
79. Lengeler B, Schroer CG, Benner B, Gerhardus A, Gunzler TF, Kuhlmann M, Meyer J, Zimprich C (2002) Parabolic refractive X-ray lenses. *J Synchrotron Radiat* 9:119–124
80. Gorelick S, Vila-Comamala J, Guzenko VA, Barrett R, Salome M, David C (2011) High-Efficiency Gold Fresnel Zone Plates for Multi-keV X-rays. In: McNulty I, Eyberger C, Lai B (eds) 10th International Conference on X-Ray Microscopy, pp 88–91
81. Sarkar SS, Sahoo PK, Solak HH, David C, Van der Veen JF (2008) Fabrication of Fresnel zone plates by holography in the extreme ultraviolet region. *J Vac Sci Technol B* 26:2160–2163
82. Alianelli L, Sawhney KJS, Barrett R, Pape I, Malik A, Wilson MC (2011) High efficiency nanofocusing kinoform optics for synchrotron radiation. *Opt Express* 19:11120–11127
83. Barrett R, Baker R, Cloetens P, Dabin Y, Morawe C, Suhonen H, Tucoulou R, Vivo A, Zhang L (2011) Dynamically-figured mirror system for high-energy nanofocusing at the ESRF. In: Proceedings of SPIE, Advances in X-Ray/EUV optics and components VI, vol 8139, p 813904. doi:10.1117/12.894735
84. Bichlmeier S, Janssens K, Heckel J, Gibson D, Hoffmann P, Ortner HM (2001) Component selection for a compact micro-XRF spectrometer. *X-Ray Spectrom* 30:8–14
85. Trentelman K, Bouchard M, Ganio M, Namowicz C, Patterson CS, Walton M (2010) The examination of works of art using in situ XRF line and area scans. *X-Ray Spectrom* 39:159–166
86. Buzanich G, Wobrauschek P, Strelcić C, Markowicz A, Węgrzynek D, Chinea-Cano E, Griesser M, Uhlir K (2010) PART II (Portable ART analyzer)—development of a XRF spectrometer adapted for the study of artworks in the Kunsthistorisches Museum, Vienna. *X-Ray Spectrom* 39:98–102

87. Vittiglio G, Bichhneier S, Klinger P, Heckel J, Fuzhong W, Vincze L, Janssens K, Engstrom P, Rindby A, Dietrich K, Jembrih-Simburger D, Schreiner M, Denis D, Lakdar A, Lamotte A (2004) A compact mu-XRF spectrometer for (in situ) analyses of cultural heritage and forensic materials. *Nucl Instrum Methods Phys Res Sect B Beam Interact Mater At* 213:693–698
88. Bronk H, Rohrs S, Bjeoumikhov A, Langhoff N, Schmalz J, Wedell R, Gorny HE, Herold A, Waldschlager U (2001) ArtTAX—a new mobile spectrometer for energy-dispersive micro X-ray fluorescence spectrometry on art and archaeological objects. *Fresenius J Anal Chem* 371:307–316
89. Rabin I, Hahn O (2013) Characterization of the Dead Sea Scrolls by advanced analytical techniques. *Anal Methods* 5:4648–4654
90. Wolff T, Rabin I, Mantouvalou I, Kanngiesser B, Malzer W, Kindzorra E, Hahn O (2012) Provenance studies on Dead Sea scrolls parchment by means of quantitative micro-XRF. *Anal Bioanal Chem* 402:1493–1503
91. Valerio P, Silva RJC, Araujo MF, Soares AMM, Barros L (2012) A multianalytical approach to study the Phoenician bronze technology in the Iberian Peninsula—A view from Quinta do Almaraz. *Mater Charact* 67:74–82
92. Figueiredo E, Araujo MF, Silva RJC, Senna-Martinez JC, Vaz JLI (2011) Characterisation of Late Bronze Age large size shield nails by EDXRF, micro-EDXRF and X-ray digital radiography. *Appl Radiat Isot* 69:1205–1211
93. Herm C (2008) Mobile micro-X-ray fluorescence analysis (XRF) on medieval paintings. *Chimia* 62:887–898
94. Cheng L, Li MT, Youshi K, Fan CS, Wang SH, Pan QL, Liu ZG, Li RW (2011) The study of chemical composition and elemental mappings of colored over-glaze porcelain fired in Qing Dynasty by micro-X-ray fluorescence. *Nucl Instrum Methods Phys Res Sect B Beam Interact Mater At* 269:239–243
95. Dietz G, Ketelsen T, Hoss M, Simon O, Wintermann C, Wolff T, Rabin I, Hahn O (2012) The Egmont Master phenomenon: X-ray fluorescence spectrometric and paper studies for art history research. *Anal Bioanal Chem* 402:1505–1515
96. Sun TX, Ding XL (2015) Confocal X-ray technology based on capillary X-ray optics. *Rev Anal Chem* 34:45–59
97. Janssens K, Proost K, Falkenberg G (2004) Confocal microscopic X-ray fluorescence at the HASYLAB microfocus beamline: characteristics and possibilities. *Spectrochim Acta Part B At Spectrosc* 59:1637–1645
98. Woll AR, Agyeman-Budu D, Choudhury S, Coulthard I, Finnefrock AC, Gordon R, Hallin E, Mass J (2014) Lithographically-fabricated channel arrays for confocal X-ray fluorescence microscopy and XAFS. In: Arp U, Reversz P, Williams GP (eds) 17th Pan-American Synchrotron Radiation Instrumentation Conference (SRI 2013)
99. Bjeoumikhov A, Erko M, Bjeoumikhova S, Erko A, Snigireva I, Snigirev A, Wolff T, Mantouvalou I, Malzer W, Kanngiesser B (2008) Capillary mu Focus X-ray lenses with parabolic and elliptic profile. *Nucl Instrum Methods Phys Res Sect A Accel Spectrom Detect Assoc Equip* 587:458–463
100. Luhl L, Mantouvalou I, Schaumann I, Vogt C, Kanngiesser B (2013) Three-dimensional chemical mapping with a confocal xrf setup. *Anal Chem* 85:3682–3689
101. Woll AR, Agyeman-Budu D, Bilderback DH, Dale D, Kazimirov AY, Pfeifer M, Plautz T, Szebenyi T, Untracht G (2012) 3D X-ray fluorescence microscopy with 1.7 mu m resolution using lithographically fabricated micro-channel arrays. In: Goto S, Morawe C, Khounsary AM (eds.) *Proceedings of SPIE, Advances in X-Ray/EUV optics and components VII*, vol 8502, p 85020K. doi:10.1117/12.944365
102. Beckhoff B, Fliegau F, Ulm G, Weser J, Pepponi G, Strelci C, Wobrauschek P, Ehmann T, Fabry L, Mantler C, Pahlke S, Kanngiesser B, Malzer W (2003) Ultra-trace analysis of light elements and speciation of minute organic contaminants on silicon wafer surfaces by means of TXRF in combination with NEXAFS. *International Society for Optical Engineering*, pp 120–128
103. Woll AR, Bilderback DH, Gruner S, Gao N, Huang R, Bisulca C, Mass J (2005) Confocal x-ray fluorescence (XRF) microscopy: a new technique for the nondestructive compositional depth profiling of paintings. In: Vandiver PB, Mass JL, Murray A (eds) *Materials issues in art and archaeology VII*
104. Woll AR, Mass J, Bisulca C, Huang R, Bilderback DH, Gruner S, Gao N (2006) Development of confocal X-ray fluorescence (XRF) microscopy at the Cornell high energy synchrotron source. *Appl Phys A Mater Sci Process* 83:235–238

105. Smit Z, Janssens K, Proost K, Langus I (2004) Confocal mu-XRF depth analysis of paint layers. *Nucl Instrum Methods Phys Res Sect B Beam Interact Mater At* 219:35–40
106. Tsuji K, Matsuno T, Takimoto Y, Yamanashi M, Kometani N, Sasaki YC, Hasegawa T, Kato S, Yamada T, Shoji T, Kawahara N (2015) New developments of X-ray fluorescence imaging techniques in laboratory. *Spectrochim Acta Part B At Spectrosc* 113:43–53
107. Polese C, Cappuccio G, Dabagov SB, Hampai D, Liedl A, Pace E (2015) 2D and 3D micro-XRF based on polycapillary optics at XLab Frascati. In: Goto S, Morawe C, Khounary AM (eds) *Proceedings of SPIE, Advances in X-Ray/EUV optics and components X*, vol 9588, p 95880E. doi:10.1117/12.2189632
108. Smolek S, Nakazawa T, Tabe A, Nakano K, Tsuji K, Strelci C, Wobrauschek P (2014) Comparison of two confocal micro-XRF spectrometers with different design aspects. *X-Ray Spectrom* 43:93–101
109. Nakazawa T, Tsuji K (2013) Development of a high-resolution confocal micro-XRF instrument equipped with a vacuum chamber. *X-Ray Spectrom* 42:374–379
110. Mantouvalou I, Lange K, Wolff T, Grotzsch D, Luhl L, Haschke M, Hahn O, Kanngiesser B (2010) A compact 3D micro X-ray fluorescence spectrometer with X-ray tube excitation for archaeometric applications. *J Anal At Spectrom* 25:554–561
111. Tsuji K, Tabe A, Wobrauschek P, Strelci C (2015) Secondary excitation process for quantitative confocal 3D-XRF analysis. *Powder Diffr* 30:109–112
112. Wrobel P, Wegrzynek D, Czyzycki M, Lankosz M (2014) Depth profiling of element concentrations in stratified materials by confocal microbeam X-ray fluorescence spectrometry with polychromatic excitation. *Anal Chem* 86:11275–11280
113. Mantouvalou I, Wolff T, Seim C, Stoytschew V, Malzer W, Kanngiesser B (2014) Reconstruction of confocal micro-X-ray fluorescence spectroscopy depth scans obtained with a laboratory setup. *Anal Chem* 86:9774–9780
114. Czyzycki M, Wrobel P, Lankosz M (2014) Confocal X-ray fluorescence micro-spectroscopy experiment in tilted geometry. *Spectrochim Acta Part B At Spectrosc* 97:99–104
115. Huber C, Smolek S, Strelci C (2014) Simulation of layer measurement with confocal micro-XRF. *X-Ray Spectrom* 43:175–179
116. Wrobel P, Czyzycki M (2013) Direct deconvolution approach for depth profiling of element concentrations in multi-layered materials by confocal micro-beam X-ray fluorescence spectrometry. *Talanta* 113:62–67
117. Mantouvalou I, Malzer W, Kanngiesser B (2012) Quantification for 3D micro X-ray fluorescence. *Spectrochim Acta Part B At Spectrosc* 77:9–18
118. Schoonjans T, Silversmit G, Vekemans B, Schmitz S, Burghammer M, Riekel C, Brenker FE, Vincze L (2012) Fundamental parameter based quantification algorithm for confocal nano-X-ray fluorescence analysis. *Spectrochim Acta Part B At Spectrosc* 67:32–42
119. Laclavetine K, Ager FJ, Arquillo J, Respaldiza MA, Scrivano S (2016) Characterization of the new mobile confocal micro X-ray fluorescence (CXRF) system for in situ non-destructive cultural heritage analysis at the CNA: mu XRF-CONCHA. *Microchem J* 125:62–68
120. Reiche I, Muller K, Mysak E, Eveno M, Mottin B (2015) Toward a three-dimensional vision of the different compositions and the stratigraphy of the painting L'Homme bless, by G. Courbet: coupling SEM-EDX and confocal micro-XRF. *Appl Phys A Mater Sci Process* 121:903–913
121. Sun TX, Liu ZG, Wang GF, Ma YZ, Peng S, Sun WY, Li FZ, Sun XP, Ding XL (2014) Application of confocal X-ray fluorescence micro-spectroscopy to the investigation of paint layers. *Appl Radiat Isot* 94:109–112
122. Woll AR, Mass J, Bisulca C, Cushi-Nan M, Griggs C, Wanzly T, Ocon N (2008) The Unique History of The Armorer's Shop an application of confocal x-ray fluorescence microscopy. *Stud Conserv* 53:93–109
123. Kanngiesser B, Malzer W, Mantouvalou I, Sokaras D, Karydas AG (2012) A deep view in cultural heritage-confocal micro X-ray spectroscopy for depth resolved elemental analysis. *Appl Phys A Mater Sci Process* 106:325–338
124. Reiche I, Mueller K, Eveno M, Itie E, Menu M (2012) Depth profiling reveals multiple paint layers of Louvre Renaissance paintings using non-invasive compact confocal micro-X-ray fluorescence. *J Anal At Spectrom* 27:1715–1724
125. Yi LT, Liu ZG, Wang K, Lin X, Chen M, Peng SQ, Yang K, Wang JB (2016) Combining depth analysis with surface morphology analysis to analyse the prehistoric painted pottery from Majiayao Culture by confocal 3D-XRF. *Appl Phys A Mater Sci Process* 122

126. Choudhury S, Hormes J, Agyeman-Budu DN, Woll AR, George GN, Coulthard I, Pickering IJ (2015) Application of a spoked channel array to confocal X-ray fluorescence imaging and X-ray absorption spectroscopy of medieval stained glass. *J Anal At Spectrom* 30:759–766
127. Kanngiesser B, Mantouvalou I, Malzer W, Wolff T, Hahn O (2008) Non-destructive, depth resolved investigation of corrosion layers of historical glass objects by 3D Micro X-ray fluorescence analysis. *J Anal At Spectrom* 23:814–819
128. Yagi R, Tsuji K (2015) Confocal micro-XRF analysis of light elements with Rh X-ray tube and its application for painted steel sheet. *X-Ray Spectrom* 44:186–189
129. Li FZ, Liu ZG, Sun TX, Yi LT, Zhao WG, He JL, Peng S, Wang LL, Zhao GC, Ding XL (2015) Application of three dimensional confocal micro X-Ray fluorescence technology based on polycapillary X-Ray lens in analysis of rock and mineral samples. *Spectrosc Spectr Anal* 35:2487–2491
130. Janssens K, Vittiglio G, Deraedt I, Aerts A, Vekemans B, Vincze L, Wei F, Deryck I, Schalm O, Adams F, Rindby A, Knochel A, Simionovici A, Snigirev A (2000) Use of microscopic XRF for non-destructive analysis in art and archaeometry. *X-Ray Spectrom* 29:73–91
131. Terzano R, Spagnuolo M, Vekemans B, De Nolf W, Janssens K, Falkenberg G, Flore S, Ruggiero P (2007) Assessing the origin and fate of Cr, Ni, Cu, Zn, Ph, and V in industrial polluted soil by combined microspectroscopic techniques and bulk extraction methods. *Environ Sci Technol* 41:6762–6769
132. Janssens K, De Nolf W, Van Der Snickt G, Vincze L, Vekemans B, Terzano R, Brenker F (2010) Recent trends in quantitative aspects of microscopic X-ray fluorescence analysis. *Trac Trends Anal Chem* 29:464–478
133. Fittschen UEA, Falkenberg G (2011) Trends in environmental science using microscopic X-ray fluorescence. *Spectrochim Acta Part B At Spectrosc* 66:567–580
134. Salome M, Bleuet P, Bohic J, Cauzid J, Chalmin E, Cloetens P, Cotte M, De Andrade V, Martinez-Criado G, Petitgirard S, Rak M, Tresserras JAS, Szlachetko J, Tucoulou R, Susini J (2009) Fluorescence X-ray micro-spectroscopy activities at ESRF. In: David C, Nolting F, Quitmann C, Stambanoni M, Pfeiffer F (eds) 9th International Conference on X-Ray Microscopy Zurich, Switzerland, pp 012014
135. Hahn O, Oltrogge D, Bevers H (2004) Coloured prints of the 16th century: non-destructive analyses on coloured engravings from Albrecht Durer and contemporary artists. *Archaeometry* 46:273–282
136. Paternoster G, Rinziavillo R, Nunziata F, Castellucci EM, Lofrumento C, Zoppi A, Felici AC, Fronterotta G, Nicolais C, Piacentini M, Sciuti S, Venditelli M (2005) Study on the technique of the Roman age mural paintings by micro-XRF with Polycapillary Conic Collimator and micro-Raman analyses. *J Cult Herit* 6:21–28
137. Bertrand L, Cotte M, Stambanoni M, Thoury M, Marone F, Schoeder S (2012) Development and trends in synchrotron studies of ancient and historical materials. *Phys Rep Rev Sect Phys Lett* 519:51–96
138. Gervais C, Thoury M, Reguer S, Gueriau P, Mass J (2015) Radiation damages during synchrotron X-ray micro-analyses of Prussian blue and zinc white historic paintings: detection, mitigation and integration. *Appl Phys A Mater Sci Process* 121:949–955
139. Bertrand L, Schoeder S, Anglos D, Breese MBH, Janssens K, Moini M, Simon A (2015) Mitigation strategies for radiation damage in the analysis of ancient materials. *Trac Trends Anal Chem* 66:128–145
140. Nuyts G, Cagno S, Bugani S, Janssens K (2015) Micro-XANES study on Mn browning: use of quantitative valence state maps. *J Anal At Spectrom* 30:642–650
141. Rietveld HM (1969) A profile refinement method for nuclear and magnetic structures. *J Appl Crystallogr* 2:65–71
142. Dik J, Janssens K, Van der Snickt G, van der Loeff L, Rickers K, Cotte M (2008) Visualization of a lost painting by Vincent van Gogh using synchrotron radiation based X-ray fluorescence elemental mapping. *Anal Chem* 80:6436–6442
143. Alfeld M, Janssens K (2015) Strategies for processing mega-pixel X-ray fluorescence hyperspectral data: a case study on a version of Caravaggio's painting Supper at Emmaus. *J Anal At Spectrom* 30:777–789
144. Dik J, Wallert A, Van der Snickt G, Janssens K (2008) Silverpoint underdrawing? A note on its visualization with synchrotron radiation based x-ray fluorescence analysis. *Zeitschrift für Kunsttechnologie und Konservierung* 22:381–384
145. Struick van der Loeff L, Alfeld M, Meedendorp T, Dik J, Hendriks E, van der Snickt G, Janssens K, Chavennes M (2012) Rehabilitation of a flower still life in the Kröller-Müller Museum and a lost

- Antwerp painting by Van Gogh. In: van Tilborgh L (ed) Van Gogh: new findings. Van Gogh Museum, Amsterdam
146. Alfeld M, Janssens K, Appel K, Thijsse B, Blaas J, Dik J (2011) A portrait by Philipp Otto Runge—visualizing modifications to the painting using synchrotron-based X-ray fluorescence elemental scanning. *Zeitschrift für Kunsttechnologie und Konservierung* 25:157–163
 147. Howard DL, de Jonge MD, Lau D, Hay D, Varcoe-Cocks M, Ryan CG, Kirkham R, Moorhead G, Paterson D, Thurrowgood D (2012) High-Definition X-ray fluorescence elemental mapping of paintings. *Anal Chem* 84:3278–3286
 148. Alfeld M, Siddons DP, Janssens K, Dik J, Woll A, Kirkham R, van de Wetering E (2013) Visualizing the 17th century underpainting in Portrait of an Old Man by Rembrandt van Rijn using synchrotron-based scanning macro-XRF. *Appl Phys A Mater Sci Process* 111:157–164
 149. Alfeld M, Pedroso JV, Hommes MVE, Van der Snickt G, Tauber G, Blaas J, Haschke M, Erler K, Dik J, Janssens K (2013) A mobile instrument for in situ scanning macro-XRF investigation of historical paintings. *J Anal At Spectrom* 28:760–767
 150. Alfeld M, De Nolf W, Cagno S, Appel K, Siddons DP, Kuczewski A, Janssens K, Dik J, Trentelman K, Walton M, Sartorius A (2013) Revealing hidden paint layers in oil paintings by means of scanning macro-XRF: a mock-up study based on Rembrandt's "An old man in military costume". *J Anal At Spectrom* 28:40–51
 151. Trentelman K, Janssens K, van der Snickt G, Szafran Y, Woollett AT, Dik J (2015) Rembrandt's An Old Man in Military Costume: the underlying image re-examined. *Appl Phys A Mater Sci Process* 121:801–811
 152. Janssens K, Van der Snickt G, Alfeld M, Noble P, van Loon A, Delaney J, Conover D, Zeibel J, Dik J (2016) Rembrandt's 'Saul and David' (c. 1652): use of multiple types of smalt evidenced by means of non-destructive imaging. *Microchem J* 126:515–523
 153. Noble P, van Loon A, Alfeld M, Janssens K, Dik J (2012) Rembrandt and/or Studio, Saul and David, c. 1655: visualising the curtain using cross-section analyses and X-ray fluorescence imaging. *Technè* 36:35–45
 154. Verslype I (2012) The restoration of Woman in Blue Reading a Letter by Johannes Vermeer. *Rijksmuseum Bull* 60:2–19
 155. Bull D, Krekeler A, Alfeld M, Dik J, Janssens K (2011) An intrusive portrait by Goya. *Burling Mag* 153:668–673
 156. Monico L, Janssens K, Hendriks E, Vanmeert F, Van der Snickt G, Cotte M, Falkenberg G, Brunetti BG, Miliani C (2015) Evidence for degradation of the chrome yellows in van gogh's sunflowers: a study using noninvasive in situ methods and synchrotron-radiation-based X-ray techniques. *Angew Chem Int Edit* 54:13923–13927
 157. Van der Snickt G, Martins A, Delaney J, Janssens K, Zeibel J, Duffy M, McGlinchey C, Van Driel B, Dik J (2016) Exploring a hidden painting below the surface of Rene Magritte's Le Portrait. *Appl Spectrosc* 70:57–67
 158. Martins A, Albertson C, McGlinchey C, Dik J (2016) Piet Mondrian's Broadway Boogie Woogie: non invasive analysis using macro X-ray fluorescence mapping (MA-XRF) and multivariate curve resolution-alternating least square (MCR-ALS). *Herit Sci* 4:22. doi:10.1186/s40494-016-0091-4
 159. Martins A, Coddington J, Van der Snickt G, Van Driel B, McGlinchey C, Dahlberg D, Janssens K, Dik J (2016) Jackson Pollock's Number 1A, 1948: a non-invasive study using macro-x-ray fluorescence mapping (MA-XRF) and multivariate curve resolution—alternating least squares (MCR-ALS) analysis. *Herit Sci* 4:33. doi:10.1186/s40494-016-0105-2
 160. Ravaut E, Pichon L, Laval E, Gonzalez V, Eveno M, Calligaro T (2016) Development of a versatile XRF scanner for the elemental imaging of paintworks. *Appl Phys A Mater Sci Process* 122
 161. Anaf W, Schalm O, Janssens K, De Wael K (2015) Understanding the (in)stability of semiconductor pigments by a thermodynamic approach. *Dyes Pigm* 113:409–415
 162. Da Pieve F, Stankowski M, Hogan C (2014) Electronic structure calculations of mercury mobilization from mineral phases and photocatalytic removal from water and the atmosphere. *Sci Total Environ* 493:596–605
 163. Vanmeert F, Van der Snickt G, Janssens K (2015) Plumbonacrite identified by X-ray powder diffraction tomography as a missing link during degradation of red lead in a Van Gogh painting. *Angew Chem Int Edit* 54:3607–3610
 164. Anaf W, Trashin S, Schalm O, van Dorp D, Janssens K, De Wael K (2014) Electrochemical photodegradation study of semiconductor pigments: influence of environmental parameters. *Anal Chem* 86:9742–9748

165. Hogan C, Da Pieve F (2015) Colour degradation of artworks: an ab initio approach to X-ray, electronic and optical spectroscopy analyses of vermilion photodarkening. *J Anal At Spectrom* 30:588–598
166. Emslie SD, Brasso R, Patterson WP, Valera AC, McKenzie A, Silva AM, Gleason JD, Blum JD (2015) Chronic mercury exposure in Late Neolithic/Chalcolithic populations in Portugal from the cultural use of cinnabar. *Sci Rep* 5
167. Radepont M, de Nolf W, Janssens K, Van der Snickt G, Coquinot Y, Klaassen L, Cotte M (2011) The use of microscopic X-ray diffraction for the study of HgS and its degradation products corderoite (α -Hg₃S₂Cl₂), kenh suite (γ -Hg₃S₂Cl₂) and calomel (Hg₂Cl₂) in historical paintings. *J Anal At Spectrom* 26:959–968
168. Cotte M, Susini J, Metrich N, Moscato A, Gratziu C, Bertagnini A, Pagano M (2006) Blackening of Pompeian cinnabar paintings: X-ray microspectroscopy analysis. *Anal Chem* 78:7484–7492
169. Cotte M, Susini J, Sole VA, Taniguchi Y, Chillida J, Checroun E, Walter P (2008) Applications of synchrotron-based micro-imaging techniques to the chemical analysis of ancient paintings. *J Anal At Spectrom* 23:820–828
170. Radepont M, Coquinot Y, Janssens K, Ezrati J-J, de Nolf W, Cotte M (2015) Thermodynamic and experimental study of the degradation of the red pigment mercury sulfide. *J Anal At Spectrom* 30:599–612
171. Keune K, Boon JJ (2005) Analytical imaging studies clarifying the process of the darkening of vermilion in paintings. *Anal Chem* 77:4742–4750
172. Da Pieve F, Hogan C, Lamoën D, Verbeeck J, Vanmeert F, Radepont M, Cotte M, Janssens K, Gonze X, Van Tendeloo G (2013) Casting light on the darkening of colors in historical paintings. *Phys Rev Lett* 111
173. Anaf W, Janssens K, De Wael K (2013) Formation of Metallic Mercury During Photodegradation/ Photodarkening of alpha-HgS: electrochemical Evidence. *Angew Chem Int Ed* 52:12568–12571
174. Neiman MK, Balonis M, Kakoulli I (2015) Cinnabar alteration in archaeological wall paintings: an experimental and theoretical approach. *Appl Phys A Mater Sci Process* 121:915–938
175. Uda M (2004) In situ characterization of ancient plaster and pigments on tomb walls in Egypt using energy dispersive X-ray diffraction and fluorescence. *Nucl Instrum Methods Phys Res Sect B Beam Interact Mater At* 226:75–82
176. Daniels V, Leach B (2004) The occurrence and alteration of realgar on ancient Egyptian papyri. *Stud Conserv* 49:73–84
177. Muralha VSF, Burgio L, Clark RJH (2012) Raman spectroscopy analysis of pigments on 16-17th c. Persian manuscripts. *Spectrochim Acta Part A Mol Biomol Spectrosc* 92:21–28
178. Deneckere A, De Reu M, Martens MPJ, De Coene K, Vekemans B, Vincze L, De Maeyer P, Vandenebeele P, Moens L (2011) The use of a multi-method approach to identify the pigments in the 12th century manuscript Liber Floridus. *Spectrochim Acta Part A Mol Biomol Spectrosc* 80:125–132
179. Brown KL, Clark RJH (2004) The Lindisfarne Gospels and two other 8th century Anglo-Saxon/ Insular manuscripts: pigment identification by Raman microscopy. *J Raman Spectrosc* 35:4–12
180. Keune K, Mass J, Meirer F, Pottasch C, van Loon A, Hull A, Church J, Pouyet E, Cotte M, Mehta A (2015) Tracking the transformation and transport of arsenic sulfide pigments in paints: synchrotron-based X-ray micro-analyses. *J Anal At Spectrom* 30:813–827
181. Vermeulen M, Sanyova J, Janssens K (2015) Identification of artificial orpiment in the interior decorations of the Japanese tower in Laeken, Brussels, Belgium. *Herit Sci* 3:9
182. Trentelman K, Stodulski L, Pavlosky M (1996) Characterization of pararealgar and other light-induced transformation products from realgar by Raman microspectroscopy. *Anal Chem* 68:1755–1761
183. MunizMiranda M, Sbrana G, Bonazzi P, Menchetti S, Pratesi G (1996) Spectroscopic investigation and normal mode analysis of As₄S₄ polymorphs. *Spectrochim Acta Part A Mol Biomol Spectrosc* 52:1391–1401
184. Bindi L, Bonazzi P (2007) Light-induced alteration of arsenic sulfides: a new product with an orthorhombic crystal structure. *Am Miner* 92:617–620
185. Kyono A, Kimata M, Hatta T (2005) Light-induced degradation dynamics in realgar: in situ structural investigation using single-crystal X-ray diffraction study and X-ray photoelectron spectroscopy. *Am Miner* 90:1563–1570

186. Macchia A, Cesaro SN, Campanella L, Maras A, Rocchia M, Roscioli G (2013) Which light for cultural heritage: comparison of light sources with respect to realgar photodegradation. *J Appl Spectrosc* 80:637–643
187. Vermeulen M, Nuyts G, Sanyova J, Vila A, Buti D, Suuronen JP, Janssens K (2016) Visualization of As(III) and As(V) distributions in degraded paint micro-samples from Baroque- and Rococo-era paintings. *J Anal At Spectrom* 31:1913–1921
188. Boon JJ, Keune K, van der Weerd J, Geldof M, de Boer J (2001) Imaging microspectroscopic, secondary ion mass spectrometric and electron microscopic studies on discoloured and partially discoloured smalt in cross-sections of 16th century paintings. *Chimia* 55:952–960
189. Panighello S, Kavcic A, Vogel-Mikus K, Tennent NH, Wallert A, Hocevar SB, van Elteren JT (2016) Investigation of smalt in cross-sections of 17th century paintings using elemental mapping by laser ablation ICP-MS. *Microchem J* 125:105–115
190. Spring M, Higgitt C, Saunders D (2005) Investigation of Pigment-Medium Interaction Processes in Oil Paint containing Degraded Smalt. *Natl Gallery Tech Bull* 26:56–70
191. Robinet L, Spring M, Pages-Camagna S, Vantelon D, Trcera N (2011) Investigation of the discoloration of smalt pigment in historic paintings by micro-X-ray absorption spectroscopy at the Co K-Edge. *Anal Chem* 83:5145–5152
192. Robinet L, Spring M, Pages-Camagna S (2013) Vibrational spectroscopy correlated with elemental analysis for the investigation of smalt pigment and its alteration in paintings. *Anal Methods* 5:4628–4638
193. Cianchetta I, Colantoni I, Talarico F, d’Acapito F, Trapananti A, Maurizio C, Fantacci S, Davoli I (2012) Discoloration of the smalt pigment: experimental studies and ab initio calculations. *J Anal At Spectrom* 27:1941–1948
194. Miliani C, Daveri A, Brunetti BG, Sgamellotti A (2008) CO₂ entrapment in natural ultramarine blue. *Chem Phys Lett* 466:141–148
195. Gambardella AA, Patterson CMS, Webb SM, Walton MS (2016) Sulfur K-edge XANES of lazurite: toward determining the provenance of lapis lazuli. *Microchem J* 125:299–307
196. Salvado N, Buti S, Aranda MAG, Pradell T (2014) New insights on blue pigments used in 15th century paintings by synchrotron radiation-based micro-FTIR and XRD. *Anal Methods* 6:3610–3621
197. Pintus V, Wei SY, Schreiner M (2016) Accelerated UV ageing studies of acrylic, alkyd, and polyvinyl acetate paints: influence of inorganic pigments. *Microchem J* 124:949–961
198. Del Federico E, Shofberger W, Schelvis J, Kapetanaki S, Tyne L, Jerschow A (2006) Insight into framework destruction in ultramarine pigments. *Inorg Chem* 45:1270–1276
199. Cato E, Borca C, Huthwelker T, Ferreira ESB (2016) Aluminium X-ray absorption near-edge spectroscopy analysis of discoloured ultramarine blue in 20th century oil paintings. *Microchem J* 126:18–24
200. Monico L, Van der Snickt G, Janssens K, De Nolf W, Miliani C, Verbeeck J, Tian H, Tan H, Dik J, Radepon M, Cotte M (2011) Degradation process of lead chromate in paintings by Vincent van Gogh studied by means of synchrotron X-ray spectromicroscopy and related methods. 1. Artificially aged model samples. *Anal Chem* 83:1214–1223
201. Monico L, Van der Snickt G, Janssens K, De Nolf W, Miliani C, Dik J, Radepon M, Hendriks E, Geldof M, Cotte M (2011) Degradation process of lead chromate in paintings by Vincent van Gogh studied by means of synchrotron X-ray spectromicroscopy and related methods. 2. Original paint layer samples. *Anal Chem* 83:1224–1231
202. Monico L, Janssens K, Miliani C, Brunetti BG, Vagnini M, Vanmeert F, Falkenberg G, Abakumov A, Lu Y, Tian H, Verbeeck J, Radepon M, Cotte M, Hendriks E, Geldof M, van der Loeff L, Salvant J, Menu M (2013) Degradation process of lead chromate in paintings by Vincent van Gogh studied by means of spectromicroscopic methods. 3. Synthesis, characterization, and detection of different crystal forms of the chrome yellow pigment. *Anal Chem* 85:851–859
203. Monico L, Janssens K, Miliani C, Van der Snickt G, Brunetti BG, Guidi MC, Radepon M, Cotte M (2013) Degradation process of lead chromate in paintings by Vincent van Gogh studied by means of spectromicroscopic methods. 4. Artificial aging of model samples of co-precipitates of lead chromate and lead sulfate. *Anal Chem* 85:860–867
204. Monico L, Janssens K, Vanmeert F, Cotte M, Brunetti BG, Van der Snickt G, Leeuwestein M, Plisson JS, Menu M, Miliani C (2014) Degradation process of lead chromate in paintings by Vincent van Gogh studied by means of spectromicroscopic methods. Part 5. Effects of nonoriginal

- surface coatings into the nature and distribution of chromium and sulfur species in chrome yellow paints. *Anal Chem* 86:10804–10811
205. Monico L, Janssens K, Cotte M, Romani A, Sorace L, Grazia C, Brunetti BG, Miliani C (2015) Synchrotron-based X-ray spectromicroscopy and electron paramagnetic resonance spectroscopy to investigate the redox properties of lead chromate pigments under the effect of visible light. *J Anal At Spectrom* 30:1500–1510
 206. Monico L, Janssens K, Cotte M, Sorace L, Vanmeert F, Brunetti BG, Miliani C (2016) Chromium speciation methods and infrared spectroscopy for studying the chemical reactivity of lead chromate-based pigments in oil medium. *Microchem J* 124:272–282
 207. Tan H, Tian H, Verbeeck J, Monico L, Janssens K, Van Tendeloo G (2013) Nanoscale investigation of the degradation mechanism of a historical chrome yellow paint by quantitative EELS mapping of Cr species. *Angew Chem Int Ed* 52:11360–11363
 208. Monico L, Janssens K, Hendriks E, Brunetti BG, Miliani C (2014) Raman study of different crystalline forms of PbCrO_4 and $\text{PbCr}_{1-x}\text{S}_x\text{O}_4$ solid solutions for the noninvasive identification of chrome yellows in paintings: a focus on works by Vincent van Gogh. *J Raman Spectrosc* 45:1034–1045
 209. Monico L, Janssens K, Alfeld M, Cotte M, Vanmeert F, Ryan CG, Falkenberg G, Howard DL, Brunetti BG, Miliani C (2015) Full spectral XANES imaging using the Maia detector array as a new tool for the study of the alteration process of chrome yellow pigments in paintings by Vincent van Gogh. *J Anal At Spectrom* 30:613–626
 210. Otero V, Pinto JV, Carlyle L, Vilarigues M, Cotte M, Melo MJ (2016) Nineteenth century chrome yellow and chrome deep from Windsor & Newton. *Stud Conserv* 61:1–27
 211. Amat A, Miliani C, Fantacci S (2016) Structural and electronic properties of the PbCrO_4 chrome yellow pigment and of its light sensitive sulfate-substituted compounds. *RSC Adv* 6:36336–36344
 212. Munoz-Garcia AB, Massaro A, Pavone M (2016) Ab Initio Study of $\text{PbCr}_{(1-x)}\text{S}_x\text{O}_4$ Solid Solution: an Inside Look at Van Gogh Yellow Degradation. *Chem Sci* 7:4197–4203
 213. Casadio F, Xie S, Rukes SC, Myers B, Gray KA, Warta R, Fiedler I (2011) Electron energy loss spectroscopy elucidates the elusive darkening of zinc potassium chromate in Georges Seurat's *A Sunday on La Grande Jatte-1884*. *Anal Bioanal Chem* 399:2909–2920
 214. Zanella L, Casadio F, Gray KA, Warta R, Ma Q, Gaillard J-F (2011) The darkening of zinc yellow: XANES speciation of chromium in artist's paints after light and chemical exposures. *J Anal At Spectrom* 26:1090–1097
 215. Rosi F, Grazia C, Gabrieli F, Romani A, Paolantoni M, Vivani R, Brunetti BG, Colomban P, Miliani C (2016) UV–Vis–NIR and micro Raman spectroscopies for the non destructive identification of $\text{Cd}_{1-x}\text{Zn}_x\text{S}$ solid solutions in cadmium yellow pigments. *Microchem J* 124:856–867
 216. Grazia C, Rosi F, Gabrieli F, Romani A, Paolantoni M, Vivani R, Brunetti BG, Colomban P, Miliani C (2016) UV–Vis–NIR and microRaman spectroscopies for investigating the composition of ternary $\text{CdS}_{1-x}\text{Se}_x$ solid solutions employed as artists' pigments. *Microchem J* 125:279–289
 217. Van der Snickt G, Dik J, Cotte M, Janssens K, Jaroszewicz J, De Nolf W, Groenewegen J, Van der Loeff L (2009) Characterization of a degraded cadmium yellow (CdS) pigment in an oil painting by means of synchrotron radiation based X-ray techniques. *Anal Chem* 81:2600–2610
 218. Van der Snickt G, Janssens K, Dik J, De Nolf W, Vanmeert F, Jaroszewicz J, Cotte M, Falkenberg G, Van der Loeff L (2012) Combined use of synchrotron radiation based micro-X-ray fluorescence, Micro-X-ray Diffraction, Micro-X-ray absorption near-edge, and micro-fourier transform infrared spectroscopies for revealing an alternative degradation pathway of the pigment cadmium yellow in a painting by Van Gogh. *Anal Chem* 84:10221–10228
 219. Mass J, Sedlmair J, Patterson CS, Carson D, Buckley B, Hirschmugl C (2013) SR-FTIR imaging of the altered cadmium sulfide yellow paints in Henri Matisse's *Le Bonheur de vivre* (1905–6)—examination of visually distinct degradation regions. *Analyst* 138:6032–6043
 220. Mass JL, Opila R, Buckley B, Cotte M, Church J, Mehta A (2013) The photodegradation of cadmium yellow paints in Henri Matisse's *Le Bonheur de vivre* (1905–1906). *Appl Phys A Mater Sci Process* 111:59–68
 221. Uffelman ES, Hobbs PA, Barisas DAG, Mass JL (2013) pXRF analyses of Louise Herreshoff's paintings in relation to CdS and other pigment degradation issues. *Appl Phys A Mater Sci Process* 111:9–14
 222. Pouyet E, Cotte M, Fayard B, Salome M, Meirer F, Mehta A, Uffelman ES, Hull A, Vanmeert F, Kieffer J, Burghammer M, Janssens K, Sette F, Mass J (2015) 2D X-ray and FTIR micro-analysis of

- the degradation of cadmium yellow pigment in paintings of Henri Matisse. *Appl Phys A Mater Sci Process* 121:967–980
223. Voras ZE, deGhetaldi K, Wiggins MB, Buckley B, Baade B, Mass JL, Beebe TP Jr (2015) ToF-SIMS imaging of molecular-level alteration mechanisms in *Le Bonheur de vivre* by Henri Matisse. *Appl Phys A Mater Sci Process* 121:1015–1030
224. Ayalew E, Janssens K, De Wael K (2016) Unraveling the reactivity of minium toward bicarbonate and the role of lead oxides therein. *Anal Chem* 88:1564–1569
225. Vila A, Monrad K, Wadum J, Filtenborg T (2014) As time passed by came sunset. Christen Købke's 'View of Lake Sortedam', its genesis and colour changes. In: Sgamellotti A, Brunetti BG, Miliani C (eds) *Science and art. The painted surface*. Royal Society of Chemistry, London, pp 354–372
226. Samain L, Silversmit G, Sanyova J, Vekemans B, Salomon H, Gilbert B, Grandjean F, Long GJ, Hermann RP, Vincze L, Strivay D (2011) Fading of modern Prussian blue pigments in linseed oil medium. *J Anal At Spectrom* 26:930–941
227. Samain L, Gilbert B, Grandjean F, Long GJ, Strivay D (2013) Redox reactions in Prussian blue containing paint layers as a result of light exposure. *J Anal At Spectrom* 28:524–535
228. Samain L, Grandjean F, Long GJ, Martinetto P, Bordet P, Strivay D (2013) Relationship between the synthesis of prussian blue pigments, their color, physical properties, and their behavior in paint layers. *J Phys Chem C* 117:9693–9712
229. Samain L, Grandjean F, Long GJ, Martinetto P, Bordet P, Sanyova J, Strivay D (2013) Synthesis and fading of eighteenth-century Prussian blue pigments: a combined study by spectroscopic and diffractive techniques using laboratory and synchrotron radiation sources. *J Synchrotron Radiat* 20:460–473
230. Gervais C, Languille M-A, Reguer S, Gillet M, Pelletier S, Garnier C, Vicenzi EP, Bertrand L (2013) Why does Prussian blue fade? Understanding the role(s) of the substrate. *J Anal At Spectrom* 28:1600–1609
231. Cotter MJ, Meyers P, Vanzelst L, Sayre EV (1973) Authentication of paintings by Blakelock, RA through neutron-activation autoradiography. *J Radioanal Chem* 15:265–285
232. Alfeld M, Laurenze-Landsberg C, Denker A, Janssens K, Noble P (2015) Neutron activation autoradiography and scanning macro-XRF of Rembrandt van Rijn's *Susanna and the Elders* (Gemaldegalerie Berlin): a comparison of two methods for imaging of historical paintings with elemental contrast. *Appl Phys A Mater Sci Process* 119:795–805
233. Seim C, Laurenze-Landsberg C, Schroeder-Smeibidl B, Mantouvalou I, de Boer C, Kanngiesser B (2014) Old traces, read anew—'The Reading Hermit' painting in the light of X-ray fluorescence. *J Anal At Spectrom* 29:1354–1360
234. Van der Snickt G, Legrand S, Caen J, Vanmeert F, Alfeld M, Janssens K (2016) Chemical imaging of stained-glass windows by means of macro X-ray fluorescence (MA-XRF) scanning. *Microchem J* 124:615–622
235. Ricciardi P, Legrand S, Bertolotti G, Janssens K (2016) Macro X-ray fluorescence (MA-XRF) scanning of illuminated manuscript fragments: potentialities and challenges. *Microchem J* 124:785–791
236. Targowski P, Pronobis-Gajdzis M, Surmak A, Iwanicka M, Kaszewska EA, Sylwestrzak M (2015) The application of macro-X-ray fluorescence and optical coherence tomography for examination of parchment manuscripts. *Stud Conserv* 60:S167–S177
237. Jackall Y, Delaney JK, Swicklik M (2015) 'Portrait of a woman with a book': a 'newly discovered fantasy figure' by Fragonard at the National Gallery of Art, Washington. *Burlingt Mag* 157:248–254
238. Bacci M, Picollo M (1996) Non-destructive spectroscopic detection of cobalt(II) in paintings and glass. *Stud Conserv* 41:136–144
239. Bacci M, Picollo M, Trumpy G, Tsukada M, Kunzelman D (2007) Non-invasive identification of white pigments on 20th-century oil paintings by using fiber optic reflectance spectroscopy. *J Am Inst Conserv* 46:27–37
240. Delaney JK, Zeibel JG, Thoury M, Littleton R, Palmer M, Morales KM, de la Rie ER, Hoenigswald A (2010) Visible and infrared imaging spectroscopy of picasso's harlequin musician: mapping and identification of artist materials in situ. *Appl Spectrosc* 64:584–594
241. Gautier G, Bezur A, Muir K, Casadio F, Fiedler I (2009) Chemical fingerprinting of ready-mixed house paints of relevance to artistic production in the first half of the twentieth century. Part I: Inorganic and organic pigments. *Appl Spectrosc* 63:597–603

242. Green AA, Berman M, Switzer P, Craig MD (1988) A transformation for ordering multispectral data in terms of image quality with implications for noise removal. *IEEE Trans Geosci Remote Sens* 26:65–74
243. Nielsen AA (2011) Kernel maximum autocorrelation factor and minimum noise fraction transformations. *IEEE Trans Image Process* 20:612–624
244. Thurrowgood D, Paterson D, de Jonge MD, Kirkham R, Thurrowgood Howard D (2016) A hidden portrait by Edgar Degas. *Scientific Reports* 6:29594. doi:10.1038/srep29594

New Frontiers in Application of FTIR Microscopy for Characterization of Cultural Heritage Materials

S. Prati¹ · G. Sciutto¹ · I. Bonacini¹ · R. Mazzeo¹

Received: 17 November 2015 / Accepted: 11 April 2016 / Published online: 28 April 2016
© Springer International Publishing Switzerland 2016

Abstract We present an overview of recent advances in the application of Fourier Transform Infrared (FTIR) microscopy for analysis of complex, multicomponent, and multilayer samples such as those typically encountered in the field of heritage materials. This technique is particularly useful since it allows identification and localization of both organic and inorganic (if IR active) compounds. New improvements have been possible thanks to the introduction of ad hoc sample preparation methods to obtain either thin or cross sections that allow both avoidance of contamination from organic embedding resin and improvement of the quality of the acquired spectra. Moreover, integrated use of spectra registered in the near-infrared (NIR) and mid-infrared (MIR) regions allows better comprehension of cross section composition. Data interpretation has been improved thanks to the development of chemometric methods for elaboration of hyperspectral data. A new and very promising field is the development of enhanced FTIR methods for detection of trace components in microextracts. These systems, allowing detection of extractable organic compounds from about 0.1 mg of sample, will be extremely useful in the future for analysis of natural and synthetic colorants, varnishes extracted, for instance, from cotton swabs used during cleaning of paintings, and organic residues on archeological remains.

This article is part of the Topical Collection “Analytical Chemistry for Cultural Heritage”.

✉ S. Prati
s.prati@unibo.it

✉ R. Mazzeo
rocco.mazzeo@unibo.it

¹ Chemistry Department, Microchemistry and Microscopy Art Diagnostic Laboratory (M2ADL), University of Bologna, via Guaccimanni 42, 48100 Ravenna, Italy

Keywords Art diagnostic field · NIR-IR region · FTIR microscopy · ATR · Imaging · Mapping · Cross section preparation · Chemometric elaboration · Enhanced FTIR

1 Introduction

The energy of most molecular vibrations corresponds to the infrared region of the electromagnetic spectrum. These vibrations may be recorded and measured in the infrared spectrum. Therefore, infrared spectroscopy can be used to characterize both organic and inorganic materials, since most functional groups have fundamental vibration frequencies in the infrared region, particularly the mid-infrared (MIR), extending from 4000 to 450 cm^{-1} . The absorption bands of most functional groups lie beyond 1500 cm^{-1} , while the region below 1500 cm^{-1} ("fingerprint" region) is characteristic of each individual chemical compound. In this region, some bands associated with functional groups are also present and may be used for interpretation of the infrared spectrum of an unknown compound. Materials that are not active in the mid-infrared region (oxide, sulfides, etc.) can be analyzed if the FTIR spectrometer is equipped with a far-infrared (FIR) detector, allowing collection of spectra in the 650 to 50 cm^{-1} spectral region.

Infrared spectroscopy allows chemical characterization of both organic (binding media, varnishes, adhesives, coatings, consolidants, etc.) and inorganic materials (pigments, corrosion products, salts, etc.). The result of infrared analysis is a spectrum, where the percentage of transmission/absorbance of the sample is plotted against the wavenumber (cm^{-1}) at which the transmission/absorbance of the analyzed sample occurred [1–3].

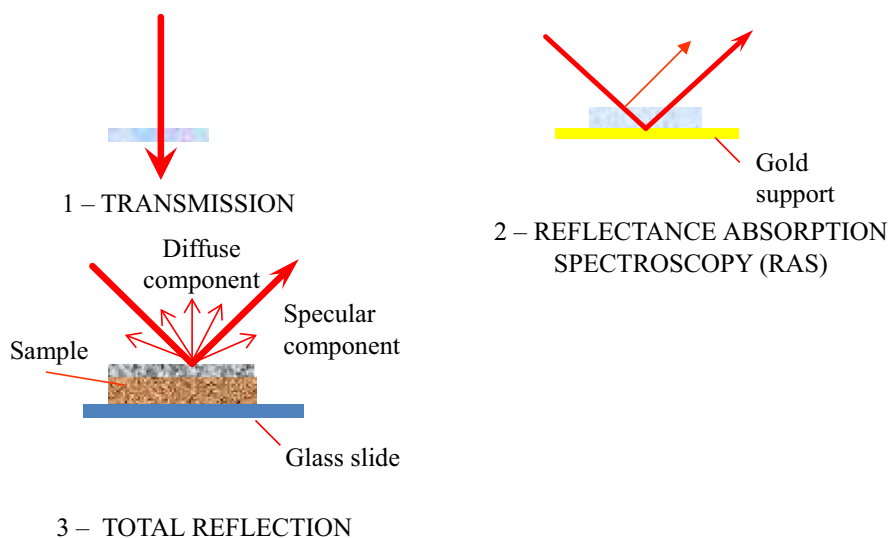


Fig. 1 Different modes for FTIR analysis of solid sample

The improvement in terms of spectral resolution and detection limit obtained with the transition from dispersive IR to FTIR instruments allowed widespread use of this technique as a suitable tool for study and conservation of cultural heritage materials [4]. Subsequently, the development in the early 1980s of FTIR microscopy represented a powerful innovation for microdestructive analysis of small samples [5].

An FTIR microscope consists of an FTIR spectrophotometer combined with an optical microscope with all reflecting optics and aspherical surfaces adapted to infrared radiation to minimize optical aberrations. A conventional infrared light source (typically a Globar silicon bar heated to 1500 K), which emits radiation from 1.5 μm up to a few tens of microns, is directly sent to the microscope rather than to the spectrophotometer sample chamber, without any modification to the interferometer. The user interface for data acquisition and processing is also the same as for conventional FTIR spectroscopy.

The microscope is designed for observation in both transmission and reflection modes. A system of dichroic mirrors allows both visible light and IR radiation to pass through the same optical system, permitting one first to observe the region of interest visually and then to record the corresponding IR spectra. Analysis by FTIR microscopy may be accomplished in several modes, depending on the amount and type (powder or fragment) of sample available (Fig. 1) [6].

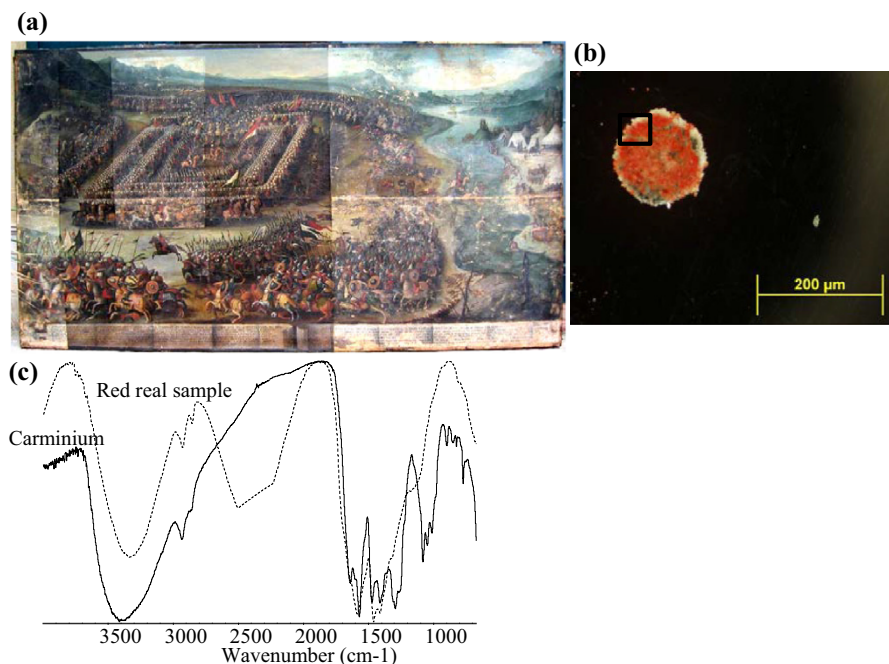


Fig. 2 **a** “Battaglia di Cialdiran,” canvas painting exhibited at the Mirto Palace Museum, Palermo, Italy; **b** optical microphotograph of a squeezed red microparticle sampled from the red robe of a warrior; **c** transmission FTIR spectrum collected from the area identified with a *square black box* in **(b)**; the squeezing of the microparticle results in partial separation of the dye from the other components, allowing identification as carmine

Transmission measurements by means of IR radiation passing through the sample benefit from high energy throughput resulting in high sensitivity. Transmission analysis is particularly suitable for small particles (sampled from larger fragments under the stereomicroscope), or thin films employing IR-transparent salts as support (i.e., NaCl window) [7], or a diamond anvil cell. In the latter case, the particle is placed onto a microcompression cell made of diamond and pressed in order to be squeezed. The hardness and inertness of diamond allow analysis of a large variety of samples without contamination. The IR spectrum of diamond presents absorption bands between 2500 and 1800 cm^{-1} , a spectral region relatively free from characteristic absorptions of common organic compounds. The diamond anvil cell is particularly useful for analysis of single organic dye particles, especially when the dye is mixed with absorbent inorganic salts and organic binders [8]. Indeed, in bulk samples, dye identification may be prevented due to overlap with bands of organic binder or other inorganic components. On the other hand, squeezing a particle enriched in dye may partially allow one to separate it from other components to record its spectrum (Fig. 2).

Transmission measurements can also be performed on thin sections obtained after polishing or microtoming a cross section. To obtain high-quality spectra, their thickness should be below 15 μm .

Alternatively, films can be analyzed using reflection–absorption spectroscopy (RAS) by applying the thin film onto a metal surface. In such conditions, the IR radiation passes through the sample and is reflected back by the metal surface. Therefore, the thin layer is crossed by the IR beam twice, yielding a high-quality spectra comparable to those recorded in transmission mode. However, reflection–absorption spectroscopy (RAS) can only be applied in some restricted cases where either the sample can be easily flattened (i.e., films, powders, particles or fibres, etc.) or where a thin layer is applied onto a metallic surface (i.e., protective coatings on metal artworks or varnish layers on gilded art objects) [9].

When the sample is not thin enough to allow transmission of IR radiation, or when it cannot be dispersed into a transparent medium, reflection techniques must be used for both surface and cross section analyses. Reflection methods are based on the principle that, when incident radiation passes through two different media, it is split into reflected and transmitted beams in different proportions according to the ratio between the refractive indexes characterizing the two materials [10].

Specular reflection is mirror-like reflection where the incident and reflected angles of the IR radiation are equal; this generates spectra characterized by Reststrahlen bands. When the analyzed surface is not totally reflecting, broadening and shift of the bands generated by diffuse-like volume reflection are also observed [10, 11]. Although the optical layout of micro-IR systems generally favors the specular component of light, both morphological and optical properties of the sample generate light containing surface and volume reflection in variable and unknown proportions. As a consequence, the usual spectral transforms that can be used on specular-like surface reflection bands, such as Kramers–Kronig and Kubelka–Munk, are not applicable [12], and the resulting spectra are difficult to interpret. Therefore, to obtain a highly reflecting surface, perfect sample planarity has to be achieved, as discussed in Sect. 3.

The total reflection mode is widely used in portable FTIR equipment [11], since it can acquire spectra in situ without the need to collect samples or be in contact with the surface under examination. In spite of the fact that total reflection has also been used to study paint cross sections [8, 13], the attenuated total reflection (ATR) mode is commonly preferred, since the recorded spectra are more easily comparable to those obtained in transmission mode.

Macro ATR tools can be coupled to bench FTIR spectrometers, allowing examination of particles and sample surfaces; the disadvantage of this method lies in the difficulty of localizing the exact area of analysis. On the other hand, slide-on micro-ATR (μ ATR) devices used in FTIR microscopy enable both surface and stratigraphical analyses.

ATR is based on the principle that total reflection is produced when incident radiation passes from a material with higher refractive index to one with a lower value, for a particular incidence angle called the critical angle. When the incidence angle (θ) is greater than the critical one, an evanescent wave is formed on the surface of the higher refractive index material (IRE, internal reflection element) and can penetrate the optically less dense medium placed in contact with it, resulting in attenuation. ATR spectra are similar to those acquired in transmission mode, but present some distortions in term of relative intensity and wavenumber shifts, principally at lower wavenumber. Indeed, the penetration depth of the evanescent wave (dp) not only depends on the refractive index of both the IRE and the analyzed material but is also a function of wavelength, as shown by Eq. 1.

$$dp = \frac{\lambda}{2\pi n_1 \sqrt{\sin^2 \theta - (n_2/n_1)^2}} \quad (1)$$

where λ is the wavelength of the incident radiation, n_1 is the refractive index of the IRE, n_2 is the refractive index of the sample, and θ is the incidence angle of the radiation on the interface [14].

This explains why absorption bands at low wavenumber are enhanced whereas absorption bands at higher wavenumber are completely absent or less intense compared with the same spectrum acquired in transmission mode. Furthermore, the refractive index of the sample is a function of wavelength, and frequency shifts are also observed, mainly at lower wavenumber.

ATR correction algorithms, as proposed in most commercially available FTIR software packages, have proved to be ineffective in the case of analysis of mixtures, corresponding to the majority of samples collected from artworks. The simplest way to compare ATR and transmission spectra is therefore to create a reference library of known compounds, whose spectra can subsequently be compared with those of unknown samples.

Spatial resolution is a crucial aspect of FTIR microscopy, especially when thin layers or small particles have to be characterized. When using a single-element mercury–cadmium–telluride (MCT) detector, the spatial resolution is related to the dimensions of the aperture, which cannot be smaller than the theoretical diffraction limit of about 10 μ m. However, it is difficult to obtain good signal-to-noise (S/N)

ratio with infrared beam aperture dimensions of $10 \times 10 \mu\text{m}^2$. Sufficient energy to collect spectra is ensured when using a $20 \times 20 \mu\text{m}^2$ aperture [6].

With respect to other acquisition modes, μATR allows investigation of smaller areas while maintaining the same aperture, thanks to the magnification factor of the IRE [15]. Indeed, the investigated area in μATR is equal to the aperture divided by the IRE refractive index, meaning that greater sensitivity can be achieved with this technique.

In recent decades, the introduction of mapping and imaging systems has allowed acquisition of chemical maps showing the distribution of different identified compounds over a selected area of the sample. FTIR mapping systems operate by sequential data collection, using a single-element mercury–cadmium–telluride (MCT) detector, adjustable apertures to select the dimensions of the investigated area, and a motorized stage. The spatial resolution is related to the aperture dimensions and the acquisition method (reflection, transmission, or μATR). Furthermore, overlap between two adjacent surface areas during data collection allows further increase in spatial resolution. The main disadvantage of such mapping systems is the long time (hours) required for acquisition, although this may not be so relevant when dealing with important cultural heritage samples. As an alternative, FTIR imaging uses a multichannel detector where small pixels of about $6 \mu\text{m}$ are distributed over a grid pattern (FPA, focal-plane array) [16, 17]. In this way, the detector collects several spectra simultaneously, thus allowing faster data collection. Typical IR-sensitive FPA detectors include 64×64 , 128×128 , and 256×256 elements (pixels) arranged in a regular pattern. Compared with mapping systems, where geometrical apertures are used, the spatial resolution in this case is determined by the pixel dimensions. Indeed, this type of detector allows one to record the optical signal over the entire field of view (FOV) and requires no aperture. Unfortunately, this also yields poor spectral quality (low signal-to-noise ratio, S/N), since the amount of photons received by each pixel is inversely related to the number of pixels. For large detectors, this means low photon quantities. The μATR configuration can provide spatial resolution of approximately $5 \mu\text{m}$, increased compared with imaging in transmission or reflection mode. Moreover, the cutoff of focal-plane array detectors at 900 cm^{-1} is a significant disadvantage in distinguishing several inorganic compounds (i.e., calcite and lead white) which show characteristic absorption bands below this wavenumber.

Linear array detectors (for raster scanning) have recently been developed, combining several mercury–cadmium–telluride (MCT) detectors with a motorized stage to scan lines sequentially. This system reduces the acquisition time by a factor corresponding to the number of detector elements. The size of individual elements is $25 \mu\text{m}$, permitting acquisition of high-quality spectra. In transmission or reflection mode, the achieved resolution of $25 \mu\text{m}$ can be reduced to $6.25 \mu\text{m}$ using an optical zoom, while in μATR the spatial resolution is reduced by the crystal magnification (to $\sim 6 \mu\text{m}$ with a germanium crystal). Recently, a new integrated FTIR microscope has been designed, offering the powerful combination of a microscope with an incorporated FTIR spectrometer (interferometer, source, laser, and detector). The main advantage of this setup is its higher energy compared with conventional

systems, where energy losses occur due to the optical path of radiation from the spectrometer to the microscope [18].

In summary, FTIR analysis can be performed using either an FTIR spectrometer or its combination with a microscope (FTIR microscopy). Different methods can be applied using both techniques, and samples can be analyzed in both transmission and reflection mode (Table 1).

2 Application of FTIR Microscopy in NIR Region

The development of near-infrared-based spectrometry dates back to the 1960s when Karl Morris of the US Department of Agriculture conceived low-noise instrumentation with computerized control of the spectrometer along with computerized data acquisition combined with use of a multivariate approach to analyze data and the use of diffuse reflectance measurements [19], allowing collection of useful spectra from a large variety of products without the necessity for pretreatment. The NIR region (13,300 to 4000 cm^{-1}) has been widely exploited in bench and portable systems for macroscopic analysis of samples in different fields (pharmaceutical, forensic, polymers, food) [20–25]. Indeed, NIR spectroscopy is a fast, noninvasive, and cost-effective analytical method, allowing noncontact measurements in reflectance mode and providing molecular information on complex matrices. Moreover, use of this spectral range may be extremely useful, as combination and overtone bands have lower absorption and are therefore not distorted by the specular reflection component. In addition, if the surface is not completely planar, these bands are enhanced by volume reflection, which often turns out to be very useful in chemical characterization of materials [26]. On the other hand, only functional groups containing N–H, C–H, O–H, C–O, and C–C bonds produce significant vibrational bands in the NIR range. Moreover, combination and overtone bands are generally broader and less well resolved than fundamental bands, and overlap with one another. For these reasons, the information obtained in this range may be less

Table 1 Different methods for FTIR analysis

	Transmission mode (analysis domain)	Reflection mode (analysis domain)
FTIR spectroscopy (MIR)	KBr, NaCl pellet, Nujol, liquid cell (bulk)	Micro-ATR (bulk, surface), Diffuse Reflectance Infrared Fourier Transform (DRIFT) spectroscopy (bulk)
FTIR spectroscopy (FIR)	Polyethylene (bulk)	Diamond micro-ATR (bulk, surface)
FTIR microscopy	Micro diamond cell, NaCl window (bulk)	Specular reflection (surface), specular reflection imaging (stratigraphic, surface), reflection–absorption spectroscopy (RAS) (surface), single-point micro-ATR (stratigraphic, surface, bulk), micro-ATR mapping (stratigraphic, surface), micro-ATR imaging (stratigraphic, surface)

specific than that obtained in the mid-infrared region, and mixtures of organic substances can barely be distinguished. For this purpose, a multivariate approach is usually required to extract useful information from spectra [27, 28].

In the field of cultural heritage, noninvasive in situ NIR spectroscopy investigations have been performed for identification of painting materials [26–30], evaluation of the long-term stability of historical papers [31], and study of degradation processes on calcareous stones [32]. Recently, Dooley et al. proposed the use of an advanced NIR reflectance imaging system for identification of organic substances in paintings, exploiting the vibrational overtones and combination bands of fundamental absorptions, which are less affected by potential pigment interference [33].

Only a few studies concerning use of FTIR microscopy in the near-infrared range for analysis of artistic multilayered samples have been reported in literature [26, 33, 34]. Rosi et al. [26] reported the application of micro-IR spectroscopy in reflection mode in the 5600 to 960 cm^{-1} range in combination with principal component analysis (PCA), for mapping the distribution of organic and inorganic materials in standard mock-ups and in a 17th century polychrome wooden sculpture. The spectra collected from different samples allowed identification of gypsum and linseed oil. Poli et al. [34] carried out micro-infrared total reflection measurements in the range from 5266 to 1000 cm^{-1} , exploiting the broad spectral response of a mercury–

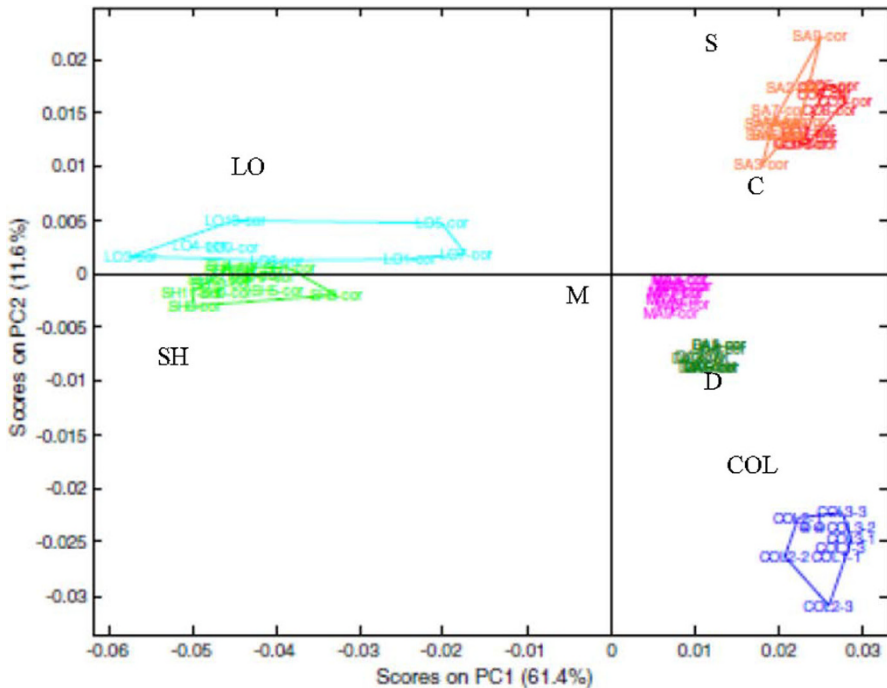


Fig. 3 PC1–2 score plot representing the separation between natural resins and linseed oil based on NIR spectra; *LO* linseed oil, *S* sandarac, *SH* shellac, *M* mastic, *D* dammar, *COL* colophony, *C* copal. Reprinted from [35], with permission from Elsevier

cadmium–telluride detector to include near-infrared information without modification of the standard mid-infrared micro-FT instrumentation. The NIR region was employed for identification of azurite on a microsample of an undated panel painting.

Recently, our research group made use of the spectral range from 8000 to 675 cm^{-1} to analyze paint cross sections in total reflection mode [35]. The main focus was to identify the type of resin employed as an ingredient in varnish layers or as a mordant for gildings in some real paint samples. A hyperspectral dataset obtained by mapping selected areas of cross sections was elaborated using chemometric methods, as illustrated in Sect. 4.

Two hyperspectral data matrices were created for the NIR and MIR regions, respectively, and subjected to specific mathematical preprocessing before chemometric elaboration. Principal component analysis (PCA) performed on the NIR matrix provided better resolution of the different layers with respect to that obtained using the MIR region. In particular, we showed how the NIR range may be particularly interesting for identification of varnish layers containing natural resin.

Indeed, MIR spectra of different natural resins show extremely similar profiles [35, 36]. Thus, it is difficult to identify not only an individual resin but also the more generic terpenoid category among: (a) sesquiterpenic resins (i.e., shellac), (b) diterpenic resins containing abietane compounds (i.e., colophony), (c) diterpenic resins containing polymerized communic acid (i.e., copal, sandarac), and (d) triterpenic resins (i.e., mastic and dammar), while it is quite easy to distinguish a resin from a siccativ oil. Conversely, FT-NIR analysis revealed the presence of bands characteristic for each investigated category. Multivariate analysis (Fig. 3) of the spectra related to the NIR range allowed separation of the different resin classes [35].

3 Optimized Preparation of Paint Cross and Thin Sections

Characterization and stratigraphic localization of the different components constituting paint layers are fundamental to achieve profound knowledge of both the painting technique and state of conservation.

In this regard, preparation of paint thin and/or cross sections represents a crucial step in examination of paintings. The procedure for mounting multilayer artistic samples as thin or cross sections for microscopic analysis was developed in the early 20th century and rapidly became a standard method in museum laboratories [37, 38]. The embedding procedure performed using wax or synthetic resins is followed by grinding, polishing, or microtoming of the embedded sample block to produce either cross or thin sections, revealing the complete layered structure to be analyzed. Prior to application of specific elemental and molecular investigations, observation of mounted cross sections under optical microscopy allows study and documentation of the structure and morphology of paint layers, providing information on the painting techniques adopted as well as presence of nonoriginal overpainting added during previous restoration interventions.

Different types of synthetic resin have been used as embedding materials. In particular, polyester resin was introduced in the mid-20th century [39], and is nowadays commonly used in many scientific laboratories all over the world. In 1994, Derrick et al. [40] published a study on different types of embedding resin used for preparation of thin and cross sections, highlighting the advantages and disadvantages of different synthetic polymers. In particular, problems related to identification of organic substances (binding media, varnishes, etc.) due to contamination that may arise from the embedding resin have been discussed. Indeed, even if synthetic resin is particularly useful for preservation of the physical integrity of samples during polishing or microtoming, it is clear that its absorption bands may interfere with the characteristic bands of organic substances used as binders or varnishes, which are usually present in very low concentrations. Consequently, in many cases, the strong absorption bands of the embedding medium in the mid-infrared region make binder identification very difficult or almost impossible. The contribution of the embedding resin can be removed by mathematical subtraction of its spectral profile from the sample spectrum [41]. However, this process is quite critical, since the bands related to contamination are less intense than those registered from the pure resin, and simply subtracting the two spectra may lead to underestimation of some bands that may derive from the sample as well. Moreover, it is worth noting that paint sample materials may show partial solubility in liquid prepolymer [38], as already reported in identification of wax-based finishing layers [1], where the high capability of the embedding resin to dissolve such natural organic substances was highlighted. Different FTIR microscopy modes can be used depending on the thickness of the cross sections; in fact, transmission modes are preferred for thin sections, whereas total or attenuated total reflection (ATR) modes have to be used with cross sections, as they are too thick for analysis in transmission.

Several strategies have been proposed to obtain thin or cross sections with the aim of preventing or reducing contamination effects induced by the embedding procedure while improving the quality of the sample surface to maximize the signal obtained by FTIR microscopy.

3.1 Thin Section Preparation

Samples prepared as thin sections provide better results than cross sections when submitted to analysis by transmission-mode FTIR microscopy, micro-X-ray diffraction (μ XRD), and micro-X-ray absorption near-edge spectroscopy (μ XANES) [42]. Nevertheless, compared with cross sections, preparation of thin sections is more destructive and difficult [42–45].

In particular, preparation of thin sections is preferred when FTIR analysis is performed using a bright and collimated synchrotron radiation (SR) source (i.e., SR-FTIR) [46]. Indeed, analysis of cross sections presents some limitations, since total reflectance spectra appear distorted and more difficult to interpret, while ATR is rarely used with a SR source due to difficulties in aligning the beam with the crystal. For these reasons, in recent years, new strategies for preparing thin sections have been proposed. Pilc et al. [41] proposed embedding paint samples on silver chloride

to obtain thin sections by microtomy. Even if this method prevented contamination of the sample, its main disadvantage is that silver chloride darkens on exposure to light, hindering localization of samples within blocks. Pilc et al. [41] also experimented with KBr as an embedding medium, but found that samples mounted in this way were difficult to microtome, as they tended to fragment and break up. Van der Weerd et al. [43] described a new method for preparing thin sections by embedding the paint chip in KBr and then polishing the obtained KBr pellet from both sides. However, this method presents some drawbacks, since samples prepared in this way are extremely fragile and difficult to handle, and without experience, it is also possible to lose the sample altogether [42].

Cotte et al. [42] proposed protecting the sample from resin infiltration by first wrapping it in aluminum foil, before embedding it with subsequent microtoming. However, this approach presents some practical difficulties when small fragments have to be handled.

Recently, application of gold coating was proposed to protect the sample from the embedding epoxy resin before microtoming [47].

Alternatively, the diamond anvil cell offers a rather classical and straightforward approach to flatten small pieces of paint and decrease their thickness [48–51]. Even if interesting results can be obtained, the layers are distorted due to the applied pressure, thus precise localization of different components may be hindered by interlayer contamination. Therefore, in studies on degradation pathways, precise localization of degradation products cannot be carried out properly.

An embedding-free technique was recently proposed for fresh and soft paintings containing organic binders at high concentration, consisting of microtoming the sample after wrapping it in two polycarbonate foils [52]. This method is particularly suitable for polymeric samples, replicas or historical paintings with strongly bound and cohesive layers. In particular, soft samples such as layers of varnishes applied on violins [45, 53, 54] can be directly microtomed without embedding. However, these embedding-free methods cannot be applied for brittle samples, since material loss can occur during microtoming. In this case, AgCl can be used as a barrier coating to protect the sample before embedding in a resin. Then, the entire block can be microtomed [52]. Use of AgCl presents two advantages: first it protects the sample from resin contamination, and secondly it provides to the sample mechanical properties suitable for microtomy.

3.2 Cross Section Preparation

To overcome problems related to preparation of thin sections, several strategies aimed at obtaining cross sections have been proposed with the aim of both avoiding resin contamination and optimizing the surface morphology to improve spectral resolution.

Use of infrared-transparent salts as embedding materials for cross sections was proposed to avoid contamination by the embedding resin and improve detection of organic substances, thanks to their transparency within the diagnostic infrared spectral region from 4000 to 400 cm^{-1} . KBr, for instance, has been proposed for

cross section preparation [55], taking inspiration from previous studies in which this salt was used to produce thin sections [43].

As KBr is a fragile material, development of a specific sample holder was proposed to improve the polishing step (Fig. 4) [55].

This method allowed significantly improved detection of organic substances as well as microscopic observations of paint cross sections under ultraviolet light, thanks to the absence of a fluorescence contribution arising from the embedding resin (Fig. 5).

However, the KBr embedding method presents some specific drawbacks, mainly related to the brittleness and hygroscopicity of the inorganic salt. In fact, Scanning Electron Microscopy (SEM)/Energy Dispersive X-ray (EDX) analysis performed on the surface of these cross sections revealed the presence of KBr resulting from the dry polishing procedure adopted [56]. This unwanted presence of KBr not only affects surface elemental analysis but also has consequences in reducing the infrared spectral quality during acquisition. This effect is particularly observed when time-consuming chemical maps are acquired and may be related to absorption of humidity by KBr present on the surface [57].

Moreover, it was observed that sample flatness was significantly dependent on operator skill. For this reason, the procedure has been modified [56] using the inorganic salt as a barrier against resin infiltration. In this way, the sample protected by KBr is embedded in synthetic resin; use of this external coating aimed to physically stabilize the fragile KBr pellet as well as protect it from atmospheric humidity (Fig. 6). More constant and reproducible results were obtained in terms of sample flatness thanks to the improved physical stability of the sample and the use of a polishing sample holder, designed to reduce the influence of the operator during the polishing procedure (Fig. 7).



Fig. 4 Sample holder for samples embedded in a KBr pellet. Reprinted from [55], with permission from Elsevier

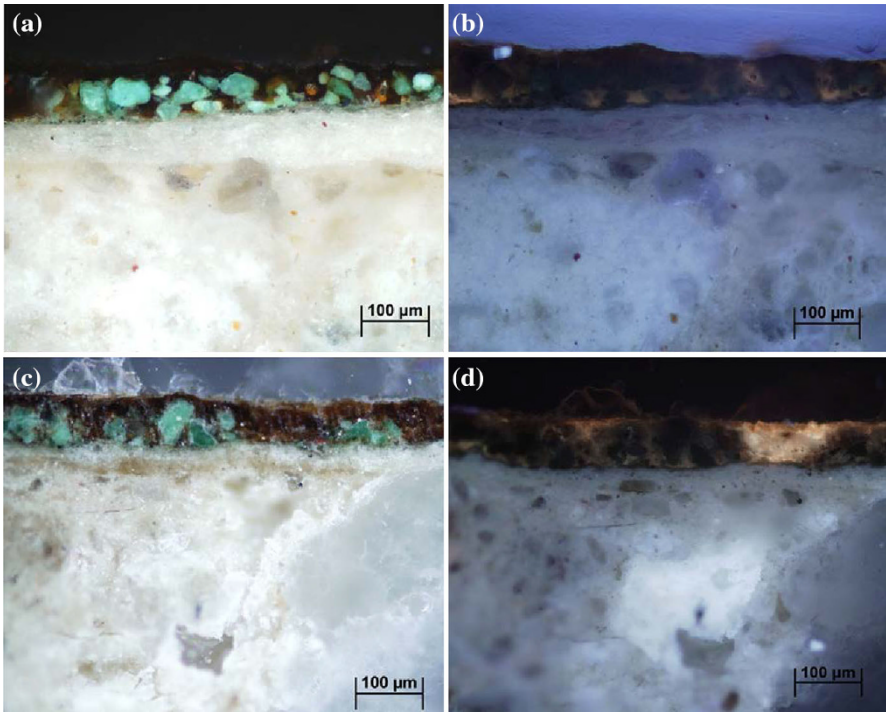


Fig. 5 Cross section photomicrographs of a sample from a Nepalese mural painting embedded in polyester resin under **a** visible and **b** UV light, and in KBr under **c** visible and **d** UV light. The fluorescence of the paint layer (**b, d**) is better documented in the sample embedded in KBr (**d**)

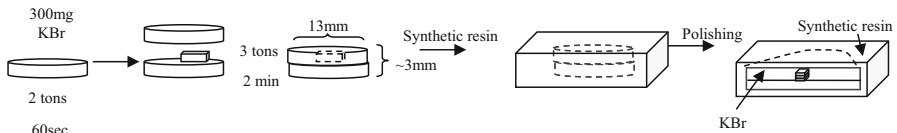


Fig. 6 Preparation of paint cross sections embedded in KBr and resin: the sample is positioned parallel to a KBr pellet, previously gently pressed. Some KBr powder is added to cover the sample, and the whole system is pressed into a new pellet, which is further embedded into a polyester resin support and polished. Reprinted from [56], with permission from Springer

It is worth noting that the planarity of the sample surface is particular important for FTIR analysis in both ATR and total reflection modes. In the first case, the improvement of the spectral quality strongly depends on the achievement of a flat surface, which optimizes the contact between the sample and the ATR crystal. In the total reflection mode, a smooth surface maximizes the specular component, allowing collection of more intense spectra.

As an alternative to KBr, sodium chloride (NaCl) has also been proposed as an embedding material, thanks to its high performance in terms of physical stability, cost, and reduced harmful effects [56]. In particular, NaCl-embedded samples



Fig. 7 Polishing sample holder. Reprinted from [56], with permission from Springer

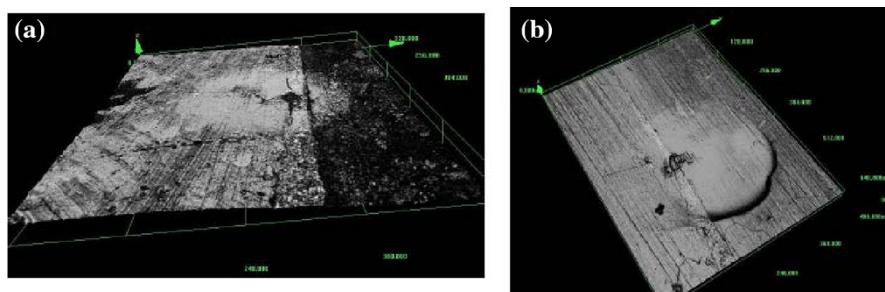


Fig. 8 Confocal image (200 \times magnification) acquired after μ FTIR-ATR analysis on standard mock-ups composed of a linseed oil–lead white paint layer applied over gypsum/glue ground, embedded in **a** NaCl and **b** KBr. Application of the same pressure on the two cross sections results in the sample embedded in NaCl appearing less damaged than the one embedded in KBr. Reprinted from [56], with permission from Springer

appear to be more resistant to ATR crystal pressure compared with similar samples embedded in KBr (Fig. 8). Moreover, NaCl-embedded samples need a lower pressure to obtain good contact and good spectral quality. In this way, problems related to displacement of the ATR crystal during mapping analysis may be reduced.

Resin contamination not only occurs due to its infiltration into the sample porosity, but is mainly due to its spreading on the surface of the cross section during the polishing step [57]. Argon-ion beam polishing can be used to reduce this

pollution effect and achieve good cross section surface quality. The system consists of a specimen chamber with a turbomolecular pump vacuum system and an optical microscope for sample positioning. After evacuating the specimen chamber, the investigated region is irradiated with a broad argon-ion beam in the accelerating voltage range between 2 and 6 kV. To prevent beam striations (curtain effect) and achieve uniform etching of heterogeneous samples characterized by the presence of materials with different hardness, the specimen stage can be rotated by 30° during ion-beam milling and rocked by 30° [58].

The main advantage of this system lies in the high quality of the sample surface, which is free from pollution by the embedding medium used. This method was first used by Boon et al. to improve the surface preparation of paint cross sections for SEM imaging [59, 60]. Recently, argon-ion milling has been applied for preparation of paint cross sections embedded in either synthetic resin [57] or KBr [56] for μ ATR analysis. In both cases, the optimized surface morphology allowed acquisition of well-resolved FTIR spectra. SEM-EDX analysis carried out on KBr-embedded samples revealed a decreased amount of KBr particles on the sample surface (Fig. 9). This may explain why the spectral quality remains quite good during mapping acquisition [56].

As an alternative to the KBr embedding system, various materials have been tested as barrier coatings against infiltration of embedding resin [40].

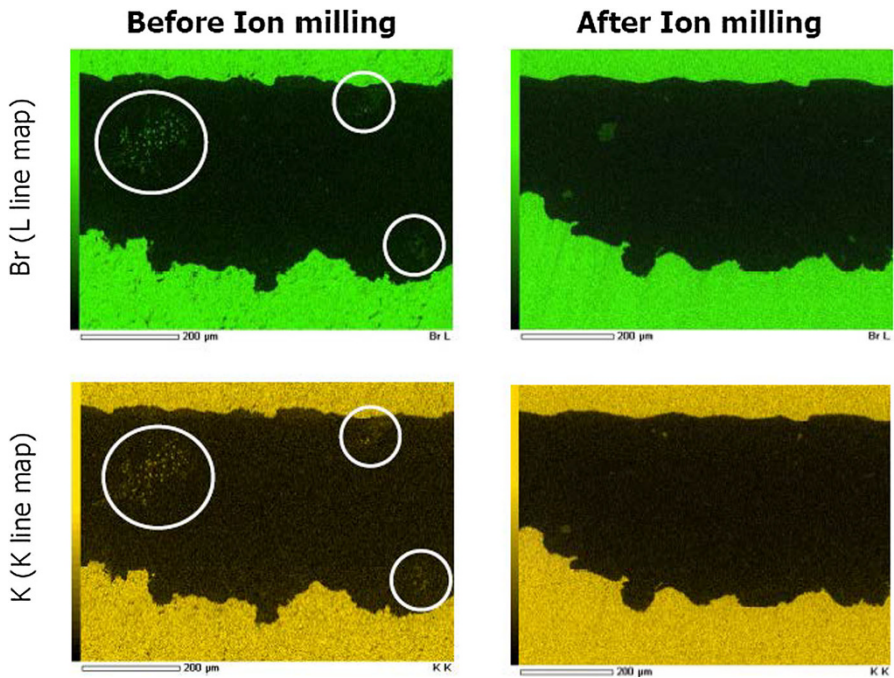


Fig. 9 SEM-EDS elemental mapping analysis performed on a standard mock-up made of a linseed oil-lead white paint layer applied over gypsum/glue ground, embedded in KBr, before and after argon-ion milling polishing procedure. *White circles* indicate presence of KBr on sample surface before polishing

For this purpose, cyclododecane ($C_{12}H_{24}$), [61], a material commonly used by conservators as a temporary consolidant, has been proposed and tested thanks to its ability to sublime at room temperature [62, 63]. Porous samples are first consolidated with saturated solution of cyclododecane in toluene (80 % w/v) or melted cyclododecane. Then, the samples are embedded in resin and cut by microtomy [61]. Cross-sections were analyzed after 24 h, after complete sublimation of cyclododecane. Even if the proposed method limits interference from embedding materials, different drawbacks were observed, including significant sample manipulation and possible reduction of sample stability after cyclododecane sublimation.

As mentioned above, the surface roughness of the paint stratigraphy is a key issue to consider when FTIR microscopy is performed in both ATR and total reflection modes. In fact, surface morphology plays a crucial role in the success of the analysis, since good contact between the ATR crystal and the surface is needed to achieve significant results. Moreover, smooth surfaces enable maximization of the specular component, responsible for the presence of distorted peaks, which appear with a first-derivative-like shape for organic substances or as inverted bands for inorganic compounds [64]. Moreover, if the surface is not completely optically flat, a diffuse reflection component whose shape is similar to transmission bands may also be observed. Corrections, such as the Kramers–Kronig (K–K) transform algorithm [65], can be applied to convert reflectance into transmission spectra when only bands with first-derivative-like shape are present. However, if organic and inorganic components are present simultaneously and the surface is not completely smooth, as in paint cross sections, it is not possible to apply a specific correction and spectra appear difficult to interpret. Therefore, maximizing the specular component results in higher intensity of the detected signal, but spectra are characterized by distorted signals.

On the other hand, the diffuse component produces bands which are not distorted and can be easily compared with transmission spectra. For this reason, even if the overall signal is reduced, an alternative strategy could be based on achieving a surface rough enough to maximize the diffuse reflection component [66].

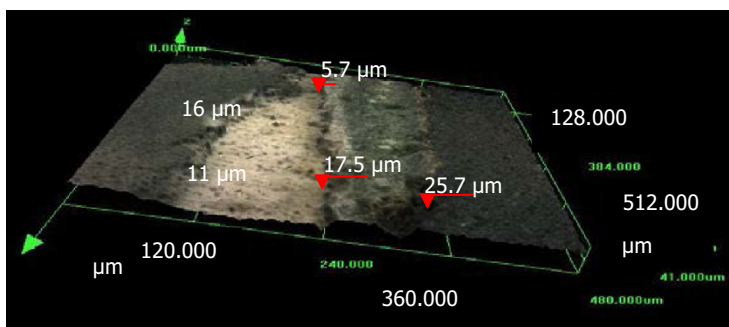


Fig. 10 Confocal image of paint cross section collected from a panel painting and prepared after pretreatment with cyclododecane. The different hardness of the paint layers and use of water as lubricant during microtomy result in production of a rough surface and material loss corresponding to the water-sensitive gypsum/glue ground. Reprinted from [57], with permission from Elsevier

In particular, the surface morphology of cross sections obtained with the cyclododecane method (Fig. 10) allows detection of diffuse bands in total reflection mode; these bands can be highly diagnostic, as they are more similar to transmission bands compared with distorted specular signals [66]. However, this embedding method presents some limitations for spectra collected in ATR mode [57], as analysis of such rough surface areas is difficult, because of the poor and uneven contact between the ATR crystal and sample.

4 Chemometric Approaches for Elaboration of ATR-FTIR Hyperspectral Data

Molecular analysis by micro-FTIR mapping and imaging allows collection of a considerable number of infrared spectra from bidimensional scanning of the sample surface, providing information about the spatial distribution of different compounds with a resolution that is a function of the objective aperture dimensions, the selected stage step, and the refraction index of air (in the case of spectra collected in total reflection mode) or the ATR crystal (in the case of μ ATR mode).

μ FTIR chemical maps/images can be obtained by plotting the intensities of characteristic absorption bands, coded on a chromatic scale (blue–red color scale), in correspondence with their spatial location within a selected sample area [67, 68]. Overlapping all of the maps/images corresponding to each wavelength, the dataset can be represented in three dimensions (two spatial dimensions plus the color-coded absorption intensity) as a hyperspectral parallelepiped, usually referred to as a hypercube (Fig. 11).

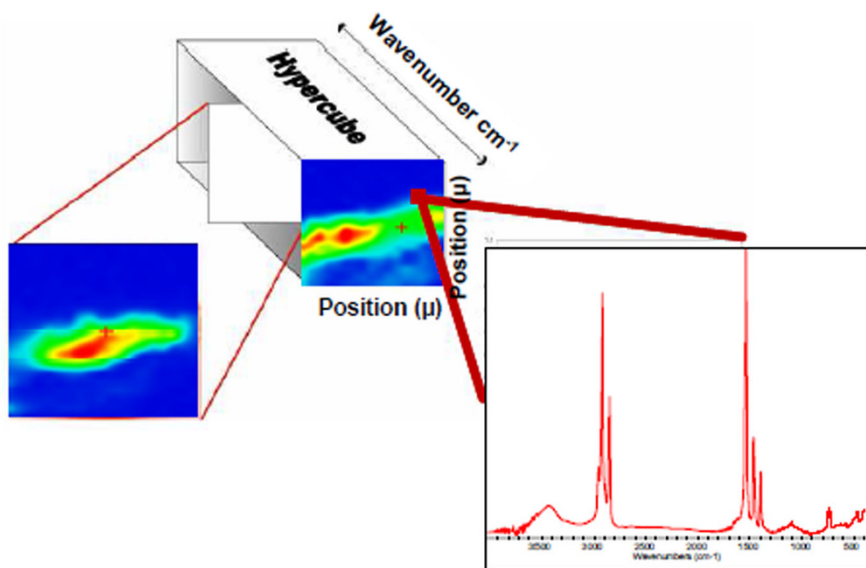


Fig. 11 Hyperspectral parallelepiped or hypercube

Nevertheless, the use of a univariate approach may result in problems related to the presence of complex mixtures, which may affect the correct identification and spatial localization of the compounds. Indeed, due to the heterogeneity and complexity of painting materials, overlapping of characteristic bands in the mid-infrared region may occur, as well as variations in their relative intensity. It has been widely demonstrated that, when datasets are constituted by multiple objects and intercorrelated variables, univariate methods—which examine one variable at a time—considerably underutilize the information contained therein. Conversely, multivariate approaches can consider and represent all the information in an easily understandable way.

Chemometrics is a chemical discipline born for interpreting and solving multivariate problems in the field of analytical chemistry. Wold used the name “chemometrics” for the first time in 1972 to identify the discipline performing extraction of useful chemical information from complex experimental systems [69]. In the last decade, chemometrics has played a crucial role in interpretation of spectroscopic data and has been increasingly used in the conservation science field.

One of the most widely employed chemometric tools is principal component analysis (PCA). PCA is an unsupervised exploratory method that looks for directions of maximum variance within a multivariate data space, based on the assumption that high variance (i.e., high variability) is synonymous with a large amount of information. The searched directions, which are called principal components (PCs), are orthogonal. This implies that they are not intercorrelated, and therefore that they never account for duplicate information [70]. From a mathematical point of view, the PCs are expressible as linear combinations of the original variables. The coefficients which multiply each variable, called loadings, represent the cosine values of the angles between the PCs and the original variables, varying between -1 and $+1$. The larger the absolute value of the loading, the larger the contribution of the corresponding original variable to the PC.

One of the main advantages of using PCA is related to the possibility of representing large amounts of complex information by way of simple bi- or tridimensional plots. Indeed, the plots obtained using two or three PCs can be used to represent the objects (score scatter plots), the original variables (loading plots), or both objects and variables (biplots). Score scatter plots may allow observation of the distribution of the objects in the plane described by two or three selected PCs, providing information about multidimensional structures existing among the objects, such as similarity, groupings, and trend patterns.

Loading plots are bidimensional representations of the loading values of the original variables on two selected PCs, providing information about the importance of the variables and about their intercorrelation, with respect to the fraction of variance (i.e., information) explained by those PCs. Relationships existing between variables and objects can be described by joint examination of loading and score plots.

4.1 Application of PCA for Elaboration of μ FTIR Maps

In the last years, several research efforts have been devoted to application of chemometric approaches for interpretation of FTIR data acquired from artistic samples [36, 71–78].

Recently, these methods were employed for interpretation of hyperspectral data obtained by FTIR mapping or imaging.

Hyperspectral data are arranged in three-dimensional matrices with dimensions $X \times Y \times W$, where X and Y are the number of vertical and horizontal measurement points, respectively, while W is the number of spectral variables recorded at each point (e.g., the different wavenumbers). Nonetheless, each point can be considered as an independent object if the three-dimensional array is unfolded into a bidimensional matrix, structured with $J = X \cdot Y$ rows and W variables. This transformation is necessary for application of usual chemometric techniques, which generally require bidimensional matrices.

After such elaboration, the objects may be refolded (Fig. 12) as in their starting configuration. This is particular useful because each point of the map can then be represented using a chromatic scale, for example, from blue (minimum) to red (maximum score value), considering the corresponding score value for a given PC. In this way, a sort of multivariate picture of the investigated sample is obtained which shows all of the information explained by that PC.

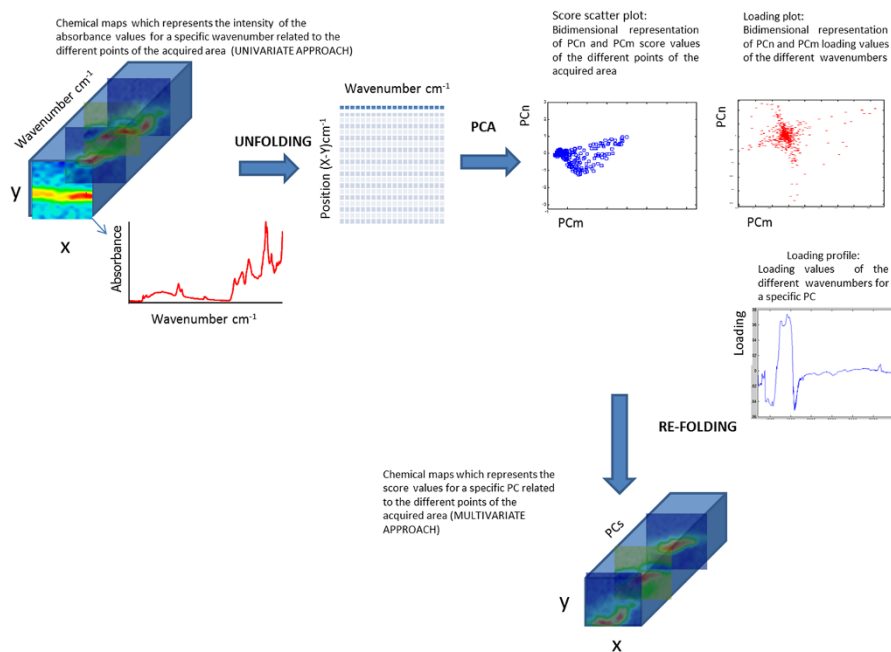


Fig. 12 Scheme of application steps of PCA multivariate approach on μ FTIR 3D data arrays

First attempts proposed interpretation of μ FTIR maps by representing score maps and by the visualization of score scatter plots, loading plots, and loading profiles (Fig. 12) [76, 77].

An improvement in data interpretation was obtained thanks to the integration of scatter plots and score maps, employing the so-called brushing approach (Fig. 13) [78]. This method allows identification of correspondences between clusters of scores (detectable in the scatter plots) and specific areas within a PC score map, thus making it possible to understand to which particular part of the investigated sample those points correspond (Fig. 13c, e). Furthermore, the spectral profiles of such objects may be extracted and interpreted by considering an average spectrum. This information can integrate analysis of the loading values, enabling identification of the spectral bands most involved in defining each subarea under investigation

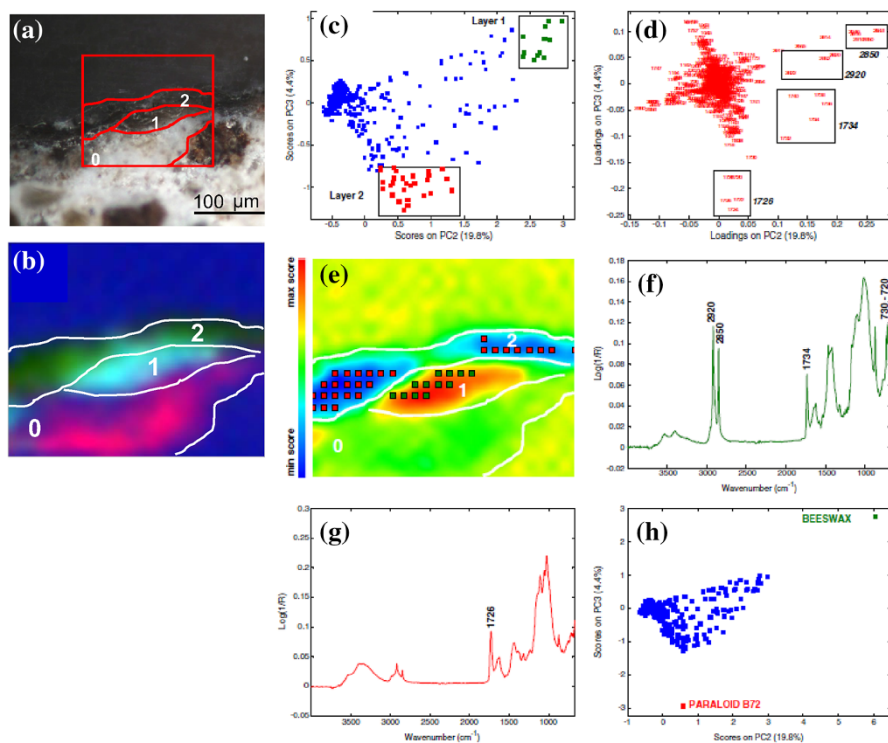


Fig. 13 PCA elaboration on μ FTIR map acquired from a real mural sample from Ercolano. **a** Photomicrograph of sample cross section, **b** PC false-color (RGB) image obtained by coding the score values on PC1, PC2, and PC3 as the intensity of the red, green, and blue channels; **c** PC2–3 score scatter plot: clusters highlighted in *green* and *red* indicate objects localized within the PC3 score map: layers 1 and 2, respectively; **d** PC2–3 loading plot, underlying the wavenumbers which mainly characterized *green points* in the PC2–3 score scatter plot (2850, 2920, and 1734 cm^{-1}) and wavenumbers which mainly characterized *red points* in the PC2–3 score scatter plot (1726 cm^{-1}); **e** PC3 score map, allowing clear distinction of the three layers present in the sample; **f** average spectral profile extracted from layer 1; **g** average spectral profile extracted from layer 2; **h** PC2–3 score scatter plot with spectra of pure standard compounds used as reference materials: Paraloid B72 (*red square*) and beeswax (*green square*). Reprinted from [78], with permission from Springer

(Fig. 13d, f–g). Finally, PC false-color (RGB) images can be obtained by coding the score values on three selected PCs as the intensity of the red, green, and blue channels (Fig. 13b). This generally allows one to illustrate the overall location of painting materials in a single image [35, 78]. As an example, Fig. 13 reports results obtained on a paint cross section collected from a mural painting from the archeological site of Ercolano (Erc3), Italy [78]. The joint interpretation of score and loading plots and the average spectra of points in the score plot corresponding to specific layers allowed identification of the protective layers present in the sample. In particular, Paraloid B72 (a commonly used acrylic consolidant and protective coating) and beeswax were identified in layer 2 and 1, respectively.

Chemometric elaboration of FTIR hyperspectral data implies use of preprocessing tools aimed at extracting the maximum useful information from the dataset. However, incorrect use of these correction tools may have negative effects in terms of amplifying noise or introducing artifacts. For this reason, the following section presents a short description of the commonest preprocessing treatments.

4.2 PCA Preprocessing Treatments

In the case of complex analytical signals arising from FTIR microscopy analysis, a number of preprocessing tools can be used with the purpose of:

1. Eliminating or reducing random noise
2. Eliminating or reducing unwanted systematic variations
3. Reducing or compressing acquired data

Unwanted systematic variations can result from instrumental difficulties, experimental conditions, and/or physical characteristics of the samples. In general, it might be advantageous to avoid unwanted signal variations by improving the experimental settings, but this approach is not always feasible.

Furthermore, in many cases, the effort that is needed (complex sample pretreatments, accurate temperature control, etc.) may be so great to become incompatible with practical and logistic issues in terms of time consumption or economic resources [79, 80]. For these reasons, when possible, it is preferable to remove signal variations afterward, by data preprocessing.

Correction of systematic differences among spectra is possible using row preprocessing treatments.

Row centering removes systematic location differences, such as baseline shifts, from a set of spectra, as shown in Fig. 14. Indeed, each absorbance value ($y_{i,v}$) referring to a specific spectrum (y_i), defined by v variables (the wavenumbers in an IR spectrum), is corrected individually by subtracting the mean absorbance value (\bar{y}_i) for spectrum y_i . The resulting values ($y_{i,v}^*$) of the row-centered spectrum are obtained as

$$y_{i,v}^* = y_{i,v} - \bar{y}_i. \quad (2)$$

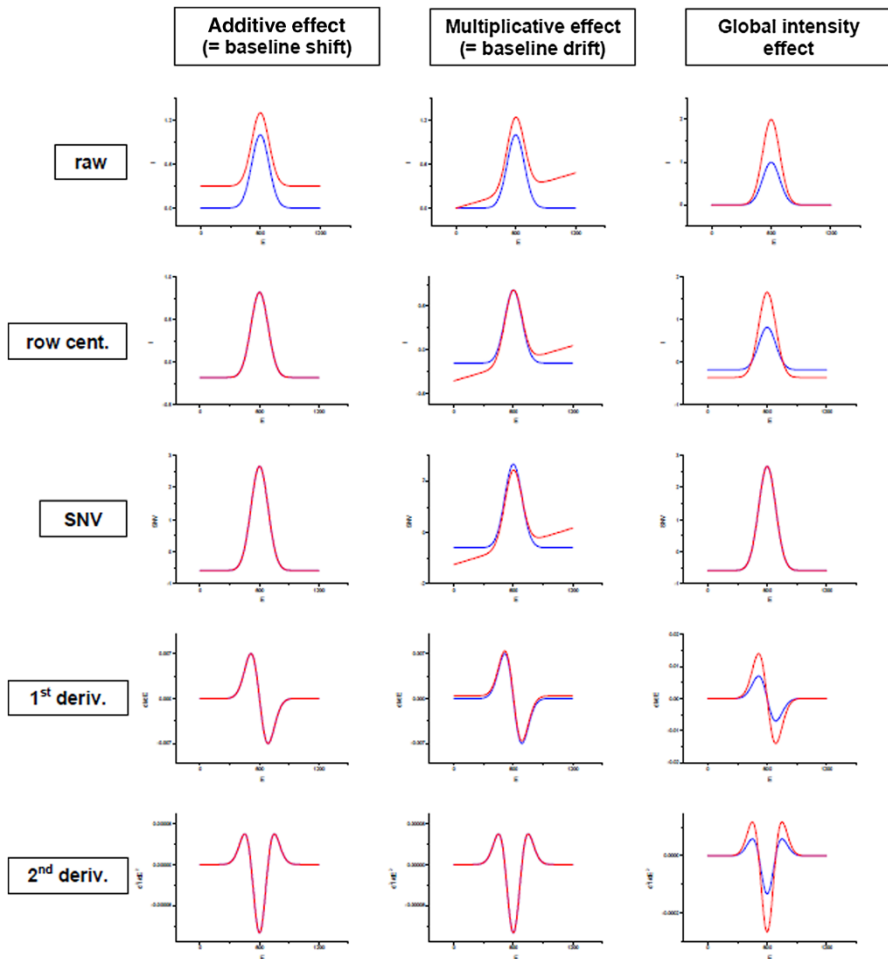


Fig. 14 Effectiveness of a number of row pretreatments in eliminating additive, multiplicative, and global intensity effects. Reprinted from [70], with permission from Elsevier

As a consequence of this transformation, the mean value of each spectrum becomes equal to 0.

Standard normal variate (SNV), or row, autoscaling corrects both location and dispersion systematic differences between spectra, thus removing baseline shifts and correcting global intensity variations (see Fig. 14). The values of an SNV-transformed spectrum are obtained by first row-centering the spectrum (y_i) then dividing the single absorbance values by the absorbance standard deviation s_i calculated considering the whole spectrum:

$$y_{i,v}^* = \frac{y_{i,v} - \bar{y}_i}{s_i} \quad (3)$$

In this way, each spectrum presents a mean value equal to 0 and a standard deviation equal to 1.

As for other corrections, SNV has to be used in a critical way; indeed, since this transformation has the peculiarity of potentially shifting informative regions throughout the signal range, interpretation of results referring to the original signals may be misleading [81].

First and second derivative treatments after smoothing increase the apparent resolution of overlapping peaks, accentuate small structural differences between nearly identical signals, and correct for baseline shifts and drifts, depending on the derivation order, as shown in Fig. 14 [70, 83].

In particular, the first derivative of a signal $y = f(x)$ is the slope of the tangent to the signal at each point:

$$y' = dy/dx. \quad (4)$$

The second derivative provides a correction for both additive and multiplicative effects and represents a measure of the curvature of the original signal. It is obtained as a further derivation of the first derivative:

$$y'' = d^2y/d^2x. \quad (5)$$

Although these transformations allow signal resolution enhancement, they may also result in enhancement of noise, which is usually characterized by high-frequency slope variations. To prevent this drawback, signals may be firstly smoothed, often using the Savitzky–Golay algorithm, to reduce the noise thanks to this moving-window averaging method [82].

Column preprocessing corrects systematic differences among variables, acting on each variable individually (the absorbance values at a certain wavenumber in all the dataset).

When column centering is performed, the absorption at a specific wavenumber for all the dataset is corrected individually by subtracting the mean absorbance value for this specific wavenumber for all the dataset (\bar{y}_v) from each individual absorbance value ($y_{i,v}$), as follows:

$$y_{i,v}^* = y_{i,v} - \bar{y}_v. \quad (6)$$

After transformation, the mean value of each column is equal to 0.

Column autoscaling eliminates systematic location and dispersion differences among heterogeneous variables. Indeed, the mean value of each single variable after such transformation is equal to 0, and the standard deviation to 1. Each variable is corrected individually by subtracting its mean (\bar{y}_v) from each of its values and then dividing by its standard deviation (s_v), as follows:

$$y_{i,v}^* = \frac{y_{i,v} - \bar{y}_v}{s_v}. \quad (7)$$

In this way, all the variables have the same a priori importance. This correction may be extremely useful in the case of signals in which all the variables have the same nature and measurement units, such as spectra, if there are relevant variables characterized by a relatively low mean value and/or standard deviation. Otherwise, this pretreatment may decrease the signal-to-noise ratio, since the same weight is given to the noisy parts.

5 New Perspectives on Application of FTIR Microscopy for Characterization of Artistic Materials: Enhanced FTIR-Based Methods

In 1980, Harstein et al. [84] discovered that, when a molecule was adsorbed on a metal surface in the form of nanoparticles or nanoislands, its infrared absorption was significantly more intense than expected. This effect, named surface-enhanced infrared reflection absorption (SEIRA), is observed in transmission, attenuated total reflection, total reflection, and diffuse reflection. Similarly to surface-enhanced Raman scattering (SERS), the enhancement is produced by a combination of electromagnetic and chemical mechanisms [85–89]. The metal islands are polarized by the incident infrared photon field through excitation of collective electron resonance, or localized plasmon modes. The dipole (p) induced in an island generates a local electromagnetic (EM) field stronger than the incident infrared photon field around the island. In particular, the intensity of the enhanced EM field decays with the distance of the analyte from the metallic surface. Moreover, in the proximity of the nanoislands, the local EM field is normally polarized at every point along the surface. The scheme reported in Fig. 15 explains the EM enhancement and the surface selection rules.

A chemical contribution to the SEIRA effect is observed when the analyte is chemisorbed on the metal surface, since additional dipoles are induced in the metal islands [89]. The enhancement factor and the prevalence of electromagnetic or

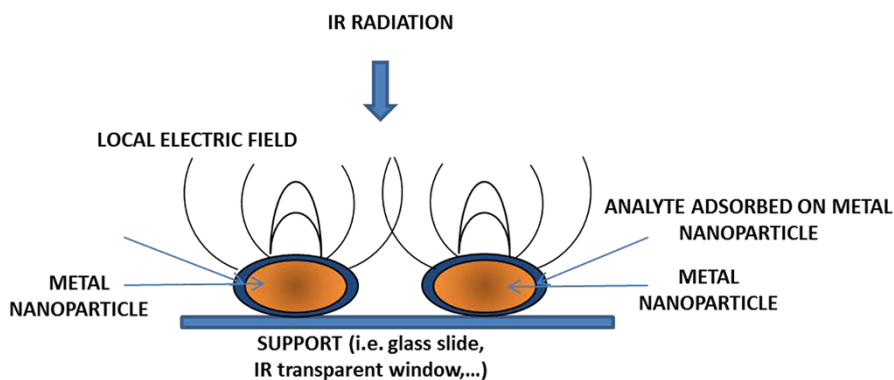


Fig. 15 Schematic representation of electromagnetic mechanism of SEIRA on metal island films

chemical contributions must be evaluated in each specific case, according to the nature of the SEIRA support used and of the molecular species investigated.

Different types of enhancing surfaces can be successfully applied to obtain such a SEIRA effect. The most widely used supports are obtained by producing island films with coinage metals [90–93]. With the advent of nanotechnology, a lot of enhancing surfaces have become available for SEIRA spectroscopy [94, 95]. Thin metal film evaporation under vacuum has been demonstrated to be an effective approach to obtain irregular surfaces (also applied for SERS analysis) [96, 97]. This is a simple and inexpensive procedure that provides a disordered, rough thin film of metal on a suitable holder. The deposition rate of the metal and the film thickness are crucial parameters in this technique to obtain an active surface. In particular, it was found that a slow rate of deposition generally provides the best enhancement [97]. An alternative method to obtain a metal film is electrochemical deposition. A suitable potential or current is applied to an electrolyte solution of salts of the metal to be deposited, under potentiostatic, galvanostatic, or potential cycling conditions. Rough electrodes obtained using this procedure have been proposed as low-cost substrates for SEIRA analysis [98].

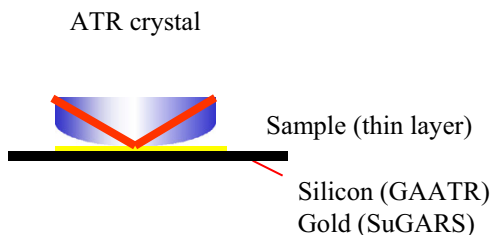
Metal colloids have become the most commonly used substrates, in both SERS and SEIRA, thanks to their easy preparation and the possibility of inducing aggregation, during and after synthesis [99, 100]. In more detail, metal colloidal nanoparticles may be produced using chemical (reactions in solution), physical (laser ablation), or photophysical (photoreduction of Au and Ag salts) methods.

For SEIRA analysis, the sample can be placed in contact with an active substrate using different methods. Using the “drop-drying method,” a dilute solution of analyte is applied onto a support and analyzed after drying. Another possibility is to form a thin film of the sample on the metal surface by evaporation under vacuum. SEIRA analysis can also be performed on Langmuir films obtained by horizontal deposition in a Langmuir balance followed by transfer to the SEIRA substrate [94]. Moreover, depending on the type of support, different configurations such as sample–metal, metal–sample, and metal–sample–metal have been successfully adopted.

Since the enhancement factors (about 10–1000 times) of SEIRA are not competitive when compared with those of SERS, little attention has been dedicated to possible applications. However, cross sections for infrared absorption are an order of magnitude larger than corresponding Raman cross sections. Thus, even if SEIRA enhancement is modest, it can be effective in practical applications, so both techniques are under development as promising optical sensor technologies [94]. Recently, two other enhanced-sensitivity FTIR methods, namely super grazing-angle reflection spectroscopy (SuGARS) and grazing-angle attenuated total reflection (GAATR), have been described [101–104].

These two techniques have in common a thin layer of sample deposited on a high-refractive-index material (a metal for SuGARS, silicon for GAATR), analyzed in “ATR mode” with a high-refractive-index internal reflection element (typically germanium) at high angle of incidence (AOI) (Fig. 16). In particular, the AOI must be greater than the critical angle for the ATR material–substrate interface for GAATR (i.e., for the germanium–silicon system, $\theta > 59.6^\circ$) and larger than the

Fig. 16 SuGARS and GAATR configurations



AOI for the Ge–sample interface for SuGARS. In the GAATR configuration, it is not possible to use lower angles (even if greater than the θ_c for the IRE–thin film system); indeed, the evanescent wave would be refracted at the interface between the thin film and the support (for example, silicon) following Snell’s law. The SuGARS configuration cannot be considered an ATR technique, because the substrate has a much higher refractive index than germanium. Nevertheless, the metal substrate confines the transmitted wave to the film, which has the consequence that the intensity of the wave in the film is greatly enhanced. When thin layers such as monolayers are applied on either silicon or a metal and analyzed in grazing conditions, the absorbance of the spectral bands is greatly amplified [101–104]. Based on simulations, the two techniques provide similar results and comparable performance. In particular, it was observed that the absorbance enhancement is high for very thin layers (about 10 nm) and then decreases to one (no enhancement) with increasing thickness [102]. Even if, to date, mainly simulation studies have been performed, these two techniques have the potential to be used in fields such as forensic, material, or conservation science, where the amount of sample is generally extremely limited.

5.1 First Applications of Enhanced FTIR Methods for Analysis of Artistic Materials

SEIRA, GAATR, and SuGARS appear to be very promising systems for analysis of thin films or in the case of very small amounts of material being available. In the field of conservation science, these methods can be applied for analysis of thin films applied on metallic surfaces such as varnished metal leaves applied in gilding techniques and protective coatings applied on metal objects, or for analysis of microextracts.

Analysis of dyes represents a possible field of application, as their characterization is a well-known challenging task, due to their inherent high tinting strength and consequent low concentration in the carrying matrix [105]. High-performance liquid chromatography (HPLC) is usually the technique chosen to precisely identify the nature of dyes and mixtures thereof [106, 107]. Alternative protocols including nondestructive investigations such as UV–Vis reflectance or fluorescence measurements conducted directly on dyed fibers prior to more invasive analysis have also been suggested [108, 109].

Vibrational spectroscopic techniques such as infrared and Raman spectroscopies have been employed as well, with consistent difficulties linked to the sample typology and the amount necessary to obtain good-quality spectra [110]. In Raman spectroscopy, problems related to the relevant fluorescence emission from dyes have been overcome by means of SERS methods which can be applied both directly on fiber or on dye extracts [111–116]. For IR spectroscopy, extractionless protocols cannot be applied because the less intense signals from dyes are completely hidden by strong bands characterizing the IR profile of the textile material onto which they are absorbed.

Therefore, dyestuffs must be extracted from their textile support, which is generally performed using the same extraction procedures applied for HPLC experiments, taking into consideration that strong acid-based extraction procedures must be avoided because they would cause hydrolysis of the fibers, forming soluble species whose IR absorption could overlap with that of the dyes.

Recently, it was shown that, starting from less than 0.1 mg of dyed fiber and employing a microextraction procedure, it was possible to identify the dye by using a SEIRA-based method [117].

In particular, 10 μL of microextract was mixed with the same aliquot of gold nanoparticle (AuNP) colloidal solution obtained by laser ablation [118]. Compared with metal colloids obtained by chemical reaction, AuNPs obtained with laser ablation avoid the presence of spurious byproducts which may affect the results. Two aliquots of the obtained solutions were spotted onto a gold-coated glass slide before and after addition of the gold nanoparticles and analyzed in RAS mode. As

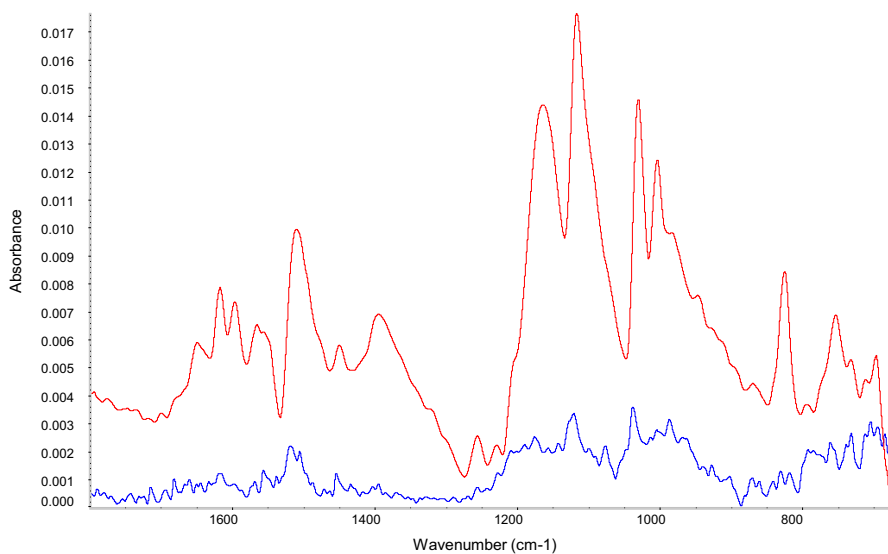


Fig. 17 SEIRA spectrum recorded on the border of a drop obtained by spotting 1 μL of solution extracted from a few millimeters of a single fiber dyed with Acid Orange 7: **a** mixed with AuNPs obtained with laser ablation (*red profile*) and **b** without addition of AuNPs (*blue profile*); full scale

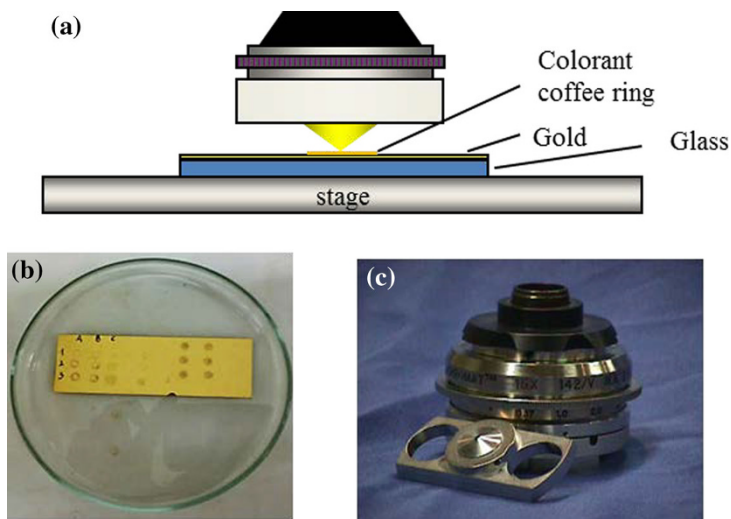


Fig. 18 ATR analysis on spot applied on a gold-coated glass slide: **a** schematic of setup; **b** gold-coated glass slide with colorants spotted on it; **c** ATR objective

reported in Fig. 17, enhancement of the signal could be observed when the analyte was added with AuNPs [117].

We recently found a greater signal enhancement when we spotted microextract onto a gold-coated glass slide and performed the analysis in μ ATR mode (Fig. 18).

This setup is similar to SuGARS, although commercial ATR systems generally have a fixed angle of incidence, which is typically selected to enable routine μ ATR analysis and is far from grazing conditions. Moreover, we found that this setup is particularly useful to analyze layers formed after evaporation of a small volume (about 1 μ L) of dye microextract, being thicker (more than 300 nm) than the monolayers suitable for SuGARS.

Our research group will shortly publish on the application of this method to analysis of dyes.

6 Conclusions and Future Perspectives

FTIR microscopy is one of the most versatile techniques for analysis of complex, multicomponent, and multilayer samples such as those typically encountered in the field of heritage materials. Indeed, even though great efforts have been devoted to development of nondestructive portable systems for in situ analysis of cultural objects over recent years, the information that these techniques can provide is still incomplete for comprehensive understanding of layer-structured artworks. For this purpose, new methods such as nuclear magnetic resonance (NMR) profilometry and terahertz spectroscopy [119, 120] have been proposed to provide nondestructive stratigraphic information, but they only allow one to obtain information on the presence and homogeneity of layered structures but not yet to chemically

characterize each layer. Therefore, the development of FTIR microscopy-based methods for analysis of artworks will provide complementary chemical information on materials used by ancient artists. More precisely, FTIR microscopy performed in the near-infrared (NIR) region in total reflectance mode can be a complementary tool for characterization of paint cross sections. Integrated use of information recorded in both NIR and MIR regions is extremely useful for molecular investigation of both organic and inorganic substances, due to the fact that combination and overtone bands present in the NIR region, even if weaker and less selective than those in the MIR region, are not distorted by reflection phenomena. Thus, NIR spectra can be efficiently used as a spectral fingerprint for stratigraphic characterization of paint cross sections.

One of the main interesting research fields will probably be further development of procedures for analysis of multilayer historical samples by means of SR-FTIR microscopy. The brightness and collimation of SR light are particularly useful for identification of complex mixtures and thin layers. The main drawback is that SR-FTIR microscopy analysis is performed either in total reflection, which produces highly distorted spectra, or in transmission, which is applicable only for thin sections. Several methods have been proposed to obtain thin sections, but the effectiveness of these preparation procedures varies with the sample composition, and in some cases sample integrity may be irretrievably compromised. Thus, further research is needed to propose more controllable procedures. On the other hand, significant improvements will be obtained by designing ad hoc ATR systems which can be easily coupled with SR light to analyze both cross and thin sections.

Chemometric elaboration allows easy interpretation of complex hyperspectral data acquired by μ FTIR mapping and imaging techniques. Further progress could be made through the development of tools that allow elaboration of hyperspectral data obtained via different molecular (i.e., Raman and FTIR) and elemental (i.e., SEM-EDX) techniques, providing an easy way to couple correctly points acquired by the different systems, considering that it will be hard to select exactly the same area and that the spatial resolution may be different.

A very interesting and promising field is the development of enhanced μ FTIR-based methods for detection of trace components in microextracts. Further efforts will be devoted to optimize microextraction procedures for different kinds of substances (i.e., natural colorants, synthetic colorants, varnishes extracted, for instance, from cotton swabs used during cleaning of paintings, organic residues on archeological remains, etc.) to improve the detection limits. At the moment, applications of these methods for identification of trace amounts of dyes in microextracts have provided the first successful results. In particular, coupling of μ FTIR to thin-layer chromatography supports used for separation of mixtures of dyes is currently under study by our research group, and results will be published in the very near future. These applications will open new frontiers in the use of FTIR microscopy for trace analysis.

Acknowledgments Part of this research has been funded by the European project “CHARISMA” FP7 Infrastructure no. 228330.

References

1. Derrick MR, Stulik DC (1999) *Infrared spectroscopy in conservation science*. The Getty Conservation Institute, Los Angeles
2. Casadio F, Toniolo L (2001) *J Cult Herit* 2:71–78
3. Gettens RJ (1952) *Sci Am* 187:22–27
4. Low MJD, Baer NS (1977) *Stud Conserv* 22:116–128
5. Messerschmidt RG, Harthcock MA (1988) *Infrared microspectroscopy. Theory and applications*. Marcel Dekker, New York
6. Prati S, Josphe E, Sciuotto G, Mazzeo R (2010) *Acc Chem Res* 6:792–801
7. Gillard RD, Hardman SM (1994) *Stud Conserv* 39:187–192
8. Bruni S, Cariati F, Casadio F, Toniolo L (1999) *Vibr Spectrosc* 20:15–25
9. Dannenberg H, Forbes JW (1960) *Anal Chem* 32:365–370
10. Griffiths P, De Haseth JA (2007) *Fourier transform infrared spectrometry*, 2nd edn. Wiley, New Jersey
11. Miliani C, Rosi F, Daveri A, Brunetti BG (2012) *Appl Phys A* 106:295–307
12. Rosi F, Federici A, Brunetti BG, Sgamellotti A, Clementi S, Miliani C (2011) *Anal Bioanal Chem* 39:3133–3145
13. Van der Weerd J, Brammer H, Boon JJ, Heeren RMA (2002) *Appl Spectrosc* 56:276–283
14. Reffner JA, Martoglio PA (1995) In: Huecki HJ (ed) *Practical guide to infrared microspectroscopy*. Marcel Dekker, New York
15. Lewis L, Sommer AJ (1999) *Appl Spectrosc* 53:375–380
16. Lewis EN, Treado PJ, Reeder RC, Story GM, Dowrey AE, Marco C, Levin IW (1995) *Anal Chem* 67:3377–3381
17. Chan KLA, Kazarian SG (2003) *Appl Spectrosc* 57:381–389
18. Joseph E, Prati S, Sciuotto G, Ioele M, Santopadre P, Mazzeo R (2010) *Anal Bioanal Chem* 396:899–910
19. Howard M (2001) In: Raghavachari R (ed) *Near-infrared applications in biotechnology*, Marcel Dekker, New York
20. Pasquini C (2003) *J Braz Chem Soc* 14:198–219
21. Blanco M, Coello J, Iturriaga H, MasPOCH S, de la Pezuela C (1998) *Analyst* 123:135–150
22. Cruz Sarraguça M, Almeida Lopez J (2009) *Vibr Spectrosc* 49:204–210
23. Reid LM, O'Donnell CP, Downey G (2006) *Trends Food Sci Tech* 17:344–353
24. Karoui R, de Baerdemaeker J (2007) *Food Chem* 102:621–640
25. Lachenal G (1995) *Vibr Spectrosc* 9:93–100
26. Rosi F, Daveri A, Doherty B, Nazzareni S, Brunetti BG, Sgamellotti A, Miliani C (2010) *Appl Spectrosc* 64:956–963
27. Bacci M, Magrini D, Picollo M, Vervat M (2009) *J Cult Herit* 10:275–280
28. Vagnini M, Miliani C, Cartechini L, Rocchi P, Brunetti BG, Sgamellotti A (2009) *Anal Bioanal Chem* 395:2107–2118
29. Milani C, Rosi F, Burnstock A, Brunetti BG, Sgamellotti A (2007) *Appl Phys A* 89:849–856
30. Rosi F, Daveri A, Miliani C, Verri G, Benedetti P, Piqué F, Brunetti BG, Sgamellotti A (2010) *Anal Bioanal Chem* 385:2097–2106
31. Trafela T, Strlic M, Kolar J, Lichtblau DA, Anders M, Pucko Mencigar D, Pihlar B (2007) *Anal Chem* 79:6319–6323
32. Nevin A, Comelli D, Osticioli I, Toniolo L, Valentini G, Cubeddu R (2009) *Anal Bioanal Chem* 395:2139–2149
33. Dooley KA, Lomax S, Zeibel JG, Miliani C, Ricciardi P, Hoenigswald A, Loew M, Delaney JK (2013) *Analyst* 138:4838–4848
34. Poli T, Chiantore O, Giovagnoli A, Piccirillo A (2012) *Anal Bioanal Chem* 402:2977–2984
35. Sciuotto G, Prati S, Bonacini I, Oliveri O, Mazzeo R (2014) *Microchem J* 112:87–96
36. Prati S, Sciuotto G, Mazzeo R, Torri C, Fabbri D (2011) *Anal Bioanal Chem* 399:3081–3091
37. Laurie AP (1914) *The pigments and mediums of the old masters*. Macmillan, London
38. Gettens RJ (1936) *Tech Stud Field Fine Arts* 5:18–22
39. Plesters J (1956) *Stud Conserv* 2:110–157
40. Derrick M, Souza L, Kieslich T, Florsham H, Stulik D (1994) *Am Instit Conserv* 33:227–245
41. Pilc J, White R (1995) *Natl Gallery Tech Bull* 16:73–84

42. Cotte M, Checron E, Mazel V, Solé A, Richardin P, Taniguchi Y, Walter P, Susini J (2009) *E-Preserv Sci* 6:1–9
43. Van der Weerd J, Heeren RMA, Boon JJ (2004) *Stud Conserv* 29:193–210
44. Tsang JS, Cunningham RH (1991) *J Am Inst Conserv* 30:163–177
45. Echard JP, Bertrand L, von Bohlen A, Le Hô AS, Paris C, Bellot-Gurlet L, Soulier B, Lattuati-Derieux A, Thao S, Robinet L, Lavédrine B, Vaiedelich S (2010) *Angew Chem Int Ed* 49:197–201
46. Janssens K, Alfeld M, Van der Snickt G, De Nolf W, Vanmeert F, Radepon M, Monico L, Dik J, Cotte M, Falkenberg G, Miliani C, Brunetti BG (2013) *Annu Rev Anal Chem* 6:399–425
47. Beltran V, Salvadó N, Butí S, Cinque G, Wehbe K, Pradell T (2015) *Anal Chem* 87:6500–6504
48. Salvadó N, Pradell T, Pantos E, Papiz MZ, Molera J, Seco M, Vendrell-Saz M (2002) *J Synch Rad* 9:215–222
49. Salvadó N, Butí S, Cotte M, Cinque G, Pradell T (2013) *Appl Phys A* 111:47–57
50. Salvadó N, Butí S, Nicholson J, Emerich H, Labrador A, Pradell T (2009) *Talanta* 79:419–428
51. Cotte M, Susini J (2008) *J Anal At Spectr* 23:820–828
52. Pouyet E, Lluveras-Tenorio A, Nevin A, Saviello D, Sette F, Cotte M (2014) *Anal Chim Acta* 822:51–59
53. Bertrand L, Robinet L, Cohen SX, Sandt C, Le Hô A, Soulier B, Lattuati-Derieux A, Echard J (2010) *Anal Bioanal Chem* 399:3025–3032
54. Echard JP, Cotte M, Dooryhee E, Bertrand L (2008) *Appl Phys A* 92:77–81
55. Mazzeo R, Joseph E, Prati S, Millemaggi A (2007) *Anal Chim Acta* 599:107–117
56. Prati S, Sciuotto G, Catelli E, Ashashina A, Mazzeo R (2013) *Anal Bioanal Chem* 405:895–905
57. Prati S, Rosi F, Sciuotto G, Mazzeo R, Magrini D, Sotiropoulou S, Van Bos M (2012) *Microchem J* 103:79–89
58. Ogura K, Kamidaira M, Asahina S, Erdman N (2007) *Microsc Microanal* 13:1518–1519
59. Boon JJ, Asahina S (2006) *Microsc Microanal* 12:1322–1323
60. Boon JJ, van der Horst J (2008) In: J Townsend (ed) *Proceedings of the ICOMCC paintings working group meeting on grounds*. Archetype, London
61. De Fonjaudran CM, Nevin A, Piqué F, Cather S (2008) *Anal Bioanal Chem* 392:77–86
62. Jäegers E, Jäegers E (1999) *Brit Mus Occas Pap* 135:37–42
63. Muros V, Hirx J (2004) *JAIC* 43:75–89
64. Hopfe V, Korte EH, Klobes P, Griihlert W (1993) *J Mol Struct* 293:245–248
65. Chalmers JM, Everall NJ, Ellison S (1996) *Micron* 27:315–328
66. Prati S, Rosi F, Sciuotto G, Oliveri P, Catelli E, Miliani C, Mazzeo R (2013) *Microchem J* 110:314–319
67. Treado PJ, Morris MD (1993) *Microscopic and spectroscopic imaging of the chemical state*. Marcel Dekker, New York
68. Krishnan K, Powell JR, Hill SL (1995) In: Humecki HJ (ed) *Practical guide to infrared microspectroscopy*. Marcel Dekker, New York
69. Wold S (1972) *Kem Tidskr* 84:34–37
70. Oliveri P, Casolino MC, Forina M (2010) *Adv Food Nutr Res* 61:57–117
71. Romero-Pastor J, Cardell C, Yebra-Rodríguez Á, Rodríguez-Navarro AB (2013) *J Cult Herit* 14:509–514
72. Sarmiento A, Pérez-Alonso M, Olivares M, Castro K, Martínez-Arkarazo I, Fernández LA, Madariaga JM (2011) *Anal Bioanal Chem* 399:3601–3611
73. Rosi F, Miliani C, Clementi C, Kahrim K, Presciutti F, Vagnini M, Manuali V, Daveri A, Cartechini L, Brunetti BG, Sgamellotti A (2010) *Appl Phys A* 100:613–624
74. Rosi F, Burnstock A, Van den Berg KJ, Miliani C, Brunetti, Navas N, Romero-Pastor JB, Manzano E, Cardell C (2008) *Anal Chim Acta* 630:141–149
75. Miliani C, Rosi F, Borgia I, Benedetti P, Brunetti BG, Sgamellotti A (2007) *Appl Spectrosc* 61:293–299
76. Rosi F, Miliani C, Federici A, Brunetti BG, Sgamellotti A, Clementi S (2010) *Anal Bioanal Chem* 399:3133–3145
77. Spring M, Ricci C, Peggie DA, Kazarian S (2008) *Anal Bioanal Chem* 392:37–45
78. Sciuotto G, Oliveri P, Prati S, Quaranta M, Lanteri S, Mazzeo R (2013) *Anal Bioanal Chem* 405:625–633
79. Valcárcel M, Cárdenas S (2005) *Trends Anal Chem* 24:67–74
80. Vlasov Y, Legin A, Rudnitskaya A, Di Natale C, D'Amico A (2005) *Pure Appl Chem* 77:1965–1983

81. Fearn T (2009) *NIR News* 20:16–17
82. Savitzky A, Golay MJE (1964) *Anal Chem* 36:1627–1639
83. Taaavitsainen VM, Brown SD, Tauler R, Walczak B (eds) (2009) *Comprehensive chemometrics*. Elsevier, Amsterdam
84. Hartstein A, Kirtley JR, Tsang JC (1980) *Phys Rev Lett* 15:201–204
85. Osawa M, Matsuda N, Yoshii K, Uchida I (1994) *Phys Chem* 98:12702–12707
86. Osawa M (2001) *Top Appl Phys* 81:163–187
87. Fasasi A, Griffiths PR, Pan HB, Wai CM (2011) *Appl Spectrosc* 7:741–745
88. Yang J, Griffiths PR (2007) *Anal Bioanal Chem* 388:109–119
89. Osawa M, Ikeda M (1991) *J Phys Chem* 95:9914–9919
90. Bjerke AE, Griffiths PR, Theiss W (1991) *Anal Chem* 71:1967–1974
91. Aroca R, Price B (1997) *J Phys Chem* 101:6537–6540
92. Hahn F, Melendres CA (2001) *Electrochim Acta* 46:3525–3534
93. Seelenbinder JA, Brown CW, Pivarnik P, Rand AG (1999) *Anal Chem* 71:1963–1966
94. Aroca F, Ross J, Domingo C (2004) *Appl Spectrosc* 58:324–338
95. Masson JF, Murray-Méhot MP, Live LS (2010) *Analyst* 135:1483–1489
96. Saito Y, Wang JJ, Smith DA, Batchelder DN (2002) *Langmuir* 18:2959–2961
97. Sockalingum GD, Beljebbar A, Morjani H, Angiboust JF, Manfait M (1998) *Biospectroscopy* 4:71–78
98. Wanzenböck HD, Mizaikoff B, Weissenbacher N, Kellner R (1998) *Fresen J Anal Chem* 362:15–20
99. Polubotko AM (1993) *Phys Lett A* 173:424–432
100. Badilescu S, Ashrit PV, Truong VV, Badilescu L (1989) *Appl Spectrosc* 43:549–551
101. Milosevic M, Berets SL, Fadeev AY (2003) *Appl Spectrosc* 57:724–727
102. Milosevic M (2012) *Internal reflection and ATR spectroscopy*. Wiley, New Jersey
103. Mulcahy ME, Berets SL, Milosevic M, Michl J (2004) *J Phys Chem B* 108:1519–1521
104. Milosevic M, Milosevic V, Berets SL (2007) *Appl Spectrosc* 61:530–536
105. Christie RM (2001) *Colour chemistry*. RSC Paperbacks, London
106. Zhang X, Laursen RA (2005) *Anal Chem* 77:2022–2025
107. van Bommel MR, Vanden Berghe I, Wallert AM, Boitelle R, Wouters J (2007) *J Chromatogr A* 1157:260–272
108. Gulmini M, Idone A, Diana E, Gastaldi D, Vaudan D, Aceto M (2013) *Dyes Pigments* 98:136–145
109. Lee J, Kim MH, Lee KB, van Elslande E, Walter P, Lee Y (2014) *Surf Interface Anal* 46:312–316
110. Vandenabeele P, Moens L (2012) *J Raman Spectrosc* 43:1545–1550
111. Casadio F, Leona M, Lombardi JR, van Duyne RP (2010) *Acc Chem Res* 43:782–791
112. Casadio F, van Duyne RP (2013) *Analyst* 138:7276–7278
113. Leona M, Decuzzi P, Kubic TA, Gates G, Lombardi JR (2011) *Anal Chem* 83:3990–3993
114. Lofrumento C, Ricci M, Platania E, Becucci M, Castellucci E (2013) *J Raman Spectrosc* 44:47–54
115. Pozzi F, Lombardi JR, Bruni S, Leona M (2012) *Anal Chem* 84:3751–3757
116. Canamares MV, Garcia-Ramos JV, Gomez-Varga JD, Domingo C, Sanchez-Cortes S (2007) *Langmuir* 23:5210–5215
117. Prati S, Quaranta M, Sciutto G, Bonacini I, Litti L, Meneghetti M, Mazzeo R (2014) *Herit Sci* 2:28
118. Amendola V, Meneghetti M (2007) *J Mater Chem* 17:4705–4710
119. Blumich B, Casanova F, Perlo J, Presciutti F, Anselmi C, Doherty B (2010) *Acc Chem Res* 43:761–770
120. Targowski P, Iwanicka M (2012) *Appl Phys A* 106:265–277

Raman Spectroscopy of cultural heritage Materials: Overview of Applications and New Frontiers in Instrumentation, Sampling Modalities, and Data Processing

Francesca Casadio¹  · Céline Daher² · Ludovic Bellot-Gurlet³ 

Received: 1 May 2016 / Accepted: 30 July 2016 / Published online: 22 August 2016
© Springer International Publishing Switzerland 2016

Abstract Rooted in the long tradition of Raman spectroscopy of cultural heritage materials, in this work we provide a personal perspective on recent applications and new frontiers in sampling modalities, data processing, and instrumentation.

Keywords Raman spectroscopy · Cultural heritage · Archaeometry · Data processing · SERS · SORS

1 Introduction

Thirty years after its first application to the study of artworks [151], Raman spectroscopy today is an established tool for the molecular investigation of cultural heritage materials. Its characteristics of high spatial resolution (typically ranging between 1 and 10 μm), both in terms of lateral resolution and depth profiling (with confocal instruments), molecular specificity (buttressed by the availability of ad-hoc built databases), non-destructivity, coupled with the ability to conduct in situ analysis, and extreme versatility in terms of the areas of applications (spanning minerals, gems, organic and inorganic pigments and their degradation products,

This article is part of the Topical Collection “Analytical Chemistry for cultural heritage”.

✉ Francesca Casadio
fcasadio@artich.edu

¹ The Art Institute of Chicago, 111 S. Michigan Ave, 60603 Chicago, IL, USA

² Centre de Recherche sur la Conservation (CRC), Muséum National d’Histoire Naturelle, Sorbonne-Universités CNRS, MCC, USR 3224, CRCC CP21, 36 rue Geoffroy Saint Hilaire, Paris 75005, France

³ Sorbonne Universités, UPMC Université Pierre et Marie Curie-Paris 6, MONARIS “de la Molécule aux Nano-objets: Réactivité, Interactions et Spectroscopies”, UMR 8233, UPMC/CNRS, 4 Place Jussieu, Paris Cedex 05 75252, France

binding media, varnishes, plastics, glass, ceramics, and conservation treatments), make Raman spectroscopy a versatile and quasi-indispensable tool in the arsenal of cultural heritage scientists. Modern, efficient detectors allow operations at very low laser powers, reducing the risk of charring or otherwise altering the sample during analysis, while the availability of several different types of instruments (including Fourier-transform Raman spectrometers and dispersive Raman microscopes equipped with confocal holes), and the rise of surface-enhanced Raman spectroscopy (SERS) have been instrumental in quenching or altogether avoiding the overwhelming phenomenon of fluorescence, which plagues Raman applications to the hierarchically complex, often organic/inorganic and aged materials that characterise works of art and archaeological artifacts.

Rooted in the long tradition of Raman spectroscopy of cultural heritage materials, in this work we provide a personal perspective on recent applications and new frontiers in sampling modalities, data processing, and instrumentation.

2 Recent Developments in Instrumentation and Sampling Modalities

2.1 Instrumentation

Since its experimental discovery [254], the instruments used to record Raman scattering radiation have witnessed numerous revolutions. These technical evolutions concern excitation sources, the interface with the sample, the scattered radiation analysis, signal recording, and the automated management of analysis or spectral handling. During these evolutions, Raman spectroscopy has broadened its areas of applications, from fundamental physics and chemistry to all fields of analytical chemistry, gaining particular relevance for the study of the cultural heritage, as illustrated in this article.

2.1.1 Laser Sources

Light sources for the Raman effect initiate with the sun (the original experiment of C.V. Raman), followed by energy lines emitted from mercury and other lamps, and then, since the 1960s, produced by lasers and all their evolutions. When introduced, lasers offered the promise of intense excitation [173], effectively counterbalancing the weakness of the Raman scattering effect. Since the 1990s, the introduction of solid laser sources (and the ensuing diversification of available lines) was one of the parameters allowing the reduction in size of Raman devices and the lowering of the barriers of the required technical environment for their operation (initially involving high-power electrical supplies, water-cooling systems and other demanding infrastructure requirements).

The most popular kinds of gas lasers are mixed helium–neon, argon, krypton and mixed argon–krypton. For helium–neon lasers, no high current or large external cooling are needed to produce sufficient power with their main emission in the red at 632.8 nm (value often rounded to 633). With its reduced size and long service life, it was a popular technical choice before the introduction of solid-state lasers. Argon

lasers' (Ar^+) most widely used line is the green at 514.5 nm (often rounded to 514). Such a laser is able to produce intense emissions, but requires a high-voltage input and an efficient external cooling system by water circulation. With the low excitation power needed for many studies of cultural heritage samples and objects, nowadays "miniaturised" argon lasers are available with air cooling and a standard power supply. The interest of such gas lasers is the ability to tune the emission wavelength, and select different emissions, which for argon, in addition to the line at 514 nm, are in the blue range at 457.9 and 488 nm. With sufficiently powerful models, an additional line in the near-ultra-violet (UV) at 363.8 nm can also be used. Tunable lasers may be appealing for Raman spectroscopy, but with a lifetime of around 10,000 h and rather high costs, these systems are not fully competitive with solid-state sources, and the manufacturers are therefore dropping this technology. For gas lasers emitting in the blue, which are more rarely used in Raman applications for the cultural heritage, a specific type is the helium–cadmium (HeCd) laser, with lines at 325 and 441.6 nm. Finally, a gas laser based on krypton is known for its deep blue lines at 406.7 and 413.1 nm, and a red one at 647.1 nm, whereas mixed argon–krypton lasers combine the blue and green lines with this additional red one.

For solid-state lasers, the most common types are based on Nd:YAG diodes (neodymium-doped yttrium aluminium garnet). The main emission of such lasers is at 1064 nm, the near-IR (IR) excitation used in Fourier-transform (FT) Raman instrumentation since the 1980s. In the 1990s, frequency-doubled Nd:YAG were introduced, with a green emission at 532 nm that is competitive with the Ar^+ lasers emitting at 514 nm, thanks to their small size, long lifetime, and stability, becoming the most popular green line in Raman spectroscopy. It should also be noted that other multiplying devices or emission lines of Nd:YAG diodes are used (see below), as, for example, the line obtained by the frequency quadrupling of their main emission, which occurs in the UV range at 266 nm.

The next generation of solid-state lasers used in Raman spectroscopy emit in the beginning of the near-IR range at around 785 nm, as is the case, for example, with gallium, aluminum, and arsenic (GaAlAs) diodes. With their affordable cost, these lasers have become very popular, also because their near-IR excitation can avoid the fluorescence of various samples from works of art and archaeology, especially organic materials. However, because of the rapid decline of CCD detector efficiency in the IR range above about 950 nm (which corresponds to a Raman shift of approximately 2220 cm^{-1} from 785 nm), no significant Raman signal can be recorded beyond about 2000 cm^{-1} . This can constitute a serious limitation when studying C–H or O–H stretching vibrations of specific samples; for example, the $\text{C}\equiv\text{N}$ stretching of Prussian blue (ferric ferrocyanide) occurring at 2102 and 2154 cm^{-1} would be out of range. Such laser diodes are also quite sensitive to temperature variations that may induce deviations of the emission wavelength; thus, a good thermal control is required for Raman applications. However, on the other hand, this specificity can be used for fluorescence removal (see Sect. 3.1). Solid-state lasers are currently regularly evolving as other diodes appear on the market, such as the GaAs diode with emission in the near-IR, around 830 nm.

For a long time, there was a lack of solid-state lasers emitting in the blue. One of the first examples to be offered on the market was a laser emitting at 473 nm based

on the frequency-doubling of a secondary emission at 946 nm of the Nd:YAG diode. Nowadays, manufacturers develop lasers for producing other wavelengths, such as, for example, at 405, 443, 488 nm. In the near future, such lasers will likely effectively replace argon or krypton gas lasers, even if they are not commonly proposed by Raman manufacturers, who still prefer systems based on green and red lines. Rather than having one gas laser emitting several wavelengths, several solid-state lasers will be used. Purchase costs (constantly reducing) and their long lifetime will make such configurations competitive.

2.1.2 *Interface with the Sample*

The tectonic shift concerning the interface with the sample took place in the 1970s with the introduction of the Raman micro-probe through coupling with a microscope [114, 115, 267]. This technical advancement allowed the reaching of several milestones: (1) it enabled micro-analysis (and, subsequently, imaging), (2) it allowed the focusing of the excitation power (thus cutting out the need for powerful lasers), and (3) it led to significant improvements in the collection of Raman scattering thanks to the high numeric aperture of microscope objectives. Using microscope objectives, analysis at the micron scale can be easily achieved, a very interesting possibility for studying ancient samples, which are typically highly heterogeneous. In addition, coupled with a motorised microscope stage and a computer control, these systems allow Raman mapping and imaging.

Several different optics are available with various magnifications (from $\times 5$ to $\times 200$), different working distances (for example, ranging from 0.38 mm to about 20 mm for a $\times 50$ objective) and thus several numerical apertures and specific wavelength working ranges (visible, IR or UV). However, the quality of the optics, as well as customised characteristics (very long working distance, high numeric aperture, special optics tailored to the red or blue range, etc.) greatly increase the price of the objectives, while multiplying the options installed on a single spectrometer requires a justified use for each of their characteristics. In any case, adapting the optics for a specific experiment may ultimately be the key to reaching the required spatial resolution, or earning the few percent of signal that will allow detection of the analyte in extreme conditions, these and others being challenges that are common when studying cultural heritage objects.

2.1.3 *Signal Analysis and Recording*

The Raman light is generally analysed by dispersive spectroscopy, initially with prisms, and, since the 1950s, with gratings. In parallel to similar developments in IR spectroscopy, the introduction of computers in the 1980s for FT calculations allowed the use of an interferometer for analysing the light, and then, in association with Rayleigh rejection, the introduction of FT-Raman. However, because of the lack of spectral resolution for “short” wavelengths, the use of this setup is restricted to excitation in the IR range, such as for the 1064 nm emission of the Nd:YAG laser. Using an interferometer also resolves the problem of an efficient IR detection by allowing the use of a single channel detector with high efficiency in the IR region

(such as ultrapure germanium crystals), circumventing the drop-off in sensitivity of multichannel Si-based CCD in the IR region.

Signal recording followed the technical evolutions of light detection. It started with photographic plates at its origin, followed by the introduction of photoelectric photomultipliers in the 1950s, which implied single channel spectrum recording (i.e. one acquisition for each point of the spectrum). Finally, CCD solid-state detectors in the 1980s have dramatically reduced the counting time, first because of their efficiency but also because of the possibility of multichannel detection. All the further improvements in CCD efficiency have regularly contributed to increasing the detection sensitivity of Raman spectroscopy. On the other hand, the possibility of obtaining an acceptable detector noise with thermoelectrical cooling by the Peltier effect (typically at -70 or -50 °C), without nitrogen cooling, has allowed a significant reduction in the system volume and its technical requirements.

Competing with FT-Raman systems, some dispersive systems with a 1064 nm excitation are currently being proposed thanks to the recent availability of more efficient multichannel detectors in the IR, such as multi-element InGaS. These developments are actually driving the miniaturisation of Raman spectrometers using an IR excitation, so that portable dispersive Raman systems with 1064 nm excitation are now commercially available.

The massive increase of system luminosity with the introduction of filter-based spectrometers in the 1990s (see below) and the availability of optic fibres has ushered in the advent of modular systems. On the one hand, the light can be transmitted without relying solely on mirrors, thus allowing the system to be subdivided into various elements linked by fibre optics, and, as a consequence, reducing the need for a whole “rigid” device and internal optical alignments. On the other hand, it has allowed moving beyond the confines of the benchtop microscope environment by using “optic probes” for interfacing the sample and the spectrometer with fibre optics. Such probes can then be brought directly to the sample or artifact without the need for the latter to be adapted to the microscope environment, allowing highly adaptable *in situ* measurements, especially interesting for cultural heritage applications.

According to the type of Raman devices used, the fibre optic probe is either an accessory with a specific exit different from the microscope in a benchtop instrument or the main entrance in the spectrometer, for example in the case of portable instruments. Each system has its own advantages according to the applications and requirements. It should be noted though that fibre optic connectors always introduce a signal loss slightly higher than a simple mirror, and applications to cultural heritage remain somehow limited to strictly *in situ* measurements when no other option is possible, while the best quality spectra are routinely obtained on benchtop Raman microscopes.

2.1.4 Rayleigh Filtering

Another key point in the functioning of a Raman spectrometer is the rejection of the Rayleigh line. This was initially done by creating an optical pathway through grating(s) and slit(s). Such systems had the advantage of working with different excitation wavelengths, accessing low frequencies close to the Rayleigh (for triple- and even higher-order of dispersion in the spectrometer) and offering high spectral

resolution. However, they had limited “luminosity” (i.e. the part of the Raman signal from the sample which reaches the detector) and could not be miniaturised.

At the end of the 1990s, the introduction of systems based on holographic filters [54, 180] constituted the latest major advance in instrumentation. The huge increase in luminosity allowed drastically reducing the counting time (thus allowing the development of imaging) or the laser power required at the sample (thus minimizing the risk of sample damage). This last parameter is the key point to unlocking the study of samples sensitive to photo-degradation by Raman spectroscopy. This is especially significant for studies in the field of the cultural heritage.

The first generation of holographic Bragg diffraction filters are “Notch” filters made of organic multilayers of gelatin. The classic ones offer a cut-off around 120 cm^{-1} , the detection of Stokes and anti-Stokes bands, and linear transmission, but suffer from a limited lifetime (of about 4 years) because of their sensitivity to humidity and photo-ageing. With time, the transmission of Notch filters is reduced and the cut-off increases to reach about 160 cm^{-1} after 2 years. When the cutoff filter capacity degrades to about 200 cm^{-1} , its replacement is mandatory for many applications because informative Raman bands from various compounds (minerals, pigments and corrosion products such as many oxides and sulfides) can be missed.

Second-generation filters, appearing commercially around 2005, are “Edge” filters made of a dielectric multilayer. When introduced, they solved the problem of durability; because such materials are stable with time, with a cut-off at around 80 cm^{-1} . Only the Stokes part of the spectra can be recorded, which is definitely not a problem for cultural heritage applications, but their main drawback is a non-linear transmission. This could be especially problematic in the field of cultural heritage as significant fluorescence is commonly present in many samples. The non-linear transmission, coupled with sample fluorescence, has the effect of creating “ripples” in the spectrum, which can hamper baseline removal of the fluorescence signal. However, these transmission characteristics can be corrected (see Sect. 3.2).

The last generation of filters appeared at the beginning of the 2010s. These ultra-narrow band filters are volume holographic Bragg gratings in photosensitive glass (with various commercial names such as “BragGrateTM” and “SureBlockTM”). Beyond their stability with time and their linear transmission, they offer a very low cut-off down to 10 cm^{-1} . Of course, to reach such low frequencies, a narrow laser line is required, as well as a spectrometer design that is highly dispersive and selective to remove the Rayleigh line. In the field of cultural heritage, as well as obtaining a linear transmission, such filters can offer the recording of Raman bands below 100 cm^{-1} which is crucial for studying some kinds of materials (such as those involving heavy metal oxides and sulfides) or recording other specific spectral features such as the Boson peak in glass. The only limitation of all holographic filters is the need of a specific filter for each excitation wavelength, but the development of filters is in parallel to the one of solid-state laser sources that deliver only one wavelength and the specialisation of devices which are devoted to one (or a limited number, i.e. two or three) configuration(s). In more general terms, the last decade has seen Raman devices move from laboratory multi-purpose, fully adjustable systems to dedicated systems specialised and optimised for specific performance and applications.

In the area of cultural heritage research, the introduction of high luminosity systems in the 2000s (in parallel to spectrometer cost reduction and their simplified use) has spurred the widespread use of Raman spectroscopy.

2.2 Approaches to Sampling

Since the early 1980s [151], the Raman microprobe has been rapidly adopted as the methodological approach of choice for the analysis of art and archaeological samples, and for in situ applications for the timely analysis of objects that could fit under the Raman microscope in its various configurations (Fig. 1). In this section, we will review the most recent and notable advances in the applications of Raman spectroscopy to the investigation of the cultural heritage.

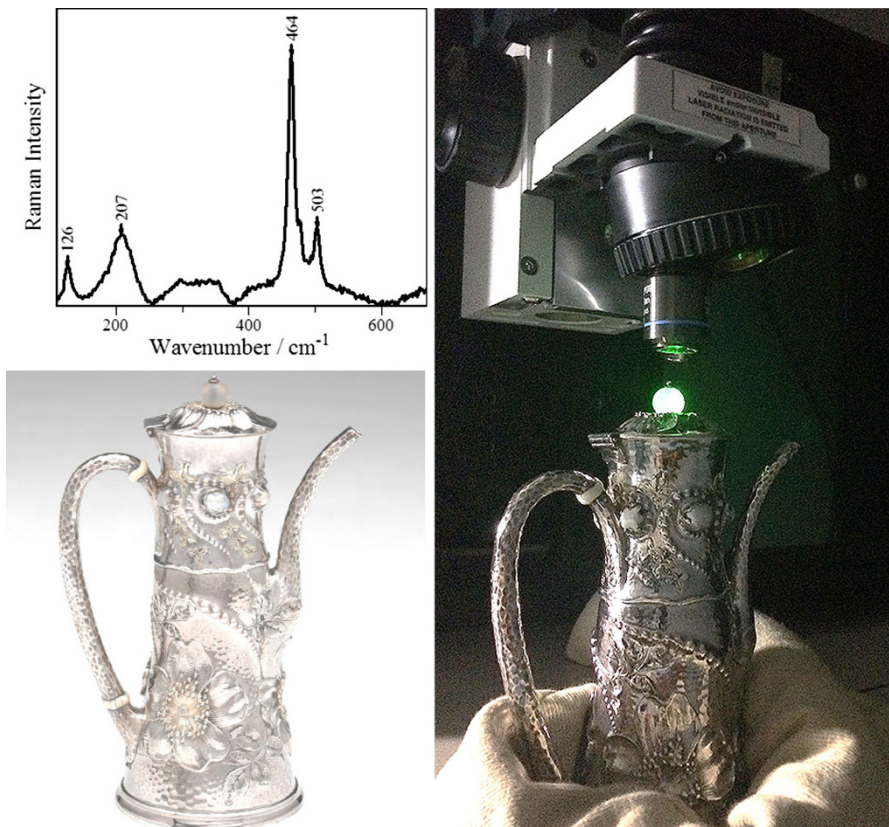


Fig. 1 Charles Osborne, Tiffany and Company, Coffee Pot, 1880–1890 (The Art Institute of Chicago, 1978.142). This silver coffee pot with inlaid pearls, and ivory insulators has a gemstone finial. Because archival records show that other similar objects by Osborne for Tiffany used nephrite, in situ Raman analysis was performed with 532-nm excitation. Analysis identified chalcedony (the peaks for quartz at 126, 207 and 463 cm^{-1} are most evident; the peak at 503 cm^{-1} can be attributed to moganite, which has been commonly found in many varieties of microcrystalline quartz) (Kingma and Hemley [172])

2.2.1 Portable Instruments

Raman spectroscopy in the cultural heritage field is increasingly valued for its portability, allowing the performing of in situ analysis, not only in museum galleries and storage facilities but also on archaeological sites including outdoors in applications such as the analysis of mural or cave paintings. New developments and improvements of the analytical setups as discussed in the previous sections have made it possible to overcome the geometrical constraints of benchtop instruments. Many reviews and research papers have extensively described and compared portable Raman spectrometers for cultural heritage analysis [85, 176, 294–296, 299, 301]. Colomban [85] traces the history of portable Raman instruments and provides a bibliographical review of the published papers on mobile/on-site Raman in the cultural heritage field, with more than 15 papers in each of 2010 and 2011. Vandenabeele et al. [295] make the distinction between transportable, mobile, portable, handheld, and palm instruments and give, for each, a brief definition of their uses. Detailed comparisons of various portable instruments are available [162, 163, 299], and specific requirements for an archaeometric use of Raman spectroscopy are discussed. These characteristics are either instrument-related, as, for example, tunability of the laser power, the speed of analysis, the analysed spot size, the spectral range (with requirements depending on the probed material) or linked to the whole setup, like the total weight of the instrument, the ease of positioning, the use of a camera, the need to work in a dark environment, and many other characteristics. Lauwers et al. [176] contributed a study on the evaluation of these characteristics for various portable instruments. Although the requirements cannot all be met, the choice of a portable Raman spectrometer relies on a compromise between the available features and the real needs of the project at hand. For example, organic substances can now be analysed in situ, as dispersive devices with near-IR excitation are available at 785 and 1064 nm; notable applications include the study of treatments with synthetic materials on the façades of historic monuments [100] and on organic minerals [162, 163], but also in the field of forensics, with 1064 nm excitation [301].

Portable Raman may also be combined with other laser-based techniques such as laser-induced fluorescence (LIF) or laser-induced breakdown spectroscopy (LIBS) [218] within the same instrument. The combination with LIBS requires a pulsed laser and thus the use of time-resolved Raman spectroscopy. The laser, grating, and CCD detector are common for both techniques, and movable filters can be added depending on the technique, with lower laser powers employed for Raman analyses. Such compact instruments have been used for the characterisation of minerals [280] and also of works of arts with applications in the analysis of pigments and binding media [224].

2.2.2 Mapping and Wide-Field Raman Spectroscopy

Raman mapping using a conventional motorised stage is used in the cultural heritage field on micro-samples and cross-sections of samples such as paint layers (in favourable cases where fluorescence is not a complete impediment to analysis)

[94, 153, 287], calcium oxalates layers deposited on the surfaces of monuments as deterioration products or as intentional mineral consolidation treatments [92, 93], iron corrosion layers [210], and other corrosion products of archaeological metal objects [18] or porcelain cards [116]. When it comes to in situ analyses, unless the object fits under the microscope and can be securely held on the motorised stage, which is not often the case, different approaches must be considered. Ropret et al. [266] proposed three analytical modes using a set of scanning mirrors placed at the horizontal exit of a benchtop Raman spectrometer that allow the laser to be moved in two dimensions instead of moving the work of art. The first mode is a step-by-step mode, very similar to conventional mapping, but with the laser moving instead of the objects. A spectrum is recorded at every step. The second mode is an averaging mode, where the mirrors oscillate to generate a macro-spot and, depending on the speed of the oscillations and on the objective, the beam size can be tuned. One average spectrum is recorded for the whole surface illuminated by the macro-spot. The third mode is the macro-mapping mode, combining the average mode and the use of the XY motorised stage. Average spectra are acquired at different positions of the moving stage, leading to a rapid scan of a large probed area. The macro-mode can be assimilated to wide-field Raman spectroscopy mapping, where the sample or object is still and images are captured in two dimensions at selected wavenumbers [274]. In other words, a band of interest is chosen thanks to a specific filter, and an image is recorded on the illuminated area using the two dimensions of the CCD detector. The filter must thus be chosen according to the excitation wavelength and the spectral region of interest of the probed material. The filters used are dielectric band pass filters that cover large energy ranges and can be tuned to select specific bands. The size of the imaged area can be changed by using different objective magnifications and by defocusing the laser. This kind of analysis can be useful in the art and archaeology field but it requires a pre-conceived idea of the probed materials in order to choose the filter accordingly. More realistically, wide-field Raman mapping could be used as a second-step technique for studying spatial organisation and composition at the macro- and mesoscale, after punctual analyses for material characterisation at the microscale. Brambilla et al. [30] have developed a transportable setup working with a 6-cm-diameter mapping surface at a distance of 20 cm from the work of art, making the system suitable for the analysis of three-dimensional objects or objects characterised by uneven surfaces such as paintings. In their instrument, a set of scanning mirrors enables the laser to move on the object surface and permits the acquisition of raster scans of a quite large area. This prototype, compared to the setup presented by Ropret et al. [266], enables in situ mapping of objects.

The difference of these setups with respect to conventional mapping on cross-sections is that, while large areas can be scanned, here only the surface of the sample or object is probed, while on cross-sections the layering of the sample is studied in depth. However, the confocality of Raman spectroscopy is preserved with the scanning mirrors setup, allowing, theoretically, the implementation of spatially offset Raman spectroscopy.

2.2.3 Spatially Offset Raman Spectroscopy (SORS)

Spatially offset Raman spectroscopy (SORS) has come to the fore in recent years as a powerful analytical tool to interrogate the chemical composition of sub-surface materials that are covered by superficial, turbid layers. First demonstrated in 2005, the principle of the method lies in collecting the Raman signal from a point in space that is displaced with respect to the point of excitation, either on the surface of the sample or deeper down on the z axis of illumination [196, 198, 199]. Subsequent data treatment can isolate the spectral contributions of the surface from those of the subsurface without requiring previous knowledge of the chemical composition of the top layer, leading to a powerful methodology that is of simpler implementation than time-gated Raman spectroscopy to achieve similar results.

Initially developed for industrial, forensics, defence, pharmaceutical and biomedical applications [42], the first demonstration for the cultural heritage used SORS to identify in a non-invasive way ivory specimens concealed under various layers of paint, varnish or other polymers, so as to assist custom protection agencies against illegal import of the material [154].

Though powerful, the technique is not applicable if the top layer is highly absorbing, if it is of a metallic nature, or if it contains analytes with Raman scattering cross-sections that are overwhelmingly higher than the lower target layer [91, 96, 101]. Also, if the target underlayer is fluorescent, SORS will suffer from fluorescence like conventional Raman microscopy. On the other hand, fluorescence of the top layer can be suppressed or significantly reduced by using this technique [99].

In recent years, the potential of SORS for the investigation of works of art has been explored in depth [95–99]. Because for art applications the layers to penetrate are much thinner (in the micrometer-size domain) than those for industrial or pharmaceutical applications (which tend to be in the millimeter-size domain), the method has been adapted, leading to the development of defocusing micro-SORS [96]. In this modality, two spatially offset measurements are collected, one at the surface, which is dominated by the spectral signature of the top layer, and one at a defocused distance obtained by lowering the sample from the microscope (i.e. at a lower position on the z axis with respect to the first measurement) to maximise signal contributions due to buried underlayers. The post-processing of the data after acquisition consists in a more or less sophisticated scaled subtraction of the spectrum obtained at point $z = 0$ from that obtained at point (or points) $z - n$ (or Δz). An alternative sampling modality, full micro-SORS, which involves the separation of excitation and collection on the x/y axis at the surface of the sample (thus requiring custom modifications to conventional Raman microscopes) has also been proposed. Compared to the defocused method, where collection and excitation points are only offset in one direction (the z -direction), full micro-SORS has been demonstrated to have the highest enhancement for the signal of the buried layer, and to have larger penetration depths (Fig. 2) [98].

Even if less effective, however, defocused micro-SORS remains attractive for its ease of implementation with conventional confocal Raman microscopes. Furthermore, various analytical strategies can be implemented to enhance the signal of

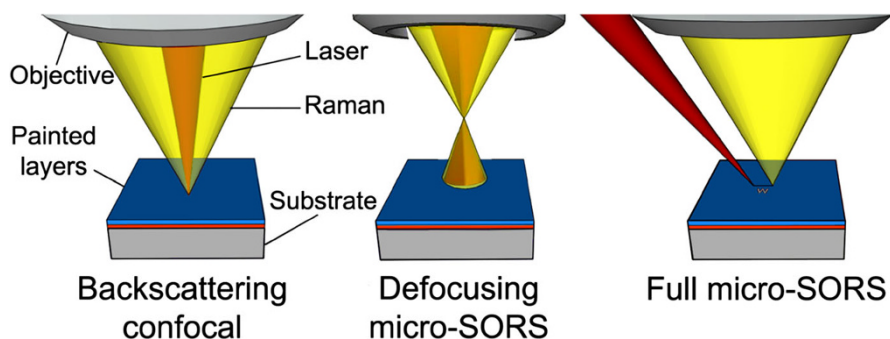


Fig. 2 Schematic representation of normal, confocal Raman, Defocusing micro-SORS and full micro-SORS measurement geometries (reproduced with permission from [200])

buried layers in defocused micro-SORS, even in light of its lower efficiency compared to its fully spatially offset variant, such as longer collection times or increased intensity of the laser excitation. Because in essence the laser spot on the surface of the object is larger in the de-focused position, concerns for laser damage of art samples due to longer irradiation times are somehow alleviated.

Compared to confocal Raman spectroscopy, which was introduced to the field several decades ago and now comes standard with most commercial Raman microscopes, defocused micro-SORS can penetrate larger depths of scattering layers (i.e. turbid media) than confocal microscopy. This has been measured in specific cases to be one or two orders of magnitude higher [98, 197]. Interestingly, Conti et al. [97] also demonstrated the capability of the technique to non-invasively assess whether two distinct chemical components (i.e. two pigments) are present mixed in one layer or individually in two subsequent layers in a stratified layering situation; the authors also demonstrate this ability to resolve mixtures through an additional surface turbid layer [97].

Most of the recent literature detailing applications of defocused micro-SORS to pigmented layers of relevance to cultural heritage studies concerns itself only with reference materials and mock-ups; however, a first application to samples from polychrome terracotta and stucco sculptures from northern Italy dating to the fifteenth–seventeenth centuries has recently been published [95]. Ultramarine blue, azurite, Prussian blue, chrome yellow, red lead, vermilion, red and yellow ochres, lead white, gypsum, anglesite and barium sulfate are documented. This is an important proof-of-concept application and good quality spectra of buried layers (down to 600 μm deep inside the paint stratigraphy) were obtained with powers at the sample of approximately 10 mW and acquisition times for the defocused positions of 100–300 s, which are about 2–6 times higher than the collection times in the focused position. On occasions, when three layers are present, and with the middle pigment being a weaker Raman scatterer than the pigments of the top and bottom layers, the researchers reported that the contribution of the pigment in the middle layer can become lost. Another limitation encountered in the analysis of actual samples is that they can be heavily degraded, have multiple layers or are highly inhomogeneous giving different results or data that are difficult to interpret

depending on the location of the analysed spot. Extremely thin layers can also be missed.

Although in principle the technique can be applied in situ, effectively bypassing the necessity of preparing cross-sections from the samples, because of the stringent requirements on focusing (and defocusing) the laser light, so far it has only been applied to samples and specimens excised from their original artifacts and not yet for in situ analysis of actual works of art. Nevertheless, the technique has potential for applications to easel paintings or small museum objects that can be placed under a Raman microscope. Compared to femtosecond pump-probe microscopy, which is also proposed as a way to obtain virtual cross-sections of paintings, but requires extremely specialised laboratory equipment [300], the instrumentation for defocusing micro-SORS is already pretty widespread in laboratories dealing with forensics and art analysis. While the data interpretation requires a certain amount of sophistication, this approach could be of wide applicability to the community of cultural heritage science researchers as it does not require more sophisticated instrumentation than conventional confocal Raman microscopes.

Interestingly, the technique is now coming full circle, as micro-SORS, which was originally developed specifically to investigate cultural heritage materials, has recently been demonstrated for industrial and research applications including the analysis of multilayer polymer samples and cellulosic or biological materials such as seeds [99].

2.2.4 Surface-Enhanced Raman Spectroscopy (SERS)

In the past 10 years, robust developments have taken place in the application of surface-enhanced Raman spectroscopy (SERS) to the characterisation of molecules of interest to the cultural heritage field.

The surface-enhanced Raman effect relies on the excitation of a surface plasmon resonance, induced when laser light of specific wavelength hits a noble-metal nanostructured surface, causing the electrons in the conduction band of the metal to oscillate in resonance with the incident light. This resonance condition is met in the visible region for Au and Ag nanoparticles. If a Raman-active molecule is in the vicinity (a few ångströms) of the nanostructured surface, the occurrence of the localised surface plasmon resonance (LSPR) causes the Raman signal of the analyte to be enormously intensified—with reported order of magnitudes of 10^8 – 10^{18} greater than normal Raman—even down to single molecule sensitivity [311]. In addition to this dominant electromagnetic effect, other chemical enhancements can occur, which are linked to molecular resonance within the analyte (leading to surface-enhanced resonance Raman scattering; SERRS) as well as electron donor/acceptor (charge transfer) phenomena between the molecule of interest and the valence level of the SERS-active substrate [188, 189, 191].

First described in the 1970s [142, 160], initially most efforts of the scientific community focused on unraveling the scientific basis for the observed phenomena. However, the potential of SERS for the ultrasensitive detection and molecular fingerprinting of analytes remained unexploited for some time, until its explosion on the analytical chemistry scene of the past 15 years, with thousands of articles

describing applications in material science, biomedicine, chemistry, and numerous reviews [203, 279].

The first application to art materials dates back to 1987, when Guineau and Guichard used a roughened silver electrode to identify madder on a textile sample [152]. However, one has to wait until 2005 to witness the portentous growth of the spectrum of applications in the cultural heritage, firmly establishing SERS as a robust tool for dye identification in the field of art analysis.

Although relevant for any Raman-active molecule, the most widely explored area of applications in cultural heritage studies has been the identification of colorants—primarily natural and, to a lesser extent, synthetic dyes and dyestuffs—with rare exceptions related to natural resins [175] and daguerreotypes [64]. The normal Raman technique, in fact, which is widely used for the identification of minerals, inorganic pigments, some organic pigments and dyes, and organometallic complexes [16, 24, 43, 61, 273], is plagued by fluorescence of the organic dyes themselves or of the paint matrix in which these weak scatterers are immersed, swamping the signal from the analyte (a notoriously weak phenomenon given that the Raman effect concerns only approximately 1 in 10^4 scattered photons). Thus, SERS has emerged as a valuable approach for the identification of colorants in art, preserving the positive aspects of the normal Raman technique, such as high spatial resolution and molecular specificity, while offering fluorescence quenching and enhanced sensitivity leading to significantly improved limits of detection.

Although to date the most comprehensive method for dyestuff identification in art is high-performance liquid chromatography (HPLC), which has the advantage of being a separation technique and can in favourable cases lead to the identification of the specific genus of plant or animal dyes [112, 309, 310], identify degradation products [111, 140, 141], and resolve complex mixtures of dozens of dyestuffs [239], SERS has emerged as a valuable alternative for severely mass-limited samples, in situ applications and when information on the main chromophore is sufficient (i.e. identification of carminic acid as opposed to determining the specific presence of Polish cochineal or Mexican cochineal). Although in recent years HPLC has significantly improved its detection limits for reduced sample sizes (of the order of 0.5 mm of dyed fibre and a few micrograms of samples from polychrome works of art), SERS maintains a sample-size and sensitivity advantage; in essence, if only one particle of colored pigment is visible, SERS can detect its colorant. However, compared to HPLC, this spectroscopic technique is severely limited in its ability to resolve complex mixtures of colorants [248, 303]. To date, only a maximum of two dyestuffs have been detected in the same sample with SERS: madder and cochineal in red lake pigments used by painters in the Impressionist circle [247], cochineal and brazilwood in textiles from the early twentieth century atelier of Mariano Fortuny [159], and quinacridone combined with quinacridone quinone in commercial pigments [192]. Alternative methodological approaches to overcome this limitation have ranged from the simple combination of SERS with thin-layer chromatography (TLC) plates [37, 53, 148, 246, 251], to advanced analytical solutions involving consecutive UV laser ablation, deposition on a SERS-active support covered in silver nanoisland film, and analysis with an optical parametric oscillator (OPO) laser system [67], and hyphenated techniques coupling HPLC with

SERS [314]. Surprisingly, the potential of combining microfluidic with SERS is still mostly unexplored in this field [248].

In the past 6 years, several comprehensive reviews of SERS for both art and forensic applications have been published [57, 148, 181, 211, 242, 248, 256, 311, 313], and the reader should refer to these for a more in-depth treatment of the subject. Here, a summary will be provided of the most notable developments in terms of substrates, excitation, sampling modalities, and other innovations, focusing on the frontiers conquered as well as illustrating challenges and areas of further development.

Sustained efforts have been focused on the synthesis of robust SERS-active substrates, ensuring reproducibility of the results and building reliable databases for the most common natural and, to a limited extent, synthetic dyes with a variety of laser excitation sources (from the blue to the near-IR) and analytical investigation conditions [40, 184, 245, 303, 315].

The most widely reported SERS-active substrate for art applications are silver colloids obtained following the method originally published by Lee and Meisel [179], which produces a random mixture of nanospheres and nanorods that are suitable for direct applications to samples from works of art with or without partial aggregation with potassium nitrate [50], poly(L-lysine) [277], sodium chloride [52] and perchlorate [40]. Modifications to this method to achieve improved performances have included centrifugation to create a concentrated paste, thus augmenting the number of nanoparticles per unit volume applied on samples varying from watercolors to textile fibres [35, 159]. To narrow the range of LSPR of the silver nanoparticles synthesised, and improve the reproducibility of the SERS spectra, glucose-assisted reduction of silver sulfate in the presence of sodium citrate as a capping agent in a microwave oven has also been proposed [181]. Other alternatives have included silver nanoparticles produced by laser photoreduction, either directly in situ on the sample under study [51, 165, 166, 257] or in solution for later use [8]. These methods are often proposed to overcome the spurious signal of the citrate that is used in the Lee–Meisel synthesis to avoid the coalescence of nanoparticles. In fact, the spectrum of citrate can appear in the SERS spectra recorded alongside, or sometimes obscuring, the analyte signal due to competing adsorption processes on the surface of the silver nanoparticles [36, 41, 184]. The main drawbacks of in situ photoreduction though are, in turn, overheating of the sample and the appearance of carbonaceous bands.

Since to be used as pigments and to dye textile fibres, most colorants need to be complexed to an inorganic substrate or thread through a metal ion, in order to free the dyestuffs of interest in these mordant dyes and lake pigments and render them more readily available to the SERS-active nanoparticles, several pre-treatment analytical steps have been proposed. By far the most amply demonstrated approach has been the non-extractive hydrolysis with hydrofluoric acid (HF) vapors. Initially proposed by Leona [181] the HF pre-treatment method is now amply validated as a fundamental step, especially to release colorants from their complexes with metal ions in lake pigments dispersed in oil binding medium [243, 247, 315]. Although direct identification of colorants with colloidal pastes on samples of pastels and watercolors has been achieved [35–37], this HF pretreatment is the most successful

analytical protocol to date to identify red lakes in glazes and oil paint layers in paintings and polychrome sculptures. Alternative pre-treatment steps with hydrochloric or sulfuric acid for the identification of yellow, red and blue colorants have also been proposed [143, 201, 221, 222], leading up to a complete flowchart including treatment with acids and solvents to identify blue (i.e. indigo, Prussian blue), and yellow organic (i.e., Reseda lake, Stil de Grain, gamboge) pigments in one sample [263], but these procedures appear more limited in scope.

Although solid state, nanofabricated substrates have been widely published and are frequently proposed for a variety of diverse applications [193], only a small number of papers have described the use of metal films over nanospheres substrates to analyse artistic dyes. Fabricated by drop-casting and self-assembly of microspheres (usually silica or polystyrene) on a glass slide, subsequently covered by a thin layer (approximately 200 nm) of vapor deposited Ag or Au, these substrates generally give high-quality spectra with higher enhancement factors than colloids [150], and can be tuned by appropriately choosing the size of the microspheres used so as to give rise to LSPRs at different wavelengths [278, 303, 304]. The major drawback of these systems is that the analyte needs to be brought into solution, and often they suffer from contamination of carbonaceous and other spurious materials that get preferentially adsorbed on the metallic coating of the microspheres.

Major efforts have recently taken place to improve the spatial resolution of SERS, which, when using colloids, is limited to the physical dimensions of the drop of colloid deposited on the sample (typically 0.5–1 mm in diameter). These have included innovative systems such as inkjet deposition of colloids (with deposition sizes 50–80 μm) and simultaneous SERS analysis [20], the first demonstration of the feasibility of tip-enhanced Raman spectroscopy for the analysis of indigo and iron gall ink [174], combining SERS analysis in a scanning electron microscope [250], and the use of OPO lasers for one-stop laser ablation and SERS analysis of samples [190, 192], including the first application on a cross-section to resolve and separate two different colorants in superimposed layers [67]. Most of these applications have been “proof-of-concept” studies (with the OPO laser approach the most widely developed to date) and in future years further developments of the methodologies are to be expected. Preliminary results attempting to identify dyestuffs on cross-sections from painting layers with lower-tech approaches have included identification of madder, carmine lake, and kermes on painting cross-sections with silver colloids [143, 158], and the identification of madder on a cross-section of a mock-up sample with direct photoreduction of silver [257].

An innovative application of SERS and SERRS for the spatially localised identification of binding media (especially proteins and gums) in samples from works of art has involved the use of metallic nanoparticles functionalised with SERS-active reporter molecules tagged to antibodies used for immunological labelling of cross-sections. Here, the antibodies provide the identification of the specific organic molecule (down to the type of animal or plant from which the binder is obtained), and these immuno-SERS nanotags are used for sensitive detection and localisation of those binders in the layer structure of the cross-section [12, 233, 276].

At present, the ultimate frontier for SERS is truly *in situ*, non- or minimally invasive analysis. To this end, a small but growing number of papers have been published demonstrating the use of flexible substrates based on acrylic gels [182, 183], methylcellulose pastes [119], gelatin [120], or agar–agar gel [187, 241], optionally loaded with a mild micro-extractant, often based on ethylenediaminetetraacetic acid (EDTA) [240]. The analytical procedure either involves mixing the gel with nanoparticles, or using the gels to extract a minute and nearly invisible amount of dye for later analysis with SERS after deposition of colloidal silver particles on the face that was previously in contact with the artifact.

Today, one can confidently say that SERS is solidly established as a reliable option for the identification of colorants in works of art and archaeological artifacts. This is also due, in part, to the wider availability of benchtop, easy-to-use Raman spectrometers, which are becoming more ubiquitous than specialised HPLC equipment in cultural heritage science laboratories.

3 Data Treatment and Chemometrics in Raman Spectroscopy Applied to Art and Archaeology

In the past decade, not only have instrumentation and sampling modalities for the Raman analysis of art and archaeological artifacts evolved but, in parallel, more sophisticated methods of spectroscopic and statistical data treatment have been proposed and are reviewed here. The first step, before comparison of spectra and further data treatment, is spectral pre-treatment in order to standardise the data. Fluorescence removal, filters' signal removal, baseline subtraction, intensity normalisation, smoothing, etc. are commonly used routines. A brief overview of the possible use of these tools is presented, as well as several ways to analyse and compare spectra: the construction of spectral libraries and automatic searches; the determination of flowcharts and criteria for the unambiguous characterisation of the studied materials; and the use of chemometrics for data classification. Some examples of studies relying on these statistical tools to advance our knowledge on the ageing of materials or the determination of individual components in mixtures are also presented.

3.1 Spectral Pretreatment: Fluorescence Signal Removal

Fluorescence is the most commonly encountered issue when working with conventional Raman spectroscopy. For cultural heritage applications, it can be due to organic materials with chromophore groups (very often conjugated double bonds) or to inclusions and impurities in some mineral compounds. To overcome this, if FT-Raman or SERS are not available or if the quenching of the fluorescence is not efficient, spectral manipulations such as subtracted shifted Raman spectroscopy (SSRS) [225, 268]; and shift excitation difference spectroscopy (SERDS) [225] can be implemented during the measurement. SERDS is performed by recording two spectra at slightly shifted laser frequencies. All constant data, considered as fluorescence, are discarded. The remaining features are the ones

affected by the laser shift, namely Raman bands. A tunable laser is required and needs to be very stable so that the frequency shifts are real. The laser frequency shifts can be affected by changing the laser's drive current or the laser temperature. SSRS, on the other hand, is a technique where the grating is significantly shifted (20 cm^{-1}), which means that the Raman bands are also shifted. When the spectral subtraction of the two obtained spectra is performed, the fluorescence background is eliminated.

For both techniques, the resulting spectrum shows derivative shape bands that can be transformed to a Raman spectrum using a specific fitting function, which considers the reconstructed spectrum as a sum of Gaussian and/or Lorentzian peaks [19]. Another mathematical procedure for recovering the Raman spectrum has been proposed by Zhao et al. [316]. A deconvolution procedure called the difference deconvolution method (DDM) is applied to obtain the final Raman spectrum. This method basically consists in considering the fluorescence signal as constant, and the Raman signal difference (due to the laser shift) as a deconvolution of the total signal, with the laser signal considered as a Dirac function using an inverse Fourier transform. The DDM technique also allows the eliminating of the signal originating from individual bad pixels. Rosi et al. [268] compare SRSS to other similar techniques such as manual shifting of the x -axis followed by the calculation of the difference between the two spectra, and a simple first derivative calculation of the spectrum. These methodologies have been applied to the analysis of various organic dyes and lakes found on textiles or parchments and appeared quite effective. The complexity lays mainly in the reconstruction of the Raman spectrum from the derivative shape peaks, a process that can create some extra bands and provide misleading results. Weis et al. [302] use a simple second-derivative processing to diminish interference from fluorescence on Raman spectra of painted works of art. In another study, [225] SERDS and SRSS techniques are applied to the analysis of blue and pink pigments and dyes and results are compared with spectra recorded on reference samples using lasers that do not induce fluorescence. Some of the samples studied nevertheless show a very intense fluorescence background preventing the application of the SERDS technique. However, in this study, the DDM procedure seems to give more viable data regarding the Raman peaks' position and intensity in comparison to the fitting procedures.

It is worth mentioning that nowadays commercial software can perform these corrections automatically. As examples, Bruker's Opus software contains a "Fluorescence Removal" tool for the Senterra spectrometer, Renishaw's WiRE software includes an "Automatic intelligent background removal" and finally HORIBA's Labspec proposes the "FLAT correction: On-the-fly automated Fluorescence Removal".

3.2 Spectral Pretreatment: Filter Signal Removal

Some filters used to reject the Rayleigh line called Edge filters (long-wave pass filters, see Sect. 2.1). Rayleigh filtering are multilayered dielectric components that present a non-linear transmission of the signal leading to very characteristic ripples

on the spectra. These ripples may hinder or be added to the Raman features of the analyte and make the baseline subtraction a critical process, especially when the analyte has a weak signal. However, it is possible to apply a simple mathematical treatment to get rid of these ripples and obtain a smooth spectrum showing the Raman bands only. The first step consists in recording a white light signal through the filter, and then without the filter (Fig. 3). The ratio of the spectrum recorded without filter to the spectrum with filter is the correcting factor. The second step is to multiply the raw spectrum by this factor in order to get a corrected spectrum. An (optional) third step is to remove a baseline from the corrected spectrum to get a final spectrum showing clear Raman bands.

Such a procedure, which could be implemented by individual users, is also nowadays proposed in their proprietary software by some manufacturers, as a specific filter correction or as a signal pretreatment option not controlled by the user.

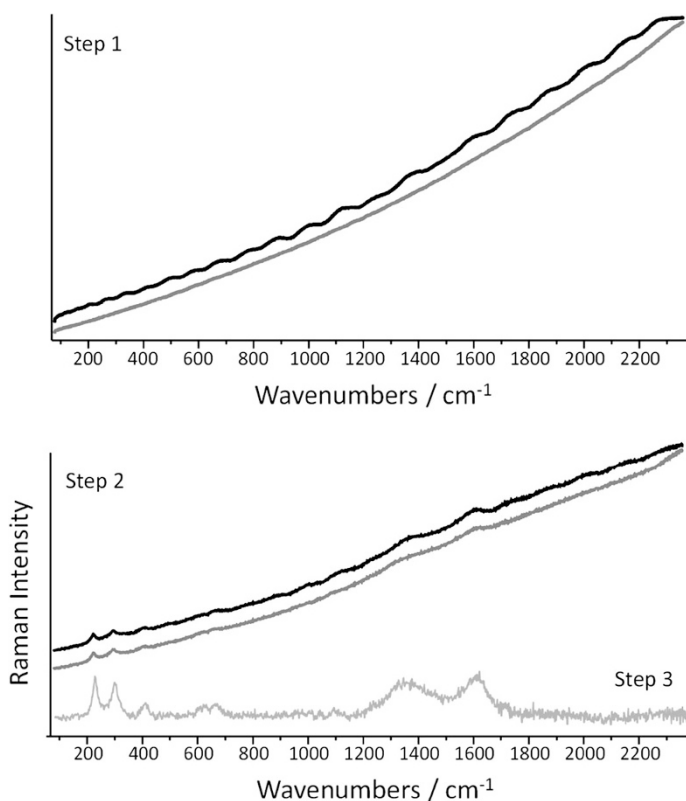


Fig. 3 Removing Edge-filter artifacts. Step 1: white light spectrum recorded with (black line) and without the edge filters in place (grey line); Step 2: multiplying the raw spectrum of the investigated sample (dark grey line) for the correction factor (i.e. ratio of the two spectra in Step 1; black line), and the latter after baseline subtraction (light grey line)

3.3 Spectral Pretreatment: First and Second Derivatives

Minerals and other inorganic materials usually show few and sharp Raman bands, and, depending on the spectral resolution of the spectrometer, band positions are obtained precisely and thus assigned. However, when it comes to organic materials and more specifically natural media, the spectra are more complicated, with broad bands that usually contain more than one vibrational feature. It is therefore much more difficult to ascertain their exact positions and to identify the chemical compounds in a straightforward way. Tools such as first and second derivatives of the Raman spectra can be used to simplify the reading of the data by separating out the peaks of overlapping bands. Thus, when the spectrum changes even slightly from a positive slope to a negative slope (due to the presence of a shoulder on a broad band for example), the feature is emphasised on the derivative spectrum. A first-order derivative passes through zero at the same wavenumber as the maximum intensity of the Raman band, and a second-order derivative is a negative band with minimum at the same position as the maximum on the zero-order band. Since it is easier to read negative peaks than imprecise slope changes or zero intensity positions, second-order derivatives are more widely employed. It is important though to add a smoothing step before the derivative transform, to avoid the enhancement of spectral noise caused by the application of the derivative function. As already discussed in this article, some studies show the use of spectral derivatives to get rid of the fluorescence background that may hinder Raman features (see Sect. 3.1), but other studies make use of these tools for other purposes. Roldan et al. [264] displayed the second derivative of normal Raman and SERS spectra of various sepia powder samples to highlight the exact position of vibrational features and assist with band assignment and comparison to previous studies. Another study [39] showed the use of vibrational spectroscopies for the identification of dyes on wool fibres. For this purpose, the authors compare second-derivative FT-Raman spectra of dyed fibres with reference dyes; but also compared the same references with the difference between the second-derivative spectra of the dyed and undyed fibres. A library-search method is then developed to include the second derivatives of ATR-FT-IR and FT-Raman spectra, and has been successfully applied on archaeological samples from Caucasian and Chinese textiles.

First derivatives can also be a first step of a more complete data-processing methodology, as is the case for several papers that focus on chemometrics (see Sect. 3.4). Navas et al. [214] applied principal component analysis (PCA) on Raman first-derivative spectra of model tempera paint samples, i.e. mixtures of different pigments with various binders. It appears that using derivative spectra, which show more evident differences than normal Raman spectra, can help in the PCA discrimination of those samples. Daher et al. [106] used the second derivative of a restricted spectral region (that of the CH band centred at 2900 cm^{-1}) to obtain the precise position of the vibrational features that are enveloped in this relatively broad band to subsequently use as parameters for a spectral decomposition procedure followed by PCA. Vandenabeele et al. [297] compared the influence of pre-processing techniques (zero-, first- and second-order derivatives) to obtain the best possible discrimination between natural and synthetic indigo pigments using

chemometrics, leading to the conclusion that second derivatives appeared to be the most accurate data pre-treatment in their study.

3.4 Material Identification and Discrimination

The widespread adoption of Raman spectroscopy as a valuable tool in laboratories involved in cultural heritage studies is also due to the availability of numerous databases of Raman spectra of interest for cultural heritage studies. These cover a wide range of materials, from pigments and minerals to organic media and plastics, and have been listed in recent reviews [61, 103, 171, 283, 284, 294, 296]. Among these, some pioneering studies and major databases are worth mentioning. An ample library of spectra of natural and synthetic pigments using visible laser excitations (632.8 and 514.5 nm) includes more than 60 pigments used prior to 1850 (also available online <http://www.chem.ucl.ac.uk/resources/raman/index.html#blue>) [16]. This study was followed and completed by the characterisation with FT-Raman of pigments that did not show any Raman signal using visible excitations, as well as some synthetic pigments [43]. More recent studies contribute to the extension of Raman spectral reference collections with more than 100 synthetic organic pigments of the twentieth and twenty-first centuries [144, 273], specific azo pigments [293], and of SERS spectra of natural dyes present in works of art [40, 41, 184, 315]. Natural organic media are also represented in depth, including binders and varnishes using either 785 nm [298] or 1064 nm excitation lines [43, 126, 129]. Collections of the spectra of plant gums [128], incenses [127], natural fibres [132] and resins are also available [32, 33].

In addition to the printed versions, many useful online databases exist, including the e-visart and e-visarch databases (<http://www.ehu.es/udps/database/database1.html>) [60] that display Raman, FT-Raman and Fourier-transform IR (FTIR) spectra of pigments and archaeological materials; the RRUFFTM Project, gathering minerals data that are downloadable or searchable online (http://rruff.info/repository/ziped_data_files/raman/); and the IRUG (IR and Raman Users Group) database, containing mainly FTIR spectra with some complementary Raman data (<http://www.irug.org/search-spectral-database>). Other examples include a database of Raman spectra of minerals, hosted at the University of Parma, Italy (<http://www.fis.unipr.it/pheviz/ramandb.php>), and an impressive and growing collection of over 270 synthetic dyes and pigments developed at the Royal Institute for Cultural Heritage (KIK-IRPA) in Brussels, Belgium (<http://modern.kikirpa.be/>).

While direct comparison of spectra of unknowns to either published databases or user-generated private databases is possible, especially after some degree of standardisation of experimental conditions for spectral acquisition, some groups have proposed further automated or semi-automated ways of simplifying spectral interpretation and matching. In recent years, the field has seen an increase in the use of statistical approaches seeking to improve material identification and discrimination. Chemometrics have the ability to extract relevant information from Raman data. In the cultural heritage field, different classification methods have been reported: unsupervised methods using calibrated models subsequently validated using an external set of data such as PCA or hierarchical cluster analysis (HCA),

and supervised methods such as partial least squares discriminant analysis (PLS-DA) also using calibrated models, but building labeled datasets.

An original approach uses fuzzy logic [59, 255] for automatic interpretation of Raman spectra. Fuzzy logic is based on the introduction of a part of imprecision, or approximation, in the reasoning to replicate a human-like decision. It is expressed in the possibility that, in a Raman spectrum, the band positions are not always exactly the same, neither is the intensity of the bands. The shifts due to natural variability of the probed materials but also to the instrumental and experimental conditions are not limiting the identification procedure. Practically, the bands characteristics of reference spectra are extracted and stored as variables in a fuzzy system that can be represented in two dimensions: the band position, and its Raman intensity. The unknown data are also extracted and added to the fuzzy system with an “uncertainty function”. Then the identification process involves computing the intersection between the fuzzy set of the unknown spectrum with each of the sets from the reference library. Finally, a score (0–1) is obtained for each band, and the system is then defuzzified using categories such as “*present*”, “*possibly present*” and “*not present*”.

By far though, the most highly used approaches rely on PCA, HCA and PLS-DA for materials classification in many contexts: to identify and discriminate pigments [214, 223, 287, 297], dyes [121] and inks [238]; to characterise organic media [105, 215–217, 229] and metallic soaps [226]; and in the related domains of forensic science [123] for the analysis of industrial paints [212]. In essence, data reduction processes using PCA for the automatic identification of pigments in works of art work by first performing data pre-treatment of a reference spectral library, including spectral range selection, baseline subtraction, linear interpolation, and intensity normalisation. Then, the preprocessed data are analysed using PCA, resulting in a condensed amount of data compiled in a reduced space (the PCs space). Spectra of unknowns undergo the same procedure and are projected on the PCs space of the references (without being included in the original PCA calculations). Finally, identification criteria based on Euclidian distances and squared cosines between the unknown spectrum and the library patterns allow the identification of the unknowns [149]. For example, Vandenabeele et al. first used PCA as a data reduction pre-treatment on raw spectra, and on first and second derivatives, then performed clustering based on Euclidian distance and LDA on this reduced dataset to separate synthetic and natural indigo of different provenance [297]. A similar approach enhanced by complementary LIBS and pulsed Raman spectroscopy demonstrates the ability to differentiate between mineral, natural and artificial ultramarine [223]. PCA has been applied for the study of tempera paint model samples made of egg yolk and nine different pigments (three reds, three blues, and three whites) using three data matrices, one for each color [214]. For each set, a specific data range is selected, according to the position of the main bands of the pigments. The results show that working on the raw Raman spectra is inconclusive, but groups can be formed if working on first derivative spectra. To study paint cross-sections of a glass painting, Staniszewska et al. [287] have performed HCA on FTIR and FT-Raman mapping data. The reconstructed cluster maps overlapping the sample image show good accuracy in the layered distribution of pigments. Raman spectroscopy coupled

to PCA used for the study of iron-based inks helps in determining which features are linked to noise and which ones are related to actual Raman data [238].

Triarylmethane dyes are molecules characterised by the presence of aromatic rings that can present several resonance forms. Their Raman spectra are therefore very similar, and, in order to differentiate between their various forms, PCA carried out on FTIR, Raman and SERS data is useful [121]. Transmission FTIR separates di-amino and tri-amino derivatives. PCA of the Raman data improves separation of the di-phenylnaphthalenes from the tri-phenylmethanes. Finally, PCA of SERS data separates the dyes based on the interaction of the silver colloids with acidic and basic dyes.

Many papers relate the use of advanced data treatment to further the spectroscopic study of natural organic media. The CH band centred at 2900 cm^{-1} has been used to separate protein-based media with PCA [216]. Clusters are formed at different scales. First, the dairy proteins (milk, casein, egg white and egg yolk) and the collagen proteins (fish glue, parchment glue, rabbit skin glue and ox bone glue) were separated. Among the dairy proteins, all the individual substances can also be separated, which is not the case for the collagen proteins. Finally, a paint sample of egg white mixed with yellow ochre was successfully identified using the proposed PCA methodology. A further study also evaluated the efficiency of that method to discriminate proteinaceous materials regardless of their ageing [215, 217]. The same spectral region (CH stretching region) has been used with PCA to distinguish between natural organic compounds from different chemical families (glues, gums, resins and oils) [105]. The statistical treatment is performed on parameters extracted from a spectral decomposition procedure (involving the precise assessment of band width, peak area, and position) that adds information closely related to the molecular structure of the media to the multivariate study. Following this procedure, the different chemical families of the organic compounds can be successfully distinguished, and different geographical provenances can even be separated within the terpenoid resins group (Fig. 4).

FT-Raman and fibre optical reflectance spectroscopy (FORS) data on several types of organic binders (egg white, egg yolk, whole egg, gum Arabic, linseed, poppy, and walnut oil) have been examined using PCA. The addition of the FORS data improved the discrimination between the binders, as supplementary information was introduced in the PCA [229]. In paint layers, depending on the pigments, organic binders such as drying oils tend to form metal soaps. In order to identify these soaps in unknown samples, Otero et al. demonstrated a methodology based on the PCA treatment on selected Raman regions of more than 20 metal carboxylates (6 cations and 4 fatty acids) [226]. The $1120\text{--}1040\text{ cm}^{-1}$ region is the most helpful in separating these soaps according to their fatty acid constituents, as it contains the vibrational features of the fatty acids chains, while the $1650\text{--}1380\text{ cm}^{-1}$ is useful in identifying the nature of the metal counterion, since it shows the bands related to the coordination of the carboxylate group with the metal cations.

While in the case of art materials the sample population is normally relatively small, in forensic science these statistical approaches have become the norm, especially when a very large number of samples need to be identified and assigned to specific categories against databases that can be massive (for example, for

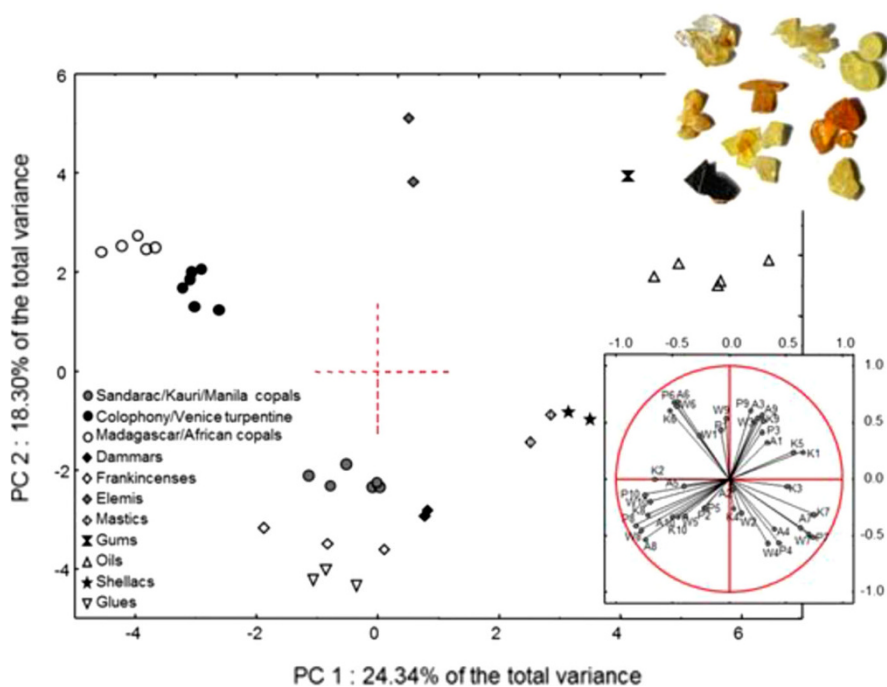


Fig. 4 Score-plot and projection of variables extracted from FT-Raman spectra of natural products on PC1 and PC2. Variables: 40 fitting parameters of the Raman CH bands. Items: 37 reference materials. The materials are clearly clustered by families. The projection of variables indicates which variables have an important contribution to each PC. Figure reprinted from [105], Copyright (2013), with permission from Elsevier

commercial industrial paints). Typically, several statistical methods are used [212]. First, the spectra are studied (in terms of noise level, variability of the measurements, etc.) before creating a reduced data matrix for PCA and HCA, or even for both PCA and HCA. Then, if the samples can be separated into different groups, score-plots or dendrograms are studied. If there is no possibility of forming more groups, the cluster is considered a single one; otherwise, the procedure is repeated to form sub-groups. This iterative method can obviously also be performed on smaller datasets as is often the case in the cultural heritage field.

All the statistical approaches mentioned so far first require the acquisition of a number of reference spectra to supplement available libraries, but also involve statistical and computational skills that are not trivial to master. Simpler tools can also be implemented for material identification.

Several papers present flowcharts to identify materials based on the presence/absence of bands, or using specific band positions that are diagnostic for a particular compound. This kind of protocol can help in the identification of materials within the same chemical family, and has proven particularly useful for organic media for which many bands are usually observed. Within the same group, compounds may have similar spectra, but slight differences related to very specific chemical bonds or

additional functional groups that are characteristic for each individual compound can help in their discrimination. A flowchart for the identification of various kinds of synthetic azo pigments, based on 21 references, allowed the distinguishing of several classes of azo pigments: β -Naphthol (lake and non-lake pigments), BON-pigments, di-arylide (di-azo) pigments, naphthol AS pigments and Hansa yellow (mono-azo) pigments [293]. This tool also successfully identified synthetic pigments from two modern art paintings by Pablo Picasso and Karel Appel. Natural organic substances including glues, oils, gums and natural resins have been extensively studied with IR and Raman spectroscopy, leading to an algorithm that identifies and discriminates the different media [107]. The proposed flowchart for material identification not only readily separates resins, oils, glues and gums based on specific bands related to their different chemical families (terpenes, triglycerides, proteins and polysaccharides) but further isolates four subgroups that are clearly set apart within the resins family: triterpenic resins, shellacs, colophony and Venice turpentine, and finally copal and sandarac. Using a similar protocol, diterpenic and triterpenic resins are differentiated in a set of archaeological resins [33].

Different Raman parameters can be very informative if wisely used. Finding the most interesting ratios or the best set of Raman features will help identifying materials, from a simple classification of compounds to a deeper characterisation of materials properties, such as, for example, their degree of crystallinity or their degree of polymerisation. This can be accomplished with the use of ratios, such as band intensities ratios, or plotting other spectroscopic parameters, such as band widths or positions. Colomban [83] links Raman features of glass to its degree of polymerisation, thereby characterizing the glass structure and the firing technologies by plotting area ratios of the Si–O bending (more intense in the case of silica-rich glasses) to the Si–O stretching vibrations (more intense for more amorphous or highly fluxed materials) (see Sect. 4.5 for more details). This ratio is then plotted as a function of the maximum intensity of the Si–O stretching vibration and results in the classification of various families of glasses, enamels and ceramic glazes that can be used as a database of spectroscopic parameters for the study of ancient artifacts [89]. Other studies directly plot the maximum intensities of the two Si–O vibrations mentioned above and also obtain a classification of glass materials according to their chemical compositions [289]. Tomasini et al. used the full width at half maximum as a function of band position for the D band (centred at 1300 cm^{-1}) and G band (at 1500 cm^{-1}) of several carbon-based black pigments (charcoal, graphite, bitumen, bistre, lampblack, ivory black, earth of Kassel and Van Dyck black), rather than adopting the more usual intensity ratio of the D and G bands [288]. This helps in grouping the pigments, simplifies their identification, and also gives an indication of the degree of graphitisation of these reference materials.

Another interesting application of Raman spectroscopy and spectral processing to determine structure–property relationships is represented by the study of the various crystalline forms of chrome yellow, an inorganic pigment that presents different structures (monoclinic, orthorhombic) depending on the amount of sulfur it contains. To better describe the spectral modifications occurring with an increase in sulfur rate, the maxima of several diagnostic bands are plotted against the percentage amount of sulfates demonstrating that the bands shift to higher

wavenumbers with increasing amount of sulfate. This is explained by the modification of the lattice introduced with the addition of sulfates, leading to a compression effect (S atoms being smaller than Cr atoms) at low percentages of sulfur and to an actual modification of the crystalline form at higher amounts.

3.5 Ageing

In addition to original, un-altered and reference materials, the study of museum or archaeological objects brings the question of the ageing and degradation of materials, particularly organic substances. Molecular transformations due to natural aging or alteration often lead to spectral modifications, and the need for databases of materials that accommodate this natural evolution has been raised in this field [61, 124].

A majority of the studies conducted with Raman spectroscopy on the alteration of organic substances concern mainly tree exudates or fossil resins such as amber. These materials are based on a terpene skeleton (diterpene) with carbon–carbon double bonds highly sensitive to oxidation [206]. To monitor these changes, the ratio of the intensities of the C=C stretching band (1650 cm^{-1}) to the C–H bending band (1445 cm^{-1}) is performed: the higher the ratio, the more advanced the degradation [32, 107, 126, 307]. However, these studies differ in how they interpret this evolution. Some works consider this ratio as a tool for potentially dating the resins [307], while others link it to issues of geological provenance (in the case of fossil resins) [32, 161]. Finally, some researchers broach the problem of the burial environment [32], or of unknown conservation conditions and its effects on band intensities. To assess the effect of unsuitable environments in museum storage on the degradation of amber, fresh and thermally aged amber samples kept in different relative humidity (RH) environments have been studied by FT-Raman and ATR-FTIR spectroscopies [281]. The results show that oxidation is likely the major degradation pathway, leading to a loss of C=C bonds (Raman) and an increase of carbonyl bonds (FTIR) on ageing regardless of the RH level. Molecular modifications can thus be monitored by looking at Raman bands intensity ratios, but the intensity is not the only spectral feature that evolves with ageing. In many cases, a broadening of the bands is also observed, linked to either the presence of new bands, or the introduction of disorder in the material, due to structural transformations. In order to better characterise all possible band evolutions and be able to explain these modifications, spectral decomposition is an accurate and powerful tool. A set of archaeological copals from a medieval excavation site in Sharma (Yemen) presenting visual differences in the bulk (fresh and transparent) and the surface (colored from yellow to red, and altered from dry to granulated, respectively) has been studied with FT-Raman and ATR-FTIR [104]. Two regions of interest showing several spectral modifications between the internal (undegraded) and external (aged) parts were used for a spectral decomposition procedure: the $1900\text{--}1400\text{ cm}^{-1}$ region, and the CH stretching region centred at 2900 cm^{-1} . This procedure requires the determination of a model or pattern. First, the number of individual bands, as well as their positions, is determined by looking at the second derivative of the spectra. Then, the adjustment procedure is launched and fitting

parameters such as the band positions, areas, half widths at half maximum and their profiles (Lorentzian or Gaussian) are extracted. The most relevant parameters are then monitored. The results show that some band variations (decreasing and broadening), and thus possible chemical reactions, correlate well with the state of conservation of the resins.

When the same set of samples are studied using PCA with spectral decomposition parameters as variables, the samples appear separated in two groups along PC1: the most altered on one side, and the less degraded on the other side [105]. Two correlated variables (band widths at half maximum) that have influenced this separation are then plotted, to arrive at the determination of a degradation index that is useful to qualify the degradation state of each copal.

3.6 Mixtures: Qualitative and Quantitative Analyses

Cultural heritage objects are heterogeneous and complex. A painting, for example, is a hierarchically complex system with multiple layers, which, starting from the support, may include the ground and paint layers and finally the varnish, and is composed of a wide variety of materials such as pigments, dyes, lakes, extenders, additives, adhesives, binders, varnishes, etc. These materials are almost invariably found as mixtures, whether heterogeneous such as paint layers or more homogenous mixtures such as varnishes or adhesives.

Raman analyses of complex samples may face many challenges. First, the presence of aged organic media in a mixture likely adds a fluorescence background to spectra recorded in dispersive mode with visible excitation lines, which may hinder the vibrational features of the analyte of interest. Second, the presence of some pigments can interfere with, for example, the identification of an organic medium, either by hiding some of the binder's bands in the spectra, but also chemically by accelerating the organic media's ageing and modifying their spectra. Finally, mixtures of organic media such as oils and resins or of synthetic dyes are often very difficult to discriminate using vibrational techniques: these materials present bands that often overlap. Looking at the unknown spectrum and comparing it with reference databases may be a way of qualitatively identifying some compounds by the presence of specific bands, but not all of them. Mathematical approaches should thus be considered to determine the mixtures' components, possibly in a (semi-)quantitative way, as can be obtained by using principal component analysis [194, 230] or spectral decomposition [10, 108, 210, 269]. PCA can be used to obtain semi-quantitative analyses of mixtures. Pallipurath et al. studied mixtures of organic media with increasing amounts of pigments: egg yolk with lead white, and poppy oil with lead–tin yellow (dark and light) [230]. Another study presented multivariate analyses of mixtures of organic media without pigmentation: linseed oil, poppy-seed oil, walnut oil and egg yolk [194]. PCA was able to clearly separate the individual media, but the mixtures were not very well discriminated, and no particular trend was observed in terms of the distribution of the binary mixtures inbetween the clusters formed by the pure materials they are made of. Overall, using an approach that applies PCA directly to determine pigments/binders or organic media proportions in mixtures still results in rather

ambiguous results. This may be because that approach considers the spectral data as a global description of the material, while other methods based on spectral decomposition aim to look at the Raman spectra from a more chemical and structural point of view. The spectral decomposition procedure consists of considering the profiles of the spectra of the binary mixtures as a linear combination of the spectra of the suspected pure materials. In other words, the sum of the pure materials spectra must fit the mixture spectrum [122]. This linear combination and fitting procedure, based on a least squares method, is performed on the intensities of the spectra. In most cases, the fitting process is performed on a selected range of wavenumbers. At the end of the procedure, a graphical result of the fitting is given, as well as the relative contribution of each pure material to the adjustment. This quantitative procedure successfully resolves the mixtures of three dyes used by the *Manufacture Nationale des Gobelins* in Paris (acid blue 258, acid yellow 169 and acid red 42) fixed on reference wool fibres, but also binary and ternary experimental mixtures with unknown proportions [269]. The authors report results of quantification that show a maximum difference of ± 4 between the theoretical and experimental percentages. A similar methodology has been applied to characterise experimental varnishes with increasing amounts of colophony in linseed oil [108], in order to determine if Raman (or FTIR spectroscopy) is efficient in detecting and quantifying such compounds in a mixture. The results showed a detection limit of 10 %, and that the relative quantification was accurate (Fig. 5a, b). The method has subsequently been demonstrated through applications to varnished objects from decorative arts museum collections in Paris [108].

A few studies have applied this same methodology on Raman mapping data [210]. In the case of mapping, the large amount of collected spectra require an automation of the fitting procedure, and the provided results consist of a matrix of data containing the relative amount of each component present in each pixel of the map, with the possibility of visualising the contribution of all the components on a false color map. This approach has been successfully applied to the study of iron corrosion [210] and more recently on the outdoor corrosion of the weathering of steel contemporary art sculptures [10].

4 Practical Raman Applications in the Cultural Heritage

4.1 Pigments, Inks and Colorants

The early years of applications of Raman spectroscopy to art and archaeology are characterised by a predominant attention to pigments and colorants. The first-ever reported study focused on the investigation of pigments on illuminated manuscripts [151], and ancient manuscripts have continued to be an area of intense investigation from the early days until the present, where, with XRF, fibre optic reflectance spectroscopy (FORS) [4, 259, 260], hyperspectral imaging and SERS [5], Raman spectroscopy has become an indispensable tool for the materials knowledge of these important objects [3, 47, 213, 292]. Published studies have not only concerned themselves with the investigation of the palette of illuminated manuscripts and

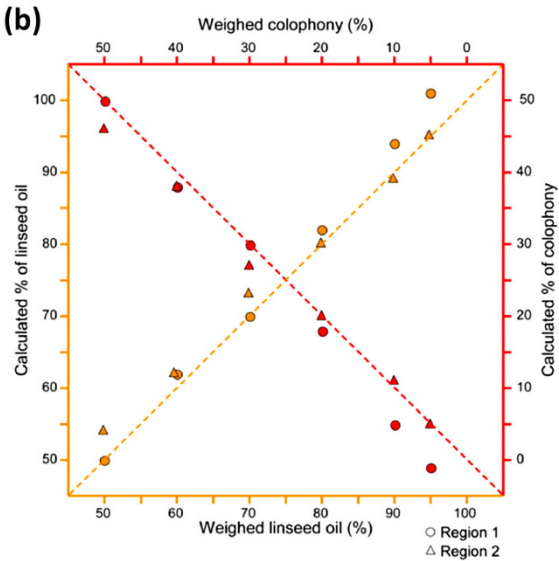
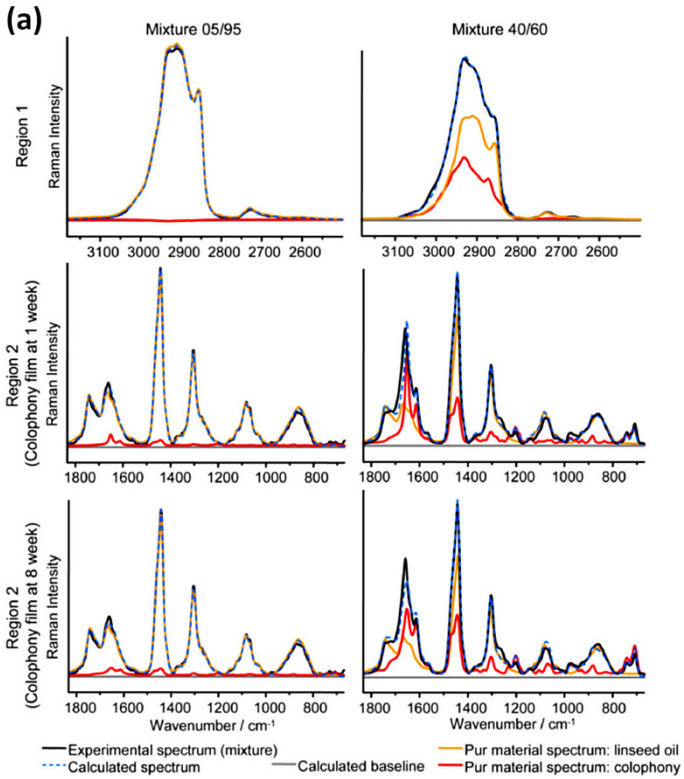


Fig. 5 a Spectral adjustment of the FT-Raman spectra (for two spectral regions) for two studied mixtures (w% of colophony/linseed oil) 05/95 and 40/60. For Region 2, two adjustments are presented: first using a 1-week dry colophony film spectrum, then an 8-week dry colophony film spectrum. It can be seen that colophony is not detected for the 05/95 varnish by exploiting Region 1 but contributes to the fitting of Region 2. It is also notable that the adjustment of Region 2 of the 40/60 mixture is better with the “oldest” colophony varnish, especially around 1650 cm^{-1} . **b** Quantitative calculation results obtained with respect to the theoretical results (weighed amounts of linseed oil and colophony) for FT-Raman data (circles Region 1, triangles Region 2). Dotted lines represent the exact correspondence between calculated and expected contents. The closer the data are to these dotted lines, the more accurate is the quantification by spectral decomposition. Figures reprinted from [108], Copyright (2014), with permission from Elsevier

assist with attribution to specific workshops [69] but they also now comprise the characterisation of degradation phenomena including, for example, the chemical and chromatic alteration of pigments based on copper [1, 2] and lead [205, 285]. In all cases, while conducting analyses, it is important to minimise the power of the laser at the sample so as not to induce the change that one is trying to measure [44, 117, 282].

After an early review on the palette of manuscript illumination [78], many foundational databases of Raman spectral signature of pigments, minerals and metal corrosion products have been published [16, 29, 43] and continue to be essential references today, together with the online databases already surveyed in Sect. 3.4.

It is well known that in the past 15 years numerous excellent reviews and special issues of journals (especially the *Journal of Raman Spectroscopy*) have been dedicated to in-depth overviews of all manners of application of Raman spectroscopy in art, archaeology, forensics, and gemology, and the reader is referred to these for a comprehensive treatment of the subject [24, 48, 77, 103, 171, 283, 284, 294, 296]. Many dedicated books are also available [68, 76, 125]. The focus of this section is rather on highlighting significant areas of interesting new research and promising future directions, as also only just carried out by Centeno [61].

In recent years, the study of pigments has evolved in two significant directions.

First, instead of reporting on isolated case studies, Raman has become a true tool to advance art history, being used, for example, for the systematic investigation of the palette of illuminated medieval manuscripts [45], or for a wide survey, using SERS, of red lake pigments employed by impressionist and post-impressionist painters [247]. Information about the identity of remnants of pigments on stone sculptures has been used to reconstruct their entire scheme of polychrome decoration [110], and, when pigments have faded, to propose re-colored visualisations of artworks [35].

Secondly, Raman spectroscopy is being used to contribute to our knowledge of pigment degradation and stability including those based on arsenic [291], lead [44, 285], copper [170], and, more recently, the lead chromates [208, 209]. Research focused on reconstructing the chemistries of production of traditional pigments following ancient recipes also includes the characterisation of deterioration products [70, 79, 101, 270]. Occasionally, spectra of pigments that have not been previously characterised are still presented in the literature and studied in depth, significantly enriching available libraries [28, 55, 290].

The study of colorants and dyes has gone hand in hand with that of mineral pigments, with FT-Raman and SERS giving an important boost to our ability to characterise synthetic and natural colorants [57, 144, 242, 273, 293, 297].

Raman being perhaps one of the very few analytical techniques that is able to characterise and distinguish black drawings, paintings and writing media, an increasing body of work has focused on these applications [81, 228, 288]. In recent years, there have also been significant advances in the identification of inks, including traditional inks such as sepia [66, 264], bistre [265], and iron gall ink [26, 27, 178, 238] and the ones used by modern artists such as the chrome logwood [34, 62, 65] and crystal violet inks used by Van Gogh [49, 244].

Overlapping with forensics, the study of modern pigments and dyes used in inks, including those used in felt-tip pens [286], lithographic inks [31, 63, 148, 202], and toned cinematographic films [186], have also benefited from the valuable contributions of Raman spectroscopy.

Of obvious interest is the use of pigment identification with Raman spectroscopy to contribute to dating and the identification of fakes and forgeries, one typical example being the identification of titanium-based whites (anatase or rutile) in works of art, which has been used to place their production after specific times in the twentieth century (Laver [177]). However, the detection of rutile or anatase in artifacts can sometimes be problematic as, due to their extremely high Raman scattering cross-sections, these polymorphs of titanium dioxide will show intense Raman peaks even when they are present in low or trace concentrations [80]. Interestingly, much of the recent published literature on fakes [46, 220] focuses on case studies related to forgeries of Russian avant garde artists, where synthetic and anachronistic pigments have often been reported (Fig. 6) [71, 271].

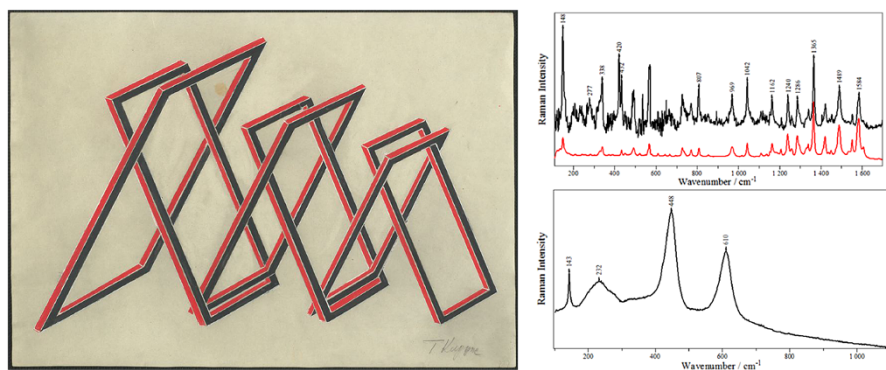


Fig. 6 Design for a Propaganda Stand (The Art Institute of Chicago 2011.880). This drawing originally entered the collection with a date of c.1922 and was previously attributed to the Russian avant-garde artist Gustav Klutis (Latvia, 1895–1938). The drawing was investigated non-invasively with Raman micro-spectroscopy with 785-nm excitation. Identification of rutile (TiO_2) white (*bottom right*) and red pigments identified as the naphthol red pigment PR9 (C. I. 12460; shown at *top right*, with the reference spectrum shown in red, as derived from [273]). According to the *color index*, A. Laska and A. Zitscher discovered PR9 only in 1922, while the first commercialisation of titanium white in its rutile form is dated to the late 1930s (Laver [177]). Both pigment findings are thus inconsistent with the presumed date of creation of this work

4.2 Minerals and Gemstones

The use of Raman spectroscopy for mineral identification/gemmological purposes can be thought of as the first application of Raman which can be relevant in the field of cultural heritage. The early applications to gemmology at the end of the 1970's [118], soon after the introduction of the Raman microprobe (see Sect. 2) may be explained by the generally high resistance of these materials to laser excitation. Here, phase identification is mainly achieved by comparison with published databases (see Sect. 3.4), which have been regularly enriched (since Schubnel et al., [276] which could be considered the first one), especially by contributions that account for slight differences in the spectrum in relation to the gem origin (i.e. variation of the chemical composition and/or the structure).

Materials of various origins are classified as gems or minerals of interest in the field of cultural heritage, from precious minerals (diamond, emerald, garnet, ruby, etc.) [22, 23, 157] to precious stones selected for their aesthetic value (Lapis Lazuli, jade, nephrite, etc.) [56, 72, 82, 155], fossilised resins (amber, copal, etc.) [104, 281] and biomaterials (corals, pearls, etc.) [21, 167, 168]. As already mentioned in this article, several dedicated reviews focused on applications in gemmology are available and should be consulted for a comprehensive overview of the field [24, 145, 171].

Recent and innovative applications in the cultural heritage involve the identification of mineral phases to help with the study of raw materials exploitation, underlining the links between past societies and their environment through use of natural resources. If the analytical characterisation allows it, the precise recognition of different quarries or geological sources may be useful for studying provenance and circulation networks. Such provenance studies by Raman spectroscopy are also relevant to other fields like, for example, the earth sciences [9]. The current wide availability of portable instruments benefits gemmology and the cultural heritage by enabling in situ measurements of precious objects, which generally require on-site analysis and often have barely accessible areas to measure [14, 237].

4.3 Natural and Synthetic Organic Materials

While the study of natural organic binding media and varnishes and the important contributions of statistical analysis to the characterisation and discrimination of such materials, both in their original and aged status, have been extensively discussed in Sects. 3.4–3.6, here, applications to biomaterials and synthetic polymers are briefly reviewed.

Early work includes the identification of lichen encrustations that are responsible for the biodeterioration of wall paintings [136, 138, 207], a subject that has been expanded to incorporate other bio-materials [308] including those that are characteristic of extremophilic environments such as are found in Antarctica or on Mars [136, 164, 312].

FT-Raman spectroscopy has been used to characterise bone, hoofs, tortoiseshell [134] and ivory [130]. Significant advancements in the characterisation of biopolymers, such as skin, callus, hair and nail [15, 305], as well as mummified

[6] and archaeological skin [133] and human hair from archaeological excavations, have been reported [249, 306].

The study of textile fibres including archaeological linen [132], as well as the FT-Raman characterisation of parchment and paper [137], are also important contributions to our knowledge of culturally significant artifacts.

Starting in the 1960s, the power of Raman spectroscopy to identify not only the type of synthetic polymers but also determine important parameters about their structures and physical–mechanical properties has been exploited within the confines of the discipline of polymer science [147, 219]. In the field of art and design, the potential of Raman spectroscopy is still somehow under-utilised [102, 231, 232, 272], but some comprehensive review of Raman applications for the identification of post-consumer plastics for recycling purposes using PCA [7], and other industrial applications are available [135, 139].

4.4 Deterioration Products and Conservation Treatments

Calcium oxalates [146, 317], a pervasive product of deterioration in outdoor sculpture and historic architecture, cave paintings and many museum and archaeological objects, were among the first deterioration products to be studied with Raman spectroscopy, where they have been characterised together with other organic byproducts of lichen metabolism such as erythrin, lecanoric acid and meso-erythritol [131].

Other pioneering work on deterioration products includes the discovery that red lead (Pb_3O_4) is responsible for the puzzling red stains observed on the Carrara marbles of the Certosa of Pavia [38], and in several other cases Raman spectroscopy has been instrumental in unraveling the chemical composition of deterioration products such as copper and calcium oxalates affecting mural paintings [215, 217].

Recent interesting developments include the use of such information to deduce the kinetics and thermodynamic processes regulating cycles of deterioration of, for example, the fresco cycles in the famous Roman archaeological site of Pompeii and other wall paintings [234]. In many of these studies, the availability of compact portable Raman instruments is extremely valuable for in situ studies where several areas can be monitored and mapped in expanded time- and length-scales [11, 195, 235].

Raman studies of the spectroscopic signatures of iron sulfates and other deterioration products of waterlogged wood have been reported [236], as well as the effect of conservation treatment, especially those based on the polyethylene glycol (PEG)/freeze-drying method [73, 74].

In recent years, oxalates have also been proposed as more compatible consolidants of stone, and micro-Raman spectroscopy has been used as a tool for mapping their penetration into the mineral substrate, an important factor for their successful application [91–94].

Synthetic polymers continue to be the most used type of treatment for outdoor architecture, and Raman spectroscopy has also been used to characterise those, together with other complementary spectroscopic techniques such as FTIR spectroscopy and nuclear magnetic resonance (NMR) spectroscopy [100].

4.5 Glass

Although glass has a disordered structure, Raman spectroscopy is one of the few techniques which allow the study of the glassy matrix. This “molecular” spectroscopy can probe the “local order” in such disordered structures, revealing information about the chemical composition of the glass and its thermal history. For the majority of cultural heritage objects, glasses are silica-based but also contain many other minor to trace elements. These trace elements play a role in the manufacturing process or are used as fluxes (Na, K), stabilisers (Ca, Mg), colorants/dicolorants, or are to be considered “pollutants” i.e. trace elements coming from raw materials or manufacturing/recycling. There are two main kinds of glassy materials that are relevant in the cultural heritage, bulk glass, constituting a whole object or its major parts, and “thin” glass, which represents coatings or other surface layers on stones or ceramics. Because it is easier to stabilise small amounts of material in the glassy state, glazes on ceramics typically exhibit a larger variety of chemical composition than bulk glass. This has allowed ancient ceramists to play with a wide range of possible melting temperatures and colors.

In addition to the composition and structure of the glassy part, the appearance and color of glass can also be adjusted by exploiting nano- to micro-crystallisation products created in situ during manufacturing (opacifiers, pigments, metallic luster), or micro-crystals added as pigments and/or opacifiers. As is the case for pigments in paintings (see Sect. 4.1) such pigments/opacifiers can be characterised by Raman spectroscopy, either directly from their spectra or, for metallic nano-particles, by their SERS effect on the glass spectrum at their surface [88]. To date, Raman spectroscopy is the only bench-top (or portable) analytical method for non-invasively characterising these micro-/nano-inclusions, often with a high sensitivity, selectivity and ease of implementation. In general, the concentration of such crystalline phases is not high enough to be detected by X-ray diffraction, and their analysis by scanning electron microscopy–energy dispersive spectroscopy or transmission electron microscopy (with elemental or diffraction analysis) requires sampling and generally the preparation of sections, which is often restricted from glass and ceramics in the fine arts museum context, but may be more readily available from archaeological objects or fragments.

In the cultural heritage, glass is mainly studied by elemental analyses to access the recipes/manufacturing techniques (major and minor elements) or provenance (trace elements from raw materials) [156]. The Raman spectrum is sensitive to major and minor element contents, and the sensitivity of the Raman bands to their surrounding environment allows the extracting of useful parameters that can assist in characterizing the glass composition. One such parameter is the polymerisation index (I_p) which is mainly related to the flux content, and thus relates to the melting temperature [83]. Further, the spectral decomposition of the Si–O stretching and bending band convolutions (Q^n massif) and some easily identified values (such as the wavenumber of the maximum of the Q^n massif) provide useful parameters for classifying glass with regards to the minor element contents [89].

Raman spectroscopy is useful in predicting the stability of ancient and historic glass by recognizing its class of composition based on the wavenumber of the

bending massif (around 550 cm^{-1}), which is correlated with the SiO_2 content, or the area ratio between some Q^n bands (specifically the 950 and the 1040 cm^{-1} bands) and the number of non-bridging oxygens per silicon atom [262].

When dealing with a particular kind of glass, various authors have provided specific methodologies for quantifying the content of some elements using Raman spectroscopy. Good correlations have been described between the lead content and Raman features of lead-based glass, as, for example the wavenumber shift of the band around 1070 cm^{-1} , which is described for a wide range of lead content (up to 20 mol%) [261]. For glass with varying iron content, correlations have been described between the bands centred around 980 and 1090 cm^{-1} (Q^2/Q^3 areas, respectively), and Fe_2O_3 amounts [13].

In addition to artificial glass, Raman spectroscopy has also been used to study natural glass (obsidians), particularly to address the problematic issue of provenance determination of obsidian artifacts. As all sources (volcano or volcanic event) should exhibit a specific elemental composition and may also be associated with a specific thermal history, the exploitation of specific Raman signatures provides clustering of the obsidian sources. Some exploratory studies using multivariate analysis (principal component analysis) of the whole spectrum [169], or of characteristic bands [17], demonstrate the possibility of determining obsidian provenance in specific geographic contexts such as the Pacific region and the western Mediterranean.

Compared to elemental analysis, the advantage of Raman spectroscopy to characterise glassy materials is being less sensitive to surface alteration when using a confocal setup, as the unaltered glass can be analysed through the weathered layers, thus easily providing microanalysis of well-defined sampled volumes. In fact, photons used in Raman spectroscopy can be accurately focused (more easily than X-rays) and the probed volume better defined and restricted thanks to the focality of the optical systems. Laser ablation (as in laser ablation inductively coupled plasma mass spectrometry or in LIBS) also provides localised analyses, but involves micro-destructive sampling that leaves behind a crater of a few tens of cubic microns. For studying thin, localised layers, such as heterogeneities in bulk glass (as effects of alteration) or glazes on ceramics (thin layers or small areas), Raman spectroscopy is not only an alternative to elemental analysis for obtaining the composition of the sample but exhibits unique capabilities.

In addition to being able to reveal glass and glaze composition, the structural features revealed by the Raman spectrum of glass also provide information on the thermal history of the glass. The manufacturing process of Roman panes has been determined by establishing calibration curves between the Raman stretching massif position (or the ratio between Q^2 and Q^3 bands) and the glass fictive temperature [252, 253]. By deducting the fictive temperature on both sides of a glass pane, it can be shown whether the glass was manufactured by blowing or casting. Apart from thermal analyses (thermo-gravimetric analysis, differential scanning calorimetry), Raman spectroscopy is, with IR spectroscopy and Brillouin scattering, the method of choice for revealing the links between the glass structure and its thermal history.

Such studies related to glass structures can thus also reveal key parameters about the ancient processes and the know-how of glass makers.

4.6 Ceramics

A large part of very-high-temperature ceramic manufacturing induces the melting of clays and then produces glassy products, the study of which has been previously described. But Raman spectroscopy can also be used to study the mineralogy of the ceramic paste and decoration. The growing use of Raman micro-spectroscopy in this area is related to its spatial resolution, its non-invasive character, the selectivity of signatures, and its convenient implementation, which are particularly attractive for applications to ceramic objects [25, 58, 109, 227]. Studies of the pigments used for ceramic glazes in soft paste, hard paste and majolica ceramics have been the subjects of numerous articles and are extensively reviewed elsewhere [68, 84, 86, 87, 90, 125, 258].

For the ceramic paste, the identification of mineral phases, especially in traces, offers a more detailed characterisation of the mineralogical assemblage, leading to the identification of the raw materials used, which can then contribute to illuminating clues about their provenance [204]. Additionally, the characterisation of the mineralogical composition reveals clues to the firing conditions (temperatures reached, firing atmosphere) to document the manufacturing process. However Raman results often need to be integrated with other results (generally obtained by optical microscopy, electron microscopy, X-ray diffraction, etc.) in order to support the interpretations and propose a comprehensive archaeometric description of the artifact.

By recognizing specific mineralogical phases in (or close to) the slip/glaze, some ceramic firing characteristics can be revealed, for example correlating the oxidising conditions and the various possible iron phases (with their corresponding redox state) present in an artifact or sample. This is the case for a rare metastable polymorph of Fe_2O_3 ($\epsilon\text{-Fe}_2\text{O}_3$) identified in the black glaze of Chinese ceramics [113] or magnetite and various features of the hematite spectrum characterised through the body and the gloss of Athenian pottery [75].

Looking at the evolution of the hematite spectrum with the firing temperature of terra sigillata, Leon et al. have highlighted that hematite from the slip carries in its spectral signatures a record of the temperature reached during firing. Diagrams involving ratios of the bands of hematite ($680/415$ vs. $680/620 \text{ cm}^{-1}$) separate terra sigillata productions from southern Gaul and Italy because of the lower firing temperature reached by the latter [185].

This short review on glass and ceramic studies involving Raman spectroscopy underlines its increasing use in the field of archaeometry and the cultural heritage. Besides mineralogical fingerprinting, the extraction of parameters from the Raman spectrum can reveal some very informative parameters in relation to ancient technologies of production and/or the raw material used. This sensitivity of Raman spectroscopy to structural order makes this analytical technique a very powerful one to study artifacts from *les arts du feu*.

5 Conclusions

The field of Raman spectroscopy in art and archaeology has experienced a massive and vital growth since its first application to illuminated manuscripts approximately three decades ago. Initially focused mostly on the identification of original constituent materials of works of art, it has evolved to include degradation and conservation products, and has experienced substantial improvements in its ability to accurately perform materials identification by benefitting from the use of advanced spectral and statistical treatments for enhanced spectral matching and attribution. Despite the many reviews available in the literature, this is the first time that an extensive coverage has been devoted to advanced spectral processing and the contributions of chemometrics to the furtherance of spectroscopic studies of works of art. In recent years, Raman spectroscopy is also increasingly being used to uncover structure–property relationships of artistic and archaeological materials at the microscale and to reconstruct ancient technologies. SERS is now an established tool in the analytical chemist’s toolkit, while new developments in SORS and wide-field imaging are to be expected.

It can be confidently said that Raman spectroscopy applications in the cultural heritage are continually pushing the envelope of the technique to impact every aspect of our knowledge of the “chaine operatoire” of art and archaeological artifacts: from manufacturing through use to degradation, burial (where applicable), collection, conservation and fruition.

The future of Raman spectroscopy in art and archaeology is still very bright: laser light bright.

Acknowledgments Research at the Art Institute of Chicago is supported through generous grants of the Andrew W. Mellon Foundation and Grainger Foundation. Grant DMR-0723053 from the National Science Foundation is also gratefully acknowledged for the acquisition of a FT-Raman spectrometer at the Art Institute of Chicago. Claudia Conti and Pavel Matousek are thanked for generously sharing the material reproduced in Fig. 2 for this review. F.C. thanks Prof. Richard P. Van Duyne of Northwestern University for several years of collaboration and inspiration in SERS.

References

1. Aceto M, Agostino A, Boccaleri E, Crivello F, Cerutti Garlanda A (2010) Identification of copper carboxylates as degradation residues on an ancient manuscript. *J Raman Spectrosc* 41:1434–1440. doi:10.1002/jrs.2650
2. Aceto M, Agostino A, Boccaleri E, Crivello F, Garlanda AC (2006) Evidence for the degradation of an alloy pigment on an ancient Italian manuscript. *J Raman Spectrosc* 37:1160–1170. doi:10.1002/jrs.1604
3. Aceto M, Agostino A, Fenoglio G, Gulmini M, Bianco V, Pellizzi E (2012) Non invasive analysis of miniature paintings: proposal for an analytical protocol. *Spectrochim Acta A* 91:352–359. doi:10.1016/j.saa.2012.02.021
4. Aceto M, Agostino A, Fenoglio G, Idone A, Gulmini M, Picollo M, Ricciardi P, Delaney JK (2014) Characterisation of colourants on illuminated manuscripts by portable fibre optic UV-visible-NIR reflectance spectrophotometry. *Anal Methods* 6:1488–1500. doi:10.1039/c3ay41904e
5. Aceto M, Arrais A, Marsano F, Agostino A, Fenoglio G, Idone A, Gulmini M (2015) A diagnostic study on folium and orchil dyes with non-invasive and micro-destructive methods. *Spectrochim Acta A* 142:159–168. doi:10.1016/j.saa.2015.02.001

6. Akhtar W, Edwards HGM (1997) Fourier-transform Raman spectroscopy of mammalian and avian keratotic biopolymers. *Spectrochim Acta A* 53:81–90. doi:10.1016/S1386-1425(97)83011-9
7. Allen V, Kalivas JH, Rodriguez RG (1999) Post-consumer plastic identification using Raman spectroscopy. *Appl Spectrosc* 53:672–681
8. Amendola V, Meneghetti M (2009) Laser ablation synthesis in solution and size manipulation of noble metal nanoparticles. *Phys Chem Chem Phys* 11:3805–3821. doi:10.1039/b900654k
9. Andò S, Bersani D, Vignola P, Garzanti E (2009) Raman spectroscopy as an effective tool for high-resolution heavy-mineral analysis: examples from major Himalayan and Alpine fluvio-deltaic systems. *Spectrochim Acta A* 73:450–455
10. Aramendia J, Gomez-Nubla L, Bellot-Gurlet L, Castro K, Paris C, Colombari P, Madariaga JM (2014) Protective ability index measurement through Raman quantification imaging to diagnose the conservation state of weathering steel structures. *J Raman Spectrosc* 45:1076–1084
11. Aramendia J, Gomez-Nubla L, Castro K, Martinez-Arkarazo I, Vega D, López Sanz, de Heredia A, Ibáñez García, de Opakua A, Madariaga JM (2012) Portable Raman study on the conservation state of four CorTen steel-based sculptures by Eduardo Chillida impacted by urban atmospheres. *J Raman Spectrosc* 43:1111–1117. doi:10.1002/jrs.3158
12. Arslanoglu J, Zaleski S, Loike J (2011) An improved method of protein localization in artworks through SERS nanotag-complexed antibodies. *Anal Bioanal Chem* 399:2997–3010. doi:10.1007/s00216-010-4378-0
13. Baert K, Meulebroeck W, Wouters H, Cosyns P, Nys K, Thienpont H, Terryn H (2011) Using Raman spectroscopy as a tool for the detection of iron in glass. *J Raman Spectrosc* 42:1789–1795
14. Barone G, Bersani D, Jehlička J, Lottici PP, Mazzoleni P, Raneri S, Vandenebee P, Di Giacomo C, Larinà G (2015) Nondestructive investigation on the 17–18th centuries Sicilian jewelry collection at the Messina regional museum using mobile Raman equipment. *J Raman Spectrosc* 46:989–995
15. Barry BW, Edwards HGM, Williams AC (1992) Fourier transform Raman and IR vibrational study of human skin: assignment of spectral bands. *J Raman Spectrosc* 23:641–645. doi:10.1002/jrs.1250231113
16. Bell IM, Clark RJH, Gibbs PJ (1997) Raman spectroscopic library of natural and synthetic pigments (pre- ≈ 1850 AD). *Spectrochim Acta A* 53:2159–2179. doi:10.1016/S1386-1425(97)00140-6
17. Bellot-Gurlet L, Le Bourdonnec F-X, Poupeau G, Dubernet S (2004) Raman micro-spectroscopy of western Mediterranean obsidian glass: one step towards provenance studies? *J Raman Spectrosc* 35:671–677
18. Bellot-Gurlet L, Neff D, Reguer S, Monnier J, Saheb M, Dillmann P (2009) Raman studies of corrosion layers formed on archaeological irons in various media. *J Nano Res* 8:147–156
19. Bell SEJ, Bourguignon ESO, Dennis A (1998) Analysis of luminescent samples using subtracted shifted Raman spectroscopy. *Analyst* 123:1729–1734
20. Benedetti DP, Zhang J, Tague TJ, Lombardi JR, Leona M (2014) In situ microanalysis of organic colorants by inkjet colloid deposition surface-enhanced Raman scattering. *J Raman Spectrosc* 45:123–127. doi:10.1002/jrs.4424
21. Bergamonti L, Bersani D, Mantovan S, Lottici PP (2013) Micro-Raman investigation of pigments and carbonate phases in corals and molluscan shells. *Eur J Miner* 25:845–853
22. Bersani D, Andò S, Vignola P, Moltifiori G, Marino I-G, Lottici PP, Diella V (2009) Micro-Raman spectroscopy as a routine tool for garnet analysis. *Spectrochim Acta A* 73:484–491
23. Bersani D, Azzi G, Lambruschi E, Barone G, Mazzoleni P, Raneri S, Longobardo U, Lottici PP (2014) Characterization of emeralds by micro-Raman spectroscopy. *J Raman Spectrosc* 45:1293–1300
24. Bersani D, Lottici PP (2010) Applications of Raman spectroscopy to gemology. *Anal Bioanal Chem* 397:2631–2646. doi:10.1007/s00216-010-3700-1
25. Bersani D, Lottici PP, Virgenti S, Sodo A, Malvestuto G, Botti A, Salvioli-Mariani E, Tribaudino M, Ospitali F, Catarzi M (2010) Multi-technique investigation of archaeological pottery from Parma (Italy). *J Raman Spectrosc* 41:1556–1561
26. Bicchieri M, Monti M, Piantanida G, Sodo A (2008) All that is iron-ink is not always iron-gall! *J Raman Spectrosc* 39:1074–1078. doi:10.1002/jrs.1995
27. Bicchieri M, Monti M, Piantanida G, Sodo A (2013) Non-destructive spectroscopic investigation on historic Yemenite scriptorial fragments: evidence of different degradation and recipes for iron tannic inks. *Anal Bioanal Chem* 405:2713–2721. doi:10.1007/s00216-012-6681-4

28. Bouchard M, Gambardella A (2010) Raman microscopy study of synthetic cobalt blue spinels used in the field of art. *J Raman Spectrosc* 41:1477–1485. doi:10.1002/jrs.2645
29. Bouchard M, Smith DC (2003) Catalogue of 45 reference Raman spectra of minerals concerning research in art history or archaeology, especially on corroded metals and coloured glass. *Spectrochim Acta A* 59:2247–2266
30. Brambilla A, Osticioli I, Nevin A, Comelli D, D'Andrea C, Lofrumento C, Valentini G, Cubeddu R (2011) A remote scanning Raman spectrometer for in situ measurements of works of art. *Rev Sci Instrum* 82:063109. doi:10.1063/1.3600565
31. Braz A, Lopez-Lopez M, Garcia-Ruiz C (2013) Raman spectroscopy for forensic analysis of inks in questioned documents. *Forensic Sci Int* 232:206–212. doi:10.1016/j.forsciint.2013.07.017
32. Brody RH, Edwards HGM, Pollard AM (2001) A study of amber and copal samples using FT-Raman spectroscopy. *Spectrochim Acta A* 57:1325–1338
33. Brody RH, Edwards HGM, Pollard AM (2002) Fourier transform-Raman spectroscopic study of natural resins of archaeological interest. *Biopolymers* 67:129–141
34. Bronzato M, Zoleo A, Biondi B, Centeno SA (2016) An insight into the metal coordination and spectroscopic properties of artistic Fe and Fe/Cu logwood inks. *Spectrochim Acta Part B* 153:522–529. doi:10.1016/j.saa.2015.08.042
35. Brosseau CL, Casadio F, Van Duyne RP (2011) Revealing the invisible: using surface-enhanced Raman spectroscopy to identify minute remnants of color in Winslow Homer's colorless skies. *J Raman Spectrosc* 42:1305–1310. doi:10.1002/jrs.2877
36. Brosseau CL, Gambardella A, Casadio F, Grzywacz CM, Wouters J, Van Duyne RP (2009) Ad-hoc surface-enhanced Raman spectroscopy methodologies for the detection of artist dyestuffs: thin layer chromatography-surface enhanced Raman spectroscopy and in situ on the fiber analysis. *Anal Chem* 81:3056–3062. doi:10.1021/ac802761v
37. Brosseau CL, Rayner KS, Casadio F, Grzywacz CM, van Duyne RP (2009) Surface-enhanced Raman spectroscopy: a direct method to identify colorants in various artist media. *Anal Chem* 81:7443–7447
38. Bruni S, Cariati F, Bianchi CL, Zanardini E, Sorlini C (1995) Spectroscopic investigation of red stains affecting the Carrara marble façade of the Certosa of Pavia. *Archaeometry* 37:249–255. doi:10.1111/j.1475-4754.1995.tb00741.x
39. Bruni S, De Luca E, Guglielmi V, Pozzi F (2011) Identification of natural dyes on laboratory-dyed wool and ancient wool, silk, and cotton fibers using attenuated total reflection (ATR) Fourier transform IR (FT-IR) spectroscopy and Fourier transform Raman spectroscopy. *Appl Spectrosc* 65:1017–1023. doi:10.1366/10-06203
40. Bruni S, Guglielmi V, Pozzi F (2011) Historical organic dyes: a surface-enhanced Raman scattering (SERS) spectral database on Ag Lee-Meisel colloids aggregated by NaClO₄. *J Raman Spectrosc* 42:1267–1281. doi:10.1002/jrs.2872
41. Bruni S, Guglielmi V, Pozzi F (2010) Surface-enhanced Raman spectroscopy (SERS) on silver colloids for the identification of ancient textile dyes: tyrian purple and madder. *J Raman Spectrosc* 41:175–180. doi:10.1002/jrs.2456
42. Buckley K, Matousek P (2011) Non-invasive analysis of turbid samples using deep Raman spectroscopy. *Analyst* 136:3039–3050. doi:10.1039/c0an00723d
43. Burgio L, Clark RJ (2001) Library of FT-Raman spectra of pigments, minerals, pigment media and varnishes, and supplement to existing library of Raman spectra of pigments with visible excitation. *Spectrochim Acta A* 57:1491–1521. doi:10.1016/S1386-1425(00)00495-9
44. Burgio L, Clark RJH, Firth S (2001) Raman spectroscopy as a means for the identification of plattnerite (PbO₂), of lead pigments and of their degradation products. *Analyst* 126:222–227. doi:10.1039/B008302J
45. Burgio L, Clark RJH, Hark RR (2010) Raman microscopy and X-ray fluorescence analysis of pigments on medieval and Renaissance Italian manuscript cuttings. *Proc Natl Acad Sci USA* 107:5726–5731. doi:10.1073/pnas.0914797107
46. Burgio L, Clark RJH, Hark RR (2009) Spectroscopic investigation of modern pigments on purportedly medieval miniatures by the “Spanish Forger”. *J Raman Spectrosc* 40:2031–2036. doi:10.1002/jrs.2364
47. Burgio L, Clark RJH, Muralha VSF, Stanley T (2008) Pigment analysis by Raman microscopy of the non-figurative illumination in 16th- to 18th-century Islamic manuscripts. *J Raman Spectrosc* 39:1482–1493. doi:10.1002/jrs.2027

48. Buzzini P, Suzuki E (2015) Forensic applications of Raman spectroscopy for the in situ analyses of pigments and dyes in ink and paint evidence. *J Raman Spectrosc*. doi:10.1002/jrs.4818
49. Cañamares MV, Chenal C, Birke RL, Lombardi JR (2008) DFT, SERS, and single-molecule SERS of crystal violet. *J Phys Chem C* 112:20295–20300. doi:10.1021/jp807807j
50. Cañamares MV, Garcia-Ramos JV, Domingo C, Sanchez-Cortes S (2004) Surface-enhanced Raman scattering study of the adsorption of the anthraquinone pigment alizarin on Ag nanoparticles. *J Raman Spectrosc* 35:921–927. doi:10.1002/jrs.1228
51. Cañamares MV, Garcia-Ramos JV, Gomez-Varga JD, Domingo C, Sanchez-Cortes S (2007) Ag nanoparticles prepared by laser photoreduction as substrates for in situ surface-enhanced Raman scattering analysis of dyes. *Langmuir* 23:5210–5215. doi:10.1021/la063445v
52. Cañamares MV, Lombardi JR, Leona M (2008) Surface-enhanced Raman scattering of protoberberine alkaloids. *J Raman Spectrosc* 39:1907–1914. doi:10.1002/jrs.2057
53. Cañamares MV, Reagan DA, Lombardi JR, Leona M (2014) TLC-SERS of mauve, the first synthetic dye. *J Raman Spectrosc* 45:1147–1152. doi:10.1002/jrs.4508
54. Carrabba MM, Spencer KM, Rich C, Rauh D (1990) The utilization of a holographic Bragg diffraction filter for Rayleigh line rejection in Raman spectroscopy. *Appl Spectrosc* 44:1558–1561
55. Casadio F, Bezur A, Fiedler I, Muir K, Trad T, Maccagnola S (2012) Pablo Picasso to Jasper Johns: a Raman study of cobalt-based synthetic inorganic pigments. *J Raman Spectrosc* 43:1761–1771. doi:10.1002/jrs.4081
56. Casadio F, Douglas JG, Faber KT (2007) Noninvasive methods for the investigation of ancient Chinese jades: an integrated analytical approach. *Anal Bioanal Chem* 387:791–801. doi:10.1007/s00216-006-0684-y
57. Casadio F, Leona M, Lombardi JR, Van Duyne R (2010) Identification of organic colorants in fibers, paints, and glazes by surface enhanced Raman spectroscopy. *Acc Chem Res* 43:782–791. doi:10.1021/ar100019q
58. Casanova Municchia A, Micheli M, Ricci MA, Toledo M, Bellatreccia F, Mastro SL, Sodo A (2016) Raman, SEM-EDS and XRPD investigations on pre-Columbian Central America “estucado” pottery. *Spectrochim Acta A* 156:47–53
59. Castans M, Perez-Pueyo R, Soneira MJ, Golobardes E, Fornells A (2011) Identification of Raman spectra through a case-based reasoning system: application to artistic pigments. *J Raman Spectrosc* 42:1553–1561
60. Castro K, Perez-Alonso M, Rodri-guez-Laso MD, Fernandez LA, Madariaga JM (2005) On-line FT-Raman and dispersive Raman spectra database of artists’ materials (e-VISART database). *Anal Bioanal Chem* 382:248–258
61. Centeno SA (2016) Identification of artistic materials in paintings and drawings by Raman spectroscopy: some challenges and future outlook. *J Raman Spectrosc* 47:9–15. doi:10.1002/jrs.4767
62. Centeno SA, Bronzato M, Ropret P, Zoleo A, Venzo A, Bogialli S, Badocco D (2016) Composition and spectroscopic properties of historic Cr logwood inks. *J Raman Spectrosc*. doi:10.1002/jrs.4938
63. Centeno SA, Buisan VL, Ropret P (2006) Raman study of synthetic organic pigments and dyes in early lithographic inks (1890–1920). *J Raman Spectrosc* 37:1111–1118. doi:10.1002/jrs.1594
64. Centeno SA, Meller T, Kennedy N, Wypyski M (2008) The daguerreotype surface as a SERS substrate: characterization of image deterioration in plates from the 19th century studio of Southworth & Hawes. *J Raman Spectrosc* 39:914–921. doi:10.1002/jrs.1934
65. Centeno SA, Ropret P, Federico ED, Shamir J, Itin B, Jerschow A (2010) Characterization of Al(III) complexes with hematein in artistic alum logwood inks. *J Raman Spectrosc* 41:445–451. doi:10.1002/jrs.2455
66. Centeno SA, Shamir J (2008) Surface enhanced Raman scattering (SERS) and FTIR characterization of the sepia melanin pigment used in works of art. *J Mol Struct* 873:149–159. doi:10.1016/j.molstruc.2007.03.026
67. Cesaratto A, Leona M, Lombardi JR, Comelli D, Nevin A, Londero P (2014) Detection of organic colorants in historical painting layers using UV laser ablation surface-enhanced Raman microspectroscopy. *Angew Chem Int Ed* 53:14373–14377. doi:10.1002/anie.201408016
68. Chalmers JM, Edwards HGM, Hargreaves MD (2012) IR and Raman spectroscopy in forensic science. Wiley, Chichester
69. Chaplin TD, Clark RJH, Jacobs D, Jensen K, Smith GD (2005) The Gutenberg bibles: analysis of the illuminations and inks using Raman spectroscopy. *Anal Chem* 77:3611–3622. doi:10.1021/ac050346y

70. Chaplin TD, Clark RJH, Scott DA (2006) Study by Raman microscopy of nine variants of the green–blue pigment verdigris. *J Raman Spectrosc* 37:223–229. doi:10.1002/jrs.1469
71. Chaplin TD, Clark RJH, Singer BW (2014) Early 20th C Russian painting? Raman identification of modern pigments on a pastel supposedly Painted by the renowned artist Natalia Goncharova. *J Raman Spectrosc* 45:1322–1325. doi:10.1002/jrs.4569
72. Chen T-H (2008) A Raman spectroscopic study of heat-treated nephrite. *Phase Transit* 81:205–216
73. Christensen M, Frosch M, Jensen P, Schnell U, Shashoua Y, Nielsen OF (2006) Waterlogged archaeological wood—chemical changes by conservation and degradation. *J Raman Spectrosc* 37:1171–1178. doi:10.1002/jrs.1589
74. Christensen M, Nielsen OF, Jensen P, Schnell U (2005) Water structure in polyethylene glycols for preservation of wooden artefacts. A NIR-FT-Raman spectroscopic investigation. *J Mol Struct* 735–736:267–270. doi:10.1016/j.molstruc.2004.10.090
75. Cianchetta I, Maish J, Saunders D, Walton M, Mehta A, Foran B, Trentelman K (2015) Investigating the firing protocol of Athenian pottery production: a Raman study of replicate and ancient sherds. *J Raman Spectrosc* 46:996–1002
76. Ciliberto E, Spoto G (2000) Modern analytical methods in art and archaeology. Wiley, New York
77. Clark RJH (2007) The scientific investigation of artwork and archaeological artefacts: Raman microscopy as a structural, analytical and forensic tool. *Appl Phys A* 89:833–840. doi:10.1007/s00339-007-4212-5
78. Clark RJH (1995) Raman microscopy: application to the identification of pigments on medieval manuscripts. *Chem Soc Rev* 24:187–196. doi:10.1039/CS9952400187
79. Clark RJH, Cridland L, Kariuki BM, Harris KDM, Withnall R (1995) Synthesis, structural characterisation and Raman spectroscopy of the inorganic pigments lead tin yellow types I and II and lead antimonate yellow: their identification on medieval paintings and manuscripts. *J Chem Soc Dalton Trans*. doi:10.1039/DT9950002577
80. Clark RJH, Wang Q, Correia A (2007) Can the Raman spectrum of anatase in artwork and archaeology be used for dating purposes? Identification by Raman microscopy of anatase in decorative coatings on Neolithic (Yangshao) pottery from Henan, China. *J Archaeol Sci* 34:1787–1793. doi:10.1016/j.jas.2006.12.018
81. Coccato A, Jehlicka J, Moens L, Vandenabeele P (2015) Raman spectroscopy for the investigation of carbon-based black pigments. *J Raman Spectrosc* 46:1003–1015. doi:10.1002/jrs.4715
82. Coccato A, Karampelas S, Wörle M, van Willigen S, Pétrequin P (2014) Gem quality and archeological green “jadeite jade” versus “omphacite jade”. *J Raman Spectrosc*. doi:10.1002/jrs.4512
83. Colomban P (2003) Polymerisation degree and Raman identification of ancient glasses used for jewelry, ceramic enamel and mosaics. *J Non Cryst Solids* 323:180–187
84. Colomban P (2004) Raman spectrometry, a unique tool to analyze and classify ancient ceramics and glasses. *Appl Phys A* 79:167–170. doi:10.1007/s00339-004-2512-6
85. Colomban P (2012) The on-site/remote Raman analysis with mobile instruments: a review of drawbacks and success in cultural heritage studies and other associated fields. *J Raman Spectrosc* 43:1529–1535
86. Colomban P, Paulsen O (2005) Non-destructive determination of the structure and composition of glazes by Raman spectroscopy. *J Am Ceram Soc* 88:390–395. doi:10.1111/j.1551-2916.2005.00096.x
87. Colomban P, Sagon G, Faurel X (2001) Differentiation of antique ceramics from the Raman spectra of their coloured glazes and paintings. *J Raman Spectrosc* 32:351–360. doi:10.1002/jrs.704
88. Colomban P, Schreiber HD (2005) Raman signature modification induced by copper nanoparticles in silicate glass. *J Raman Spectrosc* 36:884–890
89. Colomban P, Tournié A, Bellot-Gurlet L (2006) Raman identification of glassy silicates used in ceramics, glass and jewellery: a tentative differentiation guide. *J Raman Spectrosc* 37:841–852
90. Colomban P, Treppoz F (2001) Identification and differentiation of ancient and modern European porcelains by Raman macro- and micro-spectroscopy†. *J Raman Spectrosc* 32:93–102. doi:10.1002/jrs.678
91. Conti C, Aliatis I, Casati M, Colombo C, Matteini M, Negrotti R, Realini M, Zerbi G (2014) Diethyl oxalate as a new potential conservation product for decayed carbonatic substrates. *J Cult Herit* 15:336–338. doi:10.1016/j.culher.2013.08.002
92. Conti C, Aliatis I, Colombo C, Greco M, Possenti E, Realini M, Castiglioni C, Zerbi G (2012) μ -Raman mapping to study calcium oxalate historical films. *J Raman Spectrosc* 43:1604–1611

93. Conti C, Colombo C, Dellasega D, Matteini M, Realini M, Zerbi G (2011) Ammonium oxalate treatment: evaluation by μ -Raman mapping of the penetration depth in different plasters. *J Cult Herit* 12:372–379. doi:10.1016/j.culher.2011.03.004
94. Conti C, Colombo C, Matteini M, Realini M, Zerbi G (2010) Micro-Raman mapping on polished cross-sections: a tool to define the penetration depth of conservation treatment on cultural heritage. *J Raman Spectrosc* 41:1254–1260
95. Conti C, Colombo C, Realini M, Matousek P (2015) Subsurface analysis of painted sculptures and plasters using micrometre-scale spatially offset Raman spectroscopy (micro-SORS). *J Raman Spectrosc* 46:476–482. doi:10.1002/jrs.4673
96. Conti C, Colombo C, Realini M, Zerbi G, Matousek P (2014) Subsurface Raman analysis of thin painted layers. *Appl Spectrosc* 68:686–691. doi:10.1366/13-07376
97. Conti C, Realini M, Botteon A, Colombo C, Noll S, Elliott SR, Matousek P (2016) Analytical capability of defocused μ -SORS in the chemical interrogation of thin turbid painted layers. *Appl Spectrosc* 70:156–161
98. Conti C, Realini M, Colombo C, Matousek P (2015) Comparison of key modalities of micro-scale spatially offset Raman spectroscopy. *Analyst* 140:8127–8133. doi:10.1039/c5an01900a
99. Conti C, Realini M, Colombo C, Sowoidnich K, Afseth NK, Bertasa M, Botteon A, Matousek P (2015) Noninvasive analysis of thin turbid layers using microscale spatially offset Raman spectroscopy. *Anal Chem* 87:5810–5815. doi:10.1021/acs.analchem.5b01080
100. Conti C, Striova J, Aliatis I, Colombo C, Greco M, Possenti E, Realini M, Brambilla L, Zerbi G (2013) Portable Raman versus portable mid-FTIR reflectance instruments to monitor synthetic treatments used for the conservation of monument surfaces. *Anal Bioanal Chem* 405:1733–1741
101. Conti C, Striova J, Aliatis I, Possenti E, Massonnet G, Muehlethaler C, Poli T, Positano M (2014) The detection of copper resinate pigment in works of art: contribution from Raman spectroscopy. *J Raman Spectrosc* 45:1186–1196. doi:10.1002/jrs.4455
102. Cucci C, Bartolozzi G, Marchiafava V, Picollo M, Richardson E (2016) Study of semi-synthetic plastic objects of historic interest using non-invasive total reflectance FT-IR. *Microchem J* 124:889–897. doi:10.1016/j.microc.2015.06.010
103. Czamara K, Majzner K, Pacia MZ, Kochan K, Kaczor A, Baranska M (2015) Raman spectroscopy of lipids: a review. *J Raman Spectrosc* 46:4–20. doi:10.1002/jrs.4607
104. Daher C, Bellot-Gurlet L (2013) Non-destructive characterization of archaeological resins: seeking alteration criteria through vibrational signatures. *Anal Methods* 5:6583–6591. doi:10.1039/C3AY41278D
105. Daher C, Bellot-Gurlet L, Le Hô A-S, Paris C, Regert M (2013) Advanced discriminating criteria for natural organic substances of cultural heritage interest: spectral decomposition and multivariate analyses of FT-Raman and FT-IR signatures. *Talanta* 115:540–547. doi:10.1016/j.talanta.2013.06.014
106. Daher C, Drieu L, Bellot-Gurlet L, Percot A, Paris C, Le Hô A-S (2014) Combined approach of FT-Raman, SERS and IR micro-ATR spectroscopies to enlighten ancient technologies of painted and varnished works of art. *J Raman Spectrosc* 45:1207–1214
107. Daher C, Paris C, Le Ho A-S, Bellot-Gurlet L, Echard J-P (2010) A joint use of Raman and IR spectroscopies for the identification of natural organic media used in ancient varnishes. *J Raman Spectrosc* 41:1494–1499. doi:10.1002/jrs.2693
108. Daher C, Pimenta V, Bellot-Gurlet L (2014) Towards a non-invasive quantitative analysis of the organic components in museum objects varnishes by vibrational spectroscopies: methodological approach. *Talanta* 129:336–345. doi:10.1016/j.talanta.2014.05.059
109. Damjanović L, Bikić V, Šarić K, Erić S, Holclajtner-Antunović I (2014) Characterization of the early Byzantine pottery from Caričin Grad (South Serbia) in terms of composition and firing temperature. *J Archaeol Sci* 46:156–172
110. Daniel F, Mounier A, Aramendia J, Gómez L, Castro K, Fdez-Ortiz de Vallejuelo S, Schlicht M (2015) Raman and SEM-EDX analyses of the “Royal Portal” of Bordeaux Cathedral for the virtual restitution of the statuary polychromy. *J Raman Spectrosc*. doi:10.1002/jrs.4770
111. Degano I, Biesaga M, Colombini MP, Trojanowicz M (2011) Historical and archaeological textiles: an insight on degradation products of wool and silk yarns. *J Chromatogr A* 1218:5837–5847. doi:10.1016/j.chroma.2011.06.095
112. Degano I, Ribechini E, Modugno F, Colombini MP (2009) Analytical methods for the characterization of organic dyes in artworks and in historical textiles. *Appl Spectrosc Rev* 44:363–410. doi:10.1080/05704920902937876

113. Dejoie C, Sciau P, Li W, Noé L, Mehta A, Chen K, Luo H, Kunz M, Tamura N, Liu Z (2014) Learning from the past: rare e-Fe₂O₃ in the ancient black-glazed Jian (Tenmoku) wares. *Sci Rep* 4:4941
114. Delhaye M, Dhamelincourt P (1974) Laser Raman microprobe and microscope. In: *Proceeding Abstracts, Fourth international conference on raman spectroscopy* Brunswick, ME, USA
115. Delhaye M, Migeon M (1966) Intérêt de la concentration d'un faisceau laser pour l'excitation de l'effect Raman. *C R Acad Sci Paris* 262:1513–1516
116. Deneckere A, Vekemans B, Van de Voorde L, De Paepe P, Vincze L, Moens L, Vandennebee P (2012) Feasibility study of the application of micro-Raman imaging as complement to micro-XRF imaging. *Appl Phys A* 106:363–376
117. De Santis A, Mattei E, Pelosi C (2007) Micro-Raman and stratigraphic studies of the paintings on the “Cembalo” model musical instrument (A.D. 1650) and laser-induced degradation of the detected pigments. *J Raman Spectrosc* 38:1368–1378. doi:10.1002/jrs.1777
118. Dhamelincourt P, Schubnel H-J (1977) La microsonde moléculaire à laser et son application à la minéralogie et la gemmologie. *Rev Gemmol* 52:11–14
119. Doherty B, Brunetti BG, Sgamellotti A, Miliani C (2011) A detachable SERS active cellulose film: a minimally invasive approach to the study of painting lakes. *J Raman Spectrosc* 42:1932–1938. doi:10.1002/jrs.2942
120. Doherty B, Presciutti F, Sgamellotti A, Brunetti BG, Miliani C (2014) Monitoring of optimized SERS active gel substrates for painting and paper substrates by unilateral NMR profilometry. *J Raman Spectrosc* 45:1153–1159. doi:10.1002/jrs.4542
121. Doherty B, Vagnini M, Dufourmantelle K, Sgamellotti A, Brunetti B, Miliani C (2014) A vibrational spectroscopic and principal component analysis of triarylmethane dyes by comparative laboratory and portable instrumentation. *Spectrochim Acta A* 121:292–305
122. Döpner S, Hildebrandt P, Mauk AG, Lenk H, Stempfle W (1996) Analysis of vibrational spectra of multicomponent systems. Application to pH-dependent resonance Raman spectra of ferricytochrome C. *Spectrochim Acta A* 52:573–584
123. Doty KC, Muro CK, Bueno J, Halámková L, Lednev IK (2016) What can Raman spectroscopy do for criminalistics? *J Raman Spectrosc* 47:39–50. doi:10.1002/jrs.4826
124. Edwards HGM, Ali EMA (2011) Raman spectroscopy of archaeological and ancient resins: problems with database construction for applications in conservation and historical provenancing. *Spectrochim Acta A* 80:49–54
125. Edwards HGM, Chalmers JM, Royal Society of Chemistry (Great Britain) (2005) *Raman spectroscopy in archaeology and art history*. Royal Society of Chemistry, Cambridge
126. Edwards HGM, Falk MJ, Edwards HGM, Falk MJ (1997) Fourier transform Raman spectroscopic study of ancient resins: a feasibility study of application to archaeological artefacts. *J Raman Spectrosc* 28:211–218
127. Edwards HGM, Falk MJ, Edwards HGM, Falk MJ (1997) Fourier-transform Raman spectroscopic study of frankincense and myrrh. *Spectrochim Acta A* 53:2393–2401
128. Edwards HGM, Falk MJ, Sibley MG, Alvarez-Benedi J, Rull F (1998) FT-Raman spectroscopy of gums of technological significance. *Spectrochim Acta A* 54:903–920
129. Edwards HGM, Farwell DW (1996) Fourier-transform Raman spectroscopic study of natural waxes and resins. I. *Spectrochim Acta A* 52:1639–1648
130. Edwards HGM, Farwell DW, Holder JM, Lawson EE (1997) Fourier-transform Raman spectroscopy of ivory: II. spectroscopic analysis and assignments. *J Mol Struct* 435:49–58. doi:10.1016/S0022-2860(97)00122-1
131. Edwards HGM, Farwell DW, Seaward MRD (1991) Raman spectra of oxalates in lichen encrustations on Renaissance frescoes. *Spectrochim Acta Part Mol Spectrosc* 47:1531–1539. doi:10.1016/0584-8539(91)80247-G
132. Edwards HGM, Farwell DW, Webster D (1997) FT Raman microscopy of untreated natural plant fibres. *Spectrochim Acta Part* 53:2383–2392. doi:10.1016/S1386-1425(97)00178-9
133. Edwards HGM, Farwell DW, Williams AC, Barry BW, Rull F (1995) Novel spectroscopic deconvolution procedure for complex biological systems: vibrational components in the FT-Raman spectra of ice-man and contemporary skin. *J Chem Soc Faraday Trans* 91:3883–3887. doi:10.1039/FT9959103883
134. Edwards HGM, Hunt DE, Sibley MG (1998) FT-Raman spectroscopic study of keratotic materials: horn, hoof and tortoiseshell. *Spectrochim Acta A* 54:745–757. doi:10.1016/S1386-1425(98)00013-4

135. Edwards HGM, Johnson AF, Lewis IR (1993) Applications of Raman spectroscopy to the study of polymers and polymerization processes. *J Raman Spectrosc* 24:475–483. doi:10.1002/jrs.1250240803
136. Edwards HGM, Moody CD, Jorge Villar SE, Wynn-Williams DD (2005) Raman spectroscopic detection of key biomarkers of cyanobacteria and lichen symbiosis in extreme Antarctic habitats: evaluation for Mars Lander missions. *Icarus* 174:560–571. doi:10.1016/j.icarus.2004.07.029
137. Edwards HGM, Perez FR (2004) Application of Fourier transform Raman spectroscopy to the characterization of parchment and vellum. II—effect of biodeterioration and chemical deterioration on spectral interpretation. *J Raman Spectrosc* 35:754–760. doi:10.1002/jrs.1155
138. Edwards HGM, Russell NC, Seaward MRD, Slarke D (1995) Lichen biodeterioration under different microclimates: an FT Raman spectroscopic study. *Spectrochim Acta Part Mol Spectrosc* 51:2091–2100. doi:10.1016/0584-8539(95)01499-1
139. Everall N, King B (1999) Raman spectroscopy for polymer characterization in an industrial environment. *Macromol Symp* 141:103–116. doi:10.1002/masy.19991410111
140. Ferreira ESB, Hulme AN, McNab H, Quye A (2004) The natural constituents of historical textile dyes. *Chem Soc Rev* 33:329–336. doi:10.1039/b305697j
141. Ferreira ESB, Quye A, McNab H, Hulme AN, Wouters J, Boon JJ (2001) Development of analytical techniques for the study of natural yellow dyes in historical textiles. *Dyes Hist Archaeol* 16(17):179–186
142. Fleischmann M, Hendra P, Mcquilla AJ (1974) Raman-spectra of pyridine adsorbed at a silver electrode. *Chem Phys Lett* 26:163–166. doi:10.1016/0009-2614(74)85388-1
143. Frano KA, Mayhew HE, Svoboda SA, Wustholz KL (2014) Combined SERS and Raman analysis for the identification of red pigments in cross-sections from historic oil paintings. *Analyst* 139:6450–6455. doi:10.1039/c4an01581a
144. Fremout W, Saverwyns S (2012) Identification of synthetic organic pigments: the role of a comprehensive digital Raman spectral library. *J Raman Spectrosc* 43:1536–1544. doi:10.1002/jrs.4054
145. Fritsch E, Rondeau B, Hainschwang T, Karampelas S (2012) Raman spectroscopy applied to gemmology. In: Dubessy J, Caumon MC, Rull F (eds) *Raman spectroscopy applied to Earth sciences and cultural heritage*. European Mineralogical Union Mineralogical Society of Great Britain and Ireland, Twickenham, UK, pp 455–489
146. Frost RL (2004) Raman spectroscopy of natural oxalates. *Anal Chim Acta* 517:207–214. doi:10.1016/j.aca.2004.04.036
147. Gall MJ, Hendra PJ, Peacock CJ, Cudby MEA, Willis HA (1972) Laser-Raman spectrum of polyethylene: part 1. Structure and analysis of the polymer. *Polymer* 13:104–108. doi:10.1016/S0032-3861(72)80003-X
148. Geiman I, Leona M, Lombardi JR (2009) Application of Raman spectroscopy and surface-enhanced raman scattering to the analysis of synthetic dyes found in ballpoint pen inks. *J Forensic Sci* 54:947–952
149. González-Vidal JJ, Perez-Pueyo R, Soneira MJ, Ruiz-Moreno S (2012) Automatic identification system of Raman spectra in binary mixtures of pigments. *J Raman Spectrosc* 43:1707–1712
150. Greeneltch NG, Davis AS, Valley NA, Casadio F, Schatz GC, Van Duyne RP, Shah NC (2012) Near-IR surface-enhanced raman spectroscopy (NIR-SERS) for the identification of eosin Y: theoretical calculations and evaluation of two different nanoplasmonic substrates. *J Phys Chem A* 116:11863
151. Guineau B (1984) Microanalysis of painted manuscripts and of colored archaeological materials by Raman laser microprobe. *J Forensic Sci* 29:471–485
152. Guineau B, Guichard V (1987) Identification des colorants organiques naturels par microspectrométrie Raman de résonance et par effet Raman exalte de surface (SERS). ICOM Committee for Conservation: 8th Triennial Meeting, Sydney, Australia, 6–11 September, 1987. The Getty Conservation Institute, Sydney, pp 659–666
153. Halac EB, Reinoso M, Luda M, Marte F (2012) Raman mapping analysis of pigments from Proas Iluminadas by Quinquela Mart. *J Cult Herit* 13:469–473
154. Hargreaves MD, Macleod NA, Brewster VL, Munshi T, Edwards HGM, Matousek P (2009) Application of portable Raman spectroscopy and benchtop spatially offset Raman spectroscopy to interrogate concealed biomaterials. *J Raman Spectrosc* 40:1875–1880. doi:10.1002/jrs.2335
155. Hark RR, Clark RJH (2010) Raman microscopy of diverse samples of Lapis Lazuli at multiple excitation wavelengths. *AIP Conf Proc* 1267:315–316. doi:10.1063/1.3482531

156. Henderson J (2013) *Ancient glass. An interdisciplinary exploration*. Cambridge University Press, New York, USA
157. Huong LTT, Hofmeister W, Hager T, Karampelas S, Kien NDT (2014) A preliminary study on the separation of natural and synthetic emeralds using vibrational spectroscopy. *Gems Gemol* 50:287–292
158. Idone A, Aceto M, Diana E, Appolonia L, Gulmini M (2014) Surface-enhanced Raman scattering for the analysis of red lake pigments in painting layers mounted in cross-sections. *J Raman Spectrosc* 45:1127–1132. doi:10.1002/jrs.4491
159. Idone A, Gulmini M, Henry A-I, Casadio F, Chang L, Appolonia L, Duyne RPV, Shah NC (2013) Silver colloidal pastes for dye analysis of reference and historical textile fibers using direct, extractionless, non-hydrolysis surface-enhanced Raman spectroscopy. *Analyst* 138:5895–5903. doi:10.1039/C3AN00788J
160. Jeanmaire D, Vanduyne R (1977) Surface Raman Spectroelectrochemistry. 1. Heterocyclic, aromatic, and aliphatic-amines adsorbed on anodized silver electrode. *J Electroanal Chem* 84:1–20. doi:10.1016/S0022-0728(77)80224-6
161. Jehlicka J, Villar SEJ, Edwards HGM (2004) Fourier transform Raman spectra of Czech and Moravian fossil resins from freshwater sediments. *J Raman Spectrosc* 35:761–767
162. Jehlicka J, Vitek P, Edwards HGM, Hargreaves M, Capoun T (2009) Rapid outdoor non-destructive detection of organic minerals using a portable Raman spectrometer. *J Raman Spectrosc* 40:1645–1651
163. Jehlicka J, Vitek P, Edwards HGM, Heagraves M, Caapoun T (2009) Application of portable Raman instruments for fast and non-destructive detection of minerals on outcrops. *Spectrochim Acta A* 73:410–419
164. Jorge-Villar SE, Edwards HGM (2013) Microorganism response to stressed terrestrial environments: a Raman spectroscopic perspective of extremophilic life strategies. *Life Open Access J* 3:276–294. doi:10.3390/life3010276
165. Jurasekova Z, del Puerto E, Bruno G, Garcia-Ramos JV, Sanchez-Cortes S, Domingo C (2010) Extractionless non-hydrolysis surface-enhanced Raman spectroscopic detection of historical mordant dyes on textile fibers. *J Raman Spectrosc* 41:1455–1461. doi:10.1002/jrs.2651
166. Jurasekova Z, Domingo C, Garcia-Ramos JV, Sanchez-Cortes S (2008) In situ detection of flavonoids in weld-dyed wool and silk textiles by surface-enhanced Raman scattering. *J Raman Spectrosc* 39:1309–1312. doi:10.1002/jrs.2053
167. Karampelas S, Fritsch E, Mevellec J-Y, Sklavounos S, Soldatos T (2009) Role of polyenes in the coloration of cultured freshwater pearls. *Eur J Miner* 21:85–97
168. Karampelas S, Fritsch E, Rondeau B, Andouche A, Métivier B (2009) Identification of the endangered pink-to-red stylaster corals by Raman spectroscopy. *Gems Gemol* 45:48–52
169. Kelloway SJ, Kononenko N, Torrence R, Carter EA (2010) Assessing the viability of portable Raman spectroscopy for determining the geological source of obsidian. *Vib Spectrosc* 53:88–96
170. Keune K, Boon JJ, Boitelle R, Shimadzu Y (2013) Degradation of Emerald green in oil paint and its contribution to the rapid change in colour of the *Descente des vaches* (1834–1835) painted by Theodore Rousseau. *Stud Conserv* 58:199–210. doi:10.1179/2047058412Y.0000000063
171. Kiefert L, Karampelas S (2011) Use of the Raman spectrometer in gemmological laboratories: review. *Spectrochim Acta A* 80:119–124. doi:10.1016/j.saa.2011.03.004
172. Kingma KJ, Hemley RJ (1994) Raman spectroscopic study of microcrystalline silica. *Am Miner* 79:269–273
173. Kogelnik H, Porto SPS (1963) Continuous Helium-Neon red Laser as a Raman source. *J Opt Soc Am* 53:1446–1447
174. Kurouski D, Zaleski S, Casadio F, Van Duyne RP, Shah NC (2014) Tip-enhanced Raman spectroscopy (TERS) for in Situ identification of indigo and iron gall ink on paper. *J Am Chem Soc* 136:8677–8684. doi:10.1021/ja5027612
175. Lau D, Livett M, Prawer S (2008) Application of surface-enhanced Raman spectroscopy (SERS) to the analysis of natural resins in artworks. *J Raman Spectrosc* 39:545–552. doi:10.1002/jrs.1878
176. Lauwers D, Hutado AG, Tanevska V, Moens L, Bersani D, Vandennebeele P (2014) Characterisation of a portable Raman spectrometer for in situ analysis of art objects. *Spectrochim Acta A* 118:294–301

177. Laver M (1997) Titanium dioxide whites. In: FitzHugh EW (ed) *Artists' pigments: a handbook of their history and characteristics*, vol 3. National Gallery of Art, Washington & Oxford University Press, Oxford, pp 295–339
178. Lee AS, Otieno-Alego V, Creagh DC (2008) Identification of iron-gall inks with near-IR Raman microspectroscopy. *J Raman Spectrosc* 39:1079–1084. doi:10.1002/jrs.1989
179. Lee PC, Meisel D (1982) Adsorption and surface-enhanced Raman of dyes on silver and gold sols. *J Phys Chem* 86:3391–3395. doi:10.1021/j100214a025
180. Lenain BP (2000) Analytical Raman spectroscopy: a new generation of instruments. *Analisis* 28:11–14
181. Leona M (2009) Microanalysis of organic pigments and glazes in polychrome works of art by surface-enhanced resonance Raman scattering. *Proc Natl Acad Sci USA* 106:14757–14762. doi:10.1073/pnas.0906995106
182. Leona M (2006) Non-invasive identification of fluorescent dyes in historic textiles by matrix transfer-surface enhanced Raman scattering. US patent 6943031 B2
183. Leona M, Decuzzi P, Kubic TA, Gates G, Lombardi JR (2011) Nondestructive identification of natural and synthetic organic colorants in works of art by surface enhanced Raman scattering. *Anal Chem* 83:3990–3993. doi:10.1021/ac2007015
184. Leona M, Stenger J, Ferloni E (2006) Application of surface-enhanced Raman scattering techniques to the ultrasensitive identification of natural dyes in works of art. *J Raman Spectrosc* 37:981–992. doi:10.1002/jrs.1582
185. Leon Y, Lofrumento C, Zoppi A, Carles R, Castellucci EM, Sciau P (2010) Micro-Raman investigation of terra sigillata slips: a comparative study of central Italian and southern Gaul productions. *J Raman Spectrosc* 41:1550–1555
186. Lofrumento C, Prati S, Ricci M, Bonacini I, Quaranta M, Sciuotto G, Ballarin B, Cassani MC, Castellucci E, Mazzeo R (2015) Identification of dyes in toned and tinted XX century cinematographic films by surface enhanced Raman spectroscopy. *J Raman Spectrosc*. doi:10.1002/jrs.4819
187. Lofrumento C, Ricci M, Platania E, Becucci M, Castellucci E (2013) SERS detection of red organic dyes in Ag-agar gel. *J Raman Spectrosc* 44:47–54. doi:10.1002/jrs.4162
188. Lombardi JR, Birke RL (2009) A unified view of surface-enhanced Raman scattering. *Acc Chem Res* 42:734–742. doi:10.1021/ar800249y
189. Lombardi JR, Birke RL (2012) The theory of surface-enhanced Raman scattering. *J Chem Phys* 136:144704. doi:10.1063/1.3698292
190. Londero P, Lombardi JR, Leona M (2013) A compact optical parametric oscillator Raman microscope for wavelength-tunable multianalytic microanalysis. *J Raman Spectrosc* 44:131–135. doi:10.1002/jrs.4150
191. Londero PS, Leona M, Lombardi JR (2013) Definitive evidence for linked resonances in surface-enhanced Raman scattering: excitation profile of Cu phthalocyanine. *Appl Phys Lett* 102:111101. doi:10.1063/1.4794071
192. Londero PS, Lombardi JR, Leona M (2013) Laser ablation surface-enhanced Raman microspectroscopy. *Anal Chem* 85:5463–5467. doi:10.1021/ac400440c
193. Luo S-C, Sivashanmugan K, Liao J-D, Yao C-K, Peng H-C (2014) Nanofabricated SERS-active substrates for single-molecule to virus detection in vitro: a review. *Biosens Bioelectron* 61:232–240. doi:10.1016/j.bios.2014.05.013
194. Manzano E, Garcia-Atero J, Dominguez-Vidal A, Jose Ayora-Canada M, Fermin Capitan-Vallvey L, Navas N (2012) Discrimination of aged mixtures of lipidic paint binders by Raman spectroscopy and chemometrics. *J Raman Spectrosc* 43:781–786. doi:10.1002/jrs.3082
195. Martínez-Arkarazo I, Smith DC, Zuloaga O, Olazabal MA, Madariaga JM (2008) Evaluation of three different mobile Raman microscopes employed to study deteriorated civil building stones. *J Raman Spectrosc* 39:1018–1029. doi:10.1002/jrs.1941
196. Matousek P, Clark IP, Draper ERC, Morris MD, Goodship AE, Everall N, Towrie M, Finney WF, Parker AW (2005) Subsurface probing in diffusely scattering media using spatially offset Raman spectroscopy. *Appl Spectrosc* 59:393–400
197. Matousek P, Morris MD, Everall N, Clark IP, Towrie M, Draper E, Goodship A, Parker AW (2005) Numerical simulations of subsurface probing in diffusely scattering media using spatially offset Raman spectroscopy. *Appl Spectrosc* 59:1485–1492. doi:10.1366/000370205775142548
198. Matousek P, Towrie M, Parker AW (2005) Simple reconstruction algorithm for shifted excitation Raman difference spectroscopy. *Appl Spectrosc* 59:848–851. doi:10.1366/0003702054280757

199. Matousek P, Conti C, Colombo C, Realini M (2015) Monte Carlo simulations of subsurface analysis of painted layers in micro-scale spatially offset Raman spectroscopy. *Appl Spectrosc* 69:1091–1095. doi:10.1366/15-07894
200. Matousek P, Conti C, Realini M, Colombo C (2016) MicroScale spatially offset Raman spectroscopy for noninvasive subsurface analysis of turbid materials. *Analyst* 141:731–739 (Published by The Royal Society of Chemistry)
201. Mayhew HE, Fabian DM, Svoboda SA, Wustholz KL (2013) Surface-enhanced Raman spectroscopy studies of yellow organic dyestuffs and lake pigments in oil paint. *Analyst* 138:4493–4499. doi:10.1039/C3AN00611E
202. Mazzella WD, Buzzini P (2005) Raman spectroscopy of blue gel pen inks. *Forensic Sci Int* 152:241–247. doi:10.1016/j.forsciint.2004.09.115
203. McNay G, Eustace D, Smith WE, Faulds K, Graham D (2011) Surface-enhanced raman scattering (SERS) and surface-enhanced resonance raman scattering (SERRS): a review of applications. *Appl Spectrosc* 65:825–837
204. Medeghini L, Lottici PP, De Vito C, Mignardi S, Bersani D (2014) Micro-Raman spectroscopy and ancient ceramics: applications and problems. *J Raman Spectrosc* 45:1244–1250
205. Miguel C, Claro A, Gonçalves AP, Muralha VSF, Melo MJ (2009) A study on red lead degradation in a medieval manuscript Lorrão Apocalypse (1189). *J Raman Spectrosc* 40:1966–1973. doi:10.1002/jrs.2350
206. Mills JS, White R (1994) *The organic chemistry of museum objects*, 2nd edn. Butterworth Heinemann, London
207. Miralles I, Edwards HGM, Domingo F, Jorge-Villar SE (2015) Lichens around the world: a comprehensive study of lichen survival biostrategies detected by Raman spectroscopy. *Anal Methods* 7:6856–6868. doi:10.1039/C5AY00655D
208. Monico L, Janssens K, Hendriks E, Brunetti BG, Miliani C (2014) Raman study of different crystalline forms of PbCrO_4 and PbCr1 - xSxO_4 solid solutions for the noninvasive identification of chrome yellows in paintings: a focus on works by Vincent van Gogh. *J Raman Spectrosc* 45:1034–1045
209. Monico L, Janssens K, Miliani C, Van der Snickt G, Brunetti BG, Cestelli Guidi M, Radepon M, Cotte M (2013) Degradation process of lead chromate in paintings by Vincent van Gogh studied by means of spectromicroscopic methods. 4. Artificial aging of model samples of co-precipitates of lead chromate and lead sulfate. *Anal Chem* 85:860–867. doi:10.1021/ac3021592
210. Monnier J, Bellot-Gurlet L, Baron D, Neff D, Guillot I, Dillmann Ph (2011) A methodology for Raman structural quantification imaging and its application to iron indoor atmospheric corrosion products. *J Raman Spectrosc* 42:773–781
211. Muehlethaler C, Leona M, Lombardi JR (2016) Review of surface enhanced Raman scattering applications in forensic science. *Anal Chem* 88:152–169. doi:10.1021/acs.analchem.5b04131
212. Muehlethaler C, Massonnet G, Esseiva P (2011) The application of chemometrics on IR and Raman spectra as a tool for the forensic analysis of paints. *Forensic Sci Int* 209:173–182
213. Muralha VSF, Miguel C, Melo MJ (2012) Micro-Raman study of Medieval Cistercian 12–13th century manuscripts: Santa Maria de Alcobaça, Portugal. *J Raman Spectrosc* 43:1737–1746. doi:10.1002/jrs.4065
214. Navas N, Romero-Pastor J, Manzano E, Cardell C, Navas N, Romero-Pastor J, Manzano E, Cardell C (2010) Raman spectroscopic discrimination of pigments and tempera paint model samples by principal component analysis on first-derivative spectra. *J Raman Spectrosc* 41:1486–1493
215. Nevin A, Melia JL, Osticioli I, Gautier G, Colombini MP (2008) The identification of copper oxalates in a 16th century Cypriot exterior wall painting using micro FTIR, micro Raman spectroscopy and gas chromatography-mass spectrometry. *J Cult Herit* 9:154–161. doi:10.1016/j.culher.2007.10.002
216. Nevin A, Osticioli I, Anglos D, Burnstock A, Cather S, Castellucci E (2007) Raman spectra of proteinaceous materials used in paintings: a multivariate analytical approach for classification and identification. *Anal Chem* 79:6143–6151
217. Nevin A, Osticioli I, Demetrios Anglos D, Burnstock A, Cather S, Castellucci E (2008) The analysis of naturally and artificially aged protein-based paint media using Raman spectroscopy combined with principal component analysis. *J Raman Spectrosc* 39:993–1000
218. Nevin A, Spoto G, Anglos D (2012) Laser spectroscopies for elemental and molecular analysis in art and archaeology. *Appl Phys A* 106:339–361

219. Nielsen JR (1964) Raman spectra of polymers. *J Polym Sci Part C* 7:19–35. doi:10.1002/polc.5070070104
220. Nielsen SE, Scaffidi JP, Yezierski EJ (2014) Detecting art forgeries: a problem-based Raman spectroscopy lab. *J Chem Educ* 91:446–450. doi:10.1021/ed400319k
221. Oakley LH, Dinehart SA, Svoboda SA, Wustholz KL (2011) Identification of organic materials in historic oil paintings using correlated extractionless surface-enhanced Raman scattering and fluorescence microscopy. *Anal Chem* 83:3986–3989. doi:10.1021/ac200698q
222. Oakley LH, Fabian DM, Mayhew HE, Svoboda SA, Wustholz KL (2012) Pretreatment strategies for SERS analysis of indigo and Prussian blue in aged painted surfaces. *Anal Chem* 84:8006–8012. doi:10.1021/ac301814e
223. Osticioli I, Mendes NFC, Nevin A, Gil FPSC, Becucci M, Castellucci E (2009) Analysis of natural and artificial ultramarine blue pigments using laser induced breakdown and pulsed Raman spectroscopy, statistical analysis and light microscopy. *Spectrochim Acta A* 73:525–531
224. Osticioli I, Mendes NFC, Nevin A, Zoppi A, Lofrumento C, Becucci M, Castellucci EM (2009) A new compact instrument for Raman, laser-induced breakdown, and laser-induced fluorescence spectroscopy of works of art and their constituent materials. *Rev Sci Instrum* 80:076109. doi:10.1063/1.3184102
225. Osticioli I, Zoppi A, Castellucci EM (2006) Fluorescence and Raman spectra on painting materials: reconstruction of spectra with mathematical methods. *J Raman Spectrosc* 37:974–980
226. Otero V, Sanches D, Montagner C, Vilarigues M, Carlyle L, Lopes JA, Melo MJ (2014) Characterisation of metal carboxylates by Raman and IR spectroscopy in works of art. *J Raman Spectrosc* 45:1197–1206
227. Özçatal M, Yaygingöl M, İssi A, Kara A, Turan S, Okyar F, Pfeiffer Taş Ş, Nstova I, Grupçe O, Mınçeva-Şukarova B (2014) Characterization of lead glazed potteries from Smyrna (İzmir/Turkey) using multiple analytical techniques; Part I: body. *Ceram Int* 40:2153–2160
228. Pagès-Camagna S, Duval A, Guicharnaud H (2004) Study of Gustave Moreau's black drawings: identification of the graphic materials by Raman microspectrometry and PIXE. *J Raman Spectrosc* 35:628–632. doi:10.1002/jrs.1215
229. Pallipurath A, Skelton J, Ricciardi P, Bucklow S, Elliott S (2013) Multivariate analysis of combined Raman and fibre-optic reflectance spectra for the identification of binder materials in simulated medieval paints. *J Raman Spectrosc* 44:866–874
230. Pallipurath A, Vofely RV, Skelton J, Ricciardi P, Bucklow S, Elliott S (2014) Estimating the concentrations of pigments and binders in lead-based paints using FT-Raman spectroscopy and principal component analysis. *J Raman Spectrosc* 45:1272–1278. doi:10.1002/jrs.4525
231. Pastorelli G, Trafela T, Taday PF, Portieri A, Lowe D, Fukunaga K, Strlic M (2012) Characterisation of historic plastics using terahertz time-domain spectroscopy and pulsed imaging. *Anal Bioanal Chem* 403:1405–1414. doi:10.1007/s00216-012-5931-9
232. Pereira A, Candeias A, Cardoso A, Rodrigues D, Vandennebe P, Caldeira AT (2016) Non-invasive methodology for the identification of plastic pieces in museum environment—a novel approach. *Microchem J* 124:846–855. doi:10.1016/j.microc.2015.07.027
233. Perets EA, Indrasekara ASDS, Kurmis A, Atlasevich N, Fabris L, Arslanoglu J (2015) Carboxy-terminated immuno-SERS tags overcome non-specific aggregation for the robust detection and localization of organic media in artworks. *Analyst* 140:5971–5980. doi:10.1039/c5an00817d
234. Pérez-Alonso M, Castro K, Madariaga JM (2006) Investigation of degradation mechanisms by portable Raman spectroscopy and thermodynamic speciation: the wall painting of Santa María de Lemoniz (Basque Country, North of Spain). *Anal Chim Acta* 571:121–128. doi:10.1016/j.aca.2006.04.049
235. Pérez-Alonso M, Castro K, Martínez-Arkarazo I, Angulo M, Olazabal MA, Madariaga JM (2004) Analysis of bulk and inorganic degradation products of stones, mortars and wall paintings by portable Raman microprobe spectroscopy. *Anal Bioanal Chem* 379:42–50. doi:10.1007/s00216-004-2496-2
236. Petrou M, Edwards HGM, Janaway RC, Thompson GB, Wilson AS (2009) Fourier-transform Raman spectroscopic study of a Neolithic waterlogged wood assemblage. *Anal Bioanal Chem* 395:2131–2138. doi:10.1007/s00216-009-3178-x
237. Petrová Z, Jehlička J, Čapoun T, Hanus R, Trojek T, Goliáš V (2012) Gemstones and noble metals adorning the sceptre of the Faculty of Science of Charles University in Prague: integrated analysis by Raman and XRF handheld instruments. *J Raman Spectrosc* 43:1275–1280

238. Piantanida G, Menart E, Bicchieri M, Strlič M (2013) Classification of iron-based inks by means of micro-Raman spectroscopy and multivariate data analysis. *J Raman Spectrosc* 44:1299–1305
239. Pirok BWJ, Knip J, van Bommel MR, Schoenmakers PJ (2016) Characterization of synthetic dyes by comprehensive two-dimensional liquid chromatography combining ion-exchange chromatography and fast ion-pair reversed-phase chromatography. *J Chromatogr A* 1436:141–146. doi:10.1016/j.chroma.2016.01.070
240. Platania E, Lofrumento C, Lottini E, Azzaro E, Ricci M, Becucci M (2015) Tailored micro-extraction method for Raman/SERS detection of indigoids in ancient textiles. *Anal Bioanal Chem* 407:6505–6514. doi:10.1007/s00216-015-8816-x
241. Platania E, Lombardi JR, Leona M, Shibayama N, Lofrumento C, Ricci M, Becucci M, Castellucci E (2014) Suitability of Ag-agar gel for the micro-extraction of organic dyes on different substrates: the case study of wool, silk, printed cotton and a panel painting mock-up. *J Raman Spectrosc* 45:1133–1139. doi:10.1002/jrs.4531
242. Pozzi F, Leona M (2016) Surface-enhanced Raman spectroscopy in art and archaeology. *J Raman Spectrosc* 47:67–77. doi:10.1002/jrs.4827
243. Pozzi F, Lombardi JR, Bruni S, Leona M (2012) Sample treatment considerations in the analysis of organic colorants by surface-enhanced Raman scattering. *Anal Chem* 84:3751–3757. doi:10.1021/ac300380c
244. Pozzi F, Lombardi JR, Leona M (2013) Winsor & Newton original handbooks: a surface-enhanced Raman scattering (SERS) and Raman spectral database of dyes from modern watercolor pigments. *Herit Sci* 1:23. doi:10.1186/2050-7445-1-23
245. Pozzi F, Porcinai S, Lombardi JR, Leona M (2013) Statistical methods and library search approaches for fast and reliable identification of dyes using surface-enhanced Raman spectroscopy (SERS). *Anal Methods* 5:4205–4212. doi:10.1039/C3AY40673C
246. Pozzi F, Shibayama N, Leona M, Lombardi JR (2013) TLC-SERS study of Syrian rue (*Peganum harmala*) and its main alkaloid constituents. *J Raman Spectrosc* 44:102–107. doi:10.1002/jrs.4140
247. Pozzi F, van den Berg KJ, Fiedler I, Casadio F (2014) A systematic analysis of red lake pigments in French Impressionist and Post-Impressionist paintings by surface-enhanced Raman spectroscopy (SERS). *J Raman Spectrosc* 45:1119–1126. doi:10.1002/jrs.4483
248. Pozzi F, Zaleski S, Casadio F, Leona M, Lombardi JR, Van Duyn R (2016) Surface-enhanced Raman spectroscopy: using nanoparticles to detect trace amounts of colorants in works of art. In: Dillmann P, Bellot-Gurlet L, Nenner I (eds) *Nanoscience and cultural heritage*. Atlantis Press, Paris, pp 161–204
249. Prikhodko S, Fischer C, Boytner R, Lozada M, Uribe M, Kakoulli I (2007) Applications of variable pressure SEM and Raman spectroscopy for the non-destructive study of bio-specimens from pre-Columbian mummies in the Tarapacá Valley, Northern Chile. *Microsc Microanal* 13:1492–1493. doi:10.1017/S1431927607075332
250. Prikhodko SV, Rambaldi DC, King A, Burr E, Muros V, Kakoulli I (2015) New advancements in SERS dye detection using interfaced SEM and Raman spectromicroscopy (μ RS). *J Raman Spectrosc* 46:632–635. doi:10.1002/jrs.4710
251. Qiu-ju H, Li-qin W (2016) Research progress of Raman spectroscopy on Dyestuff identification of ancient relics and artifacts. *Spectrosc Spectr Anal* 36:401–407. doi:10.3964/j.issn.1000-0593(2016)02-0401-07
252. Raffaëly L, Champagnon B, Ollier N, Foy D (2008) IR and Raman spectroscopies, a way to understand how the Roman window glasses were made? *J Non-Cryst Solids* 354:780–786
253. Raffaëly-Veslin L, Champagnon B, Lesage F (2008) Thermal history and manufacturing processes of Roman panes studied by Raman spectroscopy. *J Raman Spectrosc* 39:1120–1124
254. Raman CV (1928) A new radiation. *Indian J Phys* 2:387–398
255. Ramos PM, Ferré J, Ruisánchez I, Andrikopoulos KS (2004) Fuzzy logic for identifying pigments studied by Raman spectroscopy. *Appl Spectrosc* 58:848–854
256. Rana V, Canameres MV, Kubic T, Leona M, Lombardi JR (2011) Surface-enhanced Raman spectroscopy for trace identification of controlled substances: morphine, codeine, and hydrocodone. *J Forensic Sci* 56:200–207. doi:10.1111/j.1556-4029.2010.01562.x
257. Retko K, Ropret P, Korosec RC (2014) Surface-enhanced Raman spectroscopy (SERS) analysis of organic colourants utilising a new UV-photoreduced substrate. *J Raman Spectrosc* 45:1140–1146. doi:10.1002/jrs.4533
258. Ricciardi P, Colomban P, Milande V (2008) Non-destructive Raman characterization of Capodimonte and Buen Retiro porcelain. *J Raman Spectrosc* 39:1113–1119. doi:10.1002/jrs.1918

259. Ricciardi P, Delaney JK, Facini M, Glinsman L (2013) Use of imaging spectroscopy and in situ analytical methods for the characterization of the materials and techniques of 15th century illuminated manuscripts. *J Am Inst Conserv* 52:13–29. doi:10.1179/0197136012Z.0000000004
260. Ricciardi P, Delaney JK, Facini M, Zeibel JG, Picollo M, Lomax S, Loew M (2012) near-IR reflectance imaging spectroscopy to map paint binders in situ on illuminated manuscripts. *Angew Chem Int Ed* 51:5607–5610. doi:10.1002/anie.201200840
261. Robinet L, Bouquillon A, Hartwig J (2008) Correlations between Raman parameters and elemental composition in lead and lead alkali silicate glasses. *J Raman Spectrosc* 39:618–626
262. Robinet L, Couptry C, Eremin K, Hall C (2006) The use of Raman spectrometry to predict the stability of historic glasses. *J Raman Spectrosc* 37:789–797
263. Roh JY, Matecki MK, Svoboda SA, Wustholz KL (2016) Identifying pigment mixtures in art using SERS: a treatment flowchart approach. *Anal Chem* 88:2028–2032. doi:10.1021/acs.analchem.6b00044
264. Roldán ML, Centeno SA, Rizzo A (2014) An improved methodology for the characterization and identification of sepia in works of art by normal Raman and SERS, complemented by FTIR, Py-GC/MS, and XRF. *J Raman Spectrosc* 45:1160–1171. doi:10.1002/jrs.4620
265. Roldan ML, Centeno SA, Rizzo A, van Dyke Y (2015) Characterization of bistre pigment samples by FTIR, SERS, Py-GC/MS and XRF. In: Symposium PP—materials Issues in Art and Archaeology X, pp mrsf13–1656–pp02–04 (10 pages)
266. Ropret P, Miliani C, Centeno SA, Tavzes C, Rosi F (2010) Advances in Raman mapping of works of art. *J Raman Spectrosc* 41:1462–1467. doi:10.1002/jrs.2733
267. Rosasco GJ, Etz ES, Cassatt WA (1974) Investigation of the Raman spectra of individual micron sized particles. *Proceeding Abstracts, Fourth International Conference on Raman Spectroscopy*
268. Rosi F, Paolantoni M, Clementi C, Doherty B, Miliani C, Brunetti BG, Sgamellotti A (2010) Subtracted shifted Raman spectroscopy of organic dyes and lakes. *J Raman Spectrosc* 41:452–458. doi:10.1002/jrs.2447
269. Salpin F, Trivier F, Lecomte S, Couptry C (2006) A new quantitative method: non-destructive study by Raman spectroscopy of dyes fixed on wool fibres. *J Raman Spectrosc* 37:1403–1410. doi:10.1002/jrs.1557
270. San Andrés M, de la Roja JM, Baonza VG, Sancho N (2010) Verdigris pigment: a mixture of compounds. Input from Raman spectroscopy. *J Raman Spectrosc* 41:1468–1476. doi:10.1002/jrs.2786
271. Saverwyns S (2010) Russian avant-garde... or not? A micro-Raman spectroscopy study of six paintings attributed to Liubov Popova. *J Raman Spectrosc* 41:1525–1532. doi:10.1002/jrs.2654
272. Saviello D, Toniolo L, Goidanich S, Casadio F (2016) Non-invasive identification of plastic materials in museum collections with portable FTIR reflectance spectroscopy: reference database and practical applications. *Microchem J* 124:868–877. doi:10.1016/j.microc.2015.07.016
273. Scherrer NC, Stefan Z, Françoise D, Annette F, Renate K (2009) Synthetic organic pigments of the 20th and 21st century relevant to artist's paints: Raman spectra reference collection. *Spectrochim Acta Part* 73:505–524. doi:10.1016/j.saa.2008.11.029
274. Schlücker S, Schaeberle MD, Huffman SW, Levin IW (2003) Raman microspectroscopy: a comparison of point, line, and wide-field imaging methodologies. *Anal Chem* 75:4312–4318
275. Schubnel HJ, Pinet M, Smith DC, Lasnier B (eds) (1992) *La microsonde Raman en gemmologie*. Association Française de Gemmologie, Paris
276. Sciutto G, Littl L, Lofrumento C, Prati S, Ricci M, Gobbo M, Roda A, Castellucci E, Meneghetti M, Mazzeo R (2013) Alternative SERRS probes for the immunochemical localization of ovalbumin in paintings: an advanced mapping detection approach. *Analyst* 138:4532–4541. doi:10.1039/c3an00057e
277. Shadi QT, Chowdhry BZ, Snowden MJ, Withnall R (2004) Semi-quantitative analysis of alizarin and purpurin by surface-enhanced resonance Raman spectroscopy (SERRS) using silver colloids. *J Raman Spectrosc* 35:800–807. doi:10.1002/jrs.1199
278. Sharma B, Cardinal MF, Kleinman SL, Greeneltch NG, Frontiera RR, Blaber MG, Schatz GC, Van Duyne RP (2013) High-performance SERS substrates: advances and challenges. *MRS Bull* 38:615–624. doi:10.1557/mrs.2013.161
279. Sharma B, Frontiera RR, Henry A-I, Ringe E, Van Duyne RP (2012) SERS: materials, applications, and the future. *Mater Today* 15:16–25

280. Sharma SK, Misra AK, Lucey PG, Lentz RCF (2009) A combined remote Raman and LIBS instrument for characterizing minerals with 532 nm laser excitation. *Spectrochim Acta A* 73:468–476
281. Shashoua Y, Berthelsen MBLD, Nielsen OF (2006) Raman and ATR-FTIR spectroscopies applied to the conservation of archaeological Baltic amber. *J Raman Spectrosc* 37:1221–1227
282. Smith GD, Burgio L, Firth S, Clark RJH (2001) Laser-induced degradation of lead pigments with reference to Botticelli's *Trionfo d'Amore*. *Anal Chim Acta* 440:185–188. doi:10.1016/S0003-2670(01)01053-4
283. Smith GD, Clark RJH (2001) Raman microscopy in art history and conservation science. *Stud Conserv* 46:92–106. doi:10.1179/sic.2001.46.2.92
284. Smith GD, Clark RJH (2004) Raman microscopy in archaeological science. *J Archaeol Sci* 31:1137–1160
285. Smith GD, Derbyshire A, Clark RJH (2002) In situ spectroscopic detection of lead sulphide on a blackened manuscript illumination by Raman microscopy. *Stud Conserv* 47:250–256. doi:10.1179/sic.2002.47.4.250
286. Sodo A, Bicchieri M, Guiso M, Ricci MA, Ricci G (2012) Raman investigations on marker pen inks. *J Raman Spectrosc* 43:1781–1787. doi:10.1002/jrs.4070
287. Staniszevska E, Malek K, Kaszowska Z (2013) Studies on paint cross-sections of a glass painting by using FT-IR and Raman microspectroscopy supported by univariate and hierarchical cluster analyses. *J Raman Spectrosc* 44:1144–1155
288. Tomasini EP, Halac EB, Reinoso M, Di Liscia EJ, Maier MS (2012) Micro-Raman spectroscopy of carbon-based black pigments. *J Raman Spectrosc* 43:1671–1675
289. Tournié A, Prinsloo LC, Colomban P (2011) Raman classification of glass beads excavated on Mapungubwe hill and K2, two archaeological sites in South Africa. *J Raman Spectrosc* 43:532–542
290. Trentelman K (2009) A note on the characterization of bismuth black by Raman microspectroscopy. *J Raman Spectrosc* 40:585–589. doi:10.1002/jrs.2184
291. Trentelman K, Stodulski L, Pavlosky M (1996) Characterization of pararealgar and other light-induced transformation products from realgar by Raman microspectroscopy. *Anal Chem* 68:1755–1761. doi:10.1021/ac951097o
292. Trentelman K, Turner N (2009) Investigation of the painting materials and techniques of the late-15th century manuscript illuminator Jean Bourdichon. *J Raman Spectrosc* 40:577–584. doi:10.1002/jrs.2186
293. Vandenabeele P (2000) Raman spectroscopic database of azo pigments and application to modern art studies. *J Raman Spectrosc* 517:509–517
294. Vandenabeele P, Castro K, Hargreaves M, Moens L, Madariaga JM, Edwards HGM (2007) Comparative study of mobile Raman instrumentation for art analysis. *Anal Chim Acta* 588:108–116
295. Vandenabeele P, Edwards HGM, Jehlicka J (2014) The role of mobile instrumentation in novel applications of Raman spectroscopy: archaeometry, geosciences, and forensics. *Chem Soc Rev* 43:2628–2649
296. Vandenabeele P, Edwards HGM, Moens L (2007) A decade of Raman spectroscopy in art and archaeology. *Chem Rev ACS* 107:675–686
297. Vandenabeele P, Moens L (2003) Micro-Raman spectroscopy of natural and synthetic indigo samples. *Analyst* 128:187–193
298. Vandenabeele P, Wehling B, Moens L, Edwards H, De Reu M, Van Hooydonk G (2000) Analysis with micro-Raman spectroscopy of natural organic binding media and varnishes used in art. *Anal Chim Acta* 407:261–274. doi:10.1016/S0003-2670(99)00827-2
299. Vandenabeele P, Weis TL, Grant ER, Moens LJ (2004) A new instrument adapted to in situ Raman analysis of objects of art. *Anal Bioanal Chem* 379:137–142
300. Villafana TE, Brown WP, Delaney JK, Palmer M, Warren WS, Fischer MC (2014) Femtosecond pump-probe microscopy generates virtual cross-sections in historic artwork. *Proc Natl Acad Sci USA* 111:1708–1713. doi:10.1073/pnas.1317230111
301. Vitek P, Ali EMA, Edwards HGM, Jehlicka J, Cox R, Page K (2012) Evaluation of portable Raman spectrometer with 1064 nm excitation for geological and forensic applications. *Spectrochim Acta A* 86:320–327
302. Weis TL, Jiang Y, Grant ER (2004) Toward the comprehensive spectrochemical imaging of painted works of art: a new instrumental approach. *J Raman Spectrosc* 35:813–818
303. Whitney AV, Casadio F, Van Duyne RP (2007) Identification and characterization of artists' red dyes and their mixtures by surface-enhanced Raman spectroscopy. *Appl Spectrosc* 61:994–1000

304. Whitney AV, Van Duyn RP, Casadio F (2006) An innovative surface-enhanced Raman spectroscopy (SERS) method for the identification of six historical red lakes and dyestuffs. *J Raman Spectrosc* 37:993–1002. doi:10.1002/jrs.1576
305. Williams AC, Edwards HGM, Barry BW (1994) Raman spectra of human keratotic biopolymers: skin, callus, hair and nail. *J Raman Spectrosc* 25:95–98. doi:10.1002/jrs.1250250113
306. Wilson AS, Edwards HGM, Farwell DW, Janaway RC (1999) Fourier transform Raman spectroscopy: evaluation as a non-destructive technique for studying the degradation of human hair from archaeological and forensic environments. *J Raman Spectrosc* 30:367–373. doi:10.1002/(SICI)1097-4555(199905)30:5<367:AID-JRS384>3.0.CO;2-I
307. Winkler W, Kirchner ECh, Asenbaum A, Musso M (2001) A Raman spectroscopic approach to the maturation process of fossil resins. *J Raman Spectrosc* 32:59–63
308. Withnall R, Chowdhry BZ, Silver J, Edwards HGM, de Oliveira LFC (2003) Raman spectra of carotenoids in natural products. *Spectrochim Acta A* 59:2207–2212. doi:10.1016/S1386-1425(03)00064-7
309. Wouters J (1985) High performance liquid chromatography of anthraquinones: analysis of plant and insect extracts and dyed textiles. *Stud Conserv* 30:119–128
310. Wouters J, Verhecken A (1989) The coccid insect dyes: HPLC and computerized diode-array analysis of dyed yarns. *Stud Conserv* 34:189–200. doi:10.2307/1506286
311. Wustholz KL, Brosseau CL, Casadio F, Van Duyn RP (2009) Surface-enhanced Raman spectroscopy of dyes: from single molecules to the artists' canvas. *Phys Chem Chem Phys* 11:7350–7359. doi:10.1039/b904733f
312. Wynn-Williams DD, Edwards HGM (2000) Proximal analysis of regolith habitats and protective biomolecules in situ by laser Raman spectroscopy: overview of terrestrial antarctic habitats and mars analogs. *Icarus* 144:486–503. doi:10.1006/icar.1999.6307
313. Yaffe NR, Blanch EW (2008) Effects and anomalies that can occur in SERS spectra of biological molecules when using a wide range of aggregating agents for hydroxylamine-reduced and citrate-reduced silver colloids. *Vib Spectrosc* 48:196–201. doi:10.1016/j.vibspec.2007.12.002
314. Zaffino C, Bedini GD, Mazzola G, Guglielmi V, Bruni S (2016) Online coupling of high-performance liquid chromatography with surface-enhanced Raman spectroscopy for the identification of historical dyes. *J Raman Spectrosc*. doi:10.1002/jrs.4867
315. Zaffino C, Bruni S, Guglielmi V, De Luca E (2014) Fourier-transform surface-enhanced Raman spectroscopy (FT-SERS) applied to the identification of natural dyes in textile fibers: an extractionless approach to the analysis. *J Raman Spectrosc* 45:211–218. doi:10.1002/jrs.4443
316. Zhao J, Carrabba MM, Allen FS (2002) Automated fluorescence rejection using shifted excitation Raman difference spectroscopy. *Appl Spectrosc* 56:834–845
317. Zoppi A, Lofrumento C, Mendes NFC, Castellucci EM (2010) Metal oxalates in paints: a Raman investigation on the relative reactivities of different pigments to oxalic acid solutions. *Anal Bioanal Chem* 397:841–849. doi:10.1007/s00216-010-3583-1

Immunochemical Micro Imaging Analyses for the Detection of Proteins in Artworks

Giorgia Sciotto¹ · Martina Zangheri² ·
Silvia Prati¹ · Massimo Guardigli² · Mara Mirasoli² ·
Rocco Mazzeo¹ · Aldo Roda²

Received: 19 November 2015 / Accepted: 3 May 2016 / Published online: 10 May 2016
© Springer International Publishing Switzerland 2016

Abstract The present review is aimed at reporting on the most advanced and recent applications of immunochemical imaging techniques for the localization of proteins within complex and multilayered paint stratigraphies. Indeed, a paint sample is usually constituted by the superimposition of different layers whose characterization is fundamental in the evaluation of the state of conservation and for addressing proper restoration interventions. Immunochemical methods, which are based on the high selectivity of antigen–antibody reactions, were proposed some years ago in the field of cultural heritage. In addition to enzyme-linked immunosorbent assays for protein identification, immunochemical imaging methods have also been explored in the last decades, thanks to the possibility to localize the target analytes, thus increasing the amount of information obtained and thereby reducing the number of samples and/or analyses needed for a comprehensive characterization of the sample. In this review, chemiluminescent, spectroscopic and electrochemical imaging detection methods are discussed to illustrate potentialities and limits of advanced immunochemical imaging systems for the analysis of paint cross-sections.

Keywords Paint cross-section · Immunoassay · Imaging · Proteins · Chemiluminescence · Immuno-SERS · Immuno-SECM

This article is part of the Topical Collection “Analytical Chemistry for Cultural Heritage”.

✉ Giorgia Sciotto
giorgia.sciotto@unibo.it

¹ Department of Chemistry “G. Ciamician”, Microchemistry and Microscopy Art Diagnostic Laboratory (M2ADL), University of Bologna, Ravenna Campus, Via Guaccimanni 42, 48100 Ravenna, Italy

² Department of Chemistry “G. Ciamician”, University of Bologna, Via Selmi 2, 40126 Bologna, Italy

1 Introduction

1.1 Immunochemical Micro Imaging in Conservation Science

In the last decades, many scientific efforts have been aimed at developing innovative analytical procedures for the characterization of artwork samples. Among different paint materials, organic substances—used since ancient times as binders, varnishes and adhesives—have drawn a particular attention. Indeed, even if their identification plays a crucial role in the characterization of the execution technique, in authentication studies and in the selection of adequate methodologies for conservation, the limited amount of organic materials and their sensitivity to aging processes may compromise their correct recognition.

Immunochemical techniques, widely employed in bioanalytical and clinical chemistry [1], were proposed some years ago in the field of cultural heritage as a powerful alternative for the characterization of organic materials, overcoming common drawbacks of traditional analytical approaches such as chromatographic and spectroscopic analysis in terms of selectivity, sensitivity and analyte localization. These methodologies, exploiting the high selectivity of antigen–antibody reactions, permit the discrimination of different proteins and even the determination their biological source.

In the last decades, performances of immunochemical approaches have been deeply investigated by optimizing ad hoc systems for the identification of proteins in artistic samples [2–18].

In addition to conventional enzyme-linked immunosorbent assays (ELISA), much attention has been focused on the application of immunochemical imaging methods for the sensitive and selective localization of proteins within a paint cross-section [2, 3, 7–15]. Indeed, polychrome objects are usually characterized by multi-layered structures composed by mixtures of organic and inorganic substances, whose characterization is fundamental for the determination of adequate methodologies in restoration practices.

Imaging techniques in immunochemistry are commonly used in histological laboratory for the recognition of antigens in tissues or single cells [1, 19]. The localization of the target analyte is performed at the microscopic level and it can be achieved employing fluorescent, chemiluminescent or colorimetric detection. Imaging methods are usually based on a noncompetitive immunological approach. Thus, the immunochemical reaction is accomplished by adding the specific anti-antigen antibody, which is detected by means of a species-specific secondary antibody labeled with a suitable marker. Moreover, microscopy techniques allow the localization of target antigens with a high spatial resolution. Depending on the detection technique used, it may be also possible to perform quantitative or semi-quantitative assessment of the target analyte concentration.

The transfer of this approach to cultural heritage issues may be considered as the beginning of a new research field. Thus, different markers, such as enzymes, fluorochromes and gold nanoparticles, in combination with suitable detection techniques, have been used for the visualization of antigen–antibody complexes,

thereby allowing the sensitive identification of proteins within paint cross-sections. An overview on the most recent immunochemical micro imaging approaches developed for the localization of proteins in artistic samples is reported in [Table 1](#).

These analytical methods are particularly attractive because both identification and localization of analytes can be performed, reducing the number of samples and analyses needed, preserving a high selectivity in protein detection and assuring a powerful and cost-effective approach.

Fluorescence-based imaging is probably the most widely used approach, starting from the first pioneering studies in the field of conservation science [16–18]. Nevertheless, this technique usually presents significant interferences due to intense autofluorescence produced by sample materials (such as pigments and/or binding media), and by light scattering phenomena at the sample surface, which could hamper the detection of analytes [2, 3, 14–18]. In an attempt to overcome such drawbacks, alternative detection strategies have been proposed, leading to the development of highly sensitive immunochemical methods based on chemiluminescence (CL) imaging detection. Indeed, CL detection is not affected by interferences from sample components, thanks to the absence of any excitation source. Thus, CL imaging has proved to be suitable for the localization of proteins in paint stratigraphies with a spatial resolution of the order of micrometers by using single and multiplexed immunoassays [79]. Electrochemical detection has also been investigated, as an alternative and powerful method for the identification of proteins

Table 1 Immunochemical micro imaging methods for cultural heritage

References	Analyte	Detection system
Dolci et al. [7]	Egg albumin	Chemiluminescence
Sciutto et al. [8]	Egg albumin and bovine casein (multiplex format)	Chemiluminescence
Sciutto et al. [9]	Egg albumin and animal glue (multiplex format)	Chemiluminescence
Sciutto et al. [10]	Egg albumin	Scanning electrochemical microscopy (SECM)
Arslanoglu et al. [11]	Egg albumin, bovine casein	Surface-enhanced Raman scattering (SERS)
Sciutto et al. [12]	Egg albumin	Surface-enhanced Raman scattering (SERS)
Perets et al. [13]	Egg albumin, animal glue, bovine casein	Surface-enhanced Raman scattering (SERS)
Cartechini et al. [2]	Egg albumin, animal glue, bovine casein	Fluorescence
Magrini et al. [15]	Egg albumin, bovine casein, fish glue	Fluorescence
Kockaert et al. [16]	Egg albumin	Fluorescence
Ramirez Barat et al. [17]	Egg albumin	Fluorescence
Heginbotham et al. [18]	Egg albumin	Fluorescence

in artistic samples [10]. However, similarly to fluorescence detection, electrochemical and CL approaches cannot provide information on different substances that constitute (alone or in mixtures) the paint layers. Recently, SERS-based immunochemical methods have been proposed, enabling selective mapping of the target protein and of other Raman active substances at the same time [11–13].

The present review is aimed at summarizing the most recent imaging immunochemical approaches applied to artwork samples. In particular, in the next paragraphs, together with some basic concepts related to the principles of the methods, advanced strategies are presented. Examples of chemiluminescent, spectroscopic and electrochemical detection methods are discussed, while more conventional fluorescence approaches are not treated, since they have been reported in other recent reviews [2, 3, 13].

1.2 Immunochemical Principles

Immunoassays are analytical techniques that use antibodies as specific recognition elements, relying on the high selectivity of the binding reaction of an antibody (Ab) to its specific antigen (Ag). The selectivity and avidity of an antibody allow for the development of highly efficient methods for the determination and localization of analytes, even in complex matrices [1, 19].

Antibodies are immunoglobulin proteins produced by the immune system of organisms as a response to a given antigen. Thus, they can interact with various important analytical targets, including small organic molecules (pesticides, hormones, drugs) and biopolymers (peptides, proteins, DNA). Therefore, immunoassays can be designed for a wide range of analytes and find application in different fields, such as life sciences, clinical chemistry, and pharmaceutical, toxicological, environmental and food analysis.

Monoclonal and polyclonal antibodies (mAb and pAb, respectively) are available for immunoassays. Differently from a mAb, which recognizes only one antigenic site, a pAb is a mixture of antibodies able to bind to different epitopes (molecular moiety recognized by the antibody) within the same antigen.

The detection of an antibody requires a suitable marker, according to the detection technique used. In the simplest approach (direct labeling), the marker is directly bound to the antigen-specific antibody (primary antibody). As an alternative, the primary antibody can be detected by a properly labeled secondary antibody (indirect labeling). Such labeled antibody is usually an anti-species antibody and it is directed against primary antibodies depending on their biological source (mouse, goat, sheep, rabbit, etc.). It is worth noting that the labeling process requires significant amounts of antibody, reduces its activity and it may be quite complex. Thus, detection by indirect labeling is the most used, even if this requires an additional reaction step, and thus a longer assay time (Fig. 1). Among easily detectable molecules used as markers, the most common are: (1) radioisotopes, which are sensitive labels, but present risks related to the radioactivity; (2) fluorophores, based on the emission of photons consequent to the absorption of light radiation; (3) enzymes that can be detected by chromogenic, fluorescent or bioluminescent substrates.

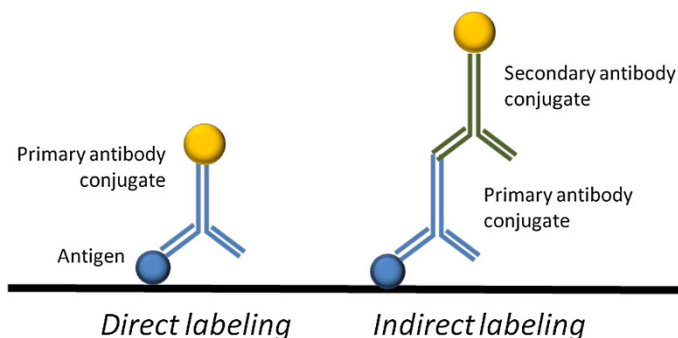


Fig. 1 Schematic of direct and indirect immunochemical approaches

Enzymes are probably the most used markers, thanks to the amplification of the analytical signal induced by their catalytic activity. Moreover, according to the substrate used, different analytical techniques may be exploited for their detection (e.g., spectrophotometry, fluorescence, chemiluminescence).

1.3 Ultrasensitive Chemiluminescent Immunochemical Analyses

Among the different techniques for the detection of immunocomplexes, chemiluminescence (CL) has shown remarkable performances in terms of spatial resolution and detection limit. Indeed, CL detection does not require an excitation source, and therefore it is not affected by the autofluorescence arising from the sample components. This characteristic is of particular relevance for the analysis of paint cross-sections, considering that several components of paintings are natively fluorescent. Thus, in the last decade, ultrasensitive CL immunochemical procedures for the detection of ovalbumin as well as for the simultaneous localization of ovalbumin and bovine casein or collagen (common proteins found in binding media or varnishes in artistic and archaeological samples) have been developed, introducing a new generation of analytical approaches in conservation science.

1.4 Chemiluminescence and Enzyme Chemiluminescent Systems

The phenomenon of CL can be defined as the emission of light (usually in the visible spectral region) originating from a chemical reaction. These reactions usually involve strong oxidant species (e.g., peroxides), and they can be divided into direct and indirect CL reactions. The direct one generates an excited-state molecule that is responsible for light emission. In indirect CL, the excited product of the chemical reaction transfers its energy to a highly fluorescent energy acceptor, which then emits. This process enables increasing the intensity of CL when the excited product is poorly fluorescent.

Chemiluminescence and bioluminescence (which is a CL reaction catalyzed by enzymes in biological system) have been widely exploited for the development of analytical and bioanalytical methods [20–26]. Thus, thanks to the sensitivity of CL

detection, it is possible to identify the target analyte within a wide concentration range (from femtomolar up to millimolar) without sample dilution or modification of the analytical procedure. On the other hand, a potential disadvantage of CL systems is that the light-emitting chemical reaction could be inhibited, enhanced or triggered by sample matrix constituents [21, 27]. Moreover, CL reactions usually have flash-type kinetics in which light emission lasts only for a few seconds. To obtain higher CL signals and steady-state emission kinetics, thus improving analytical signal handling and measurement reproducibility [28], enzymes can be used in the presence of an excess of a proper CL enzyme substrate. In addition, suitable enhancers can be added to the substrate to further improve the performance of the CL systems.

Horseshoe peroxidase (HRP) and alkaline phosphatase (AP) are the most commonly employed enzymes detectable by CL.

Substrates available for HRP are luminol (5-amino-2,3-dihydro-1,4-phthalazine-dione) derivatives. The final product of the luminol oxidation reaction is a 3-aminophthalate ion in the excited state that decays by emitting photons at a wavelength of about 425 nm (Fig. 2). The reaction takes place in alkaline environment in the presence of an oxidizing agent such as H_2O_2 . The reaction

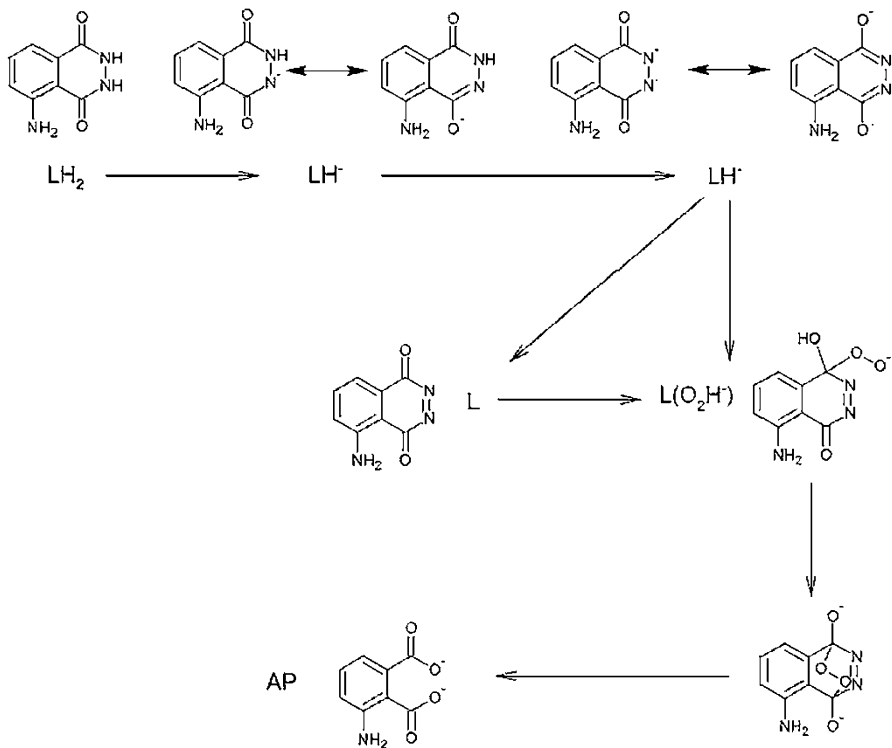


Fig. 2 Scheme of chemiluminescent luminol oxidation. Reproduced from Ref. [28] with permission from the Royal Society of Chemistry

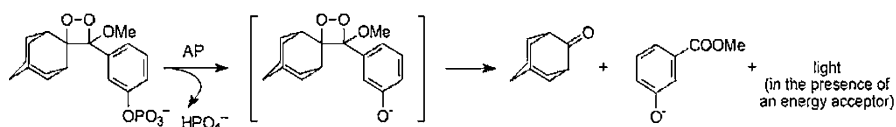


Fig. 3 Scheme of chemiluminescent reaction catalyzed by alkaline phosphatase

kinetics is usually quite fast and the maximum signal being reached in a time of the order of minutes. The presence of “enhancers,” such as substituted phenols, naphthols, phenylboronic acids, and phenothiazine derivatives, allows to stabilize and to increase the intensity of the CL signal [27].

Substrates for AP are mainly dioxetane derivatives which can be dephosphorylated by an AP-catalyzed reaction (Fig. 3). The dephosphorylated molecule decomposes, then an excited-state reaction product transfers its energy to an acceptor, which is the species responsible for the emission. The kinetics of the CL reaction catalyzed by AP is slower than that of HRP and the plateau is reached between approximately 10 and 30 min of incubation. The AP-catalyzed CL reactions are basically free of interferences, and AP itself is very stable and possesses a high turnover rate [29].

1.5 Chemiluminescent Imaging

The availability of low-light imaging devices based on high-sensitivity and high-resolution sensors—such as cooled charge-coupled devices (CCD) or complementary metal oxide semiconductor (CMOS) image sensors—has allowed the development of CL imaging methods that rely not only on the detection of light emission down to the single photon level, but also on its localization on the sample surface with good spatial resolution [30]. A wide number of applications has been described for both macro and micro samples in various fields, such as drug development, diagnostics, agrofood and environmental analysis [30–35].

Luminographs, used for the acquisition of images, employ ultrasensitive video cameras and optical systems enclosed in a light-tight box to prevent interference from ambient light. To reduce the background signal, mainly ascribable to the thermal noise, the detectors are cooled to low temperatures (down to $-100\text{ }^{\circ}\text{C}$) by means of thermoelectric or cryogenic systems. This allows for accumulation of the CL signal over long times and therefore increases the sensitivity. When connected to an optical microscope, imaging devices permit measuring and localizing of the emission on the sample with a resolution on the order of micrometers. Due to the low light intensity characteristic of the CL emissions, it is necessary to minimize the loss of signal in the optical system. Thus, suitable lens systems and objectives with high numerical aperture (NA) should be used to increase the efficiency of collection of the CL signal [35]. To correctly localize the signal in a specific area of the sample, it is also necessary to acquire an image of the sample using reflected (or transmitted) light, which is then superimposed to the pseudo-colored image of the CL emission (obtained by conversion of the gray scale of the CL image—related to

the emitted light—to a chromatic scale). The overlap between pseudo-colored and visible images allows for the clear showing of differences in the CL signals recorded from different areas of the sample surface.

1.6 Immunochemical CL Imaging for the Location of Proteins in Paint Stratigraphies

Different CL imaging assays have been developed for the immunochemical localization of proteins in paint samples, in both single and multiplexed formats.

The first attempt for the application of a CL immunochemical procedure in the field of cultural heritage was aimed at the localization of ovalbumin (chicken white egg albumin, used as binding medium in whole-egg tempera) in paint cross-sections [7]. The noncompetitive immunochemical protocol—based on the use of an anti-ovalbumin primary antibody and a horseradish peroxidase (HRP)-labeled secondary antibody—allowed the target protein to be localized on paint stratigraphies with an estimated detection limit of about 0.03 ng mm^{-2} of ovalbumin. The assay has been successfully applied on paint reconstruction as well as historical samples. Subsequently, the method has been modified for the localization of other common proteinaceous materials, and, in particular, for the simultaneous detection of different proteins in the same samples [8, 9]. Indeed, the use of different enzyme markers (HRP and AP) allowed for the separate localization of the target proteins. The possibility to simultaneously localize different analytes in the same cross-section is of particular relevance, since paint samples are usually very small and available in limited numbers, and thus, the maximum amount of information must be obtained from each sample.

Due to the complexity of the paint matrix, the preliminary set up of immunochemical procedures is usually performed on nitrocellulose membranes. Several parameters affect the performance of the assay and have to be optimized, such as: (1) antibody characteristics (e.g., selectivity), (2) antibody concentration, (3) incubation time and temperature, (4) blocking agent (i.e., nature and concentration), and (5) washing steps.

The optimization of the analytical procedure is also aimed at obtaining the highest CL signal/background ratio. However, it is worth noting that even if higher concentrations of the immunoreagents usually lead to stronger CL signals, this may be accompanied by an increment of the background signal, thus decreasing the CL signal/background ratio.

Particular attention has been paid on the evaluation of possible nonspecific interactions between paint components and immunochemical reagents. Because of the porosity of paint cross-sections, optimization of blocking and incubation steps is crucial to avoid the nonselective adsorption of the immunoreagents, which leads to high background signals and to the decrement of the target protein detectability. The blocking agents (usually proteins) are able to bind free nonspecific sites, thus preventing their interaction with the antibody. When used at the optimal concentration, the blocking agent reduces the nonspecific adsorption of the immunoreagents to the cross-section without compromising their binding to the target proteins, whereas an excessive amount will also reduce target detectability.

Table 2 Examples of blocking agents employed in immunochemical micro-imaging approaches

Analyte	Blocking agent	References
Egg albumin	Fat dried milk in water (5 % protein concentration)	Dolci et al. [7]
Egg albumin and bovine casein (multiplex format)	Soy milk and BSA (5 % total protein concentration)	Sciutto et al. [8]
Egg albumin and animal glue (multiplex format)	Fat dried milk in PBS* (5 % protein concentration)	Sciutto et al. [9]
Egg albumin	Fat dried milk in water (1 % protein concentration)	Sciutto et al. [12]
Egg albumin, animal glue, bovine casein	Soy milk (0.03 grams protein/mL) and 2.5 % BSA (w/v)	Perets et al. [13]

* *PBS* phosphate buffer solution

Some examples of blocking agents selected for the different assays are reported in Table 2. As an example, the procedure of evaluation of blocking agents for the determination of ovalbumin is reported in Fig. 4. Among the tested substances (bovine serum albumin, gelatine and dried milk), the highest signal/background ratios were obtained using a 5 % solution of nonfat dried milk in water. The nonselective binding of the immunoreagents could be reduced by careful preparation of the cross-section with appropriate dry polishing methods (which reduce the heterogeneity of the surface) and by decreasing the incubation temperature.

To assess the applicability of the assay in paint cross-sections, the possible interferences caused by common pigments have been also investigated (smalt, azurite, malachite, hematite, cinnabar, and minium). Indeed, several metal ions contained in pigments (Co^{2+} , Cu^{2+} , Fe^{3+} , Mn^{2+} , and Pb^{2+} ions) are known inhibitors of HRP [36] and the release of such ions during the CL detection step could affect the enzyme activity. In addition, metal ions can also directly influence the CL luminol reaction, either by acting as catalysts (the Co^{2+} ion is the most sensitive catalyst for the luminol- H_2O_2 reaction [37]) or inhibiting the CL process (for example, the Cu^{2+} ion [38]). However, tests aimed at evaluating such interferences did not show any detectable effects related to the catalysis or inhibition of the CL reaction (Fig. 5), suggesting the nonsignificant release of metal ions during the sample treatments.

The multiplexed approaches have been used for simultaneous detection of different pairs of target proteins, i.e., ovalbumin and casein or ovalbumin and collagen [8, 9]. The spatial distribution of the proteins in paint cross-sections has been assessed by noncompetitive immunoassays. By exploiting the specificity of the antigen–antibody reactions, selective localization of the different target proteins has been achieved by microscope CL imaging. Differently from the assay for a single protein, instead of performing sequential incubations of samples with primary and secondary antibodies, a single incubation with a preformed complex between primary and secondary antibodies (obtained by mixing appropriate dilutions of the two antibodies) has been used.

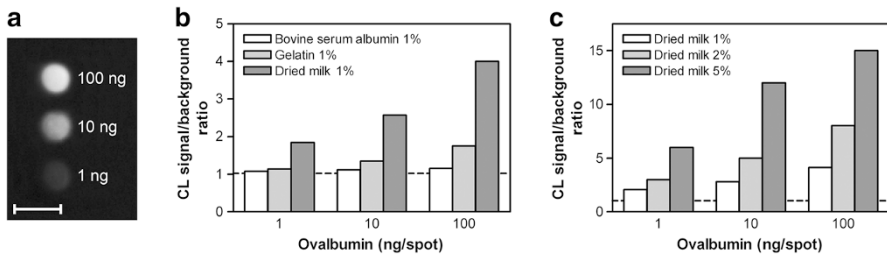


Fig. 4 Selection of **a** the blocking agent and **b** its optimal concentration performed on nitrocellulose membranes on which different amounts (1, 10 and 100 ng) of ovalbumin were spotted. Data are reported as ratios between the CL signals of the spots and the background signal of the membrane. *Panel a* shows the CL image of a nitrocellulose membrane. *Bar* represents 5 mm. Reproduced from Ref [7], by permission of Springer

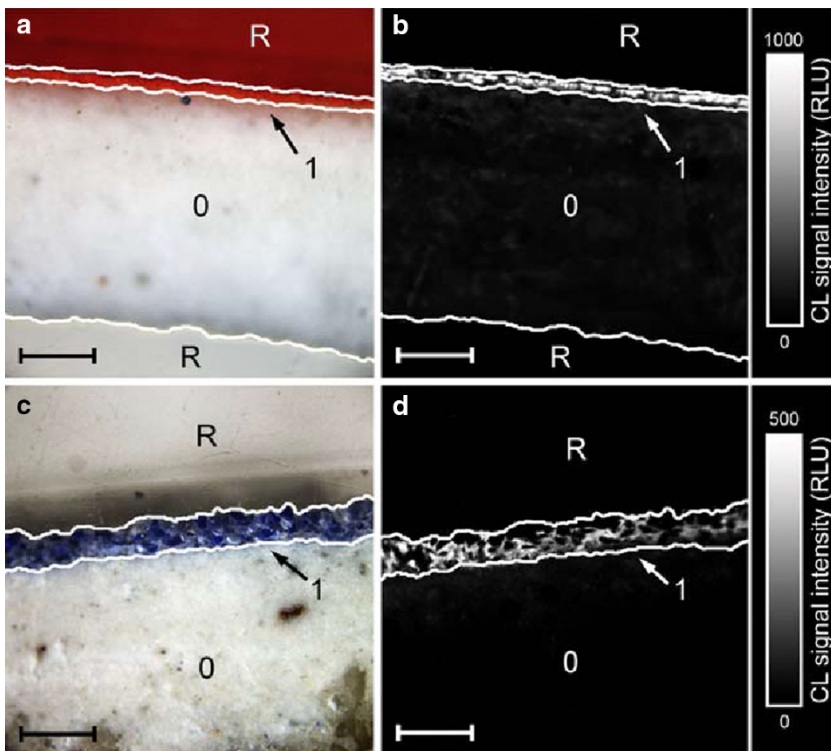


Fig. 5 Chemiluminescence immunolocalization of ovalbumin in cross-sections of standard samples with a layer of whole-egg tempera containing cinnabar (*top*) or smalt (*bottom*) pigments. *Panels a* and *c* show the live images of the cross-sections, *panels b* and *d* show the CL images, confirming the localization of the CL signal in the egg tempera layer corresponding to the binding medium. The different parts of the cross-sections are indicated (*R* resin, *O* ground layer, *1* egg tempera layer with pigments). *Bars* represent 200 μm . Reproduced from Ref. [7], by permission of Springer

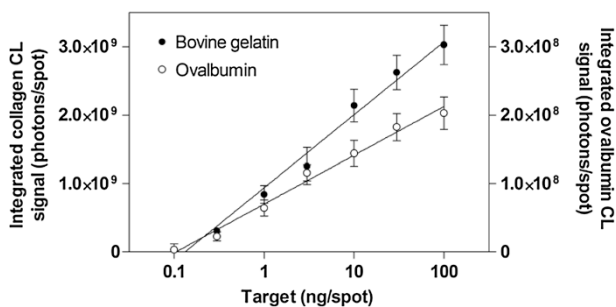


Fig. 6 Calibration curves for the multiplexed CL immunolocalization procedure obtained in nitrocellulose membrane. The limits of detection of the immunolocalization procedure (estimated as the amount of target giving a CL signal corresponding to the background plus three times its standard deviation) were about 0.3 and 0.5 ng/spot for bovine gelatin and ovalbumin, respectively. Reproduced from Ref. [9], by permission of Springer

As for HRP, inhibition of AP-catalyzed CL reaction due to metal ions has been described [39]. Thus, in the set-up of multiplexed approaches, studies on possible interferences have been carried out, demonstrating, also in this case, the absence of effects on the CL signal.

Finally, to verify the detectability of proteins using the CL immunolocalization procedures, a calibration curve has been obtained for each protein. The detection limits have been estimated as the amount of protein giving a CL signal corresponding to the background signal plus three times its standard deviation (Fig. 6).

After the evaluation of assay performance on standard paint reconstructions, historical samples have been analyzed to prove the applicability of the method for the detection of aged protein. Indeed, the degradation of the protein due to aging (high humidity and temperature conditions are known to promote hydrolysis reactions and oxidative alterations of organic components) may affect its detectability by immunochemical analysis. It has been demonstrated that ovalbumin and collagen, both in varnish layers or mixed with other paint components, can be successfully localized in real samples, thanks to the high sensitivity of the immunochemical approach (Figs. 7, 8). The efficacy of the saturation procedure and the location of the analytes with resolution of the order of micrometers are clearly demonstrated by the pseudo color images obtained by superimposition between visible and CL images.

2 Immunochemical Imaging Detection by Raman-SERS Analysis

In the last decades, SERS (Surface Enhanced Raman Scattering) probes (i.e., plasmonic nanoparticles with a Raman reporter anchored to their surface) have been used for the immunochemical detection of biomolecules related to physiological and

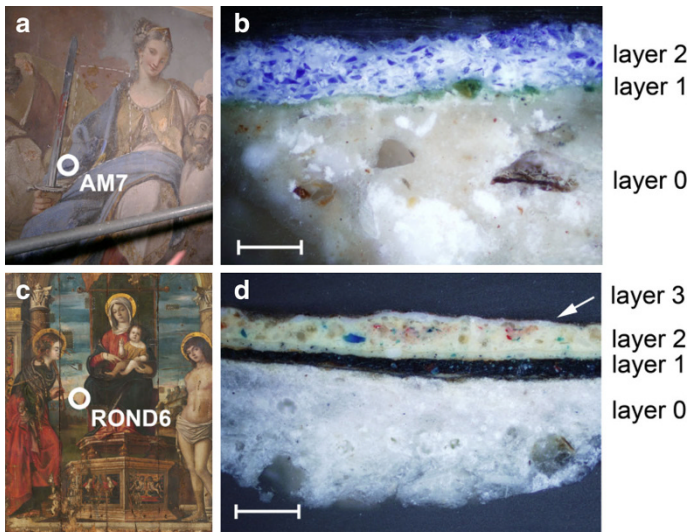


Fig. 7 **a, c** Real case studies that have been investigated with the marl of the sampling areas. **a** A wall painting attributed to Giuseppe Milani (1719–1798) and located in the Abbey of S. Maria del Monte, Cesena (Italy), dated to 1773–1774. **b** A painted wood panel by Baldassare Carrari (1460–1516), an Italian painter of the Renaissance period, representing the Virgin with the Holy baby and Saints and exhibited in the city museum of Ravenna, Italy. **b, d** *Color live* images of sample cross-sections with assignment of the different layers. The *bars* represent 100 μm . Reproduced from Ref. [9], by permission of Springer

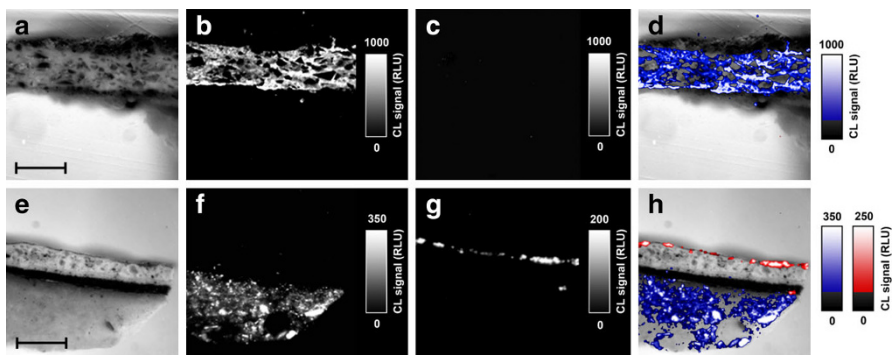


Fig. 8 **a–d** Results obtained from sample AM7 with the application of a single assay detection of collagen. The protein is present within the pigment layer. **e–h** Results obtained from sample ROND6 with the multiplexed assay for the simultaneous detection of collagen and ovalbumin. **a, e** Live images of the cross-sections. **b, f** Chemiluminescence signals corresponding to collagen. **c, g** Chemiluminescence signals corresponding to ovalbumin. **d, h** Overlay between the live images of the cross-sections and the pseudo-colored CL images in which the CL signals corresponding to collagen and ovalbumin are represented in shades of blue and red, respectively. Reproduced from Ref. [9], by permission of Springer

pathological processes in cells and tissues [40–43]. Thanks to their high capabilities, such detection systems rapidly originated one of the most promising research fields in analytical spectroscopy.

Even if the application of both SERS and SERRS (Surface Enhanced Resonant Raman Scattering) techniques is not new in the field of cultural heritage [44–48] (e.g., they have been employed for the spectroscopic investigation of organic pigments or colorants present in artistic samples in a very low amount), only few research works on the combination of SERS-based detection and immunological methods have been reported in the literature [11–13]. Nevertheless, among all the different immunochemical approaches, the use of Raman-SERS detection remains one of the most powerful methods. Indeed, this spectroscopic approach allows for the simultaneous localization of the target protein and the other paint materials through the creation of false-color chemical maps. This aspect is of paramount importance in the study of unique and precious materials, where maximum information should be achieved from the minimum number of samples.

In addition, thanks to the fact that Raman microscope is often used in conservation centers and museum laboratories, the approach could be widely and easily applied, becoming a tool for routine investigation of artistic samples.

2.1 SERS Probes

SERS probes are usually constituted by a Raman-active molecule (Raman reporter) adsorbed on the surface of a noble metal nanostructure, which is encapsulated with an external shell of polyethylene glycol (PEG), silica or bovine serum albumin in order to stabilize and protect the probe, as well as to permit its bio-conjugation [49, 50]. In biochemical approaches, this system can be used as a label of immunochemical complexes, thanks to the enhancement of the spectroscopic signal, which increases the sensitivity of the method. Thus, the probes exploit the SERS phenomena to emit unique spectral signatures indicating the presence of the immunochemical complexes.

Enhancement of the Raman signal, which has a very low scattering cross section with respect to fluorescence, usually refers to two different mechanisms: electromagnetic and chemical contribution. The electromagnetic enhancement is ascribed to the interaction between free electrons, (present on the metal surface) and the excitation light, producing a surface plasmon, which may be described as a collective oscillating electron wave. This effect provides an enhancement of the electric field in that localized area, which is greatest when the plasmon frequency is coupled with the excitation radiation [51–53]. Indeed, the plasmonic modes generate an intense absorption and scattering bands in the visible–near infrared interval. Metal particles or structures responsible for the electromagnetic mechanism should present a dimension smaller than the wavelength of the exciting light; thus, the SERS-active systems must ideally have a nanometric size (ranging between 5 and 100 nm) [54]. Moreover, the contact region between two particles (named “hot spot”) shows a very strong enhancement.

A stronger enhancement can be obtained through SERRS. Indeed, an intense Raman scattering is observed when the analyte presents a chromophore with an electronic energy close to the frequency of the excitation used. In this case, the enhancement from both plasmon and molecular resonances contribute to generate a very intense signal in SERR spectra [55]. Moreover, the fluorescence signal is

usually quenched by the nanoparticles, reducing the possible interferences with Raman scattering.

Together with the electromagnetic explanation of the SERS effect, the chemical contribution is also considered. The phenomenon is ascribed to charge transfer processes between the chemisorbed species and the metal surface, which may be responsible of an enhancement effect for system where species are able to form a chemical bond with the metal surface. This theory can be applied only in specific cases and in concert with the electromagnetic mechanism [56, 57], which, on the contrary, is also valid when molecules are only physisorbed to the surface.

The use of noble metal nanoparticles with plasmonic properties in biology and medicine fields, i.e., for the sensing of DNA and for cancer diagnosis, has increased significantly in the last decades [58–60]. Indeed, imaging investigations of cells or tissues have traditionally been performed with fluorescent probes (such as organic fluorophores), which suffer well-known limitations related to the photo bleaching effect, fluorescence background emission from the biological matrix, low stability in some extreme environments of biological systems, and bio compatibility (in particular, for quantum dots semiconductor probes). Raman reporters functionalized on the nanoparticles surface represent an alternative powerful approach for biochemical detection of target analytes. Moreover, among the various molecular imaging techniques for biomedical applications, SERS approach has become very popular, thanks to its ability to generate enhanced Raman spectra with picomolar sensitivity and multiplexing capabilities [59].

The first attempt at the application of immunochemical SERS analysis on paint samples was presented a few years ago [11]. The paper reported the use of commercial nanotags produced by Oxonica (Mountain View, CA, USA). These nanotags are constituted of a core of aggregated gold nanoparticles with a diameter of 90 nm, which is coated with a monolayer of Raman reporter and encapsulated in a silica shell, achieving a final dimension of about 120 nm. The secondary antibody is covalently bound to the nanotag for the indirect immuno-SERS protocol. The manufactured probes were selected for their reproducible SERS signal. However, several drawbacks of the proposed assay have been reported, which have been mainly ascribed to the nonspecific immuno-SERS signals arising from the paint matrix. In more detail, difficulties in removing the excess SERS nanotag complexes have been declared, either in presence or absence of the primary antibody. Even if it has not been possible to exclude nonselective interactions between probes and paint materials, the authors attributed this phenomenon mainly to the use of a feeble blocking agent and treatment. More recently, the same authors have presented an advancement of the method based on the optimization of alternative SERS nanotags. In particular, new nanotags have been proposed in an attempt to avoid nanoparticle aggregation on sample surfaces, and to reduce the nonspecific interactions between probes and paint components [13]. Such SERS probes are constituted of gold nanoparticle dimers with a Raman-active dithiolated reporter and conjugated to secondary antibodies through either amino or carboxyl groups. Moreover, nanostructures are encapsulated with amino- and carboxy-terminated PEGs ($X'-\text{PEG}-\text{SH}$: $X' = -\text{NH}_2$ or $-\text{COOH}$). Thus, hetero-bifunctional surface

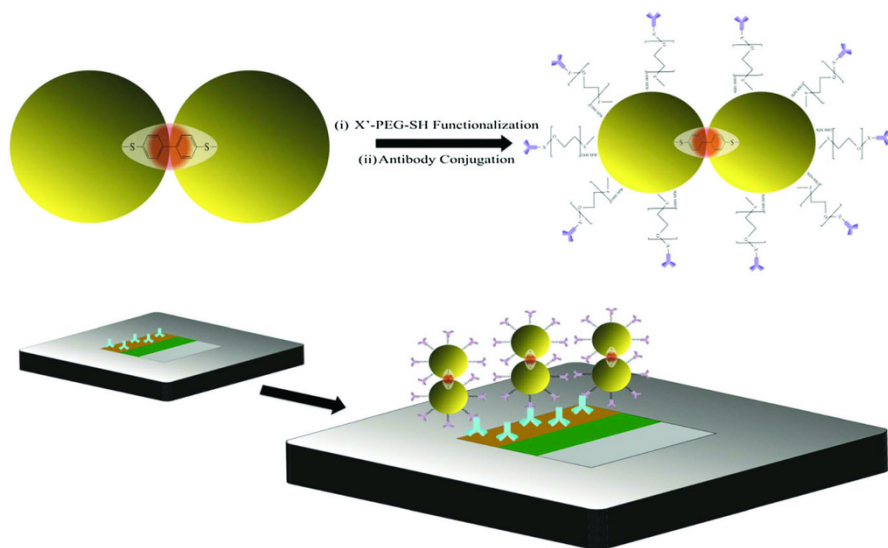


Fig. 9 Schematic of SERS-633 Au NP functionalization and immuno-SERS assay. Au NPs (*golden spheres*) are dimerized via Raman-active biphenyl-4,4'-dithiol (DBDT) reporter at the “hot spot” (*red sphere*) and surface functionalized with X'-PEG-SH coating (MW 1000, X' = -NH₂ or -COOH). Conjugation to polyclonal secondary antibody (*purple*) is achieved through DCC/NHS conjugation chemistry. First, a mounted cross-sectional sample (*bottom*) is incubated with polyclonal primary antibody (*light blue*). Next, excess primary antibody is removed with washing, and SERS-633-tagged secondary antibodies are applied. Au NPs are localized only to those regions of the sample where antigen is present. Reproduced from Ref. [13], by permission of The Royal Society of Chemistry (<http://pubs.rsc.org/en/content/articlehtml/2015/an/c5an00817d>)

coatings have been synthesized demonstrating their ability to prevent nonspecific aggregation of SERS probes on the paint sample (Fig. 9).

The technology transfer from biochemical field to conservation science allowed the application of a new generation of SERS probes, based on the laser ablation in solution (LASiS) for the preparation of metal particles, in immunochemical studies on paint cross-sections. A recent research has reported the advantages of the physical preparation of gold nanoparticles in the synthesis of SERS tracer in terms of stability, reproducibility and nonspecific interaction, providing an highly efficient detection of the target protein both in fresh and historical samples [11].

The use of the LASiS for production of nanoparticles, proposed by early research in 1993 [61], allows the obtaining of nanoparticles during the laser ablation of a bulk metal plate immersed in a liquid solution. This one-step procedure generates stable charged nanoparticles of gold, silver, platinum, copper and other materials, presenting a clean surface that can be easily functionalized without any ligand exchange reaction or extensive purification procedures. On these bases, LASiS has proved to be an excellent green and cheap alternative to traditional approaches, avoiding the presence of unreacted compounds and the formation of chemical waste [62]. It is worth reporting that one of the main drawback of LASiS is the control of average size and size distribution, which may influence the enhancement of the

signal and its reproducibility. However, by the control of condition of the laser treatment and preparation approach, the size of nanoparticles may be reduced or increased [63, 64]. In particular, a detailed study has been carried out on the characterization of aggregated AuNP solution obtained by centrifugation and used in the preparation SERS-probe, showing the reproducibility of results in terms of dimension and SERS signal [65].

The immunochemical SERS approach for the characterization of paint samples reports the use of gold nanoparticles obtained with average diameters of about 20 nm and subsequently submitted to the aggregation by means a centrifugation procedure, in attempt to maximize the efficiency of SERS enhancement through the increment of the number of “hot spots.” “Hot spots” can be described as junctions or close interactions between plasmonic objects, which can be easily obtained with the aggregation of nanoparticles [66]. The solution of NaCl in which the metal target is immersed during the laser ablation, is employed to increase the period of stability of particles, up to several months. Indeed, Cl^- ions help in opening Au-O-Au bonds formed during the ablation process in water, producing Au-O⁻ charges, which further stabilize the colloidal solution, thanks to coulombic interactions [62]. Finally, nanoparticle aggregates are functionalized with the Raman reporter and linked to the secondary antibody for the indirect immuno-SERS assay. The obtained nanostructures are coated with PEG, in order to minimize nonspecific interactions between sample matrices and SERS-nanotags. The potentialities of such system applied for the detection of ovalbumin within paint cross-section have been previously described in developing plasmonic nanostructures for ultrasensitive multiplexed identification of tumor-associated antigens [65].

Nile Blue A functionalized with liponic acid (LipNB) has been used as SERS reporter, demonstrating the efficiency of the signal with the 785 nm laser excitation for an highly sensitive identification of immuno-complexes in the heterogeneous paint substrates. The main steps of the SERS probes obtained with LASiS preparation are reported in Fig. 10.

2.2 Immuno SERS Assays for Artistic Samples

In all the researches related to the application of immunochemical SERS method to the study of paint cross-sections, a noncompetitive indirect approach has been

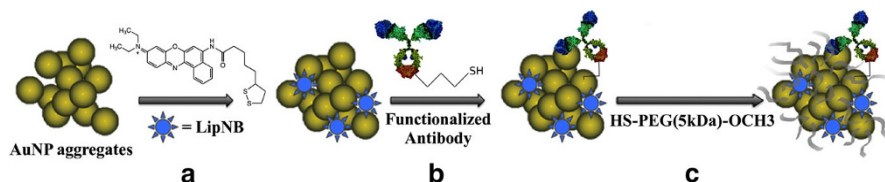


Fig. 10 Steps for the preparation of the LASiS SERS probes: **a** aggregated nanoparticles obtained by centrifugation linked with Nile Blue reporter; **b** functionalization of the secondary antibody to the nanoaggregate; **c** covering of the nanoaggregate with thiolated polyethylene glycol chains. Reproduced from Ref [12], by permission of The Royal Society of Chemistry (<http://pubs.rsc.org/en/content/articlepdf/2013/an/c3an00057e>)

proposed with the use of SERS nanotags conjugated to the secondary antibody. As previously mentioned, particular attention has been focused on the control of nonspecific interaction between SERS nanotags and paint matrices and/or embedding materials. Indeed, problems related to the inability to remove nonspecifically bound SERS nanotags, which produce false positive signals and compromise the effectiveness of the analytical response, have been indicated as the major drawback of the method [11].

To this aim, the selection of washing procedure, blocking agent and antibodies incubation conditions in immunoassays have been carefully evaluated by testing the protocol on paint sample reconstructions with or without the target protein, and applying the immunochemical assay with or without the primary antibody.

On the basis of these measurements, it has been demonstrated that the use of suitable SERS probes and a correct set up of the immune protocol allow the unambiguous identification of the analyte in paint cross-sections.

2.3 Raman-SERS Chemical Imaging

The combination between the information obtained from immunochemical methods and Raman analysis for a comprehensive characterization of paint matrices is extremely important in studies on artwork samples, to obtain the maximum amount of information from the minimum number of samples.

Nevertheless, among the scientific publications on this subject, only a research work—aimed at immunochemical detection of ovalbumin with SERS detection system—underlines the potential of the immunochemical method in combination with spectroscopic investigation of paint cross-sections [12]. In this study, mapping analyses were performed to achieve a reliable characterization of paint components in terms of molecular spectral features and spatial location, and to evaluate the

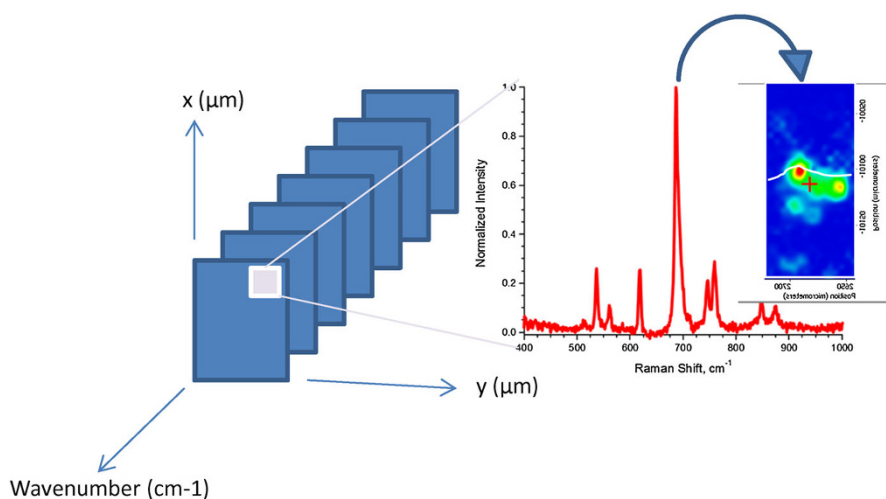


Fig. 11 Schematic of hyperspectral parallelepiped

selectivity of the approach for the target protein recognition through the creation of false color chemical maps.

Spectroscopic mapping systems allow to collect a considerable number of spectra from a bidimensional scan of sample surface, obtaining information about the spatial distribution of different compounds. The three-dimensional data structure acquired is conventionally referred to as a “hypercube,” which is composed by two spatial as well as one spectral dimension (Fig. 11). Chemical images can be obtained by coding the intensity of a characteristic band, which is diagnostic for the presence of a specific molecule (e.g., the Raman reporter of the SERS probe), by a chromatic scale. Such a false color image represents the spatial position (x, y) and the intensity of the Raman scattering (blue-red color scale) at a specific Raman shift (cm^{-1}).

In the immunochemical approach, the possibility to select a proper Raman reporter that may present a vibrational fingerprint different from all the other component, allows to obtain simultaneously a representative distribution of paint components and the selective location of the target protein. Thus, in the formulation of SERS nanotags, an important role is played by the correct selection of Raman active molecule used as reporter.

In the case of the research under examination, Nile Blue A has been proposed as Raman reporter. Thanks to its spectral feature, which is well differentiated from those of other paint components, it has been possible to obtain an unambiguous positive localization of immuno-complexes by selection of the marker band at 592 cm^{-1} with 785 nm laser excitation (Fig. 12).

As an example, chemical maps obtained on standard and historical samples (ROND12) are reported in Figs. 13 and 14. The analysis allowed the clear

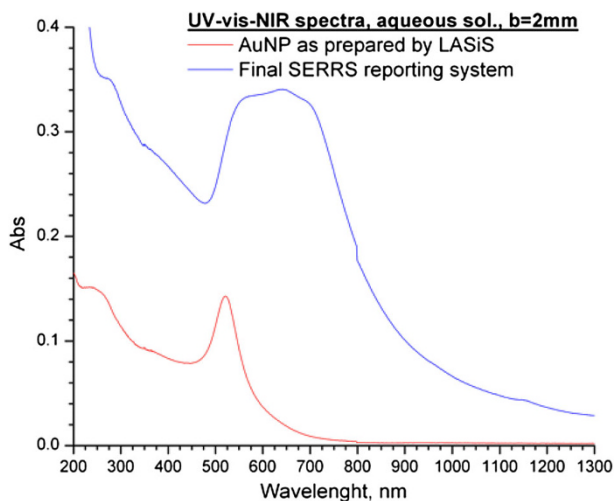


Fig. 12 Extinction spectra of the not aggregate (*red line*), and aggregated (*blue line*) gold nanoparticles after functionalization with the Nile Blue the secondary and antibody. Reproduced from Ref. [12], by permission of The Royal Society of Chemistry (<http://pubs.rsc.org/en/content/articlepdf/2013/an/c3an00057e>)

localization of ovalbumin within the whole-egg tempera red paint layer (in the standard mock-up) and in the uppermost layer of the historical sample stratigraphy. Interestingly, the result achieved for the real sample is in agreement with the previous analyses performed by CL immunochemical identification, which allowed the localization of a thin external layer of ovalbumin [7, 9]. Moreover, the immunoSERS analysis combined with the traditional Raman spectroscopy provided additional information concerning the composition of paint materials.

3 Scanning Electrochemical Microscopy for the Immunochemical Detection of Proteins

In the attempt to explore the potentialities of the immunochemical approach in the characterization of artistic samples, alternative detection techniques have also been evaluated.

In particular, a recent research study has proposed the combination of immunoassay procedures with the Scanning Electrochemical Microscopy (SECM) for the selective recognition of ovalbumin directly in paint cross-sections [10].

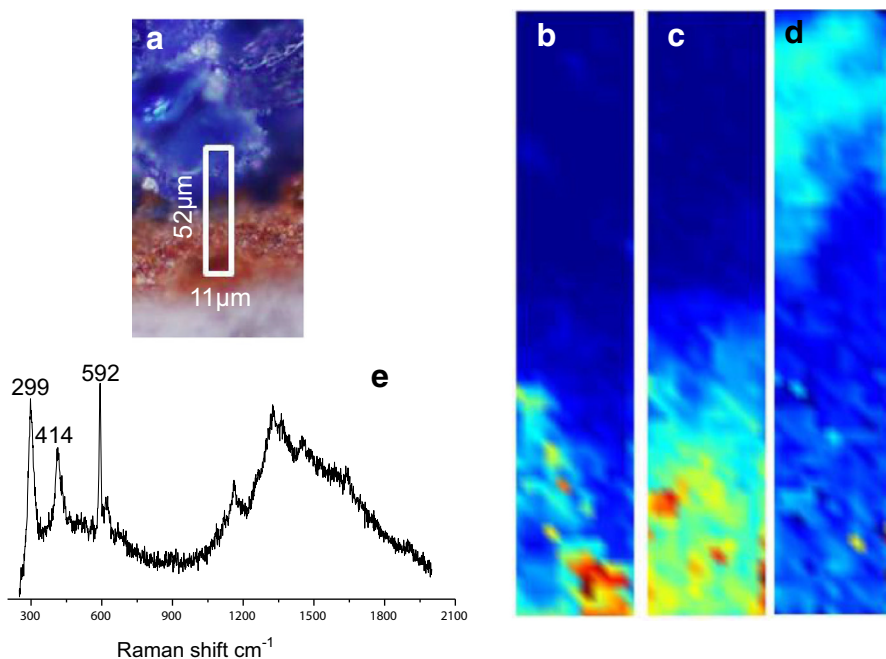


Fig. 13 **a** Cross-section microphotograph of standard sample under visible light. The *white box* indicates the selected area for Raman analysis. Chemical false *color* maps of **b** Nile Blue (band at 592 cm^{-1}); **c** *red ochre* (band at 299 cm^{-1}); **d** Azurite (band at 400 cm^{-1}); **e** Spectrum extracted from the *red paint layer* which contains ovalbumin. Bands at 299 and 414 cm^{-1} are ascribable to *red ochre*, while the band at 592 cm^{-1} is related to the Raman reporter, which indicates the presence of the target protein (ovalbumin). Reproduced from Ref. [12], by permission of the Royal Society of Chemistry (<http://pubs.rsc.org/en/content/articlepdf/2013/an/c3an00057e>)

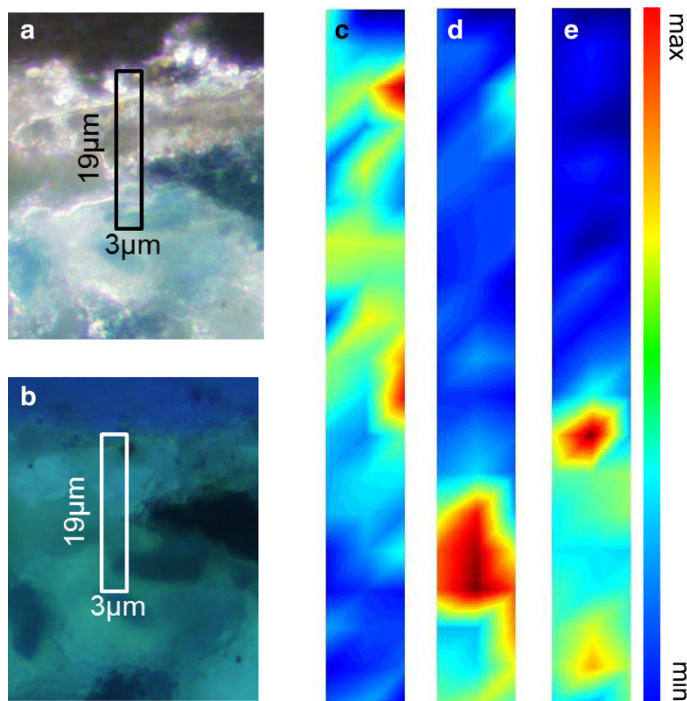


Fig. 14 Cross-section microphotographs of historical sample ROND12: **a** image under visible light; **b** image under UV illumination. *Black and white boxes* indicate the selected area for Raman analysis. Chemical false color maps of **c** Nile Blue (band at 592 cm^{-1}); **c** Azurite (band at 400 cm^{-1}); **d** lead white (band at 1051 cm^{-1}). Reproduced from Ref. [12], by permission of the Royal Society of Chemistry (<http://pubs.rsc.org/en/content/articlepdf/2013/an/c3an00057e>)

SECM allows the electrochemical detection of the analyte, obtaining information on the electrochemical process in which the target molecules are involved and providing chemical and topographic information about the investigated surfaces. Thus, it can be considered as a complementary tool in the investigation of complex substrates.

Interestingly, even if the electrochemical detection of immunocomplexes in conservation science is not new [67], the research presents the first application of SECM for paint samples investigations, opening the way for a wide application of SECM to analysis of paint cross-sections. Indeed, only very few applications of electrochemical microscopy have been reported for the characterization of heritage materials, such as ancient copper-based alloys [68].

3.1 Scanning Electrochemical Microscopy

SECM is scanning probe microscopy (SPM) based on the use of an ultramicroelectrode (UME) probe for scanning the investigated substrate and recording the current produced by electrochemical reactions. Thus, the electrochemical reaction at

the UME is spatially resolved with high resolution according to the probe diameter dimension, which is typically about 10 μm [69] for micron-sized disc-shaped electrodes sealed in glass. Sub-micron- and nanometre-scale electrodes have been also proposed in this specific study to improve the spatial resolution. The tip is connected to a positioner, which allows moving the probe across the investigated area. Even if different positioners can be employed, for high spatial resolution, a piezoelectric system is required.

SECM has been used in several types of study, such as: (1) organic and inorganic film permeability, (2) metabolites absorption in cells and (3) local surface modification [70–75].

Several operation modes can be applied for the SECM mapping approach in the investigation of electroactivity of sample surfaces, such as feedback and the generation/collection modes. However, probably the most widely employed is the feedback mode. In this case, the UME is immersed into a solution containing a redox mediator that can be oxidized or reduced according to the potential applied to the probe (e.g., if a positive potential is applied to the tip, the mediator is oxidized with a rate which depends on the diffusion of the mediator at the UME surface). Thus, the steady state current can be registered as a function of the mediator concentration and of its diffusion coefficient at the tip. When the UME is moved across the sample, the electrochemical properties, as well as the distance of the electrode from the surface, influence the variation of the mediator concentration at the UME, modifying the registered current. Indeed, an increment (positive feedback) or a decrement (negative feedback) of the current can be observed [76].

For the topographic documentation of samples, the negative feedback mode can be employed, keeping the probe at a fixed position from the investigated surface. Thus, changes in the distance between the probe and the sample surface induce a reduction of current, producing information about the morphology. However, even if the spatial resolution achieved by the SECM is not competitive with the performances of other probe scanning techniques, such as the atomic force microscopy (AFM), the most relevant advantage of this approach is the possibility to perform noncontact detection of electrochemically active species, thus preserving the analyte.

Indeed, SECM is an attractive technique for studying biological systems and processes, as well as enzyme determination in biosensing approaches and biomedical applications. In this case, the probe is used to detect the electron transfer reaction involving the immobilized enzymes, which have to be detected. In particular, a reversible redox mediator is used and converted at the tip electrode. Then the product of this reaction is regenerated by the enzymatic activity [77], producing an increment of current.

The use of immunosensing device in combination with electrochemical detection has been proposed for the study of immunochemical complexes antibodies labeled with an enzyme as recognition element [78–81]. The activity of enzymes can be precisely localized by SECM in correspondence with the target protein thanks to a catalytic production of species that are detected at the ultramicroelectrode surface. Thus, SECM imaging investigations of the enzyme activity can be applied to spatially locate the target protein.

3.2 SECM for Immunochemical Investigation of Paint Stratigraphies

In a recent research work, a new electrochemical microscope immunoassay has been developed as an innovative approach for the localization of ovalbumin in painting. The immunoassay procedure has been performed directly on paint cross-sections by using an anti-ovalbumin primary antibody and a secondary antibody, labeled with HRP and following a noncompetitive indirect approach. Subsequently, samples have been submitted to SECM measurements in feedback mode and benzoquinone (BQ) has been used as redox mediator, initially reduced into hydroquinone (H_2Q). In the presence of hydrogen peroxide (H_2O_2), the HRP-catalyzed reaction allowed the re-oxidation of H_2Q to BQ. Thus, the increment of BQ concentration in correspondence of the target protein has been detected by SECM through the reduction at the tip of the regenerated BQ (Fig. 15). The regeneration created a local concentration gradient and an increment of BQ reduction current over the layer containing the analyte. Thus, SECM measurements were carried out by approach curves and scan line analysis, both performed in presence and absence of H_2O_2 to discriminate the contribution arising from topographic features of the surface and the HRP catalyzed reaction.

The electrochemical approach has been evaluated on standard mock-ups and on a historical sample, to verify the capability of the proposed method to precisely localize HRP enzyme. As shown in Fig. 16, as an example, the scan line registered in the absence of H_2O_2 showed features mainly related to differences in surface morphology. Conversely, in the presence of H_2O_2 , an evident peak is superimposed on the signal background, revealing the catalytic activity of HRP in correspondence of the pigment layer mixed with egg. Thus, the micrometric localization of ovalbumin has been achieved by the comparison of the measurements recorded before and after H_2O_2 administration.

The study presented also the evaluation of the effect of metal ions contained in pigments (such as Co^{2+} , Cu^{2+} , Pb^{2+}) and in particular the role of Fe^{2+} due to its known interaction with H_2O_2 (Fenton reaction). However, no significant interaction with the enzyme activity have been observed.

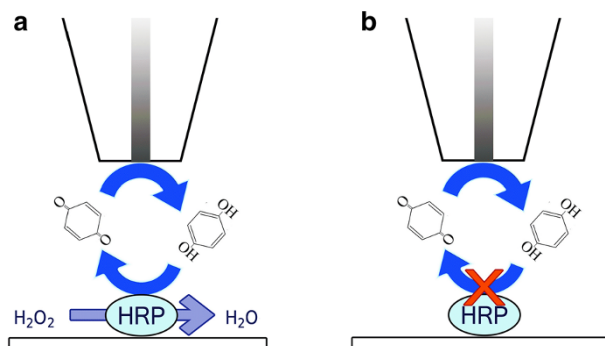


Fig. 15 Schematic representation of the BQ reaction at the tip. In the presence of H_2O_2 **a**, the immobilized HRP catalyzes the oxidation of H_2Q to BQ, consequently a regeneration current is observed. Reproduced from Ref. [10], by permission of Springer

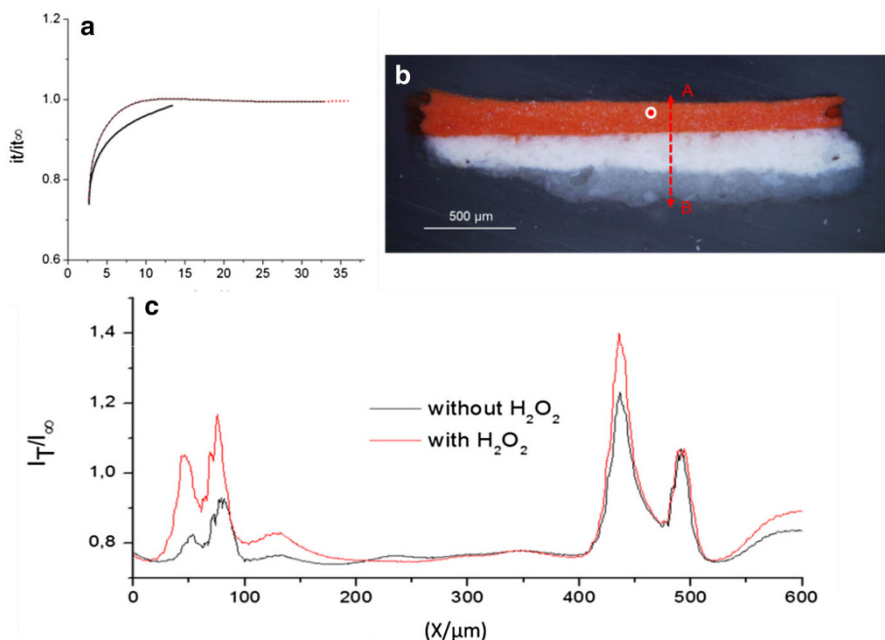


Fig. 16 **a** SECM approach curve obtained on the pigment layer without H_2O_2 (black line) and with H_2O_2 (red dashed line) recorded at $E_t = -0.35$ V, 1 mM BQ in PBS. The thin black line under the red one is the fitted curve using the theory of finite kinetics by Cornut-Lefrou. **b** Optical image of the standard sample under visible light ($100\times$). Layer 0 gypsum ground, layer 1: minimum mixed with egg whole tempera. The red spot indicates the area where the approach curve was performed, while the red dashed line represents the investigated region through scan line analysis; **c** SECM scan lines with (red line) and without H_2O_2 (black line), $E_t = -0.35$ V, 1 mM BQ in PBS. The presence of HRP-conjugated antibody can be located in correspondence of the pigment layer. Reproduced from Ref. [10], by permission of Springer

4 Conclusions and Further Perspectives

The growing interest towards new analytical strategies for the characterization of paint stratigraphies has led to the development of advanced immunochemical methods for the detection of proteins in artistic samples. In particular, the attention has been focused on micro imaging approaches for highly selective localization of target proteins within paint cross-sections. Moreover, the possibility to determine the biological source of a given protein (e.g., fish or rabbit glue) also makes the immunolocalization method relevant for authentication studies, by allowing the determination—for instance—of the production period and of the origin of painting materials.

One of the most powerful immunochemical approaches proposed in the field of conservation science is CL imaging detection. Indeed, the absence of an excitation source allowed the obtainment of high sensitivity and high spatial resolution, also working on very complex matrices (such as paint samples). The efficiency of the methods has been not experimentally proven by the detection of proteins in real samples.

Moreover, multiplexed CL assays for the simultaneous identification of different proteins have been developed. Interestingly, up to now, such CL protocols represent the only attempts reported in the literature for the simultaneous localization of two proteins within a paint stratigraphy. However, this aspect is of particular relevance in the field of cultural heritage, because paint samples are often very small and available in limited number. Therefore, from each sample, the maximum amount of information must be obtained. Nevertheless, on the basis of this principle, it is worth indicating the major limitation of the CL method, which is the inability to provide information on different organic and inorganic substances present (alone or in mixtures) within the paint layers. On the other hand, in CL investigations—as well as in all of the other immunochemical protocols presented in this review—the stratigraphic sample is not destroyed; thus, it can be submitted to other measurements just after a smooth polishing of the surface.

Thanks to the possibility to assure knowledge on different types of materials with a single type of analysis, the Raman microscopy detection approach has attracted the attention of different researchers. However, the potential of such a method is not yet completely exploited. Some studies are currently ongoing, attempting to propose a multiplex immunochemical protocol with SERS detection. Indeed, the SERS multiplexed approach is based on the use of two different SERS reporters presenting well-recognizable, enhanced spectra for the localization of different analytes within paint mixtures.

The spectroscopic approach, as well as the electrochemical approach, allows the qualitative identification of the protein investigated. However, when stratigraphic analyses are performed, quantitative investigations are not undertaken, due to the fact that only qualitative information is usually required and needed in studies on painting materials and conservation status.

Thanks to the recent developments of immunochemical methods in heritage science, the approaches described in this review appear to be suitable for routine analysis in conservation studies. Efforts are currently aiming at extending the range of detectable substances by including other proteins (e.g., casein and collagen) and organic materials (e.g., gums) used in paintings, even in a multiplexed way. However, deeper attention should be devoted to the effect of aging in the immunochemical recognition of the antigen.

Finally, it is worth underlining that, together with the optimization of microscopy imaging assays, one of the most urgent and challenging objectives is the development of user-friendly portable analytical devices to be used on site by restorers. Immunochemical systems can be applied to address such an issue in conservation science studies. In particular, it has been demonstrated that, thanks to the use of ready-to-use analytical cartridges and a portable CL detection instrument, analyses can be performed (even directly by restorers) in different working contexts (e.g., conservation and restoration laboratories or on site) where the samples are collected, reducing response time and costs of analysis [6].

References

1. Wild D (2013) *The immunoassay handbook*, 4th edn. Elsevier, Amsterdam
2. Cartechini L, Vagnini M, Palmieri M, Pitzurra L, Mello T, Mazurek J, Chiari G (2010) Immunodetection of proteins in ancient paint media. *Acc Chem Res* 43:867
3. Cartechini L, Palmieri M, Vagnini M, Pitzurra L (2016) Immunochemical methods applied to art-historical materials: identification and localization of proteins by ELISA and IFM. *Top Curr Chem*. doi:10.1007/s41061-015-0006-y
4. Palmieri M, Vagnini M, Pitzurra L, Rocchi P, Brunetti BG, Sgamellotti A, Cartechini L (2011) Development of an analytical protocol for a fast, sensitive and specific protein recognition in paintings by enzyme-linked immunosorbent assay (ELISA). *Anal Bioanal Chem* 399:3011
5. Palmieri M, Vagnini M, Pitzurra L, Brunetti BG, Cartechini L (2013) Identification of animal glue and hen-egg yolk in paintings by use of enzyme-linked immunosorbent assay (ELISA). *Anal Bioanal Chem* 405:6365
6. Zangheri M, Sciutto G, Mirasoli M, Prati S, Mazzeo R, Roda A, Guardigli M (2016) A portable device for on site detection of chicken ovalbumin in artworks by chemiluminescent immunochemical contact imaging. *Microchem J* 124:247
7. Dolci LS, Sciutto G, Guardigli M, Rizzoli M, Prati S, Mazzeo R, Roda A (2008) Ultrasensitive chemiluminescent immunochemical identification and localization of protein components in painting cross-sections by microscope low-light imaging. *Anal Bioanal Chem* 392:29
8. Sciutto G, Dolci LS, Buragina A, Prati S, Guardigli M, Mazzeo R, Roda A (2011) Development and optimization of a multiplex chemiluminescent immunochemical technique for the simultaneous detection of different proteins in paint micro cross-sections. *Anal Bioanal Chem* 399:2889
9. Sciutto G, Dolci LS, Guardigli M, Zangheri M, Prati S, Mazzeo R, Roda A (2013) Single and multiplexed immunoassays for the chemiluminescent imaging detection of animal glues in historical paint cross-sections. *Anal Bioanal Chem* 405:933
10. Sciutto G, Prati S, Mazzeo R, Zangheri M, Roda A, Bardini L, Valenti G, Rapino S, Marcaccio M (2014) Localization of proteins in paint cross-sections by scanning electrochemical microscopy as an alternative immunochemical detection technique. *Anal Chim Acta* 831:31
11. Arslanoglu J, Zaleski S, Loike J (2011) An improved method of protein localization in artworks through SERS nanotag-complexed antibodies. *Anal Bioanal Chem* 399:2997
12. Sciutto G, Littl L, Lofrumento C, Prati S, Ricci M, Gobbo M, Roda A, Castellucci E, Meneghetti M, Mazzeo R (2013) Alternative SERRS probes for the immunochemical localization of ovalbumin in paintings: an advanced mapping detection approach. *Analyst* 138:4532
13. Perets EA, Indrasekara ASDS, Kurmis A, Atlasevich N, Fabris L, Arslanoglu J (2015) Carboxy-terminated immuno-SERS tags overcome non-specific aggregation for the robust detection and localization of organic media in artworks. *Analyst* 140:5971
14. Sandu I, Schäfer S, Magrini D, Bracci S, Roque C (2012) Cross-section and staining-based techniques for investigating organic materials in painted and polychrome works of art: a review. *Microsc Microanal* 18:860
15. Magrini D, Bracci S, Sandu ICA (2013) Fluorescence of organic binders in painting cross-sections. *Proc Chem* 8:194
16. Kockaert L, Gausset P, Dubi-Rucquoy M (1989) Detection of ovalbumin in paint media by immunofluorescence. *Stud Conserv* 34:183
17. Ramirez-Barat B, de la Vinã S (2001) Characterization of proteins in paint media by immunofluorescence: a note on methodological aspects. *Stud Conserv* 46:282
18. Heginbotham A, Millay V, Quick M (2004) The use of immuno-fluorescence microscopy (IFM) and enzyme-linked immunosorbent assay (ELISA) as complementary techniques for protein identification in artists' materials. *J Am Inst Conserv* 45:89
19. Gosling JP (1990) A decade of development in immunoassay methodology. *Clin Chem* 36:1408
20. DeLuca MA (1978) *Methods in enzymology*. Academic Press, New York
21. Kricka LJ, Stanley PE, Thorpe GHG, Whitehead TP (1984) *Analytical applications of bioluminescence and chemiluminescence*. Academic Press, London, New York
22. Scott D, Dikici E, Ensor M, Daunert S (2011) Bioluminescence and its impact on bioanalysis. *Ann Rev Anal Chem* 4:297–319
23. Kamnev AA, Tugarova AV, Selivanova MA, Tarantilis PA, Polissiou MG, Kudryasheva NS (2013) Effects of americium-241 and humic substances on photobacterium phosphoreum: bioluminescence

- and diffuse reflectance FTIR spectroscopic studies. *Spectrochim. Acta Part A Mol Biomol Spectrosc* 100:171–175
24. Mirasoli M, Michelini E (2014) Analytical bioluminescence and chemiluminescence. *Anal Bioanal Chem* 406:5529–5530
 25. Alieva RR, Belogurova NV, Petrova AS, Kudryasheva NS (2014) Effects of alcohols on fluorescence intensity and color of a discharged-obelin-based biomarker. *Anal Bioanal Chem* 406:2965–2974
 26. Burakova LP, Kudryavtsev AN, Stepanyuk GA, Baykov IK, Morozova VV, Tikunova NV, Dubova MA, Lyapustin VN, Yakimenko VV, Frank LA (2015) Bioluminescent detection probe for tick-borne encephalitis virus immunoassay. *Anal Bioanal Chem* 407:5417–5423
 27. Marzocchi E, Grilli S, Della Ciana L, Prodi L, Mirasoli M, Roda A (2008) Chemiluminescent detection systems of horseradish peroxidase employing nucleophilic acylation catalysts. *Anal Biochem* 377:189
 28. Zomer J (2011) The nature of chemiluminescent reactions, chemiluminescence and bioluminescence past present and future, 1st edn. Royal Society Chemistry, Cambridge, pp 54–90
 29. Ximenes VF, Campa A, Baader WJ, Catalani LH (1999) Facile chemiluminescent method for alkaline phosphatase determination. *Anal Chim Acta* 402:99
 30. Mirasoli M, Venturoli S, Guardigli M, Dolci LS, Simoni P, Musiani M, Roda A (2011) Ultrasensitive bioanalytical imaging, chemiluminescence and bioluminescence: past, present and future. Royal Society of Chemistry, Cambridge, pp 398–424
 31. Roda A, Pasini P, Musiani M, Baraldini M, Mirasoli M, Guardigli M, Russo C (2001) Bioanalytical applications of chemiluminescent imaging. In: García-Campaña AM, Baeyens W (eds) *Chemiluminescence in analytical chemistry*. Marcel Dekker, New York, pp 473–495
 32. Roda A, Guardigli M, Pasini P, Musiani M, Baraldini M (2002) *Luminescence biotechnology: instruments and applications*. CRC Press, Florida
 33. Roda A, Guardigli M, Michelini E, Pasini P, Mirasoli M (2003) Peer reviewed: analytical bioluminescence and chemiluminescence. *Anal Chem* 75:462A
 34. Roda A, Guardigli M, Michelini E, Mirasoli M (2009) Bioluminescence in analytical chemistry and in vivo imaging. *Trends Anal Chem* 28:307
 35. Creton R, Lionel FJ (2001) Chemiluminescence microscopy as a tool in biomedical research. *Biotechniques* 31:1098
 36. Zollner H (1999) *Handbook of enzyme inhibitors*, 3rd edn. Wiley, Weinheim
 37. Price D, Worsfold PJ, Mantoura RFC (1994) Determination of hydrogen peroxide in seawater by flow injection analysis with chemiluminescence detection. *Anal Chim Acta* 298:121
 38. Yuan J, Shiller AM (1999) Determination of subnanomolar levels of hydrogen peroxide in seawater by reagent-injection chemiluminescence detection. *Anal Chem* 71:1975
 39. Rej R, Bretaudiere J-P (1980) Effects of metal ions on the measurement of alkaline phosphatase activity. *Clin Chem* 26:423
 40. Camden JP, Dieringer JA, Wang Y, Masiello DJ, Marks LD, Schatz GC, Van Duyne RP (2008) Probing the structure of single-molecule surface-enhanced raman scattering. *J Am Chem Soc* 130:12616
 41. Henry A-I, Bingham JM, Ringe E, Marks LD, Schatz GC, Van Duyne RP (2011) Correlated structure and optical property studies of plasmonic nanoparticles. *J Phys Chem* 115:9291
 42. Amendola V, Meneghetti M (2012) Exploring how to increase the brightness of surface-enhanced raman spectroscopy nanolabels: the effect of the Raman-active molecules and of the label size. *Adv Funct Mater* 22:353–360
 43. Lutz BR, Dentinger CE, Nguyen LN, Sun L, Zhang J, Allen AN, Chan S, Knudsen BS (2008) Spectral analysis of multiplex Raman probe signatures. *ACS Nano* 2:2306
 44. Lofrumento C, Ricci M, Platania E, Becucci M, Castellucci E (2013) SERS detection of red organic dyes in Ag-agar gel. *J Raman Spectrosc* 44:47
 45. Leona M, Decuzzi P, Kubic TA, Gates G, Lombardi JR (2011) Nondestructive identification of natural and synthetic organic colorants in works of art by surface enhanced Raman scattering. *Anal Chem* 83:3990
 46. Murcia-Mascarós S, Domingo C, Sanchez-Cortes S, Cañamares MV, Garcia-Ramos JV (2005) Spectroscopic identification of alizarin in a mixture of organic red dyes by incorporation in Zr-Ormosil. *J Raman Spectrosc* 36:420
 47. Doherty B, Brunetti BG, Sgamellotti A, Miliani C (2011) A detachable SERS active cellulose film: a minimally invasive approach to the study of painting lakes. *J Raman Spectrosc* 42:1932

48. Casadio F, Leona M, Lombardi JR, Van Duyne R (2010) Identification of organic colorants in fibers, paints, and glazes by surface enhanced Raman spectroscopy. *Acc Chem Res* 43:7827
49. Samanta A, Maiti KK, Soh KS, Liao X, Vendrell M, Dinish US, Yun SW, Bhuvanewari R, Kim H, Rautela S, Chung J, Olivo M, Chang YT (2011) Ultrasensitive near-infrared Raman reporters for SERS-based in vivo cancer detection. *Angew Chem* 50:6089
50. Küstner B, Gellner M, Schütz M, Schöppler F, Marx A, Ströbel P, Adam P, Schmuck C, Schlücker S (2009) SERS labels for red laser excitation: silica-encapsulated SAMs on tunable gold/silver nanoshells. *Angew Chem* 48:1950
51. Nie S, Emory SR (1997) Probing Single Molecules and Single Nanoparticles by Surface-Enhanced Raman Scattering. *Science* 275:1102
52. Aroca R (2006) Surface-enhanced vibrational spectroscopy. Wiley, West Sussex
53. Le Ru EC, Etchegoin PG (2009) Principles of surface enhanced Raman spectroscopy and related plasmonic effects. Elsevier, Amsterdam
54. Moskovits M (2005) Surface-enhanced Raman spectroscopy: a brief retrospective. *J Raman Spectrosc* 36:485
55. Lewis IR, Edwards H (2001) Handbook of Raman spectroscopy: from the research laboratory to the process line, 1st edn. CRC Press, New York
56. Lombardi JR, Birke RL, Lu T, Xu J (1986) Charge-transfer theory of surface enhanced Raman spectroscopy: Herzberg-Teller contributions. *J Chem Phys* 84:4174
57. Lombardi JR, Birke RL (2008) A unified approach to surface-enhanced Raman spectroscopy. *J Phys Chem* 112:5605
58. Maiti KK, Dinish US, Fu CY, Lee JJ, Soh KS, Yun SW, Bhuvanewari R, Olivo M, Chang YT (2010) Development of biocompatible SERS nanotag with increased stability by chemisorptions of reporter molecule for in vivo cancer detection. *Biosens Bioelectron* 26:398
59. Dykman L, Khlebtsov N (2012) Gold nanoparticles in biomedical applications: recent advances and perspectives. *Chem Soc Rev* 41(6):2256–2282
60. Khlebtsov N, Bogatyrev V, Dykman L, Khlebtsov B, Staroverov S, Shirokov A, Matora L, Khanadeev V, Pylaev T, Tsyganova N, Terentyuk G (2013) Analytical and theranostic applications of gold nanoparticles and multifunctional nanocomposites. *Theranostics* 3(3):167–180
61. Fojtik A, Henglein A (1993) Laser ablation of films and suspended particles in a solvent: formation of cluster and colloid solutions. *Ber Bunsenges Phys Chem* 97:252
62. Amendola V, Meneghetti M (2009) Laser ablation synthesis in solution and size manipulation of noble metal nanoparticles. *PCCP* 11:3805
63. Amendola V, Meneghetti M (2009) Size evaluation of gold nanoparticles by UV–vis spectroscopy. *J Phys Chem* 113:4277
64. Amendola V, Meneghetti M (2013) What controls the composition and the structure of nanomaterials generated by laser ablation in liquid solution. *Phys Chem Chem Phys* 15:3027
65. Meneghetti M, Scarsi A, Litti L, Marcolongo G, Amendola V, Gobbo M, Di Chio M, Boscaini A, Fracasso G, Colombatti M (2012) Plasmonic nanostructures for SERRS multiplexed identification of tumor-associated antigens. *Small* 8:3733
66. Kleinman SL, Frontiera RR, Henry AI, Dieringer JA, Van Duyne RP (2013) Creating, characterizing, and controlling chemistry with SERS hot spots. *Phys Chem Chem Phys* 15:21
67. Bottari F, Oliveri P, Ugo P (2014) Electrochemical immunosensor based on ensemble of nano-electrodes for immunoglobulin IgY detection: application to identify hen's egg yolk in tempera paintings. *Biosens Bioelectron* 52:403
68. Guadagnini L, Chiavari C, Martini C, Bernardi E, Morselli L, Tonelli D (2011) The use of scanning electrochemical microscopy for the characterisation of patinas on copper alloys. *Electrochim Acta* 56:6598
69. Fan FF, Demail C (2012) Preparation of tips for scanning electrochemical microscopy, scanning electrochemical microscopy. In: Marcel D (ed) New York, pp 25–52
70. Roberts WS, Lonsdale DJ, Griffiths J, Higson SPJ (2007) Advances in the application of scanning electrochemical microscopy to bioanalytical systems. *Biosens Bioelectron* 23:301–318
71. Carano M, Lion N, Girault HH (2007) Detection of proteins on membranes and in microchannels using copper staining combined with scanning electrochemical microscopy. *J Electroanal Chem* 599:349
72. Stagni S, Palazzi A, Zacchini S, Ballarin B, Bruno C, Paolucci F, Marcaccio M, Carano C, Bard AJ (2006) New family of ruthenium (II) polypyridine complexes bearing 5-aryltetrazolate ligands as systems for electrochemiluminescent devices. *Inorg Chem* 45:695

73. Zanarini S, Bard AJ, Marcaccio M, Palazzi A, Paolucci F, Stagni S (2006) Ruthenium(II) complexes containing tetrazolate group: electrochemiluminescence in solution and solid state. *J Phys Chem B* 110:22551
74. Rapino S, Valenti G, Marcu R, Giorgio M, Marcaccio M, Paolucci F (2010) Microdrawing and highlighting a reactive surface. *J Mater Chem* 20:7272
75. Valenti G, Bardini L, Bonazzi D, Rapino S, Marcaccio M, Paolucci F (2010) Creation of reactive micro patterns on silicon by scanning electrochemical microscopy. *J Phys Chem C* 114:22165
76. Sun P, Laforge FO, Mirkin MV (2007) Scanning electrochemical microscopy in the 21st century. *Phys Chem Chem Phys* 9:802–823
77. Wittstock G, Wilhelm T, Bahrs S, Steinrücke P (2001) SECM feedback imaging of enzymatic activity on agglomerated microbeads. *Electroanal* 13:669
78. Shiku H, Matsue T, Uchida I (1996) Detection of microspotted carcinoembryonic antigen on a glass substrate by scanning electrochemical microscopy. *Anal Chem* 68:1276
79. Zhang X, Peng X, Jin W (2006) Scanning electrochemical microscopy with enzyme immunoassay of the cancer-related antigen CA15-3. *Anal Chim Acta* 558:110
80. Yasukawa T, Hirano Y, Motochi N, Shiku H, Matsue T (2007) Enzyme immunosensing of pepsinogens 1 and 2 by scanning electrochemical microscopy. *Biosens Bioelectron* 22:3099
81. Kasai S, Yokota A, Zhou H, Nishizawa M, Niwa K, Onouchi T, Matsue T (2000) Immunoassay of the MRSa-related toxic protein, leukocidin, with scanning electrochemical microscopy. *Anal Chem* 72:5761

Immunochemical Methods Applied to Art-Historical Materials: Identification and Localization of Proteins by ELISA and IFM

Laura Cartechini¹ · Melissa Palmieri^{2,4} ·
Manuela Vagnini³ · Lucia Pitzurra⁴

Received: 29 September 2015 / Accepted: 8 December 2015 / Published online: 4 January 2016
© Springer International Publishing Switzerland 2015

Abstract Despite the large diffusion of natural organic substances in art-historical materials, their characterization presents many challenges due to the chemical complexity and instability with respect to degradation processes. Among natural products, proteins have been largely used in the past as binders but also as adhesives or additives in coating layers. Nevertheless, biological identification of proteins in art-historical objects is one of the most recent achievements obtained in heritage science thanks to the development of specifically tailored bio-analytical strategies. In the context of this active emerging discipline, immunological methods stand out for sensitivity, specificity and versatility for both protein recognition and localization in micro-samples. Furthermore, the growing use of immunological techniques for advanced diagnostics and clinical applications ensures continuous improvement in their analytical performance. Considering such, this review provides an overview of the most recent applications of *enzyme linked immunosorbent assay* and *immunofluorescence microscopy* techniques in the field of heritage materials. Specifically, the main strengths and potentials of the two techniques as well as their limits and drawbacks are presented and discussed herein.

Keywords ELISA · IFM · Proteinaceous binders · Heritage materials · Imaging · Painting cross-section

✉ Laura Cartechini
laura.cartechini@cnr.it

¹ Istituto di Scienze e Tecnologie Molecolari, ISTM-CNR, 06123 Perugia, Italy

² Dipartimento di Chimica, Biologia e Biotecnologie, Università degli Studi di Perugia, 06123 Perugia, Italy

³ Laboratorio di Diagnostica per i Beni Culturali di Spoleto, 06049 Spoleto, Italy

⁴ Dipartimento di Medicina Sperimentale, Università degli Studi di Perugia, 06132 Perugia, Italy

1 Introduction and Background

1.1 Immunochemical Methods in Heritage Science

Immunochemical methods encompass a set of analytical techniques relying on the selective affinity of a biological antibody for its antigen. These techniques have a long tradition [1] and are widely used analytical tools in research and clinical diagnostics for the analysis of a variety of bio-molecules (peptides/proteins, hormones, vitamins, drugs, etc.). In fact, they are capable of providing high sensitivity, accuracy and specificity for the target analyte [2]. Given these appealing features, exploration of immunological techniques in the emerging field of heritage science is, therefore, a natural step towards the use of new analytical solutions for heritage materials. In this review, we report on the most recent developments in the application of immunochemical methods in heritage science focusing on enzyme-linked immunosorbent assay (ELISA) and immunofluorescence microscopy (IFM) techniques for recognition and localisation of bio-materials for objects in this field.

In human history, natural substances have long been man's first choice as raw materials for general applications in daily life, from cosmetics, medicine, construction of functional objects to creating artworks. Proteins, polysaccharides, waxes, vegetable oils, resins, natural fibres (cotton, silk, wool, etc.) and dyes are some examples of biomaterials used since antiquity by man in his artistic productions [3–5].

The basic need of providing a detailed scientific knowledge of cultural heritage materials for scholar and conservation purposes is nowadays firmly recognised [6] and has given rise to fruitful multidisciplinary collaborations among scientists, conservators, curators, restorers and art historians [7]. However the challenging identification and characterization of natural organic substances in art-historical objects still demands great analytical efforts to fulfil this final goal [8, 9]. This is due to their intrinsic complexity and chemical instability, making them prone to alteration/degradation processes combined with their limited availability for analytical purposes when these require sampling of invaluable works of art. Furthermore, in the specific context of cultural heritage materials, natural organic substances can be found as complex mixtures in intimate contact with inorganic compounds, a fact which may seriously hamper their characterization [10].

In the attempt to look for more effective analytical strategies targeted towards the identification of organic compounds in heritage materials, modern bio-molecular techniques have been demonstrated to be particularly suited for protein analysis. Proteomics and DNA analysis [11–15] are sophisticated sensitive techniques capable of identifying species origin of proteinaceous binders. On the other hand, as shown in the following sections, immunochemical methods offer an alternative analytical approach which is simple, cost-effective, and highly versatile for identifying and localising different proteins in a single micro-sample while remaining selective with respect to their biological source. After initial sporadic works [16–18], in the last decade, a growing number of papers have appeared focusing on the application of immunological techniques in the field of heritage

Table 1 Proteins identified by immunoassays in heritage materials using different immunologic techniques

Protein	Natural material	Object	References
Chicken ovalbumin	Albumen	Paintings	[19–21, 24–27, 29, 30, 33, 34, 36–43]
		Egyptian cartonnages	[35]
Chicken egg yolk immunoglobulin	Egg-yolk	Paintings	[23, 44]
Bovine β -casein	Milk/casein	Paintings	[21, 24, 26, 27, 33, 36, 38]
		Egyptian cartonnages	[35]
Collagen	Animal glue	Paintings	[21–23, 26, 27, 30, 40]
		Egyptian cartonnages	[35]
		Polychromy on Chinese terracotta	[41]
Glycoproteins	Vegetable gum	Paintings	[21, 26, 34]
		Egyptian cartonnages	[35]
		Peruvian feathered tabard	[26]
		Water colours on paper	[26]
Fibroin	Silk	Chinese textiles	[45]

science. These include ELISA for the bulk analysis of samples (no spatial information) and immunochemical microscopy imaging techniques such as IFM, chemiluminescence and immuno surface-enhanced Raman spectroscopy (SERS) [19–30]. Examples of archaeological studies performed using immunoassays can be also found (see for example [31, 32]) but this specific application is beyond the subject of this review. **Table 1** reports the comprehensive list of biological proteins currently identified in heritage materials using different immunologic approaches along with examples of recent applications selected from literature, spanning from ancient Egyptian objects, passing through ancient Chinese polychromies and silks, up to western paintings [19–30, 33–45].

In the next paragraphs, after a brief introduction on the basics of immunoassays, a description of methodologies and variants on the use of ELISA and IFM in the study of cultural heritage materials is given.

1.2 Basic Concepts

Nature has provided living organisms with a powerful versatile defence system, composed of *innate immunity* and *adaptive immunity*, which is capable of reacting with pathogenic organisms and, in general, more so with foreign substances. By convention, the term immune response refers to the coordinated reaction of the adaptive immune system for neutralizing and eliminating these foreigner molecules, which are called *antigens* (Ag), when they overcome the innate immune defenses. Recognition of antigens takes place in specific sites (*epitopes*) through antigen receptors specifically expressed by lymphocytes, the main components of the

adaptive immune system. The immune system recognizes and acts against an enormous number of antigens by generating a wide variety of lymphocytes, each with a single antigen receptor. The most important class of antigen receptors are the immunoglobulins, also called *antibodies* (Ab). Antibodies have a characteristic Y shape (see sketch in Fig. 1 reproduced from [46]) where the binding site to the antigen (*paratope*) is located at the top of the Y arms. The mechanism which underlies the high specific interaction between antibody and antigen has been extensively studied and is still under investigation in many different aspects (kinetics, thermodynamics, structural factors, etc.). It is mainly based on non-polar interactions (van der Waals forces) but also on electrostatic and structural complementarity of the interacting protein surfaces [46–48]. The striking specificity and affinity of the Ab–Ag interaction and the ability of the immune system to generate novel protein recognition sites is not only the basic key of immunity but it also makes antibodies a fundamental tool in experimental biology, biomedical research, and diagnostics. Indeed, thanks to the adaptability of the animal immune system, it is possible to custom-produce antibodies to be used as probes for detection of biomolecules of interest in a variety of research and diagnostic

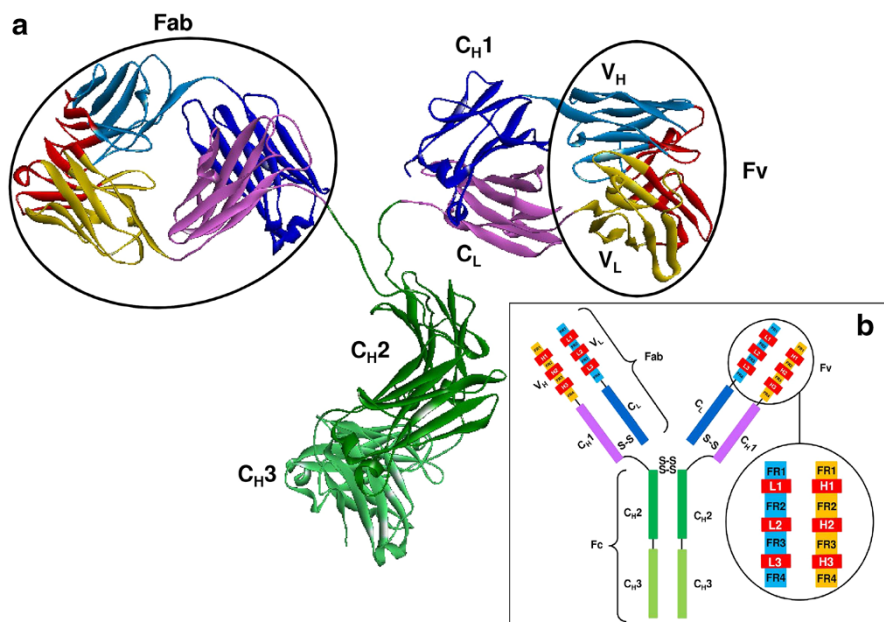


Fig. 1 **a** 3D representation of an Ab molecule and **b** schematic view of the Ab structure (reproduced from [46], a free PubMed Central [PMC] article, © 2013 Sela-Culang, Kunik and Ofra). The Y-shaped structure is formed by four polypeptide chains distinguished by two couples of identical heavy (H) and light (L) chains linked to each other by disulfide bonds. The arms of the Y-shaped structure are known as Fabs. Each Fab is composed of two variable domains (V_H in the heavy chain and V_L in the light chain) and two constant domains (C_{H1} and C_L). The Ag binding site (*paratope*) is contained in the region of the variable domains (Fv fragment) where six hyper-variable loops lie (L1, L2, and L3 in the light chain and H1, H2, and H3 in the heavy chain) forming the so-called complementarity determining regions (CDRs). Non-CDRs are distinguished as framework regions (FRs). Two additional domains of the heavy chain, C_{H2} , and C_{H3} , compose the Fc region

applications continuously in progress [49]. This branch of analytical science is called *immunoassays* [2, 50].

In immunoassays, the immuno-complex—formed by the antibody selectively bound to its antigen—is revealed by labelling the antibody in order to generate a detectable signal. Different reporter labels can be used [1]. In ELISA, the antibody is labelled with an enzyme which can react in the presence of a chromogenic or fluorogenic substrate producing a signal which is optically detected [51, 52]. Since each molecule of the enzyme can convert many molecules of the substrate, signal generation is highly amplified. In the case of IFM, the detection antibody is conjugated to a fluorophore and the immuno-complex is detected through fluorescence techniques [53]. This offers the major advantage of combining the highly specific recognition of proteins by immuno-tagging with the capability of mapping/imaging their distribution by high-resolution and high-sensitivity fluorescence microscopy and advanced micro-spectrofluorimetry techniques.

ELISA, since its invention in the 1960s [54], has rapidly developed with a number of immuno-reagents and immunoassay formats largely reviewed in literature [51, 52, 55]. It is the most common type of immunoassays in use for routine diagnostics and clinics studies; this ensures continuous advancement in assay specificity and sensitivity as well as in detection technologies. In a similar way, IFM is a fundamental research tool for imaging of biological and living systems; it is still an expanding research field which offers room for increasing development of many aspects such as: choice of fluorophores, immunoreagents, type of imaging technique, improvements in microscopes, and image computational post-processing treatments [56–59]. An extensive description of different methodologies and innovations today available in ELISA and IFM applications is out of the scope of this review since they are amply covered by the literature cited above and references therein. Instead, emphasis will be given to the emerging issues and solutions concerning the use of these immunoassays in heritage science with particular attention to the investigation of painting materials and polychromies.

1.3 Immunodetection of Aged Proteins in Heritage Materials

Proteins in heritage materials lose their native chemical physical properties as a result of the processing treatments before use and due to their prolonged exposure to environmental factors (light, humidity, temperature, oxygen, pH, etc.). In the specific case of paintings and polychromies, degradation processes are intensified owing to the interactions with pigments and other organic reactive components present in the painting matrix (for example, oxidising lipids or carbohydrates [60]). Scientific studies found that molecular modifications may vary as a result of the chemico-physical stress experienced by the system [61]: disruption of the protein–protein intermolecular interaction, oxidation, cross-linking, hydrolysis and deamidation [62–66]. Protein degradation directly influences immunoassay sensitivity due to possible losses of the active epitopes available for immuno-detection [67]. Thus, the variation of both chemical and structural properties of proteins may cause significant reduction of the antibody–antigen affinity. Furthermore, inorganic ions may inhibit enzymatic activity of the ELISA reporting system.

So far, only a few studies have focused on the systematic investigation of proteinaceous binders in laboratory painting models under different conditions in order to reveal possible hindrance effects on immunoassays due to ageing and pigment interaction [21, 23, 26, 36, 42, 43, 68]. These studies were centred mainly on ELISA investigations and are discussed in the next section, specifically dedicated to ELISA.

In consideration of the frequently occurring event of finding denatured/degraded proteins in immunoassays of heritage materials, as explained above, criteria for primary antibody selection requires particular mention. Antibodies commercially available are tailored for biotechnology and clinical applications and have been developed specifically for historical materials only rarely and are restrictedly to research studies [45, 69]. This fact limits both the choice of detectable antigens and sensitivity of the assay for non-biological samples. Antibodies against denatured proteins can offer better chances of investigating degraded samples [36]. It is, then, possible to choose between polyclonal and monoclonal primary antibodies. Polyclonal antibodies are produced in the serum of an immunized animal by different B cells and are directed against different epitopes of the antigen. Monoclonal antibodies are derived from single antibody-producing cells immortalized by fusion to a B lymphocyte tumor cell line. This class of antibodies is specific for a single epitope of the antigen. Multiple epitope recognition of polyclonal antibodies guarantees high affinity (avidity) against the antigen and increases the chances of detecting modified proteins (sensitivity); this, however, may limit assay specificity [55]. Monoclonal antibodies are, instead, highly specific but have less affinity. It is best to find the optimal compromise between antibody specificity and affinity as a function of the analytical needs. For example, high specificity is required for distinguishing biological origin of a protein in order to provide historical information on the derivation and the use of a particular proteinaceous material [23] or for authentication purposes [15]. On the other hand, to ascertain, for example, the presence of collagen (animal glue) in painting samples, species specificity is unnecessary in consideration of the ancient practise of mixing materials of different biological origin for preparation of animal glues [70].

Eventually, it is worth noting that immunologic techniques are able to identify only the searched antigen against which the used primary antibody is raised; conversely, they remain insensitive to all the other antigens possibly present in the sample. Such a limit is particularly relevant in the case of unknown samples, as is common in heritage materials. In this sense, immunological methods have to be considered as a complementary tool to other analytical techniques for an exhaustive chemical characterization of art-historical materials.

2 ELISA

2.1 The ELISA Format

Immunoassays can be classified according to different formats [51, 55] which mainly consider homogeneous or heterogeneous assays and competitive or non-

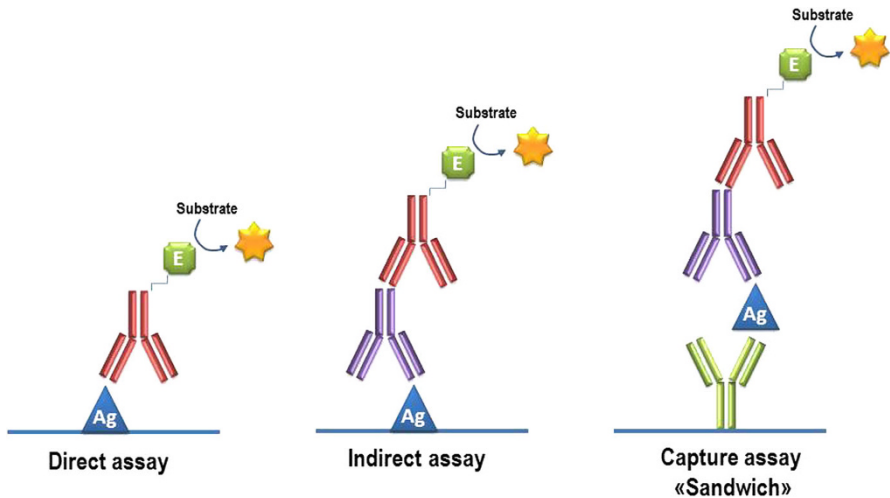


Fig. 2 ELISA formats, from *left to right*: direct, indirect and sandwich assay

competitive mechanisms. ELISA is the most widely adopted heterogeneous immunoassay format where the immuno-complex is separated from the immuno-reagents owing to its immobilisation on to a solid phase system (either the wells of a microtiter plate, cuvettes or tubes); this avoids any unspecific reaction by the unreacted reagents which are washed out before the detection step. The procedure requires the extraction into solution of the target antigen from the sample matrix.

Following such, the competitive and the non-competitive approaches are possible in ELISA. The latter is generally more sensitive [71] and can be further divided into direct, indirect, and sandwich formats [55]. **Figure 2** summarizes these three formats, configured for measuring the level of the target antigen in a sample. A full description of these formats is provided elsewhere [2, 55].

Briefly, in the direct format, the antigen is immobilised on to a solid phase and directly detected by an enzyme-conjugated primary antibody. The indirect format is, instead, a two-step method; it uses a primary antibody against the antigen while a secondary enzyme-conjugated antibody, specific to the primary one, is used for detection of the immuno-complex. In the sandwich format, the antigen is captured by a first antibody which is anchored to the solid phase system; then, a detection-labelled antibody is reacted with the bound antigen to allow detection. The sandwich format requires that the antigen contains at least two antigenic epitopes capable of binding to the capture and the detection antibodies; this limits the assay to relatively large antigens.

The indirect format is generally preferred over the direct approach due to its higher specificity and sensitivity but also as it is simpler and more flexible than the double antibody sandwich ELISA since it avoids the need of generating enzyme-antibody conjugates for each antigen to be detected.

Dot-ELISA is a further variant derived from immunoblotting techniques [72] in which proteins are 'dotted' directly onto a membrane and reacted with the antigen-

specific antibody which can be labelled with an enzyme (direct format) or recognised by a secondary tagged antibody (indirect format). The addition of the corresponding chromogenic substrate develops colour dots on the solid phase which are visually read or measured by either colorimetric or densitometric analysis after image digitalization [42, 43].

It is significant that all the applications of both conventional [19–21, 23, 26, 34–36, 40, 45] and dot-ELISA [42, 43] to heritage materials reported in literature in the last decade rely on the indirect format, mainly because it offers the best compromise with respect to specificity, sensitivity and affordability (simplicity and versatility).

2.2 ELISA Protocols for Heritage Materials

Irrespective of the approach, the development of an ELISA protocol requires optimization of different parameters, above all those influencing the equilibrium of the immuno-complex formation, such as: antibody specificity and sensitivity, antibody dilutions, incubation time and temperature and enzyme label/substrate pair; also, washing solution, buffer solution and blocking solution need to be tested [55]. Optimization is carried out to obtain high absorbance values at the lowest background signal. There is a variety of choice for these parameters which are reported in previously highlighted literature concerning applications in heritage science. However, given the choice, all manuals recommend performing in-house titration tests of reagents and cross-checking of incubation parameters in order to optimize the immunological protocol specifically for the needed application; this is because immuno-response may vary greatly from one stock of reagents to another and from one system to another.

As an example of evaluation of an immunologic procedure, Fig. 3 reports the results from tests of assay specificity and sensitivity for the immunodetection of bovine β -casein performed on samples of aged laboratory models of an easel painting made with bovine milk, chicken egg and animal glue as a binder, both pure and in the presence of different pigments [36]; the ELISA calibration curve obtained from antigen standard solutions is also shown and it gives a further estimation of the immunoassay sensitivity.

Preliminarily to all immunologic protocols, analyte *extraction* from the sample matrix is a requisite for ELISA. Note that dealing with non-biological matrices, with a variety of chemical and physical properties, means that the extraction efficiency is not predictable; thus, the procedure must be developed from the perspective of having the widest applicability for extraction and determination of any protein possibly present in unknown samples. As shown in Table 1, the largest number of applications of ELISA to heritage materials consists in the analysis of paintings. Painting materials can be very complex and heterogeneous at the micrometric level and, what is more, they usually display a composition mainly made up of inorganic compounds (pigments and fillers), whilst proteins are only a minor fraction [60]. Furthermore, natural ageing over centuries and the catalytic action of light and of metal cations from the inorganic matrix lead to important molecular modifications (see Sect 1.3) which strongly affect protein solubility. Consequently, antigen concentration available in solution to the immunoassay depends on the sample

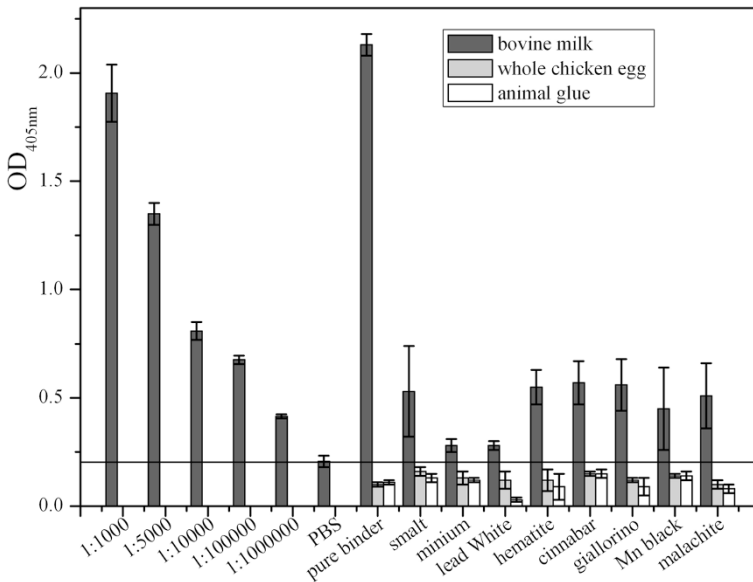


Fig. 3 ELISA calibration curve and test of antibody specificity performed for the development of an ELISA protocol for the immunodetection of bovine β -casein in paintings (see text). An indirect ELISA format was used combined with the alkaline phosphatase reporting system. Results are expressed as optical density (OD) at 405 nm $OD_{\lambda = 405\text{nm}}$ (reproduced from [36], by permission of Springer-Verlag © 2010)

extraction step. In literature, different extraction procedures have been reported to be successful for protein immunodetection in ancient painting materials, all making use of extraction in a basic buffer. [Table 2](#) gives an overview of the currently used approaches together with some information on the ELISA format and protocol respectively applied.

Another important aspect influencing assay specificity is the use of an appropriate *blocking solution* which has the function of saturating unspecific solid phase sites, avoiding unspecific bonding of the primary antibody. Normally, blocking solutions are made with proteins which compete with the antibody for attachment to the solid phase. Of course these blocking solutions should not contain any antigen recognised by the primary antibody. Non-specific antibody adsorption can be also avoided using non-ionic detergents [55]. [Table 2](#) summarizes blocking solutions reported in the immunologic studies of heritage materials here reviewed.

Typically, the immunologic protocol for indirect ELISA used in these applications is composed of the following steps:

- Step 1 Protein extraction from the sample;
- Step 2 Binding of the extracted proteins to the surface of the microtiter wells;
- Step 3 Addition of the blocking solution to saturate the unspecific sites in order to avoid false positive results;
- Step 4 Addition of the primary antibody and incubation to allow binding between the antibody and the antigen;

Table 2 Extraction conditions and blocking solutions for protein analysis in painting materials by ELISA

Elution buffer (extraction conditions)	Reporting system	Blocking solution	ELISA format [references]
10 mM Tris-HCl, 1 mM EDTA, 6 M urea, 1 % SDS—pH 7.4 (incubation for 30 min at RT)	Alkaline phosphatase/p-nitrophenyl phosphate	Powdered skim milk/ sea block buffer	Indirect ELISA [19, 20]
PBS—pH 7.4 (sonication for 4 h followed by incubation for 48 h at RT)	Alkaline phosphatase/p-nitrophenyl phosphate	Goat serum	Indirect ELISA [23]
50 mM Ambi/TFE (1:1; heating at 60 °C for 1 h with repeated vortexing)	Horse radish peroxidase/ 3,30,5,50-tetramethylbenzidine	Sea block buffer or newborn calf serum	Indirect ELISA [26]
50 mM Tris-HCl, 50 mM EDTA, 10 mM dithiothreitol, 8 M urea, 0.1 % SDS—pH 7.6 (incubation for 3 days at RT)	Indirect labelling using biotin-streptavidin system with alkaline-phosphatase/p-nitrophenyl phosphate	Horse serum	Indirect ELISA [34]
6 M urea (vortexing at RT)	Alkaline phosphatase/5-bromo-4-chloro-3-indolyl phosphate + nitro blue tetrazolium	Fish gelatine	Dot-blot ELISA [42]
25 mM Tris, 6 M urea, 191 mM glycine, 868 mM SDS (vortexing at RT)	Alkaline phosphatase/5-bromo-4-chloro-3-indolyl phosphate + nitro blue tetrazolium	Powdered skim milk	Dot-blot ELISA [43]
0.1 M phosphate buffer—pH 7 (ultrasonication for 2 h)	Horse radish peroxides/ H ₂ O ₂ + methylene blue	Bovine serum albumin	Indirect ELISA with electrochemical detection [44]

Tris-HCl tris(hydroxymethyl)aminomethane hydrochloride, *EDTA* ethylenediaminetetraacetic acid, *Tris* tris(hydroxymethyl)aminomethane, *SDS* sodium dodecylsulfate, *PBS* phosphate saline buffer, *Ambi* ammonium bicarbonate, *TFE* trioroethanol, *RT* room temperature

- Step 5 Addition of the enzyme conjugated secondary antibody and incubation to permit binding between the primary and the secondary antibody;
- Step 6 Addition of the chromogenic or fluorogenic enzyme substrate;
- Step 7 Blocking of the colouring enzymatic reaction at a fixed time. This step is necessary since colouring also depends on the time for which the enzyme is left to be active.

Between each step, wells are thoroughly rinsed in order to remove any unbound reagent leading to unspecific reactions.

Thanks to ELISA sensitivity and specificity, the optimized procedures developed for the single antigen can, then, be applied in parallel on multiple aliquots of the extract of a micro-sample for testing different proteins (multiplex detection). As an example of multiplex analysis in a single painting micro-sample (~ 1 mg), Fig. 4 reports specific recognition of bovine β -casein, chicken ovalbumin and egg yolk in

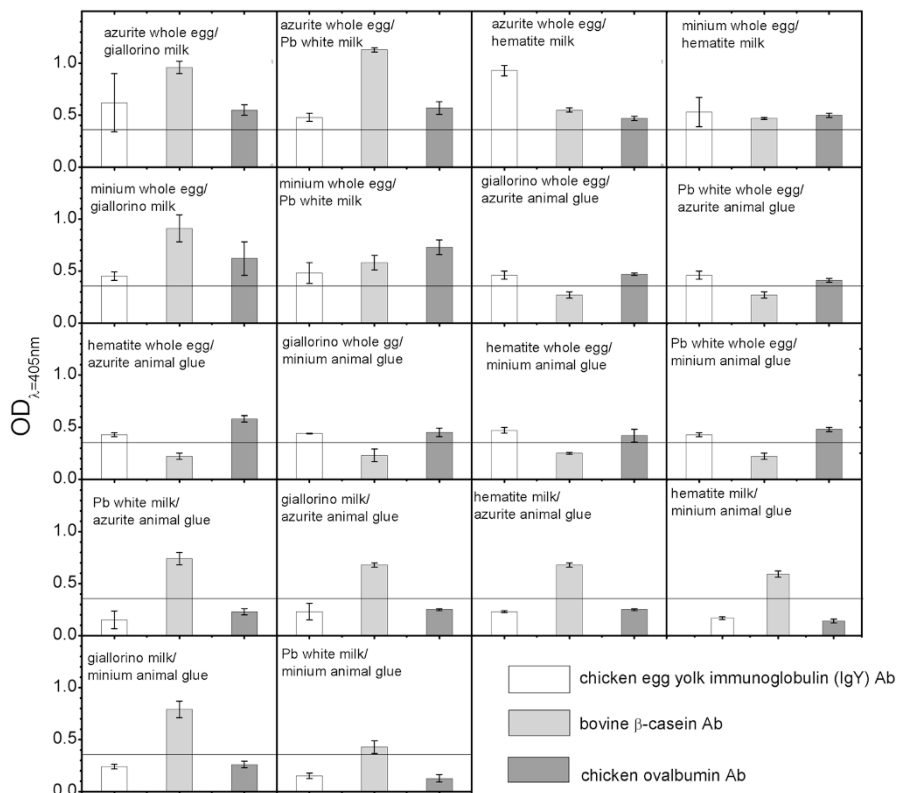


Fig. 4 Multiplex ELISA results (absorbance expressed as optical density at 405 nm $OD_{\lambda=405\text{nm}}$) obtained for protein analysis in micro-samples from aged bi-layer easel painting models treated with antibodies against chicken egg yolk immunoglobulin (IgY), bovine β -casein and chicken ovalbumin. An indirect ELISA format was used combined with the alkaline phosphatase reporting system. Standard deviation (SD) has been calculated performing three replicates for each sample. The *black line* shows the limit of detection determined for the three proteins

bi-layer model paints aged at 40° and relative humidity (RH) 85 % for 3 months according to reported protocols [23, 36]. In a similar way, ELISA results from multiple protein identification in historical samples following a similar analytical procedure are shown in Fig. 5, reproduced from [26]. Attempts for systematic investigations of the effects of ageing and of binder/pigment interactions on ELISA response are reported only in a few research papers [21, 23, 26, 36, 42, 43, 68]. These studies found a suppression of the ELISA signal depending on the ageing protocols applied to the binder (both natural and accelerated). A further reduction of the immuno-response was observed in the presence of pigments, in particular, when a basic pH environment is developed [26, 42]. This behaviour is mainly due to the direct role that metal ions have in protein degradation processes [26], although an effect of pigments without metal cations, such as bone black and cochineal red-violet lake, seems to be also present [68]. However, these sparse results do not allow inferring any clear specific action of different pigments/inorganic substrates on

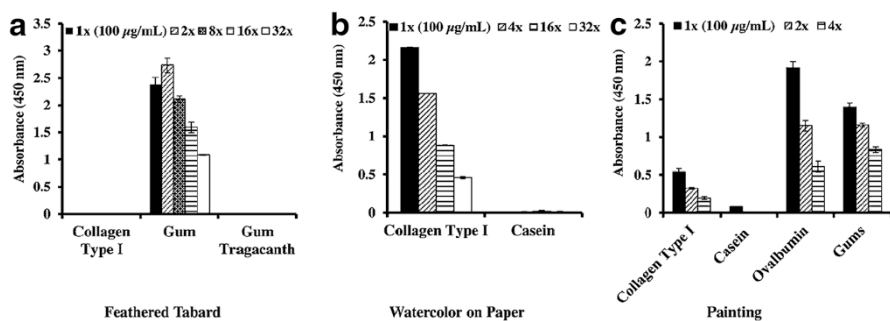


Fig. 5 Results of multiplex ELISA obtained for the identification of binders (shown in the x-axis) in micro-samples from historical materials: **a** A twelve- to thirteenth-century feathered tabard, **b** a watercolor drawing and **c** a fourteenth-century double-sided processional banner (reproduced from [26], by permission of the Royal Society of Chemistry). The legends show protein concentration in the analysed solutions. The absorbance readings of the samples are plotted after subtraction of the threshold values. In this example, an indirect ELISA format was used combined with the horse radish peroxidase reporting system (absorbance measured at 450 nm)

immunoassays in heritage materials (both as degradation promoters or immunoassay inhibitors) and deeper investigations on the subject are needed.

It is worth noting that the capability of ELISA in resolving a complex mixture of proteins and distinguishing biological origin in degraded samples provides significant basic information about materials and artistic techniques otherwise not achievable by conventional chromatographic and spectroscopic analysis. Only advanced biomolecular techniques, such as proteomics and DNA analysis, can compete with ELISA for sensitivity and specificity, but versatility and cost affordability of this immunoassay certainly open new perspectives for the investigation of art-historical materials in conservation laboratories.

3 IFM

3.1 IFM for Heritage Materials

Fluorescence is the emission of radiation following absorption of light (typically at lower wavelengths) by an atom or a molecule that returns to its ground state. The difference between excited and emitted wavelengths makes fluorescence a very sensitive analytical tool for detection of molecules with fluorescent properties. Fluorescence microscopy couples the sensitivity of fluorescence measurements with the spatial resolution of a microscope [73] and it is a good candidate for the detection and imaging of proteinaceous binders and, in general, more so of fluorescent organic components in cross-sections of polychrome samples. Protein fluorescence is usually excited from 280 to 365 nm while emission falls in the visible range [74, 75]. Unfortunately, the low specificity of the endogenous fluorescence of proteinaceous binders and the variability of the spectral properties due to ageing and to pigment interferences make binder identification by fluorescence techniques not straightforward.

As an alternative, protein tagging by visible stains or by fluorescent reporters has been used to image binder distributions in painting stratigraphies ([76, 77] and references therein). Nevertheless, this approach has the limit of not allowing for unambiguous protein identification. To overcome this limit, immunofluorescence uses fluorescent-tagged antibodies to specifically detect proteins and image their distribution by fluorescence microscopy and micro-spectrofluorimetry techniques [53, 56, 78].

Pioneering studies exploring the application of immunofluorescence microscopy to painting cross-sections [17–19] have shown promising results for future developments in heritage science. Nevertheless, so far, only a few scientific papers have been published on this thematic [21, 27, 33, 41]. This is partly due to the scarceness of combined biotechnological and micro-spectroscopy instrumental resources in conservation science laboratories, but also to some analytical drawbacks that affect the technique which are strictly related to the type of investigated materials (not biological) and which still have to be completely solved. These include unspecific fluorescence due to sample autofluorescence and to optical artefacts [27, 33, 41, 53], unspecific immunoreactions on the porous matrix of the sample and cross-section swelling as a consequence of the use of solvents during the immunologic protocol [17, 18]. In the following paragraph, an overview of the immuno-detection schemes and analytical solutions adopted to investigate heritage materials by IFM is given. Most of them were already anticipated in a research article in 2010 [21] but, since then, no improved applications of IFM to heritage materials have been published.

3.2 Immunological Protocols for IFM Applied to Heritage Materials

Immunologic protocols for application of IFM to heritage materials are all based on the indirect assay format [18, 19, 21, 27, 33, 41]. They follow the same steps of indirect ELISA (see Sect. 2.1) with the difference being that the sample is not extracted into solution but is, instead, embedded in a synthetic resin. The immuno-complex formation takes place at the exposed surface of the sample where protein epitopes are accessible to the primary antibody for immunoreaction. The secondary antibody, specific to the primary one, is conjugated with a fluorophore which, upon proper light excitation, emits, allowing for sensitive detection of the targeted molecule and, at the same time, to localize it on the sample surface [73]. Until now, chicken ovalbumin, bovine casein and animal collagen have been tested for the search of the single protein (no multiplex) by IFM both in painting models and real samples.

Standardization of the IFM methodology is much more complicated and time consuming than ELISA since it requires optimization of both the immunological protocol and the detection strategy. The former includes testing specificity and cross-reactivity of the immuno-reagents at different working conditions (incubation temperature and time, antibody concentrations, etc.) by systematic analysis of samples from laboratory models prepared as cross-sections with different binder/pigment/substrate combinations; the latter requires an accurate evaluation of the fluorophore along with the choice of the most effective detection scheme (microscope set-up). To these last two aspects, crucial for successful IFM investigations, a

specific paragraph has been dedicated in the following. Sample preparation and choice of the embedding synthetic resin are also important since they condition surface properties of the cross-section and, at the same time, define its stability during the immunologic protocol. The use of both epoxy and acrylic resins has been reported in literature [18, 19, 21, 27, 33, 41] where no light emission from the resins was observed interfering with immunofluorescence detection; as a drawback, swelling of water-soluble materials was sometimes observed after exposure to aqueous solutions during incubation [18, 19].

Concerning the immunologic procedure, the issue of unspecific antibody reactions are particularly critical in IFM with respect to ELISA. In fact, the heterogeneous porous matrix characterizing heritage materials may favour unspecific interactions with the immuno-reagents at the sample surface. The use of a blocking solution is, therefore, an indispensable step to saturate unspecific sites, combined with accurate tests of antibody specificity. Goat serum, bovin serum albumin and fat dry milk have been proposed as blocking solutions in IFM protocols [21, 27, 33, 41].

3.3 Immunofluorescence Detection

A major issue in IFM is the sensitive detection of the specific fluorescence emitted by the targeted protein avoiding interferences from unspecific fluorescence and spurious light. Given that unspecific immunofluorescence can be inhibited through focused strategies in the immunological procedure (use of blocking solution, control of antibody specificity, test of incubation temperature, etc.), unspecific fluorescence and interfering spurious light may derive from different processes: autofluorescence phenomena of the sample, light scattering at the sample surface, and infiltration of “room” light which enhance background noise [53]. Both autofluorescence and spurious light interference can be easily checked acquiring images of the sample before and after the immunostaining under the same experimental conditions of the microscope used for immunofluorescence detection. Solutions to this interference can be adopted at two different levels: choice of the fluorophore and fluorescence detection set-up.

The most significant properties of fluorescent molecules for the use as immunolabels are [57]: (1) biocompatibility for antibody conjugation, (2) photochemical stability, (3) a high molar absorption coefficient and a high fluorescence quantum yield (to be maintained also after bio-conjugation), (4) position and shape of the absorption and emission bands and (5) the Stoke shift. The Stoke shift is the difference between the spectral position of the absorption and the luminescence maxima for the same electronic transition; it, therefore, determines the overlap between the absorption and the emission bands and is relevant for the spectral separation of the fluorescence emission from the excitation light and for an efficient detection of the emission signal.

Traditional organic dyes used as fluorescent labels are fluorescein isothiocyanate (FITC, excitation with blue light, 490–495 nm; emission at 520–530 nm) and rhodamine derivative compounds such as tetramethyl rhodamine isothiocyanate (TRITC, excitation with green light, 525–540 nm; emission at 615–630 nm). Other

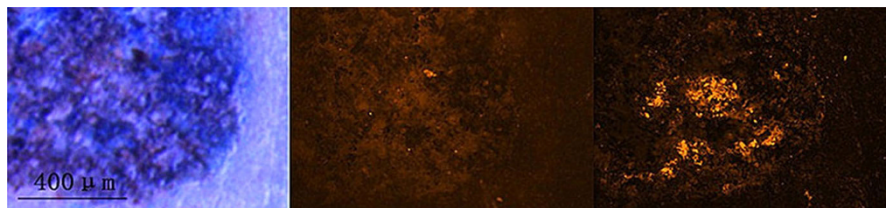


Fig. 6 IFM detection of egg albumin in a sample from a Qin Shihuang's terracotta warrior (from *left to right*: optical microscope $\times 100$ image, fluorescence $\times 100$ images before and after immuno-reaction) reprinted from [41], © 2014 Elsevier Masson SAS. All rights reserved

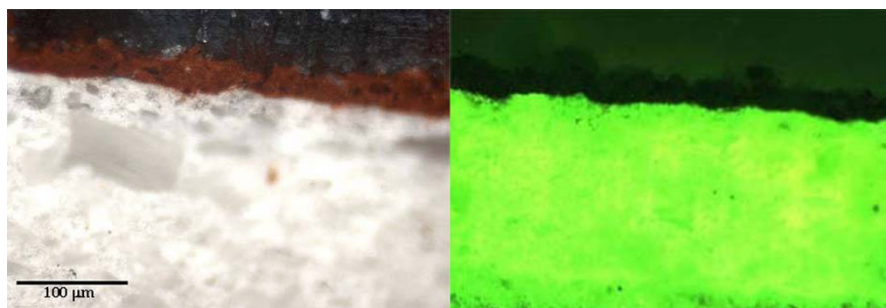


Fig. 7 *Left* optical microscope (OM) image ($\times 160$) and *right*, fluorescence image ($\times 160$)—at the same instrumental conditions of the epifluorescence microscope used for FITC detection) of a layer of hematite in egg-tempera on a gypsum/glue preparation before the immunologic protocol

new dyes have been recently introduced, such as the “Alexa” [79] or the “Dylight” [80] fluorophore series for their improved photophysical properties. As an example, Fig. 6 shows the fluorescence images of a polychrome sample from a Qin Shihuang's terracotta warrior before and after the immunostaining with an AlexaFluor 594 tagged secondary antibody for the search of chicken ovalbumin [41]. Comparing the two fluorescence images at the same position of the sample, the emission of a red–orange radiation is clearly observed after the immunologic protocol.

When using conventional wide-field fluorescence microscopes, the use of fluorophores with a reduced Stoke shift, as those above mentioned, may suffer from intense generation of spurious light from the inorganic substrate. This typically occurs when studying painting stratigraphies, as shown by Fig. 7, and it has been attributed to scattering phenomena of the excitation light incident on the sample surface [33]. In fact, the closeness in working energy range of the microscope optics used in excitation and in emission spoils detector shielding from the incident light. In order to avoid this spurious effect, new high-performance fluorescent labels based on nanocrystal inorganic chromophores are now available. In particular, quantum dots (QDs, nanoparticles of II/VI and III/V semiconductors) are the most promising materials for life science applications due to their proven photochemical and optical properties [57]: photochemical stability, high fluorescence yield, long lifetime, broadband absorption, and sharp and intense emission band. These properties are

explained by the strong confinement of electrons when the radius of the particle is smaller to the exciton Bohr radii and can be controlled by changing the particle composition, particle size and size distribution. In particular, the increased Stoke shift of QDs with respect to conventional dyes and tunability of the emission band allows improving suppression of spurious light and hinders interferences from sample autofluorescence.

Improved suppression of unspecific light is further achieved through optimization of the optical elements (objective, filters, detector, etc.) and microscope configuration. Most of the fluorescence microscopes used for diagnostic and research applications are typically wide field epifluorescence microscopes where excitation of the fluorophore and detection of the fluorescence are done through the same light path. This set-up offers the advantage over transmission microscopy for which, in the case of thin sections, only a small percentage of the exciting light is reflected off the sample along the optical path of fluorescence, improving the signal-to-noise ratio.

In recent years, the compelling need to develop new and improved fluorescence imaging systems for high-resolution and three-dimensional (3D) studies in biochemistry and cell biology gave birth to new instrumental and technological solutions that, today, have matured as super-resolution microscopy techniques which are capable of going beyond the diffraction limit [81]. Before them, laser scanning confocal fluorescence microscopy (LSCFM) has long been the most accredited technique in advanced bio-imaging studies [78]. Briefly, in LSCFM, a tightly focused spot of laser light is used to scan the sample and a pinhole in the optical path allows only light from the focal plane to arrive to the detector; while the light out of the focal plane is discarded. In this way it is possible to obtain optical sections of the specimen and reconstruct its 3D structure from the detected light independent of the position of the scanning spot. This approach is particularly valuable in the study of bulk samples, like cross-sections, to avoid detection of the excitation light reflected at the sample surface (as that shown in Fig. 7). The coupling of a laser scanning confocal microscope with a spectral detection system of the emitted light further improves recognition of specific fluorescence. This instrumental solution is fully exploitable when combined with the use of QD fluorophores. In fact, as shown by Fig. 8, the QDs' increased Stoke shift and their

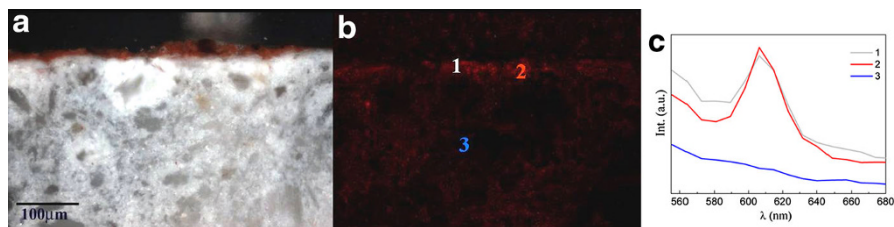


Fig. 8 Cross-section of **a** normal light and **b** fluorescence confocal microscope images (160×) from a fourteenth-century mural painting micro-sample after application of the immunologic protocol for the search of chicken ovalbumin. Protein tagging was performed with QD605 fluorophores excited at 458 nm. **c** Emission spectra collected in different fluorescent areas of the sample shown in (b). The typical QD emission at 605 nm in correspondence of the painting *red layer* allows for the unambiguous distinction between specific fluorescence and spurious background light

sharper emission band with respect to conventional organic fluorophores make easily discernible specific immunofluorescence from the light background (Fig. 8c).

At present, although QD-conjugated antibodies are commercially available and laser scanning confocal fluorescence microscopes are of daily use in many laboratories, only one application of these analytical resources to the investigation of paintings is reported in literature [21]; conversely, other recent IFM studies report about the use of conventional organic fluorophores coupled to epifluorescence microscopes despite the mentioned drawbacks [19, 27, 33, 41].

Looking to the recent advances gained in IFM relative to other disciplines, new perspectives for further developments in the field of heritage science open up. In particular, the idea of approaching simultaneous detection of more proteins in polychrome stratigraphies is very attracting. This result has been already obtained in imaging studies by chemiluminescent immunochemical microscopy [22]. However, achieving this ultimate goal by IFM poses several difficulties in terms of availability of proper primary and secondary antibodies and choice of antibody/fluorophore bio-conjugates. In fact, IFM multiplex protein recognition imposes the use of primary antibodies harvested from different species (goat, mouse, rabbit, rat, etc.) to avoid cross reactivity of the secondary antibodies. This fact limits the choice of commercial primary antibodies suitable for heritage materials. Furthermore, different secondary antibody/fluorophore bio-conjugates must be generated, having different emission wavelength for parallel fluorescence detection of multiple targets. Alternatively, direct primary antibody/fluorophore bio-conjugation can be performed. However, the loss of immunoassay specificity is a major drawback for both the solutions and many efforts still have to be made to obtain new results in this direction.

4 Summary and Future Perspectives

This review provides an overview of the most recent applications of ELISA and IFM as versatile, although very specific, tools for identification and localization of proteins in heritage materials.

Today, the proven analytical qualities of ELISA of being highly specific, sensitive and reproducible combined with the properties of being simple, fast and affordable explain the high popularity of this technique in biochemical and medical disciplines. These are, also, the reasons which make ELISA very promising for routine applications in conservation science laboratories. In fact, as shown by the examples detailed in this chapter, it can be easily implemented and used by non-specialised personnel for the multiplex recognition of proteins in historical materials [82].

On the other hand, the recent progress in organic chemistry and materials science towards the development of new fluorescent labels [83] and novel bio-conjugation strategies [84], accompanied by technical improvements achieved in microscopy [81], make immunofluorescence microscopy a promising analytical tool in heritage science [21, 33]. Analytical potentials of IFM are particularly relevant for the investigation of organic components in polychrome cross-sections, allowing further

insight to be gained into the artist's technique through the compositional study of the sample stratigraphy [85].

In spite of these considerations, until now, only a few research groups have been involved in the development of validated analytical protocols based on ELISA and IFM. In particular, many challenges still exist which hinder the diffusion of IFM in heritage science, and, thus, a more extensive experimentation of the technique is needed to make it a consolidate tool. To this purpose and also to push ELISA advancement in this field, research activities and resources must be directed towards (1) extensive experimentation of immunological protocols for different heritage materials in order to evidence analytical interferences of the matrix (either organic or inorganic) with the immunoassay; (2) enlargement of the number of commercially available antibodies dedicated to heritage materials to provide common standards to all laboratories for data comparison and exchange; (3) experimentation of new immunoassay schemes, immunoreagents and detection strategies, particularly for IFM, in order to overcome analytical obstacles here reviewed; (4) exploration of alternative imaging techniques consistently based on specific recognition of proteins for multiplex imaging.

Acknowledgments The authors acknowledge for funding support the CHARISMA project (GA228330)—funded by the European Union FP7-Research Infrastructure programme—and the project “Sviluppo delle attività di ricerca, valutazione e tutela conservativa” of the Regione Umbria—“Progetto 1 del Primo atto integrativo all'APQ: Tutela e prevenzione dei beni culturali”.

References

- Gosling JP (1990) A decade of development in immunoassay methodology. *Clin Chem* 36:1408
- Wild D (2013) *The immunoassay handbook*, 4th edn. Elsevier, Amsterdam
- Gettens RJ, Stout GL (1966) *Painting materials: a short encyclopaedia*. Dover Publication, New York
- Mills JS, White R (eds) (1994) *The organic chemistry of museum objects*, 2nd edn. Butterworth-Heinemann, London
- Colombini MP, Modugno F (2009) Organic materials in art and archaeology. In: Colombini MP, Modugno F (eds) *Organic mass spectrometry in art and archaeology*, Chapter 1. Wiley, Chichester
- Madariaga JM (2015) Analytical chemistry in the field of cultural heritage. *Anal Methods* 7:4848
- Sgamellotti A, Brunetti BG, Miliani C (2014) *Science and art : the painted surface*. The Royal Society of Chemistry, London, UK
- Domenech-Carbò MT (2008) Novel analytical methods for characterising binding media and protective coatings in artworks. *Anal Chim Acta* 621:109
- Colombini MP, Andreotti A, Bonaduce I, Modugno F, Ribechini E (2010) Analytical strategies for characterizing organic paint media using gas chromatography/mass spectrometry. *Acc Chem Res* 43:715
- Llucheras A, Bonaduce I, Andreotti A, Colombini MP (2010) GC/MS analytical procedure for the characterization of glycerolipids, natural waxes, terpenoid resins, proteinaceous and polysaccharide materials in the same paint microsample avoiding interferences from inorganic media. *Anal Chem* 8:376
- Leo G, Cartechini L, Pucci P, Sgamellotti A, Marino G, Birolo L (2009) Proteomic strategies for the identification of proteinaceous binders in paintings. *Anal Bioanal Chem* 395:2269
- Kuckova S, Hynek R, Kodicek M (2007) Identification of proteinaceous binders used in artworks by MALDI-TOF mass spectrometry. *Anal Bioanal Chem* 388:201
- Dallongeville S, Koperska M, Garnier N, Reille-Taillefert G, Rolando C, Tokarski C (2011) Identification of animal glue species in artworks using proteomics: application to a 18th century gilt sample. *Anal Chem* 83:9431

14. Calvano CD, van der Werf ID, Palmisano F, Sabbatini L (2015) Identification of lipid- and protein-based binders in paintings by direct on-plate wet chemistry and matrix-assisted laser desorption ionization mass spectrometry. *Anal Bioanal Chem* 407:1015
15. Albertini E, Raggi L, Vagnini M, Sassolini A, Achilli A, Marconi G, Cartechini L, Veronesi F, Falcinelli M, Brunetti B, Miliani C (2011) Tracing the biological origin of animal glues used in paintings through mitochondrial DNA analysis. *Anal Bioanal Chem* 399:2987
16. Johnson M, Packard E (1971) Methods used for the identification of binding media in Italian paintings of fifteenth and sixteenth centuries. *Stud Conserv* 16:145
17. Kockaert L, Gausset P, Dubi-Rucquoy M (1989) Detection of ovalbumin in paint media by immunofluorescence. *Stud Conserv* 34:183
18. Raminéz-Barat B, de la Vinã S (2001) Characterization of proteins in paint media by immunofluorescence: a note on methodological aspects. *Stud Conserv* 46:282
19. Heginbotham A, Millay V, Quick M (2006) The use of immunofluorescence microscopy (IFM) and enzyme-linked immunosorbent assay (ELISA) as complementary techniques for protein identification in artists' materials. *J Am Inst Conserv* 45:89
20. Mazurek J, Heginbotham A, Schilling M, Chiari G (2008) Antibody assay to characterize binding media in paint. *ICOM Comm Conserv* 2:678
21. Cartechini L, Vagnini M, Palmieri M, Pitzurra L, Mello T, Mazurek J, Chiari G (2010) Immunodetection of proteins in ancient paint media. *Acc Chem Res* 43:867
22. Sciuotto G, Dolci LS, Guardigli M, Zangheri M, Prati S, Mazzeo R, Roda A (2013) Single and multiplexed immunoassays for the chemiluminescent imaging detection of animal glues in historical paint cross-sections. *Anal Bioanal Chem* 405:933
23. Palmieri M, Vagnini M, Pitzurra L, Brunetti BG, Cartechini L (2013) Identification of animal glue and hen-egg yolk in paintings by use of enzyme-linked immunosorbent assay (ELISA). *Anal Bioanal Chem* 405:6365
24. Arslanoglu J, Zaleski S, Loike J (2011) An improved method of protein localization in artworks through SERS nanotag-complexed antibodies. *Anal Bioanal Chem* 399:2997
25. Sciuotto G, Prati S, Mazzeo R, Zangheri M, Roda A, Bardini L, Valenti G, Rapino S, Marcaccio M (2014) Localization of proteins in paint cross-sections by scanning electrochemical microscopy as an alternative immunochemical detection technique. *Anal Chim Acta* 831:31
26. Lee HY, Atlasevich N, Granzotto C, Schultz J, Loike J, Arslanoglu J (2015) Development and application of an ELISA method for the analysis of protein-based binding media of artworks. *Anal Methods* 7:187
27. Magrini D, Bracci S, Sandu ICA (2013) Fluorescence of organic binders in painting cross-sections. *Procedia Chem* 8:194–201
28. Pinna D, Galleotti M, Mazzeo R (2009) Scientific examination for the investigation of paintings: a handbook for conservators-restorers. Ed. Centro Di, Firenze
29. Sciuotto G, Litti L, Lofrumento C, Prati S, Ricci M, Gobbo M, Roda A, Castellucci E, Meneghetti M, Mazzeo R (2013) Alternative SERS probes for the immunochemical localization of ovalbumin in paintings: an advanced mapping detection approach. *Analyst* 138:4532–4541
30. Perets EA, Indrasekara ASDS, Kurmis A, Atlasevich N, Fabris L, Arslanoglu J (2015) Carboxy-terminated immuno-SERS tags overcome non-specific aggregation for the robust detection and localization of organic media in artworks. *Analyst* 140:5971–5980
31. Avci R, Schweitzer MH, Boyd RD, Wittmeyer JL, Terán Arce F, Calvo JO (2005) Preservation of bone collagen from the late cretaceous period studied by immunological techniques and atomic force microscopy. *Langmuir* 21:3584–3590
32. Lindgren J, Uvdal P, Engdahl A, Lee AH, Alwmark C, Bergquist C-E, Nilsson E, Ekström P, Rasmussen M, Douglas DA, Polcyn MJ, Jacobs LL (2011) Microspectroscopic evidence of cretaceous bone proteins. *PLoS ONE* 6(4):e19445
33. Vagnini M, Pitzurra L, Cartechini L, Miliani C, Brunetti BG, Sgamellotti A (2008) Identification of proteins in painting cross-sections by immunofluorescence microscopy. *Anal Bioanal Chem* 392:57–64
34. Klausmeyer PA, Albertson RP, Woodland RT, Schmidt MR, Blewett M (2009) FTIR and ELISA for the analysis of a Kees Van Dongen painting. *e-PS* 6:151
35. Scott DA, Warmlander S, Mazurek J, Quirke S (2009) Examination of some pigments, grounds and media from Egyptian cartonnage fragments in the Petrie Museum, University College London. *J Archaeol Sci* 36:923–932

36. Palmieri M, Vagnini M, Pitzurra L, Rocchi P, Brunetti BG, Sgamellotti A, Cartechini L (2011) Development of an analytical protocol for a fast, sensitive and specific protein recognition in paintings by enzyme-linked immunosorbent assay (ELISA). *Anal Bioanal Chem* 399:3011–3023
37. Dolci LS, Sciuotto G, Guardigli A, Rizzoli M, Prati S, Mazzeo R, Roda A (2008) Ultrasensitive chemiluminescent immunochemical identification and localization of protein components in painting cross-sections by microscope low-light imaging. *Anal Bioanal Chem* 392:29–35
38. Sciuotto G, Dolci LS, Buragina A, Prati S, Guardigli A, Mazzeo R, Roda A (2011) Development of a multiplexed chemiluminescent immunochemical imaging technique for the simultaneous localization of different proteins in painting micro cross-sections. *Anal Bioanal Chem* 399:2889–2897
39. Zangheri M, Sciuotto G, Mirasoli M, Prati S, Mazzeo R, Roda A, Guardigli M (2016) A portable device for on site detection of chicken ovalbumin in artworks by chemiluminescent immunochemical contact imaging. *Microchem J* 124:247–255
40. Mazurek J, Svoboda M, Maish J, Kawahara K, Fukakusa S, Nakazawa T, Taniguchi Y (2014) Characterization of binding media in Egyptian Romano portraits using enzyme-linked immunosorbent assay and mass spectrometry. *e-PS* 11:76
41. Hu W, Zhang K, Zhang H, Zhang B, Rong B (2015) Analysis of polychromy binder on Qin Shihuang's terracotta warriors by immunofluorescence microscopy. *J Cult Herit* 16:244
42. Gambino M, Cappitelli F, Cattò C, Carpen A, Principi P, Ghezzi L, Bonaduce I, Galano E, Pucci P, Birolo L, Villa F, Forlani F (2013) A simple and reliable methodology to detect egg white in art samples. *J Biosci* 38:397
43. Potenza M, Sabatino G, Giambi F, Rosi L, Papini AM, Dei L (2013) Analysis of egg-based model wall paintings by use of an innovative combined dot-ELISA and UPLC-based approach. *Anal Bioanal Chem* 405:691
44. Bottari F, Oliveri P, Ugo P (2014) Electrochemical immunosensor based on ensemble of nano-electrodes for immunoglobulin IgY detection: application to identify hen's egg yolk in tempera paintings. *Biosens Bioelectron* 52:403
45. Zheng Q, Wu X, Zheng H, Zhou Y (2015) Development of an enzyme-linked-immunosorbent-assay technique for accurate identification of poorly preserved silks unearthed in ancient tombs. *Anal Bioanal Chem* 407:3861–3867
46. Sela-Culang I, Kunik V, Ofiran Y (2013) The structural basis of antibody-antigen recognition. *Front Immunol* 4:302. doi:10.3389/fimmu.2013.00302
47. Akiba H, Tsumoto K (2015) Thermodynamics of antibody-antigen interaction revealed by mutation analysis of antibody variable regions. *J Biochem* 158:1–13
48. Moreira IS, Fernandes PA, Ramos MJ (2007) Hot spots—a review of the protein–protein interface determinant amino-acid residues. *Proteins* 68:803–812
49. Borrebaeck CAK (2000) Antibodies in diagnostics—from immunoassays to protein chips. *Immunol Today* 21:379
50. Hage DS (1995) Immunoassays. *Anal Chem* 67:455R
51. Blake C, Gould BJ (1984) Use of enzymes in immunoassay techniques. A review. *Analyst* 109:53
52. Porstmann T, Kiessig ST (1992) Enzyme immunoassay techniques. An overview. *J Immunol Methods* 150:5
53. Petty HR (2007) Fluorescence microscopy: established and emerging methods, experimental strategies, and applications in immunology. *Microsc Res Tech* 70:687
54. Lequin RM (2005) Enzyme immunoassay (EIA)/enzyme-linked immunosorbent assay (ELISA). *Clin Chem* 51:2415–2418
55. Crowther JR (2009) *The ELISA guidebook*, 2nd edn. Humana Press, Totowa, NJ
56. Giepmans BNG, Adams SR, Ellisman MH, Tsien RY (2006) The fluorescent toolbox for assessing protein location and function. *Science* 312:217
57. Resch-Genger U, Grabolle M, Cavaliere-Jaricot S, Nitschke R, Nann T (2008) Quantum dots versus organic dyes as fluorescent labels. *Nat Methods* 5:763–775
58. Rino J, Braga J, Henriques R, Carmo-Fonseca M (2009) *Frontiers in fluorescence microscopy Int. J Dev Biol* 53:1569
59. Schermelleh L, Heintzmann R, Leonhardt H (2010) A guide to super-resolution fluorescence microscopy. *J Cell Biol* 190:165
60. Colombini MP, Modugno F (2004) Characterisation of proteinaceous binders in artistic paintings by chromatographic techniques. *J Sep Sci* 27:147
61. Lai MC, Topp EM (1999) Solid-state chemical stability of proteins and peptides. *J Pharm Sci* 88:489–500

62. Karpowicz A (1981) Ageing and deterioration of proteinaceous media. *Stud Conserv* 26:153–160
63. Bonaduce I, Cito M, Colombini MP (2009) The development of a gas chromatographic–mass spectrometric analytical procedure for the determination of lipids, proteins and resins in the same paint micro-sample avoiding interferences from inorganic media. *J Chromatogr A* 1216:5931
64. Leo G, Bonaduce I, Andreotti A, Marino G, Pucci P, Colombini MP, Birolo L (2011) Deamidation at asparagine and glutamine as a major modification upon deterioration/aging of proteinaceous binders in mural paintings. *Anal Chem* 83:2056
65. Duce C, Bramanti E, Ghezzi L, Bernazzani L, Bonaduce I, Colombini MP, Spepi A, Biagi S, Tine MR (2013) Interactions between inorganic pigments and proteinaceous binders in reference paint reconstructions. *Dalton Trans* 42:5975
66. Ghezzi L, Duce C, Bernazzani L, Bramanti E, Colombini MP, Tiné MR, Bonaduce I (2015) Interactions between inorganic pigments and rabbit skin glue in reference paint reconstructions. *J Therm Anal Calorim* 122:315–322
67. Arslanoglu J, Schultz J, Loike J, Peterson K (2010) Immunology and art: using antibody-based techniques to identify proteins and gums in artworks. *J Biosci* 35:3
68. Ren F, Atlasevich N, Baade B, Loike J, Arslanoglu J (2015) Influence of pigments and protein aging on protein identification in historically representative casein-based paints using enzyme-linked immunosorbent assay. *Anal Bioanal Chem*. doi:10.1007/s00216-015-9089-0
69. Zevgiti S, Sackarellos C, Sackarellos-Daitsiotis M, Ioakimoglou E, Panou-Pomonis E (2007) Collagen models as a probe in the decay of works of art: synthesis, conformation and immunological studies. *J Pept Sci* 13:121–127
70. Brunello F (1982) *Il libro dell'arte*, Neri, Pozza edn. Vicenza, Italy
71. Ishikawa E, Hashida S, Kohno T (1991) Development of ultrasensitive enzyme immunoassay reviewed with emphasis on factors which limit the sensitivity. *Mol Cell Probes* 5:81–95
72. Towbin H, Gordon J (1984) Immunoblotting and dot immunobinding—current status and outlook. *J Immunol Method* 72:313–340
73. Lichtman JW, Conchello JA (2005) Fluorescence microscopy. *Nat Methods* 2:910–919
74. Matteini P, Camaiti M, Agati G, Baldo MA, Mutoc S, Matteini M (2009) Discrimination of painting binders subjected to photo-ageing by using microspectrofluorometry coupled with deconvolution analysis. *J Cult Herit* 10:198–205
75. Nevin A, Anglos D, Cather S, Burnstock A (2008) The influence of visible light and inorganic pigments on fluorescence excitation emission spectra of egg-, casein- and collagen-based painting media. *Appl Phys A* 92:69–76
76. Sandu ICA, Roque ACA, Matteini P, Schaefer S, Aagati G, Correia CR, Viana JFFP (2012) Fluorescence recognition of proteinaceous binders in works of art by a novel integrated system of investigation. *Microsc Microanal* 75:316–324
77. Sandu ICA, Schaefer S, Magrini D, Bracci S, Roque ACA (2012) Cross-section and staining-based techniques for investigation of organic materials in painted and polychrome works of art—a review. *Microsc Microanal* 18:860–865
78. Földes-Papp Z, Demel U, Tilz GP (2003) Laser scanning confocal fluorescence microscopy: an overview. *Int Immunopharmacol* 3:1715–1729
79. Panchuk-Voloshina N, Haugland RP, Bishop-Stewart J, Bhalgat MK, Millard PJ, Mao F, Leung W-Y, Haugland RP (1999) Alexa Dyes, a series of new fluorescent dyes that yield exceptionally bright, photostable conjugates. *J Histochem Cytochem* 47:1179–1188
80. Sarkar P, Sridharan S, Luchowski R, Desai S, Dworecki B, Nlend M, Gryczynski Z, Gryczynski I (2010) Photophysical properties of a new DyLight 594 dye. *J Photochem Photobiol, B* 98:35–39
81. Schermelleh L, Heintzmann R, Leonhardt H (2010) A guide to super-resolution fluorescence microscopy. *J Cell Biol* 190:165–175
82. Pavelka J, Kovaciková L, Smejda L (2011) The determination of domesticated animal species from a Neolithic sample using the ELISA test. *C R Palevol* 10:61–70
83. Yao J, Yang M, Duan Y (2014) Chemistry, biology, and medicine of fluorescent nanomaterials and related systems: new insights into biosensing, bioimaging, genomics, diagnostics, and therapy. *Chem Rev* 114:6130–6178
84. Day JJ, Marquez BV, Beck HE, Aweda TA, Gawande PD, Meares CF (2010) Chemically modified antibodies as diagnostic imaging agents. *Curr Opin Chem Biol* 14:803–809
85. Beltran V, Salvadó N, Butí S, Cinque G, Wehbe K, Pradell T (2015) Optimal sample preparation for the analysis of micrometric heterogeneous samples. *Anal Chem* 87:6500–6504

Trends in High Performance Liquid Chromatography for Cultural Heritage

Ilaria Degano¹ · Jacopo La Nasa¹

Received: 14 September 2015 / Accepted: 11 March 2016 / Published online: 30 March 2016
© Springer International Publishing Switzerland 2016

Abstract The separation, detection and quantitation of specific species contained in a sample in the field of Cultural Heritage requires selective, sensitive and reliable methods. Procedures based on liquid chromatography fulfil these requirements and offer a wide range of applicability in terms of analyte types and concentration range. The main applications of High Performance Liquid Chromatography in this field are related to the separation and detection of dyestuffs in archaeological materials and paint samples by reversed-phase liquid chromatography with suitable detectors. The relevant literature will be revised, with particular attention to sample treatment strategies and future developments. Reversed phase chromatography has also recently gained increasing importance in the analysis of lipid binders and lipid materials in archaeological residues: the main advantages and disadvantages of the new approaches will be discussed. Finally, the main applications of ion chromatography and size exclusion chromatography in the field of Cultural Heritage will be revised in this chapter.

Keywords HPLC · Ion chromatography · Size exclusion chromatography · RP-HPLC · Black crusts · Polymers in conservation · Dyes · Lipid binders

This article is part of the Topical Collection “Analytical Chemistry for Cultural Heritage”.

✉ Ilaria Degano
ilaria.degano@unipi.it

Jacopo La Nasa
jacopo.lanasa@for.unipi.it

¹ Department of Chemistry and Industrial Chemistry, University of Pisa, Via Moruzzi, 13, 56124 Pisa, Italy

1 Introduction

The separation, detection and quantitation of specific species contained in a sample in the field of Cultural Heritage requires selective, sensitive and reliable methods. The ability of a technique or protocol to provide information on single components of a sample, their being ions, small molecules or polymers, is of paramount importance when dealing with complex and unknown mixtures of organic and inorganic species, such as paint or archaeological samples. Moreover, analytical techniques generally need to be suitable for coupling with detectors, such as diode array spectrophotometers and mass spectrometers, which allow one to run not only quantitative, but also qualitative analyses.

Liquid chromatography is a separation technique in which the mobile phase is a liquid and the elution is, in the majority of cases, carried out in a column [1]. The systems for liquid chromatography consist of a column containing a support and a stationary phase, and a pump for solvent delivery. For analytical purposes, an injection and a detection system are included. The only requisite for an analyte to be analysed by liquid chromatography is its solubility in a proper liquid solvent: thus, several materials present in Cultural Heritage samples can be analysed by this mean. In order to separate two or more analytes, they must exhibit a different retention that depends on their interactions with both the stationary and the mobile phase. Small particles are used as stationary phase to enhance the differences in retention of the analytes, and thus to increase the efficiency of the columns. High performance liquid chromatography (HPLC) is a modern liquid-phase chromatography technique based on the use of small particles and high pressures. In the late 1980s, 5 μm particles (diameter) were developed; the newest applications entail the use of 1.8 μm particles, which may be employed to perform Ultra-High Pressure Liquid Chromatography (UHPLC, if pressures are higher than 400 bar). The main processes underlying separations in liquid chromatography are: adsorption, partition, ion exchange, size exclusion and affinity. In the field of Cultural Heritage studies, the great majority of applications of HPLC are based on partition (in particular, reversed-phase chromatography [RP-HPLC]). RP-HPLC has been widely applied in the last 20 years in the characterisation of organic dyes: the identification of dyeing sources is usually achieved by comparing the chromatographic profiles of extracts of unknown samples to those obtained for known dyeing sources. With most of the chromophore-containing molecules being polar, water-soluble compounds, RP-HPLC is the method of choice for the analysis of natural dyes. Lately, the application of liquid chromatography, most often coupled to diode array detectors (HPLC–DAD), has become a routine strategy for the characterisation of the colour palette in tapestry and textiles, and for the detection of organic lakes in paintings. The latest research trends today are mainly focused on sample preparation strategies, the employment of mass spectrometry (MS)-based techniques for the detection and identification of unknown species, and on the application of UHPLC.

Ion exchange chromatography has also been used in the field of Cultural Heritage, mainly as a step of a routine protocol aimed at identifying specific properties of particulates and deposits.

Table 1 Main applications of liquid chromatography in cultural heritage

Type of LC	Type of samples	Detectors	References
Partition (reversed- phase)	Dyes	UV/Vis detectors (UV/Vis) Diode array detector (DAD) Fluorescence detector (Fluo) API-Mass spectrometry (ESI-MS, APCI-MS)	[3–33]
	Lipids: drying oils; alkyd resins; archeological samples (amorphous residues)	Atmospheric pressure chemical ionisation (APCI) mass spectrometry Electrospray ionisation (ESI) tandem mass spectrometry	[34–50]
Ion chromatography	Inorganic salts (mainly anions) and small organic acids (formic, oxalic and acetic acids) in black crusts and generally damaged layers on stone buildings	Conductometer (with ion suppressor) and UV-Vis spectrophotometers	[51–53]
	Damaged layer due to atmospheric corrosion of historical organ pipes	Conductometer (with ion suppressor)	[54–57]
	Indoor pollutants	Conductometer (with ion suppressor)	[58, 59]
	NO ₂ , SO ₂ , acetic and formic acids in their anionic forms in air in historical buildings	Conductometer (with ion suppressor)	[60–65]
SEC/GPC	Polysaccharides (wood, paper and gums)	Refractive index detector (RID)	[69–73]
		Fourier transform infrared spectroscopy (FTIR)	
	Cellulose based materials	Diode array detector (DAD)	[74–81]
		Refractive index detector (RID)	
		Fluorescence-multiangle laser light scattering detector (MALS)	
	Protein paint binders	UV detector (UV)	[82, 83]
Diode array detector (DAD) Cold vapour generation atomic fluorescence spectrometry (CVGAFS)			
Triterpenoid resins	UV/Vis detector (UV/Vis) Refractive index detector (RID)	[84]	

Table 1 continued

Type of LC	Type of samples	Detectors	References
	Lipids	UV/Vis detector (UV/Vis) Diode array detector (DAD) Refractive index detector (RID) Fluorescence-multiangle laser Light scattering detector (MALS)	[85, 86]

Size exclusion chromatography has also been used in some peculiar case studies, which will be reviewed in this Chapter.

Table 1 lists the main type of chromatographies described in the literature in the field, along with the type of samples analysed, and the most common detectors. Each type of chromatography will be discussed in detail in the following paragraphs.

2 Reversed-Phase Chromatography

Reversed-phase chromatography is the most used mode in HPLC analysis of organic molecules (RP-HPLC). The separation is prominently based on the relative hydrophobicity of the solutes, the stationary phase being made of low polarity packings such as octadecylsilane or octylsilane phases bonded to silica or neutral polymeric beads. The mobile phase is usually water and/or water miscible solvents, such as alcohols or acetonitrile [1]. Mobile phase modifiers include acid or alkaline buffers, depending on the nature of the analyte. Several detectors may be coupled with RP-HPLC, the spectrophotometric ones being the most common (ultraviolet-visible (UV–Vis), Diode array detector [DAD], fluorescence). Mass spectrometry can be coupled to RP-HPLC separations, mainly by electrospray ionisation (ESI) or atmospheric pressure chemical ionisation (APCI) interfaces [2]. RP-HPLC is applied in the field of Cultural Heritage-related studies in four main fields:

- analysis of natural and synthetic dyes;
- analysis of lipids in archaeological samples or used as paint binders;
- proteomics;
- analysis of molecular markers in archaeological residues (e.g. wine residues, etc.).

In this chapter, we will review the main applications in the fields of natural and synthetic dye analyses and in lipidomics applied to Cultural Heritage. Being the great majority of applications related to the qualitative and quantitative analysis of dyes, a brief paragraph on their characteristics will be included.

2.1 Natural and Synthetic Dyes

Natural organic colourants were used to prepare inks and lakes and most of all to dye fabrics. They can be classified accordingly to the application method, i.e. as mordant, direct or vat dyes, or to their chemical classes, as reported in Table 2. Synthetic dyes and pigments are classified in the Colour Index, a reference record for all the commercial dyes and pigments, created in 1924 by the Society of Dyers and Colourists. The pigments are recorded by a generic name and a number, as their chemical classes are too numerous to be listed [3].

The relatively small amount of samples available, the low concentration of molecular markers in the original material, the presence of possible degradation products, and the lack of information on the original recipes are the main analytical problems that challenge the analyst in the characterisation of organic dyes in works of art by micro-destructive techniques [4]. Generally, the identification of the dye source is based on the identification of molecular markers, followed by a qualitative and semi-quantitative comparison of analytical results with the profiles of known reference materials. Reversed-phase liquid chromatography is the method of choice for the analysis of natural dyes, because most of the chromophore-containing molecules are polar, water-soluble compounds. The application of liquid chromatography to the analysis of natural dyestuffs has been reviewed in detail in [5–7]. The 2014 review contains a complete overview of latest sample treatments and analysis methods [8].

The latest applications have mainly focused on innovative sample preparation strategies and the employment of novel detection techniques (in particular, MS-based techniques), and on the characterisation of previously unreported dye sources or of minor components of known raw materials, which may help in their unambiguous identification in historical samples. With regard to synthetic dyes, organic pigments were in most cases analysed by pyrolysis coupled with GC/MS (Py-GC/MS) [9, 10], being insoluble in most solvents. Only in selected cases was RP-HPLC, mainly coupled with ESI-MS², used for their study [11, 12]. On the other hand, synthetic organic dyestuffs were analysed by RP-HPLC, either with DAD or MS detection [13–15].

Chromatographic conditions entail the use of a reversed-phase C18 or C8 (or even C4) column; to separate the most polar coloured compounds, such as phenolic acids contained in tannins, polar embedded reversed-phase columns such as RP-amide were tested in a few cases [16]. The most commonly used eluents are water, acetonitrile, and methanol. Acetonitrile has important advantages over MeOH, including lower absorbance in the 200–275 nm range, lower UV cutoff, and lower back-pressure due to lower viscosity [17]. Elution takes place in gradient mode, with a constant percentage of an acid, used to reverse the dissociation of analytes, most of which have acidic groups [17]. The nature and amount of mobile phase modifier is chosen not only on the basis of optimal peak shape and thus resolution, but also depending on the detection system adopted. Formic (FA), trifluoroacetic (TFA) and phosphoric acid are the most used modifiers in the analysis of natural dyes. In a few cases, methanesulfonic acid (MSA) has been used to improve resolution of indigoid compounds [18]. Amongst these, only MSA and FA can be

Table 2 Most common natural dyestuffs classified by their chemical class [7]

Dye source		Botanical name	Main molecular markers
Anthraquinoid dyes	Madder-type	<i>Rubia tinctorum</i> L., <i>Rubia peregrina</i> , <i>Rubia cordifolia</i> , <i>Rubia akane</i> , <i>Galium</i> species, <i>Relbunium</i> , <i>Morinda citrifolia</i> L.	Alizarin, purpurin, xanthopurpurin, munjistin, pseudopurpurin
	Armenian, Polish and American cochineal	<i>Dactylopius coccus</i> Costa, <i>Porphyrophora polonica</i> , <i>Porphyrophora haemli</i> Brandt	Carminic acid (main component), kermesic acid, flavokermesic acid, dcii, dciv, dcvii
	Kermes	<i>Kermes vermilio</i> Planchon	Kermesic acid (75–100 %), flavokermesic acid (0–25 %)
	Lac dye	<i>Kerria Lacca</i> Kerr	Laccaic acid a (71–96 %), laccaic acid b, c and d (0–20 %), flavokermesic acid (3.6–9.0 %)
Flavonoid dyestuffs	Weld	<i>Reseda luteola</i> L.	Luteolin, apigenin, chrysoeriol
	Dyer's broom	<i>Genista tinctoria</i> L.	Luteolin, (apigenin), genistein
	Sawwort	<i>Serratula tinctoria</i> L.	Luteolin, diosmetin, chlorogenic acid
	Persian berries	<i>Rhamnus</i> genus berries	Quercetin, rhamnetin, kaempferol
	Young fustic	<i>Cotinus coggygia</i> Scop.	Fisetin, fustin, sulfuretin
	Fustic	<i>Clorophora tinctoria</i> L.	Morin, maclurin, kaempferol
	Quercitron	<i>Quercus velutina</i> Lam.	Quercetin, quercitrin
	Safflower	<i>Carthamus tinctorius</i>	Carthamin, cts, safflower yellow a, safflower yellow b, and precarthamin
	Brazilwood and sappanwood	<i>Caesalpinia</i> species	Brazilin, brazilein, bw compounds
Indigoid dyestuffs	Logwood	<i>Haematoxylum campechianum</i>	Hematein, hematoxylin
	Indigo	<i>Indigofera tinctoria</i>	Indigotin, indirubin
	Woad	<i>Isatis tinctoria</i>	Indigotin
	Purple	<i>Bolinus brandaris</i> L., <i>Hexaplex trunculus</i> L., <i>Stramonita haemastoma</i> , <i>Plicopurpura patula</i> , <i>Nucella lapillus</i>	6,6'-dibromoindigotin, 6-bromoindigotin, indigotin, 6,6'-dibromoindirubin, 6-bromoindirubin, indirubin
Lichen	Orchil	<i>Rocella tinctoria</i>	Orcein
Tannins	Galls	Gallnuts from <i>Cynips</i> , or <i>Quercus sinfectoria</i> Oliv.	Galic acid, ellagic acid
	Alder bark	<i>Alnus glutinosa</i>	Galic acid, quercetin, emodin
	Sumac	<i>Rhus</i> genus	Galic acid, elladico acid, quercitrin, kaempferol
	Black walnut	<i>Juglans nigra</i> , <i>Juglans regia</i> L., <i>Juglans cinerea</i> L.	Juglone

Table 2 continued

Dye source		Botanical name	Main molecular markers
Naphto-quinones	Alkanna	<i>Alkanna tinctoria</i> Tausch.	Alkannin
	Henna	<i>Lawsonia inermis</i> L.	Lawsonone
Polymethindyes	Turmeric	<i>Curcuma longa</i> L.	Curcumin, demethoxycurcumin, bisdemethoxycurcumin
	Saffron	<i>Crocus sativus</i> L.	Crocin, crocetin
	Annatto	<i>Bixa orellana</i> L.	Bixin

reasonably used when exploiting a mass spectrometric detection. FA is indeed the most used for LC–MS analyses.

Most separations are performed on 150×4.6 , 5- μm particle-size columns. The use of narrow-bore columns can result in increased peak heights for analysed compounds [18, 19], but their application never gained much importance in the field. UHPLC was recently successfully applied [20–22], showing the potentialities of this technique in this field. Owing to instrument improvements, UHPLC allows the use of sub-2- μm porous particles while applying extreme pressures and faster flow rates, resulting, eventually, in shorter runtimes. As a consequence, lower solvent consumption and faster analyses can be achieved, while maintaining a high chromatographic efficiency. Further details on the three published applications of UHPLC to the analysis of natural dyes are reported in Table 3.

With regard to the sample treatments, most recent papers deal with the optimisation of extraction conditions by comparison of different methods. As the range of chemical classes exploited as colouring materials is surprisingly broad, the molecular markers of each dye differ in terms of solubility and reactivity in acidic and basic media [7]. In order to take into account these properties, distinct extraction procedures have been optimised for different classes of chromophores. Recent research deals with the quest for an optimal strategy to extract all type of dyestuffs from a textile, painting or ink sample. A comparative investigation of hydrolysis methods to analyse natural organic dyes by HPLC–PDA from 12 biological sources selected for the preparation of dyed fibers, pigments and paints is described in [23]. The same type of study was performed on six dyestuffs in woolen textiles by Manhita and coworkers [24], and on six dyestuffs by Karapanagiotis and coworkers [25], while Sanyova proposed a new mild procedure for anthraquinone-based organic lakes [26]. For the analysis of inks on paper, specific sampling and extraction procedures were developed, such as the direct application of a brush imbibed with SDS [27].

Extraction methods can be divided into three main classes: hydrolysis in an acidic (for HCl) methanolic solution; application of complexation agents such as HF [26, 28], formic [29], oxalic [30], trifluoroacetic, acetic, EDTA (“mild extraction methods”); extraction with organic solvents such as pyridine, dimethylsulfoxide (DMSO), or dimethylformamide (DMF) [5]. Hydrolysis in acidic methanolic solution and the application of complexation agents is most often used in case of

Table 3 Comparison of the UHPLC methods described in the literature for the characterisation of natural organic dyes

Standards and reference materials	Column(s) and detector(s)	Acquisition parameters	Advantages/disadvantages	References
Gallic acid, carminic acid, rutin, luteolin, quercetin, apigenin, alizarin, purpurin	Acquity UPLC BEH C18 100 mm × 2.1 mm ID, 1.7 μm particle size, waters (best of three UHPLC columns tested) Detector: PDA	$T = 30\text{ }^{\circ}\text{C}$ Flow rate: 0.25 mL/min Eluents: H ₂ O and ACN with 0.1 % formic acid $V = 5\text{ }\mu\text{L}$	Short runtime (6 min, gradient) LODs not reported	[16]
Standards for quantitative analysis: alizarin, apigenin, genistein, luteolin, purpurin Reference materials: cochineal, turmeric, indigo, Kermes Spectral database: 59 natural reference materials (85 compounds)	Acquity UPLC BEH C18 150 mm × 2.1 mm ID, 1.7 μm particle size, waters (best of five UHPLC columns tested) Detector: PDA	$T = 40\text{ }^{\circ}\text{C}$ Flow rate: 0.2 mL/min Eluents: H ₂ O and MeOH with 0.1 % formic acid $V = 0.1\text{--}4\text{ }\mu\text{L}$	40-min runtime (gradient) LODs (evaluated at the λ_{max} in the visible range for each analyte): <0.1 ng (injected) for flavonoids; 0.2–0.3 ng for anthraquinones; 0.3 ng for indigo and 8.1 ng for curcumin	[2]
Standards for quantitative analysis: luteolin, apigenin, genistein, chrysoeriol, diosmetin Reference material: <i>Genistainctoria</i> L.	PST BEH C18 150 mm × 2.1 mm ID, 1.7 μm particle size, waters Detectors: PDA and ESI-MS/MS	$T = 55\text{ }^{\circ}\text{C}$ Flow rate: 0.25 mL/min Eluents: H ₂ O with 0.02 % formic acid and MeOH $V = 5\text{ }\mu\text{L}$	37 min runtime (gradient) LODs (evaluated at 254 nm): 0.5–1.9 ng injected	[17]

mordant dyes and organic lakes. The extraction of brominated indigoids, known molecular markers of purple, which are vat dyes, and of carthamin, the molecular marker of safflower, is mainly performed by an organic solvent such as DMF or DMSO. Moreover, since these latter analytes are sensitive to acidic environments, the use of acids must be avoided if possible. The extractions take place at elevated temperatures, generally ranging between 40 and 120 °C, for a short time for labile dyes and up to 1 h for the mordant dyes. In few cases, the reaction is performed in an ultrasonic bath [7]. If HCl or HF is used, the extract is cooled and evaporated to dryness under vacuum or under nitrogen flow and redissolved in a small volume of the eluent, water–methanol mixture, DMF or DMSO (also in mixtures), depending on the nature of the analytes. The main difference between the use of the strong methods and the mild ones lies in the nature of the extracted compounds. In particular, the application of strong conditions leads to the breaking of glycosidic bonds [30], the decarboxylation or dehydration of molecular markers, the esterification of phenolcarboxylic compounds [7]. Moreover, the hydrolysis results in the complete disruption of the samples, leading in some cases to severe matrix effects, which may be overcome by introducing a liquid/liquid extraction step with a suitable solvent, such as ethylacetate [31, 32]. No method of election has been identified yet, which is optimal for all the investigated materials. A comparison between different sample treatments applied to the extractions of madder components from reference lakes or textiles, reported in recent papers, is presented as an example in Fig. 1.

2.2 Lipids

Vegetable oils consist of mixtures of triacylglycerols (TAGs), glycerol tri-esters of fatty acids. Their identification has proven valuable to establish the painting technique when oils are used as paint media, or to investigate ancient diet and pharmaceutical ointments when they are found as residues in potsherds. Reverse phase high pressure liquid chromatography is the preferred chromatographic approach for the separation of complex mixtures of triglycerides in oils, using several detectors including UV spectrophotometers, refractive index detectors, and mass spectrometers [33–36]. Notwithstanding, only few applications of HPLC to the characterisation of lipid materials in paints or archaeological materials have been published, mainly due to the difficulty to detect surviving TAGs after centuries of ageing, even in museum environments.

Mass spectrometry detection is fundamental for TAG profiling, since RP-HPLC is generally unable to separate the positional isomers of TAGs: mass spectrometry detects TAGs, and also identifies positional isomers [34, 37]. Both atmospheric pressure chemical ionisation (APCI) mass spectrometry and electrospray ionisation (ESI) tandem mass spectrometry have been successfully used for the differentiation of TAG positional isomers on the basis of their fragmentation patterns [35, 37–42]. An example of APCI-MS spectrum obtained for 1,3-distearoyl-2-oleoyl glycerol (SOS) is presented in Fig. 2.

In the field of archaeological materials characterisation, HPLC–APCI–MS was successfully applied for the study of the lipid fractions of residues extracted from

fr

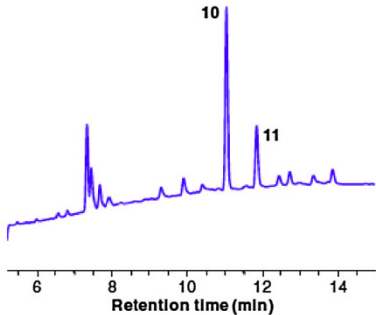
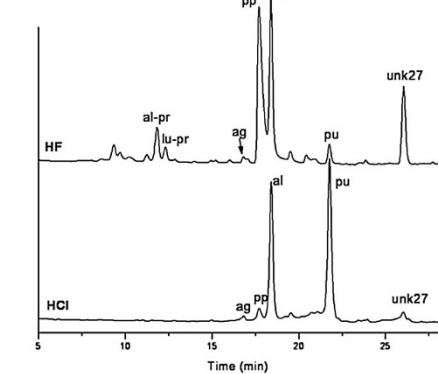
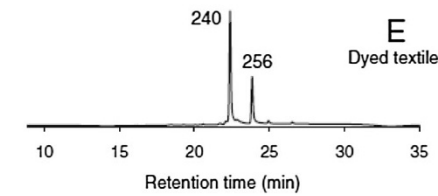
Chromatogram	Sample treatment	Ref.
 <p>reference madder-dyed wool (alum-mordanted), chromatogram shown at 290 nm</p>	<p>2 mg of dyed wool was placed in vials, and 1.0 mL of 0.1% Na₂EDTA in H₂O/DMF (1:1, v/v) solution was added. The vials were capped and kept at 100 °C for 30 min. Vials were cooled to room temperature, and the solvent was evaporated under vacuum. 10 = alizarin; 11 = purpurin.</p>	[24]
 <p>Chromatograms (at 255 nm) of extracts of home-made madder lake RT2</p>	<p>Upper chromatogram: the samples (c. 0.2 mg in glass test tubes) were dispersed at room temperature in 250 µL of a 2/1/1/1 (v/v) mixture of HF aqueous solution (HF 4 M, DTPA 4 mM, LiF 120 mM), MeOH, DMF and AcEt. The supernatants were filtered on polyethylene frits (0.5 µm) before injection. Lower chromatogram: the samples (c. 0.2 mg in glass test tubes) were dispersed in 250 µL of a 2/1/1 mixture of concentrated HCl, methanol and water, and heated for 10 min at 110 °C. After evaporation to dryness under vacuum, the residues were taken up in 50 µL of MeOH/H₂O (1:1, v/v), filtered on polyethylene frits (0.5 µm), and injected into the HPLC system.</p>	[28]
 <p>Chromatogram (at 450 nm) of extract of a textile dyed with <i>Rubia tinctorum</i> (240 = alizarin and 256 = purpurin)</p>	<p>heating approximately 0.1–1 mg of fibers in 200 µL of a solution of pyridine/water/1.0 M oxalic acid in water (95:95:10) at 100 °C for 15 min.</p>	[30]

Fig. 1 Examples of chromatograms obtained after the application of different sample treatments to reference lakes or textiles prepared with madder dyestuffs

late Roman cooking pots, along with the more traditional GC/MS approach [39]. The presence of beeswax in the residues was proven by identification of the constituting alkanes, mono- and diesters. The main contribution of HPLC-APCI-MS was the detection of high amounts of saturated triacylglycerols (TAGs) that indicated that animal fat was processed in the pots. The lipid extracts were obtained

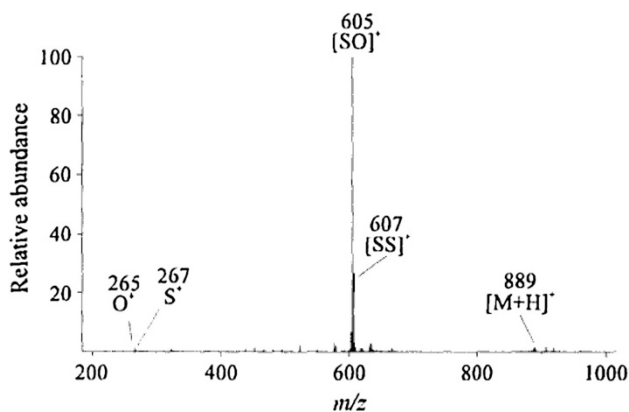


Fig. 2 The APCI mass spectrum of 1,3-distearoyl-2-oleoyl glycerol (SOS) (reprinted with permission from [38])

by extraction with *n*-heptadecane and analysed using a reversed-phase column of the type Supelcosil LC18 (25 cm × 4.6 mm, Supelco) with a gradient of methanol and *iso*-propanol as mobile phase. The same approach was used in the study of residues in ancient oil lamps found at the archaeological site of Sagalassos (South-West Turkey) [42]. HPLC–APCI–MS allowed the detection of surviving TAGs whose nature and profile suggested that olive oil was used as illuminant for the archaeological oil lamps. The presence of relative high amounts of multiply unsaturated TAGs and traces of saturated TAGs suggested that other oils and animal fat were also added.

More recently, extracts of archaeological potsherds from the same archaeological site were analysed by three complementary chromatographic and mass spectrometric procedures. GC/MS, GC–IR–MS, HPLC–APCI–MS were used and led to the identification of animal fat. The samples for liquid chromatography were extracted with chloroform/methanol and subjected to silylation derivatisation; the chromatographic set-up included a reversed phase column 15 cm Varian OmniSpher C18 with a diameter of 3 mm, which was held at 60 °C. A full 10- μ L loop of the sample was injected. The same set-up was used to characterise burned greasy deposits found inside shells of the large Nile bivalve *Chambardia rubens*, excavated in a VIII–X century AD church of the Coptic monastery of Bawit (Egypt) and supposedly used as lamps. Low concentrations of unaltered TAGs were detected by HPLC–APCI–MS, which included TAGs with at least one dihydroxylated acyl chain. The preservation of this species may be accounted by the dry climate of the excavation site. The type and distribution of the surviving TAGs suggested the illuminant was rapeseed (*Brassica napus* L.) or radish (*Raphanussativus* L.) oil.

HPLC–APCI–MS was also applied to the study of historical pharmaceutical ointments from the XVIII century [43]. The analytical protocol was set up using a comparative study based on the evaluation of TAG compositions of raw natural lipid materials, in laboratory-reproduced ointments, and was then applied to residues contained in a series of apothecary jars. In order to characterise the

triglyceride profile of the archeological samples, the chromatographic separation was performed using an Ascentis C18 column (150 × 4.6 mm, 5 μm particle size, Supelco, USA) and *iso*-propanol and methanol as mobile phase. The samples were submitted to extraction with a mixture of chloroform/methanol at reflux and the extracted material was dried, suspended in hexane and washed three times in a separator funnel with a water/ethanol solution. The final residue in hexane was then dried and diluted in the elution mixture [43].

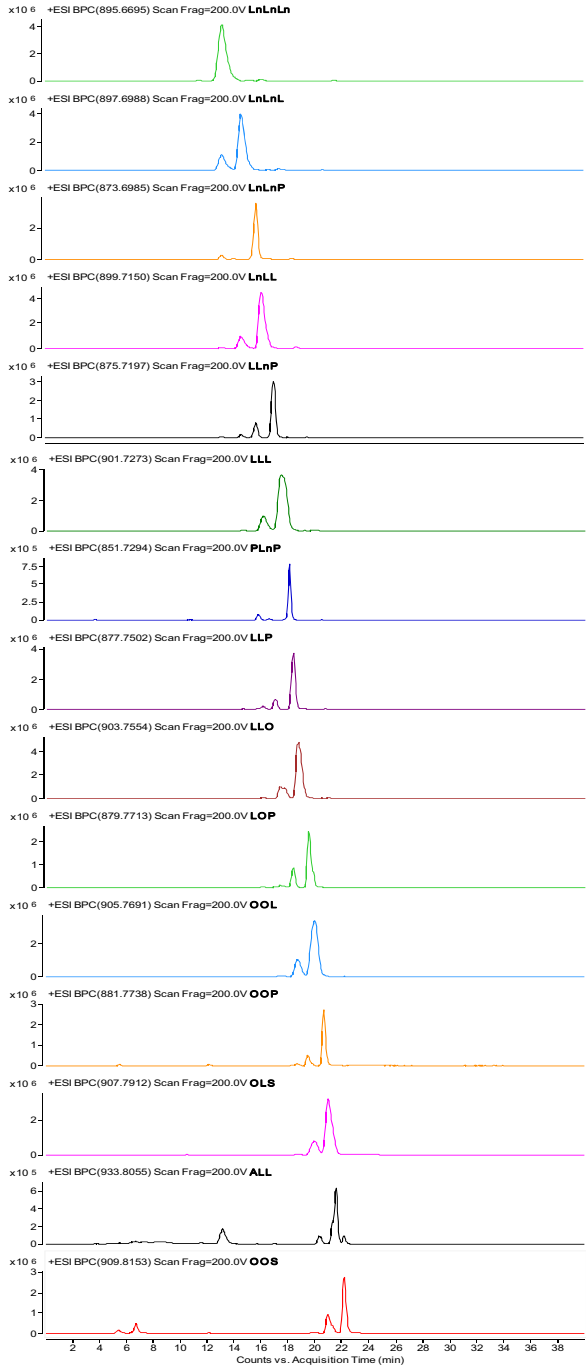
In the study of oil paints, HPLC–APCI–MS of triglycerides was performed to evaluate the effects of traditional processing methods of linseed oil on the composition of its triacylglycerols. The study aimed at evaluating how the triglyceride composition of linseed oil changed as a consequence of different oil pretreatments such as washing with water, heating or treatment with lead-based dryers. The separation of the TAGs was performed using a NovaPack C18 column (150 × 4.6 mm, Waters, USA) and acetonitrile/ethanol as eluents [44]. In order to characterise the lipid fraction of linseed oil after the processing methods, the oil samples were dissolved in a acetonitrile/*iso*-propanol/hexane mixture and injected in the chromatographic system.

Recently developed non-porous core particles stationary phases [45] were also tested for the separation of TAGs in oils, which were used as binding media or for producing ointments, and proved to have a high efficiency at lower back pressures, compared to traditional porous particles [36, 37].

In particular, HPLC–ESI–MS equipped with a core shell stationary phase was used to determine the triglycerides profile of a set of fresh reference oils commonly used in modern and contemporary art. The separation of the triglycerides was performed using a Poroshell 120 EC-C18 column (50 mm × 3.0 mm, 2.7 μm particle size, Agilent, USA) with a high-resolution ESI-Q-ToF tandem mass spectrometer as detection system using *iso*-propanol and methanol as eluents [36]. HPLC TAGs analysis allows to characterise the different species in the sample (Fig. 3). The triglycerides were extracted using *n*-hexane and the extracts were dried under nitrogen stream, diluted with the elution mixture before the injection. The optimised chromatographic method was applied for the characterisation of the triglyceride profiles of drying oils used in modern paint tubes formulations, and to characterise the lipid material in paint samples. The paint samples were submitted to a microwave extraction (600 W, 80 °C) using a *n*-hexane/chloroform solution, and the extracts were dried under nitrogen stream, diluted with the elution mixture and filtered before the injection [46].

The same analytical approach used for the characterisation of fresh oils was applied to the characterisation of the lipid composition of several alkyd resins. The characterisation of the glycerides composition allowed to discriminate between different trademarks of commercial alkyd paints, to identify the raw materials used for the production of the resin and to define the synthesis process used for their preparation [47]. The same method based on liquid chromatography coupled with high resolution mass spectrometry and hexane extraction was applied to a set of industrial alkyd resins: the application of this method allowed not only the identification of the TAGs, but also the detection of pentaerythritol and phthalic acid esters deriving from the synthesis process of the resin [48] (tandem mass spectrum

Fig. 3 Extract ion chromatograms of linseed oil for 15 identified TAGs species (reprinted with permission from [36])



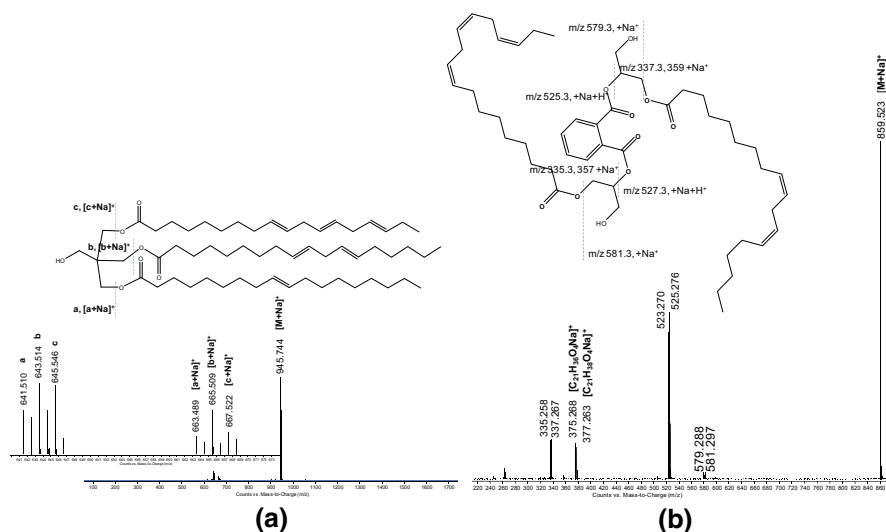


Fig. 4 Tandem mass spectrum and fragmentation pattern of **a** PenLnLO and **b** LGlyPhGlyLnsodiade adducts (reprinted with permission from [49])

of PenLnLO and LGlyPhGlyLn sodiated adducts shown in Fig. 4). The analytical approach used for the characterisation of the fresh alkyd paint and resins was also applied for the characterisation of the oxidised triglycerides in a set of alkyd paint layers exposed to acetic acid vapour. The application this HPLC procedure is suitable for the characterisation of aged and fresh alkyd resins, for discriminating between different trademarks, and to evaluate the conservation state of an artwork [49, 50].

A slightly modified method, still based on the use of a Poroshell 120 EC-C18 column with a high resolution electrospray ionisation-quadrupole-time of flight tandem mass spectrometer as detection system, was optimised for the identification of triacylglycerols in complex archaeological residues [37]. Thanks to the unprecedented chromatographic separation and detection sensitivity of the set-up, it was possible for the first time to perform TAGs profiling in archaeological residues and reference materials with a data set containing more than 500 molecular formulas. In particular, it was possible to distinguish between plant oils and animal fats, and to identify pork suet even in complex mixtures with plant oils. The archaeological organic residues were homogenised in a mixture of dichloromethane/methanol using an ultrasonic bath. Then the mixture was filtered, dried under nitrogen stream, suspended in hexane and washed three times in a separator funnel with a water/ethanol solution. The final residue was then dried over MgSO_4 , filtered and evaporated to dryness. The final material was diluted with the elution mixture and injected in the chromatographic system [37].

In conclusion, thanks to the improvements in columns efficiency and in resolution of the available mass spectrometers, HPLC-MS based techniques are gaining momentum in the analysis of triglycerides and their oxidation products in

archaeological residues and in paintings. In the last 3 years, several papers have described optimised procedure for their determination. On the one hand, the applicability of these protocols to actual case studies in the field of archaeology has been proven in several cases, in which the original lipid material was relatively well preserved, thanks to suitable conservation conditions (i.e. very dry climate and relatively anaerobic conditions, in the absence of direct light). On the other hand, the application of TAGs profiling for the identification of the binding medium is complicated by the tendency of siccativ oils to polymerise, due to the exposure to direct light and conservation in unfortunate conditions. Thus, only few successful applications of this strategy in paint analyses have been presented so far [46]. The publication of new case studies in the future will prove the actual applicability of the technique to diagnostic analyses of paintings.

3 Ion Chromatography

Ion chromatography (IC) is an ion-exchange technique in which low concentrations of organic and inorganic anions and cations are determined using ion exchangers of low ion-exchange capacity with dilute buffers [1]. IC is mostly employed to separate organic and inorganic ions, amino acids, proteins or nucleic acids. Strong or weak acids or bases can be used as stationary phases to separate cations and anions, respectively. The ion exchangers are supported on silica, polystyrene or carbohydrate-based polymers.

In the field of Cultural-Heritage-related studies, IC has been mainly used as a robust routine technique to quantify inorganic anions and cations, and small organic acids in a plethora of samples. In this chapter, a few examples of possible applications of this technique will be provided, focusing on a few classic case studies and presenting some new developments.

Several papers describe the application of IC to the study of immovable cultural heritage, i.e. stone, masonries, etc., to characterise inorganic salts in damage layers or in black crusts. It has also been applied to characterise the VOCs and the particulate determined in environmental studies in musea, in semi-confined exhibition areas, and, in general, in the urban environment where important monuments stand.

One of the first applications of ion chromatography to the characterisation of anions in damage layers of outdoor building was published in 1995 [51]. An analytical procedure was set up for the dissolution of damage layers from stone monuments with the aim of performing ion chromatography analyses. The dissolution was achieved in water and purified from cations using cation resins, and ion chromatography analysis was performed with anionic micromembrane suppressor and two serial detectors (conductometer and spectrophotometer). The separation was undertaken on an Ionpac column (AS4A-SC). Halide anions (F^- , Cl^- , Br^-), nitrates and nitrites, phosphates, oxalates and carbonates were quantitated in samples from damaged layers of stone monuments, i.e. black crusts. The same approach and instrumental setup was adopted in [52], where the formate and acetate anions were also determined, and eventually applied to the complete

characterisation of black crust in damage layers on historic buildings at different European urban sites [53]. The soluble anions, including formate, acetate and oxalate, were measured by ion chromatography analysis (IC) with a Dionex 4500i (IonPac AS14 column with a AMMS III suppressor in conjunction with a conductivity detector). Oxalates were the most abundant small (C1–C2) organic anion found at all the sites. The data reported show how OC and EC concentrations and OC/EC ratio are typical of each site and provide essential input for an exhaustive investigation of black crust formation.

Similar studies were presented in [54], where the degradation of archaeological porous stone in the medieval city of Rhodes was assessed, and in [55], which focuses on the effects of sulphation in the frame of a research study on the effects of atmospheric deposition on the cement mortar of the basement in a twentieth-century building. The results achieved by IC were complemented by analyses performed by visual observation, scanning electron microscopy, X-ray diffraction, differential and gravimetric thermal analysis and the quantitative determination of elemental carbon. Sulphation was found to be the main damage mechanism occurring on the cement mortar constituting the base section of a building, since the concentration of sulphate increases from the inner to the outer layer at the expense of the carbonate. The same approach, system setup, and similar results were obtained for the case study of Michelozzo's Courtyard in Florence (Italy) [56]. The investigation adopted a holistic approach involving thermographic measurements on the wall paintings, microclimatic analysis, gaseous pollutant monitoring, atmospheric particles characterisation and dry deposition compositional analysis. Also in this case, the surface is undergoing a sulphation process. In particular, the presence of significant amounts of sulphite (SO_3^{2-}), with concentration values well correlated to the sulphate ones, indicates that sulphate is also produced by the oxidation of sulphite at the painting surface. The effects of rising damp on the durability of a plaster were studied in [57] by means of a similar, multi-analytical approach entailing ion chromatography.

Summarising, the application of a routine analytical technique such as IC, complemented by several other microscopy- or spectroscopy-based techniques, to the characterisation of black crusts, and more generally, of superficial layers of stone and plaster, allowed the researchers to highlight specific behaviours of stone buildings depending on the environment.

A similar approach, in terms of use of a multi-analytical array of techniques (ICP-AES, SEM, ...) including ion chromatography, was adopted for the characterisation of particulate matter. This method is widely applied in environmental chemistry, so previously optimised methods are routinely applied in the field of Cultural Heritage. Notwithstanding, a few interesting case studies will be discussed. To analyse the deposition of fine particulate matter (PM) on book surfaces in the National Library in Prague, Smolik and coworkers [58] used cellulose filters to sample the PM, and SEM and IC to characterise them. Ghedini and coworkers monitored the atmospheric aerosol in the area of the Florence Baptistery [59]. Total suspended particulate (TSP) was collected using circular filters with diameter of 47 mm. Atmospheric particles were sampled for the measurement of total weight, non-carbonate carbon (NCC) and major soluble ions by ion chromatography. Interesting results were obtained by comparing the data

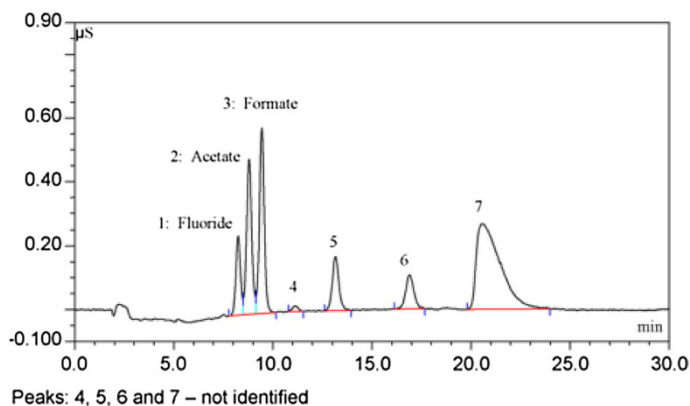


Fig. 5 Separation of fluoride, acetate and formate on an IonPac AS14 in a real sample taken at the Cathedral of Cologne (reprinted with permission from [61])

collected in different sampling points, from both a qualitative and quantitative point of view.

Besides the characterisation of damage on stone historical and modern buildings, IC was exploited to study metal corrosion in some archaeological and historical materials. A nice example is given by the evaluation by IC of the atmospheric corrosion of historical organ pipes by volatile organic acids, as described in [60]. The corrosivity of formic and acetic acid was investigated in laboratory exposed polished samples. Corrosion rate was measured gravimetrically and the corrosion products were analysed qualitatively and quantitatively by IC equipped with an IONPAC AD9-SC analytical column. The results imply that acetic acid vapour is a very important corrosive agent for lead pipes in historical organs, while formic acid is slightly less corrosive than acetic acid. Also in this case, the application of a routine analytical protocol such as IC for the quantification of small organic acids to a peculiar case study allowed the researcher to highlight important characteristics of the objects under study.

Finally, ion chromatography has also been used to quantify the above-mentioned volatile organic acids (namely, acetic and formic acid) in air samples in and outside the Cathedral of Cologne (Germany), after sampling the corresponding acids by passive Radiello[®] diffusion tubes [61]. Both acids were adsorbed by TEA and subsequently extracted with water. Four important gaseous pollutants were sampled simultaneously, i.e. NO₂, SO₂, acetic and formic acids, and their quantitation performed by IC by the same method described in [62]. The performances of two analytical columns (Allsep A-2 and IonPac) were compared in terms of detection limits, precision, and dynamic range. An example of separation is shown in Fig. 5. With regard to confined environments, few analytical methods entailing IC have been published for the detection of acetic and formic acid vapours in musea [63]; one study even focuses on the detection not only of airborne acetate and formate, but also fluoride [64].

One last example presents the application of ion chromatography, along with several other techniques (such as mercury intrusion porosimetry; Fourier transform infrared spectroscopy; scanning electron microscope with energy dispersive spectrometry), to the evaluation of the best application technique for a novel hydroxyapatite-based consolidating treatment for limestone [65].

4 Size Exclusion Chromatography

Size exclusion chromatography (SEC), often referred to as gel permeation chromatography (GPC) in the case of the analysis of hydrophilic macromolecules, is a separation technique in which molecules are separated on the basis of their hydrodynamic molecular volume or size [66].

In the SEC chromatographic system, a liquid mobile phase flows through the column at a fixed flow rate, setting up a pressure gradient across its length; the particles of the stationary phase are porous with controlled pore size. The smaller macromolecules are able to penetrate into these pores as they pass through the column, while the larger ones are too large to be accommodated and remain in the interstitial space. The smaller molecules are only temporarily retained and will flow through the column until they encounter other particles' pores to enter. Meanwhile, the larger molecules flow more rapidly through the length of the column because they cannot reside inside the pores for any period of time [67].

SEC is widely used for separation of various natural and synthetic polymers. With proper column calibration and by the use of molecular-weight-sensitive detectors, such as light scattering, viscometry, or mass spectrometry, the molecular weight distribution and the statistical molecular weight averages can readily be obtained [66–68].

In Cultural Heritage studies, SEC has been used to characterise synthetic polymers used as paint binders or consolidants; to assess the degradation of cellulosic and wooden materials and Arabic gum used as binder; to study the binder-pigment interactions in protein-based paintings; and to evaluate the polymerisation or, in general, the degradation processes undergone by terpenoid varnishes and lipid binders.

4.1 Synthetic Polymers

A number of synthetic materials have been exploited by artists and restorers, and the wide variety of formulations of synthetic resins has allowed their extensive use as paint binders, plastic materials, consolidants, adhesives, coatings and varnishes and many other applications.

Size-exclusion chromatography interfaced with a refractive index detector (SEC-RID) was applied to evaluate the modification of the molecular weight distribution of the varnishes Laropal A81, Laropal A101, Laropal K80, Regalrez 1094 and Arkon P90 during artificial ageing, and to evaluate the effects due to the addition of Tinuvin 292 as UV-stabiliser in the formulation of the resins. The resins were solubilised in tetrahydrofuran and directly injected in the LC system, and the

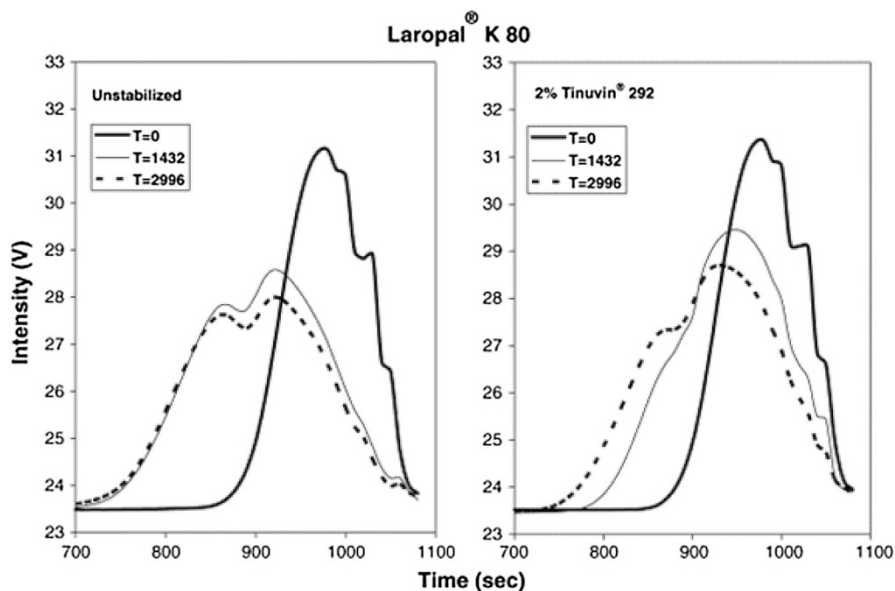


Fig. 6 Changes in SEC of unstabilised and stabilised Laropal K 80 during accelerated light aging (reprinted with permission from [69])

chromatographic separation was performed using two Polymer Laboratories (Netherlands) PL-gel 5 μm mixed-D columns (300 mm \times 7.5 mm) and tetrahydrofuran as eluent [69]. The results obtained for unstabilised and stabilised Laropal K80 during accelerated light aging are reported in Fig. 6.

The modification of the molecular weight of the ketone resin Laropal K80 during ageing was also studied with the same chromatographic approach in the commercial formulation of BEVA 371, a heat-seal adhesive containing two EVA co-polymers, the ketone resin, a phthalate ester of a hydroabietyl alcohol and a paraffin wax [70].

SEC-RID was also applied to evaluate the photochemistry processes involved in the ageing poly(vinyl acetate) paints and to evaluate the ageing effects related to the presence of pigments and fillers in the paint formulation: the information on the molecular weight distribution obtained with SEC-RID were used to identify the main chemical reactions involved in the ageing of the paint and to predict its long-term life [71].

In all these cases, SEC allowed the researchers to evaluate the behaviour of different polymeric resins upon ageing, and thus their long-term stability, and, as a consequence, suitability as conservation or restoration materials.

In one case, SEC coupled with Fourier transform infrared spectroscopy (SEC-FTIR) was applied for the characterisation of artists' acrylic emulsion paints [72]. The collection of the infrared data was performed using an off-line solvent-elimination interface. The use of the off-line interface is commonly preferred over on-line flow-cell systems, since the removal of the solvents used in the chromatographic separation allows for the increase of the signal-to-noise ratio

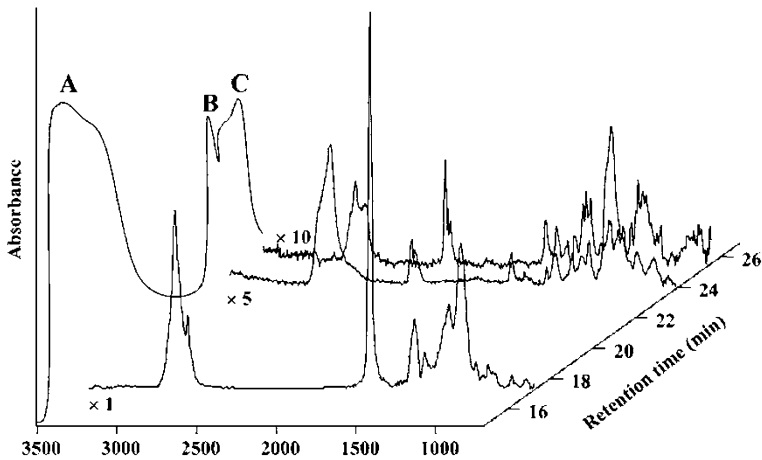


Fig. 7 3D plot obtained by SEC-FTIR of an acrylic emulsion paint. *Peak A* has been identified as a poly(nBA-co-MMA) medium, *peak B* as an alkyl aryl polyethoxylate surfactant and *peak C* as Pigment Red 5 (reprinted with permission from [72])

and decreases the limits of detections [73]. The acrylic emulsions were solubilised in tetrahydrofuran and the chromatographic separation was performed using three Polymer Laboratories (United Kingdom) PLgel 10 μm MIXED-B (300×7.5 mm) columns and tetrahydrofuran as eluent. Figure 7 reports an example of a 3D plot obtained for the characterisation of an acrylic emulsion paint [72]. The use of infrared spectroscopy as a detector system allowed the simultaneous identification of the polymer matrix and the minor components, such as the surfactants and dyes used in the acrylic paint emulsions. This approach allowed a full characterisation of the material under study, but required a relatively high amount of sample. Thus, it can only be applied for studies on reference materials or for quality control of newly produced materials (e.g. during natural or artificial ageing experiments), and not for diagnostic purposes. Examples of the application of SEC to these type of problems follow.

4.2 Polysaccharides (Wood, Paper and Gums)

The main chemical components in wood are cellulose, hemicellulose, lignin and extractives. Cellulose is a homo-polymer of β -1,4-glucose units with a highly regular H-bonded network between its layers, especially in the case of crystalline cellulose, while hemicellulose is a carbohydrate hetero-polymer consisting of different monomers. Lignin is a tridimensional macromolecular network in which the more abundant monomers are substituted phenols bonded via ether bonds.

GPC was applied to determine the chemical features and molecular weight distributions in wood and in the corresponding extracted lignin using different sample pretreatments [74, 75]. The analyses were performed on both archeological and reference wood samples in order to evaluate the change in the molecular weight

distribution occurring as an effect of ageing. The chromatographic separation of the wood components was performed using an Agilent (USA) PL 3 μm MIXED gel E (MW 220–400 K) and tetrahydrofuran as eluent. The detection of the analytes was performed using a diode array detector (DAD) set at 280 nm [74, 75]. The same analytical approach was successfully applied for the characterisation of the conservation state of archeological waterlogged wood artifacts [76].

In all these cases, GPC provided important data on the depolymerisation of lignin in different conservation conditions, which can be correlated with the conservation state of wood in archaeological context.

GPC was also used for the ageing studies of paper related to the presence of metals. The presence of copper ions that migrate from the pigments can catalyse the degradation of cellulose and discoloration of the paper. In order to evaluate the effects of this metal on paper, a GPC-Fluorescence-multi-angle laser light scattering detector (MALS) apparatus was used. The use of this system allowed to determine not only the absolute molar mass moments by MALS, but also the contents of carbonyl groups measured by a fluorescence detector after a carbonyl specific chemical labeling [77]. Gel permeation chromatography was also applied for the characterisation of cellulose nitrate, a semi-synthetic material deriving from the industrial processing of cellulose, which was one of the first semi-synthetic plastics to be commercially exploited. Many museums contain a large number of artifacts containing this plastic. In order to evaluate the main degradation pattern of this material, GPC-RID was applied for the characterisation of several samples from selected artifacts in various stages of preservation, and on a set of artificially aged reference cellulose nitrate films [78, 79].

In both cases, GPC was mainly adopted to highlight the depolymerisation reactions occurring in paper or nitrocellulose as results of hydrolysis, possibly catalysed by metal ions.

Gum Arabic, or acacia gum, is the oldest and best known of all the tree gum exudates and has been used as binder and traded for more than 5000 years. Structural studies of the proteic and polysaccharide components of gum Arabic were performed using GPC coupled with a UV-RID-MALS [80]. The effects of the ultraviolet irradiation on the physicochemical and functional properties of gum Arabic were also evaluated using GPC-RID-UV: the modification of the molecular weight distribution of the gum polymer were used to identify the cross-linking and depolymerisation processes occurring during exposure to UV light [81].

4.3 Protein Paint Binders

Historically, proteinaceous materials, such as egg, casein and animal glue, have commonly been used as paint binders.

Size exclusion chromatography was applied on paint replicas of casein and ovalbumin with cinnabar (HgS) in order to evaluate the ageing pathways of these proteins in presence of such pigment. The separation of the proteins was performed using a SEC system coupled to UV and cold vapor generation atomic fluorescence spectrometry detector (SEC–UV–CVGAFS). CVGAFS technique is based on the pre-column derivatisation of protein thiol groups with a mercurial probe in order to

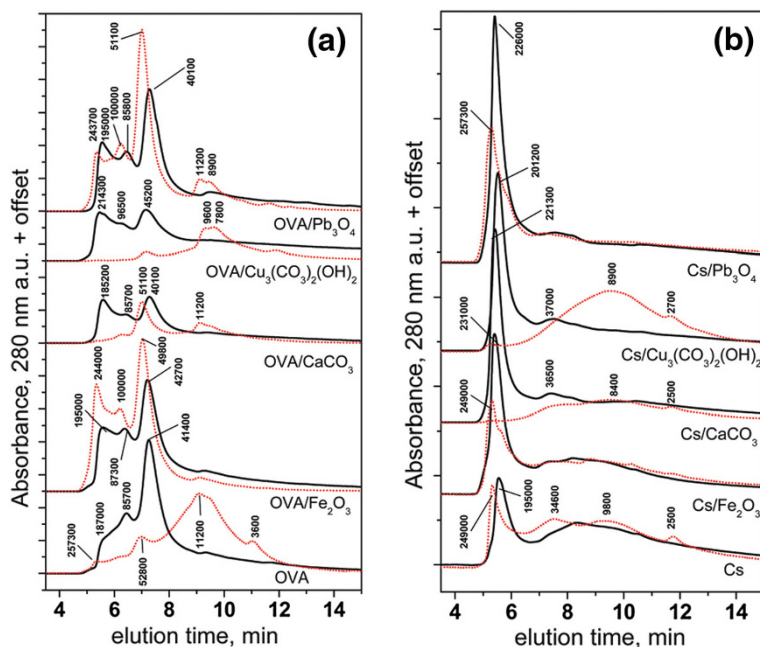


Fig. 8 SEC-UV chromatograms of the soluble fraction of unaged (*continuous line, black*) and aged (*dotted line, red*) ovalbumin/pigment (a) and casein/pigment (b) paint replica (reprinted with permission from [83])

selectively speciate and detect mercury–protein complexes by CVGAFS. The separation of the proteins was performed using a Biosep SEC S2000 column (Phenomenex, USA) and an isocratic elution in 50 mM Phosphate Buffered Saline pH 7.4, 0.15 M NaCl at 1.0 mL/min [82]. The interactions of casein and ovalbumin with azurite ($\text{Cu}_3(\text{CO}_3)_2(\text{OH})_2$), calcium carbonate (CaCO_3), hematite (Fe_2O_3) and red lead (Pb_3O_4) were also evaluated using the chromatographic conditions described above, with a DAD detector (Fig. 8) [83]. The results highlighted that pigments may act directly on the stability of the protein structure because of their interaction with amino acid functional groups, or indirectly, promoting oxidation.

4.4 Triterpenoid Resins

Triterpenoid resins are the main components of traditional varnishes used by artists and are often identified in archeological amorphous materials. Polymerisation and degradation of triterpenoid resins entails radical polymerisation, cross-linking and condensation, oxidative modifications and shortening of side-chains.

In order to evaluate the effects on the molecular weight distribution of these chemical processes, dammar and mastic resins were studied using a high performance size exclusion chromatography system (HP-SEC) coupled with RID and UV/Vis detectors [84]. This technique was not applied to other cases of

terpenoid resins due to their poor solubility in the majority of the samples. Nonetheless, the results highlighted in [84] proved that the ageing processes are related to the thickness of the varnish layer; as an example, condensation reactions that leads to cross-linking and polymerisation were identified only in the first portion of the resin layer and are related to UV wavelength exposure.

4.5 Lipids

Drying oils are one of the most ancient binders used in paints for both decorative and protective purposes. The oils used as paint binder are usually pre-processed by heating, chemical bleaching and treatment with metallic salts in order to enhance their siccative proprieties (ability to form films).

The effects of these processes on linseed oil were studied using an HP-SEC-RID-UV/Vis-DAD system. The oil samples were solubilised using tetrahydrofuran and the chromatographic separation was performed using a PLGEL 5 μm 1000 Å column (300 \times 7.5 mm, Polymer Laboratories, Netherlands) and tetrahydrofuran as eluent [85]. The application of SEC analysis allowed the identification of the main chemical modification involved during the preparation of linseed oil. Two major chemical processes were observed for the oils: oxidation and oligomerisation. This is accompanied by a relative decrease in the percentage of the triple unsaturated fatty acid, the most reactive component of the TAGs.

Alkyd paints, introduced in the 1940s, represent an evolution of modern drying oils. They are oil-modified polyesters, characterised by higher drying rates than classic drying oils. Size exclusion chromatography coupled with a MALS and a RID detector was applied to evaluate the structure of an alkyd resin produced using soybean oil at different polymerisation reaction times in [86]. The application of SEC coupled with a MALS detector provides information about the branching and on the molecular weight distribution of the resin.

5 Summary and Conclusions

This review of the several applications of liquid chromatography to the study of materials in the field of Cultural Heritage highlighted that several protocols were optimised for the detection and, in several cases, quantitation, of a great number of analytes. Almost all types of HPLC have been exploited with the aim of characterising different properties of different materials.

Until now, most of the research has focused on the application of reversed-phase HPLC to the analysis of organic dyes and lakes, which has almost become routine in diagnostic campaigns. Besides the future perspective for proteomics in this field, reviewed in another chapter, the analysis of dyes and lipid residues or binders represents the most promising application up to now. The main improvement that is currently gaining momentum is related to the development and validation of UHPLC methods for dyes analyses, which allow faster separations without losses in chromatographic resolution. Moreover, the key issue in both these applications (namely, dyes and lipid analysis) is the optimisation of sample treatment, in order

not only to avoid matrix effects, which have not been evaluated in any of the published papers, but also to lower detection and quantitation limits.

Less common applications of HPLC include ion chromatography and size exclusion chromatography, which have both been successfully applied to selected cases.

Ion chromatography has been mainly used as routine analytical technique to quantify cations and anions in damage layers and patinas, mostly on stone buildings. Robust protocols entailing sample treatment and complementation of IC results with those of other techniques have been published, which has set the standard for future applications.

Size exclusion chromatography has been applied in a few cases to the study of polymeric materials upon ageing (also thanks to accelerated ageing tests). Both natural (proteins, polysaccharides, lignin) and synthetic (alkyd binders and low molecular weight resins) polymers have been studied, with particular attention to their behaviour in the presence of inorganic salts, which may influence depolymerisation or polymerisation reactions. This technique has high potential for the characterisation of the ageing of materials, given the possibility to detect and characterise the products. On the one hand, we may expect future developments to go in the direction of coupling this technique with mass spectrometric detection that has already proven effective in the study of protein behaviour in biological studies, and in polymer chemistry for more than 10 years. On the other hand, the lack of proper standards in the field of Cultural-Heritage-related studies might represent a drawback for this kind of application.

Acknowledgments The authors graciously acknowledge the National project “PRIN 2010–2011: Sustainability in cultural heritage: from diagnosis to the development of innovative systems for consolidation, cleaning and protection”, granted by MIUR for financial support. They would also like to acknowledge their colleagues at University of Pisa, professor Erika Ribechini and professor Francesca Modugno, for the fruitful discussions.

References

1. The chromatography and sample preparation terminology guide (2013)
2. Colombini MP, Modugno F (2009) Organic mass spectrometry in art and archeology. Wiley, Chichester
3. Lomax SQ, Learner T (2006) A review of the classes, structures, and methods of analysis of synthetic organic pigments. *J Am Inst Conserv* 45(2):107–125
4. Nowik W, Desrosiers S, Surowiec I, Trojanowicz M (2005) The analysis of dyestuffs from first- to second-century textile artefacts found in the Martresde-Veyre (France) excavations. *Archaeometry* 47:835–848
5. Surowiec I (2008) Application of high-performance separation techniques in archaeometry. *Microchim Acta* 162:289–302
6. Rosenberg E (2008) Characterisation of historical organic dyestuffs by liquid chromatography–mass spectrometry. *Anal Bioanal Chem* 391:33–57
7. Degano I, Ribechini E, Modugno F, Colombini MP (2009) Analytical methods for the characterization of organic dyes in artworks and in historical textiles. *Appl Spectrosc Rev* 44:363–410
8. Pauk V, Bartak P, Lemr K (2014) Characterization of natural organic colorants in historical and art objects by high-performance liquid chromatography. *J Sep Sci* 37:3393–3410

9. Russell J, Singer BW, Perry JJ, Bacon A (2011) The identification of synthetic organic pigments in modern paints and modern paintings using pyrolysis-gas chromatography–mass spectrometry. *Anal Bioanal Chem* 400:1473–1491
10. Ghelardi E, Degano I, Colombini MP, Mazurek J, Schilling M, Learner T (2015) Py-GC/MS applied to the analysis of synthetic organic pigments: characterization and identification in paint samples. *Anal Bioanal Chem* 407:1415–1431
11. Carlesi S et al (2015) Discovering “The Italian Flag” by Fernando Melani (1907–1985). *Spectrochim Acta Part A Mol Biomol Spectrosc*
12. Lech K, Wilicka E, Witowska-Jarosz J, Jarosz M (2013) Early synthetic dyes—a challenge for tandem mass spectrometry. *J Mass Spectrom* 48:141–147
13. van Bommel MR, Vanden Berghé I, Wallert AM (2007) High-performance liquid chromatography and non-destructive three-dimensional fluorescence analysis of early synthetic dyes. *J Chromatogr A* 1157:260–272
14. Confortin D, Neevel H, Brustolon M, Franco L, Kettelarij AJ, Williams RM, van Bommel MR (2010) Crystal violet: study of the photo-fading of an early synthetic dye in aqueous solution and on paper with HPLC-PDA, LCMS and FORS. *J Phys Conf Ser* 231:1–9
15. de Keijzer M, van Bommel MR, Hofmann-de Keijzer R, Knaller R, Oberhumer E (2012). Indigo carmine: understanding a problematic blue dye. In: *Contributions to the Vienna Congress 2012 (Vienna 2012)*, pp S87–S95
16. Restivo A, Degano I, Ribechini E, Colombini MP (2014) Development and optimisation of an HPLC-DAD-ESI-Q-TOF method for the determination of phenolic acids and derivatives. *Plos One* 9:e88762
17. Halpine SM (1995) An improved dye and lake pigment analysis method for high performance liquid chromatography and diode-array detection. *Stud Conserv* 41:76–94
18. Nowik W, Marcinowska R, Kusyk K, Cardonc D, Trojanowicz M (2011) High performance liquid chromatography of slightly soluble brominated indigoids from Tyrian purple. *J Chromatogr A* 1218:1244–1252
19. Surowiec I, Quye A, Trojanowicz M (2006) Liquid chromatography determination of natural dyes in extracts from historical Scottish textiles excavated from peat bogs. *J Chromatogr A* 1112:209–217
20. Taujenis L, Olšauskaitė V (2012) Identification of main constituents of historical textile dyes by ultra performance liquid chromatography with photodiode array detection. *Chemija* 23:210–215
21. Serrano A, van Bommel M, Hallett J (2013) Evaluation between ultrahigh pressure liquid chromatography and high-performance liquid chromatography analytical methods for characterizing natural dyestuffs. *J Chromatogr A* 1318:102–111
22. Troalen LG, Phillips AS, Peggie DA, Barran PE, Hulme AN (2014) Historical textile dyeing with *Genista tinctoria* L.: a comprehensive study by UPLC-MS/MS analysis. *Anal Methods* 6:8915–8923
23. Wouters J, Grzywacz CM, Claro A (2011) A comparative investigation of hydrolysis methods to analyze natural organic dyes by HPLC-PDA. *Stud Conserv* 56:231–249
24. Manhita A, Ferreira T, Candeias A, Barrocas Dias C (2011) Extracting natural dyes from wool—an evaluation of extraction methods. *Anal Bioanal Chem* 400:1501–1514
25. Valianou L, Karapanagiotis I, Chrysoulakis Y (2009) Comparison of extraction methods for the analysis of natural dyes in historical textiles by high-performance liquid chromatography. *Anal Bioanal Chem* 395:2175–2189
26. Sanyova J (2008) Mild extraction of dyes by hydrofluoric acid in routine analysis of historical paint micro-samples. *Microchim Acta* 162:361–370
27. Blanc R, Espejo T, Lopez-Montes A, Torres D, Crovetto G, Navalón A, Vilchez JL (2006) Sampling and identification of natural dyes in historical maps and drawings by liquid chromatography with diode-array detection. *J Chromatogr A* 1122:105–113
28. Sanyova J, Reisse J (2006) Development of a mild method for the extraction of anthraquinones from their aluminum complexes in madder lakes prior to HPLC analysis. *J Cult Herit* 7:229–235
29. Lech K, Jarosz M (2011) Novel methodology for the extraction and identification of natural dyestuffs in historical textiles by HPLC–UV–Vis–ESI–MS. Case study: chasubles from the Wawel Cathedral collection. *Anal Bioanal Chem* 399:3241–3251
30. Mouri C, Laursen R (2012) Identification of anthraquinone markers for distinguishing *Rubia* species in madder-dyed textiles by HPLC. *Microchim Acta* 179:105–113
31. Zhang X, Laursen RA (2005) Development of mild extraction methods for the analysis of natural dyes in textiles of historical interest using LC-diode array detector-MS. *Anal Chem* 77:2022–2025

32. VandenBerghe I, Gleba M, Mannering U (2009) Towards the identification of dyestuffs in early iron age Scandinavian peat bog textiles. *J Archaeol Sci* 36:1910–1921
33. Colombini MP, Carmignani A, Modugno F et al (2004) Integrated analytical techniques for the study of ancient Greek polychromy. *Talanta* 63:839–848
34. Stolyhwo A, Colin H, Guiochon G (1985) Analysis of triglycerides in oils and fats by liquid chromatography with the laser light scattering detector. *Anal Chem* 57:1342–1354
35. Herrera LC, Potvin M, Melanson J (2010) Quantitative analysis of positional isomers of triacylglycerols via electrospray ionization tandem mass spectrometry of sodiated adducts. *Rapid Commun Mass Spectrom* 24:2745–2752
36. Byrdwell WC, Neff WE (2002) Dual parallel electrospray ionization and atmospheric pressure chemical ionization mass spectrometry (MS), MS/MS and MS/MS/MS for the analysis of triacylglycerols and triacylglycerol oxidation products. *Rapid Commun Mass Spectrom* 16:300–319
37. La Nasa J, Ghelardi E, Degano I, Modugno F, Colombini MP (2013) Core shell stationary phases for a novel separation of triglycerides in plant oils by high performance liquid chromatography with electrospray-quadrupole-time of flight mass spectrometer. *J Chromatogr A* 1308:114–124
38. Saliu F, Degano I, Colombini MP (2014) Identification of triacylglycerols in archaeological organic residues by core-shell reversed phase liquid chromatography coupled to electrospray ionization-quadrupole-time of flight mass spectrometry. *J Chromatogr A* 1346:78–87
39. Mottram HR, Evershed RP (1996) Structure analysis of triacylglycerol positional isomers using atmospheric pressure chemical ionisation mass spectrometry. *Tetrahedron Lett* 37:8593–8596
40. Kimpe K, Jacobs PA, Waelkens M (2002) Mass spectrometric methods prove the use of beeswax and ruminant fat in late Roman cooking pots. *J Chromatogr A* 968:151–160
41. Kimpe K, Jacobs PA, Waelkens M (2001) Analysis of oil used in late Roman oil lamps with different mass spectrometric techniques revealed the presence of predominantly olive oil together with traces of animal fat. *J Chromatogr A* 937:87–95
42. Romanus K, Van Neer W, Marinova E et al (2008) Brassicaceae seed oil identified as illuminant in Nilotic shells from a first millennium AD Coptic church in Bawit, Egypt. *Anal Bioanal Chem* 390:783–793
43. Romanus K, Poblome J, Verbeke K, Luypaerts A, Jacobs P, De Vos D, Waelkens M (2007) An evaluation of analytical and interpretative methodologies for the extraction and identification of lipids associated with pottery sherds from the site of Sagalassos, Turkey. *Archaeometry* 49:729–747
44. Saliu F, Modugno F, Orlandi M, Colombini MP (2011) HPLC APCI–MS analysis of triacylglycerols (TAGs) in historical pharmaceutical ointments from the eighteenth century. *Anal Bioanal Chem* 401:1785–1800
45. Berg JDJvd, Vermist ND, Carlyle L, Holcapek M, Boon JJ (2004) Effects of traditional processing methods of linseed oil on the composition of its triacylglycerols. *J Sep Sci* 27:181–199
46. Chester TL (2013) Recent developments in high-performance liquid chromatography stationary phases. *Anal Chem* 85:579–589
47. LaNasa J, Zanaboni M, Uldanck D, Degano I, Modugno F, Kutzke H, Tveit ES, Topalova-Casadiogo B, Colombini mp (2015) Novel application of liquid chromatography/mass spectrometry for the characterization of drying oils in art: Elucidation on the composition of original paint materials used by Edvard Munch (1863–1944). *Anal Chim Acta* 896:177–189
48. Nasa JL, Degano I, Modugno F, Colombini MP (2013) Alkyd paints in art: characterization using integrated mass spectrometry. *Anal Chim Acta* 797:4–80
49. Nasa JL, Degano I, Modugno F, Colombini MP (2015) Industrial alkyd resins: characterization of pentaerythritol and phthalic acid esters using integrated mass spectrometry. *Rapid Commun Mass Spectrom* 29:225–237
50. Nasa JL, Degano I, Modugno F, Colombini MP (2014) Effects of acetic acid vapour on the ageing of alkyd paint layers: multianalytical approach for the evaluation of the degradation processes. *Polym Degrad Stab* 105:257–264
51. Gobbi G, Zappia G, Sabbioni C (1995) Anion determination in damage layers of stone monuments. *Atmos Environ* 29:703–707
52. Sabbioni C, Ghedini N, Bonazza A (2003) Organic anions in damage layers on monuments and buildings. *Atmos Environ* 37:1261–1269
53. Bonazza A, Sabbioni C, Ghedini N (2005) Quantitative data on carbon fractions in interpretation of black crusts and soiling on European built heritage. *Atmos Environ* 39:2607–2618

54. Moropoulou A, Kouli M, Kourtelis Ch, Theoulakis P, Avdelidis NP (2001) Integrated methodology for measuring and monitoring salt decay in the medieval city of Rhodes porous stone. *Mediterr Archaeol Archaeom* 1:57–68
55. Tittarelli F, Moriconi G, Bonazza A (2008) Atmospheric deterioration of cement plaster in a building exposed to a urban environment. *J Cult Herit* 9:203–206
56. Nava S, Becherini F, Bernardi A et al (2010) An integrated approach to assess air pollution threats to cultural heritage in a semi-confined environment: the case study of Michelozzo's Courtyard in Florence (Italy). *Sci Total Environ* 408:1403–1413
57. Fassina V, Favaro M, Naccari A, Pigo M (2002) Evaluation of compatibility and durability of a hydraulic lime-based plaster applied on brick wall masonry of historical buildings affected by rising damp phenomena. *J Cult Herit* 3:45–51
58. Smolik J, Maskova L, Zikova N, Ondrackova L, Ondracek (2013) Deposition of suspended fine particulate matter in a library. *Herit Sci* 1:7
59. Ghedini N, Ozga I, Bonazza A, Dilillo M, Cachier H, Sabbioni C (2011) Atmospheric aerosol monitoring as a strategy for the preventive conservation of urban monumental heritage: the Florence Baptistery. *Atmos Environ* 45:5979–5987
60. Niklasson A, Johansson L-G, Svensson J-E (2004) Atmospheric corrosion of historical organ pipes: influence of acetic and formic acid vapour and water leaching on lead. In: *Proceedings of Metal 2004 National Museum of Australia Canberra ACT 4–8 October 2004 (Canberra 2004)*, National Museum of Australia, pp 273–280
61. Kontozova-Deutsch V, Krata A, Deutsch F, Bencs L, Van Grieken R (2008) Efficient separation of acetate and formate by ion chromatography: application to air samples in a cultural heritage environment. *Talanta* 75:418–423
62. Ghedini N, Sabbioni C, Bonazza A, Gobbi G (2006) Chemical–thermal quantitative methodology for carbon speciation in damage layers on building surfaces. *Environ Sci Technol* 40:939–944
63. Hodgkins RE, Grzywacz CM, Garrell RL (2011) An improved ion chromatography method for analysis of acetic and formic acid vapours. *e-Preserv Sci* 8:74–80
64. Kontozova-Deutsch V, Deutsch F, Bencs L, Krata A, Van Grieken R, De Wael K (2011) Optimization of the ion chromatographic quantification of airborne fluoride, acetate and formate in the Metropolitan Museum of Art, New York. *Talanta* 86:372–376
65. Franzoni E, Sassoni E, Graziani G (2015) Brushing, poultice or immersion? The role of the application technique on the performance of a novel hydroxyapatite-based consolidating treatment for limestone. *J Cult Herit* 16:173–184
66. Barth HG, Boyes BE, Jackson C (1998) Size exclusion chromatography and related separation techniques. *Anal Chem* 70:251R–278R
67. Wu CS (2003) *Handbook of size exclusion chromatography and related techniques: revised and expanded*. Taylor & Francis
68. Berek DA (2010) Size exclusion chromatography—a blessing and a curse of science and technology of synthetic polymers. *J Sep Sci* 33:315–335
69. Maines CA, Da la Rie ER (2005) Size-exclusion chromatography and differential scanning calorimetry of low molecular weight resins used as varnishes for paintings. *Prog Org Coat* 52:39–45
70. Ploeger R, De la Rie ER, McGlinchey CW, Palmer M, Maines CA, Chiantore O (2014) The long-term stability of a popular heat-seal adhesive for the conservation of painted cultural objects. *Polym Degrad Stab* 107:307–313
71. Ferreira JL, Melo MJ, Ramos AM (2010) Poly(vinyl acetate) paints in works of art: a photochemical approach. Part 1. *Polym Degrad Stab* 95:453–461
72. Scalrone D, Chiantore O (2004) Separation techniques for the analysis of artists' acrylic emulsion paints. *J Sep Sci* 27:263–274
73. Somsen GW, Gooijer C, Velthors NH, Brinkman UAT (1998) Coupling of column liquid chromatography and Fourier transform infrared spectrometry. *J Chromatogr A* 811:1–34
74. Colombini MP, Lucejko JJ, Modugno F, Orlandi M, Tolppa E-L, Zoia L (2009) A multi-analytical study of degradation of lignin in archaeological waterlogged wood. *Talanta* 80:61–70
75. Salanti A, Zoia L, Tolppa EL, Giachi G, Orlandi M (2010) Characterization of waterlogged wood by NMR and GPC techniques. *Microchem J* 95:345–352
76. Zoia L, Salanti A, Orlandi M (2014) Chemical characterization of archaeological wood: softwood Vasa and hardwood Riksapplet case studies. *J Cult Herit*
77. Ahn K, Hartl A, Hofmann C, Henniges U, Potthast A (2014) Investigation of the stabilization of verdigris-containing rag paper by wet chemical treatments. *Herit Sci* 2

78. Quye A, Littlejohn D, Pethrick RA, Stewart RA (2011) Investigation of inherent degradation in cellulose nitrate museum artefacts. *Polym Degrad Stab* 96:1369–1376
79. Quye A, Littlejohn D, Pethrick RA, Stewart RA (2011) Accelerated ageing to study the degradation of cellulose nitrate museum artefacts. *Polym Degrad Stab* 96:1934–1939
80. Islam AM, Phillipsl GO, Sljivo A, Snowden MJ, Williams PA (1997) A review of recent developments on the regulatory, structural and functional aspects of gum arabic. *Food Hydrocoll* 4:493–505
81. Kuan Y-H, Bhat R, Senan C, Williams PA, Karim AA (2009) Effects of ultraviolet irradiation on the physicochemical and functional properties of gum Arabic. *J Agric Food Chem* 57:9154–9159
82. Duce C, Ghezzi L, Onor M, Bonaduce I, Colombini MP, Tinè MR, Bramanti M (2012) Physicochemical characterization of protein–pigment interactions in tempera paint reconstructions: casein/cinnabar and albumin/cinnabar. *Anal Bioanal Chem* 402:2183–2193
83. Duce C, Bramanti E, Ghezzi L, Bernazzani L, Bonaduce I, Colombini MP, Spepi A, Biagi S, Tine MR (2013) Interactions between inorganic pigments and proteinaceous binders in reference paint reconstructions. *Dalton Trans* 42:5945–6236
84. Theodorakopoulos C, Boon JJ (2011) A high performance size exclusion chromatographic study on the depth-dependent gradient in the molecular weight of aged triterpenoid varnish films. *Prog Org Coat* 72:778–783
85. Berg JDJ, Vermist ND, Carlyle L, Holčapek M, Boon JJ (2004) Effects of traditional processing methods of linseed oil on the composition of its triacylglycerols. *J Sep Sci* 27:181–199
86. Vareckova D, Podzimek S, Lebduska J (2006) Characterization of alkyd resins by size exclusion chromatography coupled with a multi-angle light scattering photometer. *Anal Chim Acta* 557:31–36

Analytical Approaches Based on Gas Chromatography Mass Spectrometry (GC/MS) to Study Organic Materials in Artworks and Archaeological Objects

Ilaria Bonaduce¹  · Erika Ribechini¹ ·
Francesca Modugno¹ · Maria Perla Colombini^{1,2}

Received: 30 September 2015 / Accepted: 14 December 2015 / Published online: 4 January 2016
© Springer International Publishing Switzerland 2015

Abstract Gas chromatography/mass spectrometry (GC/MS), after appropriate wet chemical sample pre-treatments or pyrolysis, is one of the most commonly adopted analytical techniques in the study of organic materials from cultural heritage objects. Organic materials in archaeological contexts, in classical art objects, or in modern and contemporary works of art may be the same or belong to the same classes, but can also vary considerably, often presenting different ageing pathways and chemical environments. This paper provides an overview of the literature published in the last 10 years on the research based on the use of GC/MS for the analysis of organic materials in artworks and archaeological objects. The latest progresses in advancing analytical approaches, characterising materials and understanding their degradation, and developing methods for monitoring their stability are discussed. Case studies from the literature are presented to examine how the choice of the working conditions and the analytical approaches is driven by the

Guest Editor: Rocco Mazzeo

✉ Ilaria Bonaduce
ilaria.bonaduce@unipi.it
Erika Ribechini
erika.ribechini@unipi.it
Francesca Modugno
francesca.modugno@unipi.it
Maria Perla Colombini
maria.perla.colombini@unipi.it

¹ Department of Chemistry and Industrial Chemistry, University of Pisa, Via Moruzzi 13, 56124 Pisa, Italy

² Institute for the Conservation and Promotion of Cultural Heritage, National Research Council of Italy, Via Madonna del Piano 10, 50019 Sesto Fiorentino, Italy

analytical and technical question to be answered, as well as the nature of the object from which the samples are collected.

Keywords Gas chromatography/mass spectrometry · Wet chemical sample pre-treatment · Analytical pyrolysis · Organic materials · Paintings · Archaeological objects

1 Introduction

Gas chromatographic techniques were first used in conservation science in the 1970s, and were driven by the interest in identifying organic materials present as binders in paintings, or associated with archaeological objects. Since the pioneering work of Mills and White in the laboratories of the National Gallery in London [1–3] and of Michael Shilling at the Getty Conservation Institute in Los Angeles [4], gas chromatography coupled with mass spectrometry (GC/MS) has become an established method for investigating organic materials in art and archaeological objects.

Most organic materials encountered in cultural heritage are macromolecular. In some cases, they are natural or synthetic polymers (such as proteins, plant gums, vinyl, and acrylic resins), others undergo oligomerisation or cross-linking reactions as an effect of exposure to light and air (such as natural resins or drying oils). Organic materials in the cultural heritage are also polar and have a low volatility. Their analysis by GC/MS thus entails chemical or thermal treatments in order to reduce the original macromolecules into low polarity, low molecular weight components, thus facilitating their volatilisation and subsequent separation onto a gas chromatographic column. This can be achieved by coupling analytical pyrolysis with gas chromatography mass spectrometry (Py-GC/MS) or by a wet-chemical treatment of the samples prior to GC/MS. Common analytical approaches, method developments, advantages, and drawbacks of the different methods, as well as instrumental aspects have been discussed and overviewed in detail in the literature [5–12].

In the last 10 years, analytical research involving GC/MS and PY-GC/MS has tackled three related challenges: advancing analytical approaches, characterising materials and understanding their degradation, and developing methods for monitoring their stability. The choice of the working conditions and the analytical approaches is firstly driven by analytical and technical questions, among which: what painting or manufacturing technique has been applied? What is the object's state of conservation? Which chemical markers or features allow to detect a specific material? Which analytical procedure detects a specific analyte?

The answers clearly depend on the classes of organic materials found in the sample and the nature of the sample itself. Organic materials in archaeological contexts, in classical art objects, or in modern and contemporary works of art may be the same or belong to the same classes, but can also vary considerably, often presenting different ageing pathways and chemical environments, thus requiring different analytical approaches. Thus, the following sections discuss the recent advances in GC/MS and Py-GC/MS for the characterisation and identification of organic materials in archaeological contexts, classical art objects, and modern and contemporary works of art.

2 Organic Materials in Archaeological Contexts

Archaeological organic samples involve a range of critical characteristics, making their study an analytical challenge. Their investigation is complicated by the ageing and degradation of the molecules present in the organic substances [13–18]. This means that in order to establish the origin of the natural substances in the sample and to understand the alteration processes that have modified the materials it is essential to identify the molecular composition as well as to reveal the presence of

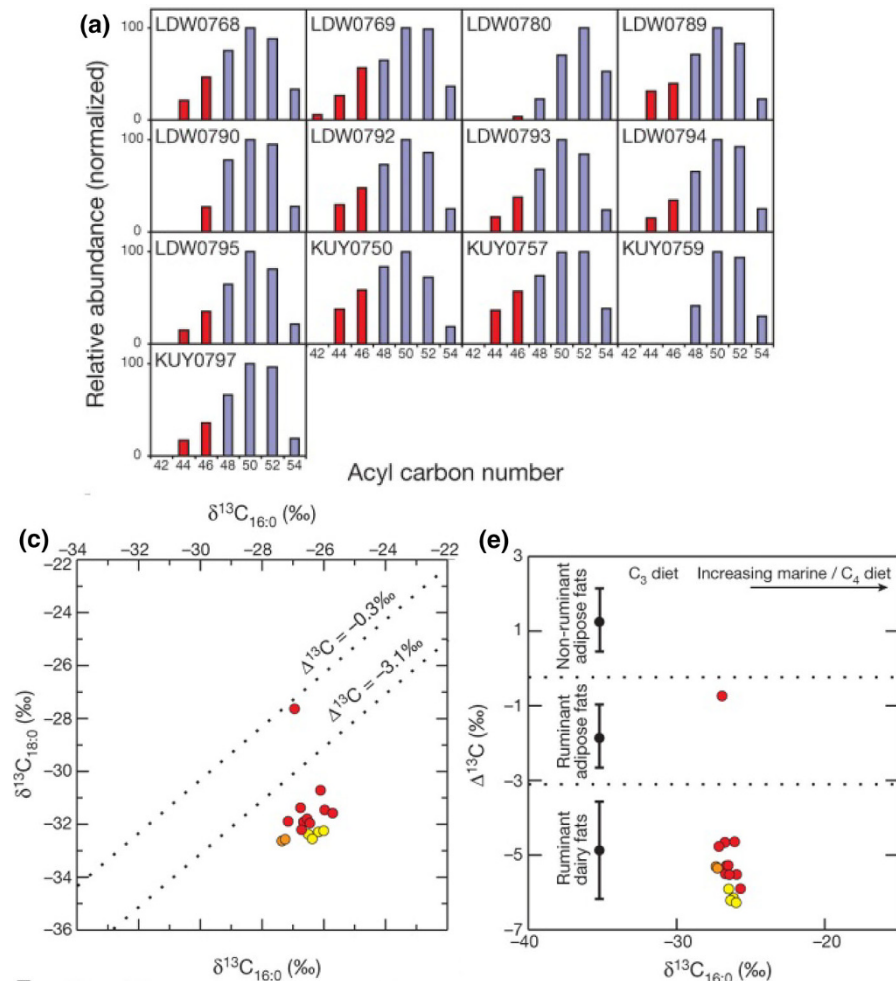


Fig. 1 TAG distributions of total lipid extracts of sieves from the region of Kuyavia (a). The blue bars denote TAGs present in both adipose and milk fats, whereas those in red are only detectable in milk fat. Plots of the $\delta^{13}\text{C}$ values for the C16:0 and C18:0 fatty acids prepared from animal fat residues extracted from sieves (b). $\Delta^{13}\text{C}$ values of the extracts plotted against their $\delta^{13}\text{C}_{16:0}$ values from the same potsherds (c). Adapted from [50]

molecular markers. Gas chromatography/mass spectrometry (GC/MS), after appropriate wet-chemical pre-treatments of the sample or using analytical pyrolysis, is thus the most commonly adopted technique.

The possibility of identifying unexpected compounds by MS detection on the basis of their mass spectra makes GC/MS particularly suitable for studying unknown matrices and/or following ageing and degradation pathways. In addition, given that gas chromatography combustion-isotope ratio mass spectrometry (GC-C-IRMS) can be used to measure the carbon stable isotope ratios ($\delta^{13}\text{C}$) of palmitic and stearic acids, the exact origin of lipid substances from archaeological findings can be identified, which is one of the greatest challenges of organic residues analysis [19]. In fact, degraded lipid substances are mainly composed of palmitic and stearic acids regardless of the original source, due to degradation processes that tend to make the fatty acid profile of archaeological samples difficult or impossible to diagnose. Isotopic analysis has proven to be a powerful tool in identifying the origin of lipid materials of a very similar composition, even in mixtures. This analysis distinguishes between ruminant and porcine adipose fats and between lipids from C3 and C4 plants. In addition, ruminant adipose and dairy fats can also be distinguished by the $\delta^{13}\text{C}$ values along with $\Delta^{13}\text{C}$ ($\delta^{13}\text{C}_{18}-\delta^{13}\text{C}_{16}$) of their fatty acids [19].

Since 2000, GC/MS, Py-GC/MS, and GC-C-IRMS have been well established techniques for identifying organic substances and materials linked to specific productions, daily life and food activities, religious or ritual practices, and cosmetic and medical activities [20–47]. In addition, the same techniques, particularly GC-C-IRMS, have been used to address some key questions concerning animal husbandry in prehistoric phases [48–52].

A particularly interesting study was recently carried out by GC/MS and GC-C-IRMS on organic residues preserved in sieves/strainers from the region of Kuyavia (Poland) and dating back to 5200–4800 cal. BC to investigate the function of these ceramic vessels [50]. The chromatographic profile along with $\delta^{13}\text{C}$ values of palmitic (C_{16}) and stearic (C_{18}) acids, and $\Delta^{13}\text{C}$ ($\delta^{13}\text{C}_{18}-\delta^{13}\text{C}_{16}$) values provided direct chemical evidence of their use in milk processing (Fig. 1). The chemical data obtained provided evidence of the high abundance of dairy products and the specific features of the ceramic shreds, characterized by the presence of several holes, led the authors to suggest that as early as 7000 years ago prehistoric people were able to make cheese.

The chemical study of organic materials from archaeological contexts is generally based on the knowledge of the behaviour of the materials under ageing and on comparisons with reference materials of a known origin. Thus, collecting reference materials for testing analytical procedures and comparing analytical data and submitting them to artificial ageing treatments are important preliminary steps in the research on ancient materials [6, 17, 18]. Further considerations are required for the potential use of unexpected materials that are not extensively used in modern society, such as the *Brassicaceae* oil used as an illuminant found in two Roman ceramic lamps (lamps 718 and 809) discovered at the archaeological site of North Necropolis of Antinoe (Egypt) [31]. The two lamps showed an adherent blackish residual deposit, which was submitted to an analytical protocol based on GC/MS

analysis. After alkaline hydrolysis, extraction, and derivatisation reaction with BSTFA, the samples produced the chromatographic patterns shown in Fig. 2.

The extracts consisted of a series of linear monocarboxylic saturated fatty acids ranging from 9 to 24 carbon atoms with hexadecanoic acid (palmitic) and octadecanoic acid (stearic) as the most prominent, and a high abundance of long chain acids (C₂₀–C₂₄), a series of α,ω -dicarboxylic acids ranging from four up to 14 carbon atoms, with nonanedioic acid (azelaic) as the main constituent of this group, a series of ω -hydroxycarboxylic acids ranging from eight up to 14 carbon atoms, and three long chain dihydroxycarboxylic acids with 18, 20, and 22 carbon atoms, namely, 9,10-dihydroxyoctadecanoic acid, 11,12-dihydroxyeicosanoic acid, and 13,14-dihydroxydocosanoic acid; each of the dihydroxycarboxylic acids were present as a pair of threo-erythro isomers. The predominance of C9 dicarboxylic acid (azelaic acid) together with the presence of 9,10-dihydroxylated acids implied high amounts of oleic acid in the original lipid material. On the other hand, the presence of 11,12-dihydroxyeicosanoic acid and 13,14-dihydroxydocosanoic acid was a very distinctive feature of these samples, and the formation of 11,12-dihydroxyeicosanoic acid and 13,14-dihydroxydocosanoic was ascribed to the oxidation of gondoic and erucic acids. Since the only seed oils that contained high amounts of gondoic and erucic acids were those derived from *Brassicaceae* [31, 53, 54], the results were interpreted as chemical evidence of the use of a seed oil derived from *Brassicaceae* species for lighting purposes. It was impossible to detect the botanical species from which the seed oil used in the examined lamps was actually produced, thus it is not known whether the oil came from radish as reported by Pliny, or from another *Brassicaceae* plant such as rapeseed. In any case, detection of the characteristic markers in lamps from Antinoe, one of the main urban

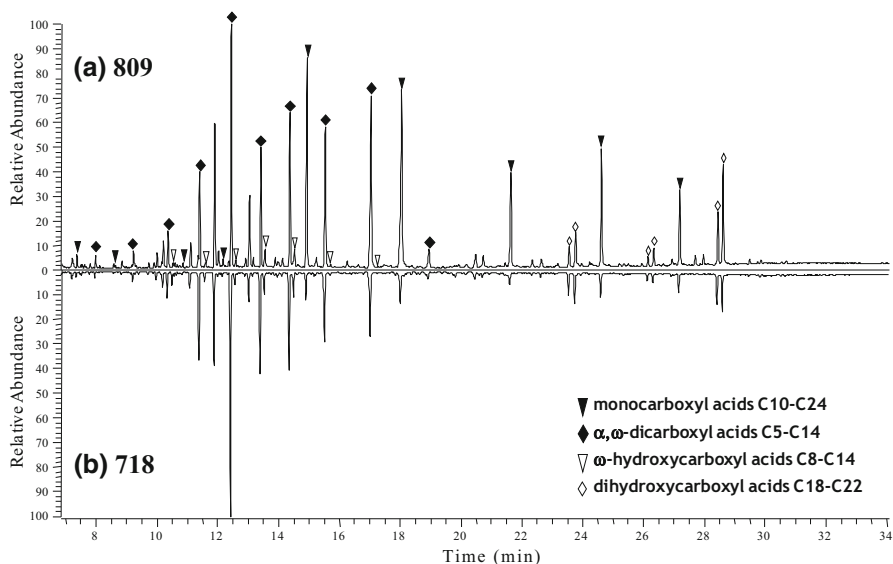


Fig. 2 GC/MS chromatogram of *a* sample 718 and *b* sample 809 [31]

centres of Roman Egypt, represents chemical confirmation of the widespread use of cruciferous oil at that time and is consistent with ancient documents [55]. This was supported by the results obtained in the aging tests and analysis performed on *Brassica juncea* oil and the pure gondoic and erucic acids. It was possible to demonstrate that 11,12-dihydroxyeicosanoic acid and 13,14-dihydroxydocosanoic acid are markers for cruciferous seed oil in archaeological residues.

Lipids of animal and plant origin as well as plant resins are the most commonly encountered substances in archaeological findings. In fact, owing to their lower susceptibility to structural modification and degradation by chemical and microbiological attacks as well as hydrophobicity, they may survive better than carbohydrates, proteins, and nucleotides in archaeological environments [13–15, 18]. A similar argument can be made for the chemical components of alcoholic beverages and wines whose water solubility limits their persistence in archaeological environments. The detection of wine and other alcoholic beverage residues has always been of great interest in the archaeological community, and although some papers have appeared in the literature [46, 56, 57], it still remains an analytical challenge. In this framework, a completely new biomarker approach entailing the detection of bacterial lipids formed during fermentation and ethanol production was recently published [58]. Correa-Ascencio et al. used gas chromatography/mass spectrometry in selected ion monitoring (m/z 191) of lipid extracts to reveal characteristic bacterio-hopanoids produced by *Zymomonas mobilis* bacterium during the fermentation of maguey plants (*Agavaceae*) in order to identify pulque residues in pottery vessels from Teotihuacan (150 B.C. to A.D. 650, Mexico).

The chemical study of organic materials from archaeological contexts is also complicated by the fact that the substances and materials used by ancient populations varied widely depending on their availability, which was strictly related to geography. On the one hand, the study and identification of plant and animal residues in European and Mediterranean artifacts are well represented and reported in the literature. On the other hand, sources of the substances used in America, in eastern countries such as China, as well as in Australia and Africa, which could differ quite substantially from those used traditionally in Mediterranean/European areas, have been studied less. In recent years, a number of papers dedicated to the GC/MS study of non-European/Mediterranean objects have appeared in the literature [58–68]. Some of these papers aim to fill the gap regarding the material composition of non-European/Mediterranean archaeological findings by carrying out systematic GC/MS investigations of reference substances that had not previously been studied.

A recent trend in the characterisation of organic materials in archaeological objects is to perform non-invasive analyses of the volatile organic compounds (VOCs) released from the organic components. VOC emissions can be characteristic of a given material and can provide information on the material composition and its state of degradation. According to the experimental asset, the analysis can provide qualitative, semiquantitative, or quantitative information. It is performed by exposing an adsorbing fiber to volatile molecules released from a surface or from a solid sample enclosed in a closed vial, in some cases with the assistance of heating to increase the concentrations of VOCs.

In the latter case, the technique is referred to as headspace solid phase microextraction (SPME) [69]. The main advantage of this approach is that it is totally non-invasive and non-destructive to the sample. This approach was used for example in the detection of phenolic derivatives and sesquiterpenoid isomers, which were recognised as the volatile biomarkers of birch bark tar. Directly at the archaeological site, these and other volatile compounds emitted were trapped as soon as the archaeological artefacts were discovered and recovered from their sediment matrix, providing a non-destructive analytical method for investigating the nature of the glues used in the past [70]. The same approach was used to determine the composition of a mummy balm in samples from the tomb of Khnoumit at Dachour in Egypt, by recognising the VOC profiles of volatile terpenes and phenols characteristic of conifer resin [69]. Another example is the investigation of the different geological origins of amber from the volatile fraction. Romanian (romanite) and Baltic (succinite) ambers were studied showing significant differences in the VOC profile [71].

Lignocellulosic polymers are a particular class of organic biomaterials in the cultural heritage. Preserved wood archaeological objects are extremely rare, due to the fragility of wood towards fire, insects, and biological agents such as fungi. Wood survives for centuries only when degrading agents are less aggressive, as is the case of waterlogged shipwrecks. In these cases, the determination of the chemical composition of wood is key in assessing its preservation and evaluating the necessity for consolidation.

Analytical pyrolysis coupled with GC/MS is a powerful tool for this purpose due to the difficulties in obtaining information on the molecular structure of lignin and cellulose by other techniques using a limited amount of sample [72]. Pyrolysis of wood produces a mixture of low molecular weight compounds derived from polysaccharides, which also leads to the formation of levoglucosan and of relatively simple phenols resulting from the cleavage of ether and C–C bonds of lignin [73–75]. The phenols produced retain their substitution patterns from the lignin polymer [76], thus it is possible to identify components from the *p*-hydroxyphenylpropanoid (H), guaiacylpropanoid (G), and syringylpropanoid (S) lignin units. Pyrolysis products of wood are polar, low volatile molecules. Consequently, specific reagents are added to the sample before pyrolysis in order to achieve the *in situ* thermally assisted hydrolysis of specific bonds and the derivatisation of polar groups present in the pyrolysis products in order to improve the chromatographic separation and analytical response of polar compounds. Thus, it is possible to separate and detect much more structurally significant products than by conventional pyrolysis techniques, with a better chromatographic performance and longer column lifetime. The most common derivatization approach in analytical pyrolysis coupled with GC/MS is a trimethylation reaction, where tetramethylammonium hydroxide (TMAH) is used simultaneously with pyrolysis [77], and silylation with hexamethyldisilazane (HMDS) [5].

Py-GC/MS, with and without derivatisation, has been used to study the chemical alterations of wood components [78–80] induced by fungi [81, 82] and also by chemical and enzymatic treatments [83, 84] and to investigate the degradation of archaeological wood [85–90]. Py-GC/MS produces semi-quantitative results on the

extent of cellulosic loss occurring in waterlogged wood artifacts such as shipwrecks and highlights the chemical modifications undergone by polysaccharides and lignin. Differences between the archaeological wood of several historical periods and sound wood have been found in the relative amounts of pyrolysis products, which, above all, show a polysaccharide degradation/depletion compared to lignin. There can be a relative loss of up to 90 % of polysaccharide pyrolysis products in terms of peak areas, from sound to archaeological wood.

The loss of polysaccharides induced by degradation can be semi-quantitatively estimated by interpreting the pyrograms and calculating parameters such as the holocellulose/lignin (H/L) pyrolytic coefficient, defined as the ratio between the relative abundances of holocellulose (cellulose and hemicelluloses) and lignin pyrolysis products [91]. H/L coefficients of different samples analyzed in the same conditions can be compared, leading to a quantitative evaluation of the decay processes. H/L coefficients reported in the literature for sound wood vary from around 1.0 for softwood up to 3.0 for hardwood, depending on the species. Pyrolytic H/L of extensively degraded archaeological wood have been reported to be significantly lower (0.2–0.3) [88, 89].

Figure 3 shows the pyrogram of sound maple wood in comparison with that of waterlogged archaeological maple wood, showing the loss of polysaccharide pyrolysis products.

The information obtained by the interpretation of pyrolysis products is not limited to the depletion of carbohydrates, because the increase in specific pyrolysis products that are markers of degradation or alteration can also be evaluated. A study carried out on archaeological oak (*Quercus* sp.) wood samples, ranging from the sixteenth century AD to 6000 BP, provided the first unequivocal evidence that the demethylation of syringyl units occurs very early in wood degradation [90]. The GC/MS pyrograms revealed a number of methoxycatechols directly related to syringyl units, which are characteristic building blocks of angiosperm lignin. A Py-GC/MS study of a sample of waterlogged beech from the excavation of the site at San Rossore (Pisa, Italy) confirmed the formation of catechols and methoxy catechols, which are derived from the demethylation of both guaiacyl and syringyl lignin [87]

In another study [89], archaeological waterlogged wood remains from the roof of a Roman villa in Herculaneum buried in AD 79 by the eruption of Vesuvius were analyzed by pyrolysis–gas chromatography/mass spectrometry (Py-GC/MS). The findings enabled the authors not only to highlight the loss of polysaccharides and the demethylation undergone by lignin, but also its oxidation. The analyzed samples contained a relatively high abundance of vanillin, acetovanillone, vanillic acid, and coniferylaldehyde, indicating that lignin monomers had also undergone oxidation reactions in the course of ageing. An O/L coefficient can be taken as a pyrolytic indicator of the degree of oxidation of lignin, calculated as the sum of the normalized areas of vanillin, acetovanillone, vanillic acid, and coniferylaldehyde, divided by the sum of the areas of all the lignin pyrolysis products. The O/L coefficient values show that the O/L for sound wood is 0.07 and most archaeological samples from Herculaneum showed a coefficient higher than 0.1, thus revealing a significant degree of oxidation [89].

Polar pyrolysis products of wood, such as vanillic acid, which are significant in evaluating the extent of oxidation of lignin, are not detected in GC without derivatisation. Although TMAH has been occasionally used for the characterization of wood and its components [92, 93], it is not the ideal reagent because the methylation of phenolic groups makes them indistinguishable from methoxylic groups, unless isotopically labelled reagents are used. Thus, the use of silylating reagents for in situ derivatisation reactions is preferred in the Py-GC/MS analysis of wood [85, 94].

3 Analysis of Organic Materials in Classical Art Objects

GC/MS is the most common technique for the molecular characterisation of organic materials in paintings, polychrome objects, and classical art in general. A plethora of studies have been reported in journals, books, and conference proceedings (see for example [95–137]). In the last 10 years some improvements in analytical procedures used by the scientific community for the analysis of organic materials in

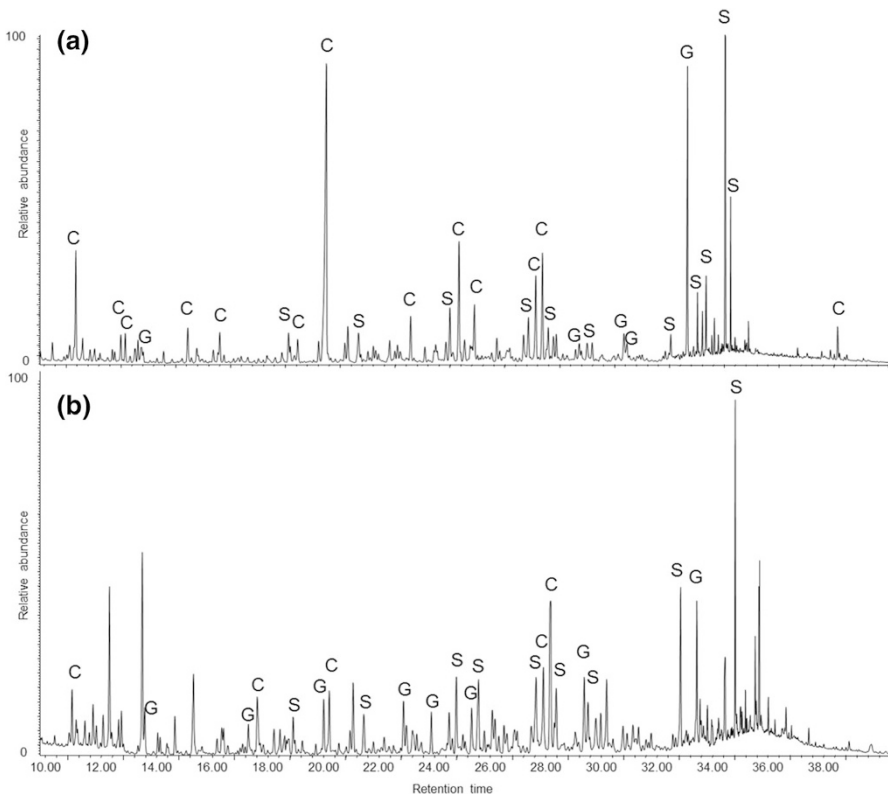


Fig. 3 Py(HMDS)-GC/MS profiles obtained for the analysis of sound maple wood (a) and archaeological maple wood (b). *C* carbohydrates, *G* guaiacyl lignin, *S* syringyl lignin [72]

art samples have been proposed [101, 138–147]. Particular focus has been on both understanding and removing analytical interference caused by inorganic constituents [148–150] and on developing methods for the simultaneous detection of more than one class of organic materials in the same micro-sample [151–155].

Proteins, glycerolipids, and polysaccharides are the main binders found in art samples [6]. In addition, natural waxes, lacquers, and terpenoid resins have been used as additives, varnish ingredients, and consolidants. These materials are mixed together with pigments and fillers. They are then subjected to ageing. All this results in extremely complex samples with a variety of molecules with different chemical reactivities.

Some organic materials cannot be chemically processed for analysis by GC/MS and require analytical pyrolysis [5]. The pool of produced fragments provides a fingerprint that is characteristic of a particular sample, in terms of both the fragment's nature and relative distribution. This approach means that the chemical composition of a sample can be reconstructed on the basis of a detailed interpretation of the chromatographic molecular profile of the thermal degradation products of the original components and on the recognition of specific molecular markers in the chromatogram or of characteristic molecular patterns, which act as molecular fingerprints of the pyrolyzed material [5, 12].

A class of material that cannot be chemically processed for analysis by GC/MS and requires analytical pyrolysis is represented by oriental lacquers, extracted from three species of the same tree belonging to the *Anacardiaceae* family. Their sap is composed of water (30 %), glycoproteins (2 %), plant gum (7 %), a laccase enzyme (1 %), and a mixture of catechol derivatives (60–65 %), which varies depending on the plant of origin [156].

The phenolic fraction of the sap is responsible of the hardening of the lacquer, which polymerises leading to the formation of C–C aromatic nucleus-side chain coupling bonds, C–O phenolic oxygen-side chain coupling bonds, and C–C bonds between side chains. This results in cross-linked polymeric structures [157, 158], which cannot be analysed by GC/MS, but require Py-GC/MS in order to characterize and identify the oriental lacquers [124, 156, 159–168] in ancient samples of unknown composition [48, 51–60]. The low volatility of acidic and alcoholic moieties of oriental lacquer pyrolysis products means that they are unsuitable for gas chromatographic analysis, as they cause a rather low reproducibility of the resulting pyrograms, low sensitivity for specific compounds, and strong memory effects. In fact, the most promising results have been achieved using thermally assisted reactions with tetramethylammonium hydroxide (TMAH) [159, 166] and hexamethyldisilazane [167] as derivatizing agents. [Figure 4](#) shows the profiles of alkyl-catechols, which are formed by thermal cleavage of C–C bonds between aromatic nuclei and side chains, obtained from the pyrolysis of two lacquer samples in the presence of HMDS ([Fig. 4a](#)) and TMAH ([Fig. 4b](#)).

In both samples urushi, the lacquer obtained from *Rhus vernicifera*, was identified. The mixture contained in the sap of *Rhus vernicifera* is called urushiol, whose principal component is 3-pentadecylcatechol [156]. The lacquer was identified based on the detection of derivatised molecular biomarkers in the

pyrogram, as well as characteristic pyrolytic profiles of derivatised alkylcatechols and alkylphenols, aliphatic hydrocarbons, and alkylbenzenes [159, 166, 167].

However, the intrinsic non-quantitative nature of the pyrolysis technique does not always lead to the unambiguous identification of the raw source of an organic material, especially in the case of mixtures. Thus, the interpretation of the pyrograms is critical, especially for aged materials, and requires not only a wide database of reference specimens, but also experience in interpreting the effect of the matrix. The simultaneous occurrence of different organic materials, the relative abundance of one material with respect to the others, the presence of inorganic materials, sample morphology, and several other factors can affect the resulting pyrograms.

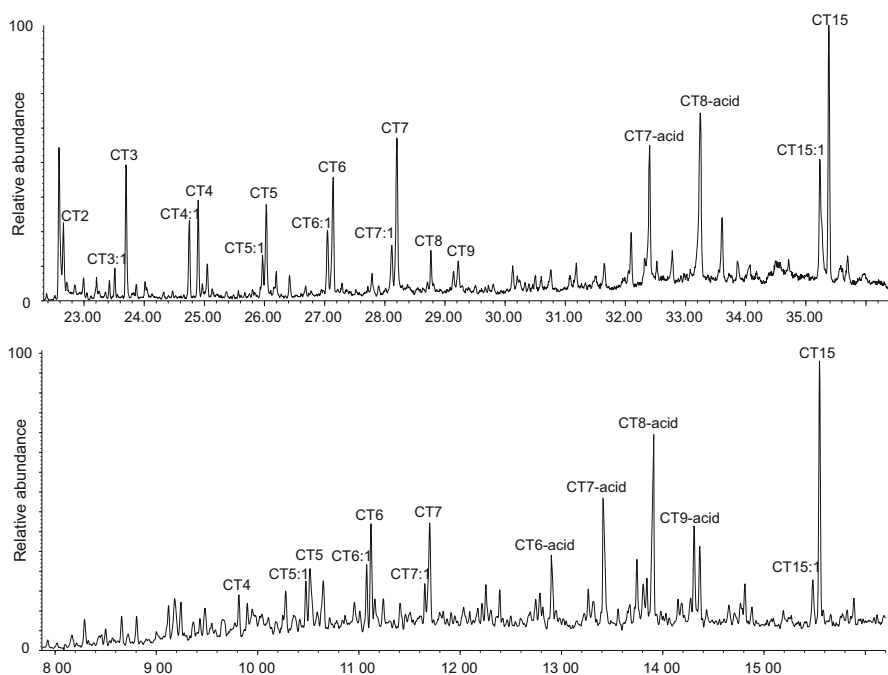


Fig. 4 **a** Py (HMDS)-GC/MS: extracted ion chromatograms of the ion with m/z 179 of a sample collected from the lacquer layer of a Chinese polychrome sculpture dating back to the twelfth century. Pyrolysis temperature was 550 °C and interface temperature was 280 °C (Sample was kindly provided by Catharina Blaensdorf). **b** Py (TMAH)-GC/MS extracted ion chromatograms of the ion with m/z 151 of a sample collected from the lacquer layer of a cabinet dating from the late nineteenth century. Pyrolysis temperature was 550 °C and interface temperature was 320 °C (Sample was kindly provided by Joanna Koryciarz Kitamikado. Analysis was carried out by Diego Tamburini at the workshop Recent Advances in Characterizing Asian Lacquer, 2014, held at the Centre de Recherche et de Restauration des Musées de France, under the supervision of Dr Michael Schilling). Legend to the Figure: *CT2* 3-ethylcatechol, *CT3* 3-propylcatechol, *CT4:1* 3-butenylcatechol, *CT4* 3-butylcatechol, *CT5:1* 3-pentenylcatechol, *CT5* 3-pentylcatechol, *CT6:1* 3-hexenylcatechol, *CT6* 3-hexylcatechol, *CT6 acid* 6-(2,3-dihydroxyphenyl)hexanoic acid, *CT7:1* 3-heptenylcatechol, *CT7* 3-heptylcatechol, *CT7 acid* 7-(2,3-dihydroxyphenyl)heptanoic acid, *CT8* 3-octylcatechol, *CT8 acid* 8-(2,3-dihydroxyphenyl)octanoic acid, *CT9* 3-nonylcatechol, *CT9 acid* 9-(2,3-dihydroxyphenyl)nonanoic acid, *CT15:1* 3-pentadecenylcatechol, *CT15* 3-pentadecylcatechol. The catechols are in the mono-TMS form in **a** and in the bis-CH3 form in **b**

Another approach to analyse the complex mixtures of natural organic materials that can be found in art samples by GC/MS is based on the wet chemical pre-treatment of the sample in order to increase the volatility of the original compounds by means of hydrolysis and derivatisation. Hydrolysis conditions for these materials are all very different. For example, glycerolipids and waxes are quantitatively hydrolysed by an alkaline solution. Proteins and polysaccharides require acidic solutions, although in very different conditions, milder for polysaccharides, harsher for proteins. This means that either the sample is divided into aliquots to be processed separately for various components, or the sample is subject to extractions and separations steps in order to obtain different fractions for the different materials. In addition to the reliability of the analytical approach chosen, the quality of the results obtained in the GC/MS analysis of art samples relies both on the characterisation of the reference materials and their degradation pathways and on the development of suitable analytical models for data analysis.

Identifying organic materials in paint samples is generally based on three main methodologies: identification in the chromatogram of specific biomarkers (chemotaxonomy), recognition of the overall chromatographic profile, or quantitative analysis of significant compounds.

Natural terpenoid resins are identified based on the presence of molecular biomarkers in the chromatogram [6]. For example, butolic, aleuritic, shellolic and laccishellolic, lacsholic, laccilacsholic acids, and relative epimers are the markers of shellac resin, a resin of animal origin from *Coccus* species, when saponification has been carried out in conditions that allow the Cannizzaro type reactions undergone by the aldehyde moieties in jalaric and laccijalaric acid to be completed [169]

Natural waxes are identified based on the recognition of their molecular profiles [6]. For example, beeswax is identified based on the detection of fatty acids in the chromatogram with an even number of carbons (from palmitic to dotriacontanoic acid), (ω -1)-hydroxy acids with an even number of carbons (from 15-hydroxyhexadecanoic acid to 23-hydroxytetracosanoic acid), long chain linear alcohols with an even number of carbons (from tetracosanol to tetratriacontanol), long chain (α,ω -1)-diols with an even number of carbons (from 1,23-tetracosandiol to 1,27 octacosandiol), and long chain linear saturated hydrocarbons with the prevalence of an odd number of carbons (from tricosane to tritriacontane) [170]. The volatility of some of beeswax components makes it possible to identify it in a museum object also by analysing its VOCs. For example, beeswax was identified as the moulding material of some sculptures by analysing the VOC composition (n-alkanes and n-carboxylic acids) of the showcase in which the sculpture was kept [171].

Proteinaceous materials can be identified based on the quantitative evaluation of the amino acidic profile obtained after hydrolysis [7]. One of the main difficulties in identifying proteinaceous materials, is that with the exception of animal glue containing hydroxyproline (which is an amino acid produced by hydroxylation of the amino acid proline with a post translational modification), the proteins of organic paint media all contain the same amino acids. Quantitative evaluations are thus necessary; however, quantitative profiles can be influenced by the inorganic pigments and fillers present [6 and references therein]. Pigments give rise to strong interactions with the organic media, modifying the thermal stability and tertiary

structure of the proteins, forming complexes, causing crosslinking and hydrolysis of the peptide chains, and favouring oxidation with ageing [172–174]. If purification procedures are not adopted, inorganic media can not only interfere in the derivatisation step and damage the GC column, but can also modify the quantitative profiles [6 and references therein].

Polysaccharide media are identified on the basis of the presence/absence of sugars and uronic acids in the chromatogram. Tragacanth, arabic, and fruit tree gums are the most commonly used gums in classical art in the Mediterranean basin and Europe, and are characterised by quite different sugar profiles. It has been shown that ageing in the presence of certain pigments can modify the sugar profiles, making the gum identification less straightforward [150]. In addition, most of the natural organic media found in artworks contain saccharides, including proteinaceous media [150]. It has also been suggested that polysaccharides from plant tissues (wood, straw, paper, etc.) may be present in particulate matter both in indoor and outdoor environments.

Four decisional schemes have thus been proposed [150] to identify the source of a plant gum (Fig. 5) to be used as alternatives when:

- a. there are no proteinaceous materials simultaneously present and there seems to be no contamination¹
- b. the presence of proteinaceous materials is unknown and there seems to be no contamination (see footnote 1)
- c. proteinaceous materials are simultaneously present and their source is known, and there seems to be no contamination (see footnote 1)
- d. the polychromy is on a wooden/paper support or contains straw, or the xylose/arabinose ratio is higher than 1, thus the samples are clearly contaminated by sugars originating from plant tissues present in the environmental particulate matter

The identification of the origin of the saccharide material in a paint sample is even more complex when considering possible sources of sugars other than polysaccharide media. One example is represented by an extensive historical and scientific investigation into commercially prepared British watercolour cakes from London based artists' colourmen Reeves, Rowney, Ackermann, and Roberson, dating from before the eighteenth through to the early twentieth century [175]. The study revealed that although arabic gum was the main binder, several other additives could be present, including smaller portions of other gums, among which the lesser known gums heder, lake, ammoniac, guttae, and guaiacum. Other additives, such as sugar or honey, starch, and other non-saccharide materials were also added, in order to obtain specific rheologies of the paint. As expected, the chromatograms of the saccharide fractions generated by such mixtures can be impossible to interpret if the possible ingredients are not known through a systematic investigation into the historical sources.

¹ This is based on the evaluation of the xyl/ara ratio: when this is higher than 1, contamination is hypothesised.

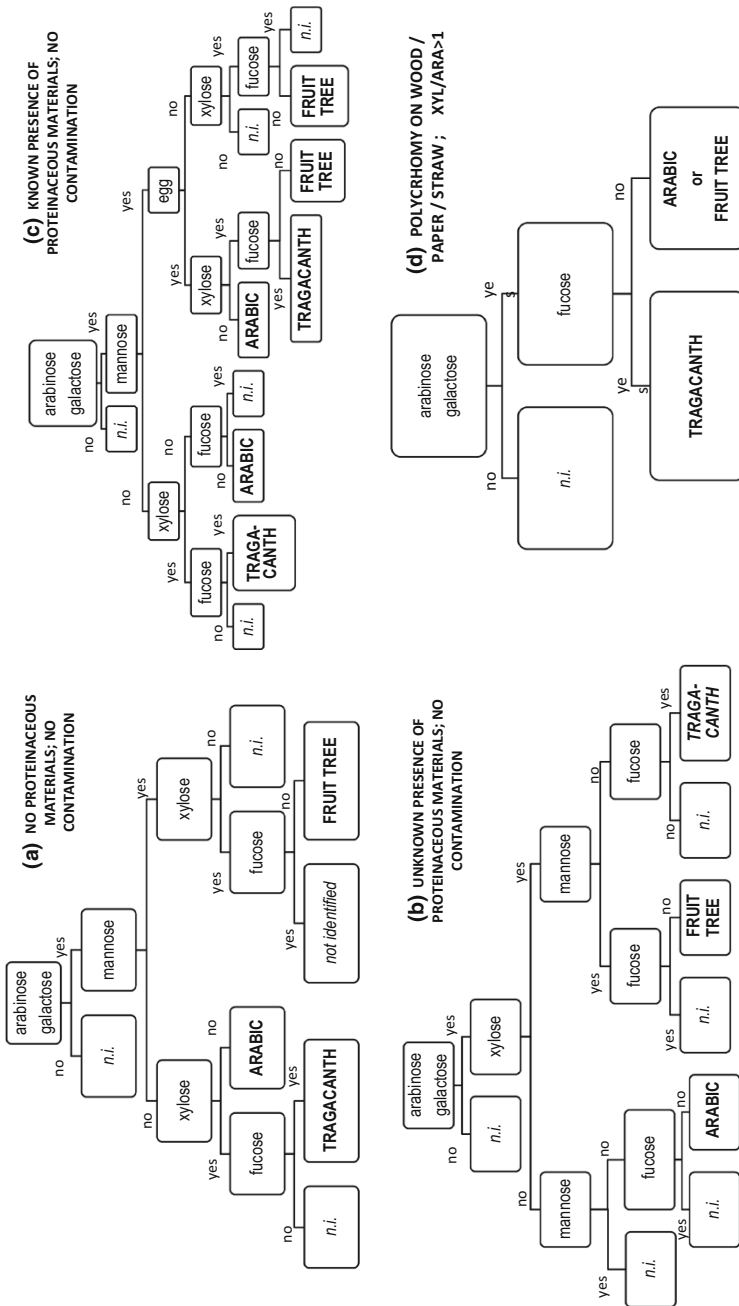


Fig. 5 Decisional schemes to identify a plant gum in a paint sample based on the knowledge of the simultaneous presence of proteinaceous materials and contamination from sugars originating from plant tissues [150]. *n.i.* not identified

Glycerolipids are identified by GC/MS based on the ratio between the relative amount of palmitic and stearic acid (P/S) and the ratio between the relative amount of azelaic and palmitic acid (A/P). An A/P ratio lower than 0.3 suggests the presence of non-drying fats, such as egg yolk, while a ratio higher than one points to the presence of a drying oil [1, 6, 11, 176 and references therein].

Azelaic acid is in fact one of the main oxidation products of polyunsaturated fatty acids, which are abundant in drying oils. The P/S ratio is used to distinguish between different drying oils. This is based on the assumption that as palmitic and stearic acids are saturated long chain acids, they are stable to ageing. Actually, using the P/S ratio to identify the source of the drying oil has several limitations. It has been recently shown that evaporation of the organic medium from the paint layers takes place during ageing at a surprisingly fast rate, depleting the paint layers of glycerol and fatty acids [177]. A weight loss of 15 % was observed in reference paint layers of linseed oil and vine black in only 12 years. When fatty acids are saponified by the pigment, such as Pb^{2+} in the lead white pigment, then evaporation does not take place [177]. Thus, the presence in the paint layers of any material, pigment, or other binder, which can form complexes or other sorts of chemical compounds with the fatty acids, hinders this phenomenon. Considering that palmitic acid evaporates four times more quickly than stearic acid [178], the P/S value is expected to significantly decrease over time. There are thus other factors of fundamental importance in determining the final P/S value of a paint sample, some of which are the direct consequence of the rapid evaporation of the free fatty acids from the paint film: the film thickness at the sampling point, the presence of any other organic materials that could hinder the evaporation of fatty acids as a consequence of the formation of non-volatile complexes (for example, protein-fatty acid complexes), the presence of pigments able to form complexes with the fatty acids [179–182], the presence of overlying layers [183, 184], the cleaning treatments [185–187], and finally the thermo-hygrometric conditions of the storage places throughout the history of the paint [178]. This means that the P/S ratio alone is not a suitable parameter for determining the source of the oil.

The identification of polysaccharide, proteinaceous, and lipidic binders is thus based on the quantitative analysis of significant compounds, that is sugars, amino acids, and long chain linear and dicarboxylic acids, respectively. The reliability of such models is based on the evaluation of blanks and calibration curves. These are two very important, but often neglected aspects, which in analytical chemistry are the basis for quantitative measurements.

Environmental blanks are often impossible to determine in samples collected from cultural heritage, as in the case of paintings. Laboratory blanks, however, can be measured and are fundamental for distinguishing between the actual sample and laboratory contamination. For example, Fig. 4 shows the chromatogram of the saccharide fraction of a sample from the mural paintings of the Nefertari tomb in Luxor, Egypt, and highlights the peaks of xylose, arabinose, mannose, and galactose obtained by GC/MS after extraction, acidic hydrolysis, desalting, and mercaptalation followed by silylation [150]. The sample did not contain any protein and showed no sign of environmental contamination. According to the decisional scheme in Fig. 5 A, the chromatographic profile suggests the presence of fruit tree gum. In fact, xylose

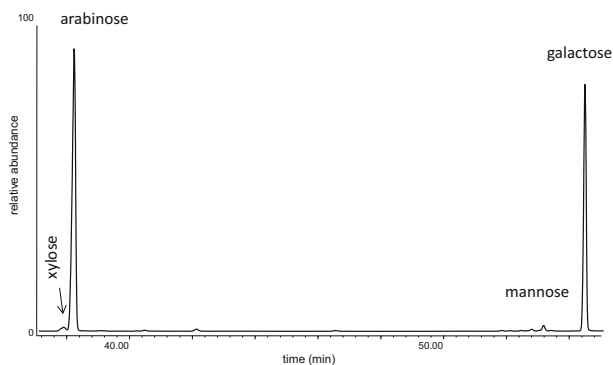


Fig. 6 GC/MS Chromatogram of the sample from the mural paintings of the Nefertari tomb, Luxor, Egypt [188] obtained by GC/MS after extraction, acidic hydrolysis, desalting, and mercaptalation followed by silylation [150]

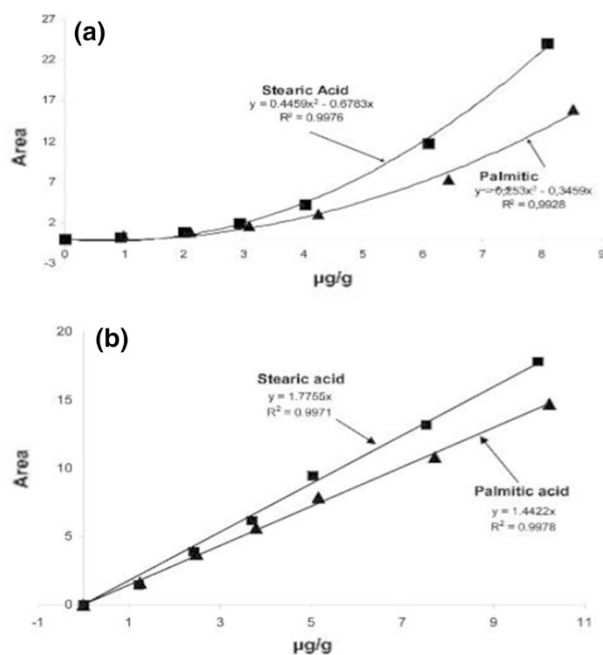


Fig. 7 Calibrations graphs acquired for palmitic and stearic acids in the case of empty glass liner (a) or glass wool-packed glass liner (b) (image from [189]). Quantification was obtained after alkaline hydrolysis, acidification, extraction, and silylation

and mannose, at a 95 % confidence level, fell under the detection limit of the analytical procedure [155], indicating that only arabinose and galactose belonged to the sample. This led to the identification of arabic gum (Fig. 6).

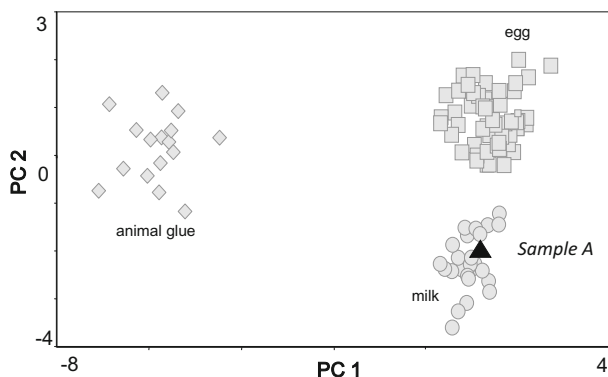


Fig. 8 Score plot obtained from the principal component analysis of the amino acid profile (Ala 7.0, Gly 6.2, Val 8.3, Leu 10.0, Ile 4.7, Ser 8.4, Pro 4.6, Phe 9.3, Asp 17.6, Glu 23.8, Hyp 0.0) of a sample from a reference paint layer of egg (Sample A) together with those of 105 reference paint samples of egg, casein, and animal glue determined by GC/MS after extraction, desalting using a C4 loaded pipette, hydrolysis, and silylation [153]

Quantification in GC/MS is also often performed based on peak areas, instead of calibration curves, and this may lead to erroneous evaluations of the relative amounts of the constituents of interest [189]. Even when a one-point calibration method is used, the linearity of the instrument response is neither controlled nor guaranteed. This was demonstrated in an evaluation of P/S ratios for the identification of the source of the drying oil. A nonlinear instrument response was obtained for both palmitic and stearic acids, which was attributed to incomplete sample evaporation in the GC/MS injector (Fig. 7).

The non-linear instrument response leads to different P/S values depending on the sample dilution. By analysing three different aliquots of the same sample (10, 20, and 30 μL), the P/S ratios obtained were 1.7, 1.9, and 2.4, respectively. The first two values suggest the identification of linseed oil in the sample, but the third value is in agreement with the literature data for walnut oil. The authors also proved that packing the glass liner with deactivated glass wool improved the sample evaporation and ensured the linearity of the instrument response and independence of the P/S ratio from sample dilution (Fig. 7).

When non-linear responses are observed, it is necessary to ensure that the areas of the analytes to be quantified fall within the portion of the calibration curve that has been experimentally measured with reference standards. For example, Fig. 8 shows the score plot obtained from the principal component analysis of the amino acid profile (Ala 7.0, Gly 6.2, Val 8.3, Leu 10.0, Ile 4.7, Ser 8.4, Pro 4.6, Phe 9.3, Asp 17.6, Glu 23.8, Hyp 0.0) of a sample from a reference paint layer of egg white (Sample A) together with those of 105 reference paint samples of egg, casein, and animal glue. Amino acid concentration were determined by GC/MS after extraction, desalting using a C4 loaded pipette, hydrolysis, and silylation [153]. The sample clearly falls within the cluster of casein. This can be explained because the concentration of the amino acids calculated from the chromatographic areas was

more than ten times higher than the highest concentrations used for the calibration curves, and thus the quantitation was erroneous.

The complexity of the data interpretation involved in the GC/MS analysis of samples from cultural heritage, both using pyrolysis and wet chemical pre-treatment, is very well exemplified by the analyses of a round robin sample performed by ten laboratories specialised in the field in the framework of the activities of the MaSC-Users Group for Mass Spectrometry and Chromatography in Cultural Heritage (<http://mascgroup.org/>) [190]. The sample contained ParaloidB82, a copolymer of ethyl acrylate and methyl methacrylate (EA/MMA), sandarac, mastic, linseed oil, egg white, gum arabic, and succinic acid. The sample was analysed using FTIR and GC/MS based analytical techniques. The materials were specifically included in the round robin blind sample in order to make the data interpretation quite complex. For example, arabic gum contains a small amount of protein with a high content of hydroxyproline, which is commonly used as marker for the presence of animal glue. Sandarac contains polycommunic acid, which is also abundant in other compounds, such as copal resin or Baltic amber, which also contains succinic acid. This compound was also added to the sample. The results of the round robin analysis can be summarised as follows: an acrylic resin (EA/MMA) was identified six times, succinic acid three times, Baltic amber (hypothesized) four times, copal once, sandarac seven times, mastic ten times, linseed oil ten times, gum arabic three times, gum (possible) twice, egg white four times, egg four times. The data clearly indicate that more than one procedure is often necessary to characterise fully such complex samples as those collected from cultural heritage, although this is not always possible given the very small sample size.

4 Analysis of Organic Materials in Modern and Contemporary Art Objects

The investigation of materials and the diagnosis of modern and contemporary art is a relatively recent field of application of analytical chemistry, to which conservation scientists have devoted increasing attention over the last 10–15 years. We decided to dedicate a specific section to the topic in this chapter due to the relative lack of textbooks on the study of materials in contemporary art, compared to the applications of analytical chemistry to classical art and archaeological objects, which are much more extensively described in the literature. However, there are a few textbooks and publications on the investigation and analysis of materials in modern art and are an excellent basis for research in this field [8, 9, 12, 191].

At the turn of the nineteenth century a staggering array of new binders were developed and used in the production of fine art paints. The new oil paints were sold in tubes, and thus contained not only oils and pigments, but also additives such as surfactants and stabilizers.

Oil sources have been investigated in paint tubes and samples from works of art [192–194]. Actually, the identification of the oil source in the case of modern oil media is even more complex, although GC/MS is still the preferred technique [192, 194–198]. The range of oils used is different in modern oil paints compared to

classic oil paints, and includes safflower, palm, soybean, and many others. The introduction of new lipid materials and oleochemicals was driven by the economic sustainability of production and the availability, workability, and possibility of improving their properties by means of additives and engineered treatments. In some cases, a specific marker for an oil can be identified in the chromatogram, permitting its identification. In a recent study, the detection of specific fatty acid markers such as ricinoleic and erucic acids led to the assessment of castor oil and rapeseed oil among the components of the oil paints used by Lucio Fontana [193]. In another work, the presence of odd-number (C7–C15) fatty acids and the observed P/S values suggested the presence of animal fats and of soybean and safflower oils in the paints used by Pablo Picasso [196]. Despite the difficulties in the interpretation of the fatty acid profile, GC/MS has proven to be a fundamental tool in assisting the evaluation of conservation practices of modern oil paints [199, 200].

Alkyd resins are another class of lipid modern paint binders in contemporary art. Alkyds are an industrial evolution of oil paint media. The adoption of these oil-based industrial polymers by artists is one of the milestones in the evolution of painting techniques in twentieth century art. Alkyds are oil-modified polyesters manufactured from poly-ols (typically glycerol or pentaerythritol), aromatic polybasic acids (phthalic anhydride and phthalic acids are the most common) and a source of fatty acids, usually a vegetable oil [201]. Drying and semi-drying oils, such as linseed, soybean, and castor oil are used for the production of alkyd resins. The lipid fraction of alkyds can be characterized by GC/MS analysis after saponification [195, 202–204]; however, Py-GC/MS with appropriate derivatising agents is a currently used approach used for the chemical characterization of these synthetic polymers for their identification in paint samples and to study their curing processes [12, 196, 203–207]

Py-GC/MS analysis of alkyd paints has been performed by online, thermally assisted hydrolysis and derivatization of the hydroxyl and carboxylic groups present in the resin components and fragments, with the same approach successfully adopted for the chemical characterization of oil paintings [12, 205]. Fatty acids derived from the lipid components and aromatic components such as phthalic anhydride and phthalic acids can be observed in the pyrograms. Benzoic acid is also often observed, derived both from phthalic acid or phthalic anhydride, but it can also be present in the resin as a terminal chain or length modifier. Phthalic anhydride can be detected in pyrogram of an alkyd without derivatising agent; however, isophthalic acid would not, leading to the possibility of incorrect identifications. In pyrolysis conditions, the reported products of pentaerythrol are 3-methoxy-2,2-bis(methoxymethyl)-1-propanol and 3-methoxy-2-methoxymethyl-1-propanol [12]. THM-GCMS has been successfully used to investigate alkyd paints in artworks by Lucio Fontana (“Concetto Spaziale” 1961) [12], Jackson Pollock (“Yellow Islands” 1952) [206], and Pablo Picasso (“Nude Woman in a Red Armchair” 1932) [196]. The results proved that Picasso experimented with alkyd resins, which was unusual for the times.

Although many artists have used these modern paints and explored their handling and optical properties, “tempera”, a classic painting technique using a protein based

binder, has also been rediscovered in the twentieth century. New editions of historical treatises increased the debate on technical issues and the use of tempera was a key topic among those artists involved in the renewal of a classicist style and traditional working methods. Consequently, numerous formulations containing proteinaceous binders were developed and commercialised. Identifying modern tempera techniques is much more complex than in classical art. By using GC/MS in the analysis of the lipid and proteinaceous fractions of artist and model samples, it has recently been demonstrated that the word “tempera” used by artists at the end of the nineteenth and beginning of the twentieth century is more related to the rheological properties of the paint, which is strongly influenced by its minor additives (such as glycerol, soaps, or tallow) more than its main constituents [208] (proteins and/or lipids).

Since the synthesis of cellulose nitrate by Schönbein and Böttger in 1846 [209], artistic experimentation has led to the introduction of synthetic resins in artistic productions: paintings, sculptures, installations, and restoration procedures have included synthetic materials and industrially elaborated natural materials. Acrylic polymers, were initially diluted with solvents and later were used as much more practical aqueous emulsions (waterborne paints), diffused as varnishes, paint binders and as material for 3D art. Similarly, vinyl resins were used as adhesives and binders, and nylon was an alternative to natural fibres. The complex composition of modern and contemporary paintings is thus the result of the rapid changes occurring in society and culture due to industrialization during the twentieth century [209–211].

Conservators are now for the first time facing problems related to the degradation and preservation of recently introduced industrial materials. A crucial aspect of the composition of modern commercial materials, affecting their stability over time and their response to conservation treatments, is the wide variety of formulations, often covered by patents. Commercial formulations of synthetic materials contain several components, including pigments, stabilisers, plasticisers, and other additives. These were added to the main polymer in order to modify its general properties, and they can strongly contribute to several degradation phenomena characteristic of plastic artefacts, including water sensitivity, brittleness, vulnerability to light, deformation, surface deposits, gloss change, cracking, and shrinkage. Their unknown composition can be a problem in the evaluation of the compatibility of the ingredients used during restoration with the different ingredients in the original material.

Advanced analytical techniques based on chromatography and mass spectrometry are now playing a key role in addressing these issues. Analytical pyrolysis is the preferred technique for the molecular characterization of synthetic organic molecules [8, 9, 212]. Py-GC/MS leads to the chemical characterization of the synthetic materials in a large range of molecular weights. The mechanisms of thermal degradation of many polymeric materials used in art are described in the literature [9, 12, 55, 213, 214], and knowledge of their pyrolytic markers can be exploited to identify them when they are present as paint binders or varnishes. Py-GC/MS has been applied to modern paint or synthetic conservation materials using different instrumental assets based on furnace, filament, and Curie point pyrolysers [8, 212, 215–218].

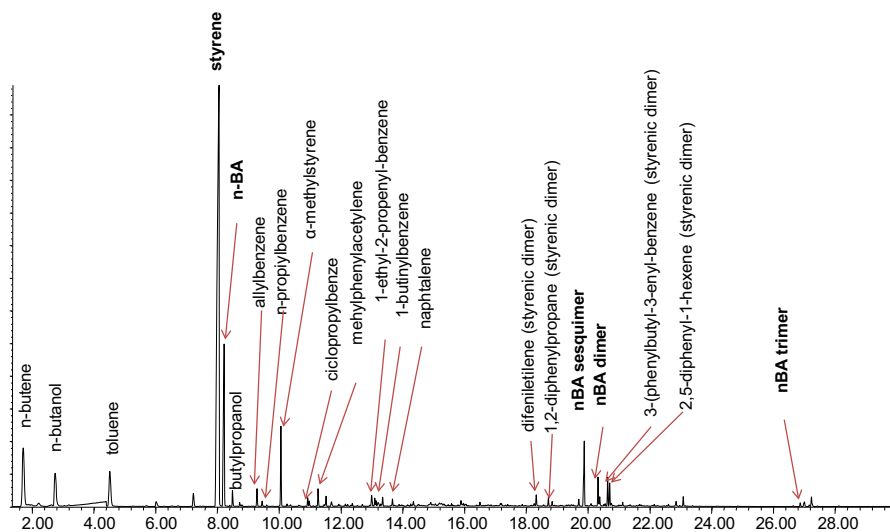


Fig. 9 Py-GC/MS chromatogram of a paint sample from the Tuttomondo mural by Keith Haring (area painted in Burgundy) [229]

Py-GC/MS identification of synthetic paint media is essential in order to understand fully the techniques of contemporary art. Identifying a synthetic binder in an artwork is in fact the first step in assessing the artist's technique, in addressing attribution and dating issues, evaluating the possible effects of cleaning, and in establishing the best conditions for conservation [219]. FTIR spectroscopy is also used to identify the type of polymer present in a sample; however, when the precise identification of the monomers is needed, for example, to discriminate between many acrylic resins, the molecular information achieved by Py-GC/MS or other mass spectrometric techniques is generally more conclusive than spectroscopic data.

As an example, a particular concern is the diagnosis of street art and outdoor murals [220, 221] where often acrylic paints have been used, because of the complete lack of established methods and protocols for the cleaning, protection, and preventive conservation of these types of artworks [222–226]. As the conservation treatment of outdoor acrylic paint is an emerging field, the identification of the original materials is necessary in order to make informed choices regarding the conservation approach.

Acrylic resins are a major class of synthetic polymers used as paint binders and varnishes. The most common monomers used in products sold for artistic applications are methyl methacrylate (MMA), ethyl acrylate (EA), n-butyl-methacrylate (nBuMA), and ethyl-hexyl-acrylate (EHA), often used as copolymers with styrenic monomers. As generally happens with macromolecules synthesized by radical addition reactions, the thermal degradation molecular profile of acrylic polymers is determined by an unzipping mechanism, which induces the scission of the polymeric chain to form the monomer or the monomers. Normally dimers and

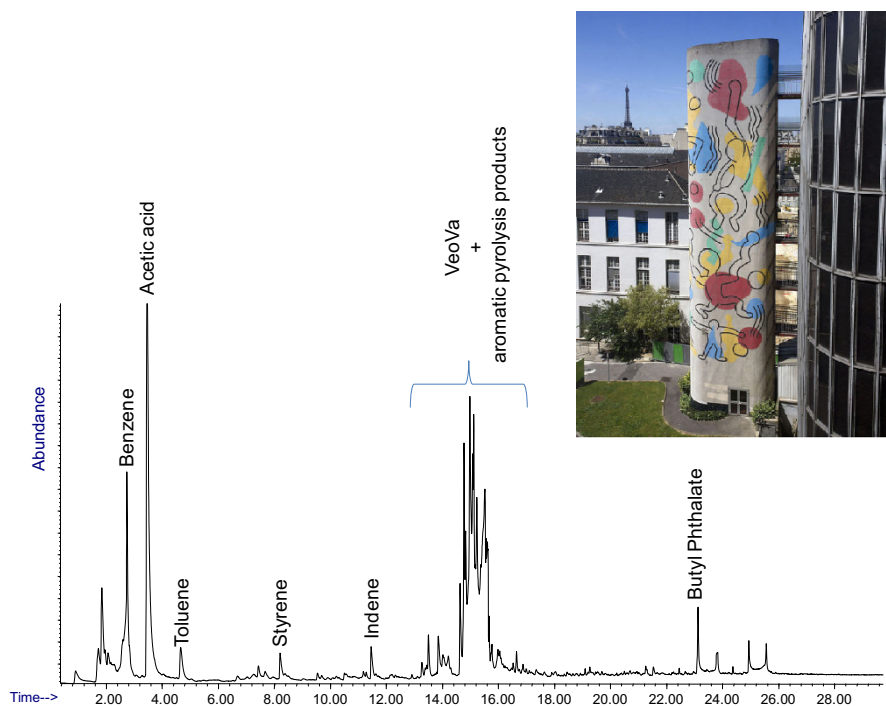


Fig. 10 Py-GC/MS chromatogram of a paint sample from Necker Hospital's mural in Paris [229]

trimers are also observed. As acrylic monomers are efficiently separated and determined by GC/MS, derivatisation is not required in their analysis [227, 228].

Figure 9 represents the chromatogram obtained in the Py-GC/MS analysis of a sample taken from the wall painting *Tuttomondo* (1989, Pisa, Italy) by Keith Haring (1958–1990) [229]. The pyrolysis profile is characterized by the presence of styrene and *n*-butylacrylate monomers as main peaks. At higher retention times, *n*-butylacrylate sesquimer, dimers and trimers are detected, which are markers of a poly-*n*-butylacrylate resin. Other significant pyrolysis products include the dimeric structures typical of a polystyrene: 1-ethyl-2-propenyl-benzene, diphenylethylene, 1,2-diphenylpropane, and 2,5-diphenyl-1-hexene. The pyrograms of the *Tuttomondo* paint samples also featured *n*-butylacrylate/styrene dimer. This molecular profile indicates that a styrene/*n*-butylacrylate copolymer is the binder in the paint materials used by Haring in Pisa [12, 213, 229].

The versatility of Py-GC/MS in studying the painting techniques in modern and contemporary artworks is illustrated by a parallel case study: the characterization of paint samples from another mural by the same artist, Keith Haring. *Necker Hospital's mural* created in 1987, (Fig. 10) is on the exterior stairwell at the Necker Children Hospital in Paris [229]. Unlike the *Tuttomondo* mural in Pisa, which is in an excellent state of conservation, the Necker Hospital mural shows conservation problems related in particular to the black paint constituting the drawing, which was

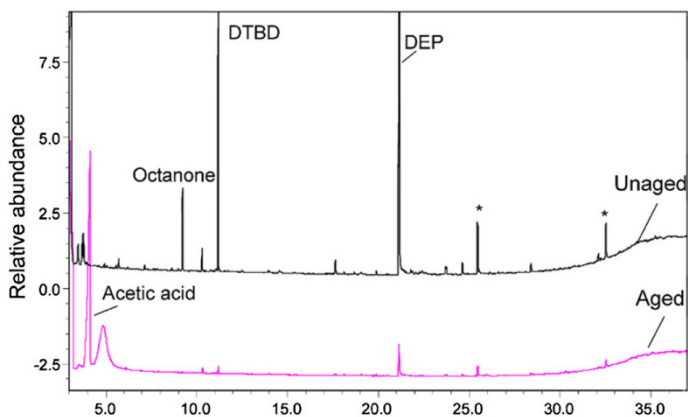


Fig. 11 Pyrograms of Mowilith(R) 50, a polyvinyl acetate, obtained by Py-GC-MS with double shot technique: in the first step—thermal desorption: DTBD, di-ter-buthyl dicarbonate; DEP, diethyl phthalate, *not identified compounds. Figure from [219]

applied over the other colour areas. The black areas have wrinkling and paint detachments, as well as degradation phenomena not present in the other colours. Seven paint samples were analysed and one of the pyrograms obtained is reported in Fig. 10 with the relative peak attribution.

The results show that in this case Haring used a different medium. The pyrolysis profiles reveal benzene and acetic acids which, together with small amounts of toluene, styrene, indene, and different aromatic compounds, are indicative of the presence of a vinyl resin [12]. The identification of a vinyl resin by Py-GC/MS requires the addition of a derivatising reagent for the thermal assistant derivatisation of acetic acid, developed in the thermal degradation of vinyl resins. In this case hexamethyldisilazane was used, so that acetic acid is separated in the form of trimethylsilyl ester. The pyrogram reveals several isomers of the vinyl ester of versatic acid (TR range 9.0–14.0 min.), a constituent of VeoVaTM, an internal plasticizer used in vinyl paint media [230]. At higher retention times, butyl phthalate, a common plasticizer added in commercial products, was also identified in all the sample. The poor conservation conditions are likely due to the composition of the binding medium: a vinyl resin containing high amounts of VeoVa as an internal plasticizer. VeoVa renders the paint layer more sensitive to daily variations in temperature, due to the decrease in the glass transition temperature of the resin. This is particularly evident in the darkest paint areas, caused by daily variations in temperature enhanced by the higher temperature reached by the dark zones due to higher absorption of light, thus promoting wrinkling, detachments, and variations in the morphology of the layer [229].

Although analytical techniques based on pyrolysis, chromatography, and mass spectrometry are a powerful tool in investigating the organic components of modern paint media, the complete characterisation of a material is not straightforward and requires specific analytical methodologies, strategies, and data analysis models to be specifically developed for each analytical problem. An interesting possibility is to

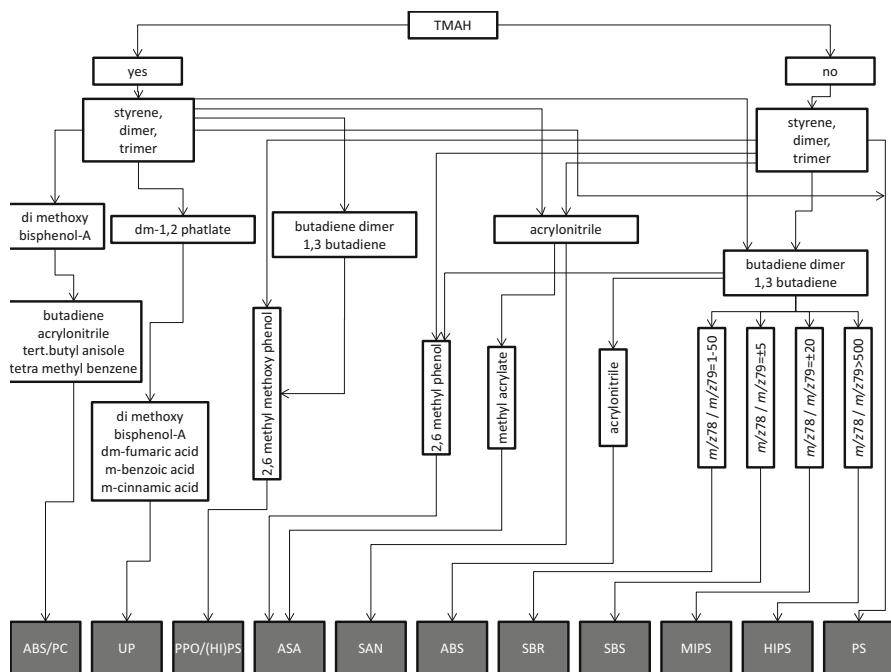


Fig. 12 Flowchart for identifying styrene-containing polymers from Py-GC/MS in the presence of TMAH. Figure adapted from [232]. *ABS/PC* acrylonitrile butadiene styrene/Polycarbonate, *UP* unsaturated polyester resin, *PPO/(HI)PS* poly(phenylene)oxide/(high impact) polystyrene, *ASA* acrylonitrile styrene acrylate, *SAN* styrene acrylonitrile, *ABS* acrylonitrile butadiene styrene, *SBR* styrene-butadiene rubber, *SBS* styrene butadiene styrene, *MIPS* medium impact polystyrene, *HIPS* high impact polystyrene, *PS* polystyrene

perform the evolved gas analysis (EGA) of the volatile products released by the sample during controlled heating at a low temperature desorption (100–250 °C) before high temperature pyrolysis. The molecular profile produced in the first and second steps are analysed separately by GC/MS in two different analytical runs. A similar approach is the double shot pyrolysis [203, 219, 231], which combines the analysis of thermally desorbed volatiles with the flash pyrolysis of the polymer. For example, in order to investigate the photochemical degradation of commercial polyvinyl acetate, Py-GC/MS in double shot mode was used to reveal the differences in the amounts of volatile components present in the specimens before and after UV ageing, including the changes in amounts of the deacetylation product acetic acid and of the content plasticizers such as diethyl phthalate (DEP) (Fig. 11) [219]. The analysis of acrylic emulsion paints after ageing highlighted the decrease in the abundance of octylphenol, which is a marker for the non-ionic surfactant octyl-phenyl-polyethoxy-ethanol in the thermal desorption chromatograms.

When using Py-GC/MS for characterising plastics, identifying the peaks in the pyrogram and deducing the structure of the original polymer is a challenging task. In fact, the same monomer can be used to produce more than one plastic, and it is

important to identify those peaks in the pyrograms that can help in differentiating between one polymer and another. This requires the development of a data analysis model to support the data interpretation. For example, styrene is the primary building block of a number of plastics, including polystyrene (PS), high impact styrene (HIPS), styrene–butadiene–styrene (SBS), unsaturated polyester resin (UP), and acrylonitrile–butadiene–styrene (ABS). In order to differentiate between these polymers using pyrolysis in the presence of TMAH, a flow chart has been proposed to assist in the pyrogram interpretation [232] (Fig. 12).

VOCs analysis by GC/MS can also be used in the conservation of plastics to better understand polymer degradation and thus the physical damage observed in plastic artifacts and artworks. For this purpose, the use of SPME sampling followed by GC/MS analysis is a non-destructive and fast tool to obtain information. The affinity of the SPME fibers toward various volatiles depends on their chemical physical properties, and different adsorbing phases are commercially available. SPME coated with a divinylbenzene/carboxen polydimethylsiloxane (DVB/CAR/PDMS) stationary phase and thickness of 50/30 μm is particularly effective in VOC trapping. It can be used to characterize the degradation state of aged paper by revealing over 50 compounds including acetic acid, a variety of aldehydes, 2-ethylhexanol, and furfural [233–235]. In fact, the degradation state of aged paper could be based on the determination of volatile compounds produced through the decomposition reactions that occur in paper upon ageing. The same approach can also be used to demonstrate that the pool of VOCs emitted by plastics is strongly influenced by the polymer formulation and by its decay, and can help in understanding how degradation takes place. Significant examples have been described for cellulose acetate as the main constituent of various objects such as dolls, laminated documents, toys, and boxes. These produced a VOC pattern, which included, in addition to the expected acetic acid, phenols, phthalates, and monoterpenes, ascribable to additives of a different nature [236–238]. Such research has also proved that HS-SPME-GC/MS is a non-invasive technique not only useful in understanding degradation phenomena, but also in identifying selected plastics at any point in their degradation, and in distinguishing between different formulations.

The analysis of VOCs by GC/MS and the investigation of the damage caused by such VOCs on the cultural heritage using GC/MS based approaches is a very powerful tool in preventive conservation. Preventive conservation not only deals with climatic considerations, but increasingly considers the effects of outdoor and indoor air pollution in cultural institutions. Museums, archives, and libraries play a special role because particular climatic requirements are needed for the well-being of visitors and at the same time to protect cultural assets against deterioration.

In this field, scientific research is aimed at assessing the complexity of the physical, chemical, and biological risks in situ, in museums, galleries, churches, and in micro-environments such as showcases and micro-climate frames [239, 240]. Recent research has focused on understanding the deterioration of art objects that make VOCs a threat to our cultural heritage. Identifying the source of a particular pollutant can be difficult, but it is now understood that modern heritage objects can act as an emissive source. The “vinegar syndrome” is an example of the production

of a volatile compound, acetic acid, as the effect of degradation phenomena of a plastic material, cellulose acetate. In cellulose acetate, upon exposure to moisture, heat, or acids, acetic acid is released (causing the characteristic vinegary smell), which has a catalytic effect on the degradation process itself, and that of other materials which are kept in the vicinity. Thus, appropriate storage conditions can be adopted in order to slow down the decay process, which include cold and moderately dry storage [240, 241]. Similarly, the chemical compounds released from a wide range of plastic objects are being investigated and how they might affect the stability of other heritage objects held in close proximity to the emitting object [237, 242–244]. In general, the emission of carboxylic acids by materials used for museum display cases has been observed [245].

Wood products, coatings, silicone-based sealants, and polyvinyl acetate adhesives, usually employed in the fabrication of frames or storage containers, emit aldehydes and organic acids that are potentially harmful to the art objects [246–248]. Acetic and formic acid are the most abundant organic acids present in museum environments. Organic acids are dangerous for monuments and buildings [249], and acetic and formic acid in museum environments corrode lead, copper, and some other metals and calcareous minerals [250–255]. However, very little is known about the possible long-term degradation impact of these gases on organic materials used in works of art, although it is clear that they can have a strong effect on the degradation of cellulose [256, 257]. Recently it has been shown that these volatile acids are also harmful to other organic materials that constitute art objects. GC/MS based approaches have shown that paint varnishes based on dammar resin and paint layers based on alkyd media are subject to accelerated degradation under exposure to acetic acid [258, 259].

5 Conclusions

An overview of the literature highlights that the analytical approach for use in GC/MS analysis of organic materials in cultural heritage samples is strongly dependent on the specific problematic posed by art historians and conservators. The complex mixtures of molecular species present in organic materials, the questions to be answered, and consequently the analytes to be searched for, determine the choice of analytical approach, especially concerning sample pretreatment.

Research on organic materials in the cultural heritage is still an open issue, and more research into analytical methodologies and data interpretation models is still necessary, based on a better understanding on the degradation processes undergone by the materials. Such research needs the support of a more systematic investigation into ancient technological and historical sources, in order to understand which materials were originally used and how they were pre-processed. In order to shed light on the various molecular and physical changes taking place in materials upon ageing, a combination of analytical techniques are being exploited including spectroscopic, thermoanalytical and spectrometric techniques. Of these, GC/MS still plays a fundamental role due to its unsurpassed ability to identify biomarkers and degradation products at a molecular level, thereby obtaining quantitative data.

HPLC and HPLC/MS are increasingly being used to study of organic materials and to supplement GC/MS data obtained from volatile components with information on higher molecular weight components. In addition, spectroscopic techniques (such as FTIR, SEM-EDX, XRF, XRD, also using synchrotron source), spectrometric (such as SIMS), and immunology-based techniques can be used to locate both organic and inorganic materials in the sample cross-section.

The number of applications of GC/MS in conservation science and archaeometry has increased every year over the two last decades, and is likely to continue to grow in the next few years thanks to improved instrumentation, the reliability of the results (given the advances in the knowledge of the community in the field), and GC/MS's versatility as the same instrumentation is able to give a molecular identification of several classes of organic materials.

References

1. Mills J, White R (2000) Organic chemistry of museum objects (2nd edn, vol 206), (Conservation and Museology). Routledge, New York
2. Mills JS (1966) The gas chromatographic examination of paint media. Part I. Fatty acid composition and identification of dried oil films. *Stud Conserv* 11(2):92–107
3. White R (1984) The characterisation of proteinaceous binders in art objects. *Natl Gallery Tech Bull* 8:5–14
4. Schilling MR, Khanjian HP (1996) Gas chromatographic analysis of amino acids as ethyl chloroformate derivatives. II. Effects of pigments and accelerated aging on the identification of proteinaceous binding media. *J Am Inst Conserv* 35:123–144
5. Bonaduce I, Andreotti A (2009) Py-GC/MS of organic paint binders. In: Colombini MP, Modugno F (eds) *Organic mass spectrometry in art and archaeology*. Wiley, New York, pp 303–326
6. Colombini MP et al (2010) Analytical strategies for characterizing organic paint media using gas chromatography/mass spectrometry. *Acc Chem Res* 395:715–727
7. Madariaga JM (2015) Analytical chemistry in the field of cultural heritage. *Anal Methods* 7(12):4848–4876
8. Peris-Vicente J et al (2009) Characterization of commercial synthetic resins by pyrolysis-gas chromatography/mass spectrometry: application to modern art and conservation. *Anal Chem* 81(8):3180–3187
9. Learner T (2004) *Analysis of modern paints*. Getty Publication, Canada
10. Edwards HG, Vandenabeele P (2012) *Analytical archaeometry: selected topic*. RCS Publishing, London
11. Andreotti A, et al (2008) Characterisation of natural organic materials in paintings by GC/MS analytical procedures, in New trends in analytical, environmental and cultural heritage chemistry. In: MP Colombini, L Tassi (eds) *Transworld Research Network: Kerala, India*. p 491
12. Scalalone D, Chiantore O (2009) Py-GC/MS of natural and synthetic resins. In: Colombini MP, Modugno F (eds) *Organic mass spectrometry in art and archaeology*. Wiley, New York, p 327
13. Serpico M, White R (2000) Ancient Egyptian materials and technology. In: Nicholson PT, Shaw I (eds) *Oil, fat and wax*. Cambridge University Press, pp 390–429
14. Pollard AM, Heron C (1996) *Archaeological chemistry*. Royal Society of Chemistry, Cambridge
15. Evershed RP (2000) Modern analytical methods in art and archaeology. In: Ciliberto E, Spoto G (eds) *Biomolecular analysis by organic mass spectrometry*. Wiley, Canada, pp 177–239
16. Ribechini E (2009) Direct mass spectrometric techniques: versatile tools to characterise resinous materials. In: Colombini MP, Modugno F (eds) *Organic mass spectrometry in art and archaeology*. Wiley, New York, pp 77–95

17. Modugno F, Ribechini E (2009) GC/MS in the characterisation of resinous materials. In: Colombini MP, Modugno F (eds) *Organic mass spectrometry in art and archaeology*. Wiley, New York, pp 215–235
18. Colombini MP, Modugno F, Ribechini E (2012) Archaeometric data from mass spectrometric analysis of organic materials: proteins, lipids, terpenoid resins, lignocellulosic polymers, and dyestuff. In: *Mass spectrometry handbook*. John Wiley & Sons, Inc., pp 797–828
19. Evershed RP (2009) Compound-specific stable isotopes in organic residue analysis in archaeology. In: Colombini MP, Modugno F (eds) *Organic mass spectrometry in art and archaeology*. Wiley, New York, pp 389–432
20. Clark KA, Ikram S, Evershed RP (2013) Organic chemistry of balms used in the preparation of pharaonic meat mummies. *Proc Natl Acad Sci* 110(51):20392–20395
21. Hansel FA, Bull ID, Evershed RP (2011) Gas chromatographic mass spectrometric detection of dihydroxy fatty acids preserved in the ‘bound’ phase of organic residues of archaeological pottery vessels. *Rapid Commun Mass Spectrom* 25(13):1893–1898
22. Evershed RP (2008) Organic residue analysis in archaeology: the archaeological biomarker revolution. *Archaeometry* 50(6):895–924
23. Copley M et al (2005) Gas chromatographic, mass spectrometric and stable carbon isotopic investigations of organic residues of plant oils and animal fats employed as illuminants in archaeological lamps from Egypt. *Analyst* 130(6):860–871
24. Evershed R et al (2004) Archaeology: formulation of a Roman cosmetic. *Nature* 432(7013):35–36
25. Buckley SA, Clark KA, Evershed RP (2004) Complex organic chemical balms of Pharaonic animal mummies. *Nature* 431(7006):294–299
26. Modugno F, Ribechini E, Colombini MP (2006) Chemical study of triterpenoid resinous materials in archaeological findings by means of direct exposure electron ionisation mass spectrometry and gas chromatography/mass spectrometry. *Rapid Commun Mass Spectrom* 20(11):1787–1800
27. Ribechini E et al (2008) Gas chromatographic and mass spectrometric investigations of organic residues from Roman glass unguentaria. *J Chromatogr A* 1183(1):158–169
28. Modugno F, Ribechini E, Colombini MP (2006) Aromatic resin characterisation by gas chromatography–mass spectrometry: raw and archaeological materials. *J Chromatogr A* 1134(1):298–304
29. Ribechini E et al (2008) An integrated analytical approach for characterizing an organic residue from an archaeological glass bottle recovered in Pompeii (Naples, Italy). *Talanta* 74(4):555–561
30. Colombini MP, Modugno F, Ribechini E (2005) Direct exposure electron ionization mass spectrometry and gas chromatography/mass spectrometry techniques to study organic coatings on archaeological amphorae. *J Mass Spectrom* 40(5):675–687
31. Colombini MP, Modugno F, Ribechini E (2005) Organic mass spectrometry in archaeology: evidence for Brassicaceae seed oil in Egyptian ceramic lamps. *J Mass Spectrom* 40(7):890–898
32. Ribechini E et al (2009) Py-GC/MS, GC/MS and FTIR investigations on LATE Roman–Egyptian adhesives from opus sectile: new insights into ancient recipes and technologies. *Anal Chim Acta* 638(1):79–87
33. Colombini M et al (2009) An Etruscan ointment from Chiusi (Tuscany, Italy): its chemical characterization. *J Archaeol Sci* 36(7):1488–1495
34. Pérez-Arantegui J et al (2009) Colorants and oils in Roman make-ups—an eye witness account. *TrAC Trends Anal Chem* 28(8):1019–1028
35. Ribechini E, Pérez-Arantegui J, Colombini MP (2011) Gas chromatography/mass spectrometry and pyrolysis-gas chromatography/mass spectrometry for the chemical characterisation of modern and archaeological figs (*Ficus carica*). *J Chromatogr A* 1218(25):3915–3922
36. Ribechini E et al (2011) Discovering the composition of ancient cosmetics and remedies: analytical techniques and materials. *Anal Bioanal Chem* 401(6):1727–1738
37. Giachi G et al (2013) Ingredients of a 2000-y-old medicine revealed by chemical, mineralogical, and botanical investigations. *Proc Natl Acad Sci* 110(4):1193–1196
38. Orsini S et al (2015) Micromorphological and chemical elucidation of the degradation mechanisms of birch bark archaeological artefacts. *Herit Sci* 3(1):2
39. Colombini M et al (2005) Characterisation of organic residues in pottery vessels of the Roman age from Antinoe (Egypt). *Microchem J* 79(1):83–90
40. Tchaplal A et al (2004) Characterisation of embalming materials of a mummy of the Ptolemaic era. Comparison with balms from mummies of different eras. *J Sep Sci* 27(3):217–234

41. Stacey R (2011) The composition of some Roman medicines: evidence for Pliny's Punic wax? *Anal Bioanal Chem* 401(6):1749–1759
42. Connan J, Nissenbaum A (2003) Conifer tar on the keel and hull planking of the Ma'agan Mikhael Ship (Israel, 5th century BC): identification and comparison with natural products and artefacts employed in boat construction. *J Archaeol Sci* 30(6):709–719
43. Brettell R et al (2015) 'Choicest unguents': molecular evidence for the use of resinous plant exudates in late Roman mortuary rites in Britain. *J Archaeol Sci* 53:639–648
44. Steele VJ, Stern B, Stott AW (2010) Olive oil or lard?: distinguishing plant oils from animal fats in the archeological record of the eastern Mediterranean using gas chromatography/combustion/isotope ratio mass spectrometry. *Rapid Commun Mass Spectrom* 24(23):3478–3484
45. Marangou C, Stern B (2009) Neolithic zoomorphic vessels from eastern Macedonia, Greece: issues of function. *Archaeometry* 51(3):397–412
46. Stern B et al (2008) New investigations into the Uluburun resin cargo. *J Archaeol Sci* 35(8):2188–2203
47. Regert M (2011) Analytical strategies for discriminating archeological fatty substances from animal origin. *Mass Spectrom Rev* 30(2):177–220
48. Cramp LJ et al (2014) Neolithic dairy farming at the extreme of agriculture in northern Europe. *Proc R Soc Lond B Biol Sci* 281(1791):20140819
49. Cramp LJ et al (2014) Immediate replacement of fishing with dairying by the earliest farmers of the northeast Atlantic archipelagos. *Proc R Soc Lond B Biol Sci* 281(1780):20132372
50. Salque M et al (2013) Earliest evidence for cheese making in the sixth millennium BC in northern Europe. *Nature* 493(7433):522–525
51. Outram AK et al (2012) Patterns of pastoralism in later Bronze Age Kazakhstan: new evidence from faunal and lipid residue analyses. *J Archaeol Sci* 39(7):2424–2435
52. Dunne J et al (2012) First dairying in green Saharan Africa in the fifth millennium BC. *Nature* 486(7403):390–394
53. Grieco D, Piepoli G (1964) Composizione degli acidi grassi contenuti nei lipidi estratti da semi e frutti oleosi. *Rivista Italiana delle Sostanze Grasse*, pp 283–287
54. O'Donoghue K et al (1996) Remarkable preservation of biomolecules in ancient radish seeds. *Proc R Soc Lond B Biol Sci* 263(1370):541–547
55. Sandy DB (1989) *The production and use of vegetable-oils in Ptolemaic Egypt*. Scholars Press, GA, Atlanta
56. McGovern PE et al (2013) Beginning of viticulture in France. *Proc Natl Acad Sci* 110(25):10147–10152
57. McGovern PE et al (2004) Fermented beverages of pre-and proto-historic China. *Proc Natl Acad Sci USA* 101(51):17593–17598
58. Correa-Ascencio M et al (2014) Pulque production from fermented agave sap as a dietary supplement in Prehispanic Mesoamerica. *Proc Natl Acad Sci* 111(39):14223–14228
59. Charrié-Duhaut A et al (2013) First molecular identification of a hafting adhesive in the Late Howiesons Poort at diepkloof Rock shelter (Western Cape, South Africa). *J Archaeol Sci* 40(9):3506–3518
60. Charrié-Duhaut A et al (2009) Molecular and isotopic archaeology: top grade tools to investigate organic archaeological materials. *C R Chim* 12(10):1140–1153
61. Buonasera TY et al (2015) Lipid biomarkers and compound specific $\delta^{13}\text{C}$ analysis indicate early development of a dual-economic system for the Arctic Small Tool tradition in northern Alaska. *J Archaeol Sci* 61:129–138
62. Crowther A et al (2015) Use of Zanzibar copal (*Hymenaea verrucosa* Gaertn.) as incense at Unguja Ukuu, Tanzania in the 7–8th century CE: chemical insights into trade and Indian Ocean interactions. *J Archaeol Sci* 53:374–390
63. Ostapkowicz J et al (2013) Birdmen, cemís and duhos: material studies and AMS ^{14}C dating of Pre-Hispanic Caribbean wood sculptures in the British Museum. *J Archaeol Sci* 40(12):4675–4687
64. Stacey R, Cartwright C, McEwan C (2006) Chemical characterization of ancient Mesoamerican 'copal' resins: preliminary results. *Archaeometry* 48(2):323–340
65. Otero JG, Schuster V, Svoboda A (2015) Fish and plants: the "hidden" resources in the archaeological record of the North–central Patagonian coast (Argentina). *Quat Int* 373:72–81
66. Kanthilatha N et al (2014) Identification of preserved fatty acids in archaeological floor sediments from prehistoric sites at Ban Non Wat and Nong Hua Raet in northeast Thailand using gas chromatography. *J Archaeol Sci* 46:353–362

67. Yuasa K et al. (2014) Analysis of Japanese ancient lacquerwares excavated from Jōmon period ruins. *J Anal Appl Pyrol* 113:73–77
68. Wei S, Song G, He Y (2015) The identification of binding agent used in late Shang Dynasty turquoise-inlaid bronze objects excavated in Anyang. *J Archaeol Sci* 59:211–218
69. Bleton J, Tchaplá A (2009) SPME/GC-MS in the characterisation of terpenic resins. In: Colombini MP, Modugno F (eds) *Organic mass spectrometry in art and archaeology*. Wiley, New York, pp 261–302
70. Regert M et al (2006) Molecular characterisation of birch bark tar by headspace solid-phase microextraction gas chromatography–mass spectrometry: a new way for identifying archaeological glues. *J Chromatogr A* 1101(1):245–253
71. van der Werf I et al (2014) A quasi non-destructive approach for amber geological provenance assessment based on head space solid-phase microextraction gas chromatography–mass spectrometry. *Talanta* 119:435–439
72. Lucejko JJ, et al (2015) Analytical instrumental techniques to study archaeological wood degradation. *Appl Spectrosc Rev* (just-accepted)
73. Sáiz-Jiménez C, De Leeuw J (1984) Pyrolysis-gas chromatography-mass spectrometry of isolated, synthetic and degraded lignins. *Org Geochem* 6:417–422
74. Faix O, Meier D, Fortmann I (1990) Thermal degradation products of wood. *Eur J Wood Wood Prod Holz als Roh- und Werkstoff* 48(7–8):281–285
75. Sáiz-Jiménez C, De Leeuw J (1986) Lignin pyrolysis products: their structures and their significance as biomarkers. *Org Geochem* 10(4):869–876
76. Boerjan W, Ralph J, Baucher M (2003) Lignin biosynthesis. *Annu Rev Plant Biol* 54(1):519–546
77. Challinor JM (2001) Review: the development and applications of thermally assisted hydrolysis and methylation reactions. *J Anal Appl Pyrol* 61(1):3–34
78. Saiz-Jimenez C et al (1987) Chemical characterization of recent and buried woods by analytical pyrolysis. Comparison of pyrolysis data with ¹³C NMR and wet chemical data. *J Anal Appl Pyrol* 11:437–450
79. Uçar G et al (2005) Analytical pyrolysis and FTIR spectroscopy of fossil *Sequoiadendron giganteum* (Lindl.) wood and MWLs isolated hereof. *Eur J Wood Wood Prod Holz als Roh- und Werkstoff* 63(1):57–63
80. Yang H et al (2005) Biomolecular preservation of Tertiary *Metasequoia* Fossil Lagerstätten revealed by comparative pyrolysis analysis. *Rev Palaeobot Palynol* 134(3–4):237–256
81. Sánchez C (2009) Lignocellulosic residues: biodegradation and bioconversion by fungi. *Biotechnol Adv* 27(2):185–194
82. Del Rio J et al (2001) Py–GC/MS study of *Eucalyptus globulus* wood treated with different fungi. *J Anal Appl Pyrol* 58:441–452
83. Oudia A et al (2009) Analytical pyrolysis study of biodelignification of cloned *Eucalyptus globulus* (EG) clone and *Pinus pinaster* Aiton kraft pulp and residual lignins. *J Anal Appl Pyrol* 85(1):19–29
84. Ibarra D et al (2004) Isolation of high-purity residual lignins from eucalypt paper pulps by cellulase and proteinase treatments followed by solvent extraction. *Enzyme Microbial Technol* 35(2):173–181
85. Colombini MP et al (2009) A multi-analytical study of degradation of lignin in archaeological waterlogged wood. *Talanta* 80(1):61–70
86. Richards V, West N (2002) The use of pyrolysis gas chromatography mass spectrometry to study the extent of degradation of waterlogged wood. In: *Proceedings of the 8th ICOM Group on wet organic archaeological materials conference, Stockholm, 11–15 June 2001*. Deutsches Schiffahrtsmuseum
87. Lucejko JJ et al (2009) Characterisation of archaeological waterlogged wood by pyrolytic and mass spectrometric techniques. *Anal Chim Acta* 654(1):26–34
88. Lucejko JJ et al (2012) Analytical pyrolysis vs. classical wet chemical analysis to assess the decay of archaeological waterlogged wood. *Anal Chim Acta* 745:70–77
89. Tamburini D et al (2014) Characterisation of archaeological waterlogged wood from Herculaneum by pyrolysis and mass spectrometry. *Int Biodeterior Biodegrad* 86:142–149
90. van Bergen PF et al (2000) Evidence for demethylation of syringyl moieties in archaeological wood using pyrolysis-gas chromatography/mass spectrometry. *Rapid Commun Mass Spectrom* 14(2):71–79
91. Tamburini D et al. (2015) Archaeological wood degradation at the site of Biskupin (Poland): wet chemical analysis and evaluation of specific Py-GC/MS profiles. *J Anal Appl Pyrol* 115:7–15

92. Fabbri D, Helleur R (1999) Characterization of the tetramethylammonium hydroxide thermochemolysis products of carbohydrates. *J Anal Appl Pyrol* 49(1):277–293
93. Kuroda K-I, Nakagawa-izumi A (2006) Tetramethylammonium hydroxide (TMAH) thermochemolysis of lignin: improvement of the distribution profile of products derived from β -aryl ether subunits. *J Anal Appl Pyrol* 75(2):104–111
94. Kuroda K-I (2000) Pyrolysis-trimethylsilylation analysis of lignin: preferential formation of cinnamyl alcohol derivatives. *J Anal Appl Pyrol* 56(1):79–87
95. Abdel-Ghani M et al (2009) Characterization of paint and varnish on a medieval Coptic-Byzantine icon: novel usage of dammar resin. *Spectrochim Acta Part A Mol Biomol Spectrosc* 73(3):566–575
96. Andreotti A et al (2014) Characterization of the organic materials used in the painting of the vaulted ceiling at the Saadian Tomb of Mulay Ahmed Al-Mansour (Marrakech). *J Cult Heritage* 15(3):300–307
97. Andreotti A et al (2009) A diagnosis of the yellowing of the marble high reliefs and the black decorations in the chapel of the tomb of Saint Anthony (Padua, Italy). *Int J Mass Spectrom* 284(1):123–130
98. Atrei A et al (2014) An integrated approach to the study of a reworked painting “Madonna with child” attributed to Pietro Lorenzetti. *J Cult Heritage* 15(1):80–84
99. Baumer U, Dietemann P (2010) Identification and differentiation of dragon’s blood in works of art using gas chromatography/mass spectrometry. *Anal Bioanal Chem* 397(3):1363–1376
100. Bersani D et al (2008) Pigments and binders in “Madonna col Bambino e S. Giovannino” by Botticelli investigated by micro-Raman and GC/MS. *J Cult Heritage* 9(1):97–102
101. Blaško J et al (2008) Gas chromatography/mass spectrometry of oils and oil binders in paintings. *J Sep Sci* 31(6–7):1067–1073
102. Bonaduce I et al (2008) The binding media of the polychromy of Qin Shihuang’s Terracotta Army. *J Cult Heritage* 9(1):103–108
103. Brécoulaki H et al (2012) Characterization of organic media in the wall-paintings of the “Palace of Nestor” at Pylos, Greece: evidence for a secco painting techniques in the Bronze Age. *J Archaeol Sci* 39(9):2866–2876
104. Caruso F et al (2007) Gas chromatography–mass spectrometry characterization of the varnish and glue of an ancient 18th century double bass. *J Chromatogr A* 1147(2):206–212
105. Cauzzi D et al (2013) Spectroscopic and chromatographic studies of sculptural polychromy in the Zhongshan Grottoes (RPC). *J Cult Heritage* 14(1):70–75
106. Čukovska LR et al (2012) Micro-Raman and GC/MS analysis to characterize the wall painting technique of Dicho Zograph in churches from Republic of Macedonia. *J Raman Spectrosc* 43(11):1685–1693
107. Daniilia S et al (2008) From Byzantine to post-Byzantine art: the painting technique of St Stephen’s wall paintings at Meteora, Greece. *J Archaeol Sci* 35(9):2474–2485
108. Daniilia S et al (2007) The Byzantine wall paintings from the Protaton Church on Mount Athos, Greece: tradition and science. *J Archaeol Sci* 34(12):1971–1984
109. Ferreira ES, Van der Horst J, Boon JJ (2005) Chemical aspects of the binding media of the Oranjezaal ensemble: an insight into 17th century Netherlandish materials and methods. In: Proceedings of the 14th ICOM-CC meeting in The Hague (I. Vergier ed), Preprint vol II
110. Guttman MJ (2013) Transylvanian glass icons: a GC/MS study on the binding media. *J Cult Heritage* 14(5):439–447
111. Kalinina KB et al (2012) An analytical investigation of the painting technique of Italian Renaissance master Lorenzo Lotto. *J Cult Heritage* 13(3):259–274
112. Ling H et al (2007) Analytical characterization of binding medium used in ancient Chinese artworks by pyrolysis–gas chromatography/mass spectrometry. *Microchem J* 85(2):347–353
113. Miliani C et al (2007) Non-invasive in situ investigations versus micro-sampling: a comparative study on a Renoirs painting. *Appl Phys A* 89(4):849–856
114. Ospitali F et al (2007) XVI century wall paintings in the “Messer Filippo” cell of the tower of Spilamberto: microanalyses and monitoring. *J Cult Heritage* 8(3):323–327
115. Pithard V, et al (2006) Study of complex organic binding media systems on artworks applying GC-MS analysis: selected examples from the Kunsthistorisches Museum, Vienna. In: Macromolecular symposia. Wiley Online Library
116. Rampazzi L et al (2007) Prehistoric wall paintings: the case of the Domus de Janas necropolis (Sardinia, Italy). *Archaeometry* 49(3):559–569

117. Rasmussen KL et al (2012) The constituents of the ink from a Qumran inkwell: new prospects for provenancing the ink on the Dead Sea Scrolls. *J Archaeol Sci* 39(9):2956–2968
118. Scott DA et al (2009) Examination of some pigments, grounds and media from Egyptian cartonnage fragments in the Petrie Museum, University College London. *J Archaeol Sci* 36(3):923–932
119. Valianou L et al (2011) Identification of organic materials in icons of the Cretan School of iconography. *J Archaeol Sci* 38(2):246–254
120. van der Werf ID et al (2013) Multi-technique chemical characterisation of a 12–13th-century painted Crucifix. *Microchem J* 106:87–94
121. van der Werf ID et al (2008) San Francesco d'Assisi (Apulia, South Italy): study of a manipulated 13th century panel painting by complementary diagnostic techniques. *J Cult Heritage* 9(2):162–171
122. Vázquez C et al (2008) Combining TXRF, FT-IR and GC-MS information for identification of inorganic and organic components in black pigments of rock art from Alero Hornillos 2 (Jujuy, Argentina). *Anal Bioanal Chem* 391(4):1381–1387
123. Wei S, Ma Q, Schreiner M (2012) Scientific investigation of the paint and adhesive materials used in the Western Han dynasty polychromy terracotta army, Qingzhou, China. *J Archaeol Sci* 39(5):1628–1633
124. Wei S et al (2011) Analytical characterization of lacquer objects excavated from a Chu tomb in China. *J Archaeol Sci* 38(10):2667–2674
125. Andreotti A et al (2007) Novel applications of the Er: YAG laser cleaning of old paintings. In: Nimmrichter J, Kautek W, Schreiner M (eds) *Lasers in the conservation of artworks*. Springer, Berlin
126. Andreotti A, et al (2006) Multianalytical study of laser pulse duration effects in the IR laser cleaning of wall paintings from the Monumental Cemetery of Pisa. *Laser Chem* 2006:11, Art ID 39046. doi:10.1155/2006/39046
127. Casoli A, Berzioli M, Cremonesi P (2013) The chemistry of egg binding medium and its interactions with organic solvents and water. *New Insights Clean Paint* 39:39–44
128. DeCruz A et al (2009) Investigation of the Er: YAG laser at 2.94 μm to remove lichens growing on stone. *Stud Conserv* 54(4):268–277
129. Kahrim K et al (2009) The application of in situ mid-FTIR fibre-optic reflectance spectroscopy and GC-MS analysis to monitor and evaluate painting cleaning. *Spectrochim Acta Part A Mol Biomol Spectrosc* 74(5):1182–1188
130. Lustrato G et al (2012) Fast biocleaning of mediaeval frescoes using viable bacterial cells. *Int Biodeterior Biodegrad* 69:51–61
131. Morrison R et al (2007) An investigation of parameters for the use of citrate solutions for surface cleaning unvarnished paintings. *Stud Conserv* 52(4):255–270
132. Osete-Cortina L, Doménech-Carbó MT (2006) Study on the effects of chemical cleaning on pinaceae resin-based varnishes from panel and canvas paintings using pyrolysis-gas chromatography/mass spectrometry. *J Anal Appl Pyrol* 76(1):144–153
133. Ranalli G et al (2005) Biotechnology applied to cultural heritage: biorestitution of frescoes using viable bacterial cells and enzymes. *J Appl Microbiol* 98(1):73–83
134. Sánchez-Ledesma A, Muro-García C, Gayo-García MD (2010) Effects of commercial soaps on unvarnished painted surfaces: a pilot study for their assessment. In: *New insights into the Cleaning of Paintings. Proceedings from the cleaning 2010 international conference, Valencia*
135. Mazzeo R, et al (2010) Scientific examination of the traditional materials and techniques used in Yuan Dynasty wall paintings. In: *Proceedings of the second international conference on the conservation of Grotto Sites, Mogao Grottoes, Dunhuang, People*
136. Riedo C, Scalarone D, Chiantore O (2010) Advances in identification of plant gums in cultural heritage by thermally assisted hydrolysis and methylation. *Anal Bioanal Chem* 396(4):1559–1569
137. Riedo C, Scalarone D, Chiantore O (2013) Multivariate analysis of pyrolysis-GC/MS data for identification of polysaccharide binding media. *Anal Methods* 5(16):4060–4067
138. Vicente JP et al (2005) Identification of lipid binders in old oil paintings by separation of 4-bromomethyl-7-methoxycoumarin derivatives of fatty acids by liquid chromatography with fluorescence detection. *J Chromatogr A* 1076(1):44–50
139. Bonaduce I et al (2007) Gas chromatographic-mass spectrometric characterisation of plant gums in samples from painted works of art. *J Chromatogr A* 1175(2):275–282
140. Hofta P (2006) Original Paper An evaluation of GC-MS and HPLC-FD methods for analysis of protein binders in paintings. *J Sep Sci* 29:2653–2663

141. Osete-Cortina L, Doménech-Carbó MT (2005) Analytical characterization of diterpenoid resins present in pictorial varnishes using pyrolysis–gas chromatography–mass spectrometry with on line trimethylsilylation. *J Chromatogr A* 1065(2):265–278
142. Piccirillo A, Scalalone D, Chiantore O (2005) Comparison between off-line and on-line derivatization methods in the characterisation of siccative oils in paint media. *J Anal Appl Pyrol* 74(1):33–38
143. Russell J et al (2011) The identification of synthetic organic pigments in modern paints and modern paintings using pyrolysis–gas chromatography–mass spectrometry. *Anal Bioanal Chem* 400(5):1473–1491
144. Sutherland K (2010) Bleached shellac picture varnishes: characterization and case studies. *J Inst Conserv* 33(2):129–145
145. Fabbri D et al (2005) Profiling fatty acids in vegetable oils by reactive pyrolysis–gas chromatography with dimethyl carbonate and titanium silicate. *J Chromatogr A* 1100(2):218–222
146. Melucci D et al (2011) Behaviour of phospholipids in analytical reactive pyrolysis. *J Therm Anal Calorim* 104(2):415–421
147. Torri C et al (2013) Py-SPME-GC-MS with on-fiber derivatization as a new solvent-less technique for the study of polar macromolecules: application to natural gums. *Microchem J* 110:719–725
148. Chiavari G, Fabbri D, Prati S (2005) Effect of pigments on the analysis of fatty acids in siccative oils by pyrolysis methylation and silylation. *J Anal Appl Pyrol* 74(1–2):39–44
149. Gautier G, Colombini MP (2007) GC–MS identification of proteins in wall painting samples: a fast clean-up procedure to remove copper-based pigment interferences. *Talanta* 73(1):95–102
150. Lluveras-Tenorio A et al (2012) Analysis of plant gums and saccharide materials in paint samples: comparison of GC-MS analytical procedures and databases. *Chem Cent J* 6(1):115
151. Singer B, McGuigan R (2007) The simultaneous analysis of proteins, lipids, and diterpenoid resins found in cultural objects. *Anal Chim* 97(7):405–417
152. Andreotti A et al (2006) Combined GC/MS analytical procedure for the characterization of glycerolipid, waxy, resinous, and proteinaceous materials in a unique paint micro-sampler. *Anal Chem* 78(13):4490–4500
153. Bonaduce I, Cito M, Colombini MP (2009) The development of a gas chromatographic–mass spectrometric analytical procedure for the determination of lipids, proteins and resins in the same paint micro-sample avoiding interferences from inorganic media. *J Chromatogr A* 1216(32):5931–5939
154. Echard J-P, Lavédrine B (2008) Review on the characterisation of ancient stringed musical instruments varnishes and implementation of an analytical strategy. *J Cult Heritage* 9(4):420–429
155. Lluveras A et al (2009) GC/MS analytical procedure for the characterization of glycerolipids, natural waxes, terpenoid resins, proteinaceous and polysaccharide materials in the same paint microsample avoiding interferences from inorganic media. *Anal Chem* 82(1):376–386
156. Niimura N et al (1996) Characterization of *Rhus vernicifera* and *Rhus Succedanea* lacquer films and their pyrolysis mechanisms studied using two-stage pyrolysis–gas chromatography/mass spectrometry. *J Anal Appl Pyrol* 37:199–209
157. Niimura N, Miyakoshi T (2003) Characterization of natural resin films and identification of ancient coating. *J Mass Spectrom Soc Jpn* 51(4):439–457
158. Kumanotani J (1995) Urushi (oriental lacquer)—a natural aesthetic durable and future-promising coating. *Prog Org Coat* 26(2–4):163–195
159. Le Hô A et al (2012) Molecular criteria for discriminating museum Asian lacquerware from different vegetal origins by pyrolysis gas chromatography/mass spectrometry. *Anal Chim Acta* 710:9–16
160. Lu R et al. (2012) Analysis of Japanese Jomon lacquer-ware by pyrolysis–gas chromatography/mass spectrometry. *J Anal Appl Pyrol* 103:68–72
161. Lu R et al (2007) Identification of Ryukyu lacquerware by pyrolysis–gas chromatography/mass spectrometry. *J Anal Appl Pyrol* 80:101–110
162. Lu R, Kamiya Y, Miyakoshi T (2006) Applied analysis of lacquer films based on pyrolysis–gas chromatography/mass spectrometry. *Talanta* 70:370–376
163. Niimura N (2009) Determination of the type of lacquer on East Asian lacquer ware. *Int J Mass Spectrom* 284:93–97
164. Niimura N, Miyakoshi T (2006) Structural study of oriental lacquer films during the hardening process. *Talanta* 70:146–152

165. Niimura N et al (1999) Identification of ancient lacquer film using two stage pyrolysis-gas chromatography/mass spectrometry. *Archeometry* 41:137–149
166. Pitthard V et al (2010) Scientific investigations of antique lacquers from a 17th-century Japanese ornamental cabinet. *Archaeometry* 52(6):1044–1056
167. Tamburini D, Bonaduce I, Colombini MP (2015) Characterization and identification of urushi using in situ pyrolysis/silylation-gas chromatography-mass spectrometry. *J Anal Appl Pyrol* 111:33–40
168. Tamburini D, Bonaduce I, Colombini MP (2015) Characterisation of oriental lacquers from *Rhus succedanea* and *Melanorrhoea usitata* using in situ pyrolysis/silylation-gas chromatography mass spectrometry. *J Anal Appl Pyrol* 116:129–141
169. Colombini MP, Bonaduce I, Gautier G (2003) Molecular pattern recognition of fresh and aged shellac. *Chromatographia* 58(5/6):357–364
170. Bonaduce I, Colombini MP (2004) Characterisation of beeswax in works of art by gas chromatography-mass spectrometry and pyrolysis-gas chromatography-mass spectrometry procedures. *J Chromatogr A* 1028(2):297–306
171. Lattuati-Derieux A, Thao S, Langlois J, Regert M (2008) First results on headspace-solid phase microextraction-gas chromatography/mass spectrometry of volatile organic compounds emitted by wax objects in museums. *J Chromatogr A* 1187:239–249
172. Duce C et al (2012) Physico-chemical characterization of protein-pigment interactions in tempera paint reconstructions: casein/cinnabar and albumin/cinnabar. *Anal Bioanal Chem* 402:2183–2193
173. Duce C et al (2013) Interactions between inorganic pigments and proteinaceous binders in reference paint reconstructions. *Dalton Trans* 42(17):5975–5984
174. Pellegrini D et al (2016) Fourier transform infrared spectroscopic study of rabbit glue/inorganic pigments mixtures in fresh and aged reference paint reconstructions. *Microchem J* 124:31–35
175. Ormsby BA et al (2005) British Watercolour cakes from the eighteenth to the early twentieth century. *Stud Conserv* 50(1):45–66
176. Colombini MP, Modugno F, Ribechini E (2009) GC/MS in the characterization of lipids. In: Colombini MP, Modugno F (eds) *Organic mass spectrometry in art and archaeology*. Wiley, London, pp 191–214
177. Bonaduce I, et al (2012) New insights into the ageing of linseed oil paint binder: a qualitative and quantitative analytical study. *PLoS One* 7(11)
178. Shilling MR, Carson DM, Khanjian HP (1998) Evaporation of fatty acids and the formation of ghost images by framed oil paintings. *West Assoc Art Conserv (WAAC) Newsletter*, 21(1)
179. Keune K, Noble P, Boon JJ (2002) Chemical changes in lead-pigmented oil paints: on the early stage of formation of protrusions. In: *Proceeding of art 2002, the 7th international conference on non-destructive testing and microanalysis for the diagnostics and conservations of the cultural and environmental Heritage*. Antwerp, Belgium
180. van der Weerd J et al (2002) Chemical changes in old master paintings: dissolution, metal soap formation and remineralization processes in lead pigmented paint layers of 17th century paintings. *Zeitschrift für Kunsttechnologie und Konservierung* 16:36–51
181. Keune K et al (2008) Comparative study of the effect of traditional pigments on artificially aged oil paint systems using complementary analytical techniques. In: Bridgland J (ed) *Preprints of 15th triennial meeting of ICOM committee for conservation*. Allied Publishers Pvt. Ltd., New Delhi, pp 833–842
182. Shilling MR, Khanjian HP (1996) Gas chromatographic determination of the fatty acid and glycerol content of lipids. I: the effects of pigments and ageing on the composition of oil paints. In: Bridgland J (ed) *ICOM committee for conservation, 11th triennial meeting in Edinburgh, Scotland, 1–6 September 1996: Preprints*. James and James: London, pp 220–227
183. Sutherland K (2000) The extraction of soluble components from an oil paint film by a varnish solution. *Stud Conserv* 45:54–62
184. Keune K, Ferreira ESB, Boon JJ (2005) Characterization and localization of the oil-binding medium in paint cross-sections using imaging secondary ion mass spectrometry. In: *ICOM committee for conservation 14th triennial meeting 2005*. James & James, The Hague, The Netherlands
185. Phenix A, Sutherland K (2001) The cleaning of paintings: effects of organic solvents on oil paint films. *Rev Conserv* 2:47–60
186. Sutherland K (2003) Solvent-extractable components of linseed oil paint films. *Stud Conserv* 48:111–135
187. Sutherland K (2006) Measurements of solvent cleaning effects on oil paintings. *J Am Inst Conserv* 45(3):211–226

188. Lluveras-Tenorio A et al (2012) The development of a new analytical model for the identification of saccharide binders in paint samples. *PLoS One* 7(11):e49383
189. Tsakalof AK, Bairachtari KA, Chrystosoulakis ID (2006) Pitfalls in drying oils identification in art objects by gas chromatography. *J Sep Sci* 29(11):1642–1646
190. van Keulen H (2009) Gas chromatography/mass spectrometry methods applied for the analysis of a Round Robin sample containing materials present in samples of works of art. *Int J Mass Spectrom* 284(1):162–169
191. Scalarone D, Chiantore O (2002) The use of pyrolysis-GC/MS for the identification of polymeric constituents in artworks, museum and collectible design objects. In: *Plastics in art: history, technology, preservation, Siegl.* pp 90–104
192. Izzo FC et al (2014) 20th century artists' oil paints: the case of the olii by Lucio Fontana. *J Cult Heritage* 15(5):557–563
193. Izzo FC, et al (2014) Modern oil paints—formulations, organic additives and degradation: some case studies. In: *Issues in contemporary oil paint.* Springer, pp 75–104
194. La Nasa J, Zanaboni M, Uldanck D, Degano I, Modugno F, Kutzke H, Tveit ES, Topalova-Casadięgo B, Colombini MP (2015) Novel application of liquid chromatography/mass spectrometry for the characterization of drying oils in art: elucidation on the composition of original paint materials used by Edvard Munch (1863–1944). *Anal Chim Acta*
195. Schilling MR, Mazurek J, Learner TJS (2007) Studies of modern oil-based artists' paint media by gas chromatography/mass spectrometry. In: *In modern paints uncovered: proceedings from the modern paints uncovered symposium.* Getty Conservation Institute, Los Angeles. pp 129–139
196. Cappitelli F, Koussiaki F (2006) THM-GCMS and FTIR for the investigation of paints in Picasso's Still Life, Weeping Woman and Nude Woman in a Red Armchair from the Tate Collection, London. *J Anal Appl Pyrol* 75:200–204
197. van den Berg KJ et al (2014) Issues in contemporary oil paint. Springer, New York
198. Ghelardi E (2014) A multi analytical approach for the characterisation of the contemporary paint materials. PhD thesis, Università degli Studi di Firenze
199. Burnstock A, et al (2007) An investigation of water-sensitive oil paints. In: *Modern paints uncovered: proceedings from the modern paints uncovered symposium.* Getty Publications
200. Bayliss S et al (2016) An investigation into the separation and migration of oil in paintings by Erik Oldenhof. *Microchem J* 124:974–982
201. Narine SS, Kong X (2005) Vegetable oils in production of polymers and plastics. *Bailey's Ind Oil Fat Prod*
202. Schilling MR, Keeney J, Leamer T (2004) Characterization of alkyd paint media by gas chromatography-mass spectrometry. *Stud Conserv* 49(Supplement-2):197–201
203. Wei S, Pintus V, Schreiner M (2013) A comparison study of alkyd resin used in art works by Py-GC/MS and GC/MS: the influence of aging. *J Anal Appl Pyrol* 104:441–447
204. La Nasa J et al (2013) Alkyd paints in art: characterization using integrated mass spectrometry. *Anal Chim Acta* 797:64–80
205. Ploeger R, Scalarone D, Chiantore O (2008) The characterization of commercial artists' alkyd paints. *J Cult Heritage* 9:412–419
206. Cappitelli F (2004) THM-GCMS and FTIR for the study of binding media in Yellow Islands by Jackson Pollock and Break Point by Fiona Banner. *J Anal Appl Pyrol* 71(1):405–415
207. Challinor J (1991) Structure determination of alkyd resins by simultaneous pyrolysis ethylation. *J Anal Appl Pyrol* 18(3):233–244
208. Dietemann P et al (1865) A colloidal description of tempera and oil paints, based on a case study of Arnold Böcklin's painting Villa am Meer II (1865). *e-Preserv Sci* 2014(11):29–46
209. Mustalish R (2004) Modern materials: plastics. In: *Heilbrunn timeline of art history.* The Metropolitan Museum of Art, New York, 2000. http://www.metmuseum.org/toah/hd/mome/hd_mome.htm
210. Altshuler B (2007) *Collecting the new: museums and contemporary art.* Princeton University Press, Princeton
211. Lavédrine B, Fournier A, Martin G (2012) Preservation of plastic artefacts in museum collections. *Comité Des Travaux Historiques Et Scientifiques*
212. Learner T (2001) The analysis of synthetic paints by pyrolysis-gas chromatography-mass spectrometry (PyGCMS). *Stud Conserv* 46:225–241
213. Tsuge S, Ohtani H, Watanabe C (2011) *Pyrolysis-GC/MS data book of synthetic polymers: pyrograms, thermograms and MS of pyrolyzates.* Elsevier, Amsterdam

214. Wampler TP (2007) *Applied pyrolysis handbook*, ed. CRC press Taylor and Francis group, New York
215. Silva MF et al (2009) Determination of the plasticizer content in poly(vinyl acetate) paint medium by pyrolysis-silylation-gas chromatography-mass spectrometry. *J Anal Appl Pyrol* 85(1–2):487–491
216. Salam LA, Matthews RD, Robertson H (2000) Pyrolysis of poly-methyl methacrylate (PMMA) binder in thermoelectric green tapes made by the tape casting method. *J Eur Ceram Soc* 20(3):335–345
217. Cortina LO, Carbò MTD (2006) Characterization of acrylic resins used for restoration of artworks by pyrolysis-silylation-gas chromatography/mass spectrometry with hexamethyldisilazane. *J Chromatogr A* 1127:228–236
218. Carbò MTD et al (2008) Characterization of polyvinyl resins used as binding media in paintings by pyrolysis-silylation -gas chromatography-mass spectrometry. *Anal Bioanal Chem* 391:1371–1379
219. Wei S, Pintus V, Schreiner M (2012) Photochemical degradation study of polyvinyl acetate paints used in artworks by Py-GC/MS. *J Anal Appl Pyrol* 97:158–163
220. Di Crescenzo MM et al (2014) The use of waterborne paints in contemporary murals: comparing the stability of vinyl, acrylic and styrene-acrylic formulations to outdoor weathering conditions. *Polym Degrad Stab* 107:285–293
221. Rainer L (2003) The conservation of outdoor contemporary murals. *GCI News* 18
222. Ormsby B, Learner T (2009) The effects of wet surface cleaning treatments on acrylic emulsion artists' paints—a review of recent scientific research. *Stud Conserv* 54(Supplement-1):29–41
223. Jablonski E et al (2003) Conservation concerns for acrylic emulsion paints. *Stud Conserv* 48(Supplement-1):3–12
224. Ormsby B, et al (2006) The effects of surface cleaning on acrylic emulsion paintings: a preliminary investigation. *Tate Papers* 6
225. Wolbers R, Norbutus A, Lagalante A (2013) Cleaning of acrylic emulsion paints: preliminary extractive studies with two commercial paint systems. In: *New insights into the cleaning of paintings: proceedings of the cleaning 2010 conference*, Smithsonian Institution Scholarly Press, Washington DC
226. Dillon CE, Lagalante AF, Wolbers RC (2014) Acrylic emulsion paint films: the effect of solution pH, conductivity, and ionic strength on film swelling and surfactant removal. *Stud Conserv* 59(1):52–62
227. Chiantore O, Scalrone D, Learner T (2003) Characterization of artists' acrylic emulsion paints. *Int J Polym Anal Charact* 8(1):67–82
228. Scalrone D, Chiantore O (2004) Separation techniques for the analysis of artists' acrylic emulsion paints. *J Sep Sci* 27:263–274
229. La Nasa J et al (2016) A chemical study of organic materials in three murals by Keith Haring: a comparison of painting techniques. *Microchem J* 124:940–948
230. Silva M et al (2010) Identification of additives in poly(vinylacetate) artist's paints using PY-GC-MS. *Anal Bioanal Chem* 397(1):357–367
231. Pintus V, Wei S, Schreiner M (2012) UV ageing studies: evaluation of lightfastness declarations of commercial acrylic paints. *Anal Bioanal Chem* 402(4):1567–1584
232. Shilling M, et al (2012) Identification and chemical composition using chromatographic methods. In: Lavédrine B, Fournier A, Martin G (eds). *Preservation of plastic artefacts in museum collections*. Comité Des Travaux Historiques Et Scientifiques, pp 61–69
233. Pedersoli JL, Ligterink F, van Bommel M (2011) Non-destructive determination of acetic acid and furfural in books by solid-phase micro-extraction (SPME) and gas chromatography-mass spectrometry (GC/MS). *Restaurator* 32(2):110–134
234. Strlič M et al (2009) Material degradomics: on the smell of old books. *Anal Chem* 81(20):8617–8622
235. Łojewski T et al (2010) Furfural as a marker of cellulose degradation. A quantitative approach. *Appl Phys A* 100(3):873–884
236. Curran K, et al (2013) Heritage smells! analysis of VOC emissions from historic plastics using SPME-GC/MS. In: 6th users' group for mass spectrometry and chromatography meeting 2013, Pisa, Italy
237. Lattuati-Derieux A et al (2013) What do plastics emit? HS-SPME-GC/MS analyses of new standard plastics and plastic objects in museum collections. *J Cult Heritage* 14(3):238–247
238. Curran K, Strlič M (2015) Polymers and volatiles: using VOC analysis for the conservation of plastic and rubber objects. *Stud Conserv* 60(1):1–14

239. Brimblecombe P (ed) (2003) The effects of air pollution on the built environment. Imperial College Press, London
240. Schieweck A et al (2007) Occurrence of organic and inorganic biocides in the museum environment. *Atmos Environ* 41(15):3266–3275
241. Godoi AF, Van Vaeck L, Van Grieken R (2005) Use of solid-phase microextraction for the detection of acetic acid by ion-trap gas chromatography–mass spectrometry and application to indoor levels in museums. *J Chromatogr A* 1067(1):331–336
242. Thiébaud B et al (2007) Application of headspace SPME-GC-MS in characterisation of odorous volatile organic compounds emitted from magnetic tape coatings based on poly (urethane-ester) after natural and artificial ageing. *Polym Testing* 26(2):243–256
243. Mitchell G, Higgitt C, Gibson LT (2014) Emissions from polymeric materials: characterised by thermal desorption-gas chromatography. *Polym Degrad Stab* 107:328–340
244. Curran K et al (2014) Cross-infection effect of polymers of historic and heritage significance on the degradation of a cellulose reference test material. *Polym Degrad Stab* 107:294–306
245. Schieweck A, Salthammer T (2011) Indoor air quality in passive-type museum showcases. *J Cult Heritage* 12(2):205–213
246. López-Aparicio S et al (2010) Measurement of organic and inorganic pollutants in microclimate frames for paintings. *e-Preserv Sci* 7:59–70
247. Risholm-Sundman M et al (1998) Emissions of acetic acid and other volatile organic compounds from different species of solid wood. *Eur J Wood Wood Prod* 56(2):125–129
248. Oikawa T et al (2005) Volatile organic compounds from wood and their influences on museum artifact materials I. Differences in wood species and analyses of causal substances of deterioration. *J Wood Sci* 51(4):363–369
249. Sabbioni C, Ghedinia N, Bonazza A (2003) Organic anions in damage layers on monuments and buildings. *Atmos Environ* 37:1261–1269
250. Tétéreault J (2003) Airborne pollutants in museums, galleries, and archives: risk assessment, control strategies and preservation management. Ottawa, Canadian Conservation Institute
251. Linnow K, Halsberghe L, Steiger M (2007) Analysis of calcium acetate efflorescences formed on ceramic tiles in a museum environment. *J Cult Heritage* 8:44–52
252. Gibson LT et al (1997) Investigation of the composition of a unique efflorescence on calcareous museum artifacts. *Anal Chim Acta* 337:253–264
253. Tétéreault J et al (2003) Corrosion of copper and lead by formaldehyde, formic and acetic acid vapours. *Stud Conserv* 48:237–250
254. Ryhl-Svendsen M (2008) Corrosivity measurements of indoor museum environments using lead coupons as dosimeters. *J Cult Heritage* 9:285–293
255. Brimblecombe P, Grossi CM (2012) Carbonyl compounds indoors in a changing climate. *Chem Cent J* 6:21
256. Dupont A-L, Tétéreault J (2000) Cellulose degradation in an acetic acid environment. *Stud Conserv* 45:201–210
257. Strlič M et al (2011) The effect of volatile organic compounds and hypoxia on paper degradation. *Polym Degrad Stab* 96:608–615
258. Bonaduce I et al (2013) The role of organic and inorganic indoor pollutants in museum environments in the degradation of dammar varnish. *Analyst* 138(2):487–500
259. La Nasa J et al (2014) Effects of acetic acid vapour on the ageing of alkyd paint layers: multi-analytical approach for the evaluation of the degradation processes. *Polym Degrad Stab* 105:257–264

DNA Sequencing in Cultural Heritage

Stefania Vai¹ · Martina Lari¹ · David Caramelli¹

Received: 30 September 2015 / Accepted: 31 December 2015 / Published online: 12 January 2016
© Springer International Publishing Switzerland 2016

Abstract During the last three decades, DNA analysis on degraded samples revealed itself as an important research tool in anthropology, archaeozoology, molecular evolution, and population genetics. Application on topics such as determination of species origin of prehistoric and historic objects, individual identification of famous personalities, characterization of particular samples important for historical, archeological, or evolutionary reconstructions, confers to the paleogenetics an important role also for the enhancement of cultural heritage. A really fast improvement in methodologies in recent years led to a revolution that permitted recovering even complete genomes from highly degraded samples with the possibility to go back in time 400,000 years for samples from temperate regions and 700,000 years for permafrozen remains and to analyze even more recent material that has been subjected to hard biochemical treatments. Here we propose a review on the different methodological approaches used so far for the molecular analysis of degraded samples and their application on some case studies.

Keywords Ancient DNA · Paleogenetics · New generation sequencing · Cultural heritage

✉ Stefania Vai
stefania.vai@unifi.it

Martina Lari
martina.lari@unifi.it

David Caramelli
david.caramelli@unifi.it

¹ Department of Biology, University of Florence, Via del Proconsolo 12, 50122 Florence, Italy

1 Ancient DNA: An Overview

About 30 years ago, the first results of recovery of genetic material from old samples were published [1, 2]. Since that time, a revolutionary development in methods, as well as an improvement in the knowledge of degraded DNA characteristics led to clear affirmation of ancient DNA (aDNA) as an investigation tool in several scientific, archaeological, and historical fields. Anthropology, archaeozoology, molecular evolution, conservation and population genetics, forensic, archaeology, and history are the disciplines that benefit from aDNA analysis. Targets of these analyses can be different and have several applications. Genetic comparison between different human groups in space and time, kinship analysis between individuals in necropolises, and genetic signature of pathogens can help to discern biological or cultural links between communities, understanding social patterns, and reconstructing the health status in past populations. On faunal or flora remains, the analysis of past genetic variability can have an important role in present day approaches for conservation and for the reconstruction of domestication processes. The evolutionary history of species can be reconstructed with more accuracy using past specimens together with modern ones, and also evolution of genes can be followed searching for their variation between different living and extinct forms. The identification of important personalities by comparison of the genetic profile with that obtained from descendants is another target for which the genetic analysis is indispensable. aDNA analysis can also permit the species identification of undetermined organic tools or objects.

Despite its name, ancient DNA actually does not refer to a particular time frame. The oldest samples analysed so far are represented by a hominin bone specimen dated around 400,000 years old from a cave in Spain [3] to a 700,000-year-old equid bone specimen preserved in permafrost [4]. But also specimens that are really close in time can present a high degree of DNA degradation due to treatments for transformation of the material and can need the same methodological approach of the most ancient ones.

Research on aDNA suffers of some issues due to degradation of the genetic material because of biochemical processes that occurred over time or treatments specimens were subjected to. Factors such as temperature, pH, and processes such as hydrolysis and oxidation, led the DNA to fragmentation into short strands, mainly by depurination [5], and to a decline of the amount of endogenous genetic material as final consequence [6]. In the meantime, the sample is enriched in exogenous DNA coming from environmental microorganisms or from people who manipulate the sample, entailing that the total genetic material recovered is due to a mixture of different biological sources from which researchers have to separate the endogenous original component [7]. Also, oxidative lesions [8] and intermolecular crosslinks can make the DNA molecules no more available for analytical steps [6]. Furthermore, the nitrous bases that constitute the DNA molecule can be affected by hydrolytic loss of amino groups, and this modification may produce misincorporations [6]. The deamination products of cytosine (uracil) and guanine (xanthine) cause incorrect base insertions (T instead of C, and A instead of G) when new DNA strands are synthesized by a DNA polymerase [8–10]. These misincorporations occurs with higher frequencies at the end of the DNA strands [7], since the overhanging single strands at fragment termini are characterized by a faster rate

of deamination [5, 7]. A correlation between the percentage of DNA molecules with misincorporations and the age of the sample has been observed (except for samples subjected to extreme environmental conditions) [11] and this pattern can be used to recognize the ancient degraded molecules from the modern contaminant ones when analyzing sequence data [12, 13].

In order to obtain reliable results, despite the degradation and the possible contamination of the samples, the genetic analysis must be performed following stringent criteria proposed for ancient DNA studies [14].

Methods for the analysis depend on the starting material and on the aim of the research: different kind of biological tissues or traces need different experimental approaches for DNA extraction, and the genetic target determine which methodology can be the more appropriate between the so called first generation or the new generation sequencing (NGS) ones that will be explained in the next paragraphs.

2 DNA Extraction

One of most used extraction methods is the phenol–chloroform-based protocol [15]. This method separates mixtures of molecules based on their differential solubility, leading proteins to isolation in an organic phase separated from an aqueous solution containing DNA.

Over time, different extraction protocols were developed in order to optimize the DNA recovery from particular degraded material. The last studies demonstrated that the sole use of EDTA and proteinase K for digestion and the binding of DNA to silica via guanidine thiocyanate or hydrochloride for purification represents the best strategy in order to recover the genetic material in term of quantity and quality [16, 17]. Especially for degraded samples where DNA is highly fragmented, this protocol is associated with the use of commercial silica columns in order to recover also really short DNA fragments that could represent the majority of the endogenous material [18, 19]. Those methods were tested especially on bone samples, since this is the most available material from which aDNA is usually recovered. For other starting materials, such as soft tissues, blood traces, hair, and vegetable materials, the same protocols as well as commercial extraction kits are available, but custom approaches with different settings for digestion are advantageous in order to optimize the cellular lysis and the release of DNA (see [20] for example, [21] for extraction from hair, [22] from plants, [23] from mummified tissues).

After DNA has been extracted, several approaches are possible in order to select the genomic regions of interest and obtain their sequence.

Since degraded DNA is often present in low copy number, an amplification of the target region represents the best strategy to be followed. Until 2005 the amplification of target regions was performed by polymerase chain reaction (PCR), then the obtained products were usually cloned and sequenced by Sanger's sequencing method. This represent the so called classical approach in the aDNA field, and it is yet the best one if the aim is to study defined DNA fragments with a minimum length of about 60 bp. Instead, if the target is represented by a large number of DNA fragments to be studied in parallel, or whole genomes, the best

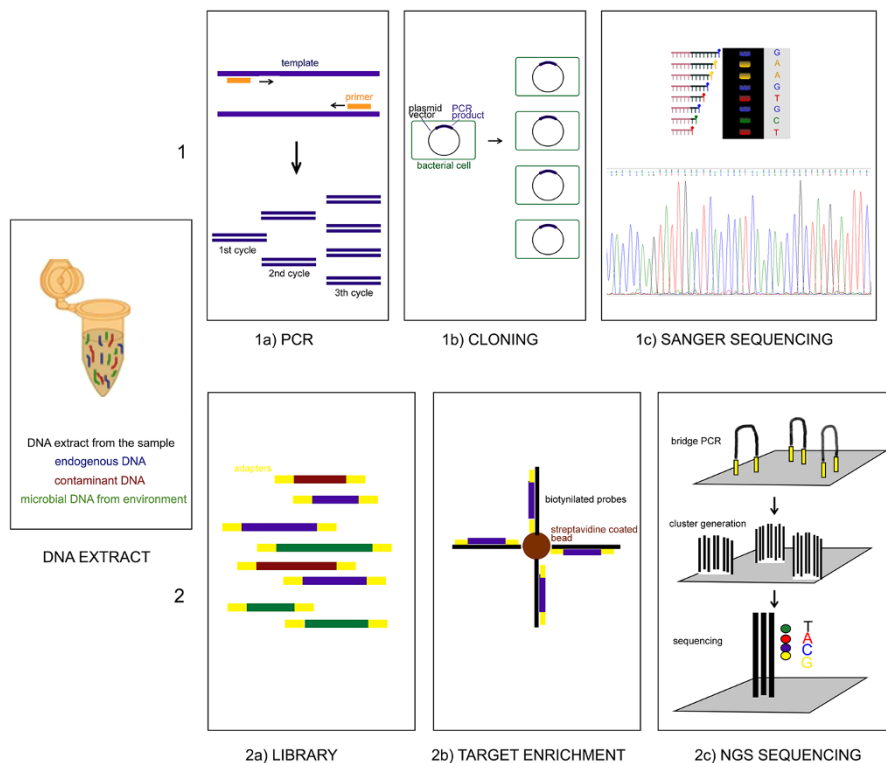


Fig. 1 Laboratory workflow for aDNA analysis. The first experimental step is represented by DNA extraction. In a degraded sample the DNA solution obtained can consist of molecules from different biological origin: so-called endogenous DNA from the sample, usually degraded, possible contaminant molecules from people who handled the sample, and microbial environmental DNA. Two different methodological approaches are possible: **1** “classical approach” based on polymerase chain reaction (PCR) and on first-generation sequencing methods (Sanger sequencing) and **2** next-generation sequencing (NGS) approach. In the first case, *1a* target DNA is selected and amplified by PCR, where the template DNA is denatured into two strands, and primers (*in orange*) permit the DNA polymerase to synthesize new complementary strands. After automated repeated thermal cycles, an exponential growth of the number of copies of the template make it available for next experimental steps. *1b* Cloning consists in the isolation of a single molecule from a PCR product into a plasmid vector that is inserted into a bacterial cell and replicated with it. *1c* Sequencing of different clones obtained from a PCR product permits comparison of different original molecules from the sample and understanding of the molecular composition, highlighting possible misincorporations due to DNA damage and possible contamination. Following the NGS approach, *2a* a library is prepared by ligation of adaptors (oligonucleotides with a universal sequence) to the original DNA molecules. *2b* possible enrichment of particular regions can be performed in order to increase the target amount and make it more available for sequencing. Target enrichment in solution by use of biotinylated DNA probes and streptavidine coated beads is shown as example [39]. *2c* NGS sequencing consist in a first step called bridge PCR, where molecules from the library are annealed to the flow cell and amplified by PCR using universal primers complementary to adaptors during the so-called cluster generation. The clonal clusters obtained represent the substratum for sequencing when at each sequencing cycle a new nucleotide position is determined by reading the fluorescent signal of each fluorescently labelled dNTP

strategy is to use the so-called next-generation sequencing methods, affirmed in the last 10 years in aDNA research, together with target enrichment by hybridization. See Fig. 1 for a schematic view of the experimental steps.

Table 1 Standard criteria for aDNA analysis required with classical approach

Criteria for aDNA analysis according to Cooper and Poinar [24]

Criteria	Explanation
Physically isolated work area	aDNA laboratory needs to be exclusively dedicated to degraded samples analysis, and the pre-amplification and post-amplification areas need to be physically separated in order to avoid possible contamination of the samples with modern DNA or amplified DNA
Control amplifications	Negative controls are needed in each experimental step in order to verify the absence of contamination in reagents and work environment
Appropriate molecular behavior	Amplification of long DNA fragments is not expected from degraded samples and if occurred it is probably due to contamination. The obtained sequence should have phylogenetic sense
Reproducibility	The result should be obtained from different extracts of the specimen
Cloning	Since a degraded sample can be represented by a mixture of DNA from different sources, direct sequencing of the PCR product can produce disturbed sequences because of overlapping of different signals or sequence of the most represented biological source that could not represent the endogenous component of the sample. Cloning the amplification products into bacterial vector permits to analyze the molecular complexity of the sample, checking for possible contamination and sequence misincorporations due to DNA damage
Independent replication	Results need to be obtained independently at least twice in different laboratories
Biochemical preservation	Other analysis (such as aminoacid racemization) can confirm the possibility of DNA preservation in the sample
Quantitation	Quantitation of the DNA in the sample can be performed by competitive or quantitative PCR (RT-PCR) in order to confirm the presence of genetic material
Associated remains	Analysis of faunal remains, for example, associated with the sample can confirm the possibility of DNA preservation and can represent a way to check for possible modern human contamination

3 Classical Approach

The classical approach based on target selection and amplification by polymerase chain reaction (PCR), still useful for some applications, was the only one available 10 years ago. Since aDNA research presents technical difficulties because of the possible minute amounts and degraded nature of surviving DNA and the risk of contamination, particular criteria need to be followed in order to authenticate the results. Standards for the analysis with classical approach were summarized by Cooper and Poinar [24]: physically isolated work area, control amplifications, appropriate molecular behavior, reproducibility, cloning, independent replication, biochemical preservation, quantitation, associated remains (Table 1).

3.1 DNA Amplification by Polymerase Chain Reaction

Polymerase chain reaction (PCR) was discovered in 1983 and represented a revolution in molecular biology [25]. This method permits a replication in vitro of

DNA fragments, simulating the one that happens *in vivo* in the cell and amplifying exponentially the target during automated repeated thermal cycles. It needs a couple of primers, oligonucleotides with a sequence complementary to the beginning and the end of the fragment of interest, from which the amplification starts with the extension of a new DNA strand complementary to the original one thanks to the activity of DNA polymerase enzyme. The amplified DNA can then be visualized by electrophoresis and can be available for sequencing.

3.2 Cloning

The DNA obtained from an ancient sample can be represented by a mixture of molecules with different origins: endogenous and contaminant DNA from the environment or people who handled the sample. For this reason, cloning of PCR products is needed in order to analyse the composition of the sample. Cloning consists in inserting single molecules obtained by PCR into a plasmid vector that will be taken over by a bacterial cell and replicated with it. Thus, single molecules from a PCR product can be isolated and independently sequenced, permitting comparison amongst each other and verifying if they come from different biological sources and/or carry signal of molecular damages (Fig. 2).

3.3 Sanger Sequencing

The sequencing method developed by Sanger in 1977 was the only one used for 30 years, and it is now considered a “first generation” technology. It is based on the synthesis of a complementary DNA template by using chain-terminating inhibitors. The sequence reaction involves DNA polymerase and both natural 2-deoxynucleotides (dNTPs) and 2,3-dideoxynucleotides (ddNTPs), the latter representing the chain-terminating inhibitors. Fluorescently labeled nested fragments, terminating at different points of the original DNA molecule, are generated [26]. After sequencing reaction, a capillary electrophoresis is needed for separating the nested fragments by size, and a laser beam causes the dyes on the fragments to fluoresce. The sequence of fluorescence signals is registered by an optical detection device producing a four-color plot since each nitrous base emits a different color. A software converts the fluorescence signal to digital data: a chromatogram that can be translated in a sequence of nitrous bases. For degraded samples, after cloning of PCR products, several clones (each deriving from a single molecule of the PCR product) need to be sequenced. From the comparison of different clones it is possible to highlight the nucleotide differences, that can be due to misincorporation or the presence of different biological sources [27]. A consensus sequence representing the original endogenous one can then be constructed from the selected clone sequences taking into account possible misincorporation and contamination from known researchers who handled the sample [28].

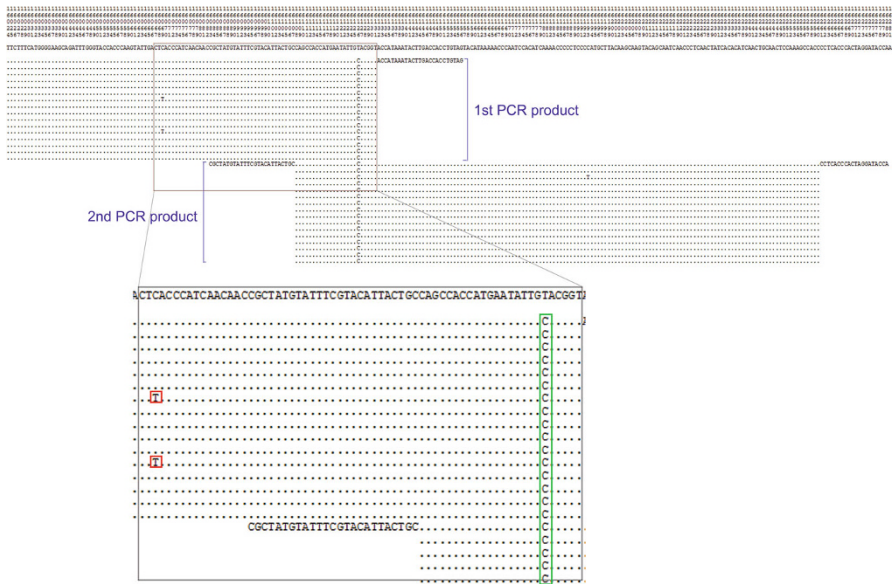


Fig. 2 Example of alignment of clones from different PCR products. Sequences of clones from two different PCRs are aligned between each other and against the reference sequence. The two PCRs are designed for amplifying two partially overlapping fragments. Sixteen clones for each PCR product are sequenced. From the *top*, numbers 16024 to 16281 represent the nucleotide positions of a fragment of the mitochondrial Hypervariable Region I (HVRI); the nucleotide sequence below the positions is the reference sequence used for comparing and describing the sample’s sequence; clone sequences, where the nucleotides identical to the reference sequence are indicated by *dots*; sequences of primers used for the PCRs are indicated for the first clone. In the enlarger box typical C to T misincorporations are highlighted in *red*, while a nucleotide mutation confirmed in all the clones and in different PCR products is highlighted in *green*

4 Next-Generation Sequencing

Since 2005, next-generation sequencing (NGS) methods are used in aDNA research [29–31], sequencing the nuclear genome of a mammoth and of a Neanderthal. NGS represented a revolution compared to the classical method based on PCR for several reasons. First of all, the high-throughput sequencing platforms used in NGS generate data from billions of DNA fragments per sequencing run, with a substantial cost reduction in front automated Sanger method [32]. Then, sample preparation for NGS permits observation of the original characteristics of the DNA molecules, such as their length and possible degradation, transforming something that represented an issue in the classical method into an advantage. In fact, shorter DNA molecules are not detectable by PCR because the method needs the whole sequence of primers (that are usually about 20 bp each) to be present before and after the target region, determining that only molecules with a minimum length of 50 bp are available to be selected. But in a degraded samples, most of the endogenous material could be represented by very short DNA molecules. Even the damage pattern can be recognizable by NGS, because the original ends of the molecules are not modified

during the sample preparation. The analysis of damage pattern can be used to assess the ancient status of the sequences, permitting the separation of them from possible modern contaminants.

Different sequencing platforms, with different procedures for template preparation, sequencing and imaging are available [33], but the one most used in the aDNA field is the Illumina/Solexa technology mainly because of its capacity to sequence shorter fragments.

4.1 Library Preparation

DNA samples need to be converted in a library before being sequenced with NGS. A library consists of a collection of DNA fragments prepared by adapter ligation and fragmentation. Adapters are represented by oligonucleotides with a known nucleotide sequence that permit immortalizing and amplifying all the molecules present in the library with universal primers. Fragmentation consists of adding a known short sequence univocally assigned to each sample (barcode or index), that permits recognizing it even if sequenced together with other samples [34]. There are commercial ready-to-use kits for library preparation, but for highly degraded samples a custom protocol was developed in order to optimize the results and have the possibility to adjust each step of the preparation according to the quality of the single sample. The first custom protocol was published by Meyer and Kircher [35] for preparation of double-stranded libraries for Illumina platforms, and consisted in separated steps of blunt-end repair of the ends of molecules, adapter ligation, and an indexing PCR for adding barcodes to each sample. In 2013 a new protocol for single-stranded library preparation demonstrated higher capacity to recover shorter endogenous sequences and to obtain a higher ration of endogenous to environmental DNA [36]. It consists of a library preparation performed by ligating a biotinylated adapter oligonucleotide to the 3' ends of heat-denatured DNA and the immobilization on streptavidin-coated beads of the resulting strands that are then copied with a polymerase before attaching a second adapter by blunt-end ligation [37].

Libraries can be also built using the enzymes uracil–DNA–glycosylase (UDG), which cleaves deaminated cytosines (uracils), and Endo VIII, which cuts at the resulting abasic sites, driving down the rate of ancient DNA errors [38]. This approach can be useful for avoiding errors of interpretation during sequence analysis due to misincorporations. But misincorporations also represent a way to differentiate ancient molecules from modern contaminant ones. For this reason a recent protocol was developed where the library is partially UDG-treated [39], with the resulting molecules presenting no more damaged nucleotides except at the terminal bases that remain available for estimation of authenticity of the DNA.

Libraries can be directly sequenced with a so-called shotgun approach consisting of sequencing the whole library representing all the molecular components of the sample. But usually the high microbial DNA content makes shotgun sequencing of ancient samples uneconomical. For this reason methods for target enrichment were developed in order to enlarge the endogenous target fraction available for sequencing compared to the exogenous one.

4.2 Target Enrichment

Methods for target enrichment are available and can be used both during library preparation and after it for selecting particular fragments of interest. The first strategy consists in preferentially incorporation of molecules characterized by damage typical of ancient DNA during library preparation [40]. The second one consists in using a set of probes, complementary to the target, in order to capture the molecules of interest by hybridization in solution [41] or on microarray [42]. Target could be the whole mitochondrial genome (see [3, 18, 43] for example), pathogenic bacterial genomes [44–46], nuclear SNPs [47], exomes [42, 48], chromosomes [49], or whole nuclear genome [50–52].

4.3 Sequencing

Sequencing on Illumina platforms consist of a first step, called cluster generation. A pool of libraries is loaded into a flow cell where the DNA fragments are captured by oligonucleotides complementary to the library adapter. Then a bridge amplification produces clonal clusters originating from a single original DNA molecule. Clusters are needed to amplify the signal emitted by the nucleotides during sequencing, in order to make it detectable. During sequencing, reversible terminator-bound dNTPs complementary to the template are incorporated at each sequencing cycle. A single fluorescently labeled nucleotide is added at each cycle, the flow cell is imaged and the emission of each cluster is recorded. Having each base a particular wavelength emission, fluorescent signals can be translated in a base sequence.

4.4 PCR and NGS

PCR is still the most efficient procedure to selectively select a target DNA region. In fact, between the methods for enrichment on libraries, none has an efficiency of 100 % for recovering the target. For this reason, PCR should still represent the best strategy when the target is a well-defined fragment or set of fragments. PCR products can be converted in libraries and sequenced by NGS approach in order to obtain a high number of sequences and a higher resolution that may help finding even a really low amount of endogenous DNA.

5 Data Analysis

Sequence data obtained with the Sanger method are represented by chromatograms and several software applications are available to visualize and explore them. Sequences converted in a text-based format (fasta) can be used for alignment with reference sequences in order to highlight possible nucleotide differences and describe the sequence motif of the sample. In aDNA, since each PCR product is usually cloned, a first alignment and comparison between clones is needed in order to produce the final consensus sequence of the sample. Alignment is the basic step for each analysis, both for comparing samples to each other or to a database and to

create phylogenetic trees or networks and to perform functional, evolutionary, or population genetic analysis. Software applications for sequence alignment are, for example, Blast [53] (for pairwise alignment), Clustal [54], Muscle [55], and Mafft [56] (for multiple alignment).

For NGS data on aDNA, some specific pipelines were developed. Tools for a primary data analysis were proposed by Kircher in 2012 [57] considering that NGS data for ancient DNA samples may include sequencing error and artefacts, damage, chimeric sequences, and ambiguities during alignment due to the short length of the molecules. For mapping against reference genomes, Mapping Iterative Assembler (MIA) [43] was developed taking into account the accumulation of misincorporations at the ends of the sequences and optimizing mapping for short reads and low quality data. After mapping, an authentication check of the sequences is needed in order to verify that they originated from the endogenous component of the sample and are not from contaminants. The typical misincorporation pattern represents one of the tools for checking authenticity of the result, even if particular diagenetic conditions can produce variable levels of damage in samples of the same age [58]. MapDamage [59] and pmdtools [13] are software applications that estimate and describe the misincorporation pattern (Fig. 3), the latter permitting the filtering out of sequences with damage signals too. Tools to estimate contamination levels in a sample are based on comparison between the sequences' profiles and the known variation across the populations or species [60–62] and are developed so far for mitochondrial data. For nuclear data the contamination could not reflect the same situation observed for the mitochondrion [63], and analysis of the heterozygosity levels on sexual chromosomes can represent an informative source [63, 64].

The Paleomix package proposed in 2014 [65] integrates in a unique pipeline adapter removal [66], mapping against reference genomes by Burrows–Wheeler Aligner (BWA) [67] or Bowtie [68], PCR duplicate removal [69], characterization of and compensation for postmortem damage by MapDamage [59], SNP calling and

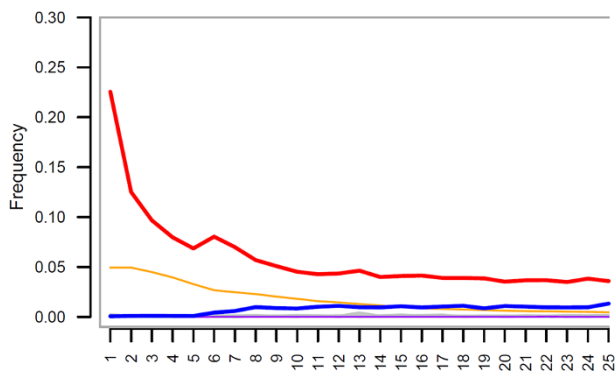


Fig. 3 Example of misincorporation pattern plot obtained with MapDamage software. Frequency percentage of sequences with nucleotide substitutions in the first 25 positions of the sequence in a Medieval human sample. The red line represent the C to T substitutions and their frequency increases towards the end of the molecule, in a typical pattern for aDNA

maximum-likelihood phylogenomic inference, and it profiles the metagenomic contents of the samples too.

Schmutzi is a software application that analyses contamination, deamination frequency, and length distribution of the molecules and infers the endogenous genome sequence even in the presence of high contamination [70]. Table 2 provides an overview of the bioinformatic tools commonly used for analyzing aDNA data.

6 Applications

The previously described methods are open to a wide range of applications in the cultural heritage field because of the variability of materials and possible topics. Materials can belong to a time range of a few years to as far back as prehistoric times. Bones are the most studied specimens since they are abundant in archeological sites and sometimes the ones with the best preservation of the genetic component, but studies on other types of materials were successfully published too. Some case studies are described in the next paragraphs.

6.1 Species Origin of Unknown Material

One of the questions aDNA analysis techniques can help to address is about which organism (animal or plant) an artefact, a tool, or a material derives from. Such determination can be defined at different taxonomic levels and sometimes also at an individual level, depending on the genetic variability (and its knowledge) of the species, being able to understand the place of origin of the individual in cases where a defined phylogeographic structure is present for the analysed genetic marker.

As summarized in Burger et al. [71] there are three important groups of starting materials: collagenous, contents of pots, vessels, and other containers, binder, glues, and oils.

DNA was successfully recovered from Egyptian papyri [72], Hellenic manuscripts [73], from modern and medieval leather samples [74], as well as a leather sample from the covering of the hammer head of a piano created in 1802 similar to that Beethoven used [75]. Genetic data were obtained from Neolithic leather legging [76], sheep wool [77], and residues on stone tools [78]. With the classical approach, genetic markers amplifiable by PCR commonly used for species identification are cytochrome b, 12 s, and 16 ribosomal RNA genes of the mitochondrion, possibly followed by determination of the D-loop mitochondrial region for analyzing intra-specific variability and individual assignment. Pangallo et al. [79] proposed a PCR-based strategy for identification of animal skin used in the manufacture of historical parchments, even if the complexity of the genetic profile of this type of sample was contemporary attested by ink and animal glues possibly used during the parchment manufacture, introducing multiple biological sources from different species and/or individuals [80]. A recent study based on the NGS approach focused on the same type of sample of seventeenth and eighteenth century northern English provenance, demonstrating that this material is a highly suitable substrate for large-scale aDNA analyses permitting the identification of the species origin and use of these data to

Table 2 Overview on the most commonly used bioinformatic tools available for aDNA analysis

Analytical step	Software	Description
Primary data analysis	FastQprocessing [55]	The package provides tools for demultiplexing of sequence reads according to their index/indexes after parallel sequencing of a pool of samples, removal of library artifacts, adapter trimming, merging of R1 and R2 reads for paired-end sequencing, and filtering for length, quality filter to avoid possible sequence errors, identification of endogenous component from environmental background, contamination estimation, removal of clonal products
Mapping	Mapping Iterative Assembler (MIA) [43]	The package provides alignment of DNA sequencing fragments to a reference then calls a consensus. The consensus is used as new reference and the process is repeated until convergence. It supports a position specific substitution matrix, which improves both alignment and consensus calling on chemically damaged aDNA
Mapping	Burrows–Wheler Alignment [67]	The package is designed for sequences against reference genomes, even large such as the human genome
Misincorporation pattern	MapDamage [59]	The software tracks and quantifies DNA damage patterns
Misincorporation pattern	PMDtools [13]	PMDtools allow the identification of degraded DNA sequences that are unlikely to originate from modern contamination and their separation in order to reduce the contamination fractions to negligible levels
Contamination check	Contamination Checker [43]	The program determines if an assembled mitochondrion is free from contamination. It looks for positions where the consensus sequence differs from a panel of known human mitochondria, then classifies each read as either belonging to the sample or a putative contaminant
Contamination check	ContamMix [62]	The method estimates the level of human DNA contamination in mitochondrial sequences, comparing the affinities of the reads to the consensus sequence, relative to their affinity to a dataset of potential contaminants represented by 311 mitogenomes from worldwide populations
Different analyses	PALEOMIX [65]	The package largely automates the analyses related to NGS data, performing a series of analyses, including read trimming, collapsing of overlapping mate-pairs, read mapping, PCR duplicate removal, SNP calling, metagenomic profiling, and quantification of post-mortem damages, misincorporation and fragmentation patterns. It provides reconstruction of maximum likelihood phylogenomic trees and evolutionary phylogenetic relationships among taxa
Different analyses	SCHMUTZI [70]	The software estimates contamination and misincorporation pattern and reconstructs endogenous mitochondrial genomes even for samples with a contamination over 50 %

obtain information about historical livestock thanks to the high resolution of NGS methodology [81]. DNA was recovered also from paintings, determining the origin of animal glues through mitochondrial DNA analysis [82].

Few published works are also available on materials preserved in different types of containers: Aztec vessels were shown to contain DNA from a vine with a pharmacological agent still used by Native Americans [71]. Also, traces of foodstuff were determined in a Celtic container made of animal skin [71]. From the residue inside one of the earliest wine jars from ancient Egypt, dating to 3000 BC, the oldest evidence of *Saccharomyces cerevisiae* associated with human activities for wine fermentation was found [83].

6.2 Personal Identification

DNA analysis permitted personal identification of famous individuals' remains by comparing their genetic profile to putative descendants.

In 2012, a skeleton was found at the presumed resting place of King Richard III. NGS analyses, based on array hybridization capture and PCRs of the skeletal remains permitted obtaining a complete mitochondrial genome that showed a perfect match with the profile of one living relative and a single-base substitution compared with a second relative. Y-chromosome SNPs were determined and differed from male-line relatives probably because of a false-paternity event in any intervening generation. Phenotypic SNPs obtained by HIRISplex system [84] predicted hair and eye color consistent with the King's appearance in an early portrait with the statistical conclusion that the evidence for the remains being those of Richard III was overwhelming [85].

Another case of remains attributed to a king is represented by a handkerchief dipped into the putative blood of the French king Louis XVI. The complete genome was sequenced with the NGS approach and the obtained profile seemed not compatible with the king's known ancestry nor with the description of the king for some phenotypic traits [86].

Even if descendants are not available for a comparison, aDNA can reveal useful information for characterization of remains. An example is that of the Italian poet Petrarca: aDNA analysis on his putative remains revealed that the skull and the postcranial skeleton belonged to different individuals, confirming the hypothesis of profanation of the grave [87]. The body attributed to the Evangelist Luke was also analysed. According to the historical written sources, the Evangelist was born in Syria, but a possible replacement of his relics could be occurred in Constantinople. The comparison between the mitochondrial data obtained from the relics with those of modern populations indicated that a Syrian origin of individual was the most likely, even if a Turkish one cannot be ruled out [88].

6.3 Study and Enhancement of Particular Samples

Some particular samples, important for the exceptionality of their preservation, their completeness, and their informative power, were in the limelight of studies designed to their enhancement and the reconstruction of details of the past history.

The Tyrolean Iceman (Ötzi) lived during the Neolithic–Copper Age transition and his mummified body was recovered in 1991, representing an exceptional finding. Several molecular studies were conducted in order to obtain as much information as possible about his life and about the environment he was living in. Analyses were carried out for the characterization of his mitochondrial [89, 90] and nuclear genomes determining some phenotypic characteristic and pathogen presence [91]; samples of the intestinal content were analysed for determining the last meals and pollen residues in order to recover information about the paleo diet and environment of 5000 years ago [92].

Another extraordinary specimen is one of the most complete hominin skeletons ever found discovered in the karst caves of Lamalunga, near Altamura (Italy). The skeleton is partly incorporated into calcite concretions and is covered by coralloid formations, then an accurate morphological study has never been possible. Ancient DNA analysis on a bone fragment permitted to define the sample as *Homo neandertalensis* [93] and the total absence of contamination due to its position in the cave and the precautions during its recovering makes this sample a special candidate to explore genetic characteristics of Neanderthals.

The Paleo–Eskimo human remains discovered in an early Greenlandic Saqqaq settlement and dated to 3400–4500 years ago represented a precious informative source for understanding migration dynamics to the New World and for an individual reconstruction thanks to the extraordinary good preservation of the DNA in permafrost. Using mitochondrial [94] and nuclear genome [95] data it was possible to identify an early migration from Siberia into the New World some 5500 years ago and not directly related to Native Americans or the later Neo-Eskimos that replaced them. Nuclear functional SNP were also used to determine phenotypic characteristics of the individual.

6.4 Ancient Populations

DNA analyses of ancient samples gave a big contribution also for understanding the past history of human populations.

Since the beginning of aDNA research, Neanderthals and their relationship with modern humans represented a main topic of interest. Thanks to several works, based both on classical methodology and NGS, focused on both mitochondrial and nuclear genomes, a lot of information is now available on this species, on its population features and dynamics, its evolutionary role in the phylogeny of the genus *Homo*, and its phenotypic and functional genetic traits [96].

A recent analysis on 101 ancient humans from Eurasia confirmed that the Bronze Age was a period of big cultural changes. Thanks to genomic data it was determined that large-scale population migrations and replacements occurred, and that probably they are responsible for the major parts of present-day demographic structure in both Europe and Asia. These migrations could also be consistent with the hypothesized and long-debated spread of Indo-European languages during the Early Bronze Age [97].

Other analyses can be conducted in order to identify the place of origin of archeologically defined populations, as well as their genealogical relationships with

the modern populations. These types of analyses are based on simulations in which ancient and modern data are put together into different possible demographic scenarios that can take into account also historical and archaeological information. Thanks to this approach, genetic continuity was found between Etruscans and some modern populations from Tuscany [98], as well as between Longobards and a modern population in Northwest Italy [99].

7 Final Remarks

Even if this chapter offers only some examples of published works in which aDNA analysis contributed to the wide world of cultural heritage, it is evident from bibliographic research that some possible application fields are still not extensively exploited. Particularly, aDNA analysis for determination of species origin of materials is not yet a routine procedure, even if it could represent an important and highly reliable test for supporting the study and enhancement of prehistoric and historic artifacts.

References

1. Paabo S (1985) Molecular-cloning of ancient egyptian mummy DNA. *Nature* 314(6012):644–645
2. Higuchi R et al (1984) DNA sequences from the quagga, an extinct member of the horse family. *Nature* 312:282–284
3. Meyer M et al (2014) A mitochondrial genome sequence of a hominin from Sima de los Huesos. *Nature* 505(7483):403–406
4. Orlando L et al (2013) Recalibrating Equus evolution using the genome sequence of an early Middle Pleistocene horse. *Nature* 499(7456):74–78
5. Lindahl T (1993) Instability and decay of the primary structure of DNA. *Nature* 362(6422):709–715
6. Paabo S (1989) Ancient DNA: extraction, characterization, molecular cloning, and enzymatic amplification. *Proc Natl Acad Sci USA* 86(6):1939–1943
7. Briggs AW et al (2007) Patterns of damage in genomic DNA sequences from a Neandertal. *Proc Natl Acad Sci USA* 104(37):14616–14621
8. Paabo S et al (2004) Genetic analyses from ancient DNA. *Ann Rev Genet* 38:645–679
9. Hansen A et al (2001) Statistical evidence for miscoding lesions in ancient DNA templates. *Mol Biol Evol* 18(2):262–265
10. Gilbert MT et al (2003) Characterization of genetic miscoding lesions caused by postmortem damage. *Am J Hum Genet* 72(1):48–61
11. Sawyer S et al (2012) Temporal patterns of nucleotide misincorporations and DNA fragmentation in ancient DNA. *PLoS One* 7(3):e34131
12. Ginolhac A et al (2011) mapDamage: testing for damage patterns in ancient DNA sequences. *Bioinformatics* 27(15):2153–2155
13. Skoglund P et al (2014) Separating endogenous ancient DNA from modern day contamination in a Siberian Neandertal. *Proc Natl Acad Sci USA* 111(6):2229–2234
14. Knapp M, Lalueza-Fox C, Hofreiter M (2015) Re-inventing ancient human DNA. *Investig Genet* 6:4
15. Lalueza-Fox C et al (2007) A melanocortin 1 receptor allele suggests varying pigmentation among Neanderthals. *Science* 318(5855):1453–1455
16. Rohland N, Hofreiter M (2007) Comparison and optimization of ancient DNA extraction. *Biotechniques* 42(3):343–352
17. Rohland N, Hofreiter M (2007) Ancient DNA extraction from bones and teeth. *Nat Protoc* 2(7):1756–1762

18. Dabney J et al (2013) Complete mitochondrial genome sequence of a Middle Pleistocene cave bear reconstructed from ultrashort DNA fragments. *Proc Natl Acad Sci USA* 110(39):15758–15763
19. Gamba C et al. (2015) Comparing the performance of three ancient DNA extraction methods for high-throughput sequencing. *Mol Ecol Resour.* doi:10.1111/1755-0998.12470
20. Cigliero SD, Edalucci E, Fattorini P (2011) DNA extraction from blood and forensic samples. In: Stanta G (ed) *Guidelines for molecular analysis in archive tissues*. Springer, Berlin, Heidelberg, pp 45–54
21. Pilli E et al (2014) Pet fur or fake fur? A forensic approach. *Investig Genet* 5:7
22. Kistler L (2012) Ancient DNA extraction from plants. *Methods Mol Biol* 840:71–79
23. Hekkala E et al (2011) An ancient icon reveals new mysteries: mummy DNA resurrects a cryptic species within the Nile crocodile. *Mol Ecol* 20(20):4199–4215
24. Cooper A, Poinar HN (2000) Ancient DNA: do it right or not at all. *Science* 289(5482):1139
25. Mullis KB, Faloona FA (1987) Specific synthesis of DNA in vitro via a polymerase-catalyzed chain reaction. *Methods Enzymology* 155:335–350
26. Sanger F, Nicklen S, Coulson AR (1977) DNA sequencing with chain-terminating inhibitors. *Proc Natl Acad Sci USA* 74(12):5463–5467
27. Hofreiter M et al (2001) DNA sequences from multiple amplifications reveal artifacts induced by cytosine deamination in ancient DNA. *Nucleic Acids Res* 29(23):4793–4799
28. Bower MA et al (2005) How many clones need to be sequenced from a single forensic or ancient DNA sample in order to determine a reliable consensus sequence? *Nucleic Acids Res* 33(8):2549–2556
29. Poinar HN et al (2006) Metagenomics to paleogenomics: large-scale sequencing of mammoth DNA. *Science* 311(5759):392–394
30. Green RE et al (2006) Analysis of one million base pairs of Neanderthal DNA. *Nature* 444(7117):330–336
31. Noonan JP et al (2006) Sequencing and analysis of Neanderthal genomic DNA. *Science* 314(5802):1113–1118
32. Schloss JA (2008) How to get genomes at one ten-thousandth the cost. *Nat Biotechnol* 26(10):1113–1115
33. Metzker ML (2010) Sequencing technologies—the next generation. *Nat Rev Genet* 11(1):31–46
34. Head SR et al (2014) Library construction for next-generation sequencing: overviews and challenges. *Biotechniques* 56(2):61–64, 66, 68, passim
35. Meyer M, Kircher M (2010) Illumina sequencing library preparation for highly multiplexed target capture and sequencing. *Cold Spring Harb Protoc* 2010(6): p. pdb prot5448
36. Bennett EA et al (2014) Library construction for ancient genomics: single strand or double strand? *Biotechniques* 56(6):289–290, 292–296, 298, passim
37. Gansauge MT, Meyer M (2013) Single-stranded DNA library preparation for the sequencing of ancient or damaged DNA. *Nat Protoc* 8(4):737–748
38. Briggs AW et al. (2010) Removal of deaminated cytosines and detection of in vivo methylation in ancient DNA. *Nucleic Acids Res* 38(6):e87
39. Rohland N et al (2015) Partial uracil—DNA—glycosylase treatment for screening of ancient DNA. *Philos Trans R Soc B Biol Sci* 370(1660):20130624
40. Gansauge MT, Meyer M (2014) Selective enrichment of damaged DNA molecules for ancient genome sequencing. *Genome Res* 24(9):1543–1549
41. Maricic T, Whitten M, Paabo S (2010) Multiplexed DNA sequence capture of mitochondrial genomes using PCR products. *PLoS One* 5(11):e14004
42. Burbano HA et al (2010) Targeted investigation of the Neandertal genome by array-based sequence capture. *Science* 328(5979):723–725
43. Briggs AW et al (2009) Targeted retrieval and analysis of five Neandertal mtDNA genomes. *Science* 325(5938):318–321
44. Devault AM et al (2014) Ancient pathogen DNA in archaeological samples detected with a Microbial Detection Array. *Sci Rep* 4:4245
45. Bos KI et al (2011) A draft genome of *Yersinia pestis* from victims of the Black Death. *Nature* 478(7370):506–510
46. Bos KI et al (2014) Pre-Columbian mycobacterial genomes reveal seals as a source of New World human tuberculosis. *Nature* 514(7523):494–497
47. Haak W et al (2015) Massive migration from the steppe was a source for Indo-European languages in Europe. *Nature* 522(7555):207–211

48. Castellano S et al (2014) Patterns of coding variation in the complete exomes of three Neandertals. *Proc Natl Acad Sci USA* 111(18):6666–6671
49. Fu Q et al (2013) DNA analysis of an early modern human from Tianyuan Cave, China. *Proc Natl Acad Sci USA* 110(6):2223–2227
50. Carpenter ML et al (2013) Pulling out the 1 %: whole-genome capture for the targeted enrichment of ancient DNA sequencing libraries. *Am J Hum Genet* 93(5):852–864
51. Enk JM et al (2014) Ancient whole genome enrichment using baits built from modern DNA. *Mol Biol Evol* 31(5):1292–1294
52. Avila-Arcos MC et al (2011) Application and comparison of large-scale solution-based DNA capture-enrichment methods on ancient DNA. *Sci Rep* 1:74
53. Camacho C et al (2009) BLAST+: architecture and applications. *BMC Bioinform* 10:421
54. Larkin MA et al (2007) Clustal W and Clustal X version 2.0. *Bioinformatics* 23(21):2947–2948
55. Edgar RC (2004) MUSCLE: multiple sequence alignment with high accuracy and high throughput. *Nucleic Acids Res* 32(5):1792–1797
56. Katoh K, Standley DM (2014) MAFFT: iterative refinement and additional methods. *Methods Mol Biol* 1079:131–146
57. Kircher M (2012) Analysis of high-throughput ancient DNA sequencing data. In: Shapiro B, Hofreiter M (eds) *Ancient DNA: methods and protocols*, vol 840. Springer, New York, pp 197–228
58. Orlando L, Gilbert MT, Willerslev E (2015) Reconstructing ancient genomes and epigenomes. *Nat Rev Genet* 16(7):395–408
59. Jonsson H et al (2013) mapDamage2.0: fast approximate Bayesian estimates of ancient DNA damage parameters. *Bioinformatics* 29(13):1682–1684
60. Green RE et al (2010) A draft sequence of the Neandertal genome. *Science* 328(5979):710–722
61. Sanchez-Quinto F et al (2012) Genomic affinities of two 7000-year-old Iberian hunter-gatherers. *Curr Biol* 22(16):1494–1499
62. Fu Q et al (2013) A revised timescale for human evolution based on ancient mitochondrial genomes. *Curr Biol* 23(7):553–559
63. Green RE et al (2009) The Neandertal genome and ancient DNA authenticity. *EMBO J* 28(17):2494–2502
64. Rasmussen M et al (2011) An Aboriginal Australian genome reveals separate human dispersals into Asia. *Science* 334(6052):94–98
65. Schubert M et al (2014) Characterization of ancient and modern genomes by SNP detection and phylogenomic and metagenomic analysis using PALEOMIX. *Nat Protoc* 9(5):1056–1082
66. Lindgreen S (2012) AdapterRemoval: easy cleaning of next-generation sequencing reads. *BMC Res Notes* 5:337
67. Li H, Durbin R (2009) Fast and accurate short read alignment with Burrows–Wheeler transform. *Bioinformatics* 25(14):1754–1760
68. Langmead B, Salzberg SL (2012) Fast gapped-read alignment with Bowtie 2. *Nat Methods* 9(4):357–359
69. <http://picard.sourceforge.net>
70. Renaud G et al (2015) Schmutzi: estimation of contamination and endogenous mitochondrial consensus calling for ancient DNA. *Genome Biol* 16(1):224
71. Burger J, Hummel S, Herrmann B (2000) Palaeogenetics and cultural heritage. Species determination and STR-genotyping from ancient DNA in art and artefacts. *Thermochim Acta* 365(1–2):141–146
72. Marota I et al (2002) DNA decay rate in papyri and human remains from Egyptian archaeological sites. *Am J Phys Anthropol* 117(4):310–318
73. Poulakakis N et al (2007) Ancient DNA and the genetic signature of ancient Greek manuscripts. *J Archaeol Sci* 34(5):675–680
74. Vuissoz A et al (2007) The survival of PCR-amplifiable DNA in cow leather. *J Archaeol Sci* 34(5):823–829
75. Merheb M et al (2016) Mitochondrial DNA, restoring Beethovens music. *Mitochondrial DNA* 27(1):355–359
76. Schlumbaum A et al (2010) Ancient DNA, a Neolithic legging from the Swiss Alps and the early history of goat. *J Archaeol Sci* 37(6):1247–1251
77. Brandt LO et al (2011) Characterising the potential of sheep wool for ancient DNA analyses. *Archaeol Anthropol Sci* 3(2):209–221
78. Shanks OC et al (2005) DNA from ancient stone tools and bones excavated at Bugas-Holding, Wyoming. *J Archaeol Sci* 32(1):27–38

79. Pangallo D et al (2010) Identification of animal skin of historical parchments by polymerase chain reaction (PCR)-based methods. *J Archaeol Sci* 37(6):1202–1206
80. Campana MG et al (2010) A Flock of sheep, goats and cattle: ancient DNA analysis reveals complexities of historical parchment manufacture. *J Archaeol Sci* 37(6):1317–1325
81. Teasdale MD et al (2015) Paging through history: parchment as a reservoir of ancient DNA for next generation sequencing. *Philos Trans R Soc B Biol Sci* 370(1660):20130379
82. Albertini E et al (2011) Tracing the biological origin of animal glues used in paintings through mitochondrial DNA analysis. *Anal Bioanal Chem* 399:2987–2995
83. Cavalieri D et al (2003) Evidence for *S. cerevisiae* fermentation in ancient wine. *J Mol Evol* 57(Suppl 1):S226–S232
84. Walsh S et al (2013) The HIRISplex system for simultaneous prediction of hair and eye colour from DNA. *Forensic Sci Int Genet* 7(1):98–115
85. King TE et al (2014) Identification of the remains of King Richard III. *Nat Commun* 5:5631
86. Olalde I et al (2014) Genomic analysis of the blood attributed to Louis XVI (1754–1793), king of France. *Sci Rep* 4:4666
87. Caramelli D et al (2007) Genetic analysis of the skeletal remains attributed to Francesco Petrarca. *Forensic Sci Int* 173(1):36–40
88. Vernesi C et al (2001) Genetic characterization of the body attributed to the evangelist Luke. *Proc Natl Acad Sci USA* 98(23):13460–13463
89. Ermini L et al (2008) Complete mitochondrial genome sequence of the Tyrolean Iceman. *Curr Biol* 18(21):1687–1693
90. Rollo F et al (2006) Fine characterization of the Iceman's mtDNA haplogroup. *Am J Phys Anthropol* 130(4):557–564
91. Keller A et al (2012) New insights into the Tyrolean Iceman's origin and phenotype as inferred by whole-genome sequencing. *Nat Commun* 3:698
92. Rollo F et al (2002) Otzi's last meals: DNA analysis of the intestinal content of the Neolithic glacier mummy from the Alps. *Proc Natl Acad Sci USA* 99(20):12594–12599
93. Lari M et al (2015) The Neanderthal in the karst: first dating, morphometric, and paleogenetic data on the fossil skeleton from Altamura (Italy). *J Hum Evol* 82:88–94
94. Gilbert MTP et al (2008) Paleo-Eskimo mtDNA genome reveals matrilineal discontinuity in Greenland. *Science* 320(5884):1787–1789
95. Rasmussen M et al (2010) Ancient human genome sequence of an extinct Palaeo-Eskimo. *Nature* 463(7282):757–762
96. Sanchez-Quinto F, Lalueza-Fox C (2015) Almost 20 years of Neanderthal palaeogenetics: adaptation, admixture, diversity, demography and extinction. *Philos Trans R Soc Lond B Biol Sci* 370(1660):20130374
97. Allentoft ME et al (2015) Population genomics of Bronze Age Eurasia. *Nature* 522(7555):167–172
98. Ghirotto S et al (2013) Origins and evolution of the Etruscans' mtDNA. *PLoS One* 8(2):e55519
99. Vai S et al (2015) Genealogical relationships between early medieval and modern inhabitants of Piedmont. *PLoS One* 10(1):e0116801

Radiocarbon Dating

Mark Van Strydonck¹

Received: 14 September 2015 / Accepted: 27 January 2016 / Published online: 25 February 2016
© Springer International Publishing Switzerland 2016

Abstract Although most historians and art historians consider the radiocarbon dating technique not to be very precise by their criteria, the method has gained much importance over the last decades. Radiocarbon dating is increasingly used in the field of textile research and old polychrome statues, but also objects made of ivory, stucco, paper, and parchment are dated with the technique. Especially after the introduction of the AMS technique, a boom of this type of research has been noticed.

Keywords Radiocarbon dating · AMS · Textiles · Polychrome statues · Stucco · IQR

1 Introduction

Chronology is the backbone of history. Without chronology, the past would be pure chaos. It is no wonder that since the dawn of civilization people have tried to order their past. This has resulted in mythological stories about the creation of the world as well as of the origin of societies and rulers. The lists of Egyptian pharaohs on the other hand were already much more exact and less mythological than most chronologies and were of great help in building the chronology of the Egyptian dynasties. Nevertheless, it was not before the 19th century that real scientific dating methods appeared. The first dating methods remained however *relative dating methods*. This implies that objects and facts are dated by means of a relationship between the items, for instance an event happening before or after the eruption of a volcano, testified by an ash layer that can be detected over large parts of a continent. So if one discovers an object under the ash layer in Italy, and another object above

✉ Mark Van Strydonck
mark.vanstrydonck@kikirpa.be

¹ Royal Institute for Cultural Heritage, Jubelpark 1, 1000 Brussels, Belgium

the same ash layer in France, it can be deduced that the Italian object is older than the French one. Objects can also be classified regarding their style or technological properties. Investigators often assume that simple and less developed artefacts are older than high-quality and technical advanced ones. This is often true, but not always the case. This can be explained very simply by a modern example. Tableware in the 19th century was precious, well made, and lasted a lifetime. Nowadays, one can buy nice-looking very cheap tableware, but it doesn't last long because the quality is low and it will be much more often replaced by a new set than in the 19th century. Also, in a further away past we can notice that common wear is often of low quality in prosperous times because it is considered as a consumable good. Furthermore, relative dating methods have the disadvantage that they depend a lot on the perception of the investigator. Two investigators belonging to a different school of thought might date the same artefact in a different period depending on their own beliefs.

Finally, in the 20th century, independent scientific dating methods began to be developed. *Absolute dating techniques* like dendrochronology have the advantage that all criteria for the analysis are in the method itself. In short: dendrochronology counts the number of tree rings in a wooden sample, measures the width of these rings, and compares this (unique) pattern of small and large rings width with a master curve made of an uninterrupted series of counted (dated) tree rings. The section in the master curve that matches with the pattern on the sample gives the age of that sample. The advantage of such a method is clear: the method is independent of the artefact in question, the presumptions of the investigator, and is only based on the properties of the material itself. Slightly different from these absolute dating methods are the *correlation dating techniques*. Just like the absolute dating methods, they use material properties from the object, but instead of giving the real age, these methods provide a result that only after correlation (or calibration) with an absolute chronology gives a calendar date. As will be explained later, radiocarbon dating is such a dating technique.

2 The Basic Principles of Radiocarbon Dating

2.1 The Origin of Radiocarbon

In nature, there are three isotopes of carbon ^{12}C (98.89 %), ^{13}C (1.11 %), and ^{14}C (10^{-10} %). The two first are stable, and the last one is radioactive. Due to β -decay, radiocarbon is transformed into nitrogen (formula 1). The half-life of ^{14}C or radiocarbon is very short compared to the age of the earth. It is only 5730 ± 40 years. This means that after 5730 years due to the radioactive decay, only half of the original amount of the isotope remains, and after two half-lives only 1/4th, etc. (Fig. 1).



After about ten half-lives, there is almost no detectable amount of radiocarbon left. This implies that radiocarbon cannot be part of the original composition of the

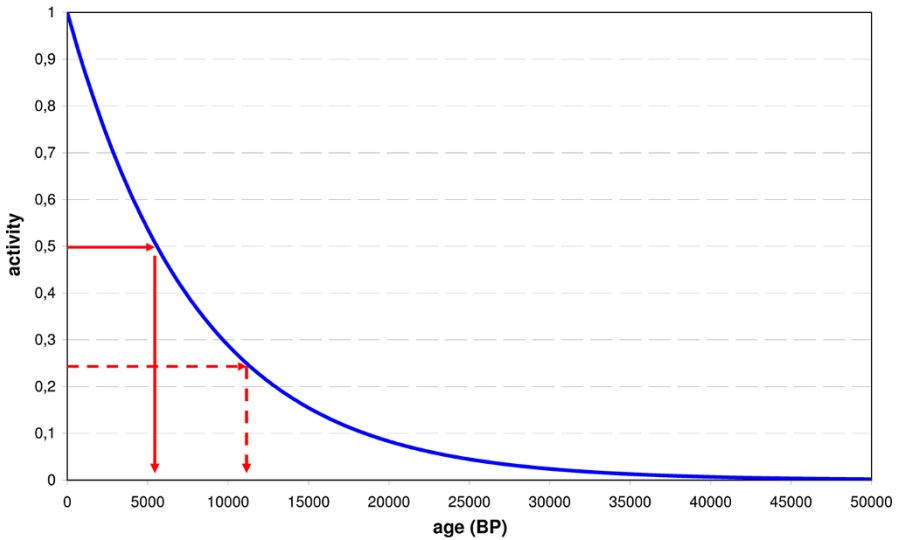


Fig. 1 Decay curve of radiocarbon: the radiocarbon activity (ordinate) in function of the conventional radiocarbon age in BP (abscissa)

earth; it must be produced in a continuous way, otherwise ^{14}C could no longer be present on earth.

Researchers found that radiocarbon is produced in the atmosphere due to a nuclear reaction between nitrogen and thermal neutrons (formula 2). These neutrons are produced by cosmic rays entering the atmosphere.



By this reaction, about 7.5 kg/year of ^{14}C or 2.2 atoms/cm² and per second are produced. Since radiocarbon is produced indirectly by cosmic rays, ^{14}C is called a cosmogenic nuclide. The radiocarbon isotope is not produced uniformly over the atmosphere. Most (ca. 60 %) is produced at about 12 km above the earth's surface because at that level the neutron density is the highest [1]. The ^{14}C production is also latitude-dependent. The earth's magnetic field is much stronger around the equator than near the poles, resulting in a lower cosmic ray flux and a lower ^{14}C production around the equator than at higher latitudes. Fortunately, the mixing is rather fast compared to the half-life of radiocarbon, so it can be stated that the ^{14}C concentration in the terrestrial biosphere is uniform [2, 3]. There is only a small difference between the northern and southern hemispheres, but this is adjusted for in the calibration programs (see below).

2.2 Radiocarbon and the Carbon Cycle

Radiocarbon in the atmosphere reacts with oxygen and forms $^{14}\text{CO}_2$. This radioactive carbon dioxide is mixed with the stable CO_2 of the atmosphere and due

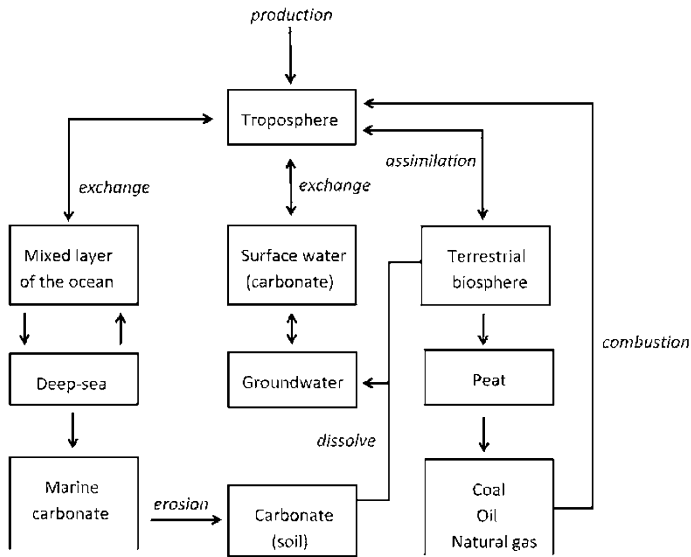


Fig. 2 Carbon cycle (after [21])

to photosynthesis, it is incorporated directly or indirectly, through the food chain, in all living material. Not only living material but also some inorganic materials like slaked lime can take up carbon dioxide (and ^{14}C) from the atmosphere.

Due to exchange mechanisms, carbon dioxide is also present in oceans, lakes, and rivers. Accordingly, living organisms in the sea will also pick up the radiocarbon signal. However, due to the fact that the mechanisms of carbon dioxide absorption are different between the terrestrial and marine biosphere, the radiocarbon content of both reservoirs is different. Furthermore, although the radiocarbon content of the terrestrial biosphere is all the same over one hemisphere, this is not so for the marine biosphere. In some parts of the ocean, there is an upwelling of 'old' water, resulting in a lower radiocarbon content of the surface waters (Fig. 2). This marine reservoir effect is very important and must be taken into consideration if one is dating for instance an object made of whale ivory instead of elephant ivory.

2.3 Radiocarbon Dating

Since the turn-over time of carbon in most living organisms is very fast compared to the half-life of radiocarbon, it can be assumed that all living organisms are in equilibrium with the ^{14}C concentration of the atmosphere. When an organism dies, all metabolic processes stop and there is no longer any renewal of the carbon in the organism and the radioactive decay will be the cause of a continuous decrease of the ^{14}C content in the remains of the organism. More generally, one can say that the radiocarbon clock starts to tick when the organism dies or has left the carbon cycle. It has to be noted here that the definition of a living organism is somewhat tricky. If

we look at a tree for instance, only the youngest growth ring can be considered as a living organism. This implies that only the last tree ring is in equilibrium with the atmosphere at the time of growth and that all rings from previous growth seasons reflect the ^{14}C content of the year of their growth. This effect can be very important in long-living trees and is called the “old-wood effect”.

Essentially, the radiocarbon dating technique will compare the remaining ^{14}C content of an organic object with the atmospheric ^{14}C content and by means of the decay curve (Fig. 1) calculate the time that has passed since the material left the carbon cycle (formula 3).

$$A = A_0 \times e^{-\lambda t} \quad (3)$$

A activity of the sample, A_0 activity of the modern atmosphere, t time, $1/\lambda = T/\ln 2$ ($T = \text{half-life}$).

2.4 Assumptions and Corrections

2.4.1 The Libby Half-Life

When James and Libby¹ [6] published their first list of dates, they assumed that the half-life of radiocarbon was 5568 ± 30 years. Later scientists discovered that this value was 3 % off, so all measurements were wrong by 3 %. By the time that the real half-life was discovered, there were already so many dates published that a change from one half-life to another would have been very confusing. So it was decided to continue to use the wrong Libby half-life.

2.4.2 Before Present (BP)

In the 1950s, Hans Suess discovered that due to the emission of fossil-fuel (coal and petroleum) derived CO_2 , the ^{14}C content of the atmosphere was lower than expected [7, 8]. As a result of this, an artificial modern radiocarbon standard was made based on the pre-industrial radiocarbon content of the atmosphere. By convention, the year 1950 was chosen as the zero year for the method. So, for example, 1900 BP (Before Present) was supposed to be 50 AD.

2.4.3 Isotopic Fractionation

Almost every chemical reaction results in isotopic fractionation. This means that the $^{13}\text{C}/^{12}\text{C}$ ratio ($^{13}\text{C}/^{12}\text{C}$) changes due to chemical reactions. For instance, the $^{13}\text{C}/^{12}\text{C}$ in the carbon dioxide of the atmosphere is different from the $^{13}\text{C}/^{12}\text{C}$ in the carbon of the cellulose made by photosynthesis (Fig. 2). The same is true for the $^{14}\text{C}/^{12}\text{C}$. This means that the ^{14}C content of the plant cellulose has changed in comparison to the atmosphere although there is no difference in age, so it is necessary to correct for

¹ Libby developed [4, 5] the radiocarbon dating method and received for this the Nobel Prize in Chemistry in 1960.

Table 1 Average $\delta^{13}\text{C}$ values for the most commonly dated materials

Material	$\delta^{13}\text{C}$ (‰)
Wood (C3-type plants like leaf trees)	-25
Plants from arid environments (C4-type plants)	-13 to -10
Charcoal	-25 to -30
Peat	-30
Bone collagen	-19 (depending on the type of diet)
Freshwater plants	-16
Marine plants	-12
Atmospheric CO_2	-8
Marine carbonate (shells)	0

this change in concentration. Fortunately, the correction is rather easy to make (formula 4).

$$\Delta t = (\delta^{13}\text{C} + 25) \times 16 \text{ year} \quad (\delta^{13}\text{C} : \text{the measured isotopic fractionation in permil}) \quad (4)$$

Table 1 represents the most common $\delta^{13}\text{C}$ values for different materials.

2.4.4 The Conventional Radiocarbon Date

Although these corrections were known for quite some time, it took the radiocarbon community a long time before finally defining a conventional radiocarbon date [9]. By definition, a conventional radiocarbon age is a radiometric age wherein the radiocarbon content of a sample is compared to that of the NBS oxalic acid standard, both normalized for isotopic fractionation. The Libby half-life is used in the age calculation and the result is expressed in BP \pm 1 standard deviation (σ).

$$t = 8033 \cdot \ln \frac{A_{\text{on}}}{A_n} \text{ (BP)} \quad (5)$$

ln: logarithm, A_{on} : the normalized activity of the modern standard, A_n : the normalized activity of the sample.

In the next paragraph, it will be shown that the conventional radiocarbon date is not a date at all. In fact, it was a historical mistake to call a radiocarbon measurement a date.

2.4.5 Calibration

One of the initial assumptions of the method was that the rate of production of radiocarbon has been constant over time. This assumption was incorrect, meaning that radiocarbon years are not equivalent to calendar years. Long-term variations in the rate of production seem to correspond to fluctuations in the strength of the earth's magnetic field. Short-term variations or "wiggles", are known as the de

Vries effect (after Hessel de Vries [10]) and may be related to variations in sunspot activity.

These temporal fluctuations in ^{14}C concentration of the atmosphere necessitate the calibration of radiocarbon results. At first, and this for approximately the last 10,000 years of the time scale, dendrochronology was used to calibrate radiocarbon results. Primarily US bristlecone pine and German and Irish oak were used to establish a calibration curve. More recently, and this for older periods until 50,000 years ago, varves (laminated lake deposits) and corals are used to construct a radiocarbon calibration curve. The most recent curve was published in 2013 [11] by an international group directed by Paula Reimer. **Figure 3c** depicts the calibration of the ^{14}C date from a Coptic textile represented in **Fig. 3a, b**. On top of the graph, the lab code (KIA-28757), the sample code (KN-1475), and the conventional date (1570 ± 25 BP) are mentioned. The radiocarbon measurement, being a Gaussian distribution represented by the mean and the standard deviation (in this case 1570

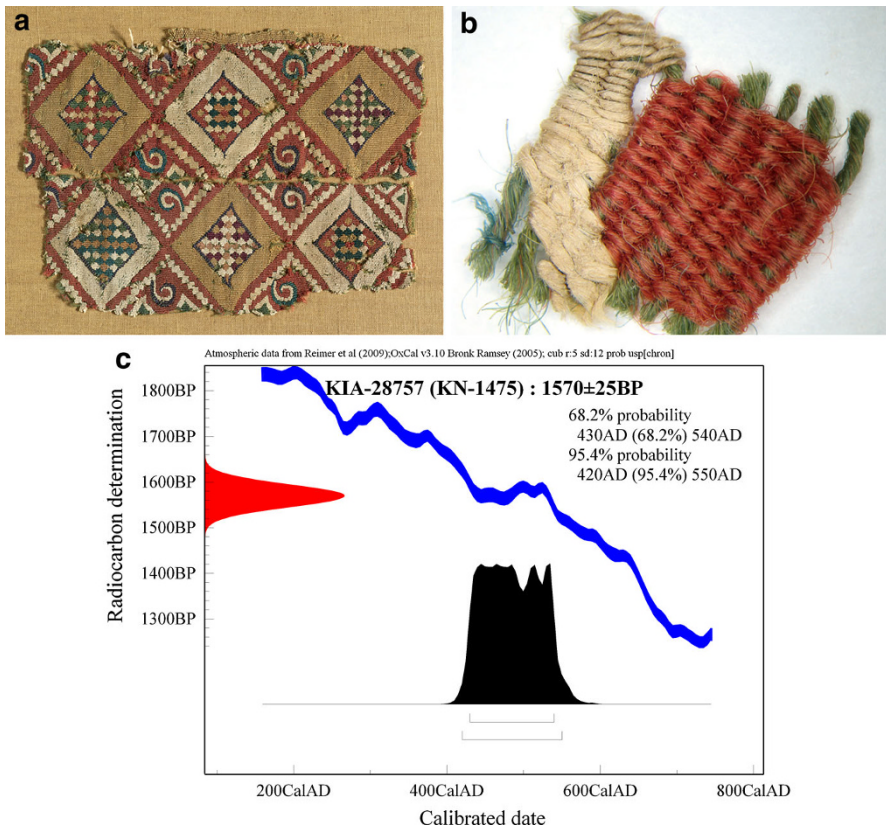


Fig. 3 **a** Polychrome tapestry, dyed with real purple (KN-1475). ©Katoen Natie, photo Hugo Maertens. **b** Detail of the sample. Samples are looked at under the microscope to reveal the presence of contaminants, mainly dust and consolidation products. If there is any doubt about the quality of the material, then a FT-IR analysis is performed ©KIK-IRPA. **c** Calibrated radiocarbon result

and 25), is represented by the curve on the vertical axis. The zigzag line represents the calibration curve. This curve gives the relationship between the radiocarbon age (vertical axis) and the calendar age (horizontal axis). The probability distribution on the horizontal axis represents the probability distribution of the calibrated age. In the upper right corner of the graph, this probability is noted in real years. So in this case, there is 95.4 % probability that the real age is between 420 and 550 cal AD. AD stands for *Anno Domini*, while the prefix ‘cal’ refers to the fact that the result is obtained by calibration of a radiocarbon date. Here the calibration was done by one of the most popular calibration programs OxCal,² but other programs do exist.

Unfortunately, due to a plateau in the calibration curve caused by changes in the solar activity [12], commonly called the Maunder minimum,³ followed by the emission of ¹⁴C free fossil CO₂ during the Industrial Revolution (Suess effect), radiocarbon is unsuitable for dating objects from ca. 1630 AD until the beginning of the second half of the 20th century.

3 Measuring ¹⁴C

Until the late 1970s, ¹⁴C could only be measured by the β -counting technique. This is a technique whereby the decay product, in this case electrons, is measured. Because of the very low content of ¹⁴C in natural materials, the amount of sample needed for the measurement and the measuring time were very important. Scientists realized, however, that it would be much more efficient to count the different radiocarbon isotopes in the sample (¹²C, ¹³C, ¹⁴C) instead of measuring the β -emission. This became possible for the first time in 1977 using the so-called accelerated mass spectrometry (AMS) technique. The first AMS measurements were conducted by teams at Rochester/Toronto and the General Ionex Corporation and soon after at the Universities of Simon Fraser and McMaster [13]. It would, however, take more than 20 years before AMS became the standard measuring technique. Not that AMS provides a priori better results than the old β -counting machines, but the counting time shrunk from ca. 2 days to 50 min, and routinely only 1 mg of carbon is needed instead of 1 g or more. AMS would really cause a revolution in the dating of precious art objects (Fig. 4).

4 Radiocarbon Dating of Cultural Objects

4.1 Dating an Object

In the ‘Notre-Dame d’el Vaux’ church in the Belgian town of Thuin, a wooden *Sedes Sapientiae* (Seat of Wisdom) called Notre Dame du Val is kept (Fig. 5a, b). Not only was the polychromy from 1891 but also important modification were made. The original chair was replaced by an impressive throne and the missing arms

² <https://c14.arch.ox.ac.uk/embed.php?File=oxcal.html>.

³ https://en.wikipedia.org/wiki/Little_Ice_Age and https://en.wikipedia.org/wiki/Maunder_Minimum.



Fig. 4 MICADAS: AMS machine made by Ionplus AG and installed at the Royal Institute for Cultural Heritage, Brussels. ©KIK-IRPA

of the Virgin and the Child were replaced. The position of the hand of the Virgin does not correspond to its original position, proven by the fact that the end of the original fingers from the left hand holding the Child around its waist are still visible. This and other multiple changes made people wonder if there was still a lot left of the original sculpture. To investigate this, a sample was taken from the main wooden trunk the statue was made of. To avoid extra damage, the sample was taken from a crack in the 19th-century polychrome painting. Before dating, the sample was scanned for consolidation products by FT-IR. The most used consolidants in restoration are animal glue, Paraloid (thermoplastic resin), PEG (polyethylene glycol) and PVA (poly vinyl acetate), but any ‘home-made’ mixture of consolidants can be found on sculptures. If one or more of these products are detected, then a special pre-treatment procedure is applied. After pre-treatment, the sample is tested again and only dated if the results are satisfactory.

The ^{14}C -results (RICH-21902: 937 ± 27 BP) gave a period between 1020 and 1160 cal AD (95.4 % probability). This is of course the age of the wood. One could argue that in the 19th century, old wood was used to create the statue. In theory, this is possible, but old wood is very difficult to work and a skilled restorer will notice the difference in almost any case. Furthermore, because the wood of the statue does not show any sapwood rings, we don’t know exactly how many rings were cut away by the artist. In fact, the age of the tree ring that was sampled was measured and not the felling date of the tree. This difference is not negligible, but in most cases only a few decades. So it was concluded that the statue, although heavily restored in the 19th century and probably already before, remains one of the rare Romanesque *Sedes Sapientiae* that survived in Belgium.

4.2 Dating a Period

It is of course very interesting to be able to date an object, but it is more interesting to be able to define a period during which a certain type of objects was in use. These



Fig. 5 **a** *Sedes Sapientiae* from Thuin (Belgium), ©KIK-IRPA. **b** X-ray picture of the *Sedes Sapientiae* from Thuin (Belgium). One can detect the nails by which new parts were added, ©KIK-IRPA. **c** Sampling point. ©KIK-IRPA

kinds of studies have been done to a great extent on textiles from the Nile Valley, roughly from the first millennium AD. This period is often called the Roman, Coptic, and Early Islamic Period. From a theoretical point of view, textiles are ideal for radiocarbon dating. Wool and silk, but also cotton, linen, and other plant fibers, are the result of only one growth season. So the radiocarbon content of the raw material reflects a very short period of assimilation of CO_2 from the atmosphere (by the food chain or by photo synthesis). Furthermore, the raw material is never stored for very long time before it is used to make a fabric. So we can state that there is a good relationship between the human event of interest (making of the fabric) and the radiocarbon event (assimilation of ^{14}C from the atmosphere) [14]. Sometimes parts of garments, like clavi, embroideries, etc., are re-used on new tunics. Even



Fig. 6 The Coptic mummy of Euphemia, the embroideress. ©KIK-IRPA

then the date of a textile fiber from the decoration will give us the age of that fabric and not of the new garment.

The radiocarbon dates are in fact the only secure dating technique because contextual as well as stylistic dating are unsecure. Often, Coptic textiles have no context. Most museum collections are derived from either old grave robberies or from 19th-century excavations. Even the context of the latter is unconfident. Late-19th century and early 20th-century excavators sold their finds to obtain funding for new excavations. When they exhibited their finds for the auction, the objects were staged. This was very well demonstrated by the study of the Coptic mummy of Euphemia, the embroideress (Fig. 6), kept in the Brussels museum of Art and History [15, 16]. The mummy was excavated by the French archaeologist Albert Gayet. More than 30 radiocarbon dates were spent on the mummy. The age of the person was obtained by dating her hair and a sample of the skin of the sole of her foot [95.4 % probability that the real age is between 440 and 490 AD (10.4 %) or between ad 530 and 610 AD (85.1 %)]. The dating of the textiles showed that the clothes she was ‘really’ wearing, in other words the ones on her body, had statistically the same age as the samples from her body, but all of the textiles draped around the mummy were from another period. Very typical of this staging was for instance the compensation of a missing mantle. Originally a mantle must have been attached to a ‘bourrelet’ (kind of headdress). This missing mantle was replaced by two other fabrics. On the right shoulder, the ‘bourrelet’ was attached by means of a thread, ^{14}C dated as modern, to a fragmentary fabric decorated with flowers and birds in a tapestry weave. It is part of a larger piece, probably a curtain, of which 18 other fragments are preserved. On the left, a fabric was sewn that was originally a pillow case. Both fragments were Coptic but were dated older than the mummy!

The traditional art-historical dates, based on typology, are not helping us either. It has been shown that those traditional dates are often wrong. Figure 7a represents the radiocarbon dates and the typological dating of 11 monochrome purple textiles from the Louvre collection (Fig. 7b). The group contains monochromatic tapestries, decorations for tunics or shawls, woven on linen tabbies,⁴ which sometimes present looped wefts. The color is obtained by dyeing the woolen wefts with a mixture of

⁴ For technical terms such as bourrelet, tapestry, weft..., see *Fabrics: a vocabulary of technical terms*, English, French, Italian, Spanish, Centre international d’Etude des textiles anciens, 34, rue de la Charité, Lyon, France.

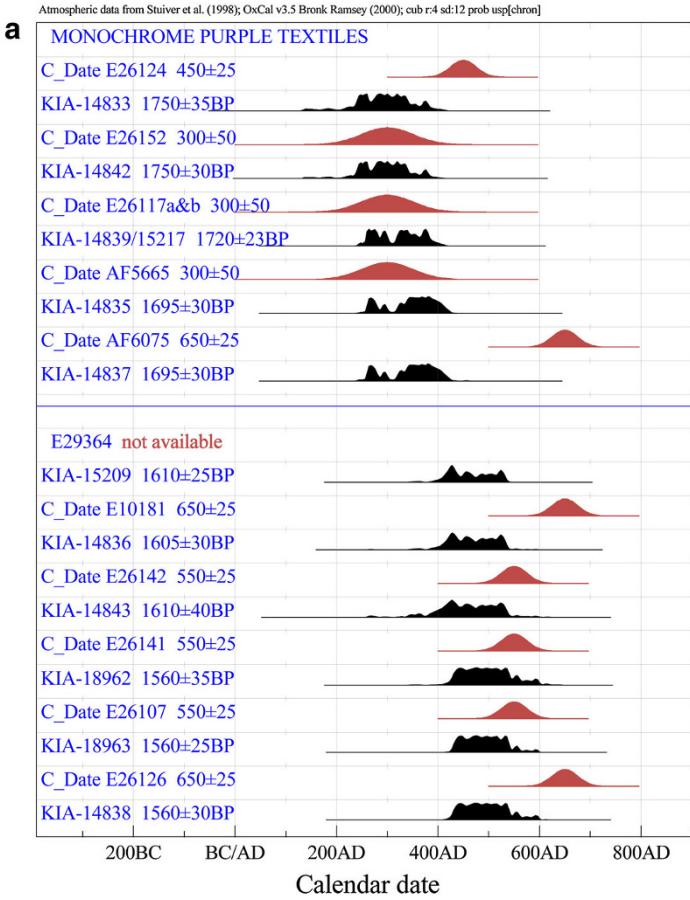


Fig. 7 **a** Radiocarbon (*black curves*) and stylistic (*red curves*) dating of monochrome purple dyed textiles. **b** Monochrome purple textile E26126 (Louvre)

madder and indigo, providing various shades of purple, violet, dark blue, etc. This “purple” color contrasts with the white natural linen. Tiny details are designed with a flying shuttle of undyed linen thread. It is obvious from Fig. 7a that there is not a good agreement between the radiocarbon and art-historical dating. Furthermore, the radiocarbon analyses show very well that there are two distinct groups, one older and one younger than 400 AD, information that is not to be retrieved from the stylistic dating.

In order to obtain information about the period in which a certain fabric was used a set of objects all having the same characteristics (type of dyestuff, weaving technique, stylistic characteristics, etc.) are dated and the probability distributions are added up to obtain a sum-probability. Of course the sample selection must be unbiased and therefore samples should be selected at random. Unfortunately, the number of textiles that survived are limited and therefore as many samples as possible should be dated, supposing that the survival of the fabrics over time was a random process. As an example, the dating series of 11 late Roman socks is represented. Samples came from the Katoen Natie (Antwerp), Royal Museums of Art and History (Brussels), Musée du Louvre (Paris), The British Museum (London), Victoria & Albert Museum (London), Petrie Museum (London). Figure 8a depicts a pair of children’s socks from the collection. The individual dates are depicted in Fig. 8b, the sum-probability in Fig. 8c. The shape of the sum-probability curve is highly influenced by the shape of the calibration curve in that particular period and therefore not much attention should be given to this curve. Much more interesting is to define the ‘floruit’ or interquartile range (IQR) and the 90 % probability range [17]. The IQR is defined by the range between the 75th percentile and the 25th percentile of the probability curve. It is a very robust indicator and represents the ‘blooming period’ or ‘floruit’. It is preceded by an ‘initial period’ and followed by a ‘decline’. In the case study represented here, the floruit is between 231 and 375 AD.

4.3 Detecting Forgeries

Sometimes it is possible to detect forgeries by means of radiocarbon. Often, recent forgeries can be detected by means of the so-called ‘bomb peak’ [18]. In the 1950s and 1960s, nuclear weapon tests were performed in the atmosphere. Consequently, the ^{14}C content of the atmosphere rose to about 100 % above normal in 1964. After the treaties between the nuclear powers in the second half of the 1960s, the ^{14}C content of the atmosphere started to decrease. Organic material that was formed in that period has a radiocarbon content that is above natural levels. This method was used to identify the fabrication date of a wooden statue supposed to be from the Tang dynasty (AD 618–690 and 705–907), called the ‘fat lady’. Traditionally, this type of statue is made of glazed or unglazed ceramics, but this was a wooden statue and a wooden statue of this kind seemed unlikely.

Figure 9 depicts the calibrated date of the analysis. Instead of OxCal, Calibomb⁵ was used to calibrate the date. The vertical axis now gives the probability

⁵ <http://calib.qub.ac.uk/CALIBomb/>.

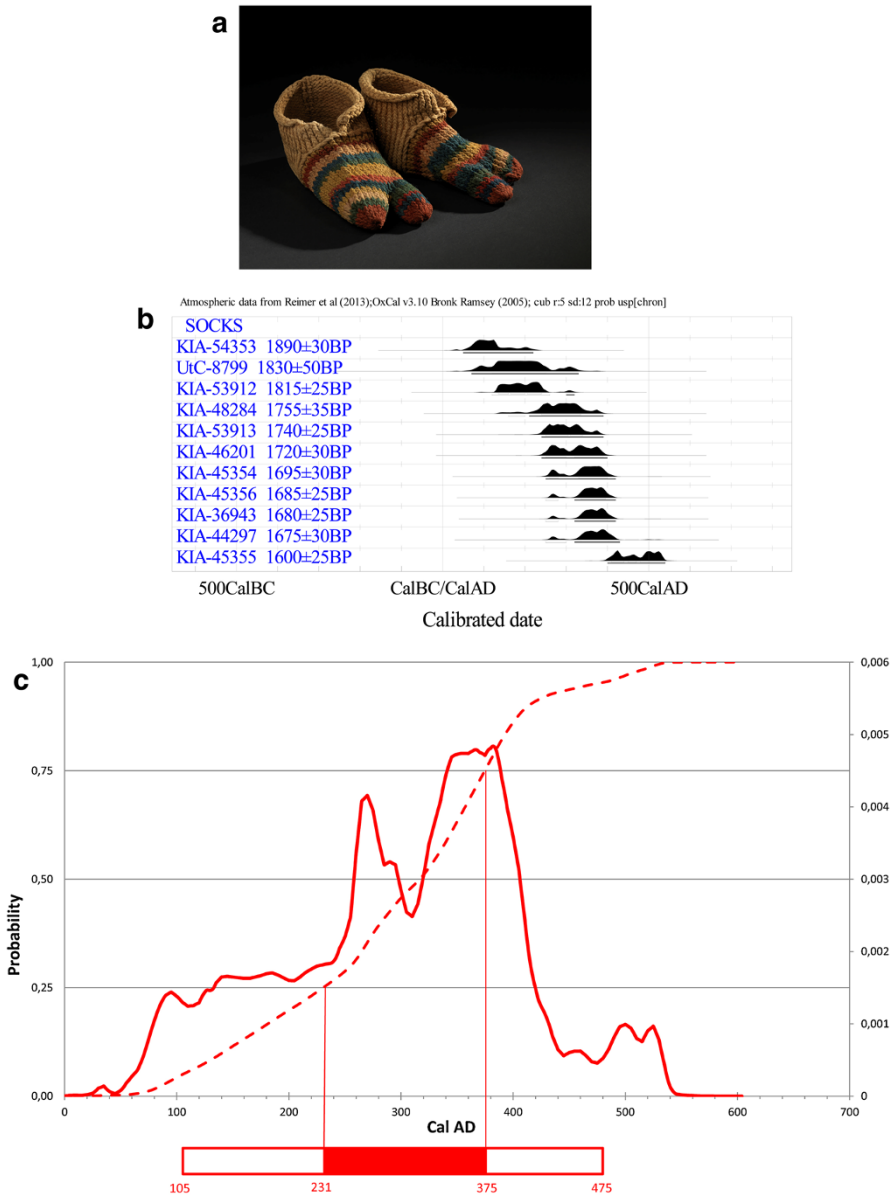


Fig. 8 **a** Late Roman children's socks. ©Katoen Natie, photo Hugo Maertens. **b** Probability distributions of 11 radiocarbon dates from late Roman socks. **c** Sum-probability and integrated probability distribution (dotted line). The interquartile range and the 90 % probability range is depicted. ©KIK-IRPA

distribution of the ^{14}C concentration and not the BP date anymore. The result [UtC-2608: $1.500 \pm 0.009 F$ (fraction modern carbon)] indicates that the radiocarbon content of the sample is 50 % above normal. The curve in the middle represents once again the relationship between the radiocarbon concentration and the calendar

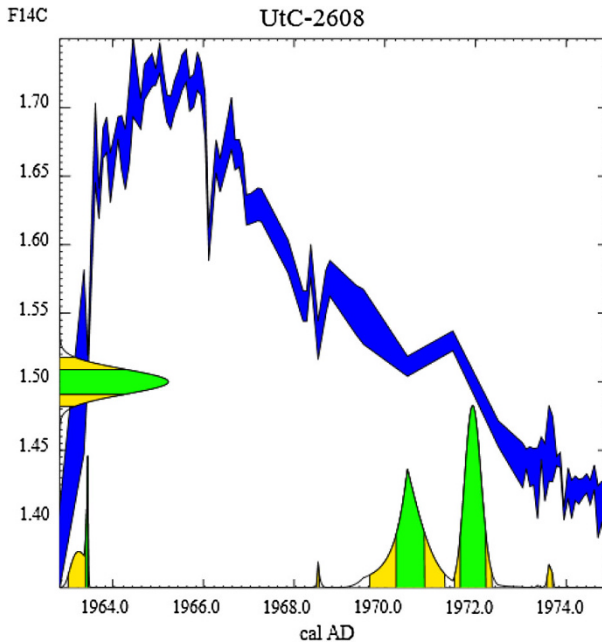


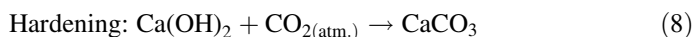
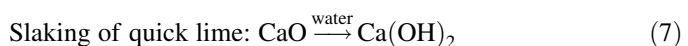
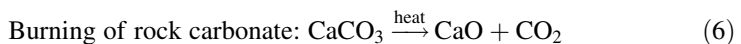
Fig. 9 Calibrated result of a wooden statue; UtC-2608: $1.500 \pm 0.009 F$

years. Note the very sharp rise in the period 1960 to 1964 due to the nuclear weapon tests and the slow decrease of the ^{14}C concentration in later periods.

The analysis shows that the wood from the statue is either from 1963 cal AD or from 1968 to 1973 cal AD, so definitely not from the Tang dynasty.

4.4 Dating Exotic Materials

Traditionally, radiocarbon dating is used to date organic material, but in fact, the method can date any material that has taken up ^{14}C from the atmosphere. So radiocarbon will also be found in shells and speleothems, but also in anthropogenic carbonates like lime mortar, plasters, and stucco. The process is more or less the same for all these materials. Rock carbonate is heated at a high enough temperature to decompose (formula 6). The formed quicklime will react with water to form slacked lime (formula 7). Finally, the slacked lime will harden by the absorption of carbon dioxide and forms calcium carbonate (formula 8).



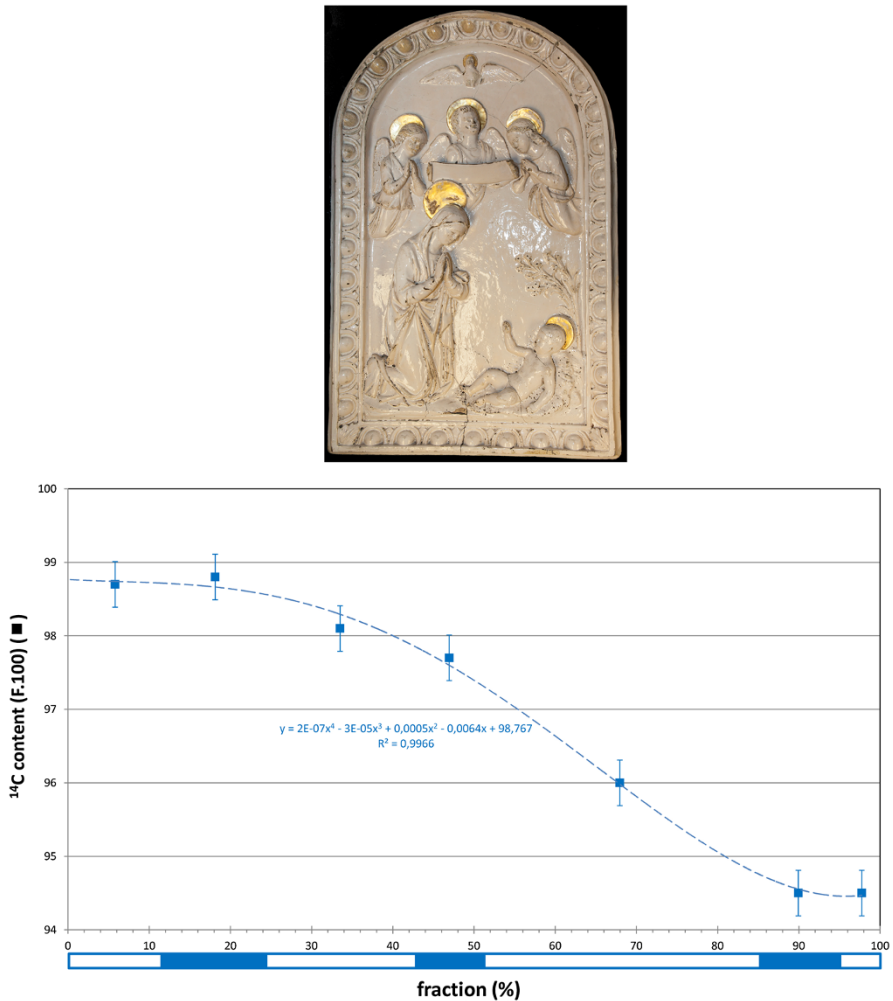
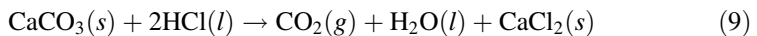


Fig. 10 **a** A supposed Italian stucco from ca. 1400 AD, ©KIK-IRPA. **b** The radiocarbon concentration of seven fractions obtained by the titration method. *Left* first fraction = more anthropogenic, *right* last fraction = less anthropogenic and more fossil rock carbonate. ©KIK-IRPA

Unfortunately, in most cases the reaction in formula 6 is not complete due to insufficient heating in the lime kiln, so the carbon in the lime is a mixture of infinite old rock carbonate and carbonate from the time the lime was made. It has, however, been proven [15, 16, 19, 20] that the softer anthropogenic lime tends to react faster with acid (formula 9) than the harder rock carbonate. So by performing a sequential or titration reaction with HCl, both carbonates can (sometimes) be separated.



This method was performed in the analysis of a stucco from Italy. Stucco or render is a material made of an aggregate, a binder and water just like a mortar. Stucco is applied wet and hardens to a very dense solid. It is used as a decorative coating for walls and ceilings and as a sculptural and artistic material in architecture. Traditional stucco is made of lime, sand, and water. Modern stucco is made of Portland cement, sand and water. Evidence of the use of stucco as a decoration material goes back to the Minoan palace of Knossos (around 1600 BC) in Crete and to Egypt during the XVIII dynasty (1543–1292 BC), but it is during the Baroque and Rococo periods that it has his maximum diffusion.

A stucco supposed to be from ca. 1400 AD was investigated. Figure 10a depicts the dated object. The sample contained only 0.32 % of carbon. This was already very suspect because traditional stucco contains much more lime, up to 30 %. It seemed already that the sample was made of cement instead of lime. Figure 10b depicts the results of the different fractions obtained by the titration method. The first fraction is left on the graph, the last fraction is right on the graph. The graph shows very well that the sample is a mixture of old and young carbonate. The two first fractions have statistically the same age; this is a strong indication that they are free of fossil carbonate. In the other fractions, one can notice an increasing content (from left to right) of fossil carbonate (older apparent age). The youngest fractions have an F value of 0.988 ± 0.004 (or 98.8 ± 0.4 % modern carbon). After calibration, this gives a calendar date between 1680 and 1940 cal AD. Consequently, the stucco cannot be made around 1400 AD.

5 Conclusions

Although radiocarbon dating is not the most obvious technique to use in the study of cultural objects, the method remains relatively un-precise and cannot be used in all periods, in many cases it can help in dating objects, establishing periods, as well as in detecting forgeries. The above-mentioned objects are only an anthology of a large variety of objects dated at the Royal Institute of Cultural Heritage in Brussels. The assemblage of dated objects also contains Japanese suits of armor (lac), wooden chests, crucifixes, oil paintings on wood and canvas, Thorahs and Korans made of parchment and paper, ink, ivory statues and medallions, etc., and they encompass a very large period from pre-historic art to the Russian Avant Garde. One must, however, always keep in mind that the method dates the material the object is made of and not the manufacturing of the object.

References

1. Ladenburg RW, Yuan LCL (1949) Distribution of slow neutrons in free atmosphere up to 67,000 feet. Colston papers, vol. I. Supplement to research, a journal of science and its applications. Butterworths Scientific Publications, London, p 35
2. Anderson EC, Libby WF, Weinhouse S, Reid AF, Kirshenbaum AD, Von Grosse A (1947) Natural radiocarbon from cosmic radiation. Phys Rev 72:931–936

3. Anderson EC, Libby WF, Weinhouse S, Reid AF, Kirshenbaum AD, Von Grosse A (1947) Radiocarbon from cosmic radiation. *Science* 106:576–577
4. Arnold JR, Libby WF (1949) Age determinations by radiocarbon content: checks with samples of known age. *Science* 110:678–680
5. Libby WF (1955) Radiocarbon dating, 2nd edn. University of Chicago Press, Chicago
6. James AR, Libby WF (1951) Radiocarbon dates. *Science* 113:111–120
7. Suess HE (1955) Radiocarbon concentration in modern wood. *Science* 122:415–417
8. Tans PP, de Jong AFM, Mook WG (1979) Natural atmospheric C-14 variations and the Suess effect. *Nature* 280:826–828
9. Stuiver M, Polach HA (1977) Discussion: reporting of ^{14}C data. *Radiocarbon* 19(3):355–363
10. de Vries HL (1958) Variation in concentration of radiocarbon with time and location on Earth. *Proc Koninklijke Nederlandse Akademie Wetenschappen* 61:94–102
11. Reimer PJ, Bard E, Bayliss A, Beck JW, Blackwell PG, Bronk Ramsey C, Buck CE, Cheng H, Edwards RL, Friedrich M, Grootes PM, Guilderson TP, Hafflidason H, Hajdas I, Hatté C, Heaton TJ, Hoffmann DL, Hogg AG, Hughen KA, Kaiser KF, Kromer B, Manning SW, Niu M, Reimer RW, Richards DA, Scott EM, Southon JR, Staff RA, Turney CSM, van der Plicht J (2013) INTCAL13 and MARINE13 radiocarbon age calibration curves 0–50,000 years CAL BP. *Radiocarbon* 55(4):1869–1887
12. Kocharov GE, Ostryakov VM, Peristikh AN, Vasil'ev VA (1995) Radiocarbon content variations and Maunder minimum of solar activity. *Sol Phys* 159(2):381–391
13. Gove HE (2000) Some comments on the accelerator mass spectrometry. *Radiocarbon* 42(1):127–135
14. Van Strydonck M, Nelson DE, Crombé P, Bronk Ramsey C, Scott EM, van der Plicht J, Hedges REM (1999) What's in a ^{14}C date. In: Evin J, Oberlin C, Daugas J-P, Salles J-F (eds) 3rd International Symposium ^{14}C and Archaeology, *Mémoires de la Société Préhistorique Française* 26, Supplément de la Revue d'Archéométrie, pp. 433–448
15. Van Strydonck M, Boudin M, Decq L, Van Den Brande T, Borms H, Ramis D, De Mulder G (2011) AMS ^{14}C dating of Balearic lime burials. *Radiocarbon* 53(4):563–574
16. Van Strydonck M, Vanden Berghe I, Boudin M, Quintelier K (2011) Euphemia: a multidisciplinary quest for the origin and authenticity of a mummy's clothes and accessories. In: De Moor A, Fluck C (eds) Dress accessories of the 1st millennium AD from Egypt. Lannoo, Tielt, pp 236–257
17. Van Strydonck M (2007) How accurate are ^{14}C dispersion diagrams in estimating a cultural period in the 1st millennium AD? In: De Moor A, Fluck C (eds) Methods of dating ancient textiles of the 1st millennium AD from Egypt and neighbouring countries. Lannoo, Tielt, pp 112–114
18. Hua Q, Barbetti M (2004) Review of tropospheric bomb ^{14}C data for carbon cycle modeling and age calibration purposes. *Radiocarbon* 46(3):1273–1298
19. Van Strydonck M, Dupas M, Dauchot-Dehon M, Pachiaudi C, Maréchal J (1982–1983) A further step in the radiocarbon dating of old mortars. *Bull Kon Inst v h Kunstpatrimonium* 19:155–171
20. Van Strydonck M, van der Borg K, De Jong AFM, Keppens E (1992) Radiocarbon dating of lime fractions and organic material from buildings. *Radiocarbon* 34(3):873–879
21. Mook WG, Waterbolk HT (1985) Handbook for archaeologists, no. 3, radiocarbon dating. European Science Foundation, Strasbourg